Ministry of
Northern Development
and Mines

Mines and
Minerals
Division

Ontario

Geoscience Research Grant Program
Summary of Research 1988–1989

Ontario Geological Survey
Miscellaneous Paper 143

edited by
V.G. Milne

1989

90-02035/

© 1989 Queen's Printer for Ontario
Printed in Ontario, Canada

ISSN 0704-2752 (Series)
ISSN 0225-5316 (Sub-series)

Publications of the Ontario Geological Survey and the Ministry of Northern Development and Mines are available from the following sources. Orders for publications should be accompanied by cheque or money order payable to the *Treasurer of Ontario*.

Reports, maps, and price lists (personal shopping or mail order):

Public Information Centre, Ministry of Natural Resources
Room 1640, Whitney Block, Queen's Park
Toronto, Ontario M7A 1W3

Reports and accompanying maps only (personal shopping):

Publications Ontario
Main Floor, 880 Bay Street
Toronto, Ontario M7A 1N8

Reports and accompanying maps (mail order or telephone orders):

Publications Ontario, Ministry of Government Services
5th Floor, 880 Bay Street
Toronto, Ontario M7A 1N8
Telephone (local calls), 965-5300
Toll-free long distance, 1-800-668-9938

Every possible effort is made to ensure the accuracy of the information contained in this report, but the Ministry of Northern Development and Mines does not assume any liability for errors that may occur. Source references are included in the report and users may wish to verify critical information.

If you wish to reproduce any of the text, tables or illustrations in this report, please write for permission to the Director, Ontario Geological Survey, Ministry of Northern Development and Mines, 11th Floor, 77 Grenville Street, Toronto, Ontario M7A 1W4.

Parts of this publication may be quoted if credit is given. It is recommended that reference be made in the following form:

Shanks, W.S. and Schwerdtner, W.M. 1989. Deformation of the Sudbury Structure; *in* Geoscience Research Grant Program, Summary of Research 1988-1989, Ontario Geological Survey, Miscellaneous Paper 143, p.4-17.

Scientific Editing: PDM Information Technology Inc. 1000-89-Deyell

Contents

Introductory Remarks, *V.G. Milne* 2

Grant 275 Deformation of the Sudbury Structure, *W.S. Shanks and W.M. Schwerdtner* 4

Grant 290 A Fast Method of Maximal Simplicity Gravity Imaging, *R.C. Bailey and W. Colangelo* 18

Grant 294 Quaternary Geology and Geochemical Exploration in the Matheson Area, *M.B. McClenaghan, O.P. Lavin, I. Nichol and J. Shaw* .. 24

Grant 300 The Genesis of Silver Vein Deposits in the Thunder Bay Area, Northwestern Ontario, *S.A. Kissin and R.L. Sherlock* 33

Grant 305 Metamorphic Petrology and Gold Mineralization of the White River Gold Prospect, Hemlo Area, *Y. Pan and M.E. Fleet* 42

Grant 310 Subsurface Radar Profiling of Two Peatlands in Southern Ontario, *D.C. Nobes, B.D. Theimer and B.G. Warner* 53

Grant 313 Hydrothermal Activity in the Kirkland Lake Intrusive Complex, *Keiko Hattori and Guy Levesque* 59

Grant 319 Gypsum Deposits of Southern Ontario, *S.J. Haynes and J. Hughes-Pearl* 68

Grant 322 Subaqueous Volcaniclastic Rocks of the Confederation Lake Area, Northwestern Ontario: Discrimination between Pyroclastic and Epiclastic Emplacement, *John Stix and Michael P. Gorton* 83

Grant 323 Lithogeochemical, Isotopic and Fluid Inclusion Studies of Hydrothermal Alteration and Breccia Veins from the Cameron Lake Gold Deposit, Northwestern Ontario, *D.R. Melling, R.P. Taylor, D.H. Watkinson and Xin Wu* 94

Grant 326 PGE Studies in the Footwall at Sudbury, *C. Li and A.J. Naldrett* 104

Grant 328 Microbial Biofilms: Colonization, Metal Uptake, and Mineralization, *F.G. Ferris, J.B. Thompson, S. Schultze, T. Witten, W.S. Fyfe and T.J. Beveridge* 114

Grant 329 The Expression of the Larder Lake Break in the Matachewan Area, *W.G. Powell, C.J. Hodgson and J.A. Hanes* 125

Grant 331 Petrology of the Springpole Lake Alkalic Volcanic Complex, *K.M. Barron, N.A. Duke and R.W. Hodder* 133

Grant 332 High-Resolution Magnetic-Susceptibility Logger and Dipmeter for Mineral Exploration Boreholes: Concept and Initial Progress, *Alfred V. Dyck, Peter V. Auchincloss and David L. Atherton* 146

Grant 336 Residence Sites of Zinc in Weathered Till from the Clyde River Prospect in Eastern Ontario, *Adrienne C.L. Larocque and H. Wayne Nesbitt* 160

Grant 341 PGE Study of the Geordie Lake and Marathon Cu–Ni–Precious Metal Deposits, Coldwell Alkalic Complex, *D.J. Good and J.H. Crocket* 186

Grant 342 Paleomagnetic Analysis of Regional and Contact Strains, *C.J. Hale and P. Lloyd* 199

Grant 343 Structural Evolution of Central and East-Central Michipicoten (Wawa) Greenstone Belt, Superior Province, *Z.G. Arias and H. Helmstaedt* 210

Grant 351 Stratigraphy and Sedimentology of the Upper Ordovician Georgian Bay Formation, Manitoulin Island and Bruce Peninsula, *M. Byerley and M. Coniglio* 227

CONVERSION FACTORS FOR MEASUREMENTS IN ONTARIO GEOLOGICAL SURVEY PUBLICATIONS

Conversion from SI to Imperial			Conversion from Imperial to SI		
SI Unit	*Multiplied by*	*Gives*	*Imperial Unit*	*Multiplied by*	*Gives*
		LENGTH			
1 mm	0.039 37	inches	1 inch	**25.4**	mm
1 cm	0.393 70	inches	1 inch	**2.54**	cm
1 m	3.280 84	feet	1 foot	**0.304 8**	m
1 m	0.049 709 7	chains	1 chain	20.116 8	m
1 km	0.621 371	miles (statute)	1 mile (statute)	**1.609 344**	km
		AREA			
1 cm^2	0.155 0	square inches	1 square inch	**6.451 6**	cm^2
1 m^2	10.763 9	square feet	1 square foot	**0.092 903 04**	m^2
1 km^2	0.386 10	square miles	1 square mile	2.589 988	km^2
1 ha	2.471 054	acres	1 acre	0.404 685 6	ha
		VOLUME			
1 cm^3	0.061 02	cubic inches	1 cubic inch	**16.387 064**	cm^3
1 m^3	35.314 7	cubic feet	1 cubic foot	0.028 316 85	m^3
1 m^3	1.308 0	cubic yards	1 cubic yard	0.764 555	m^3
		CAPACITY			
1 L	1.759 755	pints	1 pint	0.568 261	L
1 L	0.879 877	quarts	1 quart	1.136 522	L
1 L	0.219 969	gallons	1 gallon	**4.546 090**	L
		MASS			
1 g	0.035 273 96	ounces (avdp)	1 ounce (avdp)	28.349 523	g
1 g	0.032 150 75	ounces (troy)	1 ounce (troy)	**31.103 476 8**	g
1 kg	2.204 62	pounds (avdp)	1 pound (avdp)	**0.453 592 37**	kg
1 kg	0.001 102 3	tons (short)	1 ton (short)	**907.184 74**	kg
1 t	1.102 311	tons (short)	1 ton (short)	**0.907 184 74**	t
1 kg	0.000 984 21	tons (long)	1 ton (long)	**1016.046 908 8**	kg
1 t	0.984 206 5	tons (long)	1 ton (long)	**1.016 046 908 8**	t
		CONCENTRATION			
1 g/t	0.029 166 6	ounce (troy)/ ton (short)	1 ounce (troy)/ ton (short)	34.285 714 2	g/t
1 g/t	0.583 333 33	pennyweights/ ton (short)	1 pennyweight/ ton (short)	1.714 285 7	g/t

OTHER USEFUL CONVERSION FACTORS

1 ounce (troy) per ton (short)	20.0	pennyweights per ton (short)
1 pennyweight per ton (short)	0.05	ounces (troy) per ton (short)

Note: Conversion factors which are in bold type are exact. The conversion factors have been taken from or have been derived from factors given in the Metric Practice Guide for the Canadian Mining and Metallurgical Industries, published by the Mining Association of Canada in cooperation with the Coal Association of Canada.

Geoscience Research Grant Program
Summary of Research 1988–1989

edited by V.G. Milne

Director, Ontario Geological Survey.

Introductory Remarks

The Ontario Geoscience Research Grants Program was initiated in 1978 to support geoscience research at Ontario universities. By encouraging mission-oriented research, the program complements the work of the Ontario Geological Survey in carrying out its mandate:

> To stimulate exploration for, and facilitate sound planning in, all matters related to mineral and other earth resources by providing an inventory and analysis of the geology and mineral deposits of Ontario.

The program supports applied studies of up to three years duration towards: mineral deposit characterization studies of specific occurrences or groups of occurrences; petrology, rock geochemistry, structural geology, stratigraphy and geochronology studies; field and laboratory studies leading to the development of new geophysical and geochemical concepts and techniques; engineering and environmental geology studies; and methods for improving automated or manual processing to facilitate the interpretation of geoscience data.

To be eligible to receive funding, applications must be forwarded to the Ontario Geological Survey by November 15. Project proposals are subject to review by a committee reporting to the Director of the Ontario Geological Survey. This committee advises the Minister of Mines concerning geoscience research priorities at Ontario universities and of the scientific merit and relevance of the proposals submitted. The committee consists of three representatives from the minerals industry, three representatives from the university community, four representatives from the Ontario Geological Survey, and a chairperson from either industry or a university. Members of the 1988–1989 committee include:

Dr. D.J. Misener, Chairperson; Paterson, Grant and Watson Limited

Mr. C.L. Baker; Ontario Geological Survey

Dr. A.E. Beswick; Laurentian University

Dr. G. Cargill; Cargill Consulting Geologists Ltd.

Dr. M.E. Cherry; Ontario Geological Survey

Dr. J.E. Hanneson; Ontario Geological Survey

Dr. J. Legault; University of Waterloo

Dr. R. Mitchell; Lakehead University

Dr. I.G.L. Sinclair; BP Canada Inc.

Mr. H. Wallace; Ontario Geological Survey

Successful grant recipients are required to submit progress reports for publication in the annual Summary of Research and to participate in the Ontario Mines and Minerals Symposium held each December.

Publication in other scientific journals is encouraged and a final report summarizing the research results will be released as an Ontario Geological Survey Open File Report. These reports are published periodically, and are available at the Mines Library, 77 Grenville Street, Toronto, or at Ministry of Northern Development and Mines regional offices.

During 1988–1989, 25 projects were funded under this program; of these, 13 were renewal projects.

University	Value of Grants	No. of Grants
Brock	$15,930.00	1
Carleton	24,850.00	1
Lakehead	2,950.00	1
Laurentian	14,950.00	1
McMaster	69,515.00	4
Ottawa	23,040.00	1
Queen's	165,838.00	6
Toronto	80,704.00	4
Waterloo	29,347.00	2
Western	72,876.00	4
Total	$500,000.00	25

I would like to thank Dr. D.J. Misener, Committee Chairperson, and the review committee members, all of whom gave freely of their time. The efforts of the researchers are of course fundamental and are acknowledged. The following are also acknowledged for their participation in producing this volume: R.L.W. McKnight, Grants Administrator and Secretary to the Committee; staff geologists who reviewed the papers; PDM Information Technology Inc., who edited the volume; and Bojan Sifrer, who coordinated the production of this publication.

V.G. Milne

Director
Ontario Geological Survey

Grant 275 Deformation of the Sudbury Structure

W.S. Shanks and W.M. Schwerdtner

Department of Geology, University of Toronto, Toronto

ABSTRACT

The present oval map-pattern of the Sudbury Structure has previously been considered to be the result of displacement along regional-scale dislocations of the Murray fault system. Although the displacements may be appreciable, our mapping shows that a broad zone of reverse ductile shear—the Fairbank–Whitson lakes deformation zone (FWLDZ)—affects rocks of the South Range and may be principally responsible for the present geometry of the Sudbury Structure. Large-scale faulting post-dates ductile shear.

South of the FWLDZ, rocks of the Igneous Complex have escaped penetrative tectonic deformation at the Earth's surface, but are cut by numerous conjugate shears revealing that the southern Sudbury Structure was foreshortened during regional deformation. The conjugate shear zone array suggests that the bulk shortening direction was subhorizontal and directed toward the northwest.

Linear zones of ductile shear are also common in the enveloping rocks south of the Sudbury Structure. The Creighton deformation zone consists of discrete mylonite zones (30–300 m thick) linked by a through-going dislocation, the Creighton fault. Activity along the zone both predates and postdates the Sudbury event.

Mafic dikes intrude the Igneous Complex and illustrate that ductile deformation and epidote-amphibolite facies metamorphism of the South Range rocks occurred after solidification and cooling of the Igneous Complex.

INTRODUCTION

The Sudbury Structure (SS) is a large synclinorium straddling the Archean–Proterozoic unconformity (Figure 275.1). The present oval shape measures 60 by 28 km and is elongate in a northeasterly direction subparallel to the Grenville Front. The structure is divided into several segments: the North, South and East ranges.

The Igneous Complex of the SS consists of noritic, gabbroic and granophyric rocks that were emplaced along the contact between the Onaping Formation and deformed rocks of the Superior and Southern provinces. Rocks of the Igneous Complex form the margin of the SS and rocks of the Whitewater Group form the sedimentary core. From base to top, the Whitewater Group consists of heterolithic breccias of the Onaping Formation, slate of the Onwatin Formation and greywacke of the Chelmsford Formation. Contacts within the Whitewater Group are gradational and conformable (Rousell 1984b, 1972). The rocks of the South and East ranges have been deformed and metamorphosed. By contrast, the rocks of the North Range are metamorphosed, but have escaped penetrative deformation (Fleet *et al.* 1987; Card and Hutchinson 1972).

A marginal igneous phase, the Contact Sublayer, is the locus of Ni-Cu mineralization at the Igneous Complex–footwall contact. A similar rock, the Offset Sublayer, occupies radial and concentric dikes that intrude the footwall (Grant and Bite 1984).

Although studied for nearly a century, the origin of the Sudbury Structure is still hotly debated (i.e. Muir and Peredery 1984). On the one hand, proponents of an impact hypothesis point to the development of shock-metamorphic features in the enveloping rocks (e.g. shatter cones, planar structures in minerals) as evidence of a transient high-pressure shock wave that apparently could only have been produced by meteorite impact (*see* Dressler 1984). Proponents of a volcanogenic origin point mainly to its non-circular map-pattern or to its perceived relationship with regional structures (Muir 1984; Card and Hutchinson 1972).

A proper geometric restoration of the Sudbury Structure is possible only after the field of apparent total strain has been determined (*see* Shanks and Schwerdtner 1987), the kinematics of deformation assessed, and the tectonic history deciphered. In this paper, we discuss the kinematics of deformation and the tectonic history of the Sudbury Structure. In future, a geometric restoration incorporating all presently available structural data and using various hypothetical shapes of the present Igneous Complex shall be attempted in hopes of generating the initial first-order geometry of the undeformed structure.

SYNOPSIS OF FINDINGS

The paper reports progress after 11 months of field mapping and associated laboratory analysis. All data were obtained on surface, but, where possible, were supplemented by observations underground.

The 1986–1988 field seasons were devoted mainly to detailed structural and lithological mapping in the core and southern parts of the SS. Shanks and Schwerdtner (1987, 1988) summarized the pattern of apparent total strain. Field mapping

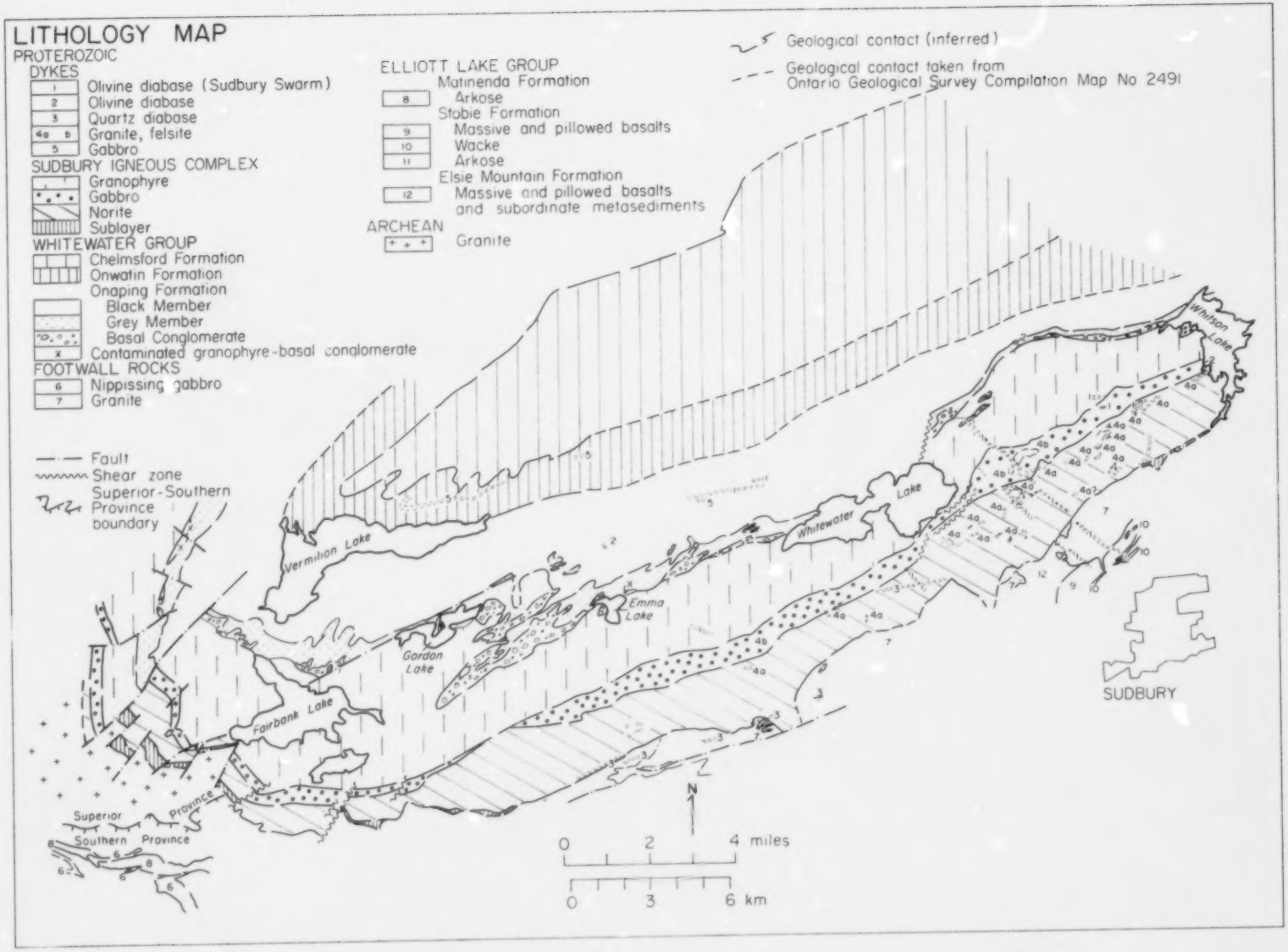

Figure 275.1. *Simplified lithological map of the Sudbury Structure project area.*

and the compilation of detailed structural maps were completed in 1988–1989 (*see* Figures 275.1–275.4). The major results of the 1988–1989 mapping session and follow-up laboratory analysis are as follows:

1. The best estimate of the near-surface dip of the FWLDZ is 40-45° southeast.
2. Assuming that the ductile strain was heterogeneous simple shear in the northwest–southeast vertical plane, the minimum estimated displacement across the middle segment of the FWLDZ exceeds 8 km. The corresponding horizontal shortening is nearly 6 km.
3. Estimates of shear magnitude derived from the angle between C- and S-surfaces (Shanks and Schwerdtner 1988) remain to be verified by alternative methods.
4. Epidote-amphibolite facies metamorphism accompanied deformation of the SS after the Igneous Complex rocks had cooled.
5. Slip on major dislocations such as the Fairbank Lake fault post-dates ductile shear in the FWLDZ.
6. Some linear zones of strongly developed rough cleavage coincide with the anticlinal crests of buckle folds in the Chelmsford Formation. Accordingly, some of these zones may not be the site of intrabasin faults as implied on published maps of the SS.
7. Displacements on the Creighton deformation zone predate and post-date the Sudbury event. Early displacements are virtually dip-slip with south side up.

DETAILED STRUCTURAL MAPPING

FAIRBANK–WHITSON LAKES DEFORMATION ZONE (FWLDZ)

The Fairbank–Whitson lakes deformation zone (FWLDZ), a major zone of reverse ductile shear, cuts the Onaping Formation and Igneous Complex in the southern Sudbury Structure. The zone has been traced for nearly 50 km along strike and passes through the southwestern footwall of the structure where it continues for an unknown distance into the Southern Province (the surficial extent of the zone is marked by schistosity trajectories on Figure 275.2). On passing through the competent norite at the southwest rim, the zone degenerates into a swarm of ductile shear zones, but regains much of its width in the wall rocks of the Southern Province. In the east, the zone extends beyond Whitson Lake. The FWLDZ may die out within the SS or turn east and leave the SS as a swarm of ductile shear zones or a series of faults. Alternatively, the zone may have caused the lobate structure of the East Range.

All rocks (except post-metamorphic dikes) are highly strained within the zone, which includes only a small portion of noritic rock. This explains the fact that almost the entire norite body of the southern Sudbury Structure is unaffected by ductile strain. The curvature of the apparent northern boundary of the FWLDZ may be real or it may be exaggerated by lack of exposure in the northeast.

Rocks of the deformation zone are L-S tectonites, whereby a schistosity which dips to the southeast throughout the entire FWLDZ is accompanied by a conspicuous stretching lineation (Figures 275.2 and 275.3). Foliation trajectories form a broad arc convex to the northwest (Figure 275.2). The stretching lineation direction varies along the zone (Figure 275.3). Near Whitson Lake, the lineation rakes steeply east, becomes subnormal over a large central zone and, in the Fairbank Lake area, rakes steeply west (Figure 275.3). This gradual change in lineation direction suggests weakly convergent flow within the deformation zone, and departs from the pattern of extension directions expected in zones produced purely by simple shear deformation. This and the apparent non-planar walls may seriously affect estimates of the magnitude of shear displacement across the zone (discussed later).

Apart from a strong schistosity, prominent planar microscale shear zones are present and interpreted as C-planes (Photo 275.1) (Shanks 1987; Escher *et al.* 1975; Berthe *et al.* 1979). Spacing of these features varies with the magnitude of strain. In some highly strained zones, a gneissic appearance is imparted to the rock. As C-planes and other shear zone fabrics have known angular relationships to zone boundaries, an indirect means exists to determine the dip of the boundary plane. Based on the average C-fabric orientation, the zone strikes 060° and has a near-surface dip of 40-45° southeast. Unfortunately, as in many large deformation zones, the dip of the boundary plane could not be measured directly.

As mine workings along the South Range have not intersected the FWLDZ, its attitude at depth is unknown. The FWLDZ may retain its 40-45° southeasterly dip as inferred from the average C-plane orientation or alternatively, it may become listric with depth. If the microscale shear zones interpreted to be C-planes are shear bands, then the inferred shear zone boundaries would dip about 65-70° to the southeast, but the deduced sense of shear would be unaffected. However, the magnitude of net displacement increases dramatically as the angle between shear zone walls and the schistosity diminishes (Ramsay and Graham 1970).

C-planes are well developed in the southern portion of the FWLDZ, notably in rocks of the Igneous Complex and Onaping Formation. However, C-planes are conspicuously absent in rocks of the upper Onaping Formation of the northern FWLDZ, yet a dramatic increase in strain from north to south is evident within the deformation zone. This indicates that either C-planes did not form in rocks of

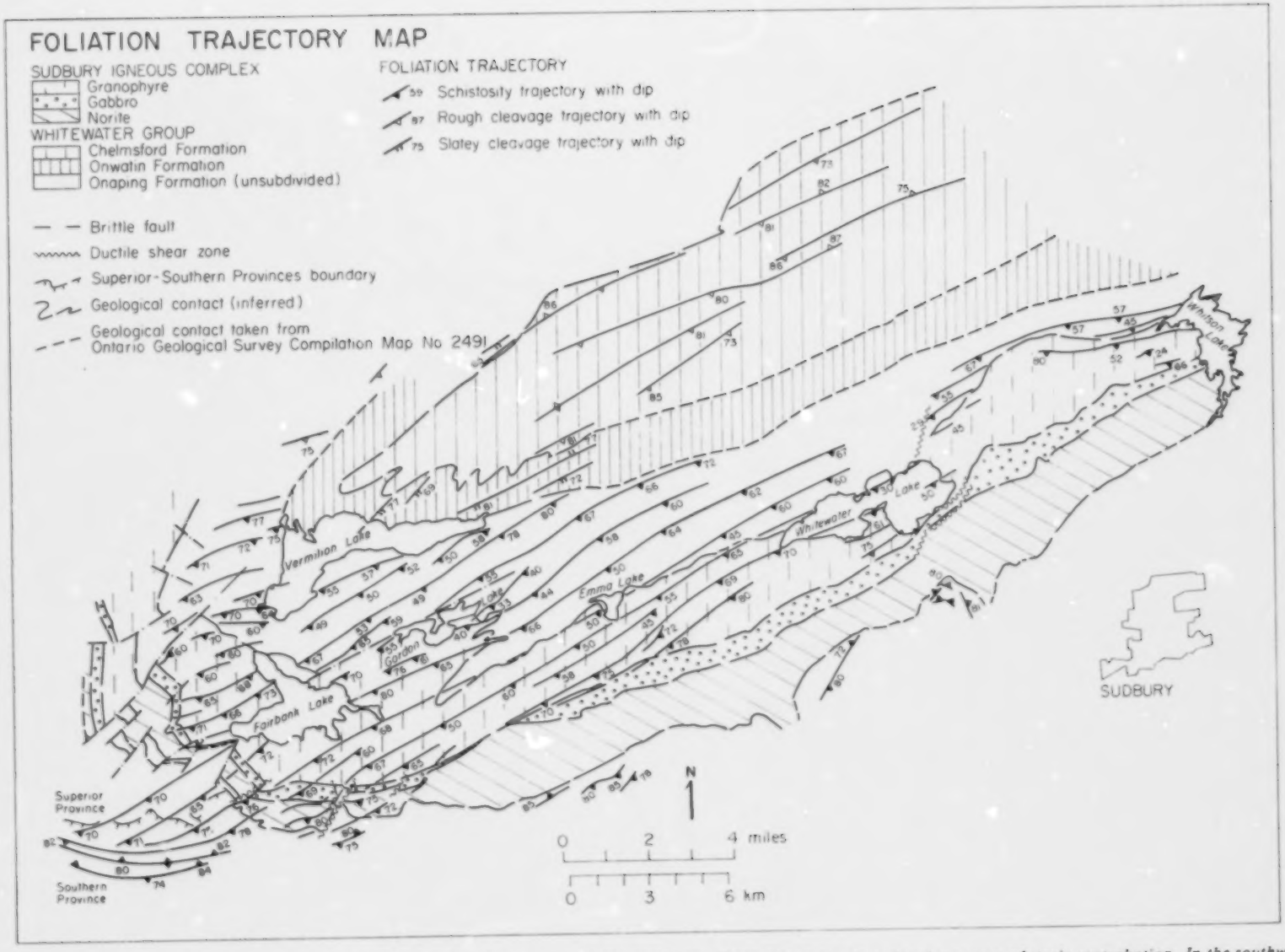

Figure 275.2. *Schistosity trajectories in the FWLDZ form a broad arc convex to the northwest. Discontinuous trajectories show areas of strain perturbation. In the southwestern Sudbury Structure, the strike of schistosity is subperpendicular to lithologic contacts.*

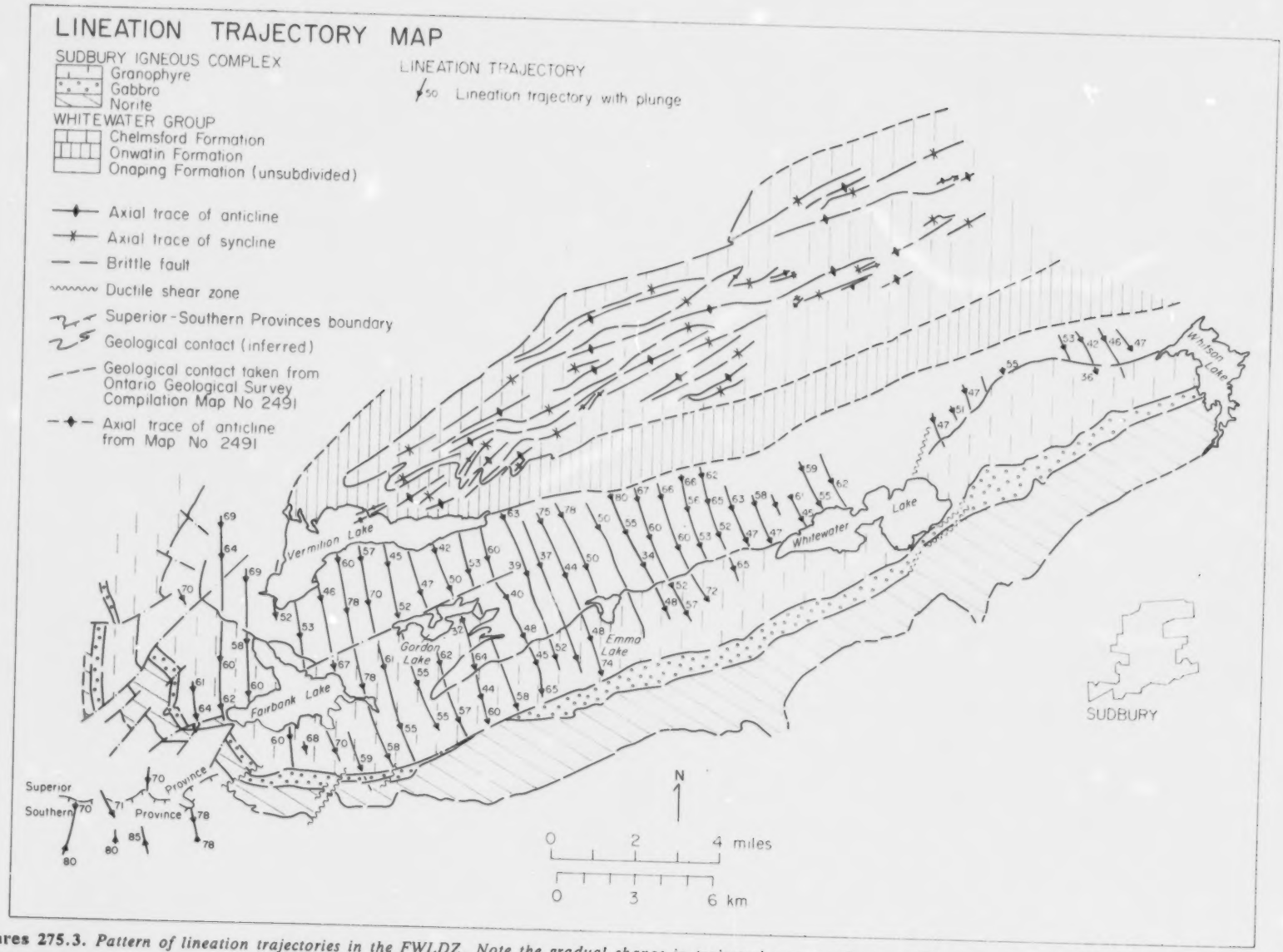

Figures 275.3. *Pattern of lineation trajectories in the FWLDZ. Note the gradual change in trajectories across the zone. The sinuous and/or bifurcating fold system of the sedimentary core is also shown.*

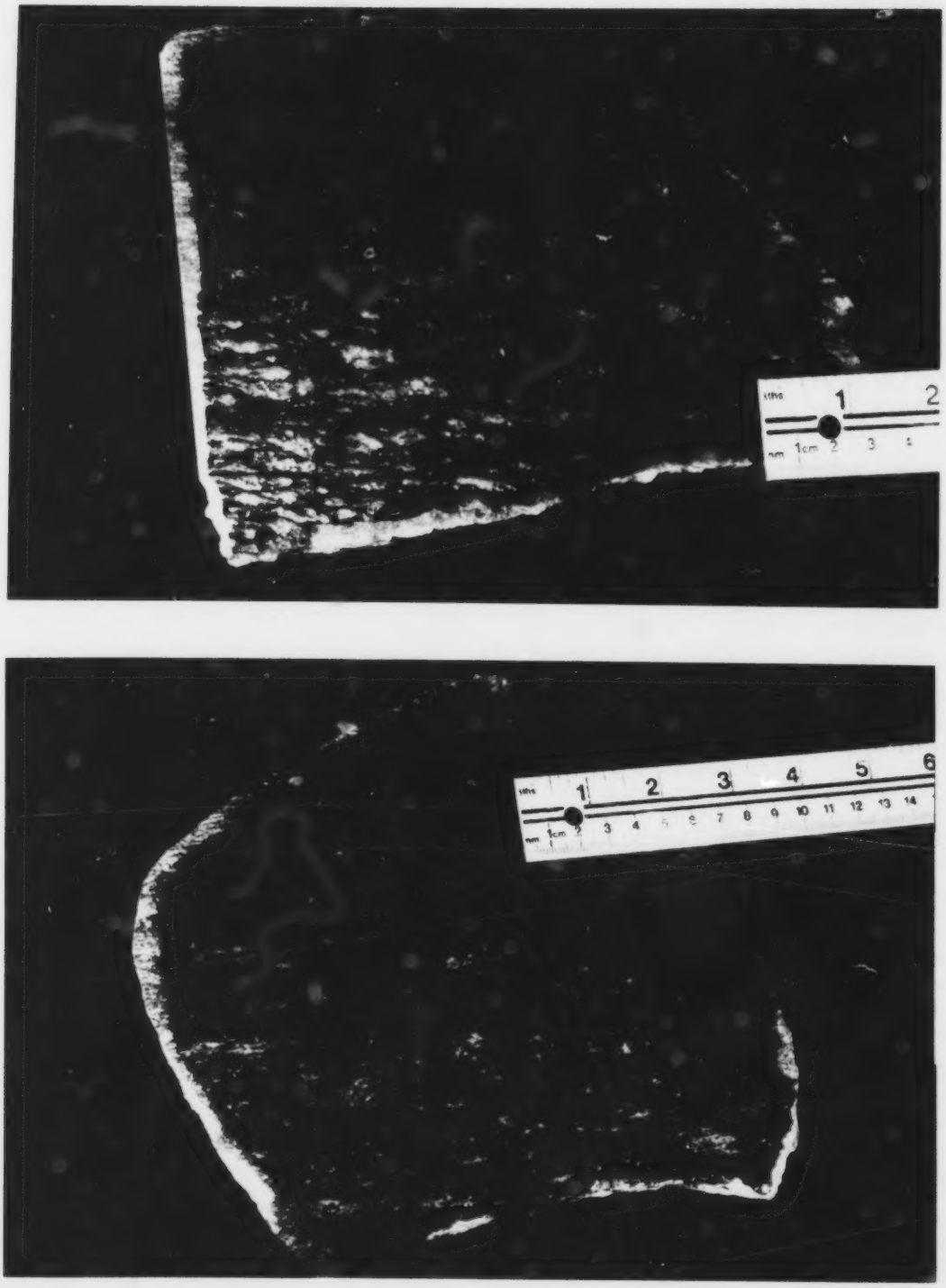

Photo 275.1. *C-S surfaces developed in (top) coarse-grained and (bottom) fine-grained granophyre.*

the upper Onaping Formation or that C-plane free rocks are fortuitously located north of the northern limit of the FWLDZ in a fold domain that encompasses much of the sedimentary core (*see also* Shanks and Schwerdtner 1988). The site of the transition zone between shear and folding regimes has not been located.

Estimate of Shear Displacement

Although ductile deformation in the FWLDZ departs from ideal simple shear, a crude estimate of displacement could be obtained from the spatial integration of shear strains across the FWLDZ (Ramsay and Graham 1970). Several shear strain profiles were constructed across the southern portion of the FWLDZ in rocks displaying C-S fabrics. The minimum estimated net displacement exceeds 8 km (assuming heterogeneous simple shear) and the associated horizontal shortening 6 km.

Because of the apparent non-planar walls and the variation of extension directions along the zone, the deformation may depart significantly from simple shear and accordingly our estimate of displacement could be in error. The obliquity between the structural framework (as defined by foliation and lineation) and the lattice-preferred orientation of quartz optic axes offers an alternative means of determining the variation in shear strain across the deformation zone (Bouchez *et al.* 1983, assuming heterogeneous simple shear). Oriented thin sections were made from two large rock specimens with well developed C-S fabrics. Similar estimates of shear strain as derived from the angle between C- and S-surfaces and that obtained from U-stage measurements would suggest that departures from simple shear might not be critical and that our estimates of net displacement are reasonable. Unfortunately, the resulting fabric diagrams are difficult to interpret in terms of shear magnitude. Accordingly, estimates of net displacement across the FWLDZ remain to be verified.

FOLD SYSTEM IN THE SEDIMENTARY CORE OF THE SUDBURY STRUCTURE

A detailed survey of the fold system in the central core of the Sudbury Structure showed that the beds of the Chelmsford Formation comprise a northeast-trending system of second-order buckle folds developed within a large first-order fold basin (Figure 275.3) (*see also* Figure 275.3 of Shanks and Schwerdtner 1988). Second-order folds are subhorizontal and nearly upright and, at the scale of individual folds, are subcylindrical. However, the enveloping surface to all second-order folds is basin-shaped, marking the first-order fold structure. Shanks and Schwerdtner (1988, Figure 275.3) presented a cross section through the central core of the SS and estimated the fold-generating strain to be less than 10%. Formation of slaty cleavage in the underlying Onwatin Formation may represent bulk shortening of nearly 30% (Ramsay 1967). Similarly, large magnitudes of layer-parallel shortening are also inferred for the Chelmsford Formation (Clendenen 1986, 1988). This suggests that the northwest-southeast bulk shortening required for making the first-order fold basin is about 40%. However, rocks of the North Range Onaping Formation and Igneous Complex appear to be virtually unstrained at surface (Fleet *et al.* 1987; Card and Hutchinson 1972). Awaiting resolution are the kinematics of fold formation, particularly of the first-order basin and a way to pinpoint the transition zone between the contrasting deformation regimes present in the SS (buckle folding in the central core vs. heterogeneous, bulk simple shear along the South Range).

DUCTILE STRAIN FEATURES SOUTH OF THE FWLDZ

Although the South Range Igneous Complex contains highly strained granophyre, its noritic to gabbroic rocks show little evidence of pervasive deformation at the surface. However, a conjugate shear zone system in rocks south of the FWLDZ demonstrates that the entire Igneous Complex was subjected to regional deformation. The shear zones separate lozenges of virtually unstrained rock, a pattern evident on both the outcrop- and map-scale (Figure 275.4).

C-planes and shear bands are well developed in some high-order shear zones. In these zones, C-planes are sub-parallel to the shear zone walls. The Mont Rouleau zone, a southeasterly dipping high-order shear zone, consists of discrete layers of ultramylonite; each is 1–3 m thick separated by less strained layers of granophyre. In the ultramylonite layers, steeper S-surfaces have largely been destroyed by C-planes, but less strained subdomains still preserve C-S surfaces together. Shear bands overprint C-S surfaces and dip more shallowly to the southeast. Shear bands are only locally developed. These fabric relationships suggest that the Mont Rouleau zone is a zone of reverse shear.

Poles to high-order shear zones have two maxima (Figure 275.5). A dominant set of shears dips steeply south and includes the largest of these high-order shear zones (the Mont Rouleau zone); a subordinate set dips steeply northward. Most of these high-order zones are only a few centimetres thick, but virtually all (on which shear sense could be determined) have a reverse sense of displacement revealing that the southern Sudbury Structure was foreshortened in bulk during regional deformation. In ductile shear zones, the obtuse bisector between the zones faces the bulk shortening direction (Ramsay 1980; Ramsay and Huber 1987). Provided that the high-order shear zones have not rotated during deformation, then the bulk shortening direction is estimated to have been subhorizontal and directed toward a bearing of 330°. Although these shear zones bound lozenge-shaped domains of virtually unstrained rock, the bulk shortening in rocks south

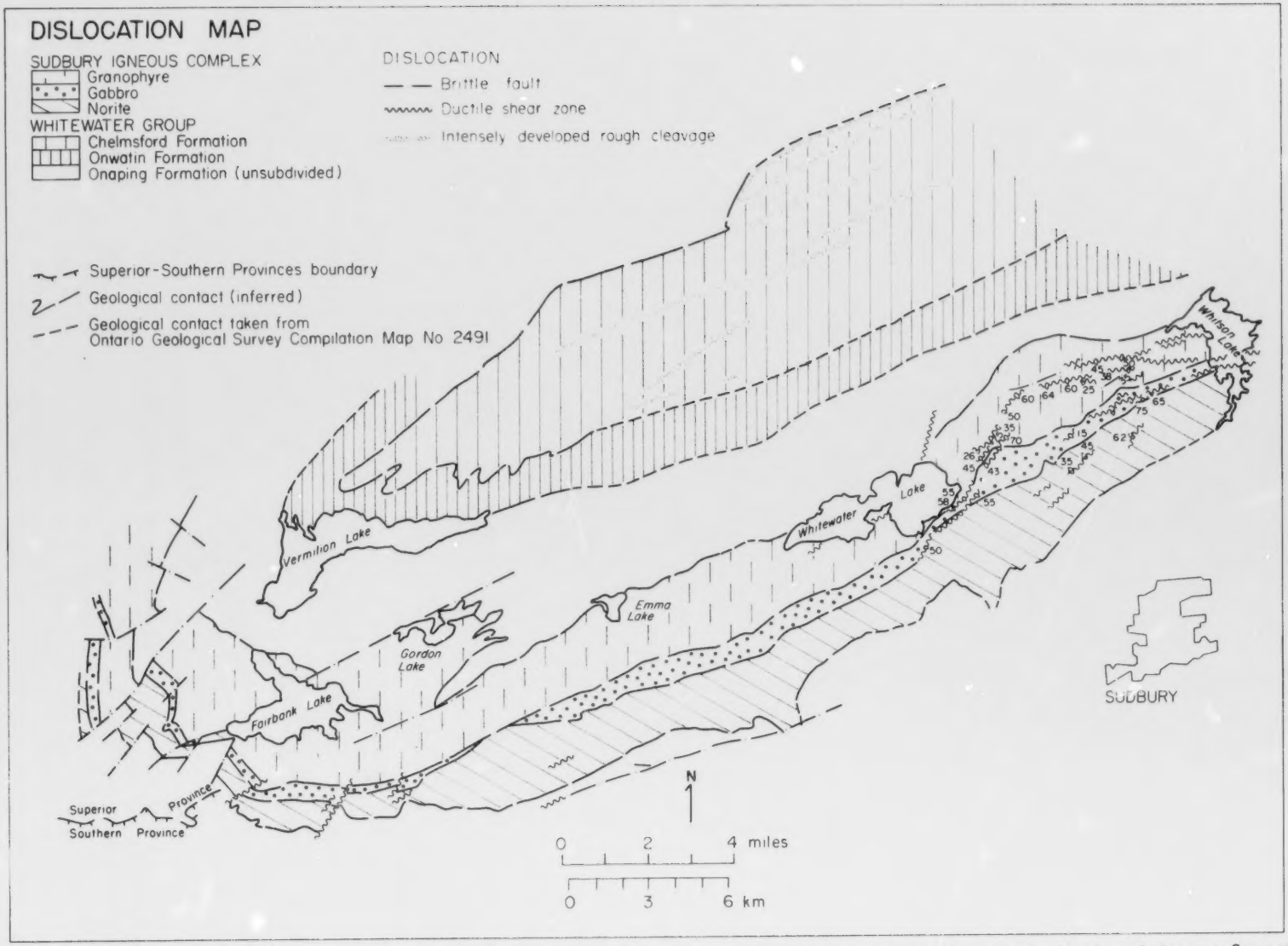

Figure 275.4. *Many dislocations shown on published maps are the site of ductile shear zones. Also shown are linear zones of strongly developed rough cleavage. Some of these zones coincide with the anticlinal crests of buckle folds in the Chelmsford Formation and may not be the site of intrabasin faults (compare with Figure 275.3).*

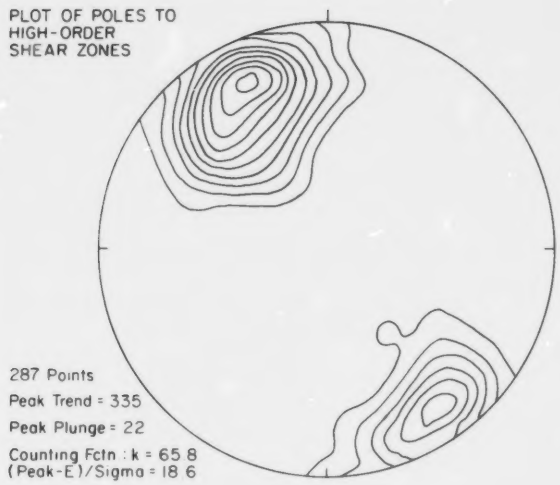

Figure 275.5. *Machine contoured stereoplot (lower hemisphere) using Gaussian weighting function (after Jowett and Robin 1988). Contours of increasing density beginning at E=3σ; increments of 2σ thereafter. Poles to high-order shear zones show two maxima. The shear zones form a conjugate array in the Igneous Complex rocks south of the FWLDZ. The obtuse bisector between the zones faces the bulk shortening direction, estimated to have been subhorizontal and directed to the northwest.*

of the FWLDZ may be appreciable (*see also* Ramsay and Huber 1987).

RELATIVE AGE OF FAULT DEVELOPMENT

Several major faults are shown to displace the Igneous Complex in the southwest portion of the Sudbury basin (Figure 275.1). A reconnaissance survey of this area confirmed that the Igneous Complex was indeed offset. Near the lineaments containing the Cameron Creek and Fairbank Lake faults, the rocks display the effects of alteration and cataclasis. The attitude of the major fault planes and of the adjacent lithologic contacts could not be determined. However, a 1/2 m zone of gouge along the Fairbank Lake fault has an orientation of 050/50SE, similar to C-planes in the surrounding rock. Ductile strain fabrics characteristic of the FWLDZ are destroyed within the fault zone. Elongate fragments of Onaping Formation have been truncated and displaced (Photo 275.2) and it is possible to find tectonically disoriented clasts and subdomains of rock preserving the earlier ductile fabric. Cataclastic deformation along the Fairbank Lake fault (and possibly the Cameron Creek fault as well) clearly post-dates ductile shear in the FWLDZ. This evidence contradicts the view that the ductile strain is solely related to faulting (Souch *et al.* 1969; Naldrett *et al.* 1970; Card and Hutchinson 1972).

These faults may not pass through the core of the SS. As noted by Rousell (1984a), many proposed faults are located in drift covered lineaments. However, some linear zones of strongly developed rough cleavage coincide with the anticlinal crests of buckle folds in the Chelmsford Formation (Figure 275.4). Accordingly, some of these zones may not coincide with intrabasin faults as inferred on published maps of the SS (Thomson 1957; Dressler 1984).

In the Mont Rouleau zone located south of the FWLDZ, pseudotachylite and cataclastite veins (Photo 275.3) crosscut the shear zone fabric. Although the absolute age of these veins is unknown, it is nonetheless worth noting that ductile shear again predates brittle deformation.

CREIGHTON DEFORMATION ZONE (CDZ)

The Creighton deformation zone (CDZ), south of the SS, consists of variably sheared (30-300 m), fractured and altered rock. The zone displaces diabase dikes of the Sudbury swarm dated at 1.25 Ga (Van Schmus 1965), and merges with the Grenville Front boundary fault to the east. The western extension of the CDZ is poorly known. However, metasediments displaying mylonitic fabric are along strike with other fault zone rocks and demonstrate the continuity of the zone to the west. Mylonitic fabric in these rocks are crosscut by Sudbury breccia dikes. The dikes, in turn, are highly deformed and possess an internal fabric similar to that of the host rock. This evidence suggests that, if the Sudbury brecciation was a single instantaneous event, ductile shear within the CDZ began prior to formation of the SS and continued for some time after.

Several linear ductile strain zones were mapped along the Creighton fault. In these high strain zones, the mineral stretching lineation is either down-dip or steeply east-raking. This coupled with microstructural evidence suggests that early displacement along the CDZ was dip-slip with south side up. In contrast, Cochrane (1988), from a study of two non-parallel offset markers, showed the Creighton fault to be a dextral transcurrent dislocation. Accordingly, the Creighton fault is considered to be a through-going transcurrent dislocation marked by alteration, cataclasis, and subordinate ultramylonites (<1 m thick) that link larger highly sheared domains having an earlier dip-slip displacement.

METAMORPHISM OF THE SOUTHERN PORTION OF THE SS

Mafic dikes intrude Igneous Complex rocks and allow the relative age of deformation and metamorphism of the SS to be established.

Quartz diabase dikes ("trap" dikes) are deformed in high-order shear zones south of the FWLDZ (Figure 275.1) and are metamorphosed to at least epidote-amphibolite grade. Petrographically,

Photo 275.2. *Micrograph of truncated Onaping fragments in the Fairbank Lake fault zone. Note also cataclastic vein carrying broken Onaping fragments. Fragments show an internal schistosity within the cataclastite vein. Brittle deformation along the fault post-dates ductile shear in the FWLDZ.*

they show polygonal quartz (2–10%) and feldspar grains, clinozoisite (1–12%), biotite (2–15%) and a strongly pleochroic amphibole (40–65%) which mantles relict cores of pyroxene and amphibole (Photo 275.4). Chill margins on some quartz diabase dikes indicate their intrusion into already cooled Igneous Complex rocks.

Macroscopically similar to quartz diabase dikes are olivine diabase "trap" dikes (perhaps fine-grained precursors to the larger Sudbury swarm dikes) (Figure 275.1). These dikes, however, are undeformed and unmetamorphosed and, in thin section, show primary igneous textures with tabular feldspar phenocrysts set in a fine-grained groundmass of olivine (5–25%), feldspar, opaques and pyroxene (Photo 275.5). Olivine-bearing trap dikes intrude deformed rocks of the FWLDZ and cut high-order shears in the Igneous Complex to the south (Figure 275.1).

From a study of metabasites at the footwall contact, Thomson *et al.* (1985) and Fleet *et al.* (1987) also suggested that the lower portion of the Igneous Complex and its footwall underwent epidote-amphibolite facies metamorphism. However, from the spatial distribution of amphibolite dikes intruding rocks of the Igneous Complex, we suggest that much of the South Range has undergone epidote-amphibolite facies metamorphism. Moreover, the FWLDZ probably separates low-greenschist facies assem-

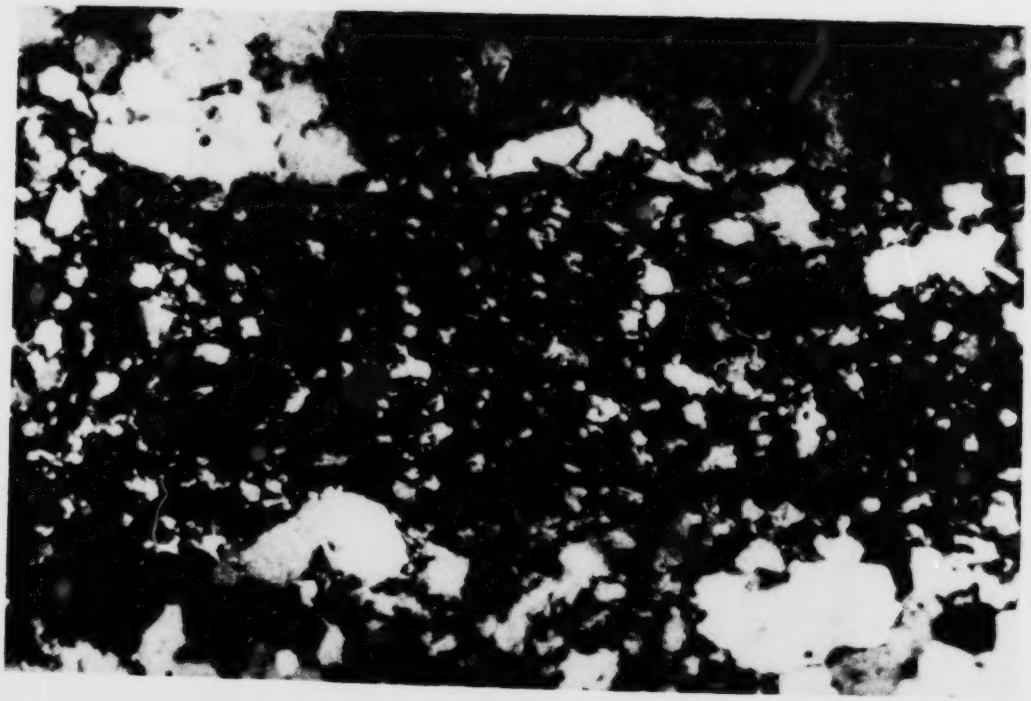

Photo 275.3. *Micrograph of cataclastite vein in granophyre of the Mont Rouleau shear zone. Vein shown horizontal and consists of finely crushed crystals between coarse grained crystals of the vein walls. Crossed polars; long edge of photo is 12 mm.*

Photo 275.4. *Micrograph of deformed and metamorphosed quartz diabase "trap" dike. Note relict cores and the alignment of metamorphic amphibole. Plane polarized light; long edge of photo is 3 mm.*

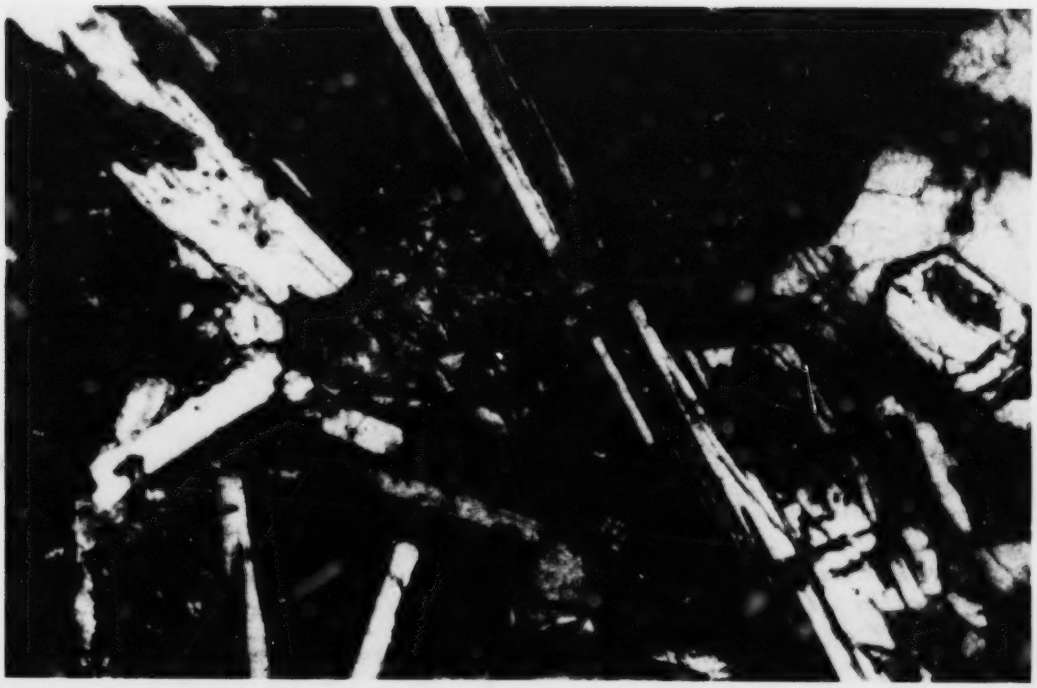

Photo 275.5. *Micrograph of undeformed and unmetamorphosed olivine diabase "trap" dike showing primary igneous texture. Anhedral, high relief mineral is olivine. Crossed polars; long edge of photo is 6 mm.*

blages of the central core from higher-grade rocks of the South Range.

Southwest of the SS, the FWLDZ coincides with a linear belt of amphibolite-facies rocks (*see* Card 1978, Figure 3; Fleet *et al.* 1987, Figure 1b) that according to Card (1978) continues west for at least 80 km. This metamorphic belt probably continues inside the Basin, but is difficult to identify because of retrograde metamorphism or a lack of suitable primary mineral assemblages.

Thomson *et al.* (1985) suggested that in mafic rocks having low permeability, the effects of low-pressure metamorphism are indistinct. This could explain why rocks of the South Range Igneous Complex are commonly thought to be unmetamorphosed (e.g., Naldrett *et al.* 1970; Naldrett and Hewins 1984).

CONCLUSIONS

The FWLDZ is a regionally extensive, broad zone of pervasive ductile shear that may account for much of the horizontal shortening of the Sudbury Structure. South of the FWLDZ, conjugate high-order shear zones formed in response to the northwest-directed compression and reveal that the entire Igneous Complex of the South Range was affected by regional deformation. The amount of shortening represented by these high-order shear zones may be appreciable. The kinematics of first-order folding are not well known, but the first-order basin may also contain an important increment of horizontal shortening.

Structural restorations attempting to determine the initial diameter ratio of the undeformed SS have not incorporated these potentially large increments of total strain. Therefore, the present oval shape of the SS cannot be used as evidence against an impact origin. Slippage on subsequent faults may be considerable and poses additional problems to a geometric restoration.

Deformation and metamorphism of the Sudbury Structure post-dates intrusion of quartz diabase dikes, but predates intrusion of small olivine diabase dikes. The evidence from mafic dikes suggest that the South Range Igneous Complex rocks underwent epidote-amphibolite facies metamorphism after they had cooled.

Linear zones of ductile shear located along the Creighton deformation zone probably represent an early dip-slip displacement history. Subsequent activation resulted in transcurrent displacement on a through-going dislocation that links linear zones of ductile shear. The evidence suggests a long and perhaps complex history of displacement on faults of the Murray system.

ACKNOWLEDGMENTS

This work is part of a PhD at the University of Toronto by W.S. Shanks and prepared under the supervision of W.M. Schwerdtner. The writers would like to thank the Ontario Geological Survey for their financial support (OGRF Grant 275 to W.M. Schwerdtner). Thanks are also extended to Inco Ltd. and Falconbridge Ltd. for permission to access their properties. The writers greatly benefitted from discussions with B.O. Dressler, P.-Y. Robin and A.J. Naldrett, and we extend our gratitude to them.

REFERENCES

Berthe, D., Choukroune, P. and Jegouzo, P.

1979: Orthogneiss, Mylonite and Non-Coaxial Deformation of Granites; Journal of Structural Geology, Volume 1, p.31-42.

Bouchez, J.L., Lister, G.S. and Nicolas, A.

1983: Fabric Asymmetry and Shear Sense in Movement-Zones; Geologische Rundschau, Volume 72, p.401-419.

Card, K.D.

1978: Metamorphism of Middle Precambrian (Aphebian) Rocks of the Eastern Southern Province; p.269-282 *in* Metamorphism in the Canadian Shield, edited by J.A. Fraser and W.W. Heywood, Geological Survey of Canada, Paper 78-10.

Card, K.D. and Hutchinson, R.W.

1972: The Sudbury Structure: Its Regional Geologic Setting; p.67-78 *in* New Developments in Sudbury Geology, edited by J.V. Guy-Bray, Geological Association of Canada, Special Paper 10.

Clendenen, W.S.

1988: Strain Studies of Cleavage Development in the Chelmsford Formation, Sudbury Basin, Ontario; Tectonophysics, Volume 145, p.191-211.

1986: Finite Strain Study of the Sudbury Basin, Ontario; unpublished MSc Thesis, Department of Geological Sciences, University of Colorado, Boulder, Colorado.

Cochrane, L.B.

1988: Control of Structural Geology on Rock Mass Failures; paper presented at Professional Development Seminar on Rock Mass Failures in Hard Rock Mining, Sudbury, Ontario.

Dressler, B.O.

1984: The Effects of the Sudbury Event and the Intrusion of the Sudbury Igneous Complex on the Footwall Rocks of the Sudbury Structure; p.97-136 *in* The Geology and Ore Deposits of the Sudbury Structure, edited by E.G. Pye *et al.*, Ontario Geological Survey, Special Volume 1, 603p. Accompanied by Map 2491, scale 1:50 000, Map NL-16/17-AM, scale 1:1 000 000.

Escher, A., Escher, J.C. and Watterson, J.

1975: The Reorientation of the Kangamiut Dike Swarm, West Greenland; Canadian Journal of Earth Sciences, Volume 12, p.158-173.

Fleet, M.E., Barnett, R.L. and Morris, W.A.

1987: Prograde Metamorphism of the Sudbury Igneous Complex; Canadian Mineralogist, Volume 25, p.499-514.

Grant, R.W. and Bite, A.

1984: Sudbury Quartz Diorite Offset Dykes: p.275-300 *in* The Geology and Ore Deposits of the Sudbury Structure, edited by E.G. Pye *et al.*, Ontario Geological Survey, Special Volume 1, 603p. Accompanied by Map 2491, scale 1:50 000, Map NL-16/17-AM, scale 1:1 000 000.

Jowett, E.C. and Robin, P.-Y. F.

1988: Statistical Significance of Clustered Orientation Data on the Sphere: An Empirical Derivation; Journal of Geology, Volume 96, p.591-599.

Muir, T.L.

1984: The Sudbury Structure: Considerations and Models for an Endogenic Origin; p.449-489 *in* The Geology and Ore Deposits of the Sudbury Structure, edited by E.G. Pye *et al.*, Ontario Geological Survey, Special Volume 1, 603p. Accompanied by Map 2491, scale 1:50 000, Map NL-16/17-AM, scale 1:1 000 000.

Muir, T.L. and Peredery, W.V.

1984: The Onaping Formation; p.139-210 *in* The Geology and Ore Deposits of the Sudbury Structure, edited by E.G. Pye *et al.*, Ontario Geological Survey, Special Volume 1, 603p. Accompanied by Map 2491, scale 1:50 000, Map NL-16/17-AM, scale 1:1 000 000.

Naldrett, A.J. and Hewins, R.H.

1984: The Main Mass of the Sudbury Igneous Complex; p.235-251 *in* The Geology and Ore Deposits of the Sudbury Structure, edited by E.G. Pye *et al.*, Ontario Geological Survey, Special Volume 1, 603p. Accompanied by Map 2491, scale 1:50 000, Map NL-16/17-AM, scale 1:1 000 000.

Naldrett, A.J., Bray, J.G., Gasparrini, E.L., Podolsky, T. and Rucklidge, J.C.

1970: Cryptic Variation and the Petrology of the Sudbury Nickel Irruptive; Economic Geology, Volume 65, p.122-155.

Ramsay, J.G.

1967: Folding and Fracturing of Rocks; McGraw-Hill, New York, 568p.

1980: Shear Zone Geometry: a Review; Journal of Structural Geology, Volume 2, p.83-89.

Ramsay, J.G. and Graham, R.

1970: Strain Variation in Shear Belts; Canadian Journal of Earth Sciences, Volume 7, p.786-813.

Ramsay, J.G. and Huber, M.I.

1987: The Techniques of Modern Structural Geology, Volume 2: Folds and Fractures; Academic Press, London, p.309-700.

Rousell, D.H.

1972: The Chelmsford Formation of the Sudbury Basin—a Precambrian Turbidite; p.79-91 *in* New Developments in Sudbury Geology, edited by J.V. Guy-Bray, Geological Association of Canada, Special Paper 10.

1984a: Structural Geology of the Sudbury Basin; p.83-95 *in* The Geology and Ore Deposits of the Sudbury Structure, edited by E.G. Pye *et al.*, Ontario Geological Survey, Special Volume 1, 603p. Accompanied by Map 2491, scale 1:50 000, Map NL-16/17-AM, scale 1:1 000 000.

1984b: Onwatin and Chelmsford Formations; p.211- 218, *in* The Geology and Ore Deposits of the Sudbury Structure, edited by E.G. Pye *et al.*, Ontario Geological Survey, Special Volume 1, 603p. Accompanied by Map 2491, scale 1:50 000, Map NL-16/17-AM, scale 1:1 000 000.

Shanks, W.S.

1987: Deformation of the Sudbury Structure, a PhD Topic Proposal; unpublished manuscript, Department of Geology, University of Toronto, Toronto.

Shanks, W.S. and Schwerdtner, W.M.

1987: Deformation of the Sudbury Structure and its Footwall; p.92-98 *in* Geoscience Research Grant Program, Summary of Research 1986-1987, edited by V.G. Milne, Ontario Geological Survey, Miscellaneous Paper 136, 241p.

1988: Deformation of the Sudbury Structure; p.46-55 *in* Geoscience Research Grant Program, Summary of Research 1987-1988, edited by V.G. Milne, Ontario Geological Survey, Miscellaneous Paper 140, 251p.

Souch, B.E., Podolsky, T. and Geological Staff,

1969: The Sulphide Ores of Sudbury: Their Particular Relationship to a Distinctive Inclusion-Bearing Facies of the Nickel Irruptive; p.252-261 *in* Magmatic Ore Deposits, edited by H.D.B. Wilson, Economic Geology, Monograph 4.

Thomson, M.L., Barnett, R.L., Fleet, M.E. and Kerrich, R.

1985: Metamorphic Assemblages in the South Range Norite and Footwall Mafic Rocks near the Kirkwood Mine, Sudbury, Ontario; Canadian Mineralogist, Volume 23, p.173-186.

Van Schmus, W.R.

1965: The Geochronology of the Blind River-Bruce Mines Area, Ontario, Canada; Journal of Geology, Volume 73, p.775-780.

Grant 290 A Fast Method of Maximal Simplicity Gravity Imaging

R.C. Bailey[1] and W. Colangelo[2]

[1]Departments of Geology and Physics, University of Toronto, Toronto

[2]Department of Physics, University of Toronto, Toronto

ABSTRACT

Previous work on maximal simplicity gravity imaging has demonstrated the feasibility of resolving the ambiguity in the inversion of continuous density models by minimizing the mean modulus of the density gradient subject to the constraints that the gravity data be fitted, that the model have specified *a priori* densities where they are known from sampling, and that density anomalies not exceed some *a priori* specified limit of plausibility. This previous work utilized a slow and cumbersome general purpose nonlinear optimization routine on a supercomputer, making it impractical for general use. The problem to be solved was converted to a classic linear programming problem, for which standard, fast reliable algorithms exist. The actual implementation used the commercially available LAMPS package on the Cray supercomputer at the University of Toronto. In addition to a 25-fold increase in speed, all the iterative interactive manipulation of the solution towards an optimum was eliminated, resulting in considerably greater ease of use.

INTRODUCTION

The imaging of the density distribution within the Earth using gravity data collected at the surface is a very non-unique problem. If a continuous density distribution is represented by a stacked array of small identical cells within each of which the density is assumed constant, models with thousands of such cells (and thus unknown density variables to be solved for) can result, even in two-dimensional (infinite strike) models. Among the various methods of selecting particular models from the infinite set that fit the data is the *maximal simplicity* method. Previous reports on this work (Bailey and Reford 1987, 1988) have shown that minimization of the mean modulus of the density model gradient selects very reasonable models, and, most importantly, allows incorporation of surface and borehole density sample values as constraints on the model. A major drawback of this modelling previously described was the amount of computation required to obtain even a relatively coarsely gridded model. Using a general purpose iterative nonlinear optimization routine required of the order of 2000 seconds of supercomputer (Cray XMP-1) time for a two-dimensional model on a grid 20 by 50 cells.

Here we report on a successful attempt to recast the mathematical problem as a linear programming problem (Kolman and Beck 1980). This achieves not only a 25-fold increase in speed of modelling, but leads to a definite and immediate statement about whether there is a feasible solution at all (i.e. one that fits both the gravity data and observed density constraints). It might still be argued that any method which requires a supercomputer is not a reasonable subject for research. This is not true; recent announcements of supercomputer chips (with 64-bit parallel processors) for personal computer use imply that methods such as that in this paper will be practical on personal computers within a very few years.

REVIEW OF THE PROBLEM

Attention here is restricted to the two-dimensional problem, in which densities are assumed invariant along strike. The density section to be modelled is then one which is perpendicular to strike. The problem to be solved is set up in the following way:

1. Divide the section into a grid of small rectangular cells (Figure 290.1), within each of which the density is assumed constant.
2. Fix the densities of those few cells which are known (i.e. because they have been sampled at the Earth's surface or by drilling).
3. Using a suitable computer algorithm, choose densities for each of the remaining cells so that the gravity data is fitted within a certain toler-

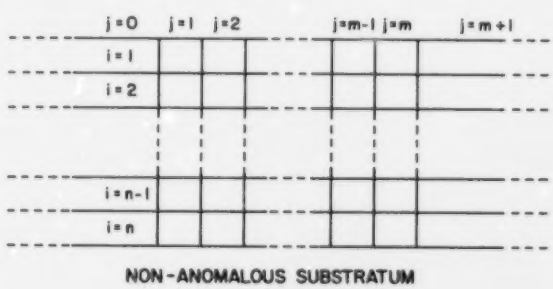

Figure 290.1. *Indexing scheme for cells of the two-dimensional density section.*

ance, *and* the sum of the sizes (absolute values) of the density differences across all cell to cell interfaces in the model is minimized. This latter minimization is a discrete celled approximation to minimizing the mean absolute value of the density gradient

$$|\nabla\varrho(x,y,z)| \qquad (1)$$

where ϱ is the density. This is equivalent to maximizing the "simplicity" of the model in a particular special way.

At least to a first approximation, the method is objective: it allows arbitrary and more or less continuous (to the extent that the cells are sufficiently small) density variations. Conventional polygonal modelling methods, on the other hand, require the density model to consist of a few polygonal bodies of uniform density, whose number and approximate location the user specifies in advance.

A FASTER COMPUTATIONAL METHOD

With the general purpose nonlinear optimization method used previously, the complexity and size of computing problem resulted in tests which were restricted to modelling a section by a coarse grid of only a few cells (e.g. 150 or fewer), and even these required many minutes of Cray supercomputer time. It was clear from these results that although the method worked, a better method of implementing step (3) above was needed. Thus, our work this year has been on converting the minimization problem of step (3) above to an exact linear programming problem, in a way detailed below.

The key points of the problem reformulation are:

- It is assumed that after the regional gravity has been subtracted from the data, the density anomalies causing the anomalous field are all above some maximum depth, z. This depth is divided into n intervals, ranging from 1 to n.
- All variations in the x direction are also limited to some range, ranging from 1 to m. (The assumption is that of a two-dimensional model with infinite strike length along the other horizontal direction y.)
- On the left and right side of the model (Figure 290.1), a layered structure is presumed, consisting of n layers extending away from the interior region to infinity on each side respectively. The leftmost cells, infinite in extent in the y and negative x direction, have the horizontal index of 0, while the rightmost cells, infinite in the y and positive x direction have the horizontal index of $m+1$. Thus there exist a total of $n(m+2)$ cells.
- Two variables are to be introduced, Δ^b_{ij} and Δ^r_{ij}, the change in density going out the bottom and the right of the ij'th cell respectively. These variables represent density changes with respect to one absolute density value, which can be that of any arbitrary cell, and which has been made to be that of the top left hand cell where $i=1$ and $j=0$ (ϱ_{10}). The right side of a vertical interface (underside of a horizontal) is the + side, and the left (upper) side is the − side.
- The sum of the gravitational effect of each cell density must be, within a certain tolerance, equal to the value of the gravity measured at certain points on the surface. This is the main constraint that will always be enforced and is expressed in equation form below (2a and 2b), where G_{tij} is the gravitational effect of cell (ij) of unit density on the vertical gravity at point t on the surface, d_t is the gravity datum at point t, e_t is the error or tolerance allowed in the datum at point t, and b_t is the regional or background gravity, also at point t.
- Two constraints may be set on every cell's bottom and right variable by setting a lower and upper range possible for that cell's density. This allows the incorporation of surface and/or borehole density values into the problem and further constrains the solution, forcing it to approach the form of the actual structure. Thus we have the following equations

$$U_{ij} \geq \varrho_{10} + \sum_{k=1}^{i-1} \Delta^b_{k0} + \sum_{l=0}^{j-1} \Delta^r_{il} \qquad (3a)$$

$$D_{ij} \leq \varrho_{10} + \sum_{k=1}^{i-1} \Delta^b_{k0} + \sum_{l=0}^{j-1} \Delta^r_{il} \qquad (3b)$$

where U_{ij} and D_{ij} are the upper and lower density limits, respectively, for cell (ij).

$$d_t - e_t \leq b_t + G_{t10}\varrho_{10} + \sum_{i=2}^{n-1}\sum_{j=1}^{m} G_{tij}\left(\varrho_{10} + \sum_{k=1}^{i-1}\Delta^b_{k0} + \sum_{l=0}^{j-1}\Delta^r_{il}\right) \qquad (2a)$$

$$d_t + e_t \geq b_t + G_{t10}\varrho_{10} + \sum_{i=2}^{n-1}\sum_{j=1}^{m} G_{tij}\left(\varrho_{10} + \sum_{k=1}^{i-1}\Delta^b_{k0} + \sum_{l=0}^{j-1}\Delta^r_{il}\right) \qquad (2b)$$

- In order to ensure that the density of any particular cell, calculated by adding ϱ_{10} with the total of the density changes along *any* path to that cell, be constant, one must have a curl free constraint for the variables. This constraint is a discrete form of Stokes' theorem, and algebraically is expressed as

$$\Delta^r_{ij} + \Delta^b_{i,j+1} - \Delta^r_{i+1,j} - \Delta^b_{ij} = 0. \quad (4)$$

- Lastly, the objective function, which is to be minimized, is

$$S = \sum_{i,j} \left(|\Delta^b_{ij}| + |\Delta^r_{ij}| \right). \quad (5)$$

By minimizing the total sum of the Δ's, subject to the above constraints, a problem in gravity inversion has essentially been converted to one in linear programming (LP). The only change necessary is to allow the anomalous densities to be negative as well as positive. Since the standard LP problem involves only non-negative real values for its variables, two transformations must be made. Allow the Δ's to be replaced by the following variables,

$$\Delta^r_{ij} = A^r_{ij} - B^r_{ij} \quad (6a)$$

and

$$\Delta^b_{ij} = A^b_{ij} - B^b_{ij} \quad (6b)$$

where

$$A^b_{ij}, A^r_{ij}, B^b_{ij}, B^r_{ij} \geq 0. \quad (6c)$$

Since the top left hand density is an anomalous density, it is allowed to range over positive and negative values also, thus we have

$$\varrho_{10} = \varrho^+_{10} - \varrho^-_{10} \quad (7a)$$

where

$$\varrho^+_{10}, \varrho^-_{10} \geq 0. \quad (7b)$$

Thus the final form of the LP problem is to minimize

$$S = \sum_{i,j} A^r_{ij} + A^b_{ij} + B^r_{ij} + B^b_{ij} \quad (8)$$

subject to the surface gravity constraints (9a and 9b), the density range constraints (10a and 10b) and the zero-curl constraint (11).

Linear programming problems are normally presented in standard form as, optimize (i.e. maximize or minimize)

$$z = \mathbf{c}^T \mathbf{x}, \quad (12a)$$

subject to

$$\mathbf{A}\mathbf{x} \leq (\geq)(=)\ \mathbf{b}, \quad \mathbf{x} \geq 0, \quad (12b)$$

where $\mathbf{A}$ is an $r \times s$ matrix, $\mathbf{c} \in R^s$, $\mathbf{x} \in R^s$, and $\mathbf{b} \in R^r$ (Kolman and Beck 1980).

Thus in order to implement a technique to properly solve the LP problem posed by equations (8), (9), (10) and (11), the two-dimensional vector representing the A's and B's must be converted to a one-dimensional vector in the form of $\mathbf{x}$ as shown in (12). The conversion is done from the bottom right hand corner of the model up through successive

$$d_t - e_t \leq b_t + G_{t10}(\varrho^+_{10} - \varrho^-_{10}) + \sum_{i=2}^{n-1} \sum_{j=1}^{m} G_{tij} \left(\varrho^+_{10} - \varrho^-_{10} + \sum_{k=1}^{i-1} (A^b_{k0} - B^b_{k0}) + \sum_{l=0}^{j-1} (A^r_{il} - B^r_{il}) \right) \quad (9a)$$

$$d_t + e_t \geq b_t + G_{t10}(\varrho^+_{10} - \varrho^-_{10}) + \sum_{i=2}^{n-1} \sum_{j=1}^{m} G_{tij} \left(\varrho^+_{10} - \varrho^-_{10} + \sum_{k=1}^{i-1} (A^b_{k0} - B^b_{k0}) + \sum_{l=0}^{j-1} (A^r_{il} - B^r_{il}) \right) \quad (9b)$$

$$U_{ij} \geq \varrho^+_{10} - \varrho^-_{10} + \sum_{k=1}^{i-1} (A^b_{k0} - B^b_{k0}) + \sum_{l=0}^{j-1} (A^r_{il} - B^r_{il}) \quad (10a)$$

$$D_{ij} \leq \varrho^+_{10} - \varrho^-_{10} + \sum_{k=1}^{i-1} (A^b_{k0} - B^b_{k0}) + \sum_{l=0}^{j-1} (A^r_{il} - B^r_{il}) \quad (10b)$$

$$A^r_{ij} - B^r_{ij} + A^b_{i,j+1} - B^b_{i,j+1} - A^r_{i+1,j} + B^r_{i+1,j} - A^b_{ij} + B^b_{ij} = 0 \quad (11)$$

rows (moving left along each one) to the top using the following transformation,

$$X_{f(i,j)+1} = B^b_{ij} \qquad (13a)$$

$$X_{f(i,j)+2} = A^b_{ij} \qquad (13b)$$

$$X_{f(i,j)+3} = B^r_{ij} \qquad (13c)$$

$$X_{f(i,j)+4} = A^r_{ij} \qquad (13d)$$

where

$$f(i,j) = 4(m+1-j) + 4(n-i)(m+2). \qquad (13e)$$

Recalling the general standard form of LP problems, given by (12), the length of the one-dimensional array **b** is bounded by $2t+n(m+1) \le r \le 2t+n(3m+5)$, where t is the number of surface gravity data points. The bounds vary according to how many cell density range constraints are applied in the LP formulation of the problem. Since i ranges from 1 to n, and j from 0 to $m+1$, then the one-dimensional arrays **c** and **x** have a length of $s = 4n(m+2)$. This value should be increased by two if $\varrho_{10} = \varrho^+_{10} - \varrho^-_{10}$ is not a given constant. It will be assumed that even when ϱ_{10} is given, $\varrho^+_{10} - \varrho^-_{10}$ will be considered variables, since the related constraint equations will have a direct effect on the (in)feasibility of the LP problem. Observe that all the A^r_{ij}'s and B^r_{ij}'s, where $j = m+2$, are at infinity, since the cells with index $(i, m+2)$ are considered to extend to infinity in the positive x direction. Therefore, the length of **c** and **x** should be decreased by $2n$, thus $s = 2n(2m+3)$.

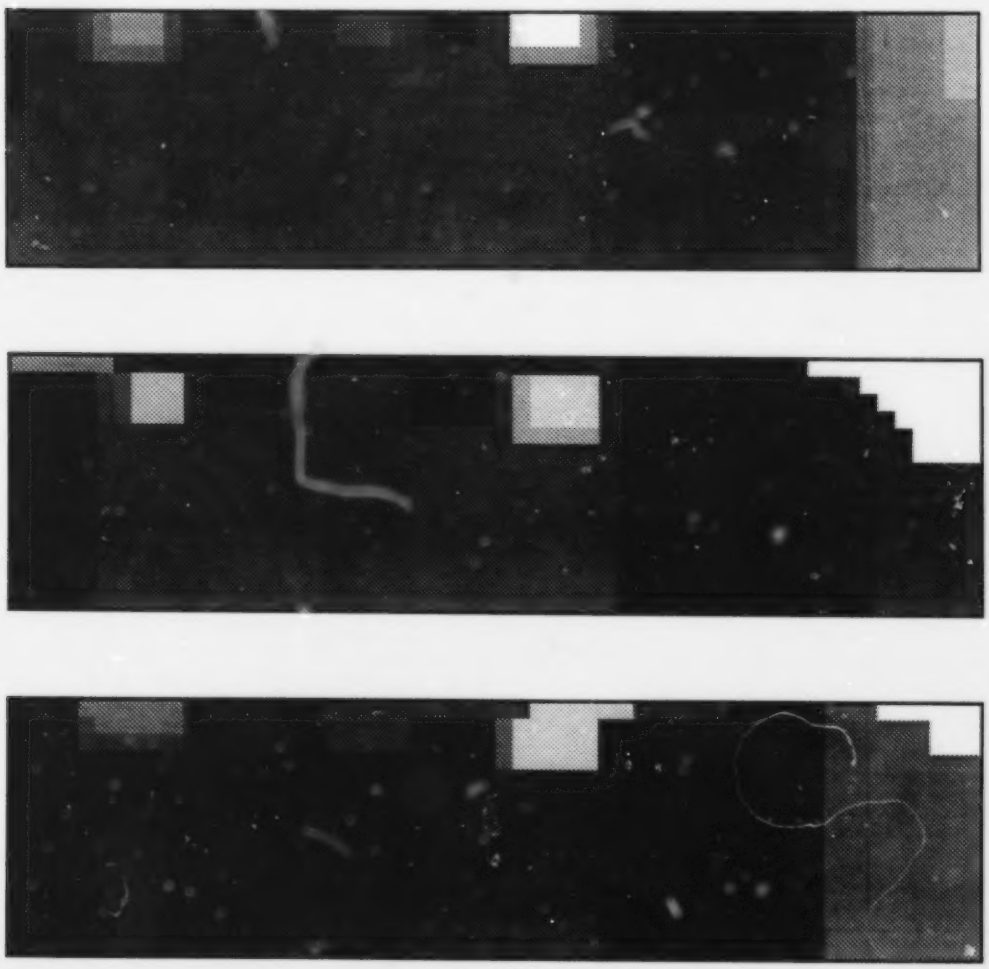

Figure 290.2. *Three grey-scale density sections obtained from the gravity profile shown as line AB in Figure 290.3. North is on the right and south on the left.*

IMPLEMENTATION

A commercial software package known as LAMPS, available on the Cray XMP-1 supercomputer at the University of Toronto, solves large LP (linear programming) problems. It requires that the problem be formulated as a classic LP problem as above, and that the matrix of coefficients of all the equations of the problem be provided in an input file. As this matrix is normally sparse for large problems, this input file must be in sparse matrix form (only the non-zero matrix elements are stored, along with their locations in the matrix). Even with such data compression, the required input file can be very large (9 megabytes for the examples shown in Figure 290.2). The creation of such a file by hand is impractical. Accordingly, a pre-processor program was written. This runs interactively on a minicomputer (such as a MicroVax), and on the basis of input from the user about the number of cells in the model, the name of the file in which the gravity data are to be found, and the name of the file in which known density

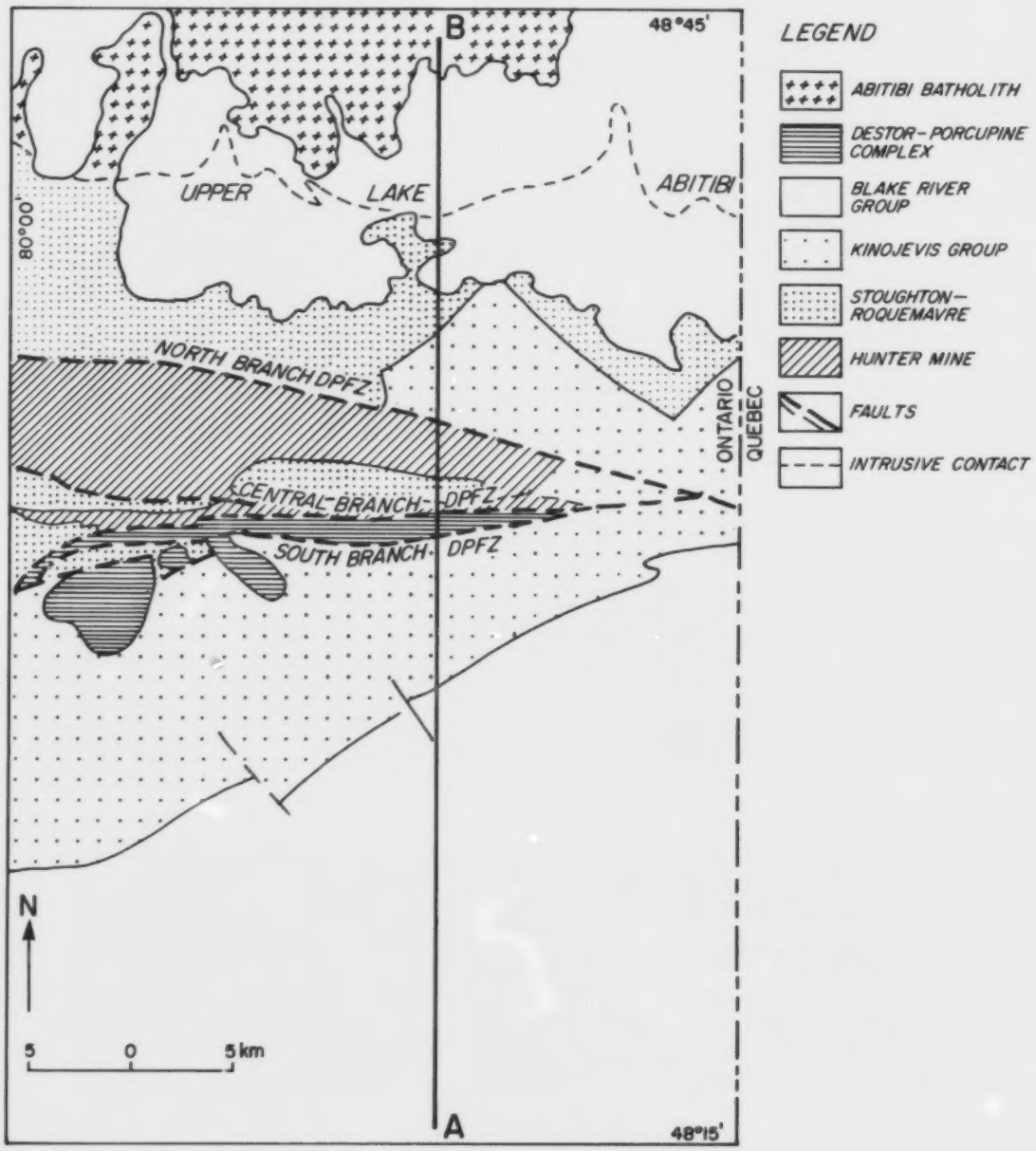

Figure 290.3. *Location of the gravity profile (line AB) on a geological map simplified from Jensen and Langford (1985).*

values are stored, constructs the required input file for the supercomputer. This is passed to the supercomputer in a batch job. The output which results is in terms of the LP problem variables defined in the preceding section, and again, is not suitable for immediate inspection. Thus a post-processor program was written. This converts the supercomputer output file to a matrix of anomalous densities, which may then be inspected or plotted using a grey-scale plotting program.

RESULTS

The main results of the above reformulation are:

a. A 25-fold speedup (a 1000 cell model now takes about 4 minutes, or about $10.00 at current academic user rates);

b. Exact solutions are obtained straightforwardly; the previous general purpose minimization routine was approximate as well as slow. Comparisons with the old algorithm on synthetic models have been completed successfully.

An idea of the speed of computation can be obtained from looking at the three solution examples shown in Figure 290.2. These are all density sections along the line AB in the Abitibi belt as shown in Figure 290.3. The anomalous density range on each is approximately −0.1 to +0.1 g/cm^3 (white to black). All these models are 56 cells across and 15 cells deep, each cell being a square kilometre in cross section. There is no vertical exaggeration. As data, gravity values were picked every kilometre from a contoured gravity dataset provided courtesy of the OGS. The only difference in the computations in each case were in the application of surface density constraints. The top model has no surface cells whose densities are constrained, whereas in each of the other two cases the surface cell densities were chosen *a priori*. For each of these three models, the above solutions required submitting a very large matrix file to the LAMPS package on the Cray supercomputer, which for the two surface constrained cases was about 9000 kilobytes containing 1048 equations, 3330 variables and about 208 000 nonzero elements. The Cray was able to solve each of these problems in about 220 seconds of cpu time.

ACKNOWLEDGMENTS

We would like to acknowledge the assistance of the staff of the Ontario Centre for Large Scale Computing, in particular Dr. A.J. Stacey, whose detailed help with the LAMPS package was invaluable.

REFERENCES

Bailey, R.C. and Reford, S.W.

1987: Improved Computer Interpretation of Gravity and Magnetic Data; *in* Geoscience Research Grant Program, Summary of Research 1986-1987, Ontario Geological Survey, Miscellaneous Paper 136.

1988: Maximal Simplicity Gravity Interpretation with Continuous Density Models; *in* Geoscience Research Grant Program, Summary of Research 1987-1988, Ontario Geological Survey, Miscellaneous Paper 140.

Jensen, L.S. and Langford, F.F.

1985: Geology and Petrogenesis of the Archean Belt in the Kirkland Lake Area, Ontario; Ontario Geological Survey, Miscellaneous Paper 123, 130p. Accompanied by Maps P.2434 and P.2435, scale 1:63 360 or 1 inch to 1 mile.

Kolman, B. and Beck, R.E.

1980: Elementary Linear Programming with Applications; Academic Press, Toronto.

Grant 294 Quaternary Geology and Geochemical Exploration in the Matheson Area

M.B. McClenaghan[1,3], O.P. Lavin[1], I. Nichol[1] and J. Shaw[2]

[1]Department of Geological Sciences, Queen's University, Kingston

[2]Department of Geography, Queen's University, Kingston

[3]Engineering and Terrain Geology Section, Ontario Geological Survey, Toronto

ABSTRACT

The Matheson area of northeastern Ontario is of great interest for mineral exploration because it is geologically similar to the adjacent Timmins gold camp. Exploration in the area is hampered by extensive and thick glacial overburden. For this reason, till geochemistry has become an important exploration method in the area. The use of till geochemistry, however, is limited by a complex glacial history and poorly documented glacial stratigraphy. The primary objective of this study is to obtain a better understanding of the Quaternary geology of the area to identify ways of making till geochemistry a more effective exploration method.

The first two years of the study focussed on the examination and interpretation of multi-element geochemical data, heavy mineral abundance data and pebble lithology data from 24 overburden drill holes from across the study area to determine both the local and regional stratigraphy. Up to three separate till units were identified in the drill holes. The uppermost till unit in most drill holes has a "felsic" composition, characterized by relatively high concentrations of SiO_2, low concentrations of MnO, Cu and Ni and by higher concentrations of felsic intrusive pebbles. Underlying till units, where present, commonly have a more "mafic" composition, characterized by lower concentrations of SiO_2 and higher concentrations of MnO, Cu and Ni and by higher concentrations of metavolcanic pebbles.

In addition to these compositional patterns, a decrease in the abundance of Paleozoic carbonate pebbles from west to east across the study area was found. This west-to-east pattern is displayed by all till units, and as a result could not be explained by current models for ice flow patterns across the area.

The third year of the study, the results of which are presented in this report, focussed on completing the examination of pebble lithology and the synthesis of all data collected during the past three years. Dispersion patterns of Paleozoic carbonate pebbles combined with the stratigraphic information from the overburden drill holes have been used to reconstruct the glacial history of the area. Two main glacial advances affected the area. An earlier flow towards the southwest was followed by a non-glacial interval. A second glacial advance (the most recent) towards the southwest later shifted towards the southeast.

Recommendations for exploration methodolgy are suggested on the basis of the results obtained from this study to make till geochemistry a more effective exploration method in the Matheson area.

INTRODUCTION

The objective of this study is to obtain a better understanding of the Quaternary geology of the Matheson area through the examination of regional characteristics of till units from sonic overburden drill holes. A better understanding of the Quaternary stratigraphy will greatly improve the effectiveness of till geochemistry as an exploration method in the search for mineral deposits in the area.

This report includes the background to the investigation, results of previous work in earlier phases of the present study, the data obtained in the third year of the program, discussion of the significance of the results, conclusions and finally recommendations for exploration.

BACKGROUND

The study area is located in the west-central portion of the Abitibi greenstone belt (Figure 294.1) and is underlain by predominantly mafic metavolcanic rocks. Two major deformation zones strike west through the area: the Destor–Porcupine fault zone and the Pipestone fault zone. In the Matheson area, numerous gold deposits are associated with these two fault zones (Whittaker 1986). Unfortunately, exploration in most of the Matheson area is hampered by extensive and thick glacial overburden. For this reason, till geochemistry has become an important exploration method in the area. In order to trace geochemical anomalies in till to their bedrock source, a knowledge of the local glacial stratigraphy and ice transport directions is essential.

Much of the Matheson area is blanketed by thick glaciolacustrine clay and silt, which limits most till sampling to costly subsurface techniques. Conse-

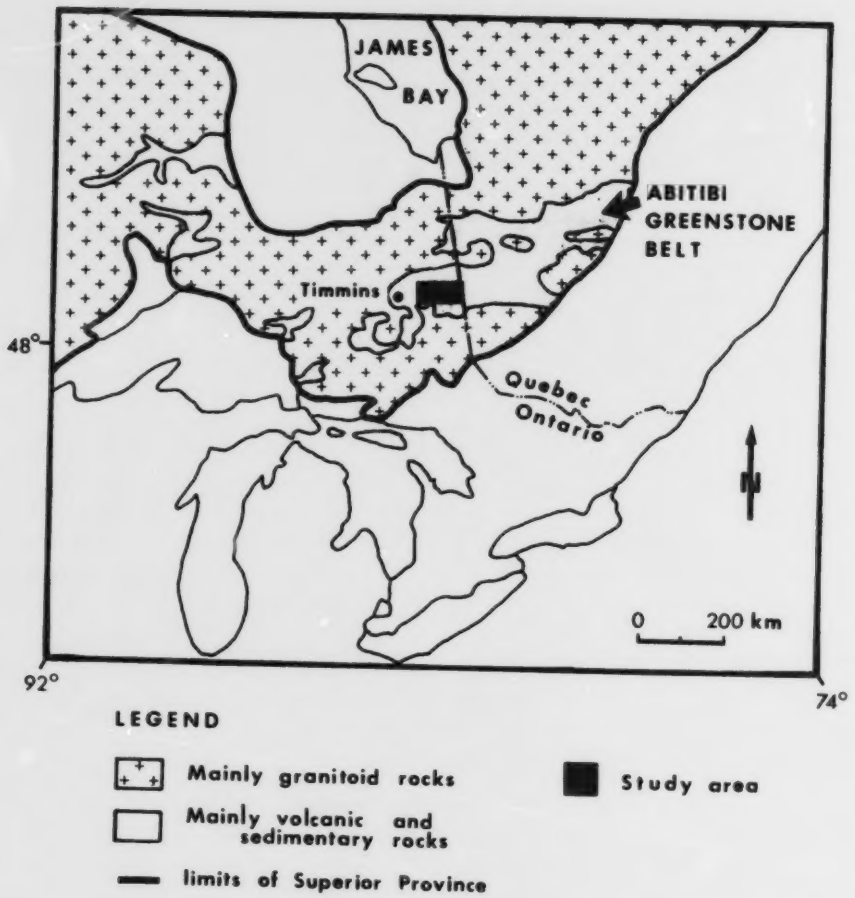

Figure 294.1. *Location of the study area in northeastern Ontario.*

quently, little is known about the glacial stratigraphy which appears complex and includes multiple tills related to multiple glacial events and ice flow directions. The youngest till sheet in the area is Matheson till (Hughes 1959) which is exposed at surface in a few places. In a few cases, Matheson till is underlain by one and possibly two distinct till units that are separated by glaciolacustrine sediments. Striations across the area record the last major ice advance toward 165°, during the Late Wisconsinan and have been correlated with the Matheson till. Rare striations oriented towards 240° and crosscut by the younger 165° striations record an earlier ice flow event.

Several factors related to the thick and varied overburden make it difficult to correlate tills and to assign ice flow directions to them. This limits the effectiveness of till geochemistry as an exploration method in the Matheson area.

1. The glacial stratigraphy is complex, including multiple till sheets probably related to more than one glacial advance, ice transport direction, and mode of deposition.
2. Knowledge of the stratigraphic relationships between tills and intercalated deposits is severely limited because thick glaciolacustrine silt and clay deposits blanket most of the area, resulting in a lack of surface exposures of underlying glacial sediments.
3. Tills below the Matheson till are rarely preserved, thus limiting the opportunity to examine and document their characteristics.
4. Dealing with these problems is made more difficult by the nature of reverse circulation drilling, the most commonly used overburden drilling technique in the area. This drilling method produces a chip and mud slurry in which all structures and most textures are destroyed, thus making identification of separate till units and interpretation of till genesis and stratigraphy extremely difficult or impossible.

An understanding of the till stratigraphy of individual drill holes is vital to the accurate interpreta-

tion and follow-up of geochemical anomalies found in them. However, as with most overburden drilling in the area, the stratigraphic information and geochemical data are often difficult to interpret. The Ontario Geological Survey (OGS) is currently involved in a multi-disciplinary, multi-year project (BRiM) designed to assist and stimulate exploration in the Black River–Matheson area (Baker *et al.* 1985). A major component of the project consists of overburden drilling and till geochemistry.

The present study involves the examination of data and analyses of till samples from selected drill holes from the first two years (1984 and 1985) of the OGS sonic overburden-drilling project in order to identify methods for interpreting drill hole stratigraphy and correlation. This will improve the overall understanding of the Quaternary history of the Matheson area and make till geochemistry a more effective exploration tool.

Data from a 15 m stratigraphic section exposed in the Maude Lake pit in Beatty Township and 24 OGS sonic drill holes comprise the data base for the study. The data were examined to address the problems of the interpretation of till stratigraphy in the area. The results presented here were obtained during the final year of a three year study. Results from the first two years of the study have been reported previously by McClenaghan *et al.* (1987, 1988a, b).

PREVIOUS WORK

Data evaluation and interpretation were carried out in three sections: 1) till geochemistry; 2) mineral abundances in the heavy mineral concentrate; and 3) pebble lithology abundances. The results from each section have been described in detail by McClenaghan *et al.* (1987, 1988b) and are summarized below.

TILL GEOCHEMISTRY

Till geochemical data examined included trace element abundances for three till fractions: 1) heavy mineral concentrate fraction; 2) <0.063 mm fraction, referred to here as the fine fraction; and 3) <2.0 mm fraction, referred to here as the total fraction. Major oxide abundances for the total fraction are also included in the data. The elements determined and those used in this study have been described in McClenaghan *et al.* (1987).

For individual drill holes the abundance patterns of most elements are, to some degree, useful for discriminating between till units. However, some measure of their geochemical similarities or differences is needed to give meaning to these identified units and to compare till units on a regional scale. Discriminant analysis provides a means by which to compare till units and categorize them into distinct groups based on their geochemical composition. In general, single trace-element distributions and a two-element discriminant function for the major oxides are efficient methods for the classification of till samples into two groups: acidic or basic. Acidic tills are characterized by lower concentrations of Cu, Ni and MnO and higher concentrations of SiO_2 while basic tills are characterized by higher concentrations of Cu, Ni and MnO and lower amounts of SiO_2. Strong inter-element correlations indicate that, in addition to the elements mentioned above, acidic tills contain greater amounts of Zr, U and Na_2O whereas basic tills contain greater amounts of Zn, Co, Ti, CaO, MgO, TiO_2 and MnO.

In general, the acidic/basic till composition is related to the stratigraphy. Across the the study area, the uppermost till unit consistently has a more acidic composition than underlying till units. This may indicate a similar provenance for this till unit. Since the upper till unit is most likely Matheson till, the acidic composition may provide a means of identifying Matheson till.

MINERAL ABUNDANCES IN HEAVY MINERAL CONCENTRATES

Dramatic differences in individual mineral abundance often coincide with contacts between till units previously identified using geochemical patterns. In many other cases, however, no distinctive changes in abundance of specific heavy minerals are present. Any patterns in mineral abundance that are discernible are not universally applicable across the entire study area. Because of analytical batch differences between sampling years, the mineral abundance data from 1984 and 1985 must be treated as two separate data sets. These factors make heavy mineral abundances of limited use as stratigraphic markers. Mineral abundance data may provide valuable information concerning the mineralogical characteristics of the bedrock source on a local scale where other analytical fractions do not.

PEBBLE LITHOLOGY ABUNDANCES

The abundance of various pebble lithologies for approximately 300 pebbles in the 4 to 90 mm size fraction of till samples from selected drill holes and the Maude Lake pit were examined to compare with the geochemical results, to help distinguish between till units and to help determine till provenance. The pebbles were grouped into one of seven categories that reflect the general bedrock lithologies within the study area and to the north: 1) felsic to intermediate intrusive pebbles, referred to here as felsic intrusive pebbles; 2) mafic intrusive pebbles; 3) metavolcanic pebbles; 4) metasedimentary pebbles; 5) ultramafic pebbles; 6) Paleozoic carbonate pebbles, referred to here as carbonate pebbles; and 7) other. These results have been described previously by McClenaghan *et al.* (1988b) and are summarized below.

A strong, negative correlation exists between the abundance of felsic intrusive pebbles and metavol-

canic pebbles. The abundances of trace elements and major oxides are strongly related to abundances of certain pebble lithologies. The associations between pebble lithologies and till geochemistry are not unexpected as the base metal content of felsic intrusive rocks is typically much lower than metavolcanic rocks, especially mafic metavolcanic rocks. Abundances of felsic intrusive and metavolcanic pebbles are the most useful for discriminating till units in individual drill holes. Discriminant analysis provides an efficient means of comparing pebble lithology composition of till units on a regional scale. As determined by discriminant analysis, the abundance of felsic intrusive pebbles is the most useful for comparing till units on a regional scale such that till units can be classified into felsic and mafic categories based on the abundance of felsic intrusive pebbles. These groupings generally display stratigraphic relationships such that the uppermost till unit in most drill holes contains more felsic intrusive pebbles than underlying till units.

The abundance of carbonate pebbles displays a consistent west-to-east decrease across the study area regardless of stratigraphic position. The Munro Esker appears to mark a transition zone between the higher abundances in the west and lower abundances in the east part of the area.

SUMMARY OF THE THIRD YEAR OF RESEARCH

Examination of the pebble fraction of till samples from selected drill holes was completed during the third year of the study. Discriminant analysis was performed on the completed pebble-frequency data set to refine the threshold determined previously (McClenaghan *et al.* 1988b). Explanations of this multivariate statistical method and training group selection procedures are described in McClenaghan *et al.* (1987). The results are summarized in Table 294.1 and indicate that a threshold of 27% felsic intrusive pebbles effectively separates till units into two compositionally distinct groups. This value is slightly higher than that previously determined for the smaller data set (McClenaghan *et al.* 1988b). The terms felsic and mafic have been adopted to describe the pebble composition of these two relatively distinct types of till units: felsic tills contain greater than 27% felsic intrusive pebbles and mafic tills contain less than 27% felsic intrusive pebbles. The two compositional groups appear to have some relationship to stratigraphy. The uppermost till unit in 23 of the 24 drill holes has a felsic composition. Underlying tills commonly have a mafic composition. An example of the relationship of felsic intrusive abundance to the 27% threshold defined by discriminant analysis is shown for drill hole 84–28 in Figure 294.2. In this drill hole, the upper two till units (till units 1 and 2) display a felsic composition while the lower till unit (till unit 3) has a mafic composition.

The felsic over mafic relationship of till units in the Matheson area is similar to those reported for till units in the Casa Berardi area, 100 km northeast of the study area. Here, Sauerbrei *et al.* (1987) reported two till units, in most cases separated by glaciolacustrine sediment. At least 80% of the cobble-sized clasts in the lower till unit are local (greenstone) bedrock lithologies. In contrast, the upper till unit contains a significantly higher percentage of foreign (intrusive) bedrock lithologies. These differences in abundance were used to distinguish between the two till units where they were found in contact with one another.

In the Selbaie Mine area, 180 km northeast of Matheson, Bouchard *et al.* (1986) have reported till units with contrasting clast compositions. The stratigraphic sequence consists of three till units separated by sand or lacustrine sediments. The lowermost till is characterized by a greater proportion of granitic (foreign) clasts than volcanic (local) clasts. The overlying till unit contains, in contrast, predominantly volcanic clasts. This is overlain by Cochrane till which has a very low clast content.

Alcock (in preparation) has reported the till at the the top of both the oldest and older packages at the Owl Creek pit are dominated by pebbles of dis-

TABLE 294.1. SUMMARY STATISTICS FOR DISCRIMINANT ANALYSIS OF THE PEBBLE LITHOLOGY ABUNDANCE DATA (N=163).

Variables in Analysis	Step	Variable Add	%Classified Correctly	F-Value**	Degrees of Freedom
Felsic intrusive	1	Felsic intrusive	84.7	130.9	1161
Mafic intrusive*	2	Mafic intrusive	84.1	79.5	2160
Metavolcanic	3	Ultramafic	87.1	55.8	3159
Metasediment*	4	Metavolcanic	87.7	44.8	4158
Ultramafic*					
Carbonate*					

** Indicates log transformed.*

*** F-value is a statistical measure of the discrimination. Higher F-values generally indicate a statistically more significant discrimination. Actual significance can be read from standard statistical tables.*

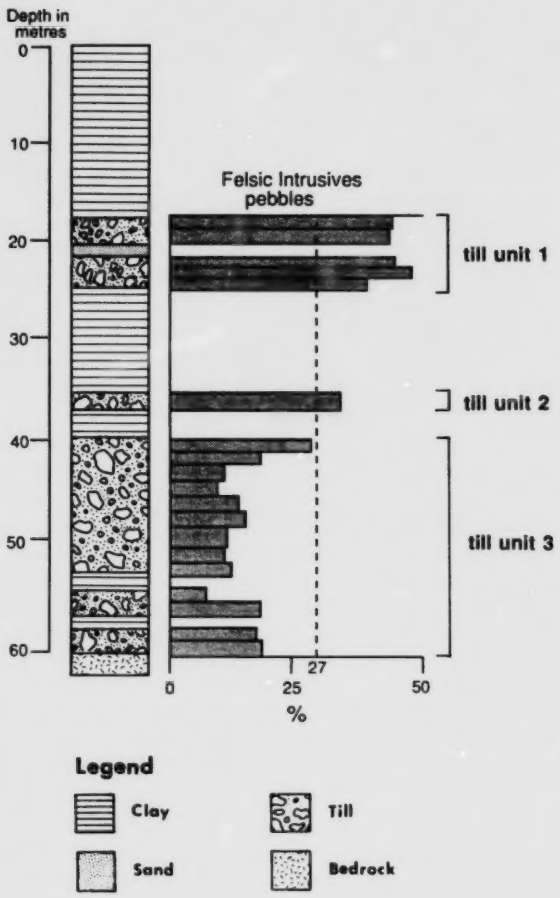

Figure 294.2. *Abundance of felsic intrusive pebbles and the 27% threshold defined by discriminant analysis for drill hole 84–28 (graphic log modified from OGS 1986).*

tally derived bedrock lithologies of felsic to intermediate intrusive rocks and Paleozoic carbonate rocks.

CARBONATE PEBBLE ABUNDANCE PATTERNS

The carbonate-pebble content only was determined for drill holes 84–13, 85–13 and 85–31 in addition to the 16 drill holes examined for all the major rock-type lithologies to provide more information on the regional distribution pattern of carbonate pebbles. The source area for the carbonate pebbles is a significant distance north of the study area in the Hudson Bay–James Bay Lowlands (Shilts 1982) as shown in Figure 294.3. The presence of these pebbles in the tills of the Matheson area indicate a minimum transport distance of approximately 200 km based on the present day distribution of Paleozoic bedrock.

Abundances of carbonate pebbles in till samples from selected drill holes across the study area and the Maude Lake pit are shown in Figure 294.4. From this figure, it is apparent that there are strong similarities in abundance of carbonate pebbles between till units within an individual drill hole. For example, drill hole 84–28, shown earlier to have marked compositional differences between till units (Figure 294.2), has a relatively uniform carbonate abundance. Even where a combination of organic material and glaciolacustrine clay and silt separates till units, as in drill holes 84–27 and 85–17, the till units contain similar abundances of carbonate.

Drill hole 85–42 displays a carbonate abundance pattern that is unique among the drill holes in the study area. As shown in Figure 294.4, the two uppermost till units contain very few to no carbonate pebbles, similar to the tills from surrounding drill holes in the east portion of the study area. The lower till unit contains between 5 and 10% carbonate pebbles. This is similar to the tills from drill holes located in the west portion of the study area. This striking contrast in carbonate abundance between till units within the same drill hole is limited to the area around drill hole 85–42. The pebble fraction from samples recovered from six holes drilled within 300 m of 85–42 by the OGS in 1988 display very similar patterns (K. Steele, Ontario Geological Survey, Toronto, personal communication, 1988).

As reported previously (McClenaghan *et al.* 1988b), carbonate-pebble abundances display a marked regional west-to-east pattern, as shown in Figure 294.4. Carbonate-pebble abundance decreases significantly from 5 to 15% in the west part of the study area to 2% or less in the east. This carbonate abundance pattern is similar to that reported by other workers in the area. Hughes (1965) found that the abundance of carbonate pebbles in the Matheson till decreased towards the southeast, from 32% in the Smooth Rock Falls area, 100 km northwest of the study area, to 1% or less in the Ramore area on the south-central edge of the study area. Shilts (1982) and, more recently, Veillette (1986) described the occurrence of carbonate till in the area south of James Bay whose eastern limit appears to be approximately the Ontario–Québec border. Thus, within the Matheson area, tills adjacent to the Ontario–Québec border should contain no carbonate pebbles. This is in agreement with the very low carbonate pebble abundances found in till samples from the easternmost drill holes. A similar west-to-east decrease is also displayed by till units below the uppermost (Matheson) till unit. No other pebble lithology displays such a striking regional pattern.

The abundance of carbonate pebbles displays a consistent west-to-east decrease across the study area regardless of stratigraphic position. The Munro Esker appears to mark a transition zone between higher abundances in the west and lower abundances in the east part of the area. Perhaps the Munro Esker marks the former location of a suture zone between two ice lobes. This may be determined through further detailed examination of material

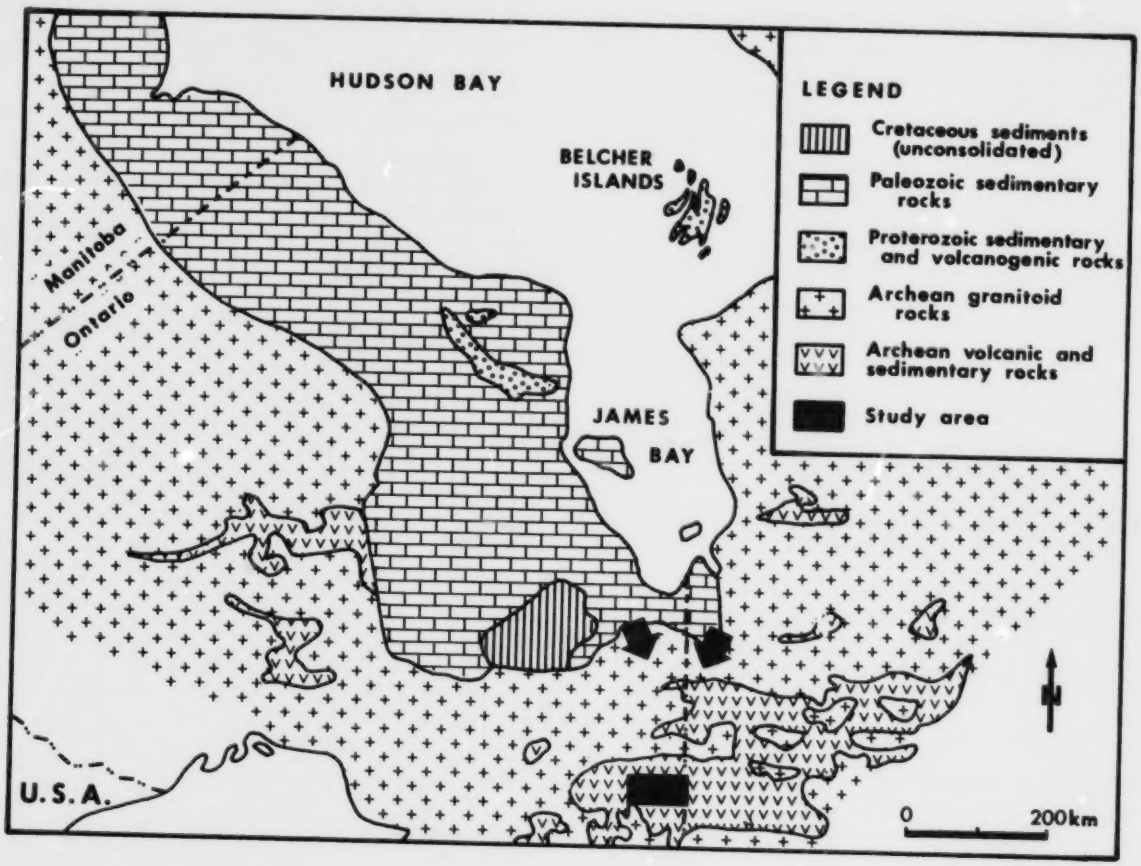

Figure 294.3. *Regional bedrock geology and ice flow directions (arrows).*

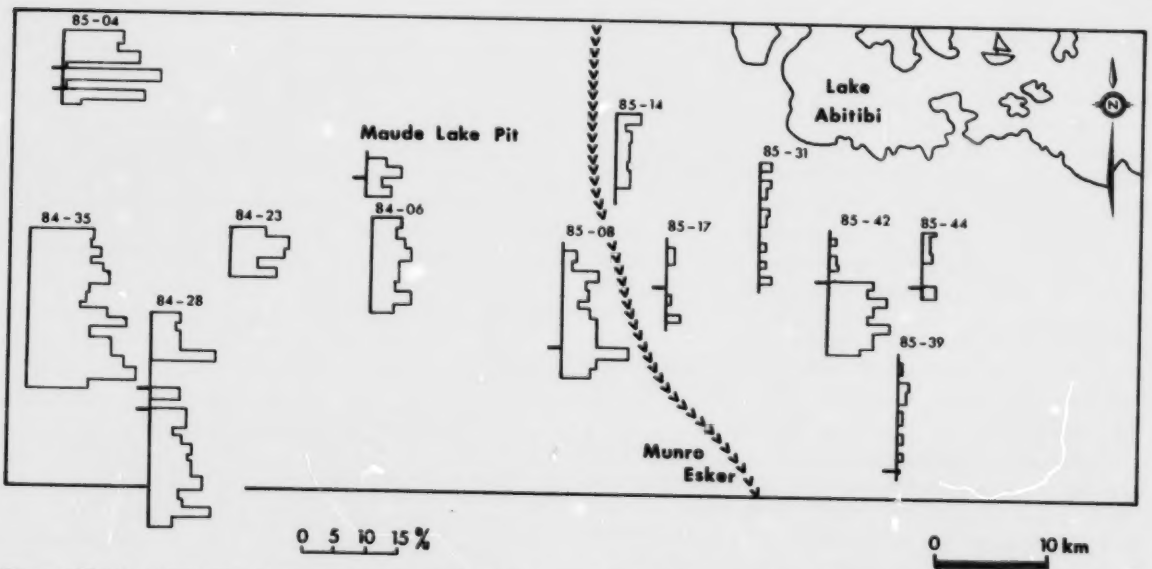

Figure 294.4. *Abundance of Paleozoic carbonate pebbles (scale bar at left) in till samples from selected drill holes across the study area and the Maude Lake pit. The top of each unit is indicated on the left side of each drill hole by a tick mark for those drill holes that contain multiple till units.*

from additional OGS sonic drill holes on both sides of the esker and any future work completed both north and south of the study area.

The similar abundances of carbonate in till units separated by organic material presumably from a non-glacial period, suggests they are of similar provenance and probably had similar ice flow patterns. Based on the present day distribution of Paleozoic bedrock north of the study area, this carbonate abundance pattern would suggest that ice flow was towards the south-southwest from an ice dome over Québec (*see* Figure 294.3).

Drill hole 85–42 is an exception to the west-to-east pattern, the reason for which is at present unclear. Unknown Paleozoic outliers north of the study area may be responsible for the unusual pattern in the vicinity of this drill hole. Alternatively, the lowest, carbonate-rich till unit may be an older till that has been protected from subsequent glacial advances that affected the rest of the area.

DISCUSSION

TILL COMPOSITION

On a regional scale, till units can be divided into two geochemically distinct groups: acidic or basic. The pebble lithology abundances indicate that the composition of these two groups is related to composition of the bedrock source. In general, till that displays an acidic chemical composition contains higher proportions of felsic intrusive pebbles and much lower proportions of metavolcanic pebbles. Till that displays a basic chemical composition contains higher proportions of metavolcanic pebbles and corresponding lower proportions of felsic intrusive pebbles. These two compositionally distinct groups are referred to hereafter as felsic and mafic. Thus, we see that the fine (<1.7 mm) and coarser (pebble) fractions of till in the Matheson area have similar compositions. Of the three analytical fractions, the fine and total matrix fractions have the strongest relationship with the pebble fraction.

The felsic and mafic compositions of the tills in the Matheson area are likely a result of local versus distal derivation of bedrock material and not two different ice flow directions. Mafic till composition probably reflects the entrainment of local, greenstone bedrock into a felsic till derived mainly from granitic and gneissic rocks north of the greenstone belt.

Regardless of which is the more viable explanation for felsic and mafic patterns, both indicate that felsic tills were derived largely from more distant bedrock sources. Since the study area is dominated by mafic metavolcanic bedrock, till of local derivation should be mafic in composition. Thus, felsic tills have had less contact with the local bedrock than mafic tills. Obviously, felsic tills are a poor indication of the composition of the local bedrock and as such are a less effective sampling medium for detecting mineralization in the local bedrock.

REGIONAL ICE FLOW PATTERNS

Only carbonate pebbles, derived from a known bedrock source area, have been used to reconstruct ice flow patterns. Based on the facts that 1) carbonate pebbles have been derived from the Hudson Bay Lowland, 2) two ice flow directions, 240° followed by 165°, are recorded by striations, and 3) the presence of regional marker horizons of clay and silt rhythmites and organic material between till units, and recent work by Veillette *et al.* (1989) in the Abitibi region, the following sequence of events has been reconstructed for the Matheson area:

1. ice advanced towards the southwest;
2. during a non-glacial interval, intertill silt and clay rhythmites and organic material were deposited;
3. the Matheson ice advanced, towards the southwest initially, shifted towards the southeast near the end of glaciation and produced glacial landforms oriented northwest;
4. the Late Wisconsinan ice sheet retreated from the area and lacustrine sediments were deposited in lake Barlow–Ojibway.

Both ice advances were probably toward similar directions as till units deposited before and after the intertill lacustrine sediment and organic material contain similar amounts of carbonate pebbles. Bedrock striations and till fabric data indicate that these ice advances were towards the southwest. Also, ice flow must have been towards the southwest in order to produce the west-to-east decrease in carbonate pebble abundance in the study area. During the final stages of deglaciation, the ice flow shifted from southwest to southeast (165°). This shift is recorded by regional striation patterns and till fabrics examined by Veillette (1986) and Veillette *et al.* (1989). What happened prior to the first southwest ice flow event mentioned above is not clear although Veillette *et al.* (1989) have proposed a southward ice flow event. Whether all these events happened during the Wisconsinan is also uncertain although Bird and Coker (1987) have suggested they all occurred during the Wisconsinan.

This model is based on the following assumptions:

1. The present day distribution of Paleozoic carbonate bedrock is similar to what it was during glaciation.
2. Silt and clay rhythmites between till units in seven drill holes indicate a similar period of lacustrine deposition between the deposition of till units.
3. Organic material associated with the above mentioned lacustrine sediments in drill holes within

the study area and in several drill holes further west in the Timmins area (DiLabio *et al.* 1988) indicate a similar non-glacial interval between the deposition of till units. This suggests a glacial retreat and deposition of the associated silts and clays in a proglacial lake.

4. The felsic or mafic character of a till is related to the entrainment of local, greenstone bedrock and not to different ice flow directions.

OVERALL CONCLUSIONS OF THE STUDY

1. Striations and till fabric data from the Maude Lake pit indicate two ice flow events affected the Matheson area: an earlier flow towards approximately 240° and a later flow toward approximately 165°. This is in agreement with regional striation patterns (Veillette 1986; Richard and McClenaghan 1985; Alcock, in preparation).

2. Till samples generally fall into one of two distinct types based on their geochemical composition: a) those with a more acidic chemical composition, and b) those with a more basic chemical composition.

3. Based on relative frequencies of pebble lithologies in till samples, two distinctive till-types are recognized in the study area: a) those with a greater percentage of felsic intrusive pebbles, and b) those with more metavolcanic pebbles.

4. Pebble lithological abundances of till samples correlate well with geochemical composition. Till of more acidic composition has higher abundances of felsic intrusive pebbles and is referred to as felsic till. Till of more basic geochemical composition has higher abundances of metavolcanic pebbles and is referred to as mafic till.

5. In general, geochemical and pebble lithological character of a till is related to stratigraphic position. The uppermost till unit in most drill holes has a more felsic composition while underlying till units commonly have a more mafic composition.

6. The mafic character of a till unit is probably related to degree of entrainment of local greenstone bedrock rather than ice flow directions.

7. Bedrock striations, till fabric data and the distribution of carbonate pebbles in the tills of the Matheson area along with the regional data of Veillette *et al.* (1989) can be used to reconstruct ice flow events. The area was affected by at least two major ice flow events towards the southwest and separated by a non-glacial event. During the final stages of the second ice advance, ice flow shifted towards the southeast.

RECOMMENDATIONS FOR EXPLORATION

The following are recommendations which will improve the effectiveness of future till geochemistry programs in the Matheson area and elsewhere in the region:

1. Where overburden drilling is required, sonic drilling is recommended over reverse circulation drilling for at least the initial stage of the overburden sampling program and ideally for the entire sampling program to provide detailed stratigraphic information about the area. Sonic drilling also allows for more precise sampling and can be stored for future reference.

2. Both heavy mineral concentrates and the fine fraction (<0.063 mm) should be analyzed geochemically. The fine fraction is the most useful for stratigraphic interpretations and correlations while both the heavy mineral fraction and the fine fraction are useful for anomaly recognition.

3. For stratigraphic interpretations and determining the felsic or mafic composition of till units, both for individual drill holes and regional correlations, the following trace elements are the most useful: Cu, Zn, Ni and Co. Although not evaluated in this study, Cr and Pb should also be useful.

4. For tracing geochemical anomalies up-ice, two ice flow directions must be considered for Matheson till: southwest flow and southeast flow. Older tills have a southwest ice flow direction.

5. Carbonate content of till samples is of little use as a regional stratigraphic tool and its mere presence or absence while logging overburden drill holes is valueless. An accurate determination of carbonate content (either of the till matrix or of the pebble fraction) may be of limited use in specific places throughout the Matheson area, such in the vicinity of drill hole 85–42.

ACKNOWLEDGMENTS

The authors would like to thank the Geophysics/Geochemistry Section of the Ontario Geological Survey, Toronto, for making all the data and samples used in this study readily available. J.M. Kuska drafted some of the figures.

REFERENCES

Alcock, P.W.
In Prep: Quaternary Geology of the Timmins Area, Districts of Cochrane, Timiskaming and Sudbury; Ontario Geological Survey, Open File Report.

Baker, C.L., Steele, K.G. and McClenaghan, M.B.
1985: Reconnaissance Till Sampling Program, Matheson-Lake Abitibi Area, Cochrane District; p.329-333 *in* Summary of Field Work and Other Activities 1985 by the Ontario Geological Survey, edited by J. Wood, O.L. White, R.B. Barlow, and A.C. Colvine, Ont-

ario Geological Survey, Miscellaneous Paper 126, 351p.

Bird, D.J. and Coker, W.B.

1987: Quaternary Stratigraphy and Geochemistry at the Owl Creek Gold Mine, Timmins, Ontario, Canada; p.267-284 *in* Geochemical Exploration 1985, edited by R.G. Garrett, Journal of Geochemical Exploration, Volume 28.

Bouchard, M.A., LaSalle, P., Lamothe, M., David, P.P. and Bouillon, J.J.

1986: Pleistocene Stratigraphy of Northwestern Abitibi from Boreholes and Excavations at Selbaie Mine, Québec; Geological Association of Canada/Mineralogical Association of Canada/Canadian Geophysical Union, Program with Abstracts, Volume 11, p.47.

DiLabio, R.N.W., Miller, R.F., Mott, R.J. and Coker, W.B.

1988: The Quaternary Stratigraphy of the Timmins Area, Ontario, as an Aid to Mineral Exploration by Drift Prospecting; p.61-65 *in* Current Research, Part C, Geological Survey of Canada, Paper 88-1C.

Hughes, O.L.

1959: Surficial Geology of Smooth Rock and Iroquois Falls Map Areas, Cochrane District, Ontario; unpublished PhD Thesis, University of Kansas, Lawrence, Kansas, 190[illegible].

1965: Surficial Geology of Part of the Cochrane District, Ontario, Canada; p.535-565 *in* International Studies on the Quaternary, edited by H.E. Wright and D.G. Frey, Geological Society of America, Special Paper 84.

McClenaghan, M.B., Lavin, O.P., Nichol, I. and Shaw, J.

1987: Quaternary Geology and Geochemical Exploration in the Matheson Area; p.200-214 *in* Geoscience Research Grant Program, Summary of Research, 1986-1987, edited by V.G. Milne, Ontario Geological Survey, Miscellaneous Paper 140, 251p.

1988a: Quaternary Geology and Geochemical Exploration in the Matheson Area, Northeastern Ontario; p.1-20 *in* Prospecting in Areas of Glaciated Terrain—1988, edited by D.R. MacDonald and K.A. Mills, The Canadian Institute of Mining and Metallurgy, 644p.

1988b: Quaternary Geology and Geochemical Exploration in the Matheson Area; p.112-123 *in* Geoscience Research Grant Program, Summary of Research, 1987-1988, edited by V.G. Milne, Ontario Geological Survey, Miscellaneous Paper 136, 241p.

Ontario Geological Survey

1986: Sonic Drillhole 84-28, Currie Township, Cochrane District; Ontario Geological Survey, Map 80760, Geophysical/Geochemical Series, Geology 1984, 1985.

Richard, J.A. and McClenaghan, M.B.

1985: Quaternary Geology of the Porquis Junction Area, District of Cochrane; Ontario Geological Survey, Map P.2949.

Sauerbrei, J.A., Pattison, E.F. and Averill, S.A.

1987: Till Sampling in the Casa-Berardi Gold Area, Québec: a Case History in Orientation and Discovery; p.297-314 *in* Geochemical Exploration 1985, edited by R.G. Garrett, Journal of Geochemical Exploration, Volume 28.

Shilts, W.W.

1982: Quaternary Evolution of the Hudson/James Bay Region; Naturaliste Canadien, Volume 109, p.309-332.

Veillette, J.J.

1986: Former Southwesterly Ice Flow in the Abitibi-Timiskaming Region: Implications for the Configuration of the Late Wisconsinan Ice Sheet; Canadian Journal of Earth Sciences, Volume 23, p.1724-1741.

Veillette, J.J., Averill, S.A., LaSalle, P. and Vincent, J.S.

1989: Quaternary Geology of the Abitibi-Temiscamingue and Mineral Exploration; Geological Association of Canada, Field Trip Guidebook, 112p.

Whittaker, P.J.

1986: Gold Metallogenesis along the Pipestone and Destor-Porcupine Deformation Zones and Associated Structures; p.404-407 *in* Summary of Field Work and Other Activities 1986, edited by P.C. Thurston, O.L. White, R.B. Barlow, M.E. Cherry and A.C. Colvine, Ontario Geological Survey, Miscellaneous Paper 132, 435p.

Grant 300 The Genesis of Silver Vein Deposits in the Thunder Bay Area, Northwestern Ontario

S.A. Kissin and R.L. Sherlock

Department of Geology, Lakehead University, Thunder Bay

ABSTRACT

Historic drill core from the Shuniah Mine and more recent drill core from the Keystone and Porcupine mines of the Thunder Bay area have provided the basis for a study of these past-producing silver mines as a function of depth. The drill-core samples were augmented by surface samples from these mines, as well as ones from the Thunder Bay Mine. Within any given stage of deposition of quartz or calcite, fluid-inclusion homogenization temperatures invariably increase with depth. Precipitation was initiated from a boiling fluid at temperatures in excess of 370°C. Cooling of the fluid and precipitation of calcite and sulphides followed generally at temperatures declining to 100°C. Several cycles of deposition occurred, separated by fracturing events. From fluid-boiling temperatures the depth of emplacement for the veins is 1 km with the pressure regime alternating between hydrostatic and lithostatic. The ore-depositing solutions appear, therefore, to have arisen from depth and to have deposited their ores in response to hydrologic factors.

Stable isotopic studies reveal that carbon in vein calcite was probably derived from organic carbon in the Gunflint and Rove Formations ($\delta^{13}C = -33‰$), which host the silver lodes. Calcite, as well, does not occur at great depth in the vein systems. $\delta^{18}O_{H_2O}$, as calculated from determinations in quartz and calcite, increases with depth, from negative to positive values, suggesting that the ore-depositing fluid was a basinal brine that became increasingly mixed with meteoric water toward the surface. Salinities are low to moderate, but invariably undersaturated, also supporting mixing.

INTRODUCTION

Previous reports from this project have dealt with a survey of fluid inclusion and sulphur isotopic studies from silver veins of the Thunder Bay area (Kissin and Jennings 1987) and a study of the silver-bearing veins of the Schreiber–Terrace Bay area (Kissin and McCuaig 1988). The silver vein deposits of the Thunder Bay and Schreiber–Terrace Bay areas were reviewed by Franklin *et al.* (1986), whose work was the starting point for this project. Briefly, silver-bearing quartz and calcite veins, with minor base metal sulphides, cut all rocks in the area. In the Thunder Bay area, the deposits occur in two northeasterly trending zones, the Mainland belt and the Island belt. The Mainland belt veins occupy northeasterly striking listric normal faults. Most deposits are hosted in the Aphebian Rove Formation shales and are closely spatially associated with capping diabase sills of Keweenawan age. A few of the deposits are hosted in the underlying Gunflint Formation or basement Archean greenstones. The Island belt veins strike northwesterly, and the northeasterly striking normal faults are occupied by diabasic and gabbroic dikes, which are cut by the veins. The host rock for these veins is again the Rove Formation. The mineralogy of the Island belt veins is often more complex than that seen in the Mainland belt, culminating in a fully developed five-element (Ag-Ni-Co-Bi-As) deposit at the famous Silver Islet Mine.

The results reported by Jennings (1986) and Kissin and Jennings (1987) indicate that formation of the veins occurred in pulses in which an initial high-temperatures phase of deposition was followed by deposition under declining temperatures. Fracturing of the first-formed vein was followed by another episode of high-temperature deposition. Thus, a single-cycle process, such as cooling of a diabase sill, could not have been responsible for the formation of the deposits. Lateral secretion from source beds such as the Rove shale, driven by the heat of the diabasic intrusions, as others had suggested previously, is thus no longer a viable hypothesis. Kissin (1988a,b) proposed that ore-depositing solutions were connate and evolved meteoric waters mobilized by anomalously high heat flow accompanying Keweenawan rifting.

The new hypothesis could be tested by the study of fluid inclusions and stable isotopes from vein systems examined at depths well below the level of the rather shallow exposures presently accessible. If ore-depositing solutions originated at depth, temperatures of trapping, as determined by fluid inclusion studies, should also increase with increasing depth below the surface. Stable isotopes in gangue minerals may also be expected to exhibit some differences with depth. Fortunately, the opportunity to study some vein systems as a function of depth was afforded by the existence of historic drill core from

the Shuniah Mine and more recent drill core from the Porcupine and Keystone mines.

GEOLOGICAL BACKGROUND

The Shuniah Mine (Figure 300.1) is located within the present city limits of Thunder Bay, immediately north of the Thunder Bay expressway. According to data compiled by Franklin *et al.* (1986), the mine was in operation in the period 1867–1868, 1870 and 1873–1881 and produced 50 000 ounces of silver. In spite of the rather low productivity, extensive undergound development was undertaken, with the sinking of four shafts and development of crosscuts at several levels (Figure 300.2). The No. 3 shaft reached a depth of approximately 800 feet (244 m), completely passing through the Rove Formation and Gunflint Formation and entering Archean granitic basement rocks (Figure 300.3). Some of the earliest known diamond drilling in North America was carried out in the period 1877–1878 (W.M Courtis, unpublished drill log), resulting in a total of 4884 feet (1488 m) of drilling with a maximum depth of 994 feet (303 m). Samples of this drill core were preserved by W.M. Courtis, the manager of the mine during much of its operation. This collection passed into the possession of the Geological Survey of Canada and was made available for study in the project.

The Thunder Bay Mine, 1.5 km east of the Shuniah Mine (Figure 300.1), operated in 1866–1869 and 1874, producing 16 000 ounces of silver (Franklin *et al.* 1986). Although little remains of underground workings that existed at one time, the vein, including showings of argentite and native silver, is exposed at the surface. The vein is hosted in Gunflint Formation shales and chert, adjacent to a capping diabase sill. Owing to the possibilities for sampling and its similar geologic setting to the Shuniah Mine, specimens from the Thunder Bay were also included in this study.

The Keystone and Porcupine mines (Figure 300.1) lie 36 km southwest of the Shuniah Mine in O'Connor and Gillies townships, respectively. The Porcupine operated intermittently in the period 1884–1911 in conjunction with the Badger Mine, 500 m to the southeast. These two mines produced a reported 400 000 ounces of silver (Franklin *et al.* 1986). The Keystone Mine, 500 m to the north of the Porcupine, operated briefly in 1891 and 1911–1912, producing 20 000 ounces of silver (Franklin *et al.* 1986). Minor efforts were made at various times to reactivate these mines; however, in the period 1965–1971 a number of patented mining properties in O'Connor and Gillies townships were assembled by Creswel Mines Ltd. In the course of various other development activities, diamond drilling of the Keystone and Porcupine mines was carried out. Samples of the drill core were preserved by

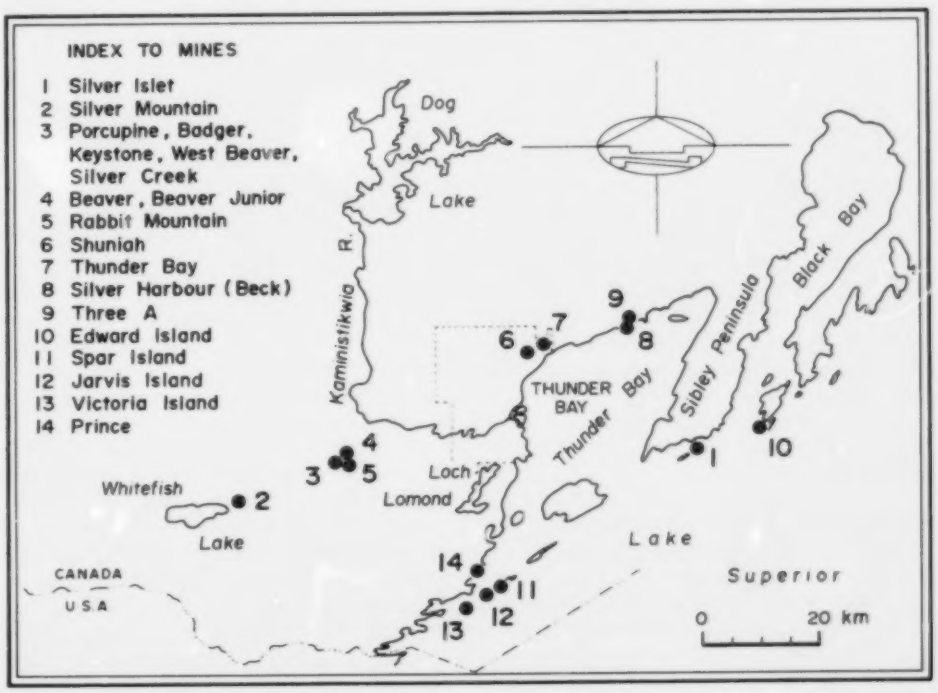

Figure 300.1. *Location map for past-producing silver mines of the Thunder Bay area. Mines studied in this report are the Shuniah (6), Thunder Bay (7) and Porcupine and Keystone (3).*

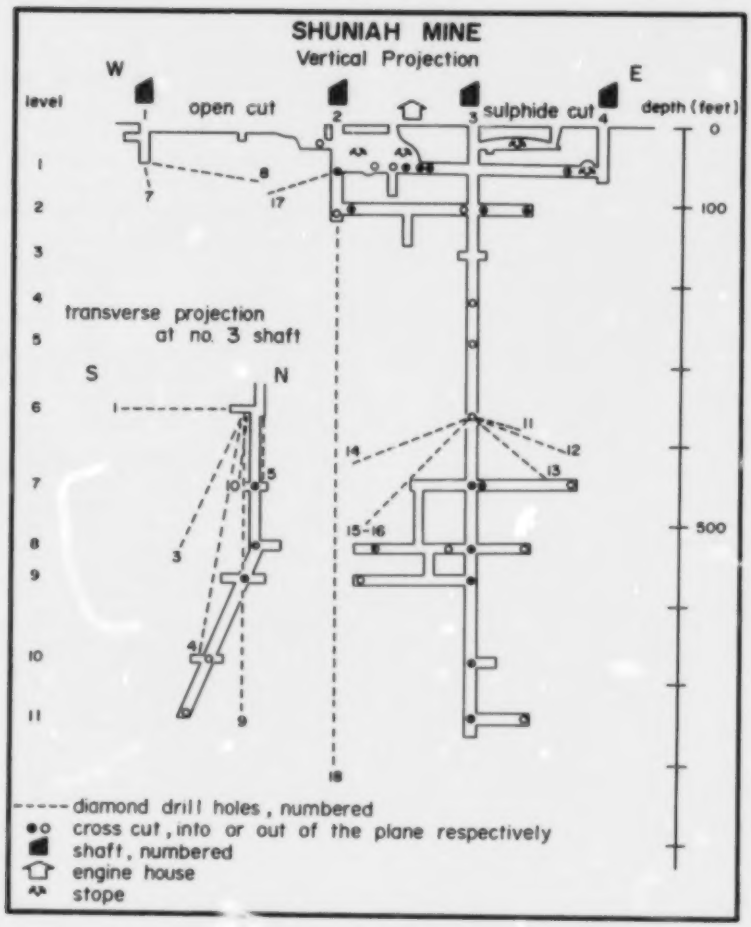

Figure 300.2. *Diagram of the maximum extent of underground development at the Shuniah Mine, showing the locations of diamond drill holes (after Courtis 1878 and Ingall 1888).*

J.M. Franklin (Geological Survey of Canada, Ottawa), who made them available for study.

Both the Keystone and Porcupine mines exploited vein systems hosted in Rove Formation shales capped by a diabase sill about 10 m thick. According to data gleaned from company records by Sherlock (1989), four holes with an aggregate length of 1132 feet (395 m) were drilled on the Porcupine and eight holes with a total length of 1350 feet (412 m) on the Keystone. The drill core sampled in this study penetrated the Rove shales completely and entered the upper portion of the underlying Gunflint Formation.

METHODOLOGY

Fluid inclusion studies were carried out using an SGE Fluid Inclusion Research System mounted on a specially adapted Leitz SM-POL polarizing microscope. The system was calibrated using standards of known melting and freezing points. As all calibration errors were $\pm 1°C$ or less, no corrections were employed.

Stable isotopic analyses were conducted by standard techniques by Geochron Laboratories Division, Kreuger Enterprises Incorporated, Cambridge, Massachusetts.

RESULTS

FLUID INCLUSION STUDIES

Fluid inclusion data from the Thunder Bay silver veins were shown by Kissin and Jennings (1987) to depend strongly on the paragenetic position of the host mineral. In each of the four mines studied in this phase of the project, a paragenetic sequence was established based on field observations and detailed examination of drill core and surface samples. The most complex relationships were observed in the Shuniah Mine, where three complete sequences of

early quartz → silver → base metal sulphides → calcite were discerned, each separated by an episode of fracturing (Figure 300.4). The precipitation of quartz occurred at the highest temperature and was accompanied by sporadic boiling. Rapid cooling followed, and fracturing preceded a new period of high-temperature crystallization. A pulse of high-temperature fluid, which precipitated fluorite and calcite, also occurred after the deposition of quartz II and calcite II, but apparently without additional fracturing. Similar paragenetic sequences were established at the Thunder Bay, Keystone and Porcupine mines, although in these cases only two sequences of crystallization separated by an episode of fracturing were observed.

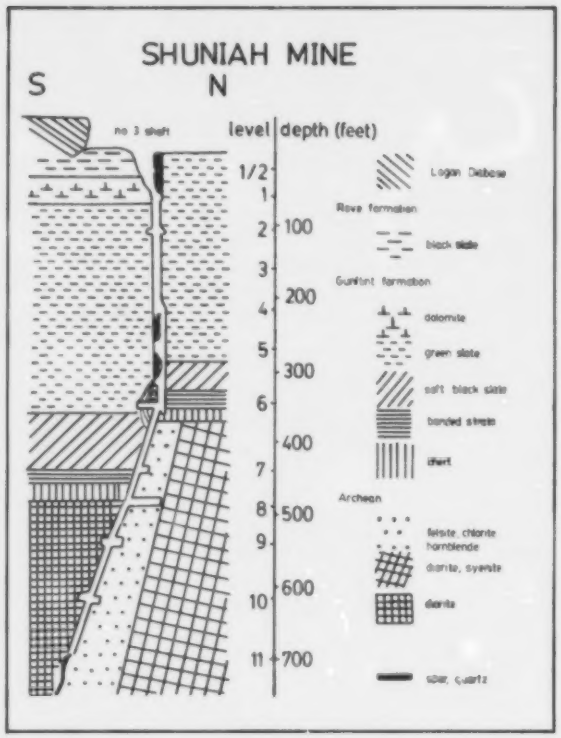

Figure 300.3. *Schematic north-south section of the No. 3 shaft of the Shuniah Mine, showing lithologies as designated by Courtis (1887).*

The fluid inclusions from all four mines are similar in that all are two-phase, liquid-vapour inclusions. All inclusions are undersaturated with respect to halides, as halide daughter crystals were not present, although in a few cases, unidentified prismatic daughter crystals, which were unreactive on heating, were present.

Freezing experiments were conducted in order to determine eutectic temperatures (T_e) and final melting temperatures (T_m) in order to establish the salt system present in the liquid phase and the salinity, respectively. The T_e for 85 inclusions from the Shuniah Mine are shown in Figure 300.5. The great amount of scatter in the data is far more than can be attributed to observational error, and it seems that in different phases of growth of the host minerals different halide systems were present. The data indicate that NaC_l, $CaCl_2$ and $MgCl_2$, in various permutations and combinations, are the dominant halides. A few inclusions with $T_e = -70°C$ are likely attributable to CO_2–H_2O vapour mixtures. These are also correlatable with late-stage calcite deposition at low temperatures. T_e determined for the other three

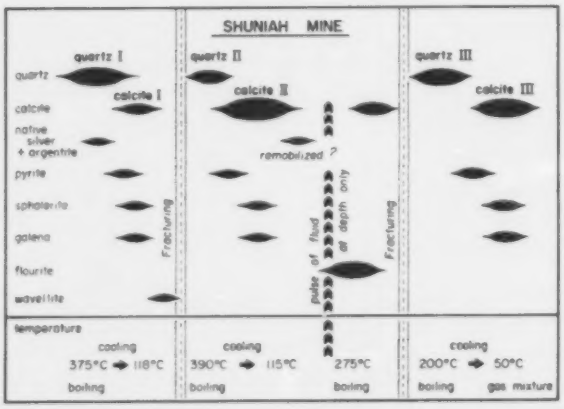

Figure 300.4. *Paragenetic sequence at the Shuniah Mine. Temperatures and the occurrence of boiling are based on fluid inclusion studies discussed in the text.*

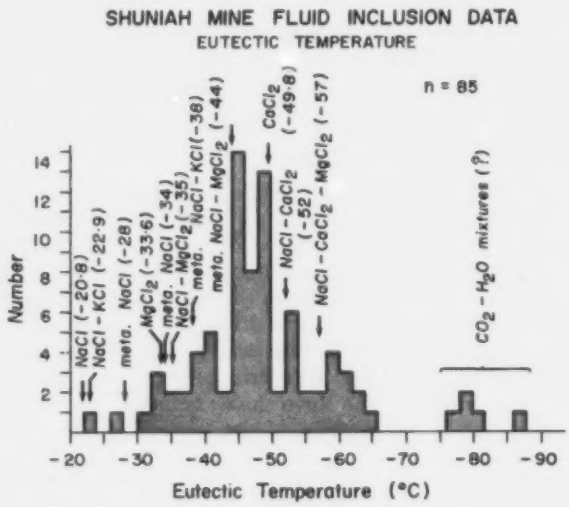

Figure 300.5. *Eutectic temperatures from 85 fluid inclusions from the Shuniah Mine plotted as a histogram. Eutectic temperatures for possible halide–H_2O systems as given by Crawford (1981) and Davis et al. (1988), are indicated (meta = metastable eutectic).*

mines show a similar scatter. Complete data are given by Sherlock (1989).

Salinities, as determined by T_m ice, are given in Figure 300.6 for 76 fluid inclusions from the Shuniah Mine. The data are presented in terms of equivalent weight percent NaCl, as determined from an equation given by Potter *et al.* (1978). The salinities vary from nearly pure water to nearly saturated, with no pronounced tendency toward any particular salt concentration. Similar data emerged from the three other mines, as well, and full details are contained in Sherlock (1989).

The T_h observed for inclusions hosted in quartz I and quartz II from the Shuniah are shown in Figures 300.7 and 300.8, respectively. Boiling, as evidenced by adjoining inclusions that homogenized to liquid and to vapour at the same temperature, occurred in zones within quartz crystals. The T_h increase with depth below surface in specimens obtained from drill core, and in all cases correlation coefficients for the linear regression equations are significant at greater than the 99% confidence level. Inclusions hosted in quartz II, which indicated boiling had occurred, homogenized at a nearly constant 43°C greater than those homogenized to liquid. The difference probably reflects the magnitude of the pressure correction applicable to the non-boiling inclusions, as will be discussed later.

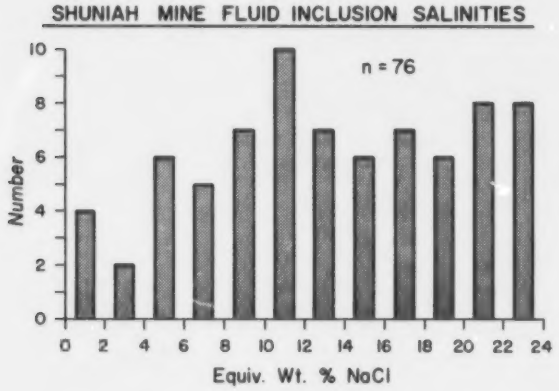

Figure 300.6. *Salinities in terms of equivalent weight percent NaCl from 76 fluid inclusions from the Shuniah Mine.*

Fluid inclusions hosted in calcite I and calcite II from the Shuniah Mine lack evidence of trapping under conditions of boiling and consistently homogenize to liquid, however, at temperatures much lower than observed for T_h in quartz (Figure 300.9 and 300.10). T_h increases with depth in the same manner as in inclusions hosted in quartz.

Calcite from the Keystone Mine (Figure 300.11) and Porcupine Mine (Figure 300.12) hosts inclusions yielding similar homogenization trends as in the Shuniah Mine. Some evidence of boiling is present in the deeper samples from the Porcupine Mine.

STABLE ISOTOPIC STUDIES

Carbon is common in the Thunder Bay area as a constituent of the sedimentary rocks, especially the Rove Formation, and as a constituent of the silver veins, deposited with quartz and calcite gangue. The Rove Formation shales are obviously carbonaceous, and analyses by Harvey (1985) revealed that they contain an average of 2 weight percent carbon. A specimen of graphitic carbon from the Rove Forma-

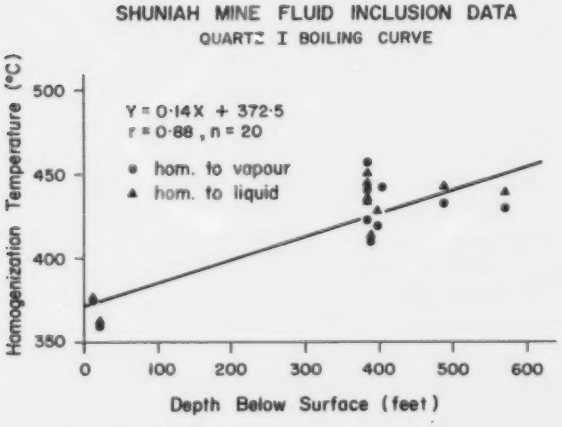
SHUNIAH MINE FLUID INCLUSION DATA
QUARTZ I BOILING CURVE
Y = 0·14X + 372·5
r = 0·88, n = 20
hom. to vapour
hom. to liquid
Homogenization Temperature (°C)
Depth Below Surface (feet)

Figure 300.7. *Homogenization temperatures (paired observations for adjoining inclusions that homogenized to liquid and to vapour) and hosted in quartz I from the Shuniah Mine. An equation of the linear regression line and the correlation coefficient r are also given for 20 observations.*

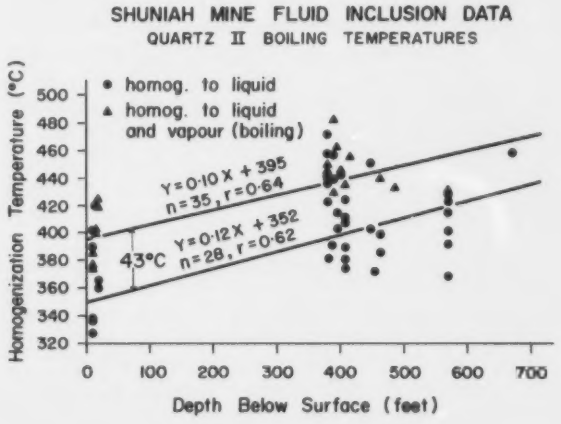
SHUNIAH MINE FLUID INCLUSION DATA
QUARTZ II BOILING TEMPERATURES
homog. to liquid
homog. to liquid and vapour (boiling)
Y = 0·10X + 395
n = 35, r = 0·64
Y = 0·12X + 352
n = 28, r = 0·62
43°C
Homogenization Temperature (°C)
Depth Below Surface (feet)

Figure 300.8. *Homogenization temperatures for 35 paired inclusions homogenizing to liquid and to vapour (triangles) and 28 inclusions homogenized to liquid (circles) and hosted in quartz II from the Shuniah Mine. Equations of the linear regression lines and correlation coefficients r are also given. A nearly constant 43°C difference between the two best fit lines is indicated.*

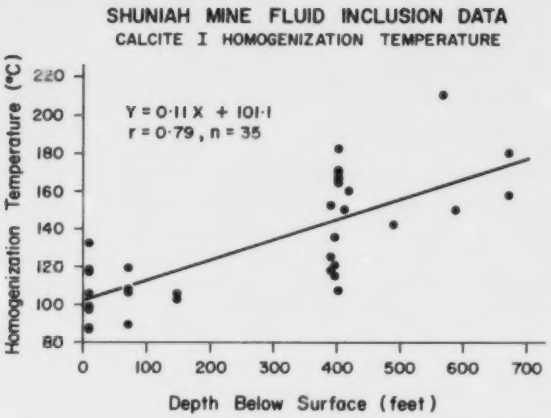
SHUNIAH MINE FLUID INCLUSION DATA
CALCITE I HOMOGENIZATION TEMPERATURE
Y = 0·11 X + 101·1
r = 0·79, n = 35
Homogenization Temperature (°C)
Depth Below Surface (feet)

Figure 300.9. *Homogenization temperatures for 35 fluid inclusions homogenized to liquid and hosted in calcite I from the Shuniah Mine. An equation of the linear regression line and the correlation coefficient r are also given.*

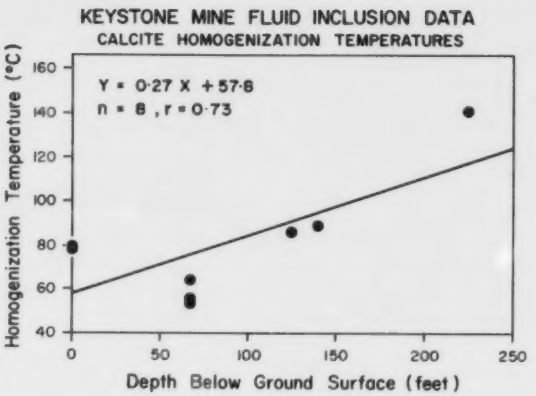
KEYSTONE MINE FLUID INCLUSION DATA
CALCITE HOMOGENIZATION TEMPERATURES
Y = 0·27 X + 57·8
n = 8, r = 0·73
Homogenization Temperature (°C)
Depth Below Ground Surface (feet)

Figure 300.11. *Homogenization temperatures for 8 fluid inclusions homogenized to liquid and hosted in calcite from the Keystone Mine. An equation of the linear regression line and the correlation coefficient r are also given.*

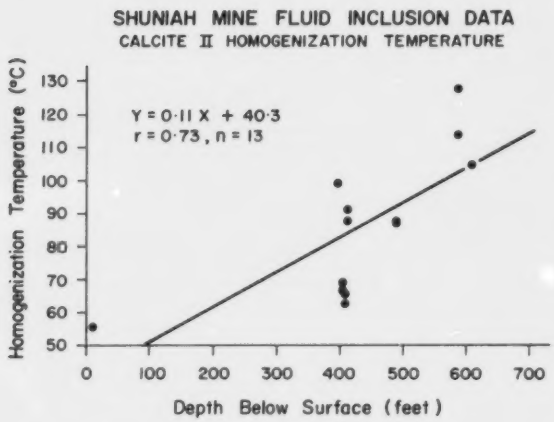
SHUNIAH MINE FLUID INCLUSION DATA
CALCITE II HOMOGENIZATION TEMPERATURE
Y = 0·11 X + 40·3
r = 0·73, n = 13
Homogenization Temperature (°C)
Depth Below Surface (feet)

Figure 300.10. *Homogenization temperatures for 17 fluid inclusions homogenized to liquid and hosted in calcite II from the Shuniah Mine. An equation of the linear regression line and the correlation coefficient r are also given.*

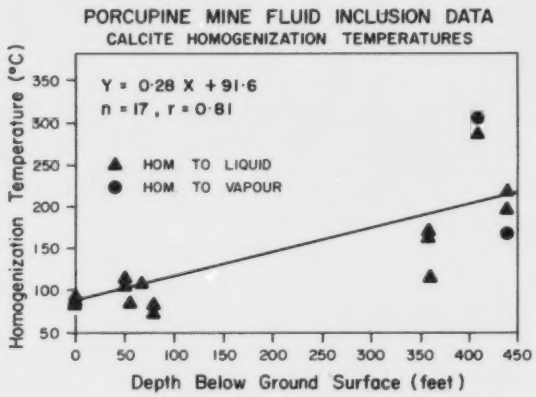
PORCUPINE MINE FLUID INCLUSION DATA
CALCITE HOMOGENIZATION TEMPERATURES
Y = 0·28 X + 91·6
n = 17, r = 0·81
HOM TO LIQUID
HOM TO VAPOUR
Homogenization Temperature (°C)
Depth Below Ground Surface (feet)

Figure 300.12. *Homogenization temperatures for 17 fluid inclusions hosted in calcite from the Porcupine Mine. Two pairs of inclusions homogenized to liquid and to vapour at depth. An equation of the linear regression line and the correlation coefficient r are also given.*

tion, obtained from a quarry containing a diabase-shale contact and located 1 km east of the Thunder Bay Mine, gave $\delta^{13}C = 31.1‰$. Carbon in the wall rock of the Thunder Bay Mine was of very similar composition of $\delta^{13}C = -31.9‰$. Carbon is much less uniformly distributed in the Gunflint Formation; however, a high content of carbon is noticeable in some of its lithologies. In particular, the Kakabeka Conglomerate member, exposed at the Archean–Proterozoic unconformity in Kakabeka Falls Provincial Park contains nodules of anthraxolite associated with silicified algal stromatolites.

The anthraxolite was determined to have $\delta^{13}C = -34.7‰$. These values are typical for organic carbon and are representative of the isotopic composition of the sedimentary units in which they occur.

Calcite from all the mines of this study was analyzed for combined $\delta^{13}C$ and $\delta^{18}O$. As fluid inclusion homogenization temperatures had been obtained for each of the 15 samples analyzed, it was possible to calculate $\delta^{13}C_{HCO^-}$ and $\delta^{18}O_{H_2O}$, utilizing an equation given by Deines *et al.* (1974) and the Changkakoti *et al.* (1986) modification of the O'Neil *et al.* (1969) equation, respectively. The results in terms of $\delta^{13}C$ calcite are plotted as a function of depth in Figure 300.13. The veins hosted in the Rove Formation show no apparent variation with depth and all values lie between $\delta^{13}C = -5$ and -9, with a mean of $-7 \pm 0.9‰$. On the other hand, the

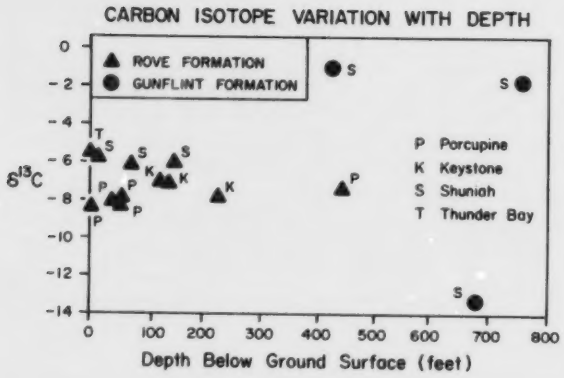

Figure 300.13. *$\delta^{13}C$ of calcite plotted as a function of depth in samples from four Thunder Bay area mines.*

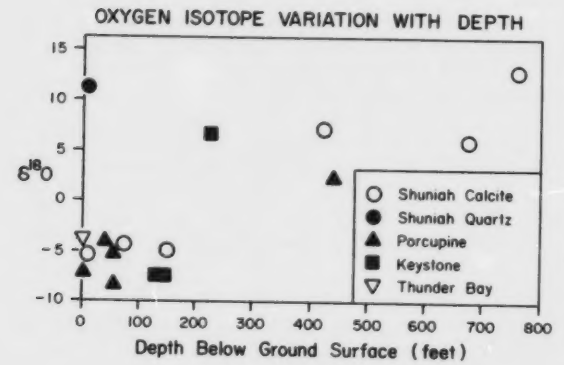

Figure 300.14. *$\delta^{18}O$ of calcite and quartz plotted as a function of depth in samples from four Thunder Bay area mines.*

Shuniah Mine samples hosted in the Gunflint Formation vary considerably.

The same 15 calcite samples and one quartz sample from the Shuniah were analyzed for $\delta^{18}O$, with results plotted in Figure 300.14 as a function of depth. Except for the quartz sample, the results appear to define a trend of increasing $\delta^{18}O$ with depth. The $\delta^{18}O$ in quartz and calcite must, however, be recalculated to yield $\delta^{18}O$ of the water from which they were precipitated.

In order to investigate the relationship between carbon and calcite or dolomite, $\delta^{13}C$ was determined in two samples from Silver Islet, one containing intergrown dolomite and carbon (SI 27) and one containing abundant carbon (SI-C). The samples yielded $\delta^{13}C = -34.8‰$ (SI 27) and $-33.3‰$ (SI-C). The Silver Islet dolomite in SI 27, with a fluid inclusion homogenization temperature of 177.5°C, yielded $\delta^{18}O = +20.4‰$ and $\delta^{13}C = 11.1‰$.

Combined δD and $\delta^{18}O$ determinations on hydrous silicate alteration minerals are very useful in interpreting the origin of hydrothermal fluids; however, typical alteration mineralization in the Thunder Bay area is weakly developed and very fine grained. Only two samples coarse enough for separation were found, sample EA 53 from the Keystone Mine as described by Jennings (1986) and a sample from the Silver Mountain Mine designated SM. Both samples consist of Rove Formation shale altered to illite and both are associated with vein minerals yielding fluid-inclusion homogenization temperatures. The results are, for EA 53, $\delta D = -68‰$, $\delta^{18}O = +12.4‰$ at 102.4°C, and for SM, $\delta D = -68‰$, $\delta^{18}O = +12.1‰$ at 129.6°C.

DISCUSSION

The fluid inclusion and stable isotopic studies of this phase of the project provide important constraints on the possible modes of genesis of the Thunder Bay area silver veins. The T_h of fluid inclusions increases with depth in each portion of the paragenetic sequence in each of the four mines studied. The conclusion that the ore-depositing solutions were heated at depth and found positions beneath Logan diabase sills to be favourable depositional sites is inescapable.

The large amount of data and good control on paragenetic position of samples from the Shuniah Mine verify the generalization of Kissin and Jennings (1987) that deposition in vein systems occurred in more than one phase, separated by a period of pronounced cooling and, usually, by additional movement in the fault that provided the initial open space. This periodicity of deposition, separated by periods of cooling, precludes a single, cooling heat source, e.g., a diabase sill or gabbroic dike, as a heating mechanism for the hydrothermal solutions.

The calculated salinities and highly variable salt compositions occurring in the fluid inclusions suggest that the sources of the fluid were heterogeneous, including various sources at depth. The uniformly undersaturated nature of the fluid inclusions in conjunction with the wide and continuous range of salinities suggests that dilution of a salt-rich solution by a low-salinity solution, probably meteoric water, occurred.

The occurrence of phases of boiling coinciding with the deposition of early, high-temperature quartz followed by a gradual decline in temperature is the typical sequence of deposition in the mines. New influxes of hot solutions initiated new episodes of boiling following movement along the faults hosting the veins. Pressures typically varied during the formation from lithostatic, on the order of 4×10^4 kPa corresponding to about 1 km depth, to hydrostatic, in the range of 5×10^3 to 10^4 kPa. Throttling due to constriction of the vein openings and crack-seal phenomena probably produced a range of intermediate

pressure conditions. Although pressure corrections of up to 25°C would apply to the T_h determined in this study, the wide variation in pressure regime makes application of pressure corrections impractical.

The carbon found in the country rock (Rove and Gunflint formations) has an average composition of about $\delta^{13}C = -33‰$, a value typical of marine organic carbon with some possible enrichment in ^{13}C due to thermal maturation (Ohmoto 1986). The carbon in the Silver Islet samples has $\delta^{13}C = -31‰$, suggesting that this carbon is recrystallized. Further calculation of the fractionation between carbon in the wall rock and calcite at the Shuniah Mine and carbon and dolomite at Silver Islet yields 26.3‰ at 95°C and 22.2‰ at 177.5°C, respectively. Although fractionation between carbon and calcite is not well known experimentally, a summary by Valley (1986) indicates that these fractionations are well within the range of observed fractionations. Thus, it is likely that the carbon in vein carbonates was derived from organic carbon in the sedimentary host rocks of the veins.

The consistency of $\delta^{13}C$ in vein carbonate hosted in the Rove Formation is probably reflective of the fairly uniform distribution of organic carbon in the unit. On the other hand, carbon in the Gunflint Formation is erratically distributed, and the scatter in $\delta^{13}C$ in vein carbonates hosted in the Gunflint Formation is attributable to variations in original carbon isotopic water/rock ratios and other factors. The hypothesis of a sedimentary source for the carbon in vein carbonates is reinforced by the observations that carbonate content decreases with depth in the vein systems and that carbonate gangue is absent when the veins are hosted by basement granites.

The oxygen isotopic composition of water, which precipitated calcite and quartz, is plotted as the cross hatched region in Figure 300.15. The δD and $\delta^{18}O$ determinations on illite samples EA 53 and SM serve to fix a hypothetical mixing curve between end-member deep basinal brines and local meteoric water. This mixing trend is further substantiated by the observed relationship between $\delta^{18}O_{H_2O}$ and depth, i.e., the isotopically heaviest waters are from the deepest samples and the lightest from the shallowest samples.

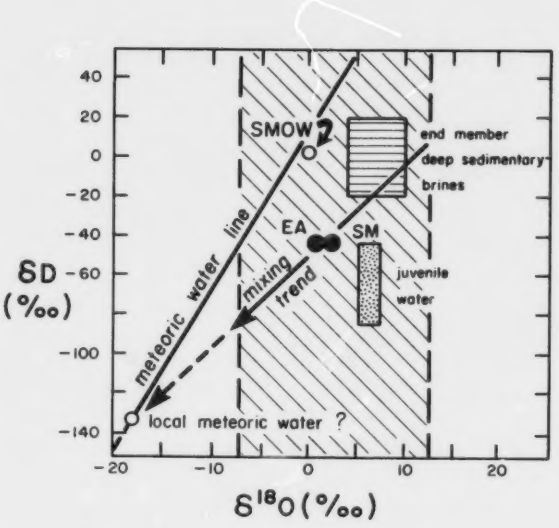

Figure 300.15. *δD vs. $\delta^{18}O$ plot showing the positions of the meteoric water line, standard mean ocean water (SMOW), end-member deep sedimentary brines and juvenile water according to Ohmoto (1986). The cross-hatched area indicates the range of values of $\delta^{18}O_{H_2O}$, as calculated from measured $\delta^{18}O$ in calcite, dolomite and quartz and fluid inclusion homogenization temperatures. The points EA and SM are illite samples from the Keystone and Silver Mountain mines and serve to fix a hypothetical mixing line between end-member deep sedimentary brines and local meteoric water.*

CONCLUSIONS

The past year's work on fluid inclusions and stable isotopes from drill-core samples from the Shuniah, Keystone and Porcupine mines, as well as surface samples from these and the Thunder Bay Mine leads us to make the following conclusions:

1. Within a given paragenetic position, fluid-inclusion homogenization temperatures increase with depth in samples from the vein systems. Thus, the ore-depositing solutions were heated at depth and deposited ores in response to boiling, cooling and dilution at depths of about 1 km below the surface.
2. The diversity of salt compositions in fluid inclusions as well as the wide range in salinities suggests mixing of a saline brine with dilute solution, probably meteoric water.
3. Carbon isotopic studies suggest that carbon in vein carbonates was derived from organic carbon in the sedimentary wall rocks.
4. Oxygen and hydrogen isotopic studies indicate progressive mixing of an end-member deep basinal brine with meteoric water.

These conclusions indicate that the ore-depositing solutions are ultimately of sedimentary origin. Kissin (1988a,b) has suggested that heat associated with Keweenawan rifting mobilized connate brines, which scavenged metals at high temperatures. The solutions rose along listric normal faults normal to the rift axis, depositing their ores in structurally favourable sites beneath diabase sills. Clearly, the special problem of the precise mechanism of ore transport is still unresolved; however, this study provides a starting point for future research in this direction.

ACKNOWLEDGMENTS

The following at Lakehead University, Thunder Bay, provided invaluable assistance in various areas: A.L. Hammond and R.L. Viitala, thin and polished section preparation; S.T. Spivak, drafting; and S.E. Millar, typing. L.M. Cumming and J.M. Franklin of the Geological Survey of Canada, Ottawa, made available the drill core from the Shuniah, Porcupine and Keystone mines.

REFERENCES

Changkakoti, A., Morton, R.D., Gray, J. and Young, C.J.

1986: Oxygen, Hydrogen, and Carbon isotopic Studies of the Great Bear Lake Silver Deposits, Northwest Territories; Canadian Journal of Earth Sciences, Volume 23, p.1463-1469.

Courtis, W.M.

1878: The North Shore of Lake Superior as a Mineral-Bearing District; Transactions of the American Institute of Mining Engineers, Volume 5, p.474-487.

1887: The Animike Rocks and Their Vein Phenomena, as shown at Duncan Mine, Lake Superior; Transactions of the American Institute of Mining Engineers, Volume 15, p.671-677.

Crawford, M.L.

1981: Phase Equilibria in Aqueous Fluid Inclusions; p.75-100 *in* Short-Course in Fluid Inclusions: Applications to Petrology, edited by L.S. Hollister and M.L. Crawford, Mineralogical Association of Canada, 304p.

Davis, D.W., Lowenstein, T.K. and Spencer, R.J.

1988: Melting Behavior of Fluid Inclusions in Laboratory Grown Halite Crystals in the Systems NaCl-H_2O, NaCl-KCl-H_2O, and NaCl-$MgCl_2$-H_2O (abstract); Geological Society of America, Program with Abstracts 1988, p.A152.

Deines, P., Langmuir, D. and Harmon, R.S.

1974: Stable Isotope Ratios and the Existence of a Gas Phase in the Evolution of Carbonate Ground Waters; Geochimica et Cosmochimica Acta, Volume 387, p.1147-1164.

Franklin, J.M., Kissin, S.A., Smyk, M.C. and Scott, S.D.

1986: Silver Deposits Associated with the Proterozoic Rocks of the Thunder Bay District, Ontario; Canadian Journal of Earth Sciences, Volume 23, p.1576-1591.

Harvey, P.L.

1985: A Test of the Lateral Secretion Hypothesis at the Rabbit Mountain Mine, Mainland Belt Silver Region, Thunder Bay District, Ontario; unpublished HBSc Thesis, Lakehead University, Thunder Bay, 75p.

Ingall, E.D.

1888: Report on Mines and Mining on Lake Superior; Geological and Natural History Survey of Canada, Annual Report for 1887-8, new series, No. 3, Part H, p.1-131.

Jennings, E.A.

1986: A Survey of the Mainland and Island Belts, Thunder Bay Silver District, Ontario: Fluid Inclusions, Mineralogy, and Stable Isotopes; unpublished MSc Thesis, Lakehead University, Thunder Bay, 159p.

Kissin, S.A.

1988a: Nickel-Cobalt-Native Silver (Five-Element) Veins: A Rift-Related Ore Type; p.268-279 *in* Proceedings Volume, North American Conference on Tectonic Control of Ore Deposits and the Vertical and Horizontal Extent of Ore Systems, edited by G. Kisvarsanyi and S.K. Grant, University of Missouri-Rolla, 567p.

1988b: The Five-Element Suite: An Indicator of Non-Magmatic Ore Types Related to Rifting and Basin Development; Explore, No. 64, p.5-7.

Kissin, S.A. and Jennings, E.A.

1987: The Genesis of Silver Vein Deposits in the Thunder Bay Area, Northwestern Ontario; p.230-241 *in* Geoscience Research Grant Program, Summary of Research, 1986-1987, edited by V.G. Milne, Ontario Geological Survey, Miscellaneous Paper 136, 241p.

Kissin, S.A. and McCuaig, T.C.

1988: The Genesis of Silver Vein Deposits in the Thunder Bay Area, Northwestern Ontario; p.146-156 *in* Geoscience Research Grant Program, Summary of Research, 1987-1988, edited by V.G. Milne, Ontario Geological Survey, Miscellaneous Paper 140, 251p.

Ohmoto, H.

1986: Stable Isotope Geochemistry of Ore Deposits; p.491-560 *in* Stable Isotopes in High Temperature Geological Processes, edited by J.W. Valley *et al.*, Reviews in Mineralogy, Volume 16, Mineralogical Society of America, 570p.

O'Neil, J.R., Clayton, R.N. and Mayeda, T.K.

1969: Oxygen Isotope Fractionation in Divalent Metal Carbonates; Journal of Chemical Physics, Volume 51, p.5547-5558.

Potter, R.W., II, Clynne, M.A. and Brown, D.L.

1978: Freezing Point Depression of Aqueous Sodium Chloride Solutions; Economic Geology, Volume 73, p.284-285.

Sherlock, R.L.

1989: A Study of the Third Dimension in the Thunder Bay Silver Veins: Fluid Inclusion and Stable Isotope Results; unpublished MSc Thesis, Lakehead University, Thunder Bay, 170p.

Valley, J.W.

1986: Stable Isotope Geochemistry of Metamorphic Rocks; p.445-490 *in* Stable Isotopes in High Temperature Geological Processes, edited by J.W. Valley *et al.*, Reviews in Mineralogy, Volume 16, Mineralogical Society of America, 510p.

Grant 305 Metamorphic Petrology and Gold Mineralization of the White River Gold Prospect, Hemlo Area

Y. Pan and M.E. Fleet

Department of Geology, University of Western Ontario, London

ABSTRACT

Polymetamorphism at the White River gold prospect of Lac Minerals Ltd., in the Hemlo–Heron Bay greenstone belt, is characterized by low to medium metamorphic grade that climaxed in two narrow zones (middle amphibolite facies) in close association with regional structures. The lower zone structurally overlies the crystalline basement (Pukaskwa gneissic complex); the upper zone encloses the regional shear zone (Hemlo shear zone) and is bounded by the Hemlo fault zone to the south. The presence of andalusite and sillimanite in metapelites classifies the peak metamorphism as typical low pressure series.

Calc-silicate rocks of distinct Cr-rich mineral assemblages formed by hydrothermal alteration from volcanogenic mafic or ultramafic rocks during peak metamorphism (epidote amphibolite facies) with significant chromium enrichment in the Cadi fracture zone. Late, low- to very low-grade hydrothermal alteration, probably associated with plutonic activity, produced some anomalously Cr-rich minerals in vesicles and crosscutting veins, as a result of the large amount of chromium in the system.

Geochemical analyses of the clastic metasedimentary rocks show chemical signatures of continental weathering processes, and suggest that the clastics were derived from intermediate to felsic volcanic materials admixed with minor amounts of mafic and ultramafic volcanic materials, and were deposited rapidly in a sedimentary basin in a continental island-arc or oceanic island-arc tectonic setting.

Anomalous gold values (up to 27 ppm) have been obtained in a local brittle-ductile shear zone. Native gold is the only gold-bearing phase and is associated with both sulphide and sheet silicate minerals. Small geochemical anomalies of As–Hg–W (–Cu) are present in the local shear zone but do not correlate with the gold anomalies. Maximum gold values occur where three stratigraphic zones, a hanging-wall sericitic zone, the anomalous zone, and a footwall pyritic zone, coalesce. Hydrothermal alteration in the local shear zone is characterized by extensive potassic and calc-silicate-like (skarn) alteration and sulphidation. Limited carbonatization is present but is not confined to the local shear zone. Clearly, the gold anomaly in the study area is directly or indirectly related to the pyritic and sericitic zones, but elucidation of its origin requires further study.

INTRODUCTION

The past year's work was a continuation of the systematic investigation of the metamorphic petrology of the Hemlo–Heron Bay greenstone belt at the White River gold prospect of Lac Minerals Ltd., in the Hemlo area.

Preliminary results were outlined by Pan and Fleet (1988) and included geological characteristics and geochemistry of the supracrustal rocks, the earlier crystalline basement (Pukaskwa gneissic complex) and the late granodioritic Cedar Lake Pluton. Particular emphasis was placed on representation of the characteristic rock units, mineral assemblages and mineral chemistry of the most important rock types including metapelites, calc-silicates, and metabasites, and the relationship of the zone of highest metamorphic grade to the Hemlo shear zone. A zone of anomalous gold values was also described briefly in respect to its stratigraphic position and relationship with the potassic and the regional calc-silicate-like alteration.

The geology and metamorphism of the study area (Pan and Fleet 1988, Figure 305.5) are summarized in Figure 305.1, which presents a complete stratigraphic section of the Hemlo–Heron Bay greenstone belt at the White River gold prospect. The figure shows the lithology of the supracrustal rocks and compositional variations in plagioclase and calcic amphiboles corresponding to both metamorphic grade and bulk rock composition. Figure 305.1 incorporates new information, most notably that unit 2 clastic metasedimentary rocks and Cr-rich calc-silicate rocks belong to the Playter Harbour Group.

This report summarizes the results of field work and laboratory investigations carried out in 1988–1989. The main objectives of the project are:

1. to improve understanding of metamorphic grade, P–T conditions, and metamorphic history of the Hemlo–Heron Bay greenstone belt, particularly the unit 1 metabasites of the Playter Harbour Group, by interpreting new petrographic evidence and mineral chemical data;

GROUP	UNIT	STRATIGRAPHY*	THICKNESS (m)	DESCRIPTION	An—CONTENT OF PLAGIOCLASE	AMPHIBOLE
CEDAR LAKE PLUTON				granodiorite	(8—10) (zoned phen.)	
HEMLO—HERON BAY GREENSTONE BELT			150	metagreywacke	26	
	9		10	amphibolite	18	Act-Hb—Hb
			100	metagreywacke	27	
			10	amphibolite	19	Act-Hb—Hb
	8		50	metapelite	29	
LSZ			8	Muscovite schist	26	Act-Hb—Hb
	7		70	intermediate metavolcanics	17	Act—Act-Hb
			80	quartz—biotite schists	42	Ay
	6		5	banded iron formation	30	(Mg,Fe) Ay+Hb+Ged+Cum
			150	biotite greywacke	22	
	5		5	lean iron formation	29	Hb+Cumm
HBZ			5	quartz-feldspar porphyry	13	
	4		60	amphibolite	39	Hb
			4	actinolite - chlorite schist	38 + 86	Act—Act-Hb
	3		120	intermediate - felsic metavolcanics	17 (12)	Act-Hb
			120	metasediments	30	Hb
			250	intermediate-felsic metavolcanics	20	Act-Hb—Hb
			150	metagreywacke	19	
PLAYTER HARBOUR	2		20	amphibolite	19	Act-Hb—Hb
			25	calc-silicates	1	Act
			30	amphibolite	18	Act-Hb—Hb
				quartz porphyry		
			50	metagreywacke	23	
			20	amphibolite	21	Act-Hb—Hb
			200	metagreywacke		
	1		300	amphibolite	35	Hb
			60	variolitic flows		Act-Hb—Hb
			450	amphibolite	38	Act-Hb—Hb
PUKASKWA GNEISS COMPLEX				granitic gneiss		

Figure 305.1. *Stratigraphic section of the Hemlo-Heron Bay greenstone belt at the White River gold prospect, showing compositional variations in plagioclase and calcic amphibole. Act - actinolite; Act-Hb - actinolitic hornblende; Hb - hornblende; Ay - anthophyllite; Ged - gedrite; Cum - cummingtonite.*
**For stratigraphic legend, see Figure 305.2.*

2. to determine mineralogical characteristics of the Cr-rich calc-silicate rocks in the Cadi fracture zone and to compare them with the well known Outokumpu skarn formation of Finland;
3. to elucidate the environment of deposition and provenance of the clastic metasedimentary rocks in a large sedimentary basin east of the Hemlo gold deposit, using new geochemical data; and
4. to determine the characteristics of gold mineralization in a local brittle-ductile shear zone based on field and polished thin section observations, and to examine the relative times of deformation, peak metamorphism, hydrothermal alteration, and gold mineralization at the White River gold prospect.

METAMORPHISM

Burk *et al.* (1986) proposed a polymetamorphic history for the Hemlo gold deposit area, based on a study of mineral assemblages, textural relations, and P–T calculations for Teck–Corona metapelites. An earlier higher pressure, moderate temperature metamorphism in response to tectonically induced crustal thickening was followed by a lower pressure metamorphism due to rapid uplifting and erosion which resulted in a substantial decrease in lithostatic pressure but only minor change in temperature. In the White River study area, however, Pan and Fleet (1988) suggested that the prograde metamorphism is more like Barrovian-type metamorphism without convincing evidence for the existence of an earlier, higher pressure metamorphism.

Work in progress on metapelites and metabasites indicates a more complete metamorphic history. An earlier, moderate pressure and low- to medium-temperature metamorphism was followed by a peak thermal metamorphism related to heterogeneous shear deformation that climaxed at medium grade (sillimanite zone in metapelites and middle amphibolite facies in metabasites) conditions in a narrow zone, which encloses the regional, Hemlo shear zone. The presence of andalusite and sillimanite in metapelites at lower metamorphic grade and higher metamorphic grade, respectively, classifies the peak metamorphism as typical low-pressure, andalusite-sillimanite facies series according to Miyashiro's (1973) scheme.

The thick mafic metavolcanic unit of the Playter Harbour Group (unit 1, Figure 305.1) largely consists of high-iron tholeiitic basalt with a few komatiitic basalt lenses. Primary textures, such as pillows, are locally well preserved. This mafic metavolcanic unit is distinguished from metabasites of other units by its coarse-grained texture and the presence of large plagioclase porphyroblasts, particularly in the lower portion close to the Pukaskwa gneissic complex.

Mineral assemblages in the metabasites consist mainly of tschermakitic/pargasitic hornblende, plagioclase, quartz, with minor biotite, chlorite, magnetite, sphene and ilmenite. Tschermakatic/pargasitic hornblende is locally rimmed by Mg-rich actinolite, and plagioclase is rimmed by epidote. The Mg-rich actinolite and epidote appear to represent late crystallization related to either retrogression after peak metamorphism or later hydrothermal alteration. Plagioclase, as large porphyroblasts, is commonly compositionally and optically zoned, in most cases with lower An content in cores and higher An content in rims. However, plagioclase in both porphyroblasts and the rock matrix is invariably of intermediate composition (An_{35-38}). Calcic amphibole, except colourless actinolite, is brown-green in colour and chemically equivalent to tschermakitic/pargasitic hornblende according to Leake's (1978) nomenclature.

The lower, mafic metabasite unit within the Playter Harbour Group is similar in mineral assemblages and mineral chemistry to the middle metabasite unit (middle amphibolite facies as defined by intercalated metapelites). Muir (1982) reported kyanite-, sillimanite- and staurolite-bearing assemblages in intercalated clastic metasedimentary rocks within this group to the west of the study area near the Heron Bay area. The aluminous assemblage was not observed in the Playter Harbour Group of this study area, possibly due to the lack of field exposures. Furthermore, samples of coarse-grained metabasite were only collected from the lower portion of this unit near the contact with the Pukaskwa gneissic complex. Therefore, it is not well understood whether the metamorphic grade changes gradationally away from the contact (a major fault, cf. Muir 1982) or in some other pattern. Nevertheless, the coarse-grained metabasites of the Playter Harbour Group have apparently been subjected to medium grade metamorphic conditions similar to those of the zone of highest metamorphic grade (units 4, 5, and 6).

Cr-RICH CALC-SILICATE ROCKS

Cr-rich calc-silicate rocks of distinct yellowish-green colour occur in the Cadi fracture zone (which is delineated from the surrounding rocks by a magnetic anomaly and is interpreted as a major structure of the study area) at or near lithological boundaries between mafic metavolcanic rocks and clastic metasedimentary rocks (Figure 305.2). These rocks have been extensively researched during the past year because of their unusual mineral assemblages related to abundant chromium and the presence of zincian chromite (up to 6.6 weight percent ZnO and 3.4 weight percent MnO) (Pan and Fleet, in press; Pan *et al.*, in preparation). They occur as conformable thin bands or lenses (1 to 10 m thick) and locally develop a crude foliation parallel to the compositional bedding.

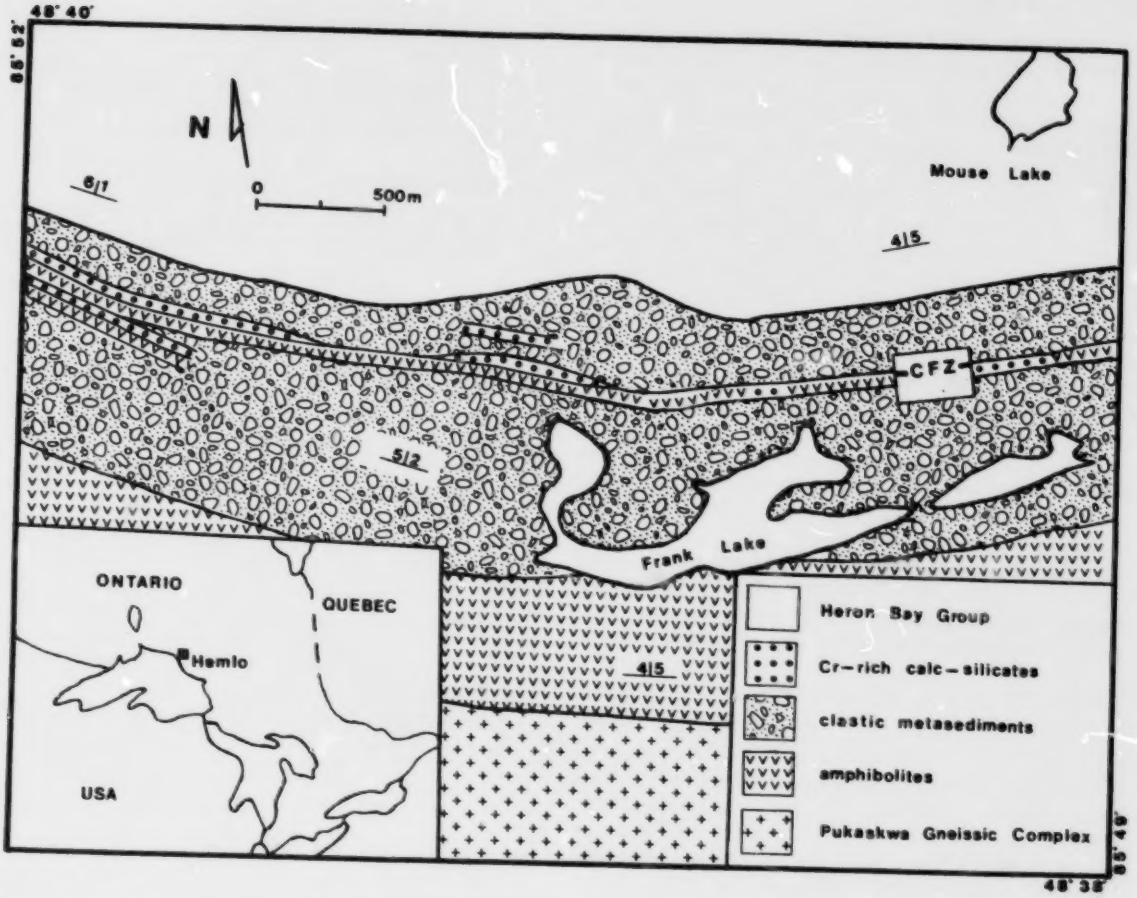

Figure 305.2. *Geological map of the Playter Harbour Group and the Cadi fracture zone (CFZ) at the White River gold prospect, Hemlo area, Ontario (prepared with assistance of Lac Minerals Ltd.).*

The characteristic silicate mineral assemblage includes clinopyroxene, grandite garnet (Cr-poor, brown and Cr-rich, green garnet), actinolite, epidote, uvarovite, prehnite, pumpellyite, chlorite, plagioclase, microcline, titanite and apatite. Variable but generally minor amounts of calcite are present. Textural and chemical evidence indicates that the main assemblage of clinopyroxene, grandite garnet, actinolite, epidote (excluding chromian epidote), plagioclase, chromite, titanite and some calcite was formed under equilibrium conditions with ambient fluids. However, the "anomalously" chromium-rich minerals, such as uvarovite (uvarovite content 64–84%), chromian epidote (up to 11.8 weight percent Cr_2O_3), chromian chlorite (up to 3.5 weight percent Cr_2O_3). prehnite (up to 1.2 weight percent Cr_2O_3), pumpellyite (up to 2.7 weight percent Cr_2O_3), as well as albite (Ab>99%) and some calcite in veins and vesicles, crystallized later than the main assemblage.

Cr-rich calc-silicates also contain a sub-economic polymetallic Fe–Ni–Co–Zn–Cu(–Mo) sulphide occurrence consisting of cobaltian pentlandite, pyrrhotite, sphalerite, chalcopyrite, Fe-rich siegenite, millerite, magnetite, goethite, and molybdenite. Cobalt is associated very largely with pentlandite (and siegenite replacing pentlandite), where lamellar cobaltian pentlandite is an exsolution product of pyrrhotite. Millerite is invariably associated with ultramafic relict fragments. Goethite containing minor Co and Ni and replacing magnetite occurs in surface samples and is apparently similar to lateritic weathering products. Molybdenite associated with cross-cutting feldspar veins apparently crystallized late in the sequence.

The sulphides and calc-silicates of the Cadi fracture zone are strikingly similar to those of the well known Outokumpu skarn formation in Finland (Von Knorring 1951; Von Knorring *et al.* 1986; Hiltunen 1982), especially in respect to the extensive Cr metasomatism, association of Zn with both chromite and sphalerite, association of Co with pentlandite, and paucity of Pb and Ag (Pan *et al.*, in preparation). However, carbonate rocks are not present in

the study area and its vicinity, and the Cr-rich calc-silicate rocks are confined to the Cadi fracture zone and are spatially associated with underlying mafic to ultramafic metavolcanic rocks. Therefore, the Cr-rich calc-silicate rocks are not of carbonate-replacement origin, but were produced by metasomatic processes which replaced volcanic or metavolcanic rocks, probably coeval with the peak metamorphism, within a major fracture zone. On the basis of contemporary studies and reviews (e.g., Einaudi *et al.* 1981; Einaudi and Burt 1982; Meinert 1984), the Cr-rich calc-silicate rocks from the study area would be regarded as a variety of skarn deposit. However, chromium (largely in zincian chromite) is more abundant than in any mafic or ultramafic metavolcanic rocks in the study area; therefore, secondary enrichment of chromium must have occurred as well. The presence of anomalously Cr-rich minerals, including uvarovite, chromian epidote, chlorite, prehnite and pumpellyite, with albite, microcline, and molybdenite in veins or cavities apparently indicates a late generation of crystallization, and these minerals probably are coeval with the regional, low- to very low-grade, calc-silicate-like alteration related to plutonic activity. The formation of the anomalously Cr-rich silicate minerals was probably dependent entirely on the presence of an adequate amount of chromium in the system.

Geothermobarometric studies reveal that the main mineral assemblage of the Cr-rich calc-silicate rocks in the Cadi fracture zone formed at a temperature of 400±50°C, a pressure of about 2–4 kbars and in the presence of a H_2O-rich fluid. PTX calculations in the system SiO_2–Al_2O_3–MgO–CaO–CO_2–H_2O further confirmed this estimation and indicated very low CO_2 fugacities ($X_{CO_2} < 0.03$, Figure 305.3) (Pan and Fleet, in press).

GEOCHEMISTRY OF THE METASEDIMENTARY ROCKS

The Hemlo gold deposit is associated with a transition from volcanic to sedimentary facies within the Hemlo–Heron Bay greenstone belt (Patterson 1984; Valliant and Bradbrook 1986). The White River gold prospect, to the east of the Hemlo gold deposit, is part of a large sedimentary basin and is mainly composed of metasedimentary rocks. Metasedimentary rocks of intermediate to felsic composition are commonly well-bedded and laminated. Primary textures, such as graded bedding and cross-bedding, which have been recognized in Heron Bay Group sedimentary rocks at the Hemlo gold deposit (T.L. Muir, Ontario Geological Survey, personal communication, 1988), are rarely observed in the study area due to extensive deformation and the lack of field exposures. However, blasto-psammitic texture with quartz and K-feldspar relics in a matrix of mafic minerals occurs in a few weakly to unfoliated domains. Some geochemical characteristics of metasediments from the study area, particularly banded iron formations, have been described previously (Pan and Fleet 1988); a number of features related to their environments of deposition and provenances will be presented in the following section.

PLAYTER HARBOUR GROUP

Clastic metasediments of the Playter Harbour Group are distinguished from those of the Heron Bay Group by the presence of calcic amphibole (actinolitic hornblende and hornblende) and the absence of banded iron formations (BIF). Pyroclastic fragments (mainly consisting of quartz and feldspars) are locally present. They are similar in texture and mineral assemblage to metasediments derived from unlithified volcanic sources and appear to be pyroclastic or volcanoclastic in origin.

Clastic sediments of the Playter Harbour Group are intermediate to felsic in composition and are geochemically comparable to typical Archean greywackes (cf. Condie 1981).

HERON BAY GROUP

Metasedimentary rocks of the Heron Bay Group are predominantly clastic with minor chemical members (oxide- and silicate-facies BIF). Clastic sedimentary rocks consist of mudstone and greywacke. The

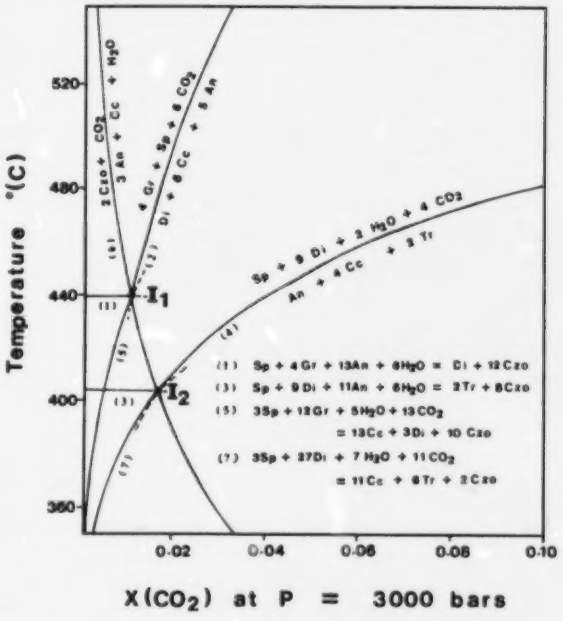

Figure 305.3. *Calculated T-X(CO_2) phase diagram in the system SiO_2-Al_2O_3-MgO-CaO-CO_2-H_2O at a pressure of 3 kbars showing mineral activities for analytical data from Cr-rich calc-silicate rocks of the Cadi fracture zone. Note that the precise positions of the invariant points I_1 and I_2 vary from sample to sample, but X(CO_2) does not exceed 0.03.*

mudstone is argillitic and recrystallized to aluminosilicate-bearing mica schist. Greywacke is feldspathic and recrystallized to quartz-feldspar schist.

The abundances of major elements are highly variable in different rock types; in particular SiO_2 (55.9–73.1 weight percent) and Al_2O_3 (12.0–21.6 weight percent) show large scale variations. The greywacke contains less Al_2O_3 and K_2O but more Na_2O and CaO relative to the mudstone. The Al_2O_3/Na_2O weight ratio (maturity index) of mudstone (average 7.1) is slightly higher than that of greywacke (average 5.2), but considerably lower than that for typical mature sediments. Although there are large scale variations in both Na_2O and K_2O content, the weight ratio of K_2O/Na_2O of all clastic sediments is typically lower than 1.0 and mostly between 0.5 and 0.7, which is comparable to common clastic sediments formed about 2.5 Ga ago (cf. Engel *et al.* 1974).

There are fairly good positive correlations between SiO_2 and ferromagnesian constituents, including TiO_2, $Fe_2O_3^*$ (total iron), MnO, and MgO, whereas Al_2O_3 and K_2O have a weak to moderate negative correlation with SiO_2. The Na_2O content shows a very weak positive correlation with SiO_2.

Like most Archean sedimentary rocks, clastic sedimentary rocks of the Heron Bay Group are characterized by high transition-metal content, especially the ferromagnesian trace elements including Ti, V, Sc, Mn, Cr, Co and Ni. This enrichment has been attributed to the more mafic and ultramafic nature of the earlier crust (Danchin 1967), although many other workers (e.g., McLennan and Taylor 1983) suggest that secondary enrichment might play an important role. The most important feature, in the present study, is that these ferromagnesian trace elements have definite positive correlations with $Fe_2O_3^*$ and MgO and negative correlations with SiO_2. This may imply a strong volcanic signature for the clastic sediments of the study area.

CHEMICAL SIGNATURES OF WEATHERING PROCESSES

The relative abundances of weathering products in sediments have been quantified using a chemical index of alteration (CIA) (Nesbitt and Young 1982). This permits a test for chemical signature of weathering processes, which can be calculated from the following oxide concentrations expressed in moles:

$$CIA = [Al_2O_3/(Al_2O_3 + CaO^* + Na_2O + K_2O)] \times 100$$

where CaO^* represents Ca associated with silicate phases only. Detailed microscopic observation reveals that Ca in sedimentary rocks from the study area occurs mainly in plagioclase and calcic amphiboles, rather than carbonates and apatite which are minor or rare. Therefore, little error is introduced by using the total CaO content for CaO^*.

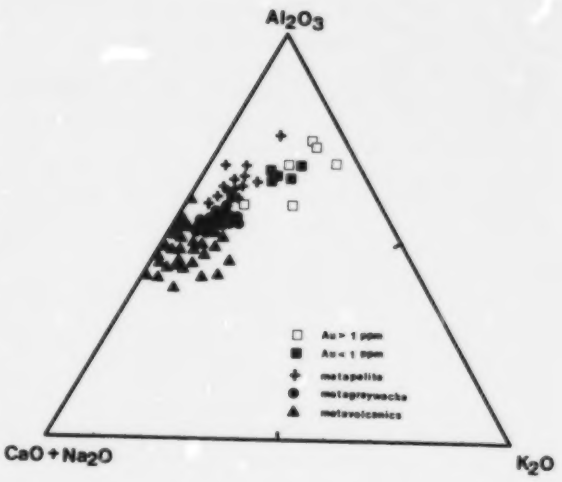

Figure 305.4. *Al_2O_3–(CaO + Na_2O)–K_2O ternary plot for all lithologies. Note the potassium enrichment in rocks from the anomalous zone (squares) and the weathering trend from volcanic rocks and metagreywackes to metapelites.*

The CIA values and the plot in Figure 305.4 for rocks of the study area reveal a well-defined weathering trend for clastic sedimentary rocks. The range of CIA values for the clastic sediments (CIA=54–69) and the average values of CIA (62) are lower than the average shale (CIA=72–75) and deep-sea mud (CIA=69). This corroborates textural and trace-element evidence that the clastic sedimentary rocks from the study area contain significant amounts of volcanic material. The expected higher CIA values of mudstone relative to greywacke indicate a higher proportion of secondary weathering products.

PROVENANCE AND TECTONIC SETTING

Clastic metasedimentary rocks from the study area are texturally and chemically immature and are generally indistinguishable from intermediate to felsic metavolcanic rocks in minor and trace element composition, particularly in regard to correlation of elements such as Sc, Co, V, Cr and Ni with $Fe_2O_3^*$ (total iron) and MgO.

Sc, V and Cr constituents are well known to be derived from simatic sources, while Th and Zr are from sialic sources. Proportions of these elements are used to distinguish various tectonic settings (Bhatia and Crook 1986; Naqvi *et al.* 1988). Figure 305.5 shows triangular plots of Th–Co–Zr/10 and Th–Sc–Zr/10. Like most Archean samples, the clastic sediments from the study area exhibit a wide spread for these geochemical discriminants, but essentially plot within or around the oceanic and continental island-arc fields. Distinct from most Archean sedimentary rocks, the clastic sedimentary rocks from the study area are intermediate to felsic in composition with enrichment of highly charged elements such as Th and Zr. The data points show a

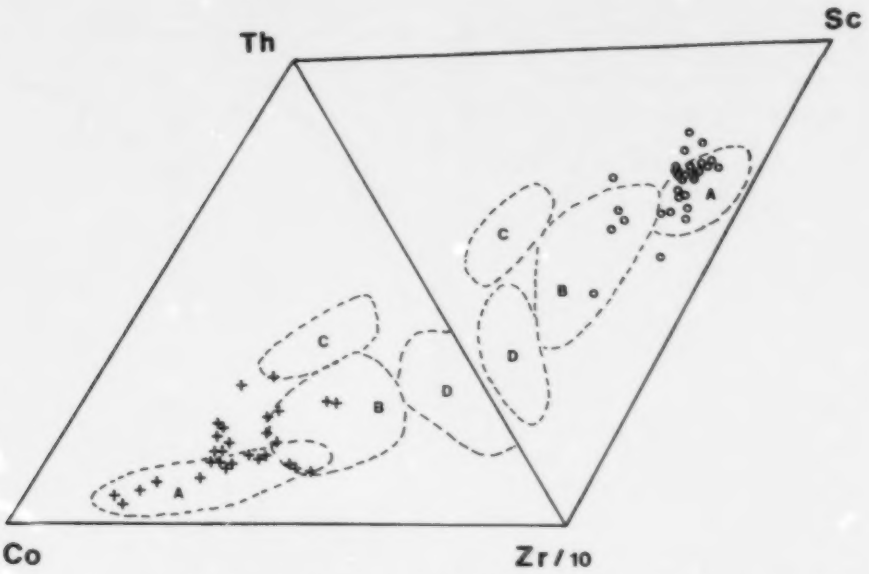

Figure 305.5. *Th-Co-Zr/10 and Th-Sc-Zr/10 triangular plots of the clastic metasedimentary rocks from the White River gold prospect for tectonic setting discrimination. Fields are indicated by dashed lines: A, ocean island arc; B, continental island arc; C, active continental margins; D, passive margins (from Bhatia and Crook 1986).*

shift towards the Th–Zr join. All geochemical discriminants indicate that these clastic sediments were mainly derived from sources of intermediate to felsic volcanics with a component of continental weathering products, admixed with minor mafic and ultramafic volcanic materials.

Pan and Fleet (1988, Figure 305.4) showed similarities of the chondrite-normalized patterns of rare earth elements (REE) between intermediate to felsic metavolcanic rocks and clastic metasedimentary rocks in the study area and a large fractionation between light REE and heavy REE as indicated by La_N/Yb_N up to 75. This also favours the hypothesis that the main source of the clastic sediments was intermediate to felsic volcanic materials.

THE ANOMALOUS ZONE AND GOLD MINERALIZATION

Previous random sampling confirmed a narrow, but laterally continuous zone with sporadic high values (up to 610 ppb) of gold at or near lithological boundaries between overlying metapelites and underlying intermediate to felsic metavolcanic rocks in the northern part of the study area at the contacts of units 7 and 8 (Pan and Fleet 1988). Gold assays of new drill-core samples taken throughout the anomalous zone returned values up to 27 ppm. Further active exploration at these locations is underway by Lac Minerals Ltd. In the following sections, new data and observations regarding the nature of the anomalous zone, gold mineralization, and geochemical characteristics and hydrothermal alteration are presented.

BRITTLE-DUCTILE SHEAR ZONE

The anomalous zone is situated within a sequence (up to 25 m thick) of muscovite schists in the lower part of lithological unit 8. Strain intensity increases progressively towards the muscovite schist unit; the increase is indicated by the tightness of fold closures, and, close to the muscovite unit, by lenses of felsic bodies with well-orientated rock fragments, which have been interpreted as mylonite (T.L. Muir, Ontario Geological Survey, personal communication, 1988). Therefore, the muscovite schist unit representing the highest strain zone is interpreted as a local shear zone (cf. Ramsay and Graham 1970; Hugon 1986). The term "local" is used here to distinguish it from the regional, Hemlo shear zone to the south (*see* Pan and Fleet 1988). The local shear zone trends at 110° in the western part of the study area, gradually changing to 085–090° in central part of the study area, and dips 45–60° north. It can be traced over a strike length of more than 2 km and attains its greatest thickness (up to 25 m) in the western part of the study area. Mineral lineation, which is generally absent within muscovite schists, is recognized in locally developed mafic boudinages within the schists and plunges to the northwest at 30°. As in the regional shear zone (HSZ), deformation within the local shear zone was predominantly ductile. However, the presence of abundant extension veins and breccia veins indicates the sporadic transition to brittle processes. Therefore, the local shear zone is brittle-ductile in nature. The sense of movement is poorly constrained due to the lack of mineral lineations. However, measurements on a number of rotated porphyroblasts in oriented sam-

ples indicate that movement on the local shear zone was probably dextral, which is similar in sense to the HSZ according to Hugon (1984, 1986).

GOLD MINERALIZATION

Within the local brittle-ductile shear zone, fine-grained muscovite schist is mainly composed of muscovite, quartz and feldspars with less abundant biotite and accessory amounts of sphene, apatite, magnetite, ilmenite and tourmaline. Elongated, euhedral to subhedral sulphide minerals (mainly pyrite and pyrrhotite with less common chalcopyrite and sphalerite) are minor phases, which are oriented parallel to subparallel to the main foliation and appear to be part of the metamorphic assemblage (these are referred to as *primary* sulphides hereafter). The local, anomalous abundance of these primary sulphides together with the presence of massive and crosscutting vein (secondary) sulphides (mainly pyrrhotite and chalcopyrite) characterize a distinct pyritic zone (up to 1 m thick), which is sporadically present in the stratigraphically lower part of the local shear zone. Correspondingly, a thin zone of abundant, randomly oriented sericite is present in the middle to upper part of the local shear zone.

Maximum gold values of 1 to 27 ppm have been obtained in localities where the zone of anomalous gold values, the hanging-wall sericite zone and the footwall pyritic zone coalesce (Figure 305.6). Native gold is the only gold-bearing phase present. Aurostibite and calaverite, which have been recognized at Hemlo (Harris 1986), have not been observed in the anomalous zone in the study area to date. Native gold commonly occurs as fine- to very fine-grained inclusions in sericites or chlorite cleavage partings or along pyrite grain fractures. It is also present as large grains (up to 100 μm) along pyrite grain fractures.

Pan and Fleet (1988) reported that gold mineralization in the study area is not associated with anomalously high Mo–Ba–Sb–Hg–As–V–W content. Trace elements correlate with lithologies rather than gold or pyrite mineralization. New geochemical data confirm this conclusion. However, slight anomalies of As, Hg and W, and locally Cu (up to 4600 ppm) (Table 305.1), are present within the muscovite schist but do not necessarily correlate with gold abundance. Moreover, these anomalies (As, Hg and W up to 390 ppm, 62 ppb and 39 ppm respectively) are considerably smaller in magnitude than those at the Hemlo gold deposit (*see* Harris 1986). Consistent with the absence of stibnite and vanadium muscovite, anomalous contents of Sb and V are not present in the study area. Barium is present as a minor constituent in biotite but occurs mainly within the margins of K-feldspar grains (up to 4.1 weight percent of BaO). In the study area, BaO content both in bulk rock and feldspar margins is considerably lower than at Hemlo (up to 15.6 weight percent BaO in feldspar; cf. Harris 1986) and is not confined to the shear zone. Molybdenite is not present in the local shear zone but occurs in minor amounts associated with late cross-cutting veins in the Cadi fracture zone.

ALTERATION

Hydrothermal alteration is well developed in the study area but less extensive than that at the Hemlo gold deposit (Pan and Fleet 1988). At the White River gold prospect, the local brittle-ductile shear zone is characterized by very fine-grained muscovite schists and anomalously high potassium content. This apparently indicates a strong potassic alteration. However, as described above, the two major potassium-bearing phases (muscovite and K-feldspar) are part of the peak metamorphic assemblage as indicated by well developed orientation of muscovite parallel to the main foliation and triple junctions of K-feldspar grains. Within the sericitic zone, the presence of randomly oriented sericite and slightly higher K_2O content may indicate further potassic en-

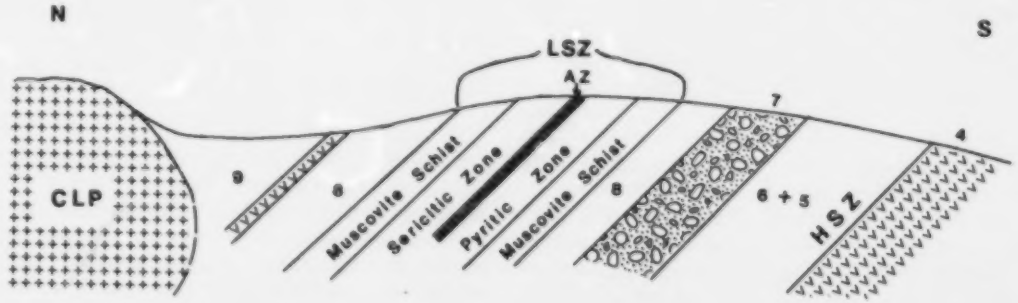

Figure 305.6. *Schematic cross-section showing stratigraphic position of the anomalous zone (AZ), the local shear zone (LSZ), Cedar Lake pluton (CLP) and the Hemlo shear zone (HSZ) at localities where maximum gold values were attained. Note that the pyritic, anomalous and sericitic zones coalesce. Not to scale.*

TABLE 305.1. REPRESENTATIVE CHEMICAL ANALYSES OF SAMPLES FROM THE LOCAL SHEAR ZONE.

Sample	PZ	MS	SZ	AZ1	AZ2	AZ3	AZ4	AZ5
				(weight percent)				
SiO_2	50.90	64.00	70.50	49.70	58.60	79.00	71.50	54.20
TiO_2	0.44	0.63	0.31	0.41	0.57	0.29	0.50	0.27
Al_2O_3	11.80	16.70	15.30	13.10	17.20	10.70	16.60	12.60
Fe_2O_3*	18.00	4.96	1.94	23.60	9.39	2.30	2.05	16.70
MgO	0.48	0.97	1.01	0.83	1.48	nd	0.10	0.93
MnO	nd	0.02	0.04	0.05	0.07	nd	nd	0.04
CaO	2.58	0.87	1.82	1.51	2.58	0.35	0.50	6.35
Na_2O	1.68	1.67	1.21	0.59	0.87	0.39	0.63	0.21
K_2O	4.48	4.23	3.98	3.45	3.93	3.34	3.34	2.40
LOI	9.10	3.80	1.70	5.40	3.80	2.20	2.80	4.30
Total	99.90	98.30	98.10	98.90	98.90	98.30	98.90	98.30
S	10.40	2.76	0.36	10.50	3.45	1.03	1.02	8.31
				(ppm)				
Ag	nd	nd	nd	nd	nd	nd	nd	8.5
As	390	110	11	3	69	120	110	38
Au (ppb)	8	5	40	300	27 000	4800	1300	14000
Ba	1200	1400	730	680	630	460	580	470
Cu	32	41	15	120	68	15	8.5	4600
Hg (ppb)	31	24	8	nd	8	nd	nd	20
Mo	nd	nd	nd	nd	nd	nd	nd	nd
Sb	0.3	0.4	0.3	0.8	0.4	0.9	1.9	0.8
V	79	100	48	58	100	48	80	58
W	39	20	9	14	17	8	14	7
Zn	74	110	74	130	100	61	32	56

Notes:
PZ – pyritic zone; MS – muscovite schist; SZ – sericitic zone; AZ – anomalous zone.
Fe_2O_3 is total iron content; nd – not detected; LOI – loss on ignition.*
ppm – parts per million; ppb – parts per billion.

richment related to a late hydrothermal event that occurred after peak metamorphism.

Sulphidation related to a late hydrothermal event is also apparent within the local shear zone and is characterized by the presence of the pyritic zone. Sulphide minerals were crystallized in at least two separate events. However, at present it is difficult to assess whether primary sulphide minerals are metamorphic in origin or diagenetic (with metamorphic recrystallization). Secondary sulphides, including pyrrhotite, pyrite and chalcopyrite in massive form or in cross-cutting veins, apparently crystallized late.

A regional scale, low- to very low-grade, calc-silicate-like alteration has been reported previously (Pan and Fleet 1988). Massive prehnite and epidote locally occur in the anomalous zone and are associated with maximum gold values. Gold mineralization associated with prominent calc-silicate alteration (skarn) has been recorded in the Southern Cross greenstone belt of Western Australia (Mueller 1988). A study of possible genetic relationship between gold mineralization and the calc-silicate alteration at the study area is underway.

The lack of carbonatization is one of the distinct features of the Hemlo gold deposit. Carbonatization occurs in the study area but is of limited development (Pan and Fleet 1988). Calcite is locally present in crosscutting veins, associated with sulphide veins and calc-silicate veins. Calcite also occurs locally in the central portion of the calc-silicate veins within the local shear zone. Massive calcite is also present in the footwall, intermediate to felsic, metavolcanic rocks immediately underlying the local brittle-ductile shear zone.

FUTURE WORK

The metamorphic history and gold mineralization of the Hemlo–Heron Bay greenstone belt are the main objectives of the present research. Further investigations into detailed aspects of metamorphic grade and P–T conditions, deformation, geochemistry of metasedimentary and metavolcanic rocks, and the nature and genesis of gold mineralization will be carried out. However, more emphasis will be placed on spatial and genetic relationships and the timing of metamorphism, deformation and alteration, relative to gold mineralization, in Archean greenstone belts, particularly the relative roles of hydrothermal and

metamorphic processes in either forming or modifying Hemlo-type gold deposits. It is hoped to establish whether the hydrothermal alteration and/or metasomatism in the study area and the nearby Hemlo gold deposit was imposed on previously metamorphosed rocks, or whether the metamorphism, metasomatism and gold mineralization were broadly contemporaneous.

ACKNOWLEDGMENTS

We thank Lac Minerals Ltd. for access to the White River property and for providing geological information and drill core. A. Campbell is especially thanked for his assistance with field work. We also thank S.M. McLennan, G.M. Young, and H.W. Nesbitt for their constructive comments on geochemical data of clastic metasedimentary rocks, L.D. Meinert, D.M. Burt, R.F. Martin, and C.V. Guidotti for suggestions on Cr-rich calc-silicate rocks. Financial support for the present study is provided by Ontario Geological Survey Research Grant 305 to M.E. Fleet.

REFERENCES

Bhatia, M.R. and Crook, K.A.W.

1986: Trace Element Characteristics of Graywackes and Tectonic Setting Discrimination of Sedimentary Basins; Contributions to Mineralogy and Petrology, Volume 92, p.181-193.

Burk, R., Hodgson, R.J. and Quartermain, A.J.

1986: The Geological Setting of the Teck-Corona Au-Mo-Ba Deposit, Hemlo, Ontario, Canada; p.311-326 *in* Proceedings of Gold '86, an International Symposium on the Geology of Gold, edited by A.J. Macdonald, Toronto, 1986.

Condie, K.C.

1981: Archean Greenstone Belt, Developments in Precambrian Geology, Volume 3; Elsevier Scientific Publishing Company, Amsterdam, 434p.

Danchin, R.V.

1967: Chromium and Nickel in the Fig Tree Shale from South Africa; Science, Volume 158, p.261-262.

Einaudi, M.T. and Burt, D.M.

1982: Introduction—Terminology, Classification, Composition of Skarn Deposits; Economic Geology, Volume 77, p.745-795.

Einaudi, M.T., Meinert, L.D. and Newberry, R.J.

1981: Skarn Deposits; Economic Geology, 75th Anniversary Volume, p.317-391.

Engel, A.E.J., Itson, S.P., Engel, C.G., Stickney, D.M. and Gray, E.J.

1974: Crustal Evolution and Global Tectonics: a Petrographic View; Geological Society of America Bulletin, Volume 85, p.843-858.

Harris, D.C.

1986: Mineralogy and Geochemistry of the Main Hemlo Gold Deposit, Hemlo, Ontario, Canada; p.297-310 *in* Proceedings of Gold '86, an International Symposium on the Geology of Gold, edited by A.J. Macdonald, Toronto, 1986.

Hiltunen, A.

1982: The Precambrian Geology and Skarn Iron Ores of the Rautuvaara Area, Northern Finland; Geological Survey of Finland, Bulletin, Volume 318, 133p.

Hugon, H.

1984: The Hemlo Deposit: Gold Mineralization within a Dextral Shear Zone; p.212-217 *in* Summary of Field Work, 1984, edited by J.Wood, O.L. White, R. Barlow and A.C. Colvine, Ontario Geological Survey, Miscellaneous Paper 119.

1986: The Hemlo Gold Deposit, Ontario, Canada: A Central Portion of a Large Scale, Wide Zone of Heterogeneous Ductile Shear; p.379-387 *in* Proceedings of Gold '86, an International Symposium on the Geology of Gold, edited by A.J. Macdonald, Toronto, 1986.

Leake, B.E.

1978: Nomenclature of Amphiboles; Canadian Mineralogist, Volume 16, p.501-520.

McLennan, S.M. and Taylor, S.R.

1983: Geochemical Evolution of Archean Shales from South Africa: I. the Swaziland and Pongola Supergroups; Precambrian Research, Volume 22, p.93-124.

Meinert, L.D.,

1984: Mineralogy and Petrology of Iron Skarns in Western British Columbia, Canada; Economic Geology, Volume 79, p.869-882.

Miyashiro, A.

1973: Metamorphism and Metamorphic Belts; Allen & Unwin, London.

Mueller, A.G.

1988: Archean Gold-Silver Deposits with Prominent Calc-Silicate Alteration in the Southern Cross Greenstone Belt, Western Australian: Analogues of Phanerozoic Skarn Deposits; Geology Department and University Extension, The University of Western Australia, Publication No. 12, p.141-163.

Muir, T.L.

1982: Geology of the Hemlo Area, District of Thunder Bay; Ontario Geological Survey, Report 218, 89p. Accompanied by Map 2439.

Naqvi, S.M., Sawkar, R.H., Subba Rao, D.V., Govil, P.K. and Gnaneswar Rao, T.

1988: Geology, Geochemistry and Tectonic Setting of Archean Greywackes from Karnataka Nucleus, India; Precambrian Research, Volume 39, p.193-216.

Nesbitt, H.W. and Young, G.M.

1982: Early Proterozoic Climates and Plate Motions inferred from Major Element Chemistry of Lutites; Nature, Volume 299, p.715-717.

Pan, Y. and Fleet, M.E.

1988: Metamorphic Petrology of the White River Gold Prospect, Hemlo, Ontario; p.165-176 *in* Geoscience Research Grant Program, Summary of Research, 1987-1988, edited by V.G. Milne, Ontario Geological Survey, Miscellaneous Paper 140, 251p.

In Press: Cr-Rich Calc-Silicates from Hemlo Area, Ontario; Canadian Mineralogist.

Pan, Y., Fleet, M.E. and Stone, W.E.

In Prep: Polymetallic (Fe-Ni-Co-Cu-Zn) Sulfides in Archean Calc-silicates from Hemlo Area, Ontario, Canada; (submitted to Mineralium Deposita).

Patterson, G.C.

1984: Exploration History and Field Stop Description of the Hemlo Area; p.66-86 *in* Gold and Copper-Zinc Metallogeny, Hemlo-Manitouwadge-Winston Lake Ontario, Canada, edited by R.H. McMillan, and D.J. Robinson, Geological Association of Canada and Canadian Institute of Mining and Metallurgy, Toronto.

Ramsay, J.G. and Graham, R.H.

1970: Strain Variation in Shear Belts; Canadian Journal of Earth Sciences, Volume 7, p.786-813.

Valliant, R.I. and Bradbrook, C.J.

1986: Relationship between Stratigraphy, Faults and Gold Deposits, Page-Williams Mine, Hemlo, Ontario, Canada; p.355-361 *in* Proceedings of Gold '86, an International Symposium on the Geology of Gold, edited by A.J. Macdonald, Toronto, 1986.

Von Knorring, K.

1951: A New Occurrence of Uvarovite from Northern Karelia in Finland; Mineralogical Magazine, Volume 29, p.594-601.

Von Knorring, K., Condliffe, E. and Tong. Y.L.

1986: Some Mineralogical and Geochemical Aspects of Chromium-Bearing Skarn Minerals from Northern Karelia, Finland; Geological Society of Finland, Bulletin, Volume 58, p.277-292.

Grant 310 Subsurface Radar Profiling of Two Peatlands in Southern Ontario

D.C. Nobes, B.D. Theimer and B.G. Warner

Department of Earth Sciences, and Quaternary Sciences Institute, University of Waterloo, Waterloo

ABSTRACT

Data processing has been completed for a ground penetrating radar (GPR) survey from Ellice Swamp, near Stratford, Ontario. The results confirm that three distinct stratigraphic units in the bog are identifiable in the radar records. The GPR data show a strong reflector at the interface of the basal peat and minerogenic sediments. Gyttja near the base is defined indirectly. The acrotelm and catotelm transition is well defined near the surface. Good correlations between arrival time and depth were achieved using the radar-derived signal velocity. Semblance processing of the radar profiles was found to enhance dramatically the identification of reflectors.

A second site, the Mer Bleue bog near Ottawa was investigated. Conventional coring was conducted at seven stations along a 550 m transect. Each core was analyzed for organic matter, water and ash content, wet and dry bulk density, and von Post humification. GPR surveys were made at two frequencies. A complete survey of the cored transect was performed at 100 MHz, and a 300 m portion of this transect was remeasured at 200 MHz. Eleven common midpoint (CMP) surveys were completed also. In addition, an EM–31 survey and two Wenner resistivity spreads were carried out to gauge distributions in subsurface electrical conductivity. Mer Bleue is much more conductive than the Ellice Swamp, leading to two highly contrasting radar profiles from the two sites.

INTRODUCTION

Peat is a valuable natural resource within Ontario, but the size of the peat inventory is not well known. The necessity of having a tool for rapidly evaluating the extent and internal character of peatlands is important as industries become increasingly interested in using peat for fuel or horticulture, and in peat by-products such as biodegradable consumer goods. The structure and quality of the peatlands are strong controlling factors in identifying optimal exploitation strategies. Ground penetrating radar (GPR) can be a fast and effective method for constructing profiles of the major stratigraphic units within peatlands, and for tracing the depth and extent of the continuity of these units. We have tested the utility of GPR on two *Sphagnum* peatlands in southern Ontario, one near Stratford and one near Ottawa.

ELLICE SWAMP, STRATFORD

The bog is developed in a shallow depression impounded on the east flank of the Milverton Moraine. Within the basin, the peatland is about 2 m thick and underlain by silt and clay. A thin, sometimes discontinuous unit of gyttja, silty gyttja, and limnic peat rests above the silt and clay. The main body of the peatland is composed of a thick mixture of cyperaceous remains and pleurocarpous mosses. Above this, there is a thin layer of amorphous black detrital peat with abundant woody remains at the base of the acrotelm, and finally, *Sphagnum* at the surface. More detailed profiles for the various physical parameters of the peatland and a preliminary radar profile have been reported in Warner and Nobes (1988).

GPR data have been acquired for a 1500 m long transect across the bog. Radar records were made at 1 m spacings using common offset shooting. Each GPR record consists of the response to 400 V pulses at 200 MHz. The survey data have been completely processed. Several methods borrowed from seismic reflection techniques were applied to the data. The records were static-corrected so that the reflection interpreted as the base of the ice layer (the survey was conducted during winter) occurs simultaneously for every trace. The average of every block of 12 traces was removed from each individual trace in an attempt to eliminate the appearance of multiple reflections. The attenuation in signal strength that occurs due to resistive losses was compensated for by using values derived empirically from the data (Figures 310.1 and 310.2). Changes in the character of the basal reflector, which are not clearly visible in this reduced illustration, occur where the limnic peat and gyttja are absent.

Profiles of peat bulk-density, humification, and the organic matter and water content show several interfaces within the main body of the peatland. However, the GPR record contains no reliably significant event that can be identified with any of these interfaces because the radar responds to marked differences in moisture content. Examination of the changes in water content within the bog reveal that the main body of the peatland has only gradual changes in moisture content. Rapid changes are apparent in the acrotelm and catotelm transition where there are changes in moisture content of more than 5%.

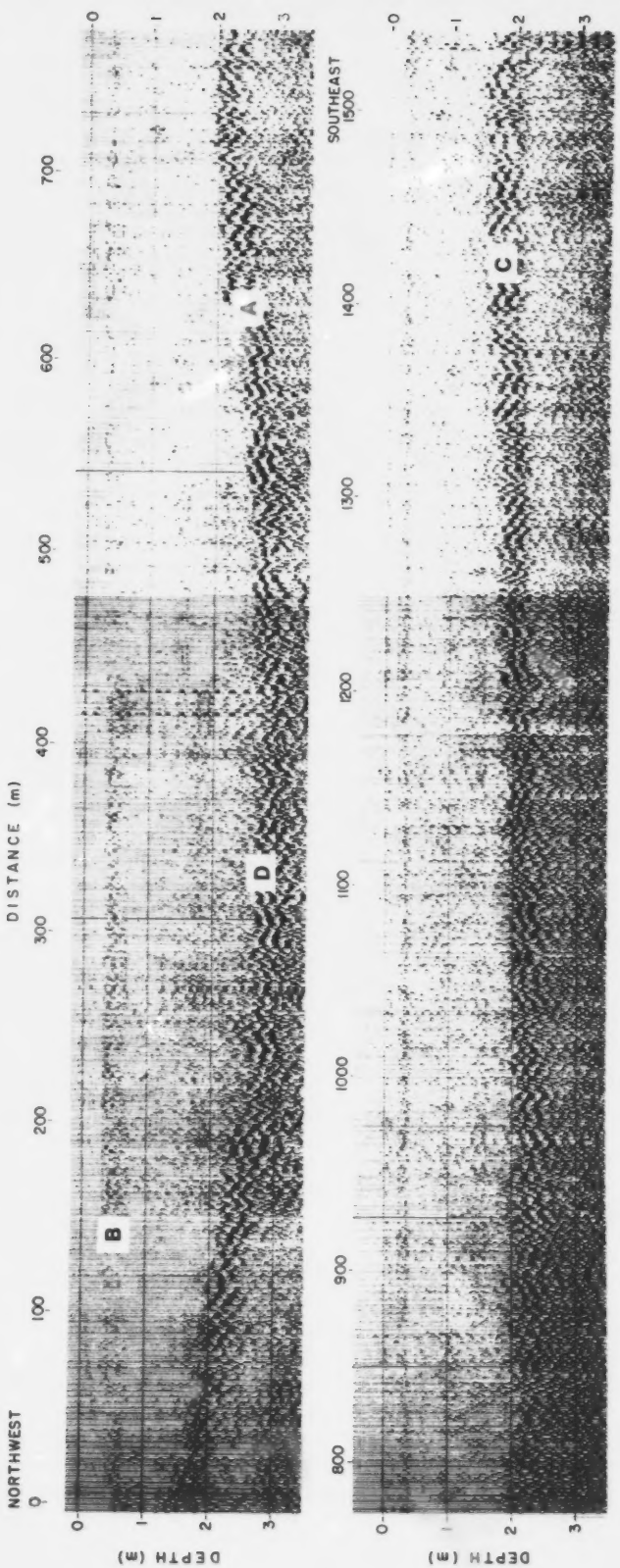

Figure 310.1. *Processed GPR profile for the transect through the Ellice Swamp. Compare equivalent points A, B, C and D on Figure 310.2.*

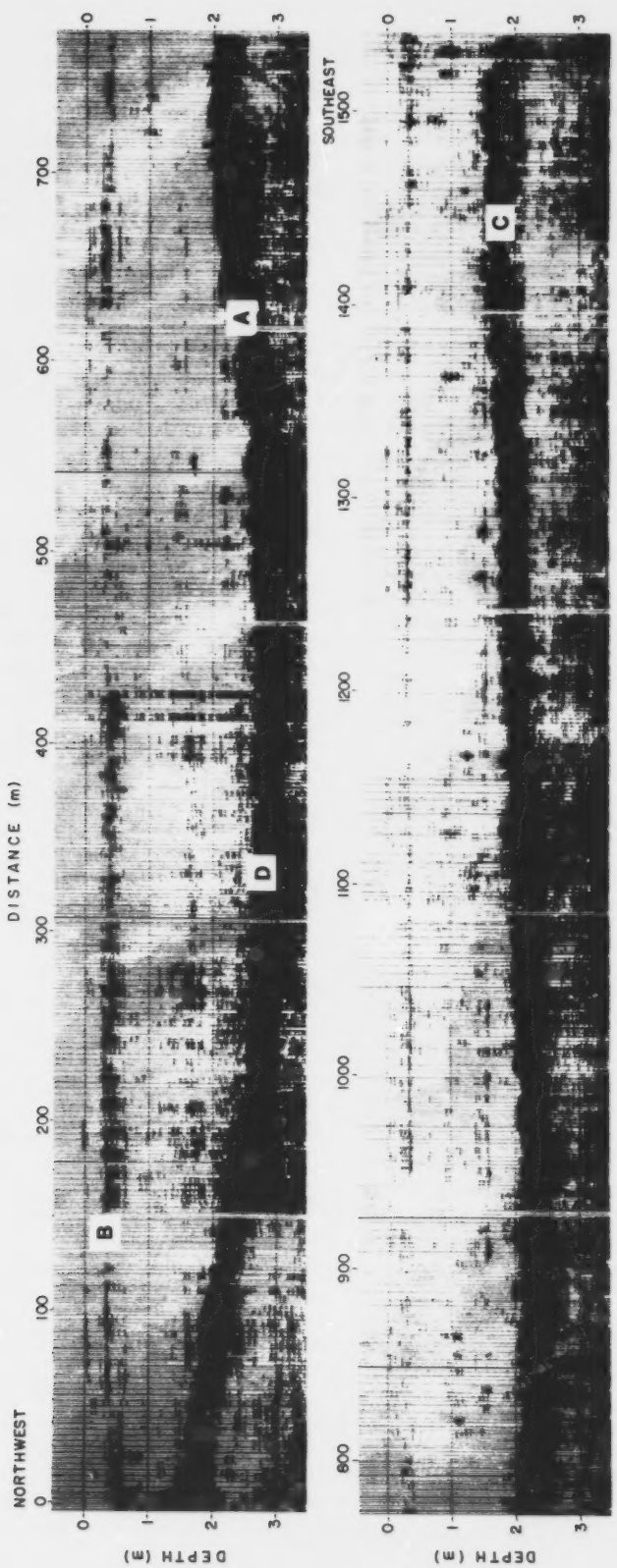

Figure 310.2. *Semblance processed GPR profile for the transect through the Ellice Swamp. Compare equivalent points A, B, C and D on Figure 310.1.*

Common midpoint (CMP) surveys were conducted at two points on the transect (398 m and 1018 m). These surveys produced two important parameters. Firstly, the CMP surveys gave values for the average electromagnetic pulse speed within the bog. This allowed reliable time-to-depth conversions to be made from the GPR profiles. This is a preferable alternative to the conventional core-to-signal calibration performed by other workers. Secondly, the CMP data allowed the attenuation constant to be calculated for proper compensation of the traces.

MER BLEUE BOG, OTTAWA

The Mer Bleue bog is a large peatland complex, occupying an area of more than 20 km², near Ottawa (Figure 310.3). The main peatland basin has three small fingers extending from its westward side. The transect for this study was conducted across the most southern one, where access was good and there were no interferences such as power lines. Mer Bleue is a raised ombrotrophic basin bog, with a variable depth along the study transect of up to 4.4 m.

A 550 m long transect was completed in July 1988. Seven cores were taken, generally at 100 m intervals. The cross section reveals a westward skewed profile. A grey-blue clay underlies the main basin. The peat attains a maximum thickness of 4.4 m on the western side of the profile (Figure 310.4), and is composed of a mixture of cyperaceous and *Sphagnum* peat. The stratigraphy of these peat units is rather variable with depth and extent along the transect (Figures 310.4 and 310.5).

Geophysical surveys were run in January 1989 when the frozen surface provided a solid working surface. A 100 MHz common-offset GPR survey was run over the summer traverse for a length of 600 m. Survey lines, each 200 m, perpendicular to the main line were taken to intersect the 100 and 300 m stations. GPR data at the 200 MHz frequency were acquired along a line from 0 to 300 m. Three CMP profiles were shot for comparison at 100, 300, and 500 m. Additional CMP surveys were taken from 298 to 308 m stepped 1 m apart.

The raw GPR profiles from the Mer Bleue bog transect are different in character from those at Elice Swamp. The basal reflection is not readily visible. Differences occur in average amplitude from trace to trace. Multiples seem less continuous. A number of point object reflectors are also apparent. As yet, data processing has not been attempted. The differences are hypothetically linked with the

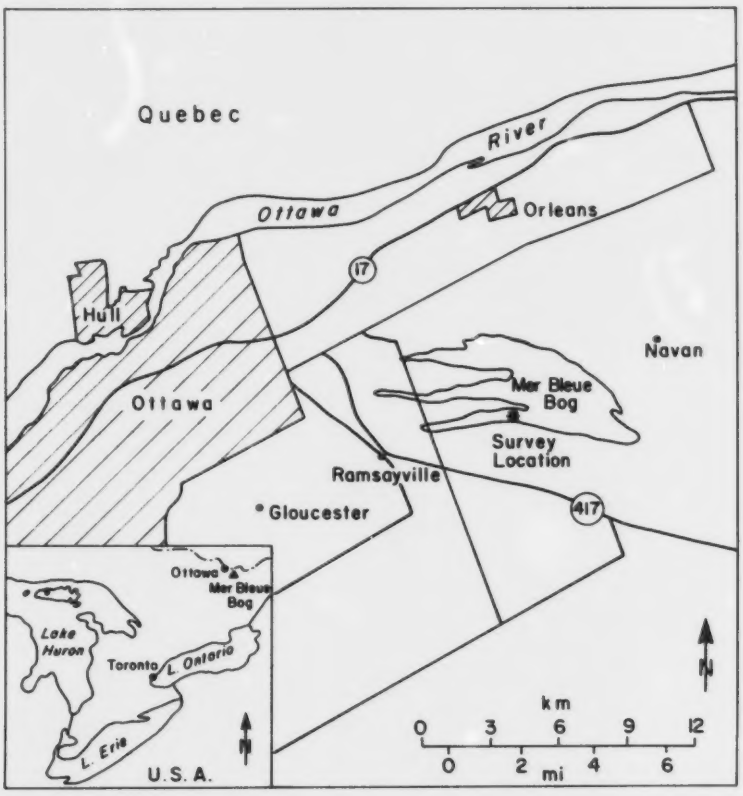

Figure 310.3. *Location of the Mer Bleue study site.*

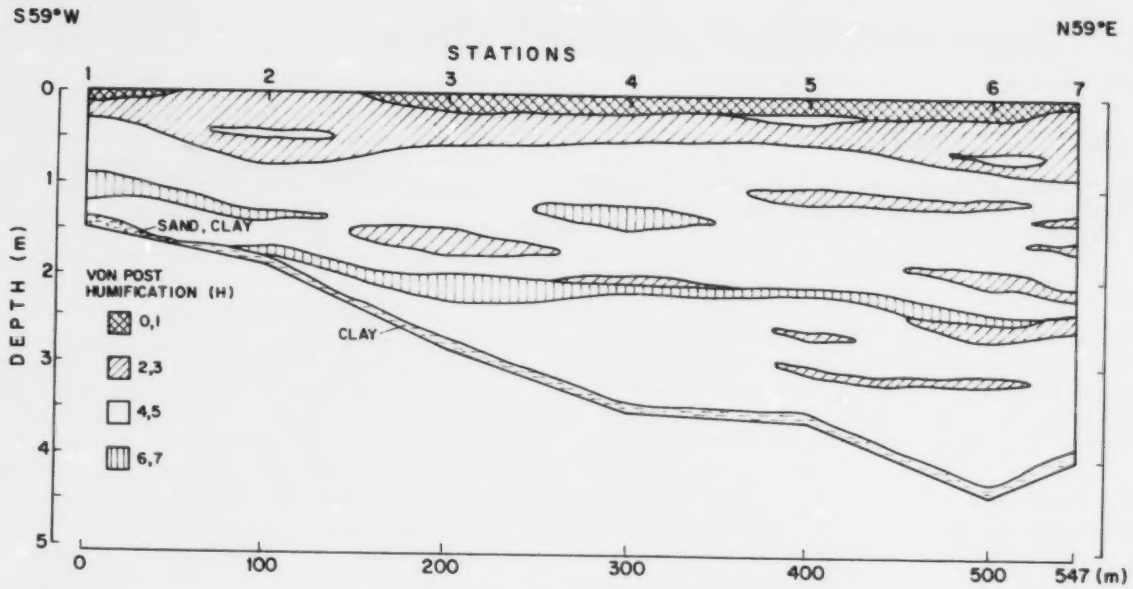

Figure 310.4. *Basin profile for peat humification (von Post scale) along the study transect.*

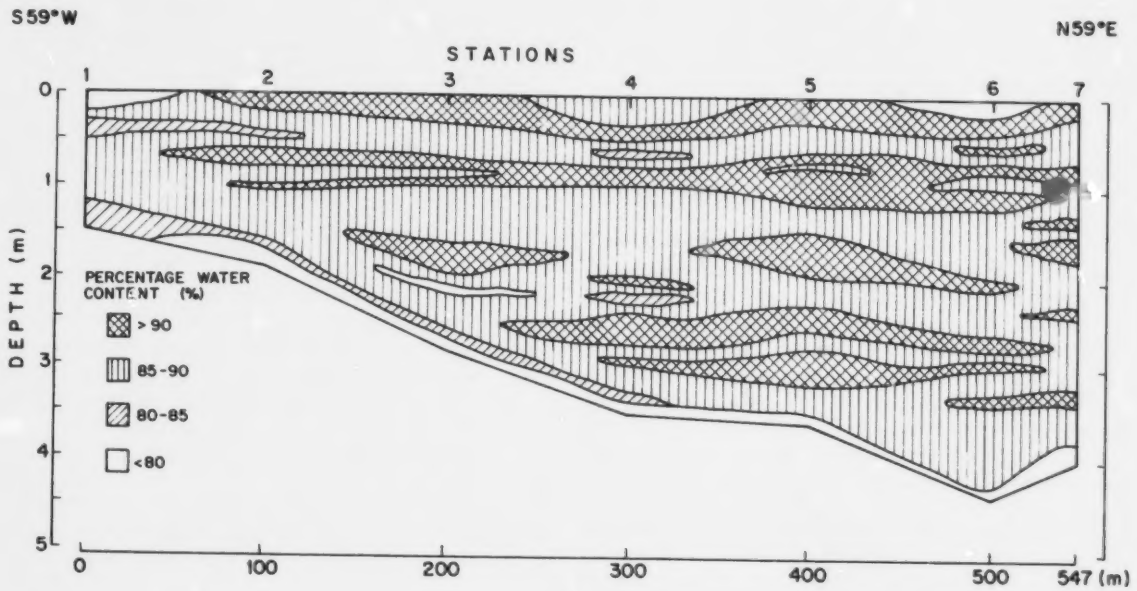

Figure 310.5. *Basin profile for peat moisture content (as percent) along the study transect.*

marked increase in electrical conductivity seen at Mer Bleue. Wenner resistivity array surveys and EM–31 measurements reveal that this bog is highly conductive. Preliminary conductivity measurements on one core segment at 300 cm depth gave values around 250 mS/m. One hypothesis that will be tested is the effect of possible high, dissolved-mineral content in pore waters from the underlying Champlain Sea clays in the peat waters. It is expected that the increase in conductivity due to salinity might result in much more attenuation of the radar pulse.

The Mer Bleue study promises to be a good test site for the application of GPR. Mer Bleue is highly conductive, has thick peat deposits, has a wide range

of reflectors, and is stratigraphically more complex than the Ellice Swamp. The contrasts between the Mer Bleue and Ellice peatlands are sharp.

ACKNOWLEDGMENTS

Our thanks go to George Schneider who provided geophysical field assistance, and Nadia Bahar who drafted the figures.

REFERENCE

Warner, B.G. and Nobes, D.C.

1988: Application of Surface Radar Sounding Techniques in Peatland Inventories, Southern Ontario: Preliminary Results; p.182-187 *in* Geoscience Research Grant Program, Summary of Research 1987-1988, edited by V.G. Milne, Ontario Geological Survey, Miscellaneous Paper 140, 251p.

Grant 313 Hydrothermal Activity in the Kirkland Lake Intrusive Complex

Keiko Hattori and Guy Levesque

Ottawa-Carleton Geoscience Centre, Department of Geology, University of Ottawa, Ottawa

ABSTRACT

The Kirkland Lake intrusive complex, a major host of gold in the Kirkland Lake camp, was developed from intrinsically oxidized magmas, evidenced by early crystallization of magnetite in augite syenite and felsic syenite, and titanite in later porphyritic units. The augite syenite and felsic syenite are hypersolvus intrusions, while the younger two porphyry units are subsolvus intrusions. This differs from the hypersolvus intrusions of the neighboring Otto, Lebel and Murdock Creek composite stocks.

The complex displays two cryptic alterations: alteration I was due to the intrusions themselves, and alteration II was related to later lamprophyre intrusion. The former is documented as hematitization and titanization of magnetite and biotitization of mafic minerals. Subsequently, the already cooled intrusions underwent alteration due to volatiles released from lamprophyres. This formed minerals of unusual chemical compositions, including Cr-, Ba- and F-rich phlogopitic micas, chromititic oxides and Sr-rich feldspars. Auriferous hydrothermal activity, which postdated alteration II, had a focussed flow regime along the present vein system and resulted in wall-rock alteration adjacent to the veins.

Augite syenite and feldspar porphyry show different wall-rock alteration mineralogy. The difference is due primarily to different Fe and K contents in the two rock units. The augite syenite unit contains secondary magnetite in the outer part and K-feldspar and pyrite closer to the gold vein. The porphyry unit is altered to chlorite and hematite in the outer aureole and sericite, carbonate and pyrite adjacent to the veins. The different mineralogies in the two units where in contact suggests fracture-controlled fluid flow during this stage of hydrothermal activity.

The alteration mineralogy indicates that vein-forming fluids were oxidizing. Pyrite adjacent to veins was introduced under a hematite-stable field. This is supported by low $\delta^{34}S$ in sulphides.

As in many gold camps, gold in the Kirkland Lake camp was introduced into re-crystallized and deformed quartz veins during the last stage of hydrothermal activity at temperatures over 340°C. It was, however, followed by hydrothermal activity of ~300°C, forming abundant crosscutting veins and barren quartz-carbonate veins.

INTRODUCTION

The Kirkland Lake gold camp occurs along the Kirkland Lake break within the Larder Lake–Cadillac deformation zone (Toogood and Hodgson 1985). Gold in the camp is hosted mostly within a series of late-kinematic felsic intrusions (Kirkland Lake intrusive complex).

This project was initiated to characterize the Kirkland Lake intrusive complex and to examine the temporal variation of hydrothermal activity in which gold mineralization took place. Petrological and mineralogical studies of the feldspar porphyry units of the complex, which hosts the central part of the camp, were reported in Hicks and Hattori (1988). The work has been extended to study the older intrusive units of the complex, augite syenite and felsic syenite, to compare the alteration in the units, and to evaluate the temporal relations of at least three separate episodes of hydrothermal alteration observed in the intrusive complex.

PETROGRAPHY OF THE KIRKLAND LAKE INTRUSIVE COMPLEX

The igneous complex displays intense alteration and deformation near the auriferous veins. However, rocks far from the veins, obtained mainly from drill cores, display preserved textures and relicts of primary mineralogy. The mineralogies of four lithological units of the complex are summarized in Table 313.1. The earlier two units, augite syenite and felsic syenite, have similar textures and mineralogies, with low amounts of mafic minerals in felsic syenite unit. The occurrence of perthitic alkali feldspar in the two older units contrasts with the presence of phenocrysts of two separate alkali feldspars in the two younger units. This suggests that the earlier two units are hypersolvus and that the later two intrusive units are subsolvus. This differs from the hypersolvus nature of all phases in the neighboring Otto (Smith and Sutcliffe 1988), Murdock Creek (Rowins *et al.* 1989) and Lebel stocks.

AUGITE SYENITE

Least altered specimens of this unit are dark grey and display equigranular and porphyritic phases. The porphyritic phase contains ~40 volume percent phenocrysts of augite and biotite set in a groundmass composed mainly of fine-grained K-feldspar. A foliated porphyritic phase in which augites are aligned is

TABLE 313.1. PRIMARY MINERALOGY OF THE KIRKLAND LAKE INTRUSIVE COMPLEX (IN DECREASING ORDER OF ABUNDANCE).

Augite Syenite	Felsic Syenite	Feldspar Porphyry	Quartz-Feldspar Porphyry
Augite (X_{Mg}* = 0.77 to 0.88)	K-feldspar with albite lamellae	Albite-Oligoclase (An_4 to An_{12})	Albite
K-feldspar with albite lamellae	Biotite	Biotite (X_{ph} = 0.6)	Biotite
Biotite (X_{ph} # = 0.6; TiO_2, <6.5%)	Augite	Green hornblende	K-feldspar
Magnetite (TiO_2 <9.1%)	Magnetite	K-feldspar (~Ab_{10})	Green hornblende
Apatite	Apatite	Apatite	Quartz
		Titanite	Titanite
		Magnetite (TiO_2 <6%)	Magnetite
		[Zircon]	Apatite
		[Monazite]	[Zircon]

[minerals]: very minor
X_{Mg} = molecular ratio of $Mg^{2+}/(Mg^{2+}+Fe^{2+})$
#X_{ph} = phlogopite molecule

also observed at the Macassa property. There are no systematic differences in mineralogy or chemical compositions between the texturally different phases of the unit. The different textures within the intrusion appear to reflect a dynamic environment at the time of emplacement; some parts could have cooled rapidly due to the movement along the Kirkland Lake break.

Primary minerals are euhedral augite (25 to 30 volume percent) and perthitic K-feldspar (60 to 70%); other minerals are Ti-rich magnetite (2 to 5%), biotite (2 to 4%) and minor apatite. Augite ranges in size from 2 to 15 mm and is commonly zoned (Table 313.2), displaying Fe-rich cores and rims 20–40 μm wide. It encloses primary magnetite and apatite. The early crystallization of magnetite reflects high ratios of (Fe^{3+}/total Fe) in the magma, indicating an oxidized source magma.

Primary biotite in the augite syenite is high in TiO_2, up to 6.5 weight percent, and its compositions are similar to those of primary biotites in the feldspar porphyry (Hicks and Hattori 1988). Rare clusters (<5 mm) of green hornblende (grain size <1 mm) are interpreted as basaltic xenoliths.

Perthite displays exsolution lamellae less than 2 μm wide in least altered specimens. Albite, previously reported as a primary mineral, is interpreted as an alteration product because of the lack of albite grains in least altered specimens. Alteration causes destruction of lamellae by re-crystallization of feldspars to form albite and K-feldspar grains. This is further supported by the presence of abundant primary CO_2 inclusions (<1 μm) in augite phenocrysts. They are single phase at room temperature.

FELSIC SYENITE

Felsic syenite is richer in K-feldspar and poorer in augite and biotite than the augite syenite; this reflects its lower MgO and FeO contents. The gradation between the two units is displayed in drill core at the Macassa Mine (DDH 42-350, at approximately 1920-foot depth; G. Nemcsok, Macassa Division, Lac Minerals Ltd., written communication, 1989). However, in some underground exposures (6400-foot level, Macassa Mine), the contact appears to be sharp. Consanguinity of the two units is also supported by a smooth line in Larsen variation diagrams (Levesque and Hattori 1989).

FELDSPAR PORPHYRY AND QUARTZ-FELDSPAR PORPHYRY

Detailed descriptions of the texture, mineralogy and mineral chemistry of the feldspar porphyry are given in Hicks and Hattori (1988). The quartz-feldspar porphyry is very similar to the feldspar porphyry in mineralogy and chemical composition. The former contains up to 8 volume percent partially resorbed quartz grains. Miarolitic cavities, commonly found in the feldspar porphyry, are rare in the quartz-feldspar porphyry.

Larsen variation diagrams of major and minor elements vs. SiO_2 show a straight line between the two units, suggesting their co-magmatic nature (Levesque and Hattori 1989).

TABLE 313.2. CHEMICAL COMPOSITIONS OF AUGITE IN AUGITE SYENITE.

	Grain I			Grain II			Grain III		
	core	mantle	rim	core	mantle	rim	core	mantle	rim
SiO_2	51.07	53.97	51.70	51.37	54.47	50.66	51.00	54.26	51.34
TiO_2	.80	.24	.70	.77	.17	.80	.80	.18	.82
Al_2O_3	3.13	1.02	3.23	2.69	1.13	3.75	3.10	1.44	3.11
Cr_2O_3	.00.	.28	.03	.01	1.13	.05	.01	.77	.03
FeO	7.73	4.10	7.75	8.28	5.18	8.57	8.13	7.38	7.28
MnO	.18	.05	.21	.23	0.10	.20	.20	.04	.15
MgO	13.98	13.59	14.22	13.50	16.84	13.59	13.70	17.11	14.42
CaO	22.44	21.38	21.88	22.16	21.86	21.38	21.40	22.04	22.24
Na_2O	.49	.72	.62	.61	.54	.72	.65	.53	.50
K_2O	.02	.01	.02	.02	.04	.01	.01	.00	.02
Total	99.84	99.73	100.36	99.64	100.58	99.73	100.00	100.36	100.21
Cation based on O = 16									
Si^{4+}	5.08	5.473	5.103	5.129	5.249	5.053	5.111	5.165	5.087
Ti^{4+}	.060	.018	.052	.058	.012	0.060	0.060	.013	.061
Al^{3+}	.360	.122	.367	.317	.128	.441	.366	.162	.363
Cr^{3+}	.000	.022	.002	.001	.086	.004	.001	.058	.002
Fe^{2+}	.643	.348	.640	.691	.417	.7145	.681	.587	.603
Mn^{2+}	.015	.004	.018	.019	.008	.017	.017	.003	.013
Mg^{2+}	2.073	2.055	2.093	2.009	2.419	2.021	2.047	2.428	2.130
Ca^{2+}	2.391	2.323	2.314	2.370	2.257	2.285	2.298	2.248	2.361
Na^{+}	.094	.142	.119	.118	.101	.139	.126	.098	.096
K^{+}	.003	.001	.003	.003	.005	.001	.001	.000	.003
SUM	10.726	10.508	10.717	10.715	10.684	10.735	10.709	10.761	10.719

CRYPTIC ALTERATION IN THE INTRUSIONS

At least two cryptic alterations are recognized in the intrusions. One is related to the intrusive activity (alteration I) and the other is related to younger lamprophyre intrusion (alteration II). The former is more profound in H_2O-rich subsolidus feldspar porphyry and quartz-feldspar porphyry units.

It appears that the second hydrothermal activity took place after the cooling of the intrusions, judging from the occurrence of coarse phlogopite replacing chlorite aggregates in feldspar porphyry unit.

INTRUSION-RELATED ALTERATION (I)

Alteration I is primarily expressed as titanization and hematitization of primary magnetite and biotitization of mafic minerals. Secondary biotite is mostly fine grained and characterized by low TiO_2 (<1 weight percent). Secondary magnetite is also low in TiO_2 and the release of Ti from primary biotite and magnetite during re-crystallization resulted in the formation of rutile needles. The details of this alteration are reported in Hicks and Hattori (1988).

LAMPROPHYRIC ALTERATION (II)

Alteration II is characterized by the formation of F-, Ba- or Cr-rich phlogopite (Table 313.3), fine Zn-bearing chromititic oxides (Table 313.4) and feldspars extremely rich in Sr and Ba. The micas are

TABLE 313.3. CHEMICAL COMPOSITIONS OF REPRESENTATIVE MICAS.

	1	2	3	4
SiO_2	35.57	36.80	38.72	38.22
TiO_2	6.42	4.66	3.67	0.76
Al_2O_3	13.49	14.09	13.34	14.40
Cr_2O_3	n.a.	0.00	0.00	2.20
FeO	15.91	17.81	15.72	13.97
MnO	0.00	n.a.	0.11	n.a.
MgO	14.34	15.42	14.78	17.59
CaO	0.00	0.00	0.00	0.00
Na_2O	0.00	0.00	0.00	0.06
K_2O	10.09	9.41	9.30	9.54
Cl	n.a.	0.00	n.a.	0.00
F	n.a.	0.00	n.a.	1.41
TOTAL	98.09	98.19	95.64	97.56
X_{ph}*	0.616	0.664	0.626	0.692

**Phlogopite molecule in the mica*
n.a.: not analyzed.

1. *Typical primary biotites in the augite syenite unit, sample LS*
2. *Primary biotite in augite syenite, sample CT6*
3. *Primary biotite in feldspar porphyry unit*
4. *Large flake of secondary lamprophyric mica (~12 mm) in feldspar porphyry, 6900' Level, Macassa Mine (sample 880427-10).*

Analysis was carried out McGill University (Sample 1), National Museum of Natural Sciences (Samples 2, 3, 4).

commonly coarse (<15 mm) and display unusual light green pleochroism. The colour appears to reflect the presence of Cr^{3+} in the mica. The compositions of micas are extremely heterogeneous within a single thin section. Even single grains show there is chemical inhomogeneity and zoning within a distance of less than 1 μm (Photo 313.1).

TABLE 313.4. CHEMICAL COMPOSITIONS OF OXIDE MINERALS.

	1	2	3	4	5
MgO	1.39	0.08	0.02	0.14	0.24
MnO	1.75	0.00	0.03	1.91	2.01
FeO*	75.61	76.29	93.05	29.97	30.42
ZnO	n.d.	0.10	0.00	9.61	9.81
Al_2O_3	2.14	0.10	0.10	7.34	8.47
Cr_2O_3	0.60	0.10	0.01	49.33	48.04
TiO_2	9.14	15.62	0.04	0.20	0.29
SiO_2	2.16	0.59	0.26	0.22	0.14
V_2O_3	n.d.	0.82	0.06	0.04	0.10
Total	92.79	93.79	93.59	98.76	99.52
Cation based on O = 16					
Ti^{4+}	1.231	2.078	0.006	0.023	0.032
Si^{4+}	0.387	0.104	0.053	0.033	0.021
Al^{3+}	0.452	0.021	0.024	1.302	1.485
Cr^{3+}	0.085	0.027	0.002	5.872	5.649
V^{3+}	0.000	0.096	0.008	0.004	0.010
Mg^{2+}	0.371	0.021	0.006	0.031	0.053
Mn^{2+}	0.265	0.000	0.005	0.244	0.253
Fe^{2+}	11.323	11.288	15.809	3.744	3.784
Zn^{2+}	0.000	0.014	0.003	1.068	1.078
Ulvospinel Base**					
Fe^{3+}	5.457	4.515	10.45	0.515	0.564
Fe^{2+}	5.866	6.773	5.36	3.229	3.220
Fe_2O_3	40.45	33.87	68.26	4.58	5.03
FeO	39.17	45.78	31.56	25.85	25.89
Total	96.81	97.52	100.36	99.23	100.02

* *Total Fe was expressed as FeO.*
** *Fe_2O_3 and FeO calculated after the method in Carmichael (1967)*

Samples:

1. *Typical magnetite microphenocryst in augite syenite unit, sample LC-1.*
2. *High-Ti primary magnetite in feldspar porphyry, (sample 880427-10), 6900'level, Macassa Mine.*
3. *Typical secondary magnetite formed during intrusive activity (sample 86-18), DDH 8-12, 177'.*
4. *Cr-bearing chromite enclosed in secondary biotite within feldspar porphyry (sample 86-18), DDH 8-12, 177', Lake Shore property.*
5. *Cr-bearing chromite within feldspar porphyry (sample 86-17), DDH 8-12, 140'.*

Analyses:
1. EDS analysis, McGill University;
2,3,4,5. wave-length analysis, The National Museum of Natural Sciences, Ottawa.

This alteration is attributed to volatile emanation from lamprophyres because 1) it is difficult to form minerals of such compositions by the release of fluids from the host intrusions, especially Cr-bearing ones, 2) phlogopite and feldspars of identical compositions are found in minette dikes in the area, 3) identical chemical zoning of mica is also found in minette dikes in the area, 4) alteration of this type, over several metres, is recognized, underground, in feldspar porphyry adjacent to a vogesite dike approximately 10 cm wide (4250-foot level, Macassa Mine) and 5) oxides of unusual compositions, especially Zn-bearing chromite, are reported from minette and vogesite dikes (e.g., Wagner and Velde 1985).

This alteration was overlooked before, probably because of its cryptic nature in most cases. Identification of Cr-micas and very fine oxides is almost impossible under the ordinary microscope. Reported occurrences of 'ilmenite' in the intrusive complex and wall rocks (e.g., Thomson 1950; Kerrich and Watson 1984) may be chromitic oxides formed by this alteration.

Compositional variations of a single mineral are common within individual lamprophyre dikes, reflecting changes in fluid compositions. This makes it difficult to determine whether an particular alteration product belongs to alteration I or II. At present, micas of normal compositions and without conspicuous chemical zoning are classified as an alteration

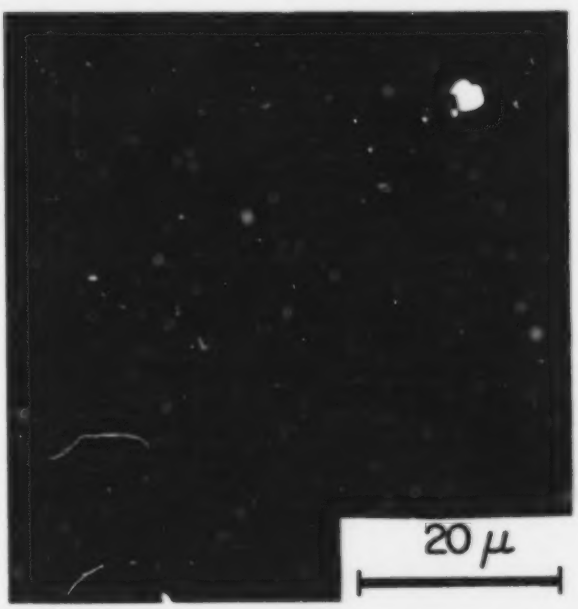

Photo 313.1. *Back scattered electron image of mica, which is interpreted to be a product of lamprophyric alteration (alteration II). Intragrain compositional inhomogeneity is shown in different shades of the image. Brighter portion corresponds to Fe-rich and darker portion to Mg-rich.*

product of alteration I. However, some may belong to alteration II.

Further work is required to understand the extent of this alteration. It appears that the volatiles infiltrated throughout the central part of the complex because almost all specimens of least-altered porphyry collected at the Lake Shore, Kirkland Lake Gold and Macassa properties display this type of alteration. SiO_2–undersaturated, probably CO_2–rich, fluids could have advanced pervasively within the intrusions without apparent fractures. It is, however, difficult to envisage the extensive alteration caused by very minor volumes of lamprophyres currently exposed in the area. Large amounts of volatiles may have migrated through the existing lamprophyre dikes or main breaks.

WALL-ROCK ALTERATION RELATED TO AURIFEROUS VEINS

Three kinds of wall-rock alteration were documented within the feldspar porphyry units (Hicks and Hattori 1988): chlorite facies, hematite-phlogopite facies and sericite-carbonate-pyrite-fuchsite facies. Further study has indicated that the occurrence of fuchsite is isolated and that the surrounding fine sericite, a product of the vein formation, is free from Cr. This suggests that Cr-bearing micas formed before the main stage of vein formation.

A detailed study of wall-rock alteration of augite syenite was carried out at the Macassa Mine in the 42–S–2 stope, which exposes a tension vein off the main break. This location was chosen because of weak deformation in the host rocks and very minor displacement of the host rocks along the vein. The vein in the stope is narrower, <30 cm, than the main vein and consequently the extent of the alteration is also minor. However, the alteration in the stope is representative of the main veins because of the occurrence of similar vein mineralogy, including visible gold, in the stope.

Alteration recognized in the augite syenite unit is classified into three facies (Levesque 1989): chlorite-carbonate facies (spotted green zone), magnetite facies and K-feldspar-pyrite facies. Within the chlorite-carbonate facies, green spots represent former augite phenocrysts, which are now composed of chlorite, carbonate and minor secondary Ti-poor magnetite. Minor hematitization is observed in primary magnetite. Titanium released during this alteration formed rutile needles. Primary biotite has been altered to chlorite.

The magnetite facies is brownish grey and characterized by destruction of augite phenocrysts (<20 volume percent). Abundant secondary magnetite was formed by oxidation of Fe^{2+} released from augite. Perthite was re-crystallized to albite and K-feldspar grains. Primary magnetite is extensively hematitized in this zone.

The K-feldspar-pyrite facies occurs adjacent to gold-bearing veins and in wall-rock fragments incorporated within the veins. Due to intense replacement, primary mineralogy and textures have been completely obliterated. Iron oxides have been replaced by pyrite due to introduction of sulphur. Primary feldspar is completely re-crystallized to K-feldspar.

Wall-rock alterations in the augite syenite unit and the feldspar porphyry unit have different appearances due to different alteration mineralogy. For example, brick red colouration in feldspar porphyry near the veins due to extensive hematitization is not observed in the augite syenite. This is explained by high total iron content in augite syenite. Apparently, the fluids oxidized a certain amount of Fe^{2+} to Fe^{3+}, forming magnetite from augite in augite syenite and hematite from magnetite in feldspar porphyry. Another major difference is K-bearing phases. Hydrothermal K-feldspar has formed in augite syenite, whereas sericite has formed in feldspar porphyry. This is due to high K_2O contents in augite syenite, which kept high K^+/H^+ ratios in the fluids, thus stabilizing K-feldspar instead of sericite.

The difference in alteration mineralogy in different host rock lithologies is maintained where the two rock units are in direct contact at 42–S–2 stope (Figure 313.1). This appears to support the notion that the fluid flow for auriferous hydrothermal activity was fracture controlled.

VEINING

Main vein formation started with the precipitation of quartz, which was subsequently fractured, re-crystallized and the fractures filled by sulphides, tellurides and gold (Photos 313.2 and 313.3). As documented in many gold deposits (e.g., Colvine *et al.* 1988), gold in the Kirkland Lake camp was introduced in the late stages of vein development. The preliminary measurements of filling temperatures of quartz indicate that the main vein formation took place at temperatures above 340°C (Gallimore 1988).

Although the upper section of the Lake Shore deposit is considered to be one of the shallowest examples of Archean gold mineralization (Colvine *et al.* 1988), there are no obvious textures indicative of open fissure filling, as is common in many shallow vein deposits in geologically younger terrains. Instead, the textures of the vein quartz reflect the hydrothermal activity and deformation under a ductile regime (Photo 313.2). This difference may be attributed to higher temperatures and deeper environments for Archean gold mineralization.

The main veins are commonly cut by barren quartz veins. Fluid inclusions in the veins show similar filling temperatures, ~330°C, and clearly late carbonate-quartz veins show filling temperatures of

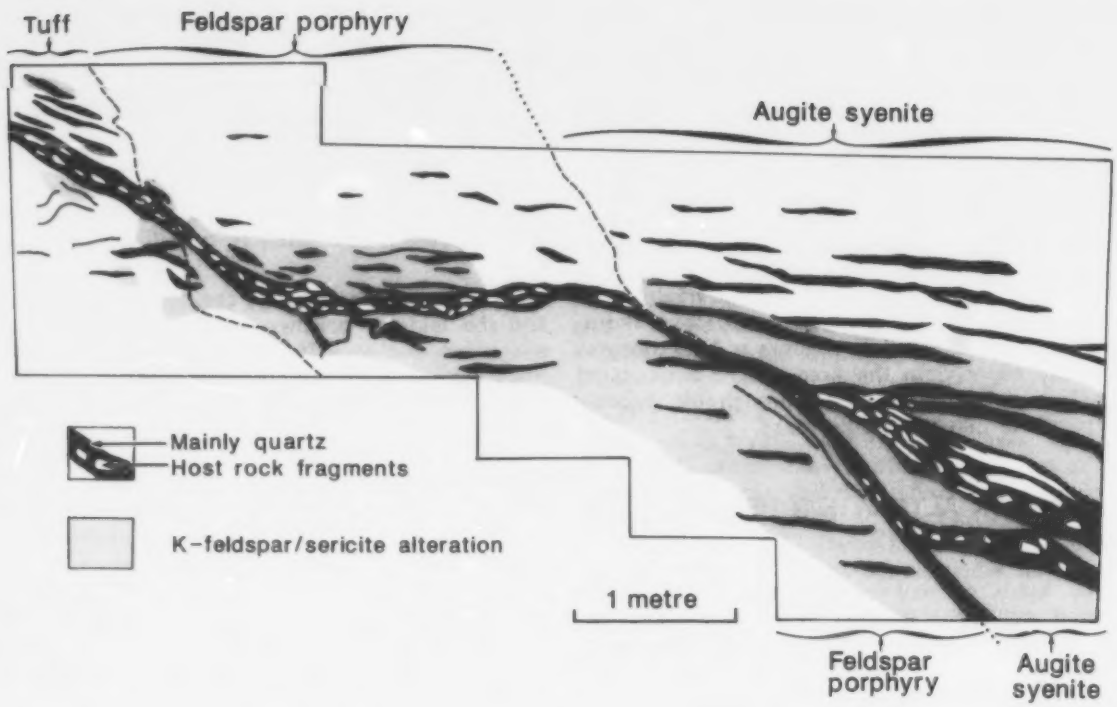

Figure 313.1. *Vertical section of a tension vein at 42-S-2 Stope, Macassa Mine (modified after a map by C. Madore, University of Ottawa). The sharp contrast in alteration mineralogy in augite syenite and feldspar porphyry units suggests fracture-controlled fluid flow with limited mixing of fluids in host rocks.*

~280°C. The data suggest that the post-gold hydrothermal activity took place at significantly higher temperatures.

The hydrothermal fluids for the main vein contained S^{2-} which was depleted in ^{34}S (Table 313.5). The values appear to be independent of grain size, mineral phase and location in the Kirkland Lake gold camp. Molybdenite, chalcopyrite and pyrite have all $\delta^{34}S$ near −9‰. The values are quite different from those for common disseminated pyrite, possible diagenetic sulphides, within trachyte tuffs and Timiskaming conglomerates in the area (Table 313.5).

The consistent $\delta^{34}S$ values from the gold-bearing veins negates the possibility of *in situ* oxidation of hydrothermal fluids in the Kirkland Lake gold camp. Instead, the fluid had a large reservoir of isotopically fractionated sulphur at depth. Different $\delta^{34}S$ values in sulphides from veins off the main break (Table 313.5) suggest a focussed fluid passage of the auriferous fluid. Sulphides in the barren veins did not undergo isotopic fractionation as sulphur in the auriferous veins.

SUMMARY

Mineralogy and chemical compositions of the Kirkland Lake intrusive complex indicate that the magmas for the complex were intrinsically oxidized, evidenced by early crystallization of magnetite in the augite syenite unit, early crystallization of titanite in the porphyry phase (e.g., Noyes *et al.* 1983), and high $Mg^{2+}/(Mg^{2+} + Fe^{2+})$ ratios of augite and biotite.

Major element compositions of the intrusions indicate that the older syenite units and younger porphyritic units were formed from different magmas (e.g., Cooke and Moorhouse 1969; Levesque and Hattori 1989). This study suggests that the two magmas had different volatile components. The two older units are hypersolvus CO_2-rich intrusions, whereas the later porphyry units are subsolvus intrusions. This differs from the hypersolvus nature of porphyritic intrusions within neighboring intrusive complexes, such as Otto, Lebel and Murdock Creek stocks.

Two styles of cryptic alteration are identified; one is related to intrusion itself and the other is due to lamprophyre intrusion. The first one includes hematitization and titanization of magnetite and

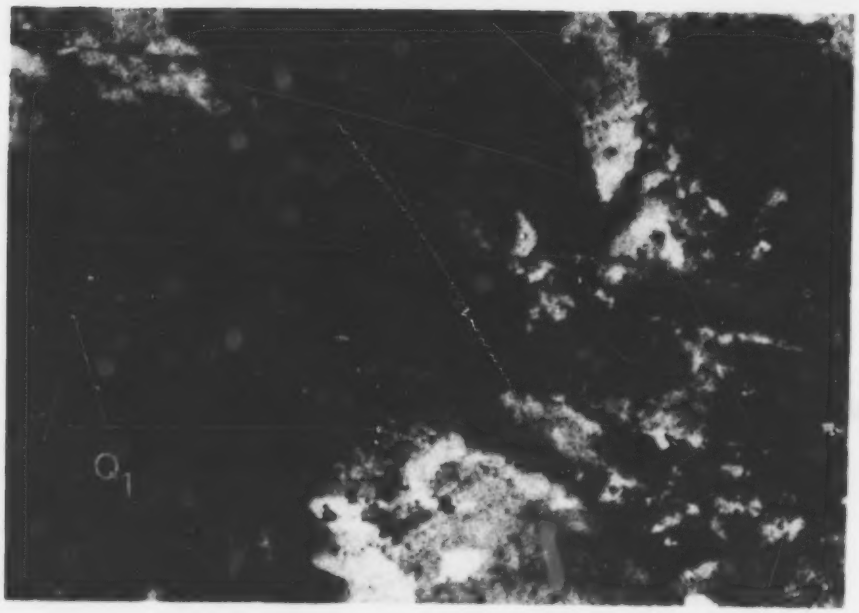

Photo 313.2. *Coarse, re-crystallized quartz grains (Q1) transected and displaced by veinlets containing sulphides (Q2). The sample was collected from the North vein, 800-foot level, Lake Shore Mine. Photo by R. Theriault.*

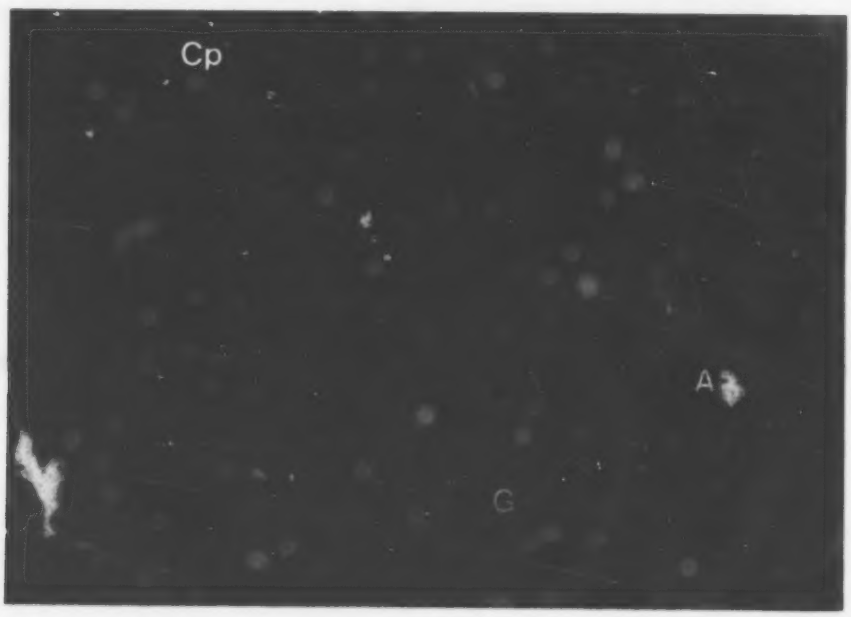

Photo 313.3. *A mixture of gold, chalcopyrite, altaite, and coloradoite fills fractures within recrystallized coarse quartz grains. The sample was collected from the North vein, 1200-foot level, Lake Shore Mine. A=altaite, Cp = chalcopyrite, G = native gold. Photo by R. Theriault.*

TABLE 313.5. SULPHUR ISOTOPE COMPOSITIONS OF DISSEMINATED SULPHIDES IN WALL ROCKS AND VEINS.

Sample Number	Description	$\delta^{34}S$ (‰)
Pyrite in sericite-carbonate-pyrite facies		
860529-09	In feldspar porphyry, 1 ft from South vein No.1 shaft pillar, Lake Shore Mine	-9.4
RT-5	In porphyry, North vein, 800'L, Lake Shore Mine	-10.3
87041406	In feldspar porphyry, North vein, 600'L, Lake Shore Mine	-9.0
Auriferous veins		
85022011	North vein, 201 E stope, Lake Shore	-12.7
86052910	No.1 shaft crown pillar, South vein, Lake Shore	-10.4
85022071	Highly sheared carbonate rich vein, Lake Shore	-9.6
86052908	South vein	-11.9
88042714	6900'L, 6936 TDB, ore zone, Macassa	-7.2
870415-33	Molybdenite, the underground garage, Lake Shore	-9.5
880427-16	Molybdenite-rich seam at 6900' L, 6936 stope, Macassa	-9.1
Post-ore carbonate-quartz vein		
85022031	244 stope, carbonate vein at the West block, Lake Shore	-7.0
850220-41	Coarse chalcopyrite, in the West Block, Lake Shore	-13.0
88042707	Barren quartz-pyrite veinlet (5 mm) parallel to the ore, Macassa	-5.6
Other occurrences		
88042704	In tuff, near Tegren fault (cutting ore veins) on 4250'L, Macassa Mine	+1.4
°8042706	In trachytic tuff, at 4200', Macassa	+1.7
[illegible]2720	In tuff at 6700 E drift, Macassa	-0.2
[illegible]0-10	In Timiskaming conglomerate,	-1.3
[illegible]2715	Coarse pyrite in fracture, 2 m to the ore, 6936TDB, Macassa	-6.7

biotitization of mafic minerals. The second one is characterized by the formation of phlogopite, oxides and feldspar of unusual compositions, including Cr-rich phlogopite. The occurrence of phlogopite replacing chloritized mafic minerals at the Lake Shore property indicates that this alteration took place after the cooling of the intrusive complex.

The hydrothermal activity related to auriferous veins postdated the above pervasive alteration. The occurrence of fuchsite (Cr-mica) adjacent to the auriferous zone is attributed to Cr-mica formation during the lamprophyric alteration before the veining.

The fluids for the veining were oxidized and sulphur-rich, resulting in magnetitization of augite in augite syenite and hematitization of magnetite and pyritization of Fe-oxides in both augite syenite and feldspar porphyry units. Low $\delta^{34}S$ values in pyrite from wall rocks and veins confirm the oxidized nature of the fluids.

The introduction of gold occurred during late stages of vein formation, however the hydrothermal activity continued in the area, producing barren quartz veins and post-ore veins at temperatures over 280°C.

The sequence of hydrothermal activity and geological events in the central part of the Kirkland Lake camp can be summarized as follows:

- augite syenite and co-magmatic felsic syenite intrusions
- intrusion of porphyry units from a different magma source
- cryptic subsolidus alteration (alteration I)
- cooling of the intrusion (chloritization of mafic minerals)
- lamprophyre emplacement and alteration (alteration II)
- main vein formation: quartz formation, re-crystallization followed by introduction of gold
- post-ore vein formation.

ACKNOWLEDGMENTS

The authors thank George Nemcsok, Chief Area Geologist, Macassa Division, Lac Minerals Ltd. and Len Cunningham, L. Cunningham and Associates, for their assistance during the field work. Thanks are also extended to Scott Ercit of The National Museum of Natural Sciences, Ottawa, and Moyra MacKinnon, McGill University, for their help during the electron microprobe work. Funding was provided by an Ontario Geoscience Research Grant to K. Hattori.

REFERENCES

Carmichael, I.S.

1967: The Iron-Titanium Oxides of Salic Volcanic Rocks and their Associated Ferromagnesian Silicates; Contributions to Mineralogy and Petrology, Volume 14, p.36-64.

Colvine, A.C., Fyon, J.A., Heather, K.B., Marmont, S., Smith, P.M. and Troop, D.G.

1988: Archean Lode Gold Deposits in Ontario; Ontario Geological Survey, Miscellaneous Paper 139, 136p.

Cooke, D.L. and Moorhouse, W.W.

1969: Timiskaming Volcanism in the Kirkland Lake Area, Ontario, Canada; Canadian Journal of Earth Sciences, Volume 6, p.117-132.

Gallimore, N.J.

1988: Study of Fluid Inclusions in Hydrothermal Veins at Macassa and Lake Shore Mines, Kirkland Lake, Ontario; unpublished BSc thesis, University of Ottawa, 79p.

Hicks, K.H. and Hattori, K.

1988: Magmatic-Hydrothermal and Wall Rock Alteration Petrology at the Lake Shore Gold Deposit, Kirkland lake, Ontario; p.192-204 *in* Geoscience Research Grant Program, Summary of Research, 1987-1988, edited by V.G. Milne, Ontario Geological Survey, Miscellaneous Paper 140, 251p.

Kerrich, R. and Watson, G.P.

1984: The Macassa Mine Archean Lode Gold Deposit, Kirkland Lake, Ontario: Geology, Pattern of Alteration and Hydrothermal Regimes; Economic Geology, Volume 79, p.1104-1130.

Levesque, G.

1989: The Kirkland Lake Intrusive Complex: A Petrographical and Chemical Approach; unpublished BSc (Honours) Thesis, University of Ottawa, 83p.

Levesque, G. and Hattori, K.

1989: Late Archean Alkaline Intrusive Complex Hosting the Kirkland Lake Gold Camp, Abitibi Greenstone Belt (abstract); Geological Association of Canada, Program with Abstracts, Volume 14, p.A-81.

Noyes, H.J., Wones, D.R. and Frey, F.A.

1983: A Tale of Two Plutons: Petrographic and Mineralogical Constraints on the Central Sierra Nevada, California; Journal of Geology, Volume 91, p.353-379.

Rowins, S.M., Lalonde, A.E. and Cameron, E.M.

1989: Geology of the Archean Murdock Creek Intrusion, Kirkland Lake, Ontario; p.313-323 *in* Current Research, Part C, Geological Survey of Canada, Paper 89-1C.

Smith, A.R. and Sutcliffe, R.H.

1988: Plutonic Rocks of the Abitibi Subprovince; p.188-196 *in* Summary of Fields Work and Other Activities 1988 by the Ontario Geological Survey edited by A.C. Colvine *et al.*, Ontario Geological Survey, Miscellaneous Paper 141, 498p.

Theriault, R.D.

1988: A Study of Gold Mineralization at the Lake Shore Mine, Kirkland Lake, Ontario; unpublished BSc thesis, University of Ottawa, 83p.

Thomson, J.E.

1950: Geology of Teck Township and Kenogami Lake Area, Kirkland Lake Gold Belt; Ontario Department of Mines, Annual Report for 1948, Volume 57, Pt. 5, p.1-53.

Toogood, D.J. and Hodgson, C.J.

1985: A Structural Investigation between the Kirkland Lake and Larder lake Gold Camps; p.200-205 *in* Geoscience Research Grant Program, Summary of Research 1984-1985, edited by V.G. Milne, Ontario Geological Survey, Miscellaneous Paper 127.

Wagner, C. and Velde, D.

1985: Mineralogy of Two Peralkaline Arfvedsonite-Bearing Minettes, A New Occurrence of Zn-Rich Chromite; Bulletin of Mineralogy, Volume 108, p.173-187.

Grant 319 Gypsum Deposits of Southern Ontario

S.J. Haynes and J. Hughes-Pearl

Department of Geological Sciences, Brock University, St. Catharines

ABSTRACT

This paper details the stratigraphy and facies changes of the mined gypsum bed and enclosing Upper Silurian Salina A Unit sedimentary rocks at the Westroc Industries Ltd. mine at Drumbo (Westroc), and compares them with equivalent strata at the Domtar Ltd. mine at Caledonia (Domtar). At both localities, the Salina A consists of three sedimentary cycles, each terminating with gypsum. The three cycles at Domtar constitute similar sequences of lagoonal muds capped by subaqueous gypsiferous lagoonal sediments. However, at Westroc, the cycles undergo a significant change from subaqueous deposition in a coastal salina, in the first cycle; to erosion, followed by mixed freshwater/hypersaline water deposition in a coastal or lacustrine salina, in the second cycle; to desiccation, followed by intertidal to subaerial deposition in a sabkha, in the third cycle.

The mined gypsum bed (Main Gypsum Bed) at Westroc forms the top of Cycle 1 and marks the first appearance of gypsum beds in the Salina Formation, above the contact with the underlying Guelph Formation. Stratigraphically, the Main Gypsum Bed correlates with the base of the Salina A-2 Unit. At Westroc, the two overlying gypsum beds in the Salina A-2 are uneconomic. In contrast, the economic gypsum bed at Domtar marks the base of the overlying Salina B anhydrite (top of Cycle 4) and is underlain by three uneconomic gypsum beds (stratigraphic equivalents of the three Salina A-2 gypsum beds at Westroc).

A modern analogue which explains the difference in Salina A facies sequences between Westroc and Domtar (55 km apart), is the semi-arid coast of northern Egypt, adjacent to the Nile delta, where gypsum is depositing in both sabkha-fringed coastal salinas and large lagoons/coastal lakes within distances equivalent to that across the Algonquin Arch.

INTRODUCTION

This paper is the second in a continuing study of the gypsum deposits of southwestern Ontario. These deposits are all located in the Upper Silurian Salina Formation on the eastern flank of the Algonquin Arch, which separates the Michigan and Appalachian (Allegheny) basins (Figure 319.1). Although numerous small mines were in operation throughout the 19th century, present production is restricted to three mines: Caledonia (Domtar Construction Materials Ltd.), Drumbo (Westroc Industries Ltd.), and Hagersville (Canada Gypsum Company). In 1988, these produced 1 458 800 tonnes of gypsum, valued at C$19 712 000 (preliminary figures, McKnight and Fell 1989). The largest producer, the Domtar Construction Materials (Domtar) deposit at Caledonia (annual production about 700 000 tonnes), was the subject of the previous study (Haynes *et al.* 1988, and in press).

This study details the geology of the host rocks and the mined gypsum bed at the Westroc Industries Ltd. (Westroc) deposit at Drumbo, where annual production is about 350 000 tonnes. In addition, textures and lithologies present at Westroc are contrasted with equivalent stratigraphic units at the Domtar deposit, 55 km to the southeast. The purpose of this study is to determine the relationship of economic gypsum beds to facies variations in the Salina Formation, and their likely environments of deposition from comparison of the facies variations at Westroc and Domtar with modern coastal subaqueous evaporites (coastal salinas and lagoons), fringed by intertidal to subaerial sabkhas, in southern Australia and northeastern Egypt.

STRATIGRAPHY OF THE SALINA FORMATION

The Upper Silurian Salina Formation constitutes a thick carbonate-evaporite sequence in the Michigan Basin, and a thick carbonate-evaporite-clastic sequence in the Appalachian Basin; these sequences thin over the intervening broad marginal platform of the northeast-trending Algonquin Arch. As a consequence, the area of the Niagara Peninsula (Figure 319.1) contains Upper Silurian sequences that are a mixture of the marginal facies of both the Michigan and Appalachian basins. This has resulted in considerable complexity in stratigraphic correlation. Stratigraphic interpretation is further complicated by controversy as to whether reef facies, present within the Michigan and Appalachian basins, represent Niagaran strata later overgrown by the basal Salina Formation, or contemporaneous growth of reefs during early Salina time. (*See* Haynes *et al.* 1988, and in press, for more detailed discussions.)

Although it does not resolve disputes over diachroneity, a practical solution to stratigraphic correlation of the Salina Formation over the Algonquin Arch is the use of drill-hole gamma-ray logs by Carter (1987). Carter (1987) presents evidence that Landes' (1945) subdivision of the Salina Formation in the Michigan Basin, into (in ascending order) A,

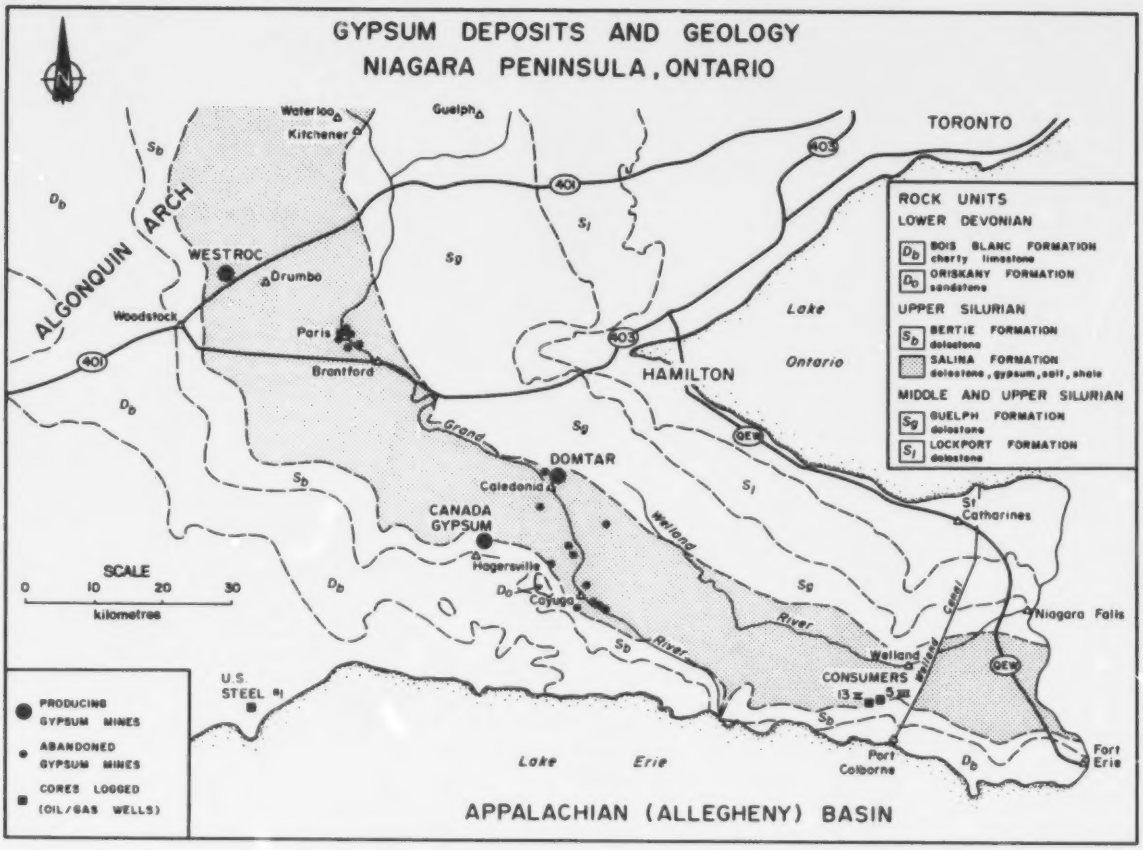

Figure 319.1. *Regional geology and location of gypsum deposits, southern Ontario.*

B, C, D, E, F and G Units, can be correlated across the Algonquin Arch and Niagara Peninsula to the Appalachian Basin, although Unit D is thin or absent over the Algonquin Arch and Niagara Peninsula. He also shows that Evans' (1950) subdivision of the Salina A Unit of the Michigan Basin into A-1 and A-2 can be extended east to the Niagara Peninsula, but not to the deeper parts of the Appalachian Basin. Carter demonstrates that the Salina A-1 changes progressively eastward from anhydrite and dolostone in the Michigan Basin, to dolostone over the Algonquin Arch (Westroc mine), to dolomitic shale in the Niagara Peninsula (Domtar mine), to shale and sandstone in the lower A Unit of the Appalachian Basin; Carter also shows that Evans' (1950) division of the Salina A-2 Unit of the Michigan Basin, into a lower A-2 evaporite and upper A-2 carbonate, can be correlated eastward to the Niagara Peninsula. The basal A-2 evaporite is the mined gypsum bed at Westroc and the Lower Gypsum bed at Domtar (Haynes *et al.* 1988, and in press). At both Westroc and Domtar, the basal A-2 gypsum is overlain by shales that correspond with a gamma-ray peak at the same stratigraphic level in Carter's logs. The A-2 carbonate is present as dolomitic shales, dolostones and gypsum beds at both Westroc and Domtar. Carter (1987) distinguishes the base of the Salina B Unit in the Algonquin Arch and Niagara Peninsula as a prominent bed of anhydrite (B anhydrite), overlain by dolomitic shales, that can be traced westward into the Michigan Basin. The B anhydrite constitutes the mined gypsum bed at the Domtar mine, but is not exposed at the Westroc mine.

GEOLOGY OF THE WESTROC DEPOSIT

MINE STRATIGRAPHY AND HOST-ROCK LITHOLOGIES

The Westroc deposit is the newest gypsum mine in southern Ontario (production commenced 1978) and the only gypsum mine that is accessed via a vertical shaft. The shaft extends 116 m from surface and terminates in dolostones of the Guelph Formation (Hartviksen 1983). Although no drill core was available, a 15.8 m semi-continuous vertical exposure of the Salina A Unit is present at the production level, near the shaft (Sections 1 and 2, Figure 319.2). This consists of a 4.9 m section in the shaft, below the mined bed (here termed the Main Gyp-

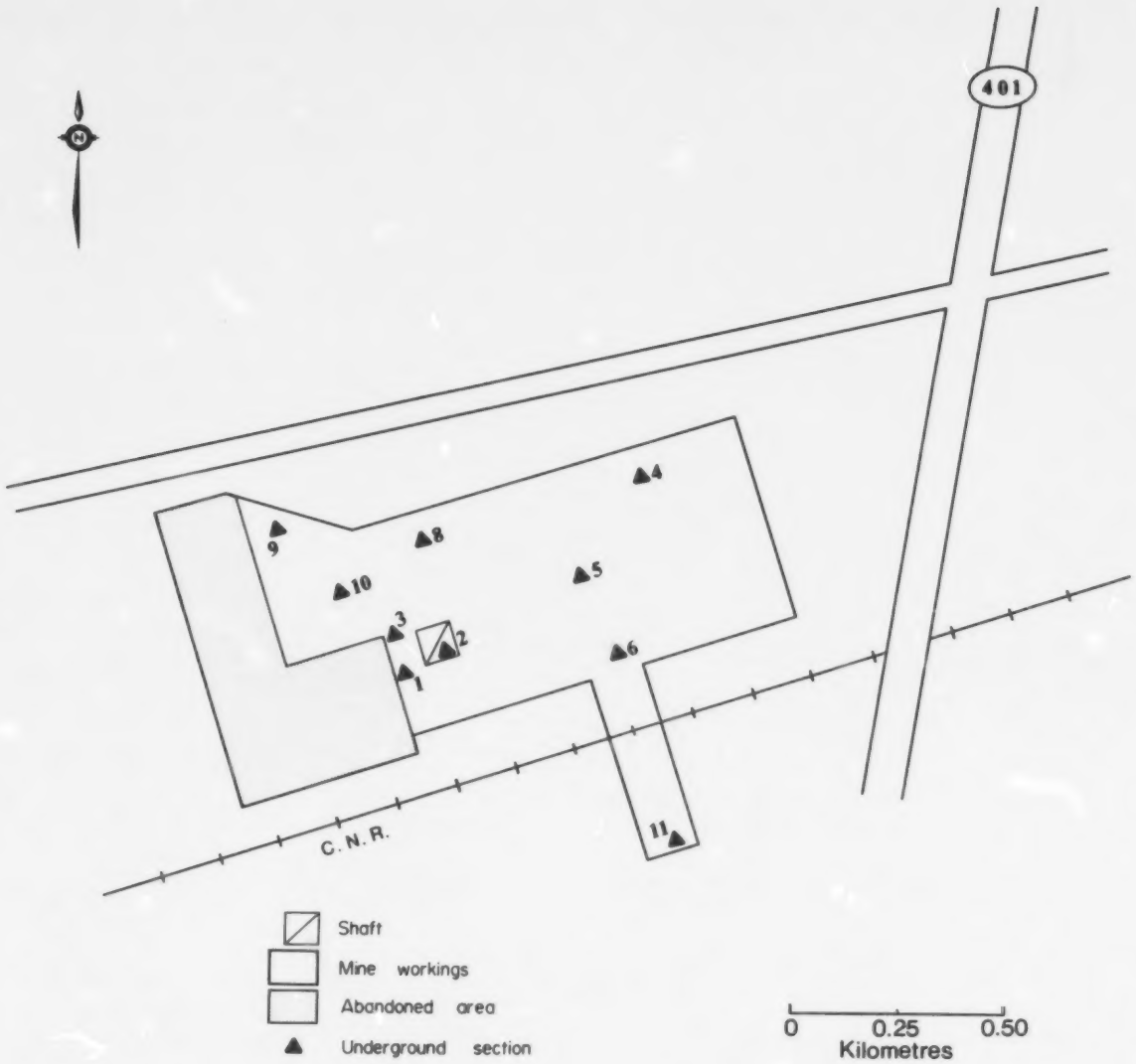

Figure 319.2. *Plan of Westroc Industries Ltd. property at Drumbo, showing positions of underground sections*

sum Bed) and a 10.9 m section of the walls in the crusher/loading bin area (adjacent to the shaft) of the Main Gypsum Bed and overlying units. The stratigraphic setting of the deposit was determined from mapping of this vertical section (Figure 319.3) at a scale of 1:10. A summary of lithology, stratigraphic position and postulated depositional environment is presented in Figure 319.4. The postulated depositional environment of each lithology is presented in this section but discussed in more detail later in the paper.

In keeping with mining terminology previously used in papers on the Domtar deposit (Haynes *et al.* 1988, and in press) *gypsite* is defined as a rock containing between 40 and 70% gypsum.

Although the Guelph–Salina contact is covered in the shaft, its location is known, from the initial shaft installation, to be 4 m below the mined gypsum bed (Kirk Scheifele, mine manager, personal communication, 1989). There is little variation between the dolomites at the top of the Guelph Formation and the dolomites of the Salina A-1 exposed in the shaft (Figures 319.3 and 319.4). The dolomites of both formations are generally massive, with colour banding varying from grey-brown to light, to dark brown. However, the Salina A-1 is marked by an increase in the amount of gypsum present in the form of stringers, laminations, bands, selenite eyes and occasional nodules. A 0.5 cm thick layer of chocolate brown fissile shale, (locally kinked) occurs at the base of the unit underlying the base of the

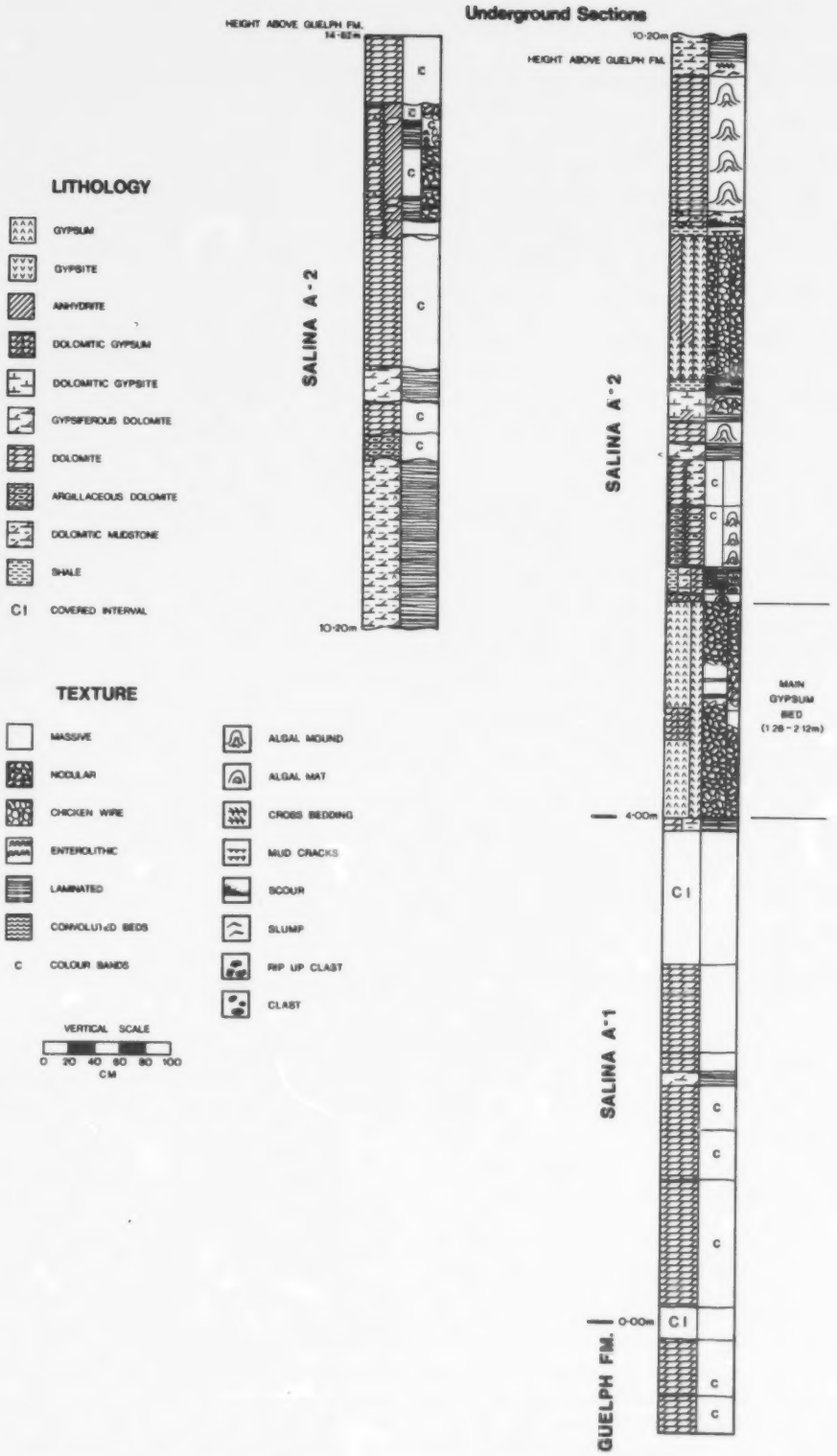

Figure 319.3. *Stratigraphy, lithology and texture of the Main Gypsum Bed and adjacent units, underground sections 1 and 2, Westroc mine.*

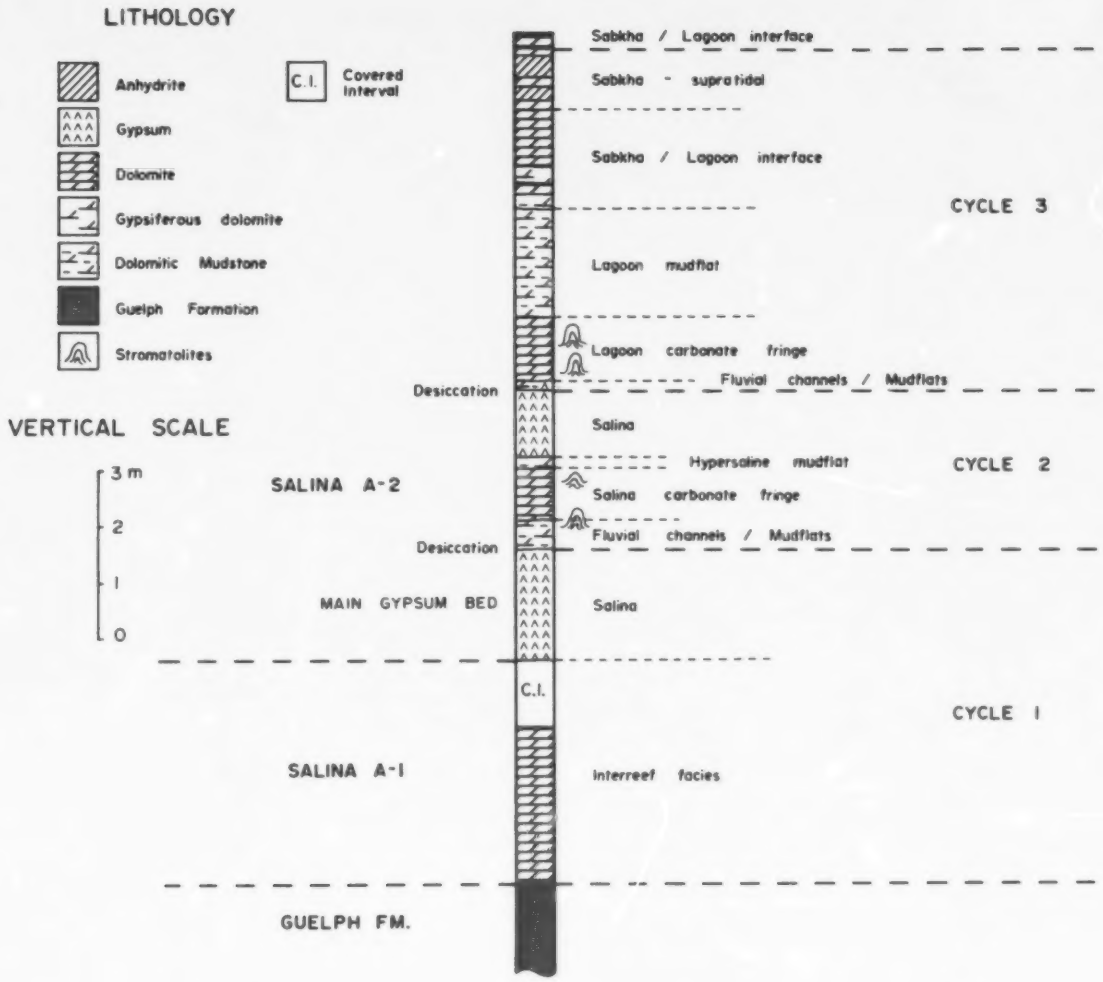

Figure 319.4. *Simplified stratigraphic section and probable depositional environments of lithologies at the Westroc mine.*

shaft collar (covered interval below Main Gypsum Bed, Figure 319.3). The Salina A-1 at Westroc appears to represent continuation of Guelph reef/interreef facies (Figure 319.4).

The unit immediately underlying the Main Gypsum Bed was only observed at two locations in the mine. One is about 40 m west of Section 11 (Figure 319.2) where the floor of the gypsum has locally domed up. Here, the unit is a pink-brown laminated dolomite which appears to be either an algal mat or a stromatolitic mound. The other locale is at Section 1 where laminated shale and dolomite is present.

The Main Gypsum Bed is the basal lithology of the Salina A-2 Unit, corresponding to the stratigraphic position of the A-2 evaporite, on the Algonquin Arch, defined by Carter (1987). The Main Gypsum Bed ranges in thickness from 1.28 m to 2.12 m, with an overall grade of 88% gypsum. It consists of gypsum and dolomitic gypsum that exhibit primarily nodular texture, although laminated, massive, hassock and chicken-wire mosaic textures are present in varying proportions throughout the mine. The Main Gypsum Bed is described in the next section. Textures and lithologies suggest that it is a coastal salina sequence. The Salina A-1 dolomites and the basal Salina A-2 evaporite constitute the lowermost of the sedimentary cycles exposed at Westroc (Cycle 1, Figure 319.4).

The Main Gypsum Bed is overlain by an approximately 8 cm thick bed of pink-brown laminated dolomite to dolomitic gypsite. This bed is remarkably consistent throughout the mine and forms an easily recognized marker. Algal structures are common. It appears to represent an algal mat that formed on filling of the coastal salina. The top of this algal mat is ripped up by dolomitic shales and mudstones, and siltstones that are locally arenaceous or conglomeratic, containing clasts of the dolomitic

algal mat. Although thickness, texture and lithology vary greatly throughout the mine, the unit is about 20 cm thick and varies from massive with some colour banding to laminated and fissile. Colour varies from grey to grey-brown to green. In general, clastic sediments are common at the base. Within this unit, graded beds are present at Sections 1, 6 and 8. At Section 6, a micro-conglomerate is overlain by a sequence of micro-turbidites comprising thin (4 to 5 cm), fining-upward, sand-silt-mudstone/shale beds. Cross-bedding is present at Sections 1, 4 and 8. At Section 1, an erosional lower contact with the underlying algal mat is evident, accompanied by rapid lateral changes of facies and local development of small-scale ripples. The clastic unit contains more arenaceous lithologies (sand and silt) in the northwestern (Sections 3, 8, 9a and 10) and eastern (Section 6) parts of the mine. At several localities isolated stromatolite mounds (up to 1 m in diameter) have sunk into the clastics, compacting the underlying sediments. This unit is overlain by a sequence, approximately 50 cm thick, of coalesced dolomitic stromatolite mounds that interfinger with a variety of dolomitic sediments. These consist of laminated dolomitic mudstone with minor gypsum nodules, or massive colour-banded argillaceous dolomite (with clasts), overlain by massive dolomite. This is capped by massive colour-banded argillaceous dolomite. Lateral variation of these three units overlying the Main Gypsum Bed is presented in Figures 319.5, 319.6, 319.7 and 319. 8. The clastic unit and the isolated stromatolite mounds probably represent mudflats and fluvial channelways on the fringes of a coastal salina or small lagoon. These may have formed either during a period of marine regression or, alternatively, during a period of unusually high rainfall. Coalesced stromatolitic mounds have been reported by Warren (1982) from areas of groundwater resurgence in the modern coastal salinas of South Australia, forming a carbonate fringe around the salina.

The Salina A-2 succession above the stromatolite mounds is exposed only at Section 1. Above the stromatolite mounds, 36 cm of massive colour-banded dolomite, grading laterally to dolomitic mudstone, is overlain by about 13 cm of laminated gypsiferous dolomite. This is capped by a 17 cm thick layer of dolomitized algal mounds exhibiting domal upper contacts. As these sequences of dolomites (including those parts of the underlying unit, where the stromatolites form continuous coalesced layers) are similar to the carbonate fringe of coastal salinas, reported by Warren (1982) from South Australia, it is likely that they formed in an equivalent environment (Figure 319.4).

The dolomites are overlain by 24 cm of laminated dolomitic gypsite with intervals of nodular gypsum in which anhydrite nodules and enteroliths are occasionally preserved. This passes upward into a thin (6 cm to 8 cm) bed of mudstone that exhibits facies and textural variation, from massive dolomitic mudstone, to laminated silty mudstone in local scour channels. These laminated gypsite and mudstone units are considered to represent a hypersaline mudflat.

Cycle 2 terminates with a 1.05–1.35 m thick bed of gypsum and anhydrite (Figures 319.3 and 319.4). Textures change laterally from nodular to chicken-wire mosaic. Where present, nodular anhydrite is underlain by blebs and stringers of gypsum in a laminated dolomite matrix. Lenses of green mudstone are present in the basal 20 cm of the chicken-wire mosaic gypsum. These lithologies and textures are consistent with deposition in a coastal salina environment.

The gypsum bed is capped by a 7 cm thick bed of mudstone containing minor dolomite. Gypsum-infilled radial tension cracks are common where the gypsum has locally domed upward (presumably due to expansion on hydration of anhydrite to gypsum). However, upward-widening desiccation cracks, filled with material from overlying lenses of argillaceous material are present where the contact with the gypsum is flat or down-warped. The upper contact of the mudstone is erosional; it is overlain by 13 cm of dolomite containing irregular layers and lenses of silt or sand that display slumps, scours and rip-ups (Figure 319.3). This basal sequence of Cycle 3 indicates that a period of intermittent flooding/erosion and subaerial desiccation took place after filling of the coastal salina. The depositional environment was probably a tidal mudflat cut by fluvial channelways (Figure 319.4). This sequence is overlain by about 1.10 m of stromatolitic dolomite that was probably deposited as a carbonate fringe on the shore of a lagoon.

This is followed by 30 cm of thin-bedded green dolomitic shales and laminated silts exhibiting graded and cross-bedding, and small slump structures. These pass upward into a 1 m thick unit of dolomitic mudstone, composed of alternating layers of laminated dolomite and mudstone. Gypsum is present locally as scattered bands, patches and blebs. This succession appears to represent lagoonal muds (Figure 319.4) with intermittent development of mesosaline conditions.

The mudstones are overlain by a 1.8 m thick sequence of dolostones consisting of (from bottom to top): 21 cm of argillaceous dolomite comprising massive colour-banded dolomite, undulating bands and lenses of mudstone, and layers and lenses of gypsum; 26 cm of massive dolomite, occasionally colour-banded; about 26 cm of laminated gypsiferous dolomite; and, 1.05 m of massive colour-banded dolomite with bands of selenite eyes. Although the internal features of these dolostones are consistent with several depositional environments, their stratigraphic position, between an underlying succession of lagoonal muds (subaqueous) and an overlying sequence (see below) of sabkha sediments

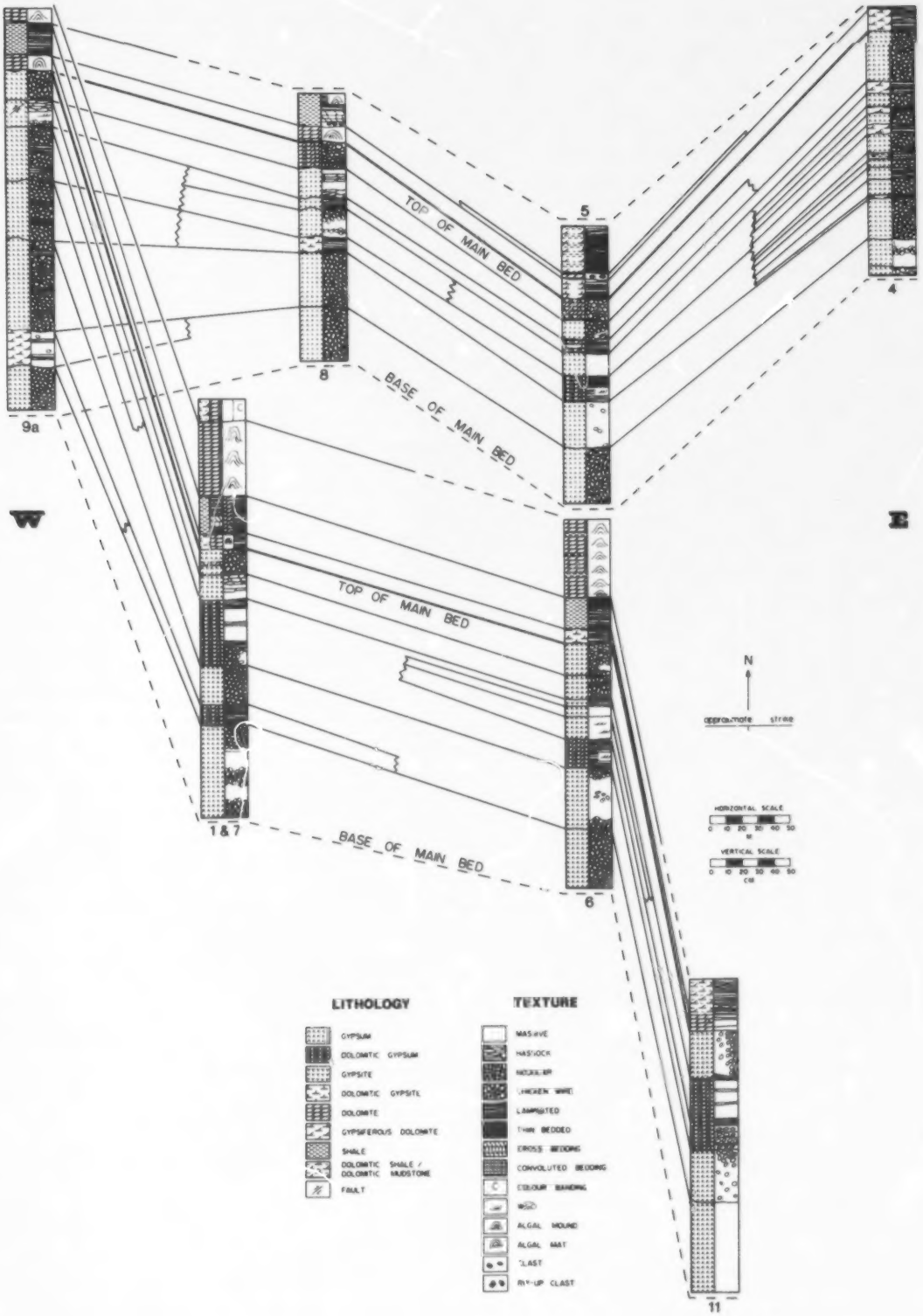

Figure 319.5. *Fence diagram of lithological and textural variations within the Main Gypsum Bed, Westroc mine. Locations of underground sections are given in Figure 319.2.*

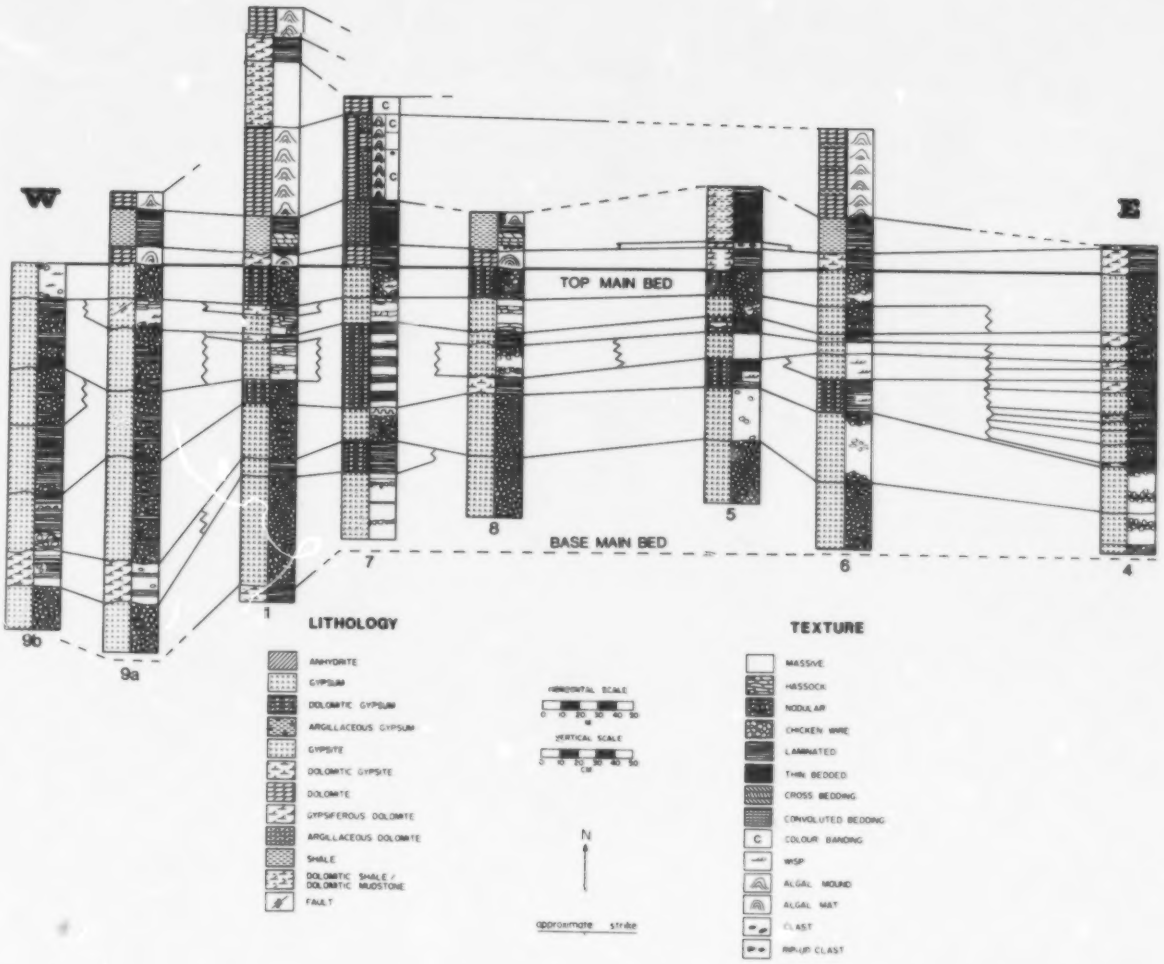

Figure 319.6. *East-west section of the Main Gypsum Bed, Westroc mine, illustrating along-strike variation of lithology and texture. Locations of underground sections are given in Figure 319.2.*

(supratidal), suggests they were deposited at a sabkha-lagoon interface as a mixture of subaqueous and intertidal sediments.

The remaining 0.8 m to 1.1 m of Cycle 3 (Figures 319.3 and 319.4) consists primarily of dolomite containing lenses of anhydrite. Where gypsum is present as minor eyes and laminations, the dolomites are massive, but display local colour banding. Elsewhere, the dolomite is laminated to thin-bedded. The anhydrite interbeds are usually nodular or massive, but enterolithic textures are present in the upper part of this sequence. By consideration of the differences between subaerial (sabkhas) and subaqueous (coastal salinas and lagoons) environments of deposition, as described by Warren (1989), this sequence was probably deposited in a supratidal sabkha environment.

The remaining 30 cm to 50 cm, overlying the sabkha sequence, consists of massive colour-banded dolomite with selenite eyes. At the base, black gypsum laminations and stringers are present above underlying dolomite and anhydrite; whereas mudstone bands are present above underlying dolomite and gypsiferous dolomite. The lack of exposure of overlying lithologies makes interpretion of the depositional environment of this unit difficult. We tentatively suggest that it may represent a new marine incursion and deposition at a sabkha-lagoon interface.

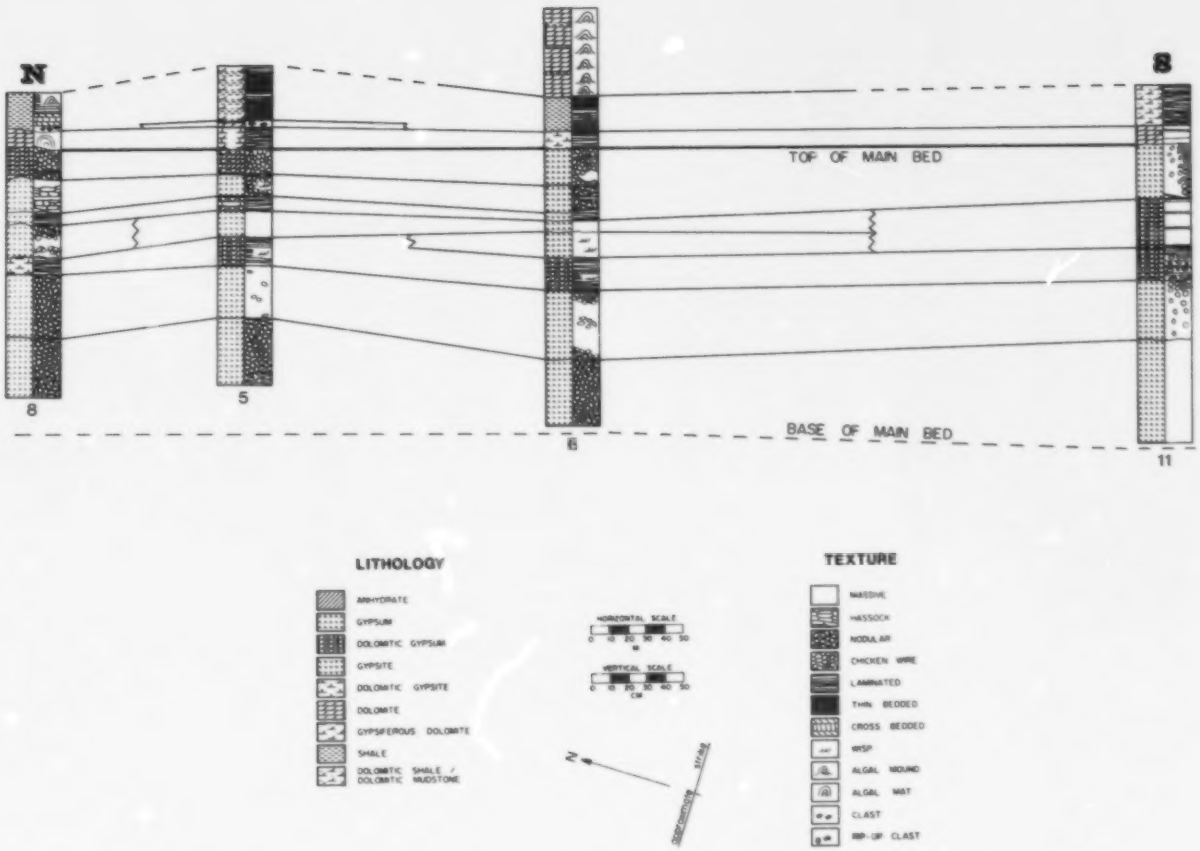

Figure 319.7. *North-south section of the Main Gypsum Bed, Westroc mine, illustrating down-dip variation of lithology and texture. Locations of underground sections are given in Figure 319.2.*

In summary, the Salina A Unit exposed underground at Westroc forms three separate cycles of subaqueous to subaerial conditions with a progressive increase in subaerial sediments from Cycle 1, at the base, to Cycle 3. This is accompanied by a progressive decrease in the thickness and gypsum content of the gypsum beds, from Cycle 1 to Cycle 3.

MAIN GYPSUM BED

The Main Gypsum Bed was mapped at 1:10 scale at 12 stations where the overlying units were exposed and the walls of the pillars could be cleaned. An overall compilation of the lithologies and textures of the Main Gypsum Bed is presented in Figure 319.3. The Main Gypsum Bed is composed of several units and subunits, of which the uppermost unit and the two lowermost units can be correlated throughout the mine. The central units correlate only over short distances. Changes of lithology and texture in the Main Gypsum Bed (and immediately overlying units) are shown in the fence diagram (Figure 319.5), an east-west (along strike) cross section (Figure 319.6), a north-south (down-dip) cross section (Figure 319.7), and a northwest-southeast (at right angles to the trend of the Algonquin Arch) section of the northwest part of the mine (Figure 319.8). These diagrams form the basis of the following description of the Main Gypsum Bed. The units were correlated on the basis of a combination of stratigraphic position, lithology and texture. The colour of different units served as a useful guide but cannot be used as a primary factor as colour changes (particularly from black to brown) may occur laterally within a few metres, and vertically within a few centimetres.

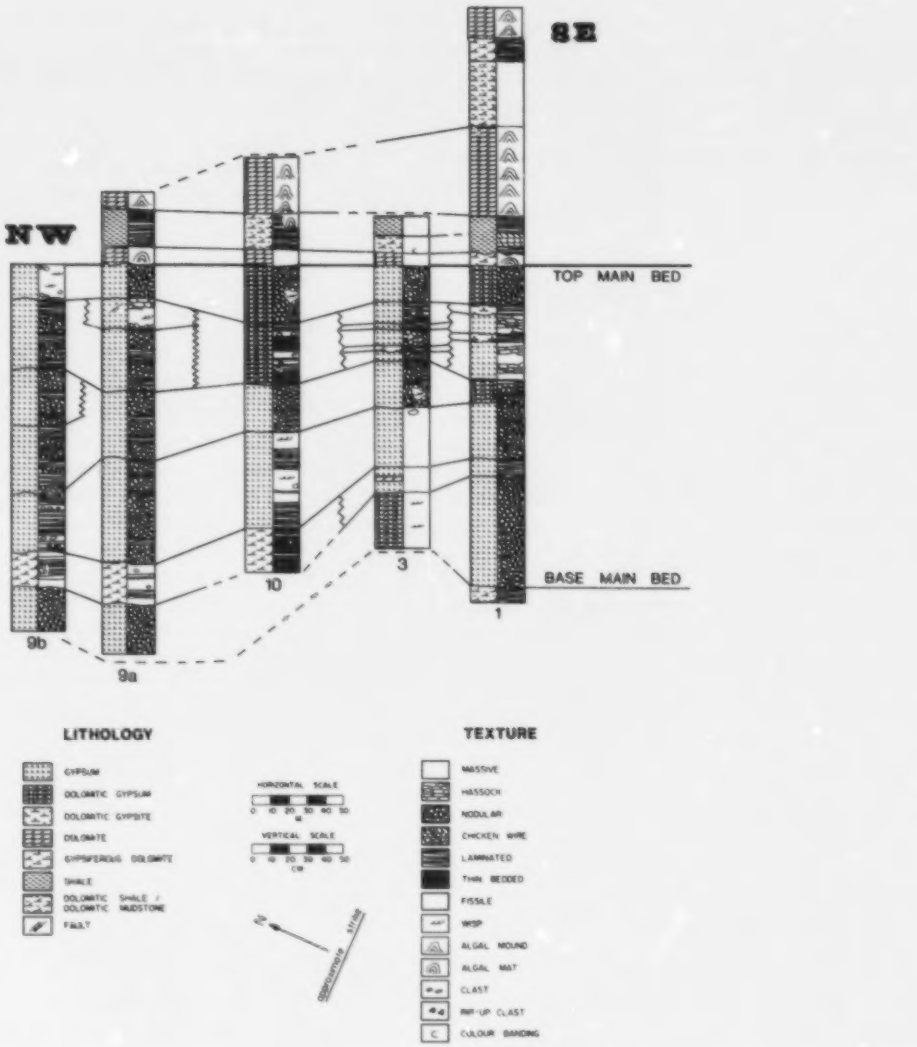

Figure 319.8. *Northwest-southeast section of the Main Gypsum Bed, northwest part of the Westroc mine, illustrating variation of lithology and texture away from the Algonquin Arch. Locations of underground sections are given in Figure 319.2.*

The two lower units are composed primarily of nodular gypsum. The basal unit ranges in thickness from 23 cm at Section 4, to 60 cm at Section 1, and 67 cm at Section 11; however, the base of this unit is only exposed at Section 1. In general, the basal unit appears as a distinctive layer of large white nodules set in a black to brown gypsum matrix. Variations from this occur in the central part of the mine: massive with minor nodules and dolomite laminations at Section 7; nodular and chicken-wire mosaic at Section 5; and massive with dolomite wisps at Section 3. In the northeast part of the mine, at Section 4, massive, nodular with laminations, and chicken-wire mosaic textures are present. At two localities (Sections 3 and 11), it is difficult to ascertain whether the texture is nodular or massive (as indicated on Figures 319.5, 319.7 and 319.8) due to lack of colour difference between possible nodules and matrix. Clastics are present in this unit in the northwest part of the mine at sections 9a and 9b. Section 9a contains silt and sand laminations; 9b contains mud laminations.

The unit above the basal unit consists of nodular gypsum, with white or brown nodules in a brown-grey-black gypsum matrix. Usually, it displays a mot-

tled or speckled appearance. The unit has an average thickness of 35 cm, ranging from 18 cm at Section 7, to 55 cm at Sections 9a and 10. At Sections 3, 5, 6 and 11, massive texture predominates over nodular. At Section 3, the gypsum is brown throughout this unit and textures are difficult to ascertain. North-south (down-dip) variation of this unit in the central area of the mine is shown in Figure 319.7: Section 5 comprises 28 cm of massive black gypsum, with occasional white nodules; Section 6, 38 cm of massive (black) and nodular (black with white nodules) gypsum; and Section 11, massive brown gypsum at the base and white nodules, in a brown gypsum matrix, at the top. In the northwestern part of the mine, white and brown laminations are present (Sections 1, 9a, 9b, and 10; Figures 319.2, 319.5, 319.6 and 319.8). This varies from complete lamination of the unit (Section 10), occasional lamination (Section 1), to alternating laminated and nodular layers (Sections 9a and 9b). Occasional enteroliths are present at Section 9a, and dolomite wisps at Sections 7 and 9a. Clastic lithologies are present in the laminated parts of this unit in the northwest of the mine; Section 9a has occasional silt and sand laminations. The presence of clastics, in the northwest part of the mine, corresponds with a general thickening of the Main Gypsum Bed and the appearance of an additional subunit between the two basal units of the Main Gypsum Bed at Sections 1, 3, 7, 9a, 9b and 10 (Figures 319.5, 319.6 and 319.8). This subunit consists of gypsiferous dolomite with mud laminations at Sections 9a and 9b, and dolomitic mudstone with minor gypsum at Section 10. Between Sections 10 and 7, there appears to be a facies change to laminated dolomitic gypsum, with occasional nodules. Laminated gypsum is present at Section 1 and massive gypsum, with a thin dolomite layer, at Section 3. The subunit pinches out eastward before Section 8.

The third unit from the base can be correlated over most of the mine, except the northeast part (Section 4). Average thickness is 22 cm, ranging from 9 cm at Section 8 to 37 cm at Sections 9a and 9b. In general, it consists of nodular or laminated brown gypsum/dolomitic gypsum, with white nodules in a brown gypsum matrix. Nodular gypsum is present at Sections 3 and 10, and nodular and laminated gypsum at Sections 9a and 9b. Dolomitic gypsum is present at Section 1 and 11 as nodules and laminations, at Sections 5 and 6 as laminations and wisps, and at Section 7 as alternating massive and laminated layers. Dolomitic gypsite (laminated) is present only at Section 8. Higher dolomite content of this unit (dolomitic gypsum and gypsite) appears to be located in a north-trending belt in the centre of the mine (Sections 1, 5, 6, 7, 8 and 11). A small algal dome of pink dolomite occurs in laminated gypsite at the locality where the floor of the Main Gypsum Bed has domed up and is underlain by pink algal dolomite (about 40 m west of Section 11). Also, thin layers of pink-brown dolomite (2 to 3 cm thick) are present near the base of laminated dolomite gypsum in the abandoned western part of the mine.

The units between the third unit up from the base and and the top unit are complex and correlate only over short distances (Figures 319.5, 319.6, 319.7 and 319.8). The total thickness of these central units averages 55 cm, ranging from 34 cm (at Section 5) to 87 cm (at Section 9a). A range of lithologies and textures form lensoid pods. At Section 9a, a fault is present. Dolomite near the fault is stylolitic. The unit below the fault is nodular and laminated gypsum, locally with silt and mud in the laminations and th matrix.

The top unit of the Main Gypsum Bed can be correlated throughout the mine. It consists of nodular gypsum with an average thickness of 22 cm, ranging from 14 cm at Section 5 to 32 cm at Sections 4 and 10. Colour varies from white to brown to black. Usually the lithology is gypsum but dolomitic gypsum occurs at Sections 1, 5 and 8, and dolomite wisps are present at Sections 7, 9a, 9b and 10. Texture varies from nodular to chicken-wire mosaic to massive. In some localities, e.g. Section 6, all three textures may be present. At Section 11, the texture changes laterally, within 0.5 m, from nodular gypsum (white nodules in a brown matrix) to massive brown gypsum (with occasional white nodules). As the transition zone is marked by a change in colour of the nodules from white through buff to brown, it is probable that the massive textures present in this unit (both here and elsewhere) are coalesced nodules of the same colour as the matrix gypsum. Blue gypsum is present at Section 6. Minor blue anhydrite occurs in dolomitic gypsum at Section 5.

In summary, the Main Gypsum Bed consists of gypsum, dolomitic gypsum and gypsite, with an average grade of 88% gypsum. Within the limits of the active mine workings (up to March 1989), the Main Gypsum Bed exhibits a general westward thickening from 1.5 m in the east to 2.1 m in the west. The bed appears to thin to about 1.5 m in the abandoned area at the western border of the mine (Figure 319.2), although unsafe conditions prevented detailed observations. Fewer, but thicker, units tend to occur in the west and south of the mine, while there are more, but thinner, units in the east. However, an additional subunit associated with an influx of clastic sediments in the basal units, is present in the west part of the mine, separating the two basal units. The texture of the Main Gypsum Bed is chiefly nodular, but laminated, massive and chicken-wire mosaic textures are present. Dolomite wisps and enteroliths are rare. The only units of the Main Gypsum Bed that can be correlated throughout the mine are the top unit of nodular/chicken-wire mosaic/massive gypsum and the two basal units of nodular/massive/laminated gypsum. The third unit from the base can be correlated across the mine, with the exception of the

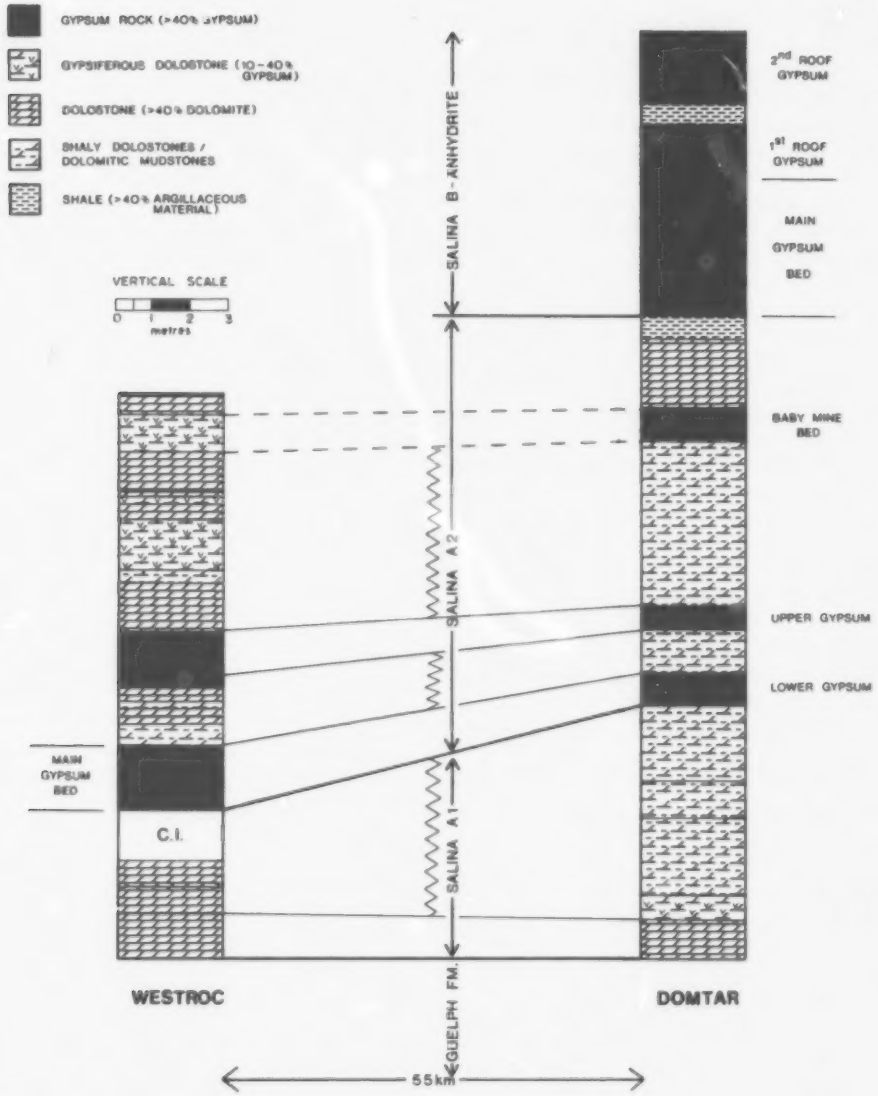

Figure 319.9. *Stratigraphic correlation of the major gypsum beds at the Domtar and Westroc deposits.*

northeastern corner. In the south, and the abandoned west parts of the mine, pink-brown dolomite occurs in this unit as thin layers and an algal mound within laminated gypsum/gypsite. Within the four correlatable units, textural variations are more pronounced along strike (east-west) than down-dip. The central units correlate only over short distances; the different lithologies forming lenses or pods with a wide variation of texture.

STRATIGRAPHIC COMPARISON OF THE DOMTAR AND WESTROC DEPOSITS

In previous publications on the Domtar deposit (Haynes *et al.* 1988, and in press), information on the Salina A Unit was available only from drill cores. However, recent tunnelling operations for the new Mine 3 access has exposed units underlining the Main Gypsum Bed (Salina B anhydrite), to about 1 m below the Salina A-1/A-2 contact. This has allowed for more detailed comparison of the Salina A-2, and the top of the Salina A-1, to be made between Westroc and Domtar (Figure 319.9).

The base of the Salina A-2 is the base of the Main Gypsum Bed at Westroc and the base of the Lower Gypsum at Domtar (Figure 319.9). The Lower Gypsum at Domtar is about 0.9 m thick (0.75 to 1.70 m) and is characterized by bands of lenticular nodules (2–4 cm thick) within a laminated

gypsite. The laminated gypsite consists of laminae (about 5 cm thick) of brown gypsiferous dolomite interspaced with white gypsum. The basal 14 cm comprises nodular to massive gypsite, with lenticular nodules (up to 8 cm in thickness) in a dark-brown gypsiferous dolomite matrix. Dark layers of laminated dolomitic mudstone/gypsiferous dolomite, about 4 cm thick, are present in the upper part of the Lower Gypsum. In the access tunnel, the Lower Gypsum is underlain by about 30 cm of grey to brown dolomite, then 9 cm of nodular to massive gypsum. This is followed, to the floor of the tunnel, by a 0.8 m sequence of grey, green and brown dolomitic mudstones with thin layers and lenses of nodular gypsum, and numerous satin spar seams. A similar sequence of dolomite mudstones overlays the Lower Gypsum and continues to the Baby Mine Bed. These mudstones enclose the Upper Gypsum (Figure 319.9), which consists of 0.35 to 0.65 m of nodular and laminated gypsite similar to the Lower Gypsum. The Baby Mine Bed is a remarkably uniform bed (0.88 to 1.04 m thick) of nodular gypsum, consisting of large white gypsum nodules (often coalesced) in a minor matrix of brown dolomitic mudstone. It is overlain by about 1.80 m of thinly laminated dolomite and dolomitic mudstone, containing numerous gypsum laminae.

Except for the basal dolomites, the Salina A Unit at Westroc is considerably different from that at Domtar (Figure 319.9). The Salina A-1 comprises massive colour-banded dolostones at Westroc, but laminated dolomitic mudstones at Domtar. The Main Gypsum Bed at Westroc can be correlated with the Lower Gypsum at Domtar, although they differ in thickness, gypsum content, and texture: about 1.5 m, mainly nodular gypsum, at Westroc; about 0.9 m, mainly laminated gypsite, at Domtar.

The Salina A-2 above the Main Gypsum Bed at Westroc consists of a complex sequence of algal dolomites, argillaceous to arenaceous clastics, stromatolitic dolomites, gypsiferous mudstones, gypsum and thinly interbedded dolomites and anhydrite. At Domtar, the equivalent stratigraphic interval is the essentially continuous sequence of dolomitic mudstones, described above. The Upper Gypsum bed at Domtar can be correlated with a gypsum bed at Westroc (Figure 319.9), although differences in thickness, gypsum content and texture are comparable to those between the Lower Gypsum (Domtar) and the Main Gypsum Bed (Westroc).

As the Salina B anhydrite (Main Gypsum Bed at Domtar) is not exposed at Westroc, the upper lithologies of the Salina A-2 Unit at Domtar (Baby Mine Bed to Main Gypsum Bed) can not be correlated directly with those at Westroc.

DISCUSSION AND CONCLUSIONS

The Salina A Unit at Westroc can be divided into three sedimentary cycles (Figures 319.4 and 319.10). The mined gypsum bed (Main Gypsum Bed) marks the termination of the first cycle. Lithologies and textures of the gypsum, and the immediately underlying and overlying host rocks, indicate that it was probably deposited in the shallow subaqueous environment of either a coastal salina, or a hypersaline lagoon, as described by Warren (1989). This coastal salina was developed on a substrate of Salina A-1 dolomites. These probably represent continued erosion of emergent pinnacle reefs as they are very similar to the inter-reef facies of the immediately underlying Guelph Formation. The top of the gypsum is marked by a laterally consistent pink-brown algal dolomite. This is similar to the algal and veneer boundstones that prograde across the modern coastal salinas of South Australia, during their final stages (Warren 1982).

The second cycle (Figures 319.4 and 319.10), commences with erosion and oxidation of the algal/veneer boundstone. This is followed by a sequence of sediments that can by equated with fluvial channelways, growth of stromalites, and deposition of lacustrine muds at the margins of a salina. The cycle closes with deposition of gypsum in a shallow subaqueous environment (using the criteria given in Warren 1989). Whether this was a coastal salina or lacustrine salina could not be determined.

The third cycle (Figures 319.4 and 319.10), commences with desiccated mudflats and stromatolitic dolomites that probably represent the shoreward fringe of a lagoon or coastal lake. This is followed by a sequence of dolomitic mudstones suggestive of lagoonal or lacustrine mudflats. These pass upward into a series of argillaceous and gypsiferous dolostones that are overlain by dolomite. The third cycle finishes with a sequence of thin-bedded dolomite and anhydrite displaying enterolithic textures. The textures of this final unit indicate deposition in the vadose and shallow phreatic conditions of the supratidal zone of a coastal sabkha (using the criteria of Warren 1989). The underlying unit was probably deposited as a mixture of subtidal and intertidal sediments at the sabkha-lagoon interface.

Three sedimentary cycles, each terminating with gypsum, also constitute the Salina A Unit at Domtar (Figure 319.10). However, the Salina A succession at Domtar is characterized by deeper-water shelf or lagoonal environments: each cycle commencing with a thick sequence of muds and terminating with laminated gypsite (intercalated layers of nodular gypsum and dolomite mud).

The upward change, from shallow water facies (salinas) to subaerial facies (sabkhas), at Westroc is identical to the modern gypsum-depositing environment on the coast of South Australia (Warren 1989). In contrast, the lagoonal facies of the Salina A Unit at Domtar are similar to modern deposition of gypsum in the hypersaline lagoons and coastal lakes about the Nile delta of northern Egypt (Levy 1980; West *et al.* 1983). Furthermore, the separa-

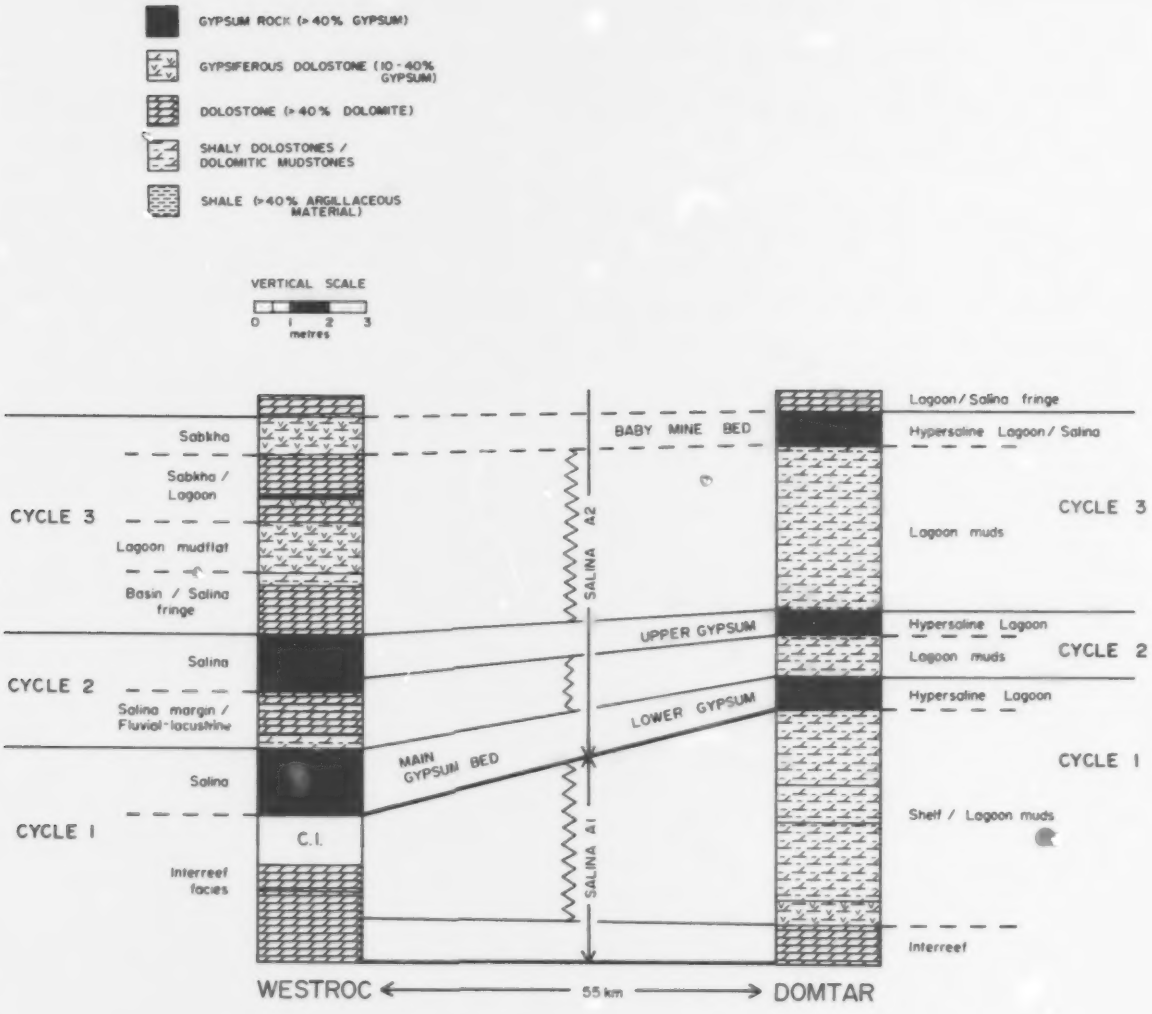

Figure 319.10. *Correlation of probable depositional environments in the Salina A Unit at the Domtar and Westroc deposits.*

tion of Domtar and Westroc by 55 km is comparable with distances along the coast of northern Egypt between lagoons/coastal lakes (e.g., Lake Maryut) and adjacent coastal salina/sabkha settings (e.g., El-Alamein lagoons). Although the Salina B anhydrite (the Main Gypsum Bed at Domtar) is not exposed at Westroc, this study provides further evidence that the modern analogue for the Salina Formation, across the Algonquin Arch, is the coast of northern Egypt, as previously suggested by Haynes *et al.* (1988, and in press).

ACKNOWLEDGMENTS

We are especially grateful to Kirk Scheifele (Operations Manager), Westroc Industries Ltd., who not only interrupted his busy operations schedule by allowing us to map the base of the shaft, and providing staff when needed, but also showed an active interest in our studies. Mike Lozon is thanked for the considerable work required in drafting the diagrams. Frances Citrigno and Wendy Morris are thanked for word processing the text.

REFERENCES

Carter, T.

1987: A Comparison of the Middle Proterozoic Balmat Evaporite Sequence with Niagaran and Cayugan Strata in the Michigan–Appalachian Basin; Proceedings of the Ontario Petroleum Institute, Twenty Sixth Annual Conference, p.1-42.

Evans, C.S.

1950: Underground Hunting in the Silurian of Southwestern Ontario; Proceedings of the Geological Association of Canada, Volume 3, p.55-85.

Haynes, S.J., Boland, R. and Hughes-Pearl, J.

1988: Gypsum Deposits of Southern Ontario; p.217-230 *in* Geoscience Research Grant Program, Summary of Research 1987-88, edited by V.G. Milne, Ontario Geological Survey, Miscellaneous Paper 140, 251p.

In Press: Depositional Setting of Gypsum Deposits, Southwestern Ontario: Domtar Mine; Economic Geology.

Hartviksen, R.C.

1983: Development of the Drumbo Mine: A New Gypsum Mine in Ontario; Canadian Institute of Mining and Metallurgy, Bulletin, Volume 76, Number 849, p.79-82.

Landes, K.K.

1945: The Salina and Bass Island Rocks in the Michigan Basin; United States Geological Survey, Oil and Gas Inventories, Preliminary Map 40, scale 1 inch to 23 miles.

Levy, Y.

1980: Evaporitic Environments in Northern Sinai; p.131-143 *in* Hypersaline Brines and Evaporitic Environments, Elsevier, New York.

McKnight, R. and Fell, V.

1989: Mineral Production in Ontario; COMDA Review, Communications Branch, Energy Mines and Resources Canada, and Ontario Ministry of Northern Development and Mines, Toronto, Volume 2, Number 2, 2p.

Warren, J.K.

1982: The Hydrological Significance of Holocene Tepees, Stromatolites, and Boxwork Limestones in Coastal Salinas in South Australia; Journal of Sedimentary Petrology, Volume 52, p.1171-1201.

1989: Evaporite Sedimentology; Prentice Hall, Englewood Cliffs, New Jersey, 285p.

West, I., Ali, Y.A. and Hilmy, M.E.

1983: Facies Associated with Primary Gypsum Nodules of Northern Egyptian Sabkhas; Sixth Symposium on Salt, Northern Ohio Geological Society, Volume 1, p.171-183.

Grant 322 Subaqueous Volcaniclastic Rocks of the Confederation Lake Area, Northwestern Ontario: Discrimination between Pyroclastic and Epiclastic Emplacement

John Stix and Michael P. Gorton

Department of Geology, University of Toronto, Toronto

ABSTRACT

A sequence of Archean, subaqueous volcaniclastic rocks outcrops in Lost Bay, Confederation Lake, in northwestern Ontario. The deposits occur within Thurston's Cycle II metasupracrustal rocks. The rocks consist dominantly of intermediate to felsic lapilli tuff, tuff breccia, tuff, and fine-grained epiclastic rocks that have a strong turbidite association; minor lavas are also present.

The coarse-grained rocks are volcaniclastic mass flow deposits that are massive, matrix-supported, and consist of light coloured clasts set in a darker matrix rich in crystals, and juvenile and lithic fragments. Juvenile clasts consist of andesitic, pumiceous and dense fragments that exhibit a range of vesicularities and may represent a continuum. Quartz-feldspar porphyry fragments with highly enriched trace element compositions are found within lapilli tuff and tuff breccia near the top of the Cycle II strata. The andesitic composition, abundant unvesiculated and pumiceous clasts, and relatively thin flow deposits characteristic of the coarse rocks imply dome growth and fragmentation. Dome growth and eruptions may have been subaqueous as well.

Turbiditic, fine-grained rocks outcrop in much of Lost Bay. The rocks range from very fine-grained, cherty tuff to coarse-grained clastic deposits. Many of the very fine-grained units lack quartz, while coarser-grained, volcaniclastic rocks may contain as much as 15% detrital quartz. Both massive and bedded units are present. Normal grading, Bouma sequences, convoluted bedding, rip-up clasts, and flame structures are common. The units lack sedimentary structures indicative of deposition above wave base. Detrital quartz within the coarser grained deposits may have been derived from the reworking of quartz-feldspar porphyry fragments in the lapilli tuff and tuff breccia. These quartz-rich units thus appear epiclastic, not pyroclastic.

INTRODUCTION

A sequence of Archean metavolcanic and metasedimentary rocks outcrops in and around Confederation Lake, northwestern Ontario (Figure 322.1). The area is located in the Uchi Subprovince of the Superior Province. The metasupracrustal rocks are bounded to the south by the English River Subprovince, to the north by the Berens Subprovince, and to the east and west by granitoid batholiths within the Uchi Subprovince. The supracrustal package is generally metamorphosed to greenschist facies.

Thurston (1985) has interpreted the structure in the Confederation Lake area as a broad synclinorium within which the metasupracrustal rocks have been folded. Within this synclinorium Thurston (1985) mapped and described three major mafic to felsic cycles. Each cycle begins with basalt and an-

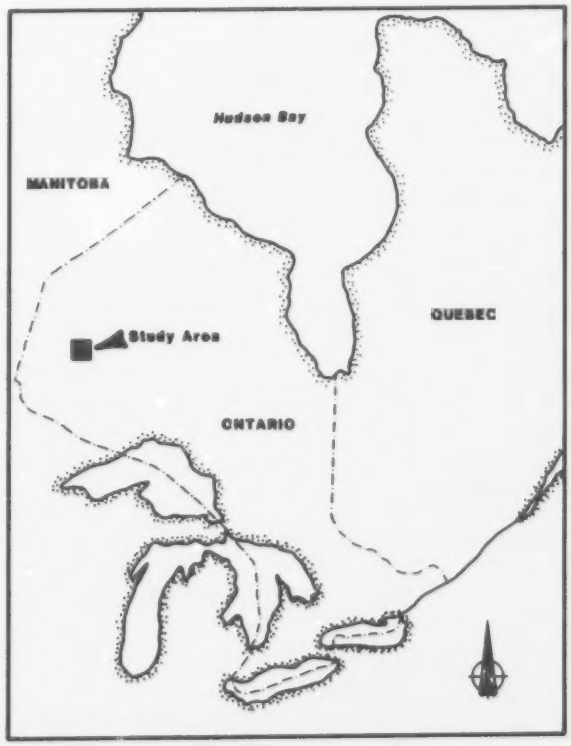

Figure 322.1. *Map showing the location of the study area in northwestern Ontario.*

desite lava flows at the base, followed up-section by andesitic and rhyolitic pyroclastics and minor lava flows. Nunes and Thurston (1980) dated Cycle I at 2959 Ma, Cycle II at 2794 Ma, and Cycle III at 2739 Ma. Thurston (1980, 1985) interpreted these cycles in terms of caldera development. Cycle I represents the platform stage, Cycle II the early stages of caldera development, and Cycle III the central graben of a caldera, post-caldera resurgent volcanism, and late-stage hydrothermal activity and ore deposition.

This paper discusses the subaqueous pyroclastic and epiclastic deposits of Cycle II in Lost Bay east of Thurston's (1985) synclinorium axis. This study examines 1) facies relations of volcaniclastic rocks in Lost Bay, 2) eruptive and depositional environments, 3) transport of pyroclastic and epiclastic debris, 4) reworking and mixing of the volcaniclastic material, and 5) the application of lithofacies codes for descriptive mapping and genetic interpretation (Stix and Gorton 1988; Stix, in preparation).

This work will provide a better understanding of 1) intermediate to silicic explosive subaqueous volcanism, 2) differences between subaerial and subaqueous pyroclastic and epiclastic deposits, 3) reworking and redeposition of pyroclastic debris in the subaqueous environment, and 4) silicic subaqueous volcanism with respect to massive sulphide deposition.

CYCLE II PYROCLASTIC AND EPICLASTIC DEPOSITS IN LOST BAY

Metasupracrustal rocks in Lost Bay strike north-northeast, dip steeply to the east, and have stratigraphic tops to the west. The rocks are thus slightly overturned. The Lost Bay package appears to be a homoclinal sequence.

Thurston (1985) has divided Cycle II rocks into five informal formations (Table 322.1). Formations E and F at the base consist primarily of mafic and intermediate lava flows. Formations G and H are composed dominantly of intermediate and felsic lapilli tuff, respectively. Formation J at the top of Cycle II consists of marble, chert, and iron formation.

This paper focusses upon the pyroclastic and epiclastic rocks of formations G and H in Lost Bay. The rocks are highly pumiceous andesites to rhyolites. At least seven sequences of unbedded lapilli tuff and tuff breccia grade upward into bedded finer-grained material (Thurston 1985). There are likely many more. The contact between formations G and H in Lost Bay is marked by the abrupt appearance of 1) abundant quartz-feldspar porphyry clasts and 2) pyroclastic and epiclastic rocks with high trace-element contents (Table 322.2). Thurston (1985) has tentatively correlated these rocks with those at Narrow and Mosier lakes to the west of the synclinorium axis which may be more proximal deposits. He has suggested these sequences are products of pyroclastic flow eruptions.

LOST BAY: MINOR LITHOLOGIES

MAFIC TO INTERMEDIATE LAVA, HYALOCLASTITE AND INTRUSIVE ROCKS

Basaltic andesites at the top of formation F outcrop along the eastern shores of Lost Bay. These rocks are flows and, in the northeastern corner of Lost Bay, hyaloclastite. The hyaloclastite is poorly sorted and framework-supported. The majority of fragments exhibit marginal quenching (Photo 322.1a). Some fragments are vesicular. The fine-grained material may represent unrimming of the margins of the larger fragments (Photo 322.1b). A few fragments show pseudo-pillow shapes with angular forms and unquenched rims.

The above evidence suggests these rocks are products of subaqueous, fire fountaining at relatively shallow depths (Carlisle 1963; Schmincke *et al.* 1983). Fire fountaining implies high rates of extrusion. The lack of tapered ballistic fragments indicates rapid quenching and/or low height of fountaining. A continuum may exist between hyaloclastites from fire fountaining and pillow breccias and may depend upon the rate of extrusion, depth of eruption, and volatile content of the magma. High erup-

TABLE 322.1. CYCLE II FORMATIONS AND LITHOLOGIES.

Formation (informal)	Lithology
J	marble; chert; iron formation
H	felsic lapilli tuff, tuff, tuff breccia; porphyritic flows
G	intermediate lapilli tuff, tuff, tuff breccia; lapillistone; metasediments
F	mafic flows; felsic tuff; mafic hyaloclastite
E	mafic, intermediate flows; intermediate, felsic tuff; chert; iron formation

Modified from Thurston (1985)

TABLE 322.2. TRACE ELEMENT GEOCHEMISTRY OF SELECTED LITHOLOGIES, LOST BAY.

Lithology	Zr (ppm)	Y (ppm)
Quartz-feldspar porphyry clast, formation H	511	100
White vitric tuff, base of formation G	132	6
Average of 3 very fine-grained, tuffaceous rocks, formation G	168	11
Average of 3 coarse-grained, quartz-bearing rocks, formation H	556	139

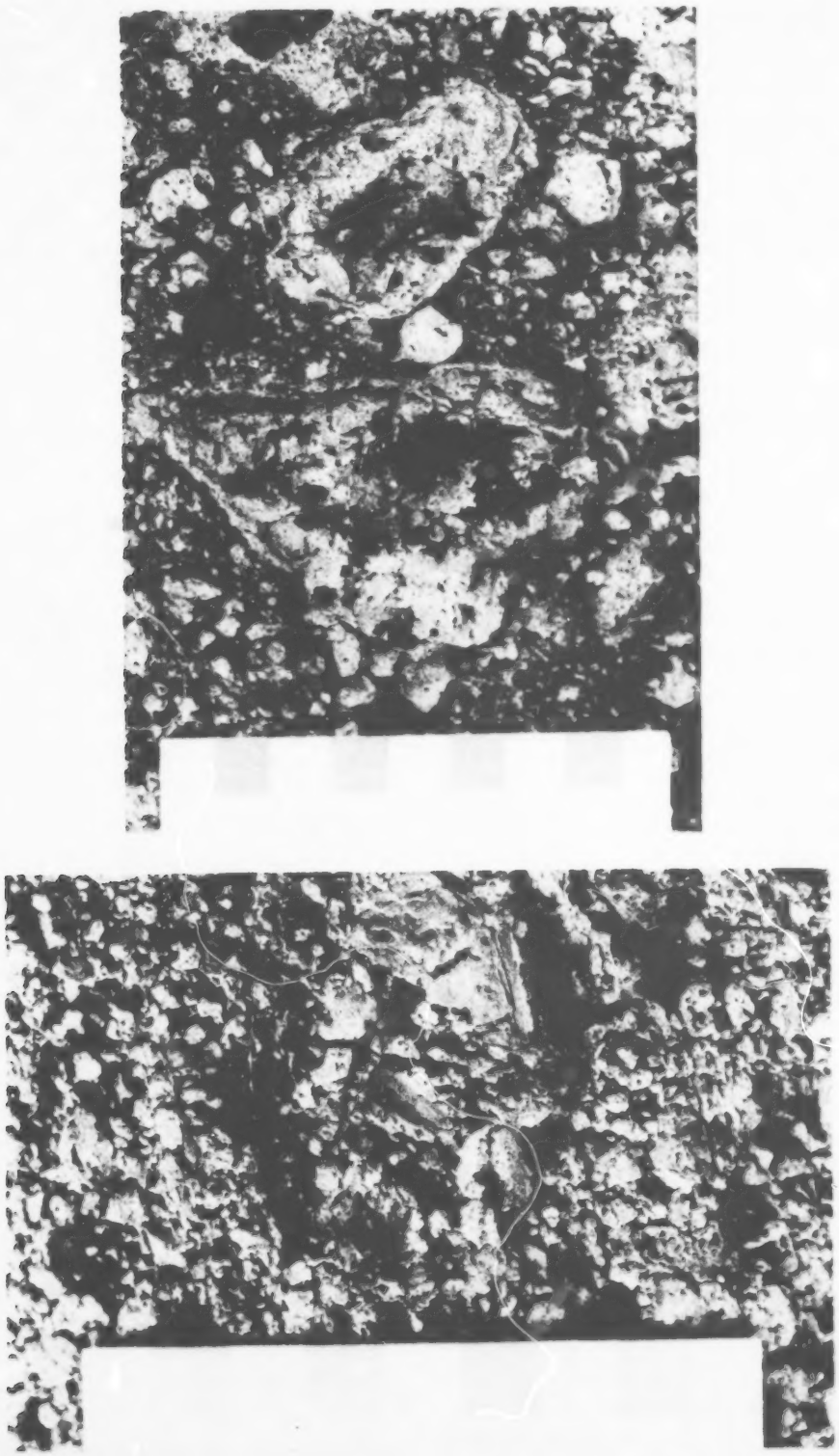

Photo 322.1. *Hyaloclastites with poorly sorted fragments that show marginal quenching.* **(a)** *Globular, partly rounded fragments that have distinct rims which were once glassy. The clasts do not resemble broken pillows.* **(b)** *Quenched, finer grained fragments that probably spalled off from the larger clasts.*

tion rates, shallow depths, and high volatile contents may favour fire fountaining, while lower eruption rates, greater depths, and lower volatile contents may result in pillow lavas and their associated breccias.

Mafic and ultramafic intrusive rocks also outcrop in the northeast corner of Lost Bay at the top of formation F and at the base of formation G. These consist of pyroxenite, gabbro, and diorite which may represent variably fractionated layered intrusions.

Oxide-facies iron formation, chert, and wackes of formation J outcrop in the southwest corner of Lost Bay at the top of Cycle II. These deposits appear to indicate a hiatus in volcanism between Cycle II and the overlying basalts of Cycle III.

LOST BAY: MAJOR LITHOLOGIES

LAPILLI TUFF AND TUFF BRECCIA

Lapilli tuff and tuff breccia of formations G and H are ubiquitous within Lost Bay. The rocks are generally massive, matrix-supported, and consist of light coloured clasts set in a darker matrix rich in crystals, and juvenile and lithic fragments. The deposits frequently are capped by fine-grained debris. Individual beds may be ungraded, normally graded, and/or inversely graded. These observations, as well as the turbidite association (see below), suggest the units are subaqueous, pyroclastic and/or epiclastic, mass flow deposits. Interbedded coarse-grained and fine-grained deposits with convoluted bedding outcrop in the southeast corner of Lost Bay, indicating mixing with water and rapid deposition with little time for dewatering.

Juvenile clasts consist of andesitic pumiceous and dense fragments that exhibit a range of vesicularities and may represent a continuum (Photo 322.2). In certain cases the colour of a fragment may be correlated with its original vesicularity. Darker, greener clasts indicate relatively high chlorite contents in amygdules and thus relatively high vesicularity. Lighter-coloured fragments are more dense and have lower vesicularities. On occasion rounded quartz grains fill vesicles instead of chlorite. The range of vesicularities of clasts and their andesitic composition may indicate an origin by dome growth and fragmentation, possibly partly phreatomagmatic.

Quartz-feldspar porphyry fragments with highly enriched trace element compositions (Table 322.2) are found within lapilli tuffs and tuff breccias of formation H near the top of Cycle II stratigraphy. These fragments are very rare in formation G, stratigraphically beneath formation H. It is difficult to determine whether these fragments are juvenile or lithic, and whether they represent eruption from new source volcanic domes and/or unroofing of hypabyssal intrusions.

TUFF AND FINE-GRAINED EPICLASTIC ROCKS

Turbiditic fine-grained grey rocks outcrop in much of Lost Bay. They are particularly abundant along the north shore of the bay. The rocks range from very fine-grained cherty tuff to coarse-grained tuff. Many of the very fine-grained units lack quartz, while coarse-grained tuffs may contain as much as 15% detrital quartz. The deposits are both massive and bedded. Normal grading, Bouma sequences, convoluted bedding, rip-up clasts, and flame structures are common (Photo 322.3). The units lack sedimentary structures indicative of deposition above wave base. Based on this evidence, these rocks have a clear turbidite association. The fine-grained units commonly outcrop above lapilli tuff and tuff breccia mass flow deposits, and the fine-grained material may be genetically related to the coarser units. However, it is usually extremely difficult to differentiate fine-grained, primary pyroclastic material from fine-grained epiclastic debris.

An unusual sequence of tuffs outcrops at the base of formation G in the northeast corner of Lost Bay. A series of very fine-grained, very finely laminated cherty white tuff bands, ranging in thicknes from less than 1 cm to more than 10 cm thick, is interbedded within grey fine-grained tuffaceous material. At least 20–30 individual tuff bands are exposed. These appear to be distal, fallout vitric tephras that have not undergone significant reworking. Their chemistry thus may represent that of the original magma. The tuffs have extremely low trace element contents (Table 322.2).

Along the north shore of Lost Bay, there are abundant fine-grained deposits that change in character up-section. Within formation G very fine-grained clastic rocks outcrop that generally lack quartz and have relatively low trace element concentrations similar to the white fallout tephras already described. Stratigraphically above and within formation H these deposits give way to coarser tuffs that contain abundant detrital quartz and have much higher trace element contents (Table 322.2). This change occurs at approximately the same stratigraphic level as the first appearance of abundant quartz-feldspar porphyry fragments, with similarly high trace element contents (Table 322.2), in the lapilli tuffs and tuff breccias. These observations indicate that detrital quartz within the fine-grained deposits may have been derived from the reworking of quartz-feldspar porphyry fragments. These quartz-rich, fine-grained units thus appear to be epiclastic, not pyroclastic.

INTERMEDIATE TO SILICIC LAVAS (?)

A series of enigmatic rocks outcrop in the southwestern part of Lost Bay at the top of formation G and within formation H. They are very fine grained, es-

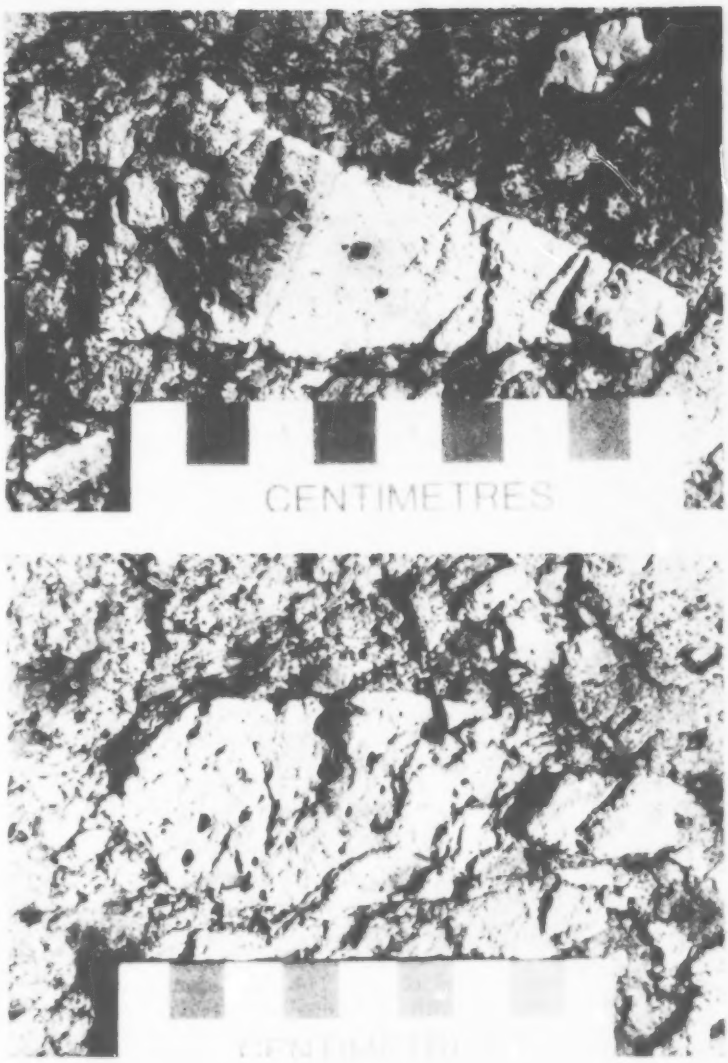

Photo 322.2. *Fragments that exhibit a range of vesicularities within lapilli tuffs and tuff breccias:* (a) *dense, angular fragment;* (b) *slightly vesiculated clast;* (c) *pumiceous, rounded fragment.*

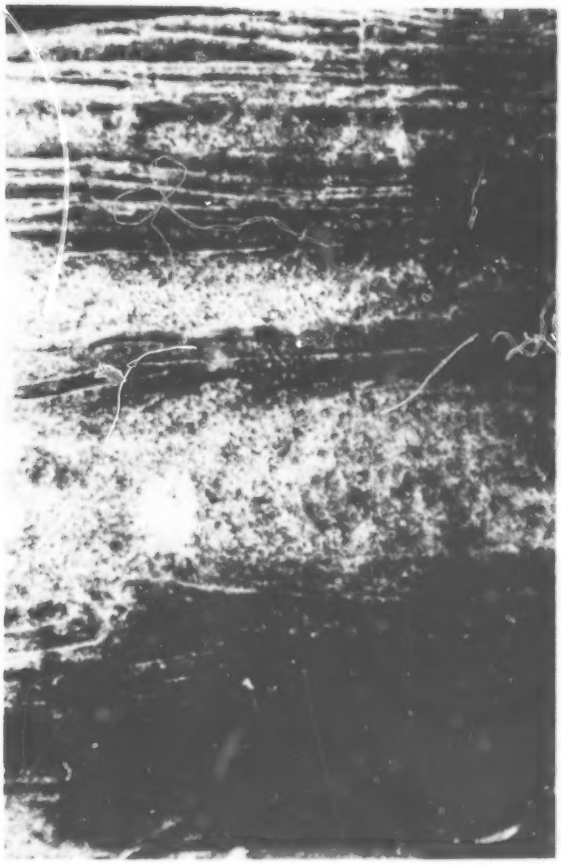

Photo 322.3. *Massive, graded and finely laminated turbidites that exhibit convoluted bedding and flame structures.*

sentially aphyric, very dark grey in colour, and contain spherulites in places. These deposits may be intermediate to silicic lavas, but the rocks are relatively highly sheared and preserved primary textures are rare. Quartz veins, sulphide mineralization and possible autoclastic breccias also are exposed. In places dense white rock outcrops, which may represent chert, hydrothermally altered rock, and/or dense unvesiculated lava. The evidence above may indicate proximity to a vent area.

DETAILED EXAMINATION OF VOLCANICLASTIC FLOW DEPOSITS IN LOST BAY

We have measured six detailed stratigraphic sections in Lost Bay, ranging in thickness from 2.1 to 10.2 m, that are representative of the pyroclastic and epiclastic rocks observed in the area (Figure 322.2). These sections provide detailed information about vertical and lateral facies changes and clues as to the eruptive and transport history of the deposits.

SECTIONS 1, 2, 3

Because Sections 1, 2, and 3 are at similar stratigraphic levels near the base of formation G (Figure 322.2a-c), they may be correlative. However, no marker beds exist to make firm connections between sections. All deposits are highly pumiceous but lack quartz-feldspar porphyry fragments.

Section 1 is pumiceous. The fragments have a range of vesicularities, suggesting incomplete vesiculation and retention of volatiles, possibly by quenching with water. In addition, highly vesiculated (>60% vesicles) pumices are absent, which may indicate flotation and loss of this material. This also implies subaqueous eruption.

The basal lapilli tuff unit at 0–1 m in Section 2 is inversely graded with the largest pumices in the top 20 cm. Coarse units in Section 2 are separated by laminated fine-grained beds. The uppermost unit at 1.5–2.6 m consists of alternating beds of well bedded lapilli tuff, suggesting segregation of material within one flow and/or discrete pulses of debris. The lack of associated fine-grained material indicates little time for fine-grained sediment to accumulate between coarser grained flows.

Coarse-grained units in Section 3 are separated by fine-grained material. The lapilli tuffs at 1.2–2.2 m are pumiceous but also contain fragments with a range of vesicularities.

SECTION 4

Section 4, located near the base of formation H, is the thickest section measured (Figure 322.2d). It consists almost entirely of lapilli tuff; very little fine-grained material is present. The beds are composed of lapilli stringers with rapidly alternating grain sizes over 20 cm or less. The clasts consist of rounded pumices with a range of vesicularities (Photo 322.4a). The pumices are not highly vesicular (<60% vesicles), suggesting flotation and loss of these fragments from the flow or flows. The pumices are relatively large (maximum 19 cm diameter) and are inversely graded in certain units (Photo 322.4b). There are also abundant quartz-feldspar porphyry fragments present. The unit at 5.65–6.2 m contains quartz-feldspar porphyry fragments that are ungraded and pumices that are clearly inversely graded, possibly because of their low bulk density compared to that of the quartz-feldspar porphyry clasts and the flow itself.

It appears very unlikely that this section represents one large flow unit because of the numerous grain size changes vertically, the inverse grading of pumices and concentrations of quartz-feldspar porphyry fragments within discrete units. The section more likely represents a series of flows. The lack of fine-grained material suggests that these flows were pulses of coarse fragmental debris deposited in rapid succession. The presence of inversely graded pumices also may indicate rapid deposition without suffi-

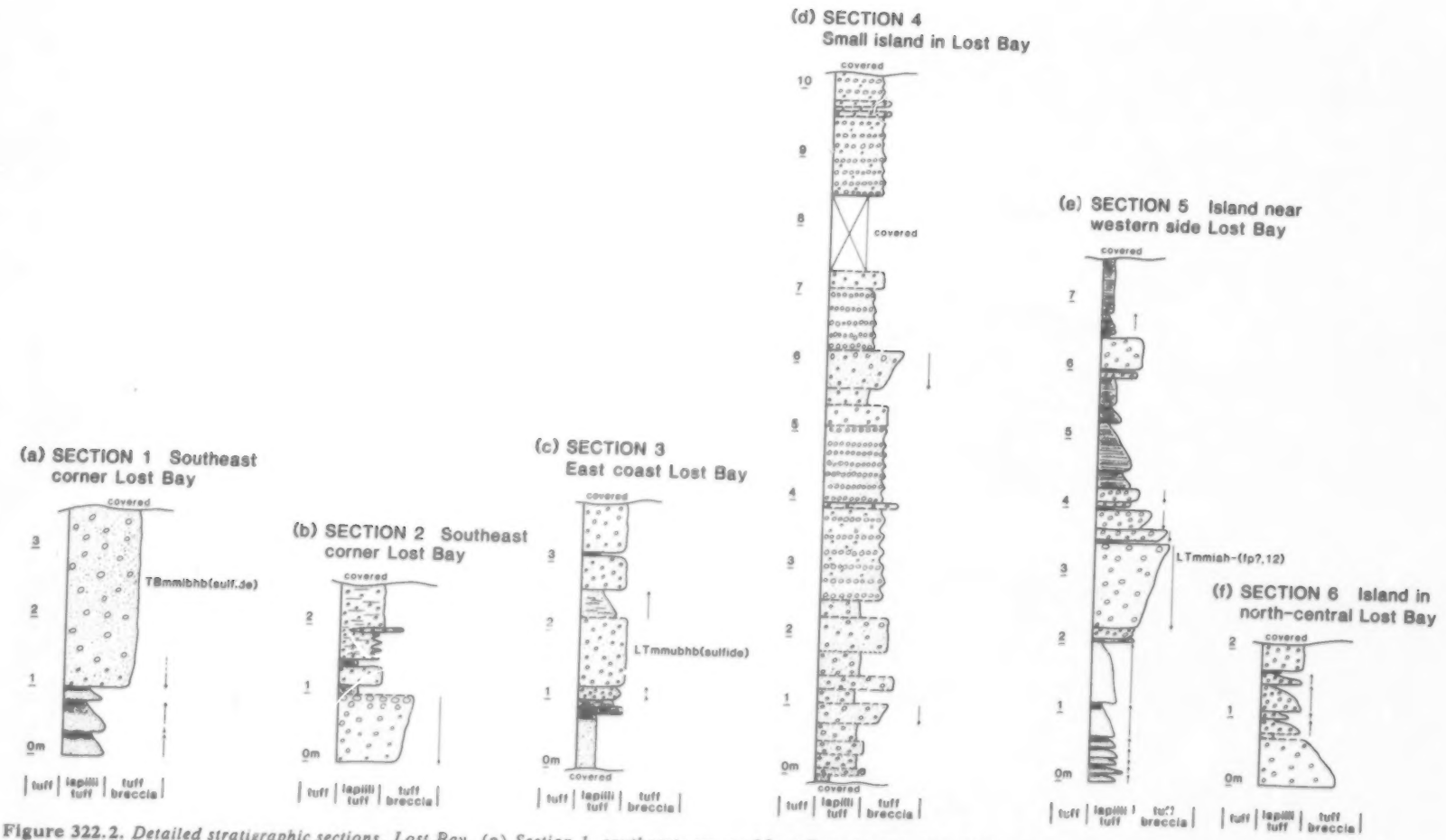

Figure 322.2. *Detailed stratigraphic sections, Lost Bay.* (a) *Section 1, southeast corner of Lost Bay. A series of turbidites are overlain by a tuff breccia, inversely graded at the base. The tuff breccia is classified with the lithofacies code TBmmibhb(sulphide) (Stix and Gorton 1988). Sections 1-3 are at approximately the same stratigraphic level.* (b) *Section 2, southeast corner of Lost Bay. An inversely graded tuff breccia is overlain by a series of well bedded lapilli tuffs.* (c) *Section 3, east coast of Lost Bay. A sequence of alternating fine-grained and coarser-grained rocks is displayed. The lapilli tuff unit at 1.2–2.2 m is coded LTmmubhb(sulphide).* (d) *Section 4, small island in Lost Bay. A thick sequence of comparatively well bedded, alternating lapilli tuffs and tuff breccias suggests rapid pulses of deposition. This section lacks fine-grained material. The unit at 5.65–6.2 m contains rounded pumices that are inversely graded (see Photo 322.4).* (e) *Section 5, island near the western side of Lost Bay. This section is noted for its normally graded turbidites at the base, overlain by inversely graded lapilli tuffs and tuff breccias at 2.25–4.3 m that become finer grained up-section and are capped by doubly-graded, fine-grained deposits.* (f) *Section 6, island in the north-central part of Lost Bay. The sequence consists of normally graded lapilli tuffs.*

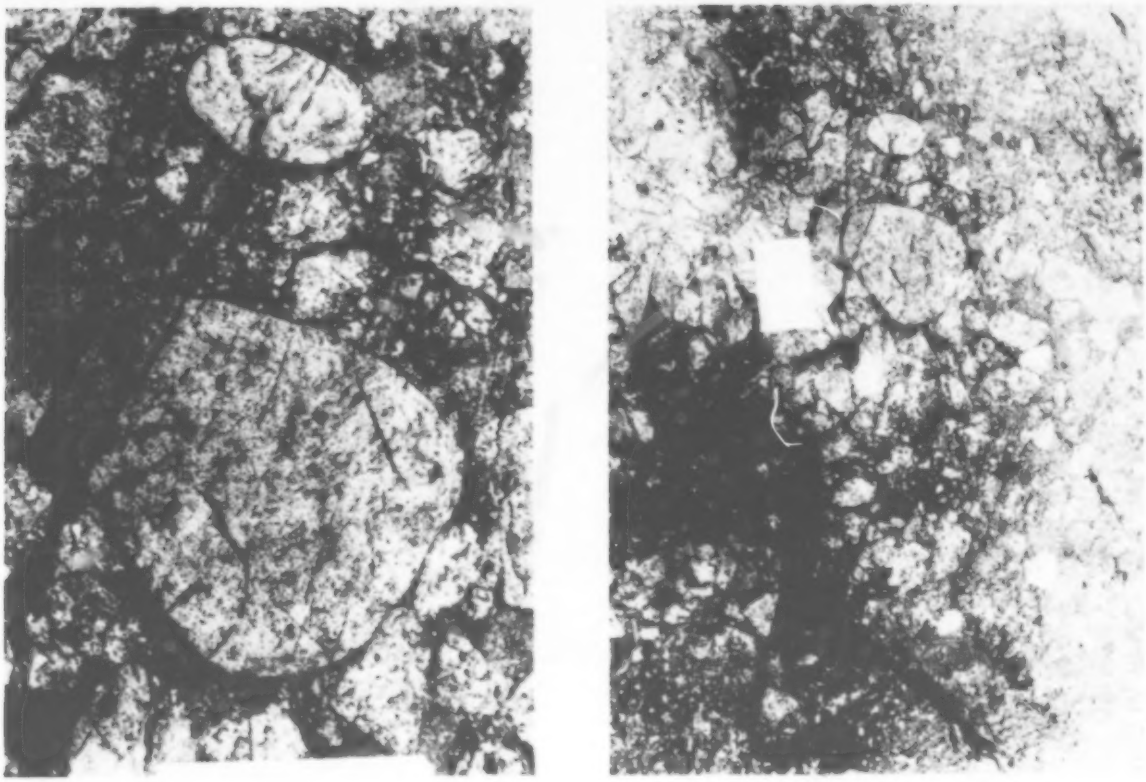

Photo 322.4. (a) *Detail of well rounded, poorly vesiculated pumiceous fragments. There are also smaller, angular quartz-feldspar porphyry clasts present.* (b) *The pumices occur at the top of an inversely graded unit 0.55 m thick within Section 4 (see Figure 322.2d). Direction of stratigraphic tops is to the top of the photo.*

cient time for the pumices to become waterlogged (Fisher 1977, 1984). These deposits may be direct products of explosive eruptions; each pulse may represent a single eruption. This must be balanced, however, against evidence for reworking, such as rounded pumices and the presence of both pumices and quartz-feldspar porphyry fragments. On the other hand, pumices can be rounded and abraded in a primary pyroclastic flow (cf. Wilson 1985, Figure 33); and the pumices and quartz-feldspar porphyry fragments may both be juvenile in origin.

SECTION 5

Section 5 also outcrops within formation H. Unlike Section 4, however, Section 5 contains abundant fine-grained material as well as lapilli tuffs and tuff breccias (Figure 322.2e). Section 5 is notable for 1) presence of double grading (Fiske and Matsuda 1964), 2) inverse grading of the lapilli tuff and tuff breccia units and 3) occurrence of both fine-grained pumices and quartz-feldspar porphyry fragments.

Lapilli tuffs and tuff breccias at 2.25–4.3 m become finer grained up-section from the unit at 2.25–3.5 m to the uppermost unit at 4.1–4.3 m. The deposits are separated by very thin fine-grained material at 3.5 m and 4.0 m. Maximum clast size of the lapilli tuffs and tuff breccias within this interval also decreases up-section from 12 cm to 2.5 cm.

The series of fine-grained beds at 4.3–5.9 m that overlie the coarse-grained material may be graded in three ways: 1) the four fine-grained units become successively finer grained up-section; 2) the three lower fine-grained units at 4.3–5.5 m are each normally graded and thinner bedded up-section; and 3) individual laminae within these three lower units may themselves be size- and/or density-graded. These deposits thus appear doubly graded.

Similarly, fine-grained material at 6.6–6.85 m, which directly overlies lapilli tuffs, both fines upward and becomes progressively thinner bedded up-section. Basal beds are 4 cm thick, while the topmost beds are approximately 1 cm thick.

Because the lapilli tuffs and tuff breccias in Section 5 appear to be 1) discrete units with very rapid changes in grain size, 2) inversely graded within each lapilli tuff and tuff breccia unit, and 3) sometimes separated by thin fine-grained material, these deposits likely do not result simply from segregation of material within one mass flow. Instead, this se-

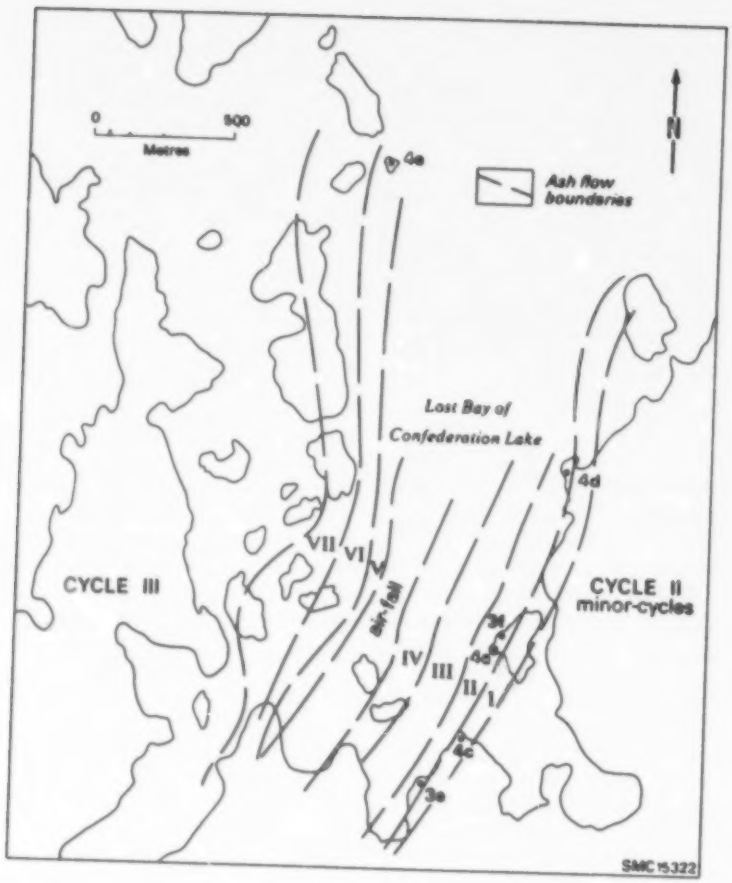

Figure 322.3. *Map showing Thurston's (1985) seven subaqueous ignimbrite sequences (I-VII) at the southern end of Lost Bay. From Thurston (1985).*

quence probably formed from a series of flows, similar to the sequence in Section 4.

The deposits at 2.05–5.9 m, as well as at 6.0–6.85 m, may be genetically related with respect to grain size and grading relations discussed above. These stratigraphic intervals may be direct products of explosive eruptions. The fact that each unit from 2.25 m to 5.9 m, including tuff breccias, lapilli tuffs, and fine-grained units, appears to be finer grained than the one below suggests they are products of a series of successively smaller eruptions. The general lack of fine-grained material between the lapilli tuffs and tuff breccias implies rapid emplacement of the coarse-grained rocks. The large proportion of non-vesicular fragments observed in these deposits suggests dome growth and fragmentation. The initial explosion may have been the most powerful, followed by a series of progressively less intense eruptions.

Alternatively, these observations may be interpreted, in whole or in part, as a series of progressively more dilute flows generated from an initially high concentration mass flow, as envisaged by Lowe (1982).

ANALYSIS OF THURSTON'S SEVEN SUBAQUEOUS PYROCLASTIC FLOW DEPOSITS IN LOST BAY

It is generally very difficult to substantiate Thurston's (1985) basis for definition and correlation of seven subaqueous ignimbrites in the southern part of Lost Bay (Figure 322.3) because of a lack of outcrop and marker beds with which to correlate the individual flow deposits.

Ignimbrite I is actually dominantly mafic lava flows. Ignimbrite II appears to be the only unit that can be reasonably correlated, although there are no distinct marker beds present. The deposits, sedimentary structures and textures, grading relations, and clast types are very similar for Sections 1–3 (Figure 322.2a-c) within ignimbrite II. But as can be seen from the sections, there are a series of units within this 'ignimbrite', not simply one. The units are relatively thin (<10 m thick), nowhere near the

thickness (70–130 m) proposed by Thurston (1985).

Ignimbrites III, IV and V also do not appear to be three simple flow units but instead a series of flow deposits within each 'ignimbrite'. There is a lack of outcrop in this area with which to define and correlate the different flow units. The airfall unit located between ignimbrites IV and V appears, instead, to be massive matrix-supported lapilli tuffs and tuff breccias.

Because of relatively intense shearing, it is difficult to evaluate ignimbrite VII. This is possibly an area of intermediate to silicic lavas (see above). It is very difficult to define or correlate a single pyroclastic flow unit here.

PYROCLASTIC AND EPICLASTIC PROCESSES IN LOST BAY

The bedding, sorting and grading relations observed in Lost Bay clearly indicate a turbidite association. There is no evidence in the area for reworking and deposition above wave base. Substantial mixing and dilution of the volcaniclastic debris with water is indicated by the abundant bedding and grading, the relatively good sorting, and the rapidly changing grain sizes within adjacent deposits. The comparative thinness of coarse-grained flow units in Lost Bay (<10 m thick) implies deposition outside a caldera and/or dome growth and fragmentation. Dome growth and fragmentation commonly is associated with andesitic compositions, relatively small-scale volcanism and small-volume pyroclastic flows, abundant juvenile and cognate, lithic, unvesiculated fragments, as well as pumiceous fragments (Smith and Roobol 1982; Stix, in press). The Lost Bay sequence fits these criteria well. Juvenile fragments generally appear andesitic in composition, flow deposits are thin and probably small-volume, and juvenile fragments have a range of vesicularities.

However, it remains extremely difficult to distinguish deposits derived directly from explosive eruptions (pyroclastic) from those that have been subjected to subsequent reworking and redeposition (epiclastic). For example, the deposits observed in Section 5 (Figure 322.2e) may be the result of eruptive processes (Fiske and Matsuda 1964), flow processes (Lowe 1982), or both. Section 4 may provide better evidence for pyroclastic character due to the presence of 1) many individual flow units, 2) abundant inversely graded pumice and 3) the lack of associated fine-grained material. In general, however, the amount of reworking of pyroclastic material in Lost Bay must have been relatively minor because of the abundance of pumice, juvenile material and coarse-grained debris.

It is also difficult to infer eruptive environments, i.e., subaerial or subaqueous. Observations which suggest subaqueous eruptions include 1) pillowed lavas and hyaloclastites of formation F which can contain 20-30% vesicles, 2) the lack of highly vesicular pumices, implying flotation, and 3) the abundance of dense fragments which may not have vesiculated due to quenching.

Based on evidence of more proximal deposits at Mosier and Narrow Lakes, Thurston (1985) has suggested that the source volcanoes were located to the north or northeast of Lost Bay. Limited paleocurrent data from flame structures in Lost Bay also suggest a component of flow to the south or southwest. On the other hand, the probable silicic lavas that outcrop in the southwestern part of Lost Bay also may indicate source vents.

The abrupt appearance of quartz-feldspar porphyry fragments in formation H is enigmatic. The fragments may be juvenile and may indicate the appearance of new magmas and sources, or they may be lithic and reflect the unroofing of older hypabyssal intrusions. The quartz-feldspar porphyry clasts have textures and chemistry very similar to those found in Cycle III. If these fragments are indeed lithic and derived from Cycle III, this implies that Cycle III is older than Cycle II, not younger as is currently thought (Thurston 1985).

ECONOMIC SIGNIFICANCE OF THE LOST BAY DEPOSITS

To assess the economic potential of the Lost Bay area requires, in part, an understanding of 1) where the deposits lie in relation to their source vents and 2) the amount of reworking that has occurred since eruption. The volcaniclastic material appears to have been deposited outside a vent area or areas and has undergone some reworking, based on several independent lines of evidence: 1) the lapilli tuff and tuff breccia volcaniclastic flow units are thin and have been mixed with water; 2) there is abundant quartz-rich fine-grained material associated with the coarser units, which is probably epiclastic; 3) the deposits are likely derived from dome point sources, rather than deposited within caldera structures; and 4) quartz-feldspar porphyry fragments found in the Lost Bay deposits may be lithic, not magmatically derived, and therefore may bear no relation to the presence of massive sulphides. By contrast, the quartz-feldspar porphyries of Cycle III are clearly magmatic and are associated with massive sulphide orebodies.

On the other hand, the Lost Bay volcaniclastic material does not appear to have suffered significant post-eruptive modification. Furthermore, there are indications of silicic lavas in the southwestern part of Lost Bay which may indicate proximity to a small vent or vents. In sum, the combined volcanological evidence suggests that Lost Bay is an unlikely candidate for economically important massive sulphide deposits.

In conclusion, we note that the presence of abundant quartz in Archean supracrustal and hypabyssal rocks may be the result of very different processes. Quartz in quartz-feldspar porphyries indicates a silicic magma that may host massive sulphides. By contrast, quartz in volcaniclastic deposits may have been concentrated by epiclastic processes, resulting in reworked rocks that have no association with vent-related ore deposits.

ACKNOWLEDGMENTS

We thank Phil Thurston and Moe Lavigne of the Ontario Geological Survey for continued support of this research. This work was funded by Ontario Geoscience Research Grant 322.

REFERENCES

Carlisle, D.

1963: Pillow Breccias and Their Aquagene Tuffs, Quadra Island, British Columbia; Journal of Geology, Volume 71, p.48-71.

Fisher, R.V.

1977: Geologic Guide to Subaqueous Volcanic Rocks in the Nipimo, Pismo Beach and Avila Beach Areas; Unpublished Report, Geological Society of America Penrose Conference, The Geology of Subaqueous Volcanic Rocks, 29p.

1984: Submarine Volcaniclastic Rocks; p.5-27 *in* Marginal Basin Geology, edited by B.P. Kokelaar and M.F. Howells, Geological Society of London, Special Publication, Volume 16.

Fiske, R.S. and Matsuda, T.

1964: Submarine Equivalents of Ash Flows in the Tokiwa Formation, Japan; American Journal of Science, Volume 262, p.76-106.

Lowe, D.R.

1982: Sediment Gravity Flows: II. Depositional Models with Special Reference to the Deposits of High-Density Turbidity Currents; Journal of Sedimentary Petrology, Volume 52, p.279-297.

Nunes, P.D. and Thurston, P.C.

1980: Two Hundred Twenty Million Years of Archean Evolution: A Zircon U-Pb Stratigraphic Study of the Uchi-Confederation Lakes Greenstone Belt, Northwestern Ontario; Canadian Journal of Earth Sciences, Volume 17, p.710-721.

Schmincke, H.-U., Rautenschlein, M., Robinson, P.T. and Mehegan, J.M.

1983: The Troodos Extrusive Series of Cyprus: A Comparison with Oceanic Crust; Geology, Volume 11, p.410-412.

Smith, A.L. and Roobol, M.J.

1982: Andesitic Pyroclastic Flows; p.415-433 *in* Andesites, edited by R.S. Thorpe, Wiley, New York.

Stix, J.

In Press: Subaqueous Intermediate to Silicic-Composition Explosive Volcanism: A Review and Development of Conceptual Frameworks; Earth-Science Reviews.

In Prep: Lithofacies Types and Order Within Subaqueous Pyroclastic Rocks; American Journal of Science.

Stix, J. and Gorton, M.P.

1988: Physical and Chemical Processes of Archean Subaqueous Pyroclastic Rocks; p.231-238 *in* Geoscience Research Grant Program, Summary of Research 1987–1988, edited by V.G. Milne, Ontario Geological Survey Miscellaneous Paper 140, 251p.

Thurston, P.C.

1980: Subaerial Volcanism in the Archean Uchi-Confederation Volcanic Belt; Precambrian Research, Volume 12, p.79-98.

1985: Physical Volcanology and Stratigraphy of the Confederation Lake Area, District of Kenora (Patricia Portion); Ontario Geological Survey, Report 236, 117p.

Wilson, C.J.N.

1985: The Taupo Eruption, New Zealand, II. The Taupo Ignimbrite; Philosophical Transactions of the Royal Society of London, Volume A 314, p.229-310.

Grant 323 Lithogeochemical, Isotopic and Fluid Inclusion Studies of Hydrothermal Alteration and Breccia Veins from the Cameron Lake Gold Deposit, Northwestern Ontario

D.R. Melling[1], R.P. Taylor[1], D.H. Watkinson[1] and Xin Wu[2]

[1]Department of Earth Sciences and Ottawa-Carleton Geoscience Centre, Carleton University, Ottawa

[2]CRPG Mineraux, Orleans, France

ABSTRACT

The Cameron Lake deposit is an Archean vein-type deposit which occurs in deformed basaltic rocks of the Cameron Lake shear zone. The introduction of gold into the shear zone, via a fluid of external derivation, was accompanied by the addition of large amounts of CO_2, K, Rb, Ba, Ca, Sr, Ag and S. Lithogeochemical and statistical analysis of samples of potentially ore-grade material (Au = 2.25 to 7.00 g/t) from the deposit demonstrates that, of these elements, only S, Ag, Sr and Ba have a positive correlation with gold, and that CO_2, K, Rb and Ca are non-correlated with gold. These data corroborate the results of textural studies which established that, of the most common alteration minerals ankerite, sericite and pyrite, only pyrite has a close spatial relationship with gold.

Fluid inclusion petrography indicates the ubiquitous presence of CO_2–H_2O bearing inclusions, some of which contain daughter minerals, in quartz from the breccia veins and other auriferous structures. Heating-freezing experiments on these inclusions demonstrate the presence of a moderately high temperature (T>230°C), low salinity (<3 weight percent equivalent NaCl), low density (0.73 g/cm^3) fluid in the shear zone during vein formation and hydrothermal alteration. Isotopic analysis of vein and alteration minerals suggests that this fluid carried isotopically light carbon ($\delta^{13}C \simeq -5‰$), and had an initial $^{87}Sr/^{86}Sr$ isotopic ratio in the range 0.7012 to 0.7016.

INTRODUCTION

The Cameron Lake gold deposit is located in the Kenora Mining District about 80 km southeast of Kenora (49°17'N, 94°44'W). It has been the subject of a comprehensive program of field-based research that has provided an overview of the deposit in terms of structural control, deposit geometry, vein paragenesis, alteration mineralogy, and their relationships to gold distribution (Melling 1986; Melling *et al.* 1986; Melling 1987). This program has provided the framework for detailed studies of the alteration lithogeochemistry and the light stable isotopic compositions of selected alteration and gangue minerals (Melling *et al.* 1988, and this report), and for Rb/Sr isotopic and fluid inclusion analysis (this report).

Together with several other prospects (Monte Cristo, Victor Island, Wampum Lake) the Cameron Lake deposit is one of a number of shear zone–hosted gold occurrences that occur within the Cameron–Rowan lakes greenstone terrane at the western extremity of the Archean Savant Lake–Crow Lake metavolcanic-metasedimentary belt in the Wabigoon Subprovince (Melling *et al.* 1986).

LITHOGEOCHEMISTRY

Geochemical analyses of potentially ore-grade material from tower samples composed of pervasively altered and gold-bearing rock from the Cameron Lake deposit are presented in Table 323.1, together with the assay data for gold in each of the samples. All of the elements (with the exception of Rb, Sr, Y, Zr, Nb and Ba) were analyzed at the Bondar-Clegg Laboratories, Ottawa, using a combination of total acid digestion (HF–$HClO_4$–HNO_3–HCl) followed by direct coupled plasma (DCP) spectrometry, sample fusion (borate flux) followed by DCP spectrometry, or specific techniques (i.e., selective ion electrodes for the halogens, dichromate titration for ferrous iron). Rb, Sr, Y, Zr, Nb and Ba were analyzed at the Ottawa–Carleton Geoscience Centre laboratory with a Philips 1410 automated X-ray fluorescence spectrometer using duplicate fused discs ($Li_2B_4O_7$, Li_2CO_3 and the sample). The gold assays were performed by Lakefield Research Ltd. using conventional fire assay procedures. The geochemical data were subjected to statistical analysis; interpretation of all of the results is beyond the scope of this paper, but part of the correlation matrix is presented in Table 323.2.

The rock samples used in this geochemical study were selected to cover the range of gold tenors (2.25 to 7.00 g/t) typically encountered in the Cameron Lake deposit. Melling *et al.* (1988) presented a detailed analysis of the chemical gains and losses that

TABLE 323.1. GOLD ASSAYS AND GEOCHEMICAL ANALYSES OF MINERALIZED SAMPLES FROM THE CAMERON LAKE DEPOSIT.

Sample	3	48	13	43	19311	26	47	19	19303	29
					Assay in grams per tonne					
Au	2.30	2.52	2.76	2.90	3.36	3.49	3.73	4.01	4.22	4.50
					Concentrations in weight percent					
SiO_2	48.80	68.80	45.60	55.50	51.80	46.50	50.70	48.10	51.00	48.00
TiO_2	0.80	0.37	0.73	0.63	0.65	0.84	0.68	0.77	0.70	0.72
Al_2O_3	11.05	6.30	11.20	8.50	10.90	10.60	9.38	10.60	10.70	10.90
Fe_2O_3	3.84	2.50	2.61	3.24	3.25	4.86	2.86	3.86	3.35	2.69
FeO	7.07	3.52	7.96	6.02	6.73	6.80	6.94	6.62	6.64	7.68
MnO	0.17	0.08	0.15	0.13	0.14	0.19	0.14	0.17	0.14	0.16
MgO	3.41	1.93	4.00	3.19	3.19	3.62	3.55	3.56	3.24	3.76
CaO	7.18	4.12	7.68	6.05	6.42	7.63	6.83	7.24	6.34	7.79
Na_2O	2.53	0.96	2.71	1.82	1.94	2.48	1.90	3.06	2.04	2.12
K_2O	1.54	0.90	1.61	1.30	1.25	1.79	1.44	1.28	1.29	1.48
P_2O_5	0.06	0.01	0.11	0.02	0.03	0.02	0.09	0.17	0.20	0.18
S	1.56	1.29	1.26	1.49	1.51	1.91	1.16	2.02	1.49	1.20
H_2O+	0.10	0.10	0.10	0.05	0.05	0.10	0.10	0.10	0.10	0.15
CO_2	14.03	7.94	15.34	12.14	13.18	13.86	13.44	13.00	12.96	14.54
F	0.06	0.03	0.04	0.04	0.04	0.05	0.04	0.04	0.04	0.04
Total	102.20	98.85	101.10	100.12	101.03	101.25	99.25	100.59	100.23	101.41
					Concentrations in parts per million					
Cl	30	70	40	40	30	30	30	10	40	20
V	228	114	237	188	199	242	213	208	197	229
Cr	270	423	208	294	255	226	277	245	278	241
Co	38	20	45	33	38	41	36	40	34	41
Ni	50	32	71	51	56	53	58	55	51	66
Cu	196	67	155	121	130	176	127	141	130	140
Zn	172	50	106	74	90	99	79	89	80	92
As	<5	<5	<5	<5	<5	<5	<5	<5	<5	<5
Se	<5	<5	<5	<5	<5	<5	<5	<5	<5	<5
Rb	56	25	52	52	45	65	42	42	47	54
Sr	166	113	171	140	155	165	152	194	159	153
Y	21	11	15	24	21	22	16	15	15	33
Zr	56	26	47	42	51	54	44	51	48	40
Nb	<5	<5	<5	20	<5	<5	<5	<5	<5	38
Mo	7	10	6	12	10	16	8	8	8	6
Ag	0.5	0.6	0.9	0.8	1.8	1.4	0.7	1.4	0.9	0.8
Cd	<1	<1	<1	<1	<1	<1	<1	<1	<1	<1
Sb	<5	<5	<5	<5	<5	<5	<5	<5	<5	<5
Te	<10	<10	<10	<10	<10	<10	<10	<10	<10	<10
Ba	135	87	121	106	111	114	87	88	119	117
W	16	14	10	16	16	16	10	16	14	10
Pb	84	34	73	47	60	76	57	73	50	74
Bi	<2	<2	<2	<2	<2	<2	<2	<2	<2	<2

TABLE 323.1. CONTINUED.

Sample	19345	8	9	30	19367	33	24	23	14	41
					Assay in grams per tonne					
Au	4.78	4.98	5.26	5.50	5.71	5.96	6.34	6.52	6.81	6.93
					Concentrations in weight percent					
SiO_2	53.00	49.90	49.00	53.00	52.10	51.30	50.00	50.20	48.40	49.00
TiO_2	0.66	0.73	0.70	0.67	0.70	0.63	0.82	0.71	0.79	0.71
Al_2O_3	9.50	10.20	11.00	10.30	10.10	10.10	10.50	10.85	11.00	10.90
Fe_2O_3	2.79	3.38	3.26	4.17	3.12	3.83	4.34	3.21	4.11	4.89
FeO	6.57	6.33	6.72	5.18	6.70	6.14	6.90	6.55	7.05	5.54
MnO	0.14	0.16	0.16	0.14	0.16	0.16	0.19	0.16	0.17	0.17
MgO	3.27	3.10	3.32	2.96	3.40	3.27	3.11	3.24	3.19	2.85
CaO	6.45	6.87	6.75	6.32	6.72	6.68	6.71	6.64	6.63	6.06
Na_2O	1.75	3.16	3.15	3.11	2.14	2.90	2.04	2.16	2.28	2.89
K_2O	1.35	1.10	1.18	1.07	1.29	1.28	1.84	1.48	1.57	1.26
P_2O_5	0.01	0.20	0.22	0.17	0.22	0.23	0.22	0.17	0.12	0.14
S	1.45	1.93	2.08	2.42	1.54	1.91	1.65	1.53	2.10	2.56
H_2O+	0.05	0.05	0.10	0.10	0.05	0.05	0.10	0.10	0.05	0.05
CO_2	12.49	12.57	13.42	11.66	12.50	13.68	13.16	13.31	14.10	12.70
F	0.04	0.05	0.04	0.04	0.03	0.03	0.05	0.04	0.04	0.05
Total	99.52	99.73	101.10	101.31	100.77	102.19	101.63	100.35	101.60	99.77
					Concentrations in parts per million					
Cl	10	30	30	30	30	30	10	30	30	30
V	212	216	205	185	204	212	245	220	246	213
Cr	316	290	280	315	277	281	212	266	220	235
Co	38	41	40	37	39	43	41	40	46	35
Ni	57	53	57	53	56	74	51	59	56	54
Cu	127	139	139	131	126	146	163	136	163	130
Zn	86	94	90	83	82	83	98	85	96	89
As	<5	<5	<5	<5	<5	<5	<5	<5	<5	<5
Se	<5	<5	<5	<5	<5	<5	<5	<5	<5	<5
Rb	40	31	42	29	44	46	68	49	56	44
Sr	129	205	203	159	157	191	148	154	190	203
Y	13	17	16	15	17	19	20	15	17	18
Zr	41	54	51	44	48	48	58	49	55	56
Nb	<5	<5	<5	<5	<5	<5	<5	<5	<5	<5
Mo	10	10	8	12	8	18	12	9	8	12
Ag	0.8	1.0	1.6	1.6	0.8	1.0	1.0	1.4	1.7	1.5
Cd	<1	<1	<1	<1	<1	<1	<1	<1	<1	<1
Sb	<5	<5	<5	<5	<5	<5	<5	<5	<5	<5
Te	<10	<10	<10	<10	<10	<10	<10	<10	<10	<10
Ba	96	122	102	96	100	129	143	98	124	167
W	16	16	14	16	16	12	14	14	16	20
Pb	71	70	68	60	76	73	83	76	100	65
Bi	<2	<2	<2	<2	<2	<2	<2	<2	<2	<2

Note: the concentrations of the trace elements Cr, Cu, Ni and Zn may contain a contribution from the chrome steel and high carbon steel grinding media used during sample preparation (cf., Hickson and Juras 1986).

TABLE 323.2. CORRELATION MATRIX FOR SELECTED ELEMENTS IN MINERALIZED SAMPLES (N=20) FROM THE CAMERON LAKE GOLD DEPOSIT.

	Au	Ag	S	CO_2	K_2O	CaO	FeT	TiO_2	MgO	Rb	Ba	Sr
Au	1.00	0.47	0.57	0.13	0.07	0.02	0.25	0.25	-0.11	0.06	0.34	0.41
Ag	0.47	1.00	0.68	0.18	-0.01	0.10	0.30	0.27	-0.02	0.02	0.08	0.49
S	0.57	0.68	1.00	-0.02	-0.19	-0.02	0.23	0.27	-0.21	-0.13	0.36	0.68
CO_2	0.13	0.18	-0.02	1.00	0.70	0.91	0.89	0.79	0.90	0.66	0.37	0.47
K_2O	0.07	-0.01	-0.19	0.70	1.00	0.66	0.79	0.75	0.62	0.93	0.36	-0.01
CaO	0.02	0.10	-0.02	0.91	0.66	1.00	0.85	0.83	0.95	0.57	0.18	0.42
FeT	0.25	0.30	0.23	0.89	0.79	0.85	1.00	0.96	0.76	0.78	0.49	0.50
TiO_2	0.25	0.27	0.27	0.79	0.75	0.83	0.96	1.00	0.70	0.70	0.42	0.49
MgO	-0.11	-0.02	-0.21	0.90	0.62	0.95	0.76	0.70	1.00	0.54	0.04	0.29
Rb	0.06	0.02	-0.13	0.66	0.93	0.57	0.78	0.70	0.54	1.00	0.47	0.03
Ba	0.34	0.08	0.36	0.37	0.36	0.18	0.49	0.42	0.04	0.47	1.00	0.44
Sr	0.41	0.49	0.68	0.47	-0.01	0.42	0.50	0.49	0.29	0.03	0.44	1.00

Note: Assays and geochemical analyses for the samples are contained in Table 323.1 of this report; FeT is total iron as Fe_2O_3; the numbers contained in the matrix are correlation coefficients and are represented in the text by the symbol r.

accompanied the pervasive hydrothermal alteration of basaltic protolith in the Cameron Lake deposit. This analysis, utilizing the isocon method of Grant (1986), indicated that S, K, Ag, Rb, Ba, CO_2, Sr and Ca were the most important mobile components introduced during hydrothermal alteration and gold deposition (*see* Figure 323.3 in Melling *et al.* 1988). The behaviour of these elements with respect to increasing gold tenor in samples from Cameron Lake is illustrated in Figure 323.1.

Of the elements that were apparently added to the rock during alteration and gold deposition only S (correlation coefficient, r=0.57), Ag (r=0.47), Sr (r=0.41) and Ba (r=0.34) have a positive correlation with gold. In contrast K_2O, CO_2, CaO and Rb are essentially non-correlated with Au (Table 323.2). Of these elements, S (in pyrite), K_2O (in sericite), and CO_2 and CaO (in ankerite) are all essential components of the pervasive alteration assemblage that is spatially associated with the breccia veins and zones of gold enrichment. Such a low correlation between Au and K_2O, CO_2 and CaO suggests that although the alteration minerals ankerite and sericite are spatially associated with zones of gold mineralization, their relative abundances should not be used as an indication of gold tenor (cf., Whitehead *et al.* 1980). The lack of any significant correlation of these elements with S (Table 323.2) also supports such a conclusion. In contrast, the positive correlation of S with Au in the mineralized samples further corroborates the importance of the close textural relationship that exists between gold and pyrite in the Cameron Lake deposit (Melling *et al.* 1986).

SULPHUR ISOTOPE COMPOSITIONS OF PYRITE

Pyrite samples for isotopic analysis were separated from 1) breccia vein fragments, and 2) pervasively altered wall rocks, by microdrilling, and were purified using conventional methods. Sulphur isotope analyses were made at the Ottawa–Carleton Geoscience Centre stable isotope facility using conventional procedures (Faure 1986), after the conversion of the sulphide to SO_2 gas by reaction with CuO at 1000°C. The results of the sulphide analyses, presented in Table 323.3, supplement those in Table 323.2 (Melling *et al.* 1988). Histograms of the sulphur isotope data (Figure 323.2) show a range of values from 0.1 to 3.7‰ for the Cameron Lake deposit, and a similar range of −0.5 to 3.2‰ for the other occurrences.

CARBON AND OXYGEN ISOTOPE COMPOSITIONS OF CARBONATES

Carbonate samples for isotopic analysis were separated by microdrilling from vein and alteration material. After separation they were purified by conventional methods, and their composition verified by X-ray diffraction. Carbon and oxygen isotope ratio measurements were made at the Ottawa–Carleton Geoscience Centre stable isotope facility using conventional procedures (Craig 1957; Faure 1986) after the application of a selective chemical separation that involved the sequential extraction of CO_2 at 50°C using 100% phosphoric acid (Al-Aasm *et al.* 1988). The results of the carbonate analyses in Table 323.4 supplement those in Table 323.3 (Melling *et al.* 1988).

Histograms of carbon isotope data (Figure 323.3) show a range of values for hydrothermal ankerite from 0.0 to −5.9‰ for the Cameron Lake deposit, and a range of values from −1.6 to −4.5‰ for the other gold occurrences. These compare with values of −0.1 to −1.6‰ in calcite from least altered basalt at Cameron Lake (Table 323.4). Figure 323.4 is a plot of $\delta^{18}O$ versus $\delta^{13}C$ for carbonates from the Cameron Lake deposit. The trend to lighter carbon and oxygen isotope values as a result of hydrothermal alteration and mineralization is consistent with

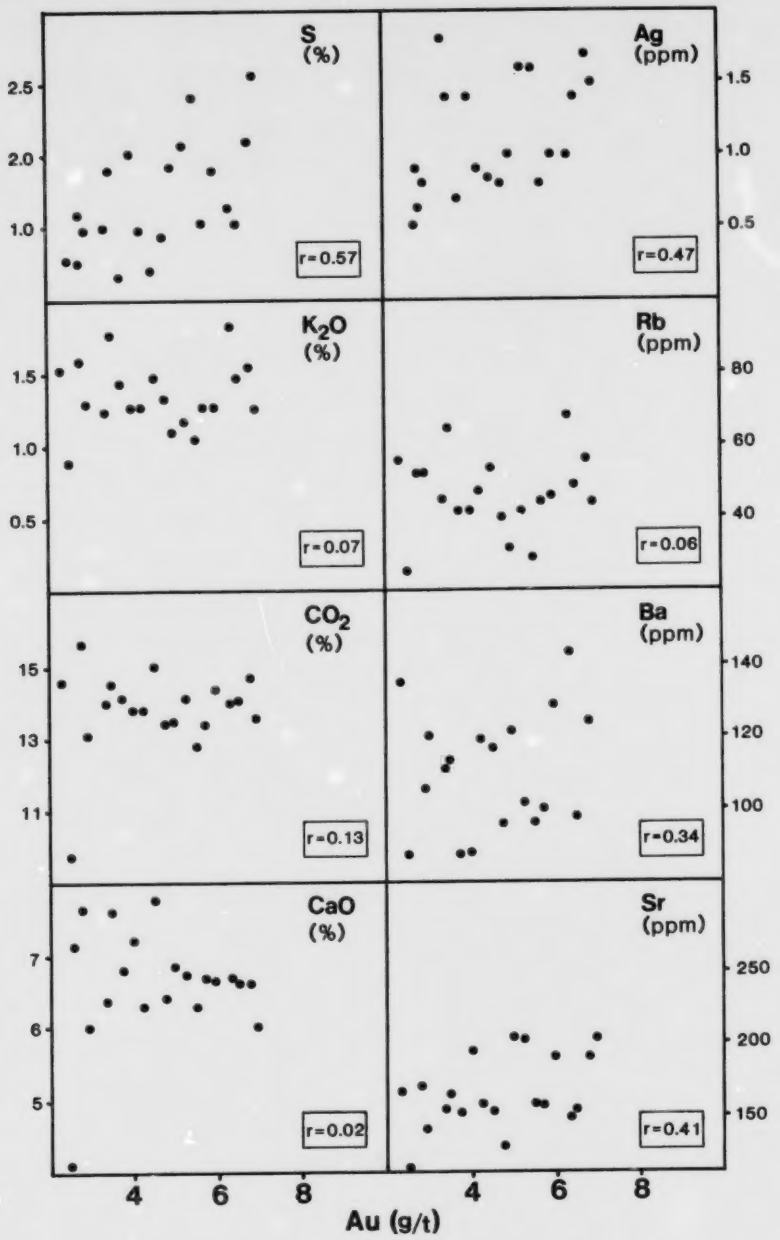

Figure 323.1. *Plots of the concentrations of selected major and trace elements as a function of the gold tenor (in g/t) of mineralized rock samples from the Cameron Lake gold deposit.*

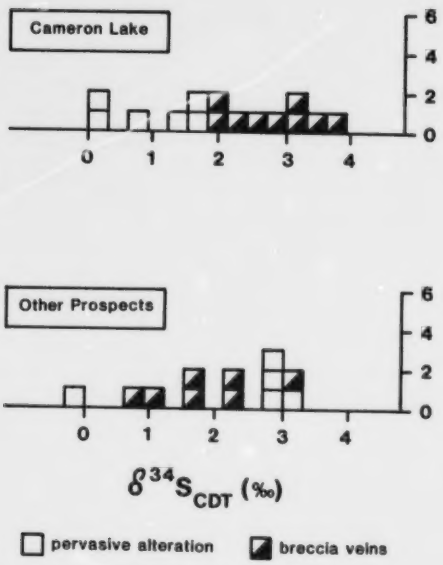

Figure 323.2. *Histogram of $\delta^{34}S$ values (in per mil relative to the CDT international standard) for pyrite from gold occurrences in the Cameron–Rowan lakes area.*

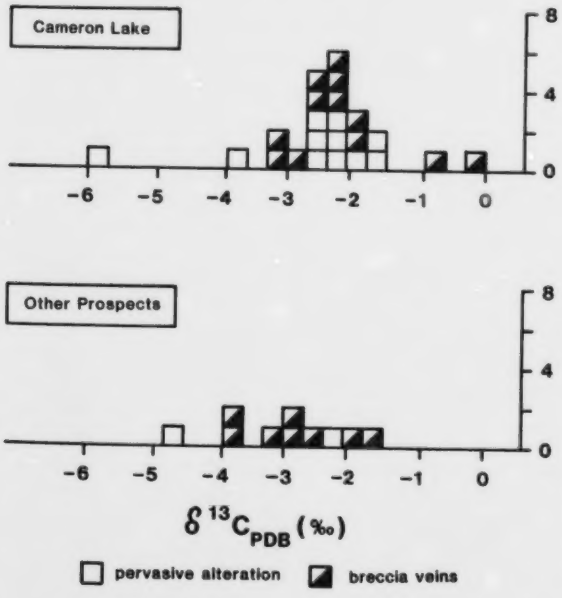

Figure 323.3. *Histogram of $\delta^{13}C$ values (in per mil relative to the PDB international standard) for ankerite from the gold occurrences in the Cameron–Rowan lakes area.*

TABLE 323.3. SULPHUR ISOTOPE RATIOS IN PYRITE FROM GOLD OCCURRENCES IN THE CAMERON–ROWAN LAKES AREA.

Sample	Lithology/alteration	$\delta^{34}S_{CDT}$
Cameron Lake deposit		
RPT–77P	breccia vein, fragment	2.3
RPT–82WP	breccia vein, fragment	2.9
Monte Cristo prospect		
RPT–71FP	pervasively altered basalt	3.2
Wampum Lake prospect		
RPT–74FP	breccia vein, fragment	1.6
RPT–79FP	breccia vein, fragment	1.7

Note: all isotopic values are reported in per mil relative to the Canyon Diablo meteorite (CDT) international reference standard (O'Neil 1986).

the introduction, along the shear zone, of a fluid carrying isotopically light carbon ($\delta^{13}C < -5.0‰$) and subsequent isotopic exchange with the host rocks ($\delta^{13}C = 0‰$).

Rb/Sr ISOTOPIC ANALYSIS

Concentrations of Rb and Sr in the mineral separates were determined by isotope dilution analyses at Carleton using ^{87}Rb– and ^{84}Sr–enriched spikes. Sr was run as a phosphate using single Ta filaments. Rb was analysed using a double Re filament technique. Sr isotope ratios were measured on a Finnegan-MAT 261 fixed multicollector solid-source mass spectrometer capable of simultaneously collecting masses 85 through 88 (Bell and Blenkinsop 1984). Reproducibility, including chemical separation, of the $^{87}Sr/^{86}Sr$ ratios is considered to be 0.004% of the quoted value at the 2σ level. Uncertainties in the Rb and Sr concentrations are less than 0.5% of the quoted values.

Results of the Rb, Sr and $^{87}Sr/^{86}Sr$ isotope analyses are contained in Table 323.5. U–Pb zircon geochronological determinations for rocks from the Savant–Crow lakes region of the Wabigoon greenstone terrane range from 2755 to 2703 Ma (for volcanic rocks) to 2695 Ma (for plutonic rocks) (Davis *et al.* 1981, summarized by Colvine *et al.* 1988). Age-corrected initial $^{87}Sr/^{86}Sr$ ratios (at 2700 Ma) for the vein albites are: RPT–1MV, 0.70164; RPT–59VC, 0.70286; RPT–27V, 0.70144; RPT–51VC, 0.70124. Although the absolute ages of the gold deposits in the Cameron–Rowan lakes area are uncertain, the low Rb/Sr ratios of the hydrothermal albite serve to minimize the age correction needed to account for the decay of ^{87}Rb present in the mineral. Consequently the calculated initial Sr ratios vary little from the measured $^{87}Sr/^{86}Sr$ isotopic ratios.

These initial strontium isotope ratios probably reflect those of the hydrothermal fluid which do-

TABLE 323.4. CARBON AND OXYGEN ISOTOPE RATIOS IN CARBONATES FROM GOLD OCCURRENCES IN THE CAMERON-ROWAN LAKES AREA.

Sample	Lithology/alteration	Mineral	$\delta^{13}C_{PDB}$	$\delta^{18}O_{SMOW}$
Cameron Lake deposit				
LD-13	least altered basalt	ankerite	0.80	12.48
LD-17.5	least altered basalt	calcite	-1.34	12.13
LD-29	least altered basalt	calcite	-1.62	11.70
LD-33	least altered basalt	calcite	-0.42	11.52
LD-43.5	least altered basalt	calcite	-0.09	11.77
		ankerite	0.07	10.86
LD-50	least altered basalt	calcite	-1.34	11.43
RPT-12MV	auriferous quartz-carbonate vein	ankerite	-2.97	11.48
RPT-46FC	breccia vein, fragment	ankerite	-2.30	11.16
RPT-47VC	breccia vein, matrix	ankerite	-2.37	11.16
RPT-65VC	auriferous quartz-carbonate vein	ankerite	-2.35	11.18
RPT-83C	auriferous quartz-carbonate vein	ankerite	-2.03	11.25
RPT-84C	incipiently altered basalt	ankerite	-1.78	12.81
Monte Cristo prospect				
RPT-69VC	auriferous quartz-carbonate vein	ankerite	-1.94	11.08
RPT-70FC	pervasively altered basalt	ankerite	-2.13	10.96
Wampum Lake prospect				
RPT-76VC	breccia vein, matrix	ankerite	-3.73	11.23
RPT-80FC	breccia vein, fragment	ankerite	-3.84	11.36
RPT-81VC	breccia vein, matrix	ankerite	-3.82	10.67

Note: all isotopic values are reported in per mil relative to either the Peedee Belemnite (PDB) or Standard Mean Ocean Water (SMOW) international reference standards (O'Neil 1986). Conversion of $\delta^{18}O$ from the PDB to the SMOW reference standard was accomplished by using the equation given by Friedman and O'Neil (1977).

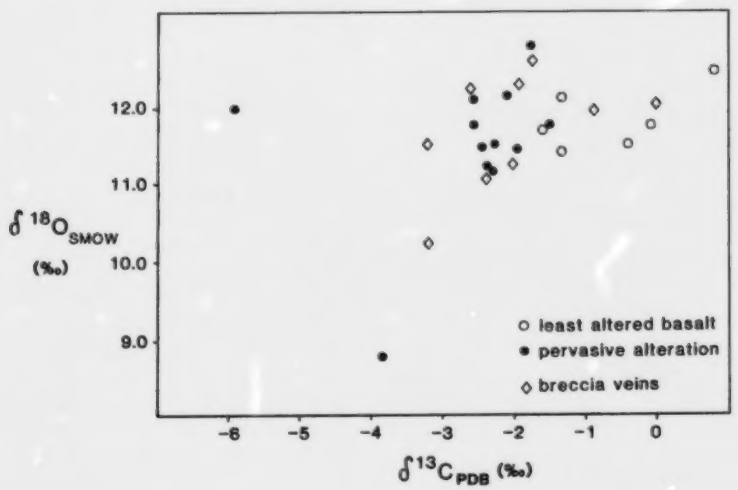

Figure 323.4. *Plot of $\delta^{18}O_{SMOW}$ versus $\delta^{13}C_{PDB}$ for carbonates from the Cameron Lake gold deposit and its immediate host rocks. All of the carbonates are ankerite with the exception of the samples from least altered basalt which are calcite.*

TABLE 323.5. Rb/Sr ISOTOPIC DATA FOR MINERALS FROM THE GOLD OCCURRENCES IN THE CAMERON-ROWAN LAKES AREA.

Sample	Lithology/alteration	Mineral	Rb (ppm)	Sr (ppm)	Rb/Sr	$^{87}Sr/^{86}Sr$ measured
Cameron Lake deposit						
RPT-1MV	breccia vein, matrix	albite	0.16	40.0*	0.020	0.70164
RPT-59VC	post-mineralization vein	albite	0.32	35.6	0.026	0.70388
Victor Island prospect						
RPT-36V	post-mineralization vein	ankerite	na	na	-	0.70133
Wampum Lake prospect						
RPT-27V	breccia vein, matrix	albite	0.63	906.2	0.002	0.70144
RPT-51VC	breccia vein, matrix	albite	0.44	657.3	0.002	0.70124

*Note: Precision of isotopic ratios is 0.004% (2 standard deviations of a measurement); NBS 987: $^{87}Sr/^{86}Sr = 0.71023 \pm 0.00003$; Eimer and Amend: $^{87}Sr/^{86}Sr = 0.70802 \pm 0.00002$; Sr ratios normalized to $^{86}Sr/^{88}Sr = 0.1194$. * - high uncertainty in measurement due to large spike:sample ratio; na - not analyzed.*

nated Sr to the host rock during the formation of the pervasive alteration that is spatially associated with gold in all of the occurrences. Although the range of initial Sr isotope ratios is small (0.7012 to 0.7029), the differences are analytically distinct and it is of interest to note that albite from the post-mineralization vein at Cameron Lake has a higher initial Sr ratio (0.7029) than the albites from the auriferous breccia veins at Cameron Lake and the other occurrences (0.7012 to 0.7016).

Initial Sr ratios recorded for vein minerals from other gold deposits hosted by large regional shear zones include: 0.7013 to 0.7015 (Kirkland Lake district, Kerrich *et al.* 1987); 0.7010 to 0.7020 (Timmins district, Kerrich 1986); and 0.7008 to 0.7041 (Val d'Or, Kerrich *et al.* 1987).

FLUID INCLUSION ANALYSIS

Fluid inclusions in quartz from all main vein types at the Cameron Lake deposit were studied. Typically the inclusions are equant with negative crystal shapes, and less than 20 μm in length. Many of the inclusions show some evidence for necking down, but all studied inclusions were selected to avoid this problem as much as possible. None of the inclusions could be characterized unambiguously as primary because of the absence in the quartz crystals of discernible growth zoning. However, all of the inclusions studied occupy fractures within, and restricted to, single quartz grains (i.e., of pseudosecondary origin, Roedder 1984). Two types of fluid inclusion were studied: 1) inclusions with two fluids and a solid phase (i.e., a liquid aqueous solution against the walls, a large bubble of liquid CO_2, and a daughter mineral) and 2) inclusions with three fluids (i.e., a liquid aqueous solution against the walls, a large bubble of liquid CO_2 within the water, and a smaller bubble of gaseous CO_2 within the liquid CO_2. In addition to microthermometric analysis using a Chaixmeca heating-cooling stage undertaken at CRSCM in Orleans, France, the composition of the gaseous and solid phases in selected inclusions was also identified using a UMIL Jobin-Yvon Raman microprobe, and a Cameca scanning electron microscope with an energy dispersive spectrometer (SEM-EDS).

The microthermometric analysis was divided into cooling and heating experiments. The temperature of melting of solid CO_2 (T_M CO_2) in all of the analyzed inclusions varied between −56.4 and −57.0°C, with a mean value of −56.6±0.2°C (n=17) which is identical to the melting temperature of pure CO_2. The average temperature of CO_2 clathrate dissociation (T_M clt) was 8.5±0.6°C (n=40), which according to the method of Collins (1979) gives a salinity of 3 weight percent NaCl equivalent for the aqueous phase. The temperature of partial homogenization of the CO_2-rich phase (T_H CO_2) varied between 16 and 30°C with an average value of 23.0±3.5°C (n=25), thus yielding an average density of 0.73 g/cm^3 for the CO_2 fluid. The measurement of the total homogenization temperature (T_H tot) of the fluid inclusions was inhibited in many instances by the occurrence of decrepitation in the temperature range 210 to 310°C.

More than 20 inclusions in quartz from all of the vein types were analyzed for CO_2, CH_4, N_2 and H_2S using the Raman microprobe. Carbon dioxide was the only gas detected (Figure 323.5), which is in agreement with the results of the analysis of the melting temperatures of solid CO_2 in the fluid inclusions.

Analysis by Raman microprobe also identified the presence of the mineral nahcolite ($NaHCO_3$) as a solid phase in an inclusion in quartz (Figure 323.6) from an auriferous vein; and SEM-EDS analysis of solid phases in fractured samples of quartz from breccia veins indicated the presence of sericite,

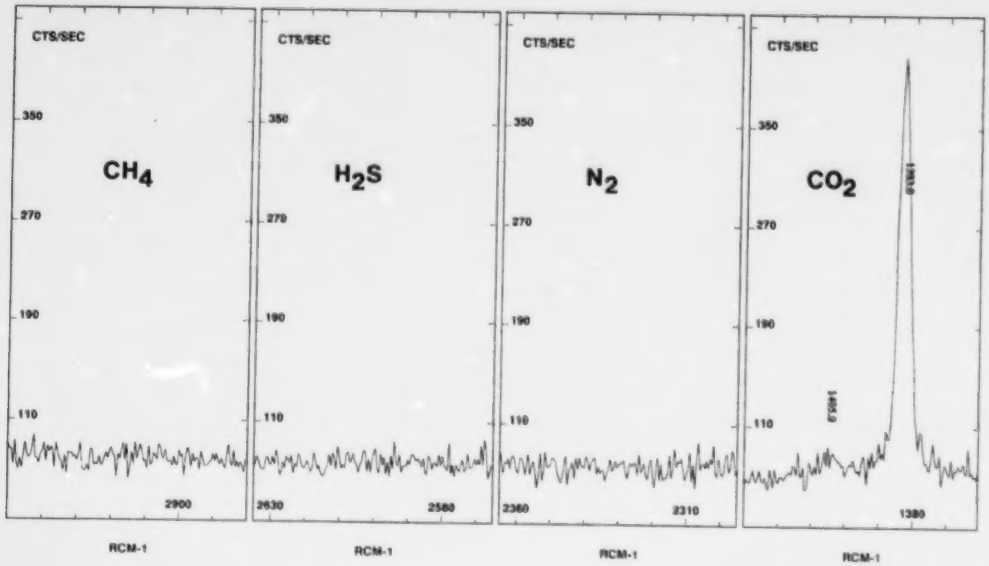

Figure 323.5. *Raman microprobe spectrum of the gas phase in a CO_2–H_2O fluid inclusion in quartz from an auriferous quartz-carbonate vein, Cameron Lake deposit (NC-16-432).*

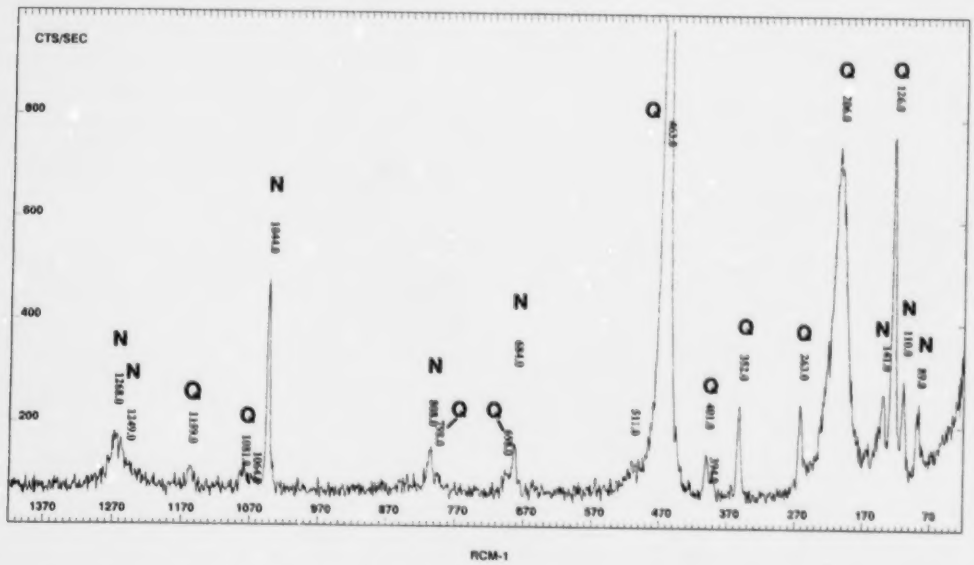

Figure 323.6. *Raman microprobe spectrum of nahcolite (N) which occurs as a daughter mineral in a CO_2–H_2O fluid inclusion in quartz from an auriferous quartz-carbonate vein, Cameron Lake deposit (NC-16-432). The peaks related to the host quartz are labelled with the letter Q.*

ankerite and calcite as either daughter minerals or accidentally trapped grains.

SUMMARY

The fluid activity that accompanied the development of the shear zone at Cameron Lake introduced massive amounts of CO_2, K, S and Au and resulted in hydrothermal carbonatization, sericitization and sulphidation of the wall rocks adjacent to breccia veins, the loci of gold mineralization in the deposit. Lithogeochemical and statistical analysis of potentially ore-grade material from pervasively altered and gold-bearing rock indicates that, of these elements, only S has a strong positive correlation with Au; a finding in keeping with the close spatial association

of pyrite with gold in the Cameron Lake deposit as evidenced in textural studies (Melling 1986; Melling *et al.* 1986).

Fluid inclusion and isotopic analyses indicate that the fluid present during shear zone development, vein formation, and hydrothermal alteration at Cameron Lake 1) was CO_2–H_2O bearing, of moderately high temperature (>230°C), low salinity (<3 weight percent equivalent NaCl, and low density (0.73 g/cm^3); and 2) was carrying isotopically light carbon ($\delta^{13}C \simeq -5‰$), and had an initial $^{87}Sr/^{86}Sr$ isotopic ratio of 0.7014 to 0.7016.

ACKNOWLEDGMENTS

Paul Nagerl, Dan Marshall and Larryn Diamond are thanked for their help with sample collection and preparation. We are also grateful to C. Beny for her assistance with the Raman microprobe analysis.

REFERENCES

Al-Aasm, I.S., Taylor, B.E. and South, B.

1988: Chemical Separation Techniques Appraisal for Isotopic Analysis of Multiple Carbonate Samples (abstract); Geological Association of Canada, Annual Meeting Program with Abstracts, Volume 13, p.A2.

Bell, K. and Blenkinsop, J.

1984: Multiple Collection in Mass Spectrometry; Geoscience Canada, Volume 11, p.50-52.

Collins, P.L.F.

1979: Gas Hydrates in CO_2-Bearing Fluid Inclusions and the Use of Freezing Data for Estimation of Salinity; Economic Geology, Volume 74, p.1435-1444.

Colvine, A.C., Fyon, J.A., Heather, K.B., Marmont, S., Smith, P.M. and Troop, D.G.

1988: Archean Lode Gold Deposits in Ontario; Ontario Geological Survey, Miscellaneous Paper 139, 136p.

Craig, H.

1957: Isotopic Standards for Carbon and Oxygen and Correction Factors for Mass Spectrometric Analysis of Carbon Dioxide; Geochimica et Cosmochimica Acta, Volume 12, p.133-149.

Faure, G.

1986: Principles of Isotope Geology; John Wiley & Sons, New York, 589p.

Friedman, I. and O'Neil, J.R.

1977: Compilation of Stable Isotope Fractionation Factors of Geochemical Interest, Data of Geochemistry; United States Geological Survey, Professional Paper 440-KK, 12p.

Grant, J.A.

1986: The Isocon Diagram—A Simple Solution to the Gresens' Equation for Metasomatic Alteration; Economic Geology, Volume 81, p.1976-1982.

Hickson, C.J. and Juras, S.J.

1986: Sample Contamination by Grinding; Canadian Mineralogist, Volume 24, p.585-589.

Kerrich, R.

1986: Fluid Transport in Lineaments; Philosopical Transactions of the Royal Society of London, Volume A317, p.219-251.

Kerrich, R., Fryer, B.J., King, R.W., Willmore, L.M. and Van Hees, E.

1987: Crustal Outgassing and LILE Enrichment in Major Lithosphere Structures, Archean Abitibi Greenstone Belt—Evidence on the Source Reservoir from Strontium and Carbon Isotope Tracers; Contributions to Mineralogy and Petrology, Volume 97, p.156-168.

Melling, D.R.

1986: The Geological Setting, Structure and Alteration Associated With Gold-Pyrite Mineralization at Cameron Lake, Wabigoon Subprovince, Northwestern Ontario; unpublished MSc Thesis, Carleton University, Ottawa, Ontario, 112p.

1987: The Occurrence of Gold in the Cameron-Rowan Lakes Area: Preliminary Report on the Monte Cristo and Victor Island Gold Prospects in the Monte Cristo Shear Zone; p.252-260 *in* Summary of Fieldwork and Other Activities 1986, edited by P.C. Thurston *et al.*, Ontario Geological Survey, Miscellaneous Paper 132, 435p.

Melling, D.R., Watkinson, D.H., Poulsen, K.H., Chorlton, L.B. and Hunter, A.D.

1986: The Cameron Lake Gold Deposit, Northwestern Ontario, Canada—Geological Setting, Structure, and Alteration; p.149-169 *in* Proceedings of Gold '86 Symposium, edited by A.J. Macdonald, Toronto, 517p.

Melling, D.R., Taylor, R.P. and Watkinson, D.H.

1988: Lithogeochemistry and Light Stable Isotope (Carbon, Oxygen and Sulphur) Geochemistry of Hydrothermal Alteration and Breccia-Veins from the Cameron Lake Gold Deposit, Northwestern Ontario; p.239-251 *in* Geoscience Grant Program Summary of Research 1987-1988, edited by V.G. Milne, Ontario Geological Survey, Miscellaneous Paper 140, 251p.

O'Neil, J.R.

1986: Terminology and Standards; p.561-570 *in* Stable Isotopes in High Temperature Geological Processes, edited by J.W. Valley *et al.*, Reviews in Mineralogy, Volume 16, Mineralogical Society of America, 570p.

Roedder, E.

1984: Fluid Inclusions; Reviews in Mineralogy, Volume 12, Mineralogical Society of America, 644p.

Whitehead, R.E.S., Davies, J.F. and Cameron, R.A.

1980: Carbonate and Alkali Alteration Patterns in the Timmins Gold-Mining Area; p.244-256, *in* Geoscience Research Grant Program, Summary of Research 1979-1980, edited by E.G. Pye, Ontario Geological Survey, Miscellaneous Paper 93, 262p.

Grant 326 PGE Studies in the Footwall at Sudbury

C. Li and A.J. Naldrett

Department of Geology, University of Toronto, Toronto

ABSTRACT

Ni–Cu sulphide ore deposits in the Strathcona Mine, on the North Range of the Sudbury Igneous Complex, are zoned, with Cu, Pt, Pd, Au and to a lesser extent Ni increasing toward the footwall and Co, Rh, Ru, Ir and Os showing the reverse trend.

The Deep Copper Zone at the Strathcona Mine occurs as a system of multiple veins and veinlets cutting the Sudbury breccia and the footwall gneisses, parallel to and 400-500 m away from the contact of the Sudbury Igneous Complex (SIC). It is richer in platinum group elements (PGE) than other ore types of this deposit. PGE concentrations vary considerably within the zone. Generally, Pt and Pd increase in areas where Os, Ir, Ru and Rh decrease in abundance. This zonation is visible across the vein system as a whole with Pt, Pd increasing and Os, Ir, Ru, Rh decreasing away from the contact. The same trend of increasing Pt and Pd is also observed on passing from the main veins to some small branching veins and also at the terminations of the veins. This zoning is believed to be the result of the fractionation of sulphide liquid as it was expelled progressively away from the contact of Sudbury Igneous Complex.

INTRODUCTION

The purpose of this project is to investigate the distribution of PGE within and near Cu-rich veins which occur in the footwall of the North Range of the Sudbury Igneous Complex in the vicinity of the Strathcona deposit (the Deep Copper Zone).

It is known that PGE are concentrated in these veins. In certain deposits on the South Range they are also concentrated external to massive Ni–Cu ore in hydrothermally emplaced mineralization (Zurbrigg *et al.* 1957). One of the objectives of this pro-

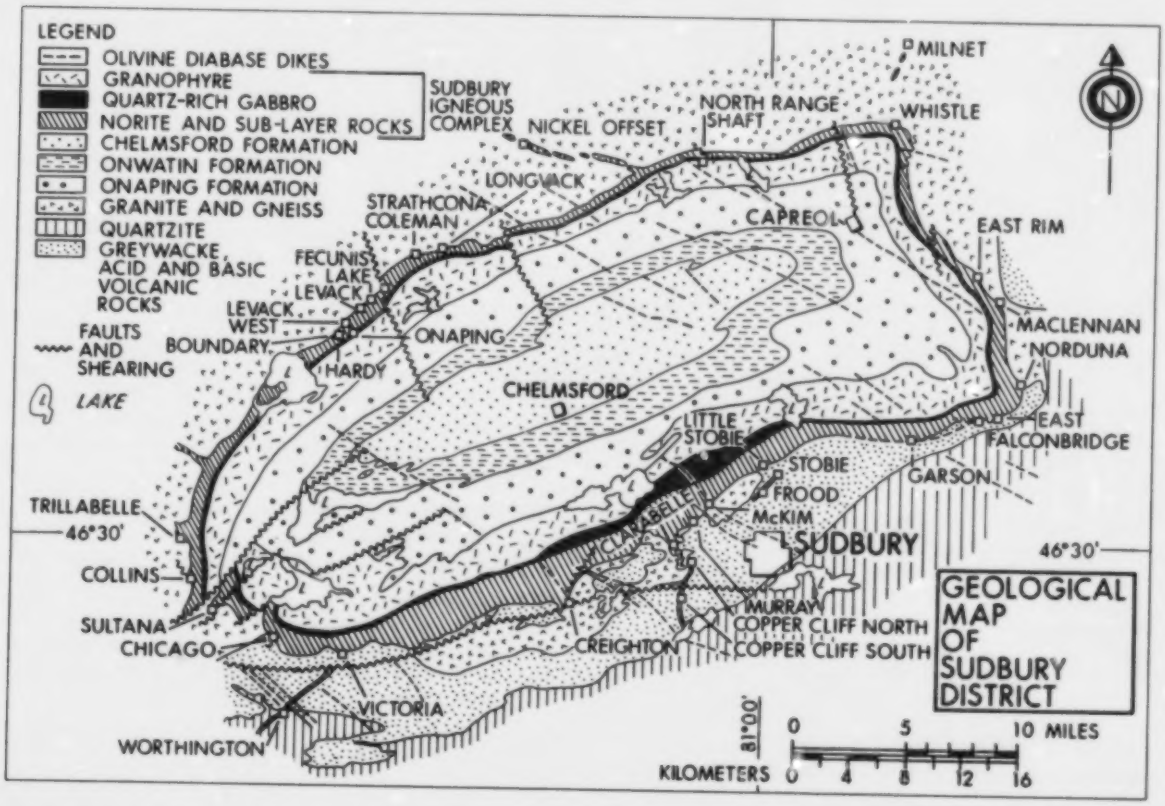

Figure 326.1. *Geological map of the Sudbury Igneous Complex and surrounding area.*

ject is to study the process of this concentration on the North Range, and to see if similar, hitherto undiscovered, hydrothermal mineralization is also present there.

During the first year of the project, the main emphasis has been given to determining possible chemical variation trends based on available mine data for Pt, Pd, Au, Cu, Ni and Co, and developing a system for analyzing Cu-rich samples for the full spectrum of PGE.

GEOLOGICAL BACKGROUND

The Sudbury Igneous Complex (Figure 326.1) is Canada's principal source of platinum group elements. The PGE are distributed widely throughout the deposits of the area.

The Sudbury ores are associated with a particular phase of the Sudbury Igneous Complex known as the Sublayer, and with a particular phase of the Sublayer which carries mafic and ultramafic inclusions (Naldrett 1984). The ore deposits fall into three main groupings:

1. North Range contact deposits, in which the ore occurs primarily in "footwall breccia" and, to a lesser extent, occurs both disseminated in overlying Sublayer and as a massive filling of fractures in the underlying gneiss.
2. South Range contact deposits, in which the ore is found mostly as massive lenses and as the matrix to a breccia of mafic and ultramafic fragments along the footwall contact, and to a lesser extent, as a dissemination in overlying sublayer.
3. Offset deposits, in which the ore occurs associated with zones rich in mafic and ultramafic inclusions in dike-like bodies of Sublayer.

Variations of these three basic types also occur, particularly where orebodies have been affected by faulting.

THE STRATHCONA MINE

This deposit has been described by Naldrett *et al.* (1967), Cowan (1968), Abel *et al.* (1979) and Coats and Snajdr (1984). The ore lies at the base of the North Range of the Sudbury Igneous Complex which dips about 35°S (Figure 326.2 and 326.3). Four ore types are observed. Disseminated sulphides of the Hanging-Wall Zone ore occur within an inclu-

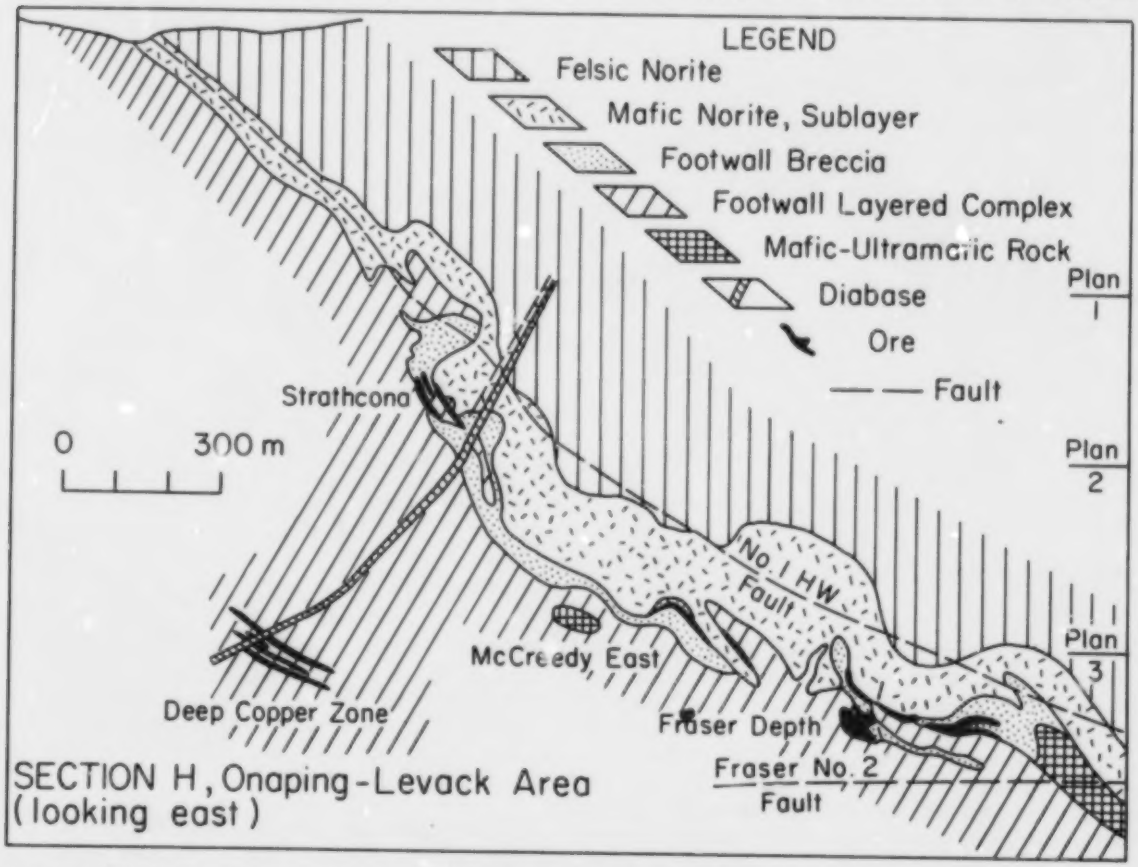

Figure 326.2. *Geological cross section of the North Range of the Sudbury Igneous Complex in the Onaping-Levack area (looking east).*

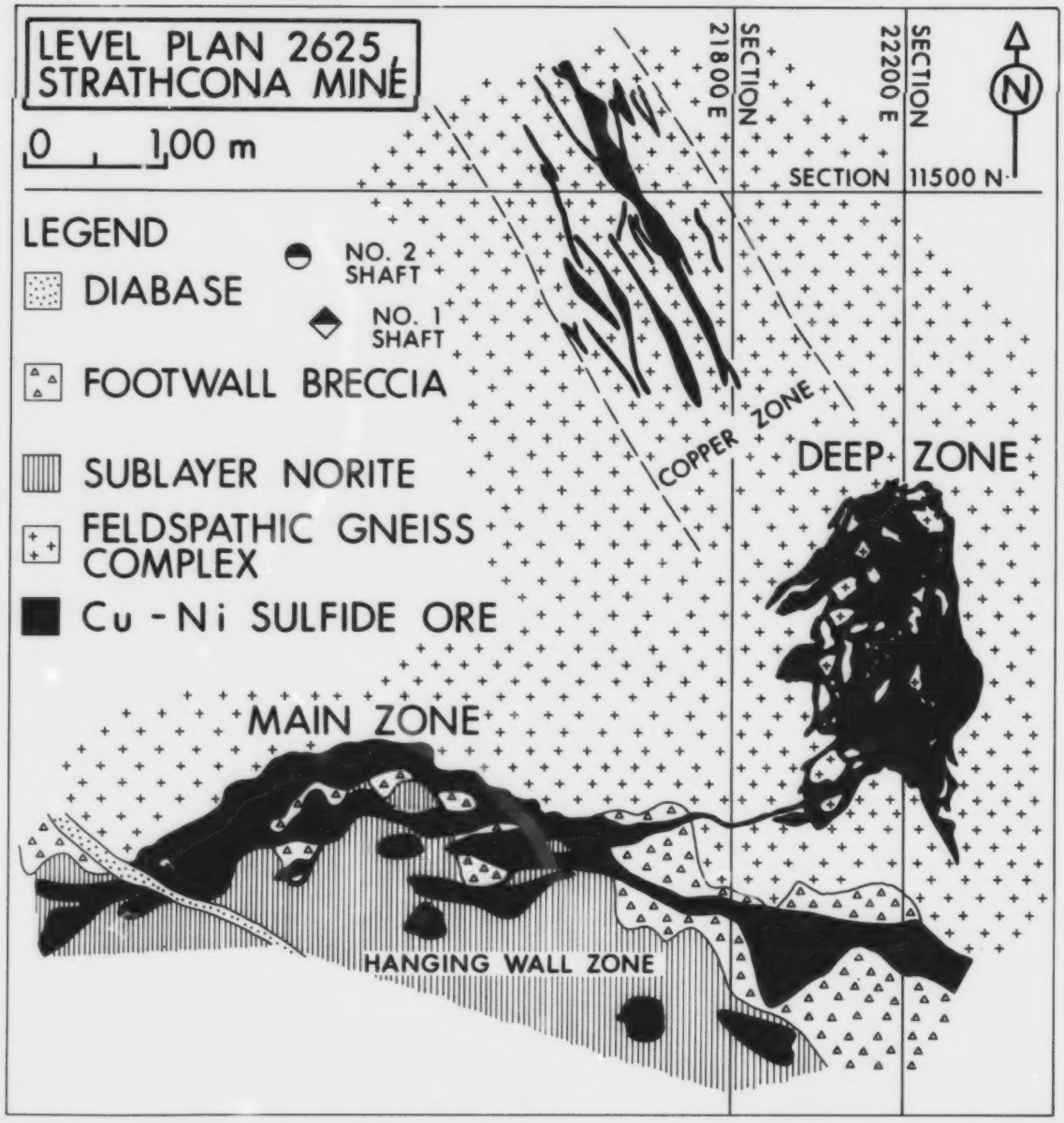

Figure 326.3. *Geological plan of the Strathcona Mine at the 2625 level.*

sion-bearing facies of the Sublayer. This is underlain by the Main Zone ore which consists of massive and disseminated ore within the Footwall Breccia which is composed of fragments of gneiss, and the Deep Zone ore which consists of stringers of massive sulphide emplaced in fractures within the gneisses forming the footwall. Pyrrhotite, chalcopyrite, magnetite and pyrite are the main minerals in each of the preceding ore zones. Very rich stringers of massive chalcopyrite (Cu Zone) with minor magnetite (5%), pyrrhotite (3.5%), pentlandite (1.5%) and sphalerite (0.5%) have long been known to occur 100–200 m into the footwall. In 1979, 15 years after mining commenced, a second more extensive zone of Cu-rich stringers, the Deep Copper Zone, (*see* Figure 326.2) was discovered up to 500 m from the contact into the footwall.

The Main Zone ore is confined to a specific type of footwall breccia characterized by a higher proportion of ultramafic fragments and a more mafic matrix than most of this breccia. The contact of this

breccia unit with the overlying Sublayer is gradational. Naldrett *et al.* (1967) believed that the ore at the Strathcona Mine was emplaced together with the Sublayer, that it settled into the footwall breccia, and that some sulphides penetrated fractures in the footwall to form the Deep Zone ore.

THE DEEP COPPER ZONE

The host rocks of the Deep Copper Zone are footwall gneisses (believed to be the metamorphosed remnants of an ancient layered complex, Coats and Snajdr 1984) which was extensively brecciated prior to intrusion of the SIC to form Sudbury Breccia. The Deep Copper Zone has an arcuate form in section (*see* Figure 326.2) parallel to the contact of the SIC and 400–500 m away from it. The sulphide ore occurs as massive veins and veinlets cutting the Sudbury Breccia and the footwall gneisses (Figure 326.4). Although there is some apparent continuity of the veins in dip length, attitudes of individual veins within the zone are not well known (the underground development was only just intersecting the veins in September 1988). The orientations of the veins are varied, but the principal directions are northwesterly and easterly. The zone as a whole appears to strike northwest and to plunge southwest. It is likely that the zone consists of a complex, multivein, interconnecting system. The veins range in width from minute stringers to a maximum of about 6 m.

Common sulphide minerals in the Deep Copper Zone include chalcopyrite, cubanite, pentlandite, millerite, pyrrhotite and bornite. Magnetite is also a common mineral together with ilmenite. Accessory minerals include galena, altaite, hessite, native silver and gold, parkerite, chalcocite, mackinawite and sphalerite. A number of platinum group minerals, mostly bismuthides and tellurides, are present as extremely small grains (1–5 μm). Although the contacts are sharp, the chalcopyrite is dispersed a distance of several millimetres to several centimetres into the wall rocks. The dispersion is often accompanied by chlorite, epidote, amphibole and Mn-rich silicates, which give rise to visible dark selvage bands along the sulphide veins.

METAL DISTRIBUTION

Both Cowan (1968) and Naldrett *et al.* (1967) noted the pronounced and systematic zoning in metal values across the Strathcona deposit with Ni, Cu and the Cu/(Cu+Ni) ratio in the sulphides in-

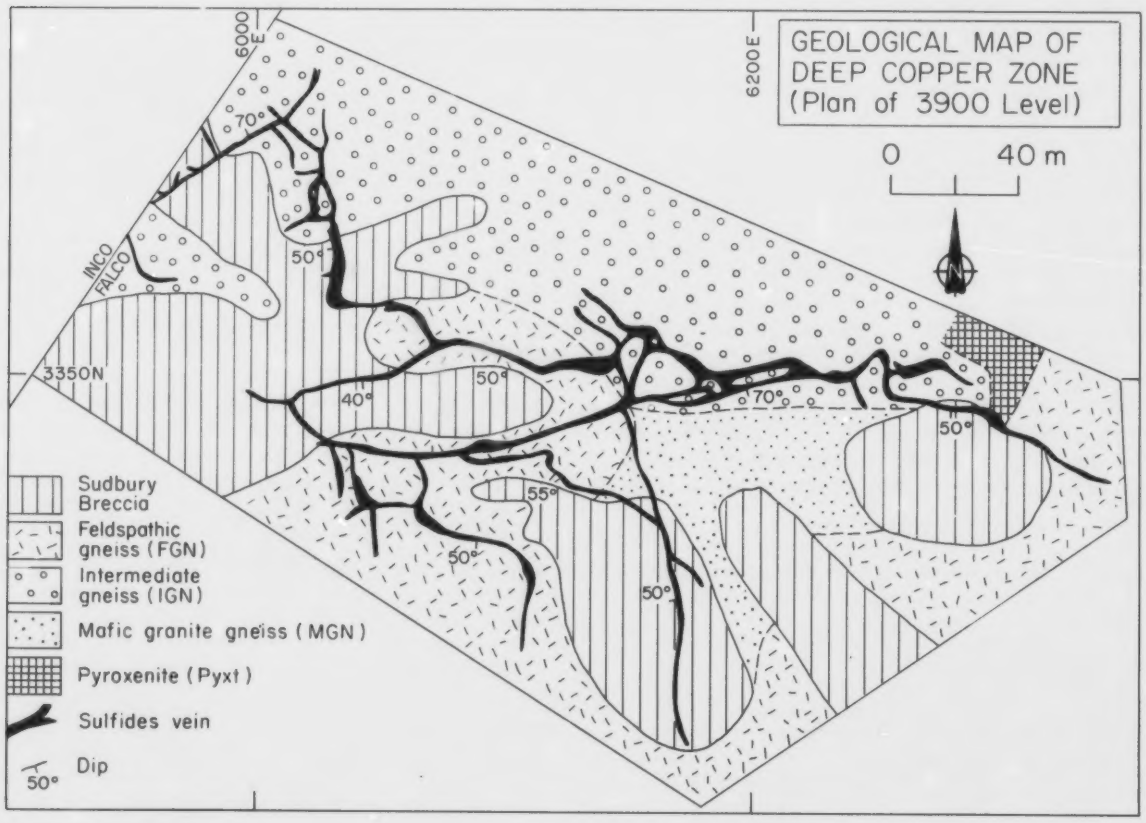

Figure 326.4. *Geological plan of Deep Copper Zone at the 3900 level of the Strathcona Mine.*

creasing from hanging wall to footwall. This zoning is particularly apparent across the Main Zone. The Hanging-Wall Zone ore is generally Ni and Cu-poor, with a low Cu/(Cu+Ni) ratio. The Cu Zone and Deep Copper Zone represent a continuation of this zoning trend.

Naldrett *et al.* (1982) drew attention to the co-variation of PGE with the base metals throughout the Sudbury ores. They showed that individual PGE in the ores are fractionated from each other, with Pt and Pd increasing with Cu and Au progressively away from the hanging wall toward the footwall, and Rh, Ru, Ir and Os showing the reverse trend. This trend is particularly demonstrated at the Strathcona Mine, where the lowest (Pt+Pd)/(Ru+Ir+Os) ratios are in the Hanging-Wall Zone ore and the highest ratios in the Cu-rich stringers of the Cu Zone. The available data from the mine has indicated that Pt and Pd are extremely rich in the Deep Copper Zone.

SAMPLES AND ANALYTICAL TECHNIQUES

Samples have been collected at 3900 underground exposures along, across and around the veins in such a way as to be representative of the different ore types, and also to detect any variation that might be present within the ore zone.

An additional 60 samples have been collected to date for full-spectrum PGE analysis and so far 15 analyses have been completed for Cu, Co, Ni, S, Au and PGE. Cu, Co, Ni and S analyses were by X-Ray fluorescence (XRF) at X-Ray Assay Laboratory, Don Mills, Ontario. The PGE and Au were determined by a fire-assay and neutron-activation procedure modified after that described by Hoffman *et al.* (1978) at the SLOWPOKE Laboratory and the Department of Geology Laboratory, University of Toronto. Since our samples are extremely Cu-rich, it is necessary to reduce the massive sulphide ore samples to 10–20 g and add additional Ni to achieve a ratio of Ni/Cu of more than 5. In this way a good fire assay button is obtained which can be dissolved easily in hydrochloric acid. Samples with low levels of Os, Ir and Ru, and high Pt and Au require an additonal count for Os, Ir and Ru approximately a month after the end of the irradiation. Information on detection limits, precision, and accuracy is given by Hoffman *et al.* (1978). It is necessary to count for more than 15 000 seconds for these elements in our samples. In accordance with the practice reported in previous papers, some duplicate analyses for each sample have been averaged. The duplicate analyses agree to within 20% for Pd, Pt, Au and Ir, and 90% for Os, Ru and Rh. The poor reproducibility for the last three elements is because their concentrations are close to background.

Since the deposits are believed to have been formed by the crystallization of a sulphide liquid, it has been our aim to characterize the composition of this liquid. Naldrett and Duke (1980) introduced a method to recalculate the analyses to 100% sulphides, in which they assumed that the mineralogy is dominantly pentlandite, chalcopyrite and pyrrhotite. The factor (F) for this calculation is:

$$F = 0.45Ni + 0.36Cu + 2.5S.$$

This is not suitable for our Deep Copper Zone ores. If we used this factor, the massive sulphide ore would calculate to have up to 120% of sulphides. This is due to significant amounts of Fe-poor or S-rich minerals, such as pyrite, millerite and bornite, in the ores. A better method to calculate F is to use pyrite instead of pyrrhotite as the iron sulphide. In this case, the factor is:

$$F = 0.83Ni + 0.97Cu + 1.89S,$$

but this is still too high to adequately describe the Deep Copper Zone massive ores. Based on a number of massive sulphide ore analyses, we found that the factor that statistically best described the Deep Copper Zone is:

$$F = 1.7S + 0.97Cu + 0.83Ni.$$

The recalculated data presented in Table 326.3 are based on this factor.

PRELIMINARY RESULTS AND DISCUSSION

The Ni, Cu, Co, Au, Pt, Pd, Ag and Pb contents of 439 analyses of massive sulphide ore, collected at the 3900 m level of the Deep Copper Zone, have been composited and examined in terms of the vari-

TABLE 326.1. METAL CONTENT (IN 100% SULPHIDES) IN DEEP COPPER ZONE.

Region	No. of Samples	wt.%			ppm					wt.% (Cu+Ni)	ppm (Pt+Pd)
		Ni	Cu	Co	Pt	Pd	Au	Ag	Pb		
I	135	1.95	27.27	0.04	4.01	6.56	0.41	167.2	0.08	29.22	10.57
II	49	1.94	26.91	0.03	4.93	6.72	0.45	186.4	0.06	28.85	11.65
III	137	2.19	28.19	0.03	4.5	7.62	0.31	154.5	0.05	30.38	12.12
IV	57	1.64	29.01	0.02	5.57	7.89	0.59	131.2	0.04	30.65	13.46
V	55	1.7	31.21	0.01	6.69	9.25	0.59	113.4	0.09	32.91	15.92
VI	6	3.19	29.49	<0.01	7.9	9.32	0.62	155.7	0.06	32.68	17.22
Average	439	1.97	28.27	0.03	4.86	7.47	0.43	138.5	0.06	30.24	12.32

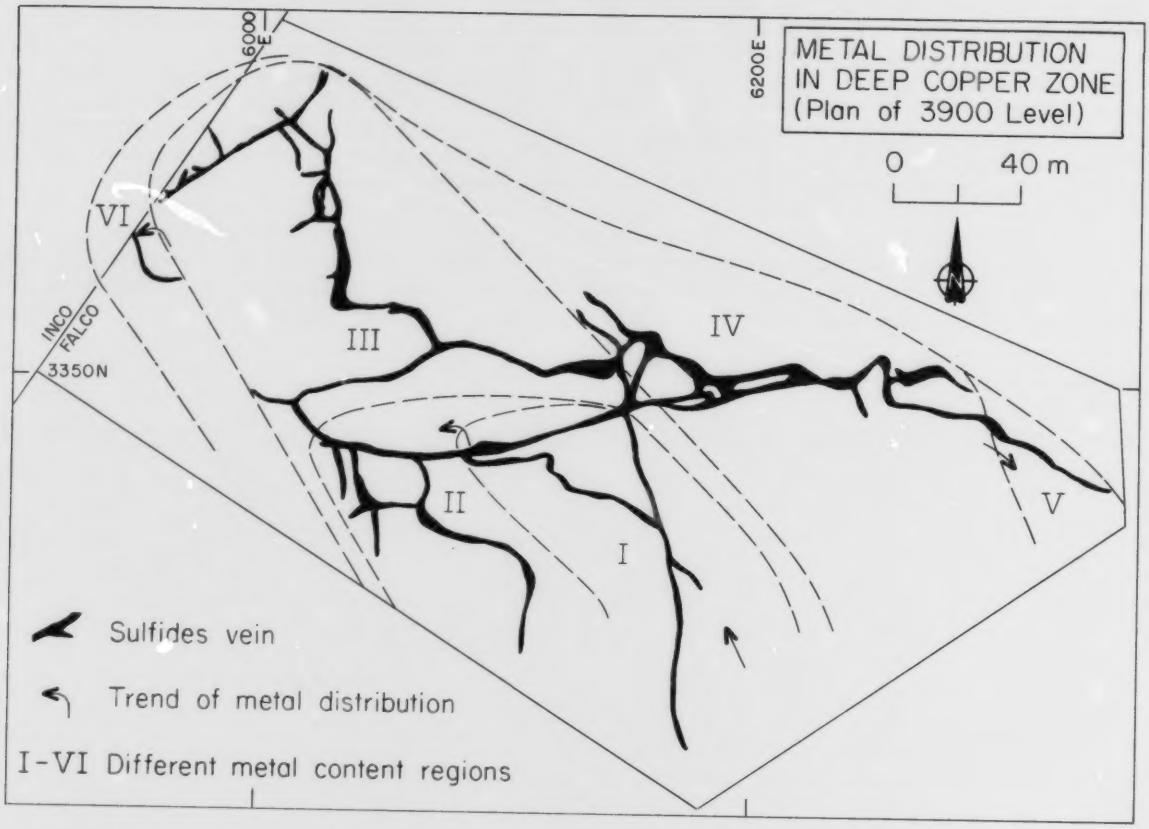

Figure 326.5. *Metal distribution in Deep Copper Zone (plan of 3900 level).*

ations that they display across the zone. The regions within which composites were calculated are numbered I to VI in Figure 326.5. Results of the analyses are illustrated in Table 326.1. The data indicate that Co decreases and that (Cu+Ni), Pt, Pd and Au increase in a direction directly away from the contact of the Sudbury Igneous Complex, and then in a northwesterly and southeasterly direction along the vein system. These compositional variations are consistent with the progressive fractional crystallization of a sulphide liquid (Naldrett *et al.* 1982), and may therefore indicate the direction in which the sulphide liquid entered and moved along the system.

A total of 3000 analyses for Ni, Co, Cu, Pt, Pd and S from the 3900–10 horizontal drilling level have been composited in the terms of width of the veins intersected by drill holes. Veins thicker than 0.4 m are described as "main veins", and those that are narrower as "small veins". The results indicate that disseminated sulphides occurring within some small veins and terminations of veins branching off main veins are richer in (Pt+Pd) and, to a lesser extent, in (Cu+Ni) than the main veins. This is illustrated in Figure 326.6, where it is seen that (Cu+Ni)

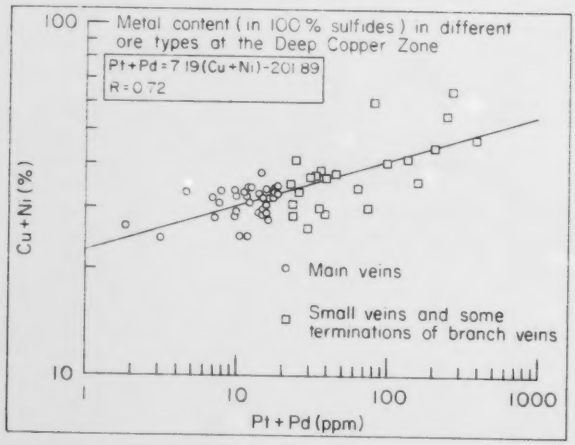

Figure 326.6. *Metal content (in 100% sulphides) in different ore types at the Deep Copper Zone.*

varies between 24% and 36% in the main veins and between 25% and 60% in the small veins and branches. From the main veins to some of the small veins, (Pt+Pd) increases with (Cu+Ni) with a correlation coefficient of 0.72. The extreme enrichment in PGE's toward what appear to be the terminations of veins is important from the point of view that these may be the end-product of sulphide liquid fractionation.

Our initial 15 full-spectrum PGE analyses are given in Table 326.2 and the values recalculated to 100% sulphides in Table 326.3. The data indicate that Os, Ir, Ru and Ru are extremely low, with Os less than 9 ppb, Ir less than 1 ppb, Ru less than 9 ppb and Rh less than 60 ppb for all the samples. The average value for the analyses is also given in the Table 326.3. The detection limits (Os<1 ppb, Ru<0.1 ppb and Rh<0.5 ppb) were used for those samples occurring at less than the detection limits on computing the averages. On the other hand, Pt, Pd and Au are very high. In comparison with other zones of the Strathcona deposit, the Deep Copper Zone shows significant Pt and Pd enrichment and Os, Ir, Ru and Rh depletion, and high ratios of Cu/(Cu+Ni) and (Pt+Pd)/(Os+Ir+Ru) (Table

TABLE 326.2. PGE CONTENT OF THE DEEP COPPER ZONE ORES.

	ppb						
Sample	Os	Ir	Ru	Rh	Pt	Pd	Au
2a	0.2	0.07	-	0.06	3948.5	1356.11	1323.3
2b	1.2	0.1	-	0.45	4247.9	1202.29	1441.6
3a	2.1	0.08	1.7	14.38	744.4	9137.28	7.1
3b	0.7	0.07	1.3	0.71	676.1	8766.63	58
4	1.7	0.03	0.1	-	2670.3	740.37	151.5
6	-	0.05	2.2	-	1101.5	3202.73	36.4
8	-	0.1	-	1.81	3219.3	4879.04	202.3
10	8.8	0.11	5.4	-	5606.9	9213.59	158.7
11	-	0.31	4.3	52.5	3466.7	8167.18	243.7
12a	-	0.05	0.6	-	3572.8	3475.32	2220.7
12b	7	0.14	0.8	0.94	2968.2	3590.69	2881.5
14	-	0.24	2.6	44.9	2052	4402.11	20.1
16	-	0.04	7.6	0.45	5296.7	7445.55	483.3
17	-	0.01	-	-	4130.6	6784.62	241.5
18	2.7	0.12	-	-	4138.9	4703.39	186.6
19a	0.2	0.07	5.7	2.77	9489.9	4987.86	258
19b	9.4	0.17	6.5	3.57	10553.6	5208.17	274.2
20	1.6	0.17	0.5	-	2214.4	4151.22	166
21	-	0.03	4.2	-	3260.6	5169.44	46.1

	wt.%				
Sample	Ni	Cu	Co	S	F
2a	4.85	1.15	0.022	4.45	7.87
2b	4.85	1.15	0.022	4.45	7.87
3a	49	0.16	0.37	31.3	1
3b	49	0.16	0.37	31.3	1
4	0.42	36	0.028	43.1	1
6	1.43	36	0.038	42.5	1
8	0.32	31.8	0.028	40.6	1
10	1.06	32.5	0.03	41.5	1
11	0.44	29.3	0.033	42.7	1
12a	5.05	11.2	0.047	25.2	1.73
12b	5.05	11.2	0.047	25.2	1.73
14	0.47	32.8	0.032	25.7	1.32
16	2.64	23.4	0.041	37.6	1.13
17	1.06	21.4	0.029	37.7	1.17
18	0.4	25.9	0.028	41.9	1.03
19a	6.84	19.3	0.05	40.8	1.07
19b	6.84	19.3	0.05	40.8	1.07
20	0.64	24.9	0.032	36.8	1.15
21	0.45	25.2	0.031	40.5	1.07

a and b are duplicate analyses

326.4). This trend is well illustrated in Figure 326.7. It can be seen that the Deep Copper Zone falls at one extremity of the compositional variation shown by the deposit. We believe that this is due to the fractionation during the cooling of an Fe-rich sulphide melt, with the fractionated liquid being expelled progressively away from the contact. The early crystallization of monosulphide solid solution concentrated Fe, Co, Ru, Rh, Ir and Os, leading to an enrichment in Ni and, even more so, in Cu, Pt, Pd and Au in the residual liquid (*see* Naldrett *et al.* 1982; Makovicky *et al.* 1986).

It has been known that ores in the Deep Copper Zone fall into four types: chalcopyrite ore, pentlandite ore, millerite ore and chalcopyrite-quartz ore. It is also known that PGE distribution in the zone is not uniform. However, so far, time and limited data have not permitted a coupling of the distribution of the full spectrum of PGE with ore types within the zone. Future studies will include analyzing additional samples and evaluating the co-variation of both PGE and ore minerals with the major compositional variations of the ore zones.

TABLE 326.3. METAL CONTENT OF THE DEEP COPPER ZONE ORES (RECALCULATED TO METAL CONTENT IN 100% SULPHIDES).

	ppb						
Sample	Os	Ir	Ru	Rh	Pt	Pd	Au
2	5.5 ± 3.9	0.67 ± 0.12	-	2.01 ± 1.54	32214 ± 1175	10055 ± 605	12716 ± 1385
3	1.4 ± 0.7	0.08 ± 0.01	1.5 ± 0.2	7.55 ± 6.84	710 ± 34	895 ± 185	32 ± 27
4	1.7	0.03	0.1	-	2670	740	1515
6	-	0.05	2.2	-	1102	3203	36
8	-	0.1	-	1.81	3219	4879	202
10	8.8	0.11	5.4	-	5606	9214	159
11	-	0.31	4.3	52.5	3467	8167	244
12	7.07 ± 5.05	0.17 ± 0.08	1.44 ± 0.4	0.8 ± 0.6	5658 ± 523	6112 ± 100	4214 ± 772
14	-	0.32	3.43	59.27	2709	5811	27
16	-	0.05	8.59	0.51	5985	8413	546
17	-	0.01	-	-	4832	7938	283
18	2.8	0.12	-	-	4263	4870	192
19	5.13 ± 4.93	0.13 ± 0.06	6.53 ± 0.43	3.39 ± 0.43	10723 ± 569	5455 ± 118	285 ± 9
20	1.84	0.2	0.58	-	2547	4774	191
21	-	0.03	4.49	-	3489	5531	49
Average	<2.75	0.16	<2.6	<8.76	5946	5737	1379

	wt.%				wt.%	ppb	Cu/	Pt/	(Pt+Pd)/	Pd/(Ir
Sample	Ni	Cu	Co	S	(Cu+Ni)	(Pt+Pd)	(Cu+Ni)	(Pt+Pd)	(Ir x 1000)	x 1000)
2	38.12	9.04	0.173	34.98	47.16	42269	0.19	0.76	6.3	1.5
3	49	0.16	0.37	31.3	49.16	9662	0.003	0.07	12.08	11.2
4	0.42	36	0.028	43.1	36.42	3411	0.99	0.78	11.37	2.5
6	1.43	36	0.038	42.5	37.43	4304	0.96	0.26	8.61	6.4
8	0.32	31.8	0.028	40.6	32.12	8098	0.99	0.4	8.09	4.9
10	1.06	32.5	0.03	41.5	32.56	14820	0.78	0.38	13.34	8.4
11	0.44	29.3	0.033	42.7	29.74	11634	0.99	0.3	3.75	2.6
12	8.74	19.38	0.081	43.6	28.12	11770	0.69	0.48	6.92	3.6
14	0.62	43.4	0.042	33.92	43.92	8519	0.96	0.32	2.66	1.8
16	2.98	26.44	0.046	42.49	29.42	14399	0.9	0.42	28.8	16.8
17	1.24	25.04	0.034	44.11	26.08	12771	0.96	0.38	127.71	79.4
18	0.41	26.68	0.029	43.16	27.09	9133	0.98	0.47	7.61	4.1
19	7.32	20.65	0.05	43.66	27.97	16178	0.74	0.66	12.44	4.2
20	0.74	28.64	0.037	42.32	29.38	7320	0.97	0.35	3.66	2.4
21	0.48	26.96	0.033	43.34	27.44	9020	0.62	0.39	30.07	18.4
Average	7.55	26.13	0.07	40.89	33.68	11683	0.78	0.51	7.3	3.6

TABLE 326.4. COMPARISON OF AVERAGE METAL CONCENTRATION IN DIFFERENT ORE TYPES AT STRATHCONA.

Ore Type	No. of Samples	wt.%			ppb						
		Ni	Cu	Co	Pt	Pd	Rh	Ru	Ir	Os	Au
Hanging-wall ore	10	3.1	0.37	0.21	114	105	60	52	29	20	19
Breccia ore	18	3.4	1.2	0.14	413	380	20	12	7	4	78
Footwall ore	8	4	2.3	0.13	750	701	16	4	4	3	112
Copper zone*	1	0.39	29.6	0.02	2551	890	4	3	0.2	2	189
Deep copper zone*	15	1.97	28.3	0.03	4860	7470	<8.76	<2.6	0.16	<2.75	430
Chondrites (CI)**					1020	545	200	690	540	514	152

Ore Type	No. of Samples	Cu/ (Cu+Ni)	Pt/ (Pt+Pd)	(Pt+Pd)/ (Ru+Ir+Os)
Hanging-wall ore	10	0.11	0.52	1.2
Breccia ore	18	0.26	0.52	3.4×10
Footwall ore	8	0.37	0.52	1.3×10^2
Copper zone*	1	0.99	0.74	6.6×10^2
Deep copper zone*	15	0.93	0.4	3.9×10^3

* *This study.* ** *Ehmann and Gillum (1972); Krähenbühl et al. (1973); Mason (1971); Wolf and Anders (1980). Other data from Naldrett et al. (1982).*

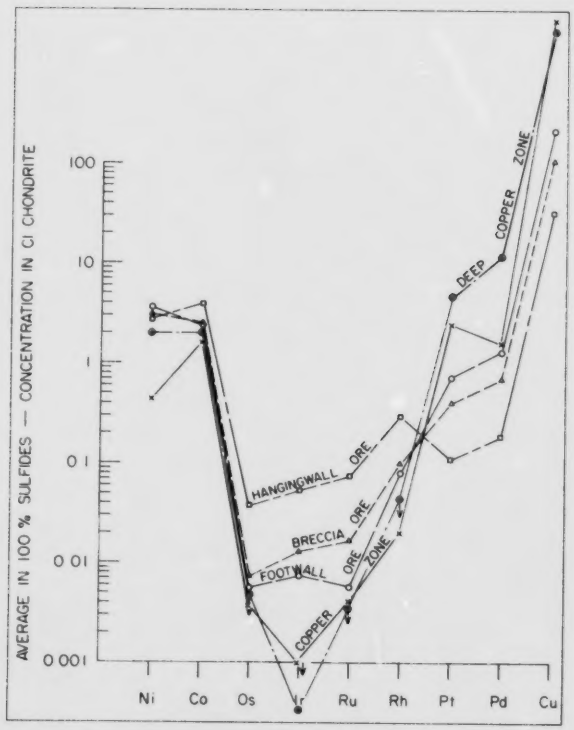

Figure 326.7. ***Average metal content (chondrite normalized) in sulphides in different ore types.***

CONCLUSIONS

Several conclusions can be drawn on the basis of the work to date.

1. PGE concentration in the Deep Copper Zone is consistent with the trend of variations shown by other ore zones at the Strathcona Mine. Significant enrichment of Pt and Pd occurs along with the depletion of Os, Ir, Ru and Rh with an increase in Cu/(Cu+Ni) and decrease in Co.
2. Within the vein system, Pt, Pd and Au increase with (Cu+Ni) and decrease of Co in a direction directly away from the contact of Sudbury Igneous Complex, and then in a northwesterly and southeasterly direction along the veins system. These compositional variations are consistent with the progressive fractional crystallization of a sulphide liquid, and may therefore indicate the direction in which the sulphide liquid entered and moved along the system.
3. Disseminated ore within some smaller veins branching off the main vein system is very much richer in Pt, Pd, and slightly richer in (Cu+Ni) than the main veins. Therefore, this may be the end product of sulphide liquid fractionation.

ACKNOWLEDGMENTS

The authors would like to thank R.G.V. Hancock (SLOWPOKE Laboratory, University of Toronto) for the use of the reactor and counting facilities and M.J. Gorton (Department of Geology, University of Toronto) for access to INAA counting equipment in the Department of Geology Laboratory. We are most grateful to C.J.A. Coats, P. Johannessen,

N.K. Abel and S. B. Nikolic (Falconbridge Limited, Sudbury Operations) and other staff at the Strathcona Mine for the support during field work.

REFERENCES

Abel, M.K., Buchan, R., Coats, C.J.A. and Penstone, M.E.

1979: Copper Mineralization in the Footwall Complex, Strathcona Mine, Sudbury, Ontario; Canadian Mineralogist, Volume 17, p.275-286.

Coats, C.J.A. and Snajdr, P.

1984: Ore Deposits of the North Range, Onaping-Levack Area, Sudbury; p.327-346 *in* The Geology and Ore Deposits of the Sudbury Structure, edited by E.G. Pye *et al.*, Ontario Geological Survey, Special Volume 1.

Cowan, J.C.

1968: The Geology of the Strathcona Ore Deposit, Sudbury District, Ontario; Canadian Institute of Mining and Metallurgy, Bulletin, Volume 61, p.38-54.

Ehmann, W.D. and Gillum, D.E.

1972: Platinum and Gold in Chondritic Meteorites; Chemical Geology, Volume 9, p.1-11.

Hoffman, E.L., Naldrett, A.J., Van Lan, J.C., Hancock, R.G.V. and Mason. A.

1978 The Determination of the Platinum Group Elements and Gold in Rocks and Ore by Neutron Activation Analysis after Preconcentration by a Nickel Sulfide Fire-assay Technique on Large Sample Sizes; Analytica Chimica Acta, Volume 102, p.157-176.

Krähenbühl, U.R., Morgan, W., Ganapathy, R. and Anders, E.

1973: Abundance of Seventeen Trace Elements in Carbonaceous Chondrites; Geochimica et Cosmochimica Acta, Volume 37, p.2353-1370.

Makovicky, M., Makovicky, E. and Rose-Hansen, J.

1986: Experimental Studies on the Solubility and Distribution of Platinum Group Elements in Base-metal Sulfides in Platinum Deposits; p.415-426 *in* Metallogeny of Basic and Ultrabasic Rocks, edited by M.J. Gallagher, R.A. Ixer, C.R. Neary and F.M. Pritchard, Institute of Mining and Metallurgy, London, Special Publication.

Mason, B. (editor)

1971: Elemental Abundances in Meteorites; Gordon and Breach Science Publishing, New York, 555p.

Naldrett, A. J.

1984: Summary, Discussion and Synthesis; p.533 *in* The Geology and Ore Deposits of the Sudbury Structure, edited by E.G. Pye, A.J. Naldrett and P.E. Giblin, Ontario Geological Survey, Special Volume 1.

Naldrett, A.J. and Duke, J.M.

1980: Platinum Metals in Magmatic Sulfide Ores; Science, Volume 208, p.1417-1428.

Naldrett, A. J., Craig, J. and Kullerud, G.

1967: The Central Portion of the Fe-Ni-S System and its Bearing on Pentlandite Solution in Iron-Nickel Sulfide Ores; Economic Geology, Volume 62, p.826-847.

Naldrett, A.J., Innes, D.G., Sowa, J. and Gorton, M.

1982: Compositional Variation within and between 5 Sudbury Ore Deposits; Economic Geology, Volume 77, p.1519-1534.

Wolf, R. and Anders, E.

1980: Moon and Earth. Compositional Differences inferred from Siderophiles, Volatiles and Alkalies in Basalts; Geochimica et Cosmochimica Acta, Volume 44, p.211-2124.

Zurbrigg, H.F. and Geological Staff

1957: The Frood-Stobie Mine; p.341-350 *in* Structural Geology of Canadian Ore Deposits 2, (Congress Vol.) Canadian Institute of Mining and Metallurgy.

Grant 328 Microbial Biofilms: Colonization, Metal Uptake, and Mineralization

F.G. Ferris[1], J.B. Thompson[2], S. Schultze[2], T. Witten[2], W.S. Fyfe[1] and T.J. Beveridge[2]

[1]Department of Geology, University of Western Ontario, London

[2]Department of Microbiology, University of Guelph, Guelph

ABSTRACT

Microbial biofilms from various natural rock surfaces and limestone and granite blocks placed in two Ontario rivers exhibited a communal mode of growth in which heterotrophic bacteria were attached to the surface of algae, cyanobacteria, and organic detritus on the substrates examined. Heterotrophic bacterial counts were 10 to 100 times more abundant on limestone (10^6 to 10^7 CFU/cm^2)* than corresponding counts from granite, gabbro, rhyolite, basalt, and quartz. Heterotrophic bacteria were an order of magnitude more abundant than either cyanobacteria or algae. Microbial population density was inversely related to rock (mineral) hardness.

Microbial biofilms, grown on *in situ* settling strips submerged at both neutral (pH $\approx$ 6.8) and acidic (pH $\approx$ 3.0) sites in a metal-contaminated watershed, bound Mn, Fe, Ni and Cu in excess of the amount adsorbed by control strips. Planktonic bacteria increased from 10^1 to 10^3 CFU/ml at all sites during the 17-week study period. Biofilm counts leveled off at 10^4 CFU/cm^2 at the neutral sites and 10^3 CFU/cm^2 at the acidic sites. Microbial biofilm metal-uptake at the neutral sites were enhanced by up to 12 orders of magnitude over acidic sites. Extracellular polymers contained iron oxide precipitates (ferrihydrite) that exhibited a granular morphology and incorporated trace amounts of silica at neutral pH sites, whereas acicular crystalloids containing sulphur developed at acidic sites.

INTRODUCTION

Microbial attachment and growth on submerged substrates is common in aquatic environments (Geesey *et al.* 1977, 1978; Mills and Maubrey 1981; Mills and Mallory 1987) and generates so-called "biofilms". These biofilms are composed mainly of prokaryotic and eukaryotic microorganisms and are common to almost all natural fluid-solid interfaces. Attachment by epilithic microbial populations at these interfaces often results in an enriched nutrient status and increased metabolic activity over planktonic counterparts (Fletcher 1985). Micro-topography of the substrate (rock surface) strongly influences colonization as microorganisms preferentially attach to microstructures in quartz grains (Weise and Rheinheimer 1978). The topography of natural rock surfaces is partially determined by erosion and abrasion along with other physical and chemical weathering processes (Tennissen 1974; Leeder 1982).

Microorganisms and their extracellular polymers (including the organic matrix in which they are contained) are among the most efficient scavengers of metallic ions (Costerton *et al.* 1981; Beveridge and Fyfe 1985). Planktonic microbial forms and bacterial capsular material have been implicated in metal ion uptake within marine and freshwater environments (Cowen and Bruland 1985; Cowen *et al.* 1986; Mittelman and Geesey 1985). The complexing of metals in solution by bacteria results in these metals being partitioned into the sediments where they subsequently contribute to authigenic mineral formation during the course of early diagenesis (Forstner 1982; Nissenbaum and Swaine 1976).

Previous investigators have used microbial surface colonization for studies involving *in situ* growth (Caldwell *et al.* 1981), nutrient uptake (Mills and Mallory 1987), and biomass determinations (Palumbo *et al.* 1987). A similar approach is taken in this investigation on the interactions between substrate hardness and microbial population density and between metallic ions and microorganisms in their native environment. Most of our information, to date, concerning microbial immobilization of metals comes from laboratory experiments on isolated bacterial cell walls and extracellular polymers (Beveridge and Fyfe 1985; Rudd *et al.* 1984). Therefore, it is important to develop a better understanding of the reactivity between metallic ions and natural microbial populations.

NATURAL BIOFILMS IN THAMES AND SPEED RIVERS, SOUTHWESTERN ONTARIO

SAMPLING PROCEDURES

Rocks submerged (10 to 20 cm depth) in rapidly flowing (~10 cm/sec) portions of the Thames River near London and the Speed River near Guelph, Ontario, were carefully removed and sampled for

*CFU = colony forming units.

their adherent microbial biofilms. Biofilm samples were collected, in triplicate, by scraping 4.0 cm^2 areas of the rock surface with sterile scalpels. For each rock specimen, two samples were placed into separate tubes containing 4.0 ml of M–9 salts for serial dilution and plate counts. The remaining sample was preserved in the field with 1.0% (vol./vol.) glutaraldehyde in river water for electron microscopy. The rock specimens were subsequently broken open and identified from freshly exposed hand samples using a field magnification lens.

Rock types sampled in the Thames River included limestone, granite, gabbro, rhyolite, basalt, and quartz. In contrast, granite and limestone were the only available rock types in the Speed River. Freshly prepared blocks of commercial limestone and granite were submerged in the Speed River so that *in situ* microbial colonization could be followed through time. The granite blocks were polished on one half of the upper surface and abraded on the other half by using coarse corundum sand paper (Photo 328.1). These blocks were sampled in the same fashion as the natural rock surfaces after 21 and 42 days of exposure in the Speed River.

RESULTS AND DISCUSSION

A dense mucilaginous coating, greenish brown in colour, covered the exposed surfaces of natural limestone in both rivers. In contrast, all other rock types examined, including the granite and limestone blocks placed *in situ* for up to 42 days, appeared to be relatively clean to the naked eye. However, scraping removed a thin biofilm similar to that removed from the native limestone. Examination of the sample material by phase light microscopy and scanning electron microscopy revealed an abundance of bacteria, cyanobacteria, eukaryotic algae, and diatoms (Photos 328.2 and 328.3). Small detrital grains (<5.0 μm diameter) were also evident.

Commonly the bacteria present were encapsulated and enmeshed in microcolonies of morphologically identical cells (Photo 328.4). Microcolony-forming bacteria were also observed as a secondary colonization on algae, cyanobacteria, and detrital organics on the rock surfaces. This multiple level of colonization established large communal aggregates of microorganisms (Photos 328.2 and 328.3). Manganese-oxidizing bacteria within communal aggregates were easily discernible by electron microscopy due to the increased electron density caused by a Mn-oxide deposit around the cells (Photo 328.5). These electron-dense precipitates generated characteristic peaks for manganese at 5.894 and 6.489 keV in energy dispersive X-ray spectra.

Typically, cyanobacterial and algal population densities were an order of magnitude less abundant than the corresponding bacterial population densities. Speed River counts were also generally lower than the corresponding counts from the Thames

Photo 328.1. *Scanning electron micrographs of: (A) a smooth granite surface and (B) an abraded granite surface. These different surface textures were emplaced in situ in the Speed River for up to 42 days (bar scale = 25 μm).*

Photo 328.2. *Scanning electron micrographs of the microbial biofilms from (A) natural granite rock surface (bar scale = 1 μm) and (B) from an abraded granite surface placed in situ in the Speed River for 42 days (bar scale = 5 μm).*

Photo 328.3. *Scanning electron micrographs of microbial biofilms from (A) natural limestone surface and (B) a limestone block emplaced in the Speed River for 42 days (bar scales = 5 μm).*

Photo 328.4. *Thin-section transmission electron micrograph of a bacterial microcolony removed from a submerged quartz cobble in the Thames River (bar scale = 500 nm).*

Photo 328.5. *Thin-section transmission electron micrograph of a communal aggregate of epilithic microorganisms from a limestone surface in the Thames River. Note manganese-oxidizing bacterium with associated manganese-oxide deposit around the cell (arrows) (bar scale = 250 nm).*

River. However, the epilithic microbial densities reported here are similar to those reported for small, flowing alpine streams (Geesey *et al.* 1978), in terms of both cell number and distribution of organisms. Further evaluation of the results revealed an inverse relationship between cell density and substrate (mineral) hardness (Figure 328.1).

Diverse microbial communities are common on submerged substrates in aquatic environments (Geesey *et al.* 1977, 1978; Marszalek *et al.* 1979) and they have been reported to promote microbial growth rates through nutrient recycling, a result of the metabolic coupling of closely juxtaposed organisms (Fletcher 1985).

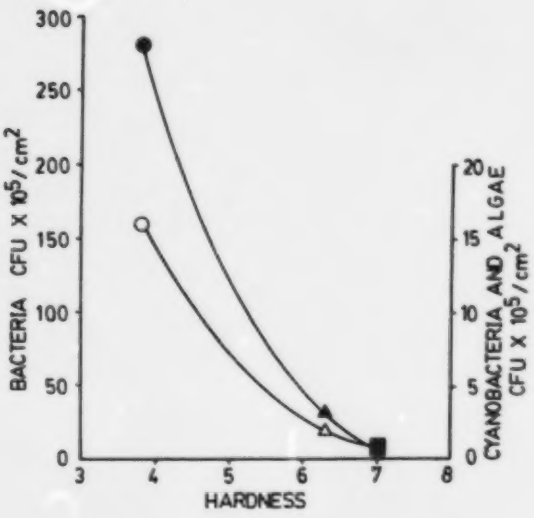

Figure 328.1. *Mean bacterial (solid symbols) and cyanobacterial-algal (open symbols) population densities on limestone (●), alkali feldspar–plagioclase based rocks (▲), and quartz (■) versus mineral substrate hardness (Moh's scale).*

Significant variations in surficial biofilm population densities were observed between the different rock types (Table 328.1). However, microorganisms removed from all rock surfaces exhibited a similar structural mode of growth (Photos 328.2 and 328.3). Limestone substrates, in both rivers, were the heaviest colonized surfaces (10^8 to 10^7 CFU/cm^2) and seem to support 10- to 100-fold more bacteria than any other rock type examined. The heavily colonized limestone contains both calcite and dolomite and has a hardness between 3 and 4 on Moh's scale of hardness. Intermediate population-density values were recorded for the alkali feldspar–plagioclase based rocks examined including granite, rhyolite, gabbro, and basalt. The hardness of this group of feldspar-rich rocks is approximately 6. Quartz cobbles examined had both the highest hardness value (7.0) and lowest microbial population density (Table 328.1, Figure 328.1).

The granite and limestone blocks submerged in the Speed River exhibited a similar density of adherent microorganisms after 21 days of *in situ* exposure (Table 328.2). This observation is consistent with the results of Mills and Maubrey (1981), in which they found that freshly prepared specimens of quartz and calcite were colonized at approximately the same rate. However, the limestone blocks supported densities of bacteria, cyanobacteria, and algae greater than the granite blocks after 42 days of exposure (Table 328.2). Similarly, the abraded halves of the granite blocks were colonized more heavily than the polished halves. These results indicate that substrate (mineral) hardness has little effect on microbial colonization rates, but does have an affect on the final population density of epilithic microorganisms.

The results provide strong evidence for the significant role of abrasive processes in determining the extent of microbial growth on mineral substrates. The physical abrasive processes in flowing streams constantly etch submerged rocks and effectively

TABLE 328.1. POPULATION DENSITY VALUES FOR BACTERIAL AND CYANOBACTERIAL-ALGAL POPULATIONS ON ROCKS SUBMERGED IN THE THAMES AND SPEED RIVERS.

River	Mineral Substrate	Number of Specimens	Viable Counts (CFU* x 10^5/cm^2)	
			Bacteria	Cyanobacteria-Algae
Thames	limestone	3	280.0 ± 47.3	16.0 ± 4.9
	granite	3	40.3 ± 8.2	3.5 ± 1.4
	basalt	2	55.5 ± 14.5	0.4 ± 0.2
	gabbro	2	15.8 ± 11.4	0.2 ± 0.03
	rhyolite	2	15.9 ± 15.3	1.3 ± 0.6
	quartz	2	3.6 ± 0.2	0.3 ± 0.1
Speed	limestone	7	26.6 ± 12.3	1.3 ± 0.4
	granite	7	4.2 ± 0.8	0.4 ± 0.3

* *CFU, colony forming units* ± *standard error.*

TABLE 328.2. POPULATION DENSITY VALUES FOR BACTERIAL AND CYANOBACTERIAL-ALGAL POPULATIONS ON LIMESTONE AND GRANITE BLOCKS SUBMERGED IN THE SPEED RIVER.

Substrate	Days of Exposure	Viable Counts (CFU x 10^5/cm^2)	
		Bacteria	Cyanobacteria-Algae
cut limestone	21	1.2 ± 0.9	0.04 ± 0.01
	42	5.7 ± 3.8	0.16 ± 0.06
polished granite	21	0.9 ± 0.2	ND
	42	1.6 ± 0.5	0.03 ± 0.02
abraded granite	21	2.3 ± 0.8	0.03 ± 0.01
	42	3.0 ± 0.9	0.04 ± 0.01

ND, not detected.

sculpture all exposed surfaces (Tennissen 1974; Leeder 1982). These highly textured surfaces afford stronger attachment for microorganisms and provide a measure of protection from fluid turbulence and shear stress (Weise and Rheinheimer 1978; Shimp and Pfaender 1982). Minerals prone to abrasion provide a better substrate for microbial attachment and growth, particularly over longer periods of time.

Our results emphasize the importance of substrate conditioning of hard smooth surfaces for the attachment and growth of microorganisms (Marszalek *et al.* 1979). They also provide a convenient parameter to use as a measure of the degree to which different rock types may be colonized, which ultimately controls ecosystems dominated by epilithic microbial forms.

MOOSE LAKE WATERSHED, ONAPING, ONTARIO

ENVIRONMENTAL SETTING

Studies of metal adsorption by adherent microbial populations were carried out within acidic and neutral pH environments of the Moose Lake watershed located northwest of Sudbury at Onaping, Ontario (Figure 328.2). Oxidation of pyrrhotite and other metal sulphides present in the Fraser Mine tailings cause the acidic conditions in portions of the Moose Lake watershed. Acidic metal-laden mine drainage collects in the upper regions of Upper Moose and Cranberry lakes. The acid waters of Upper Moose Lake are treated with a crushed limestone slurry to restore neutral pH conditions and to reduce dis-

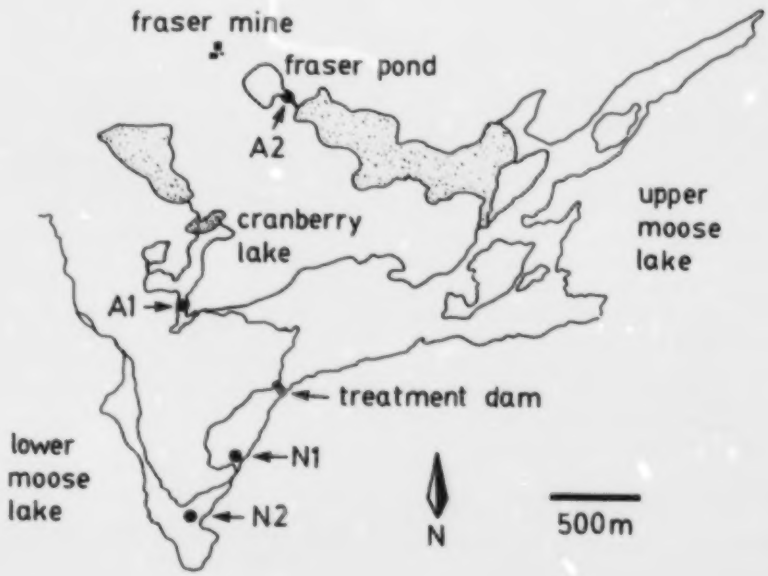

Figure 328.2. *Location map of sample stations in the Moose Lake watershed area. Fraser Mine tailing impoundments shown by shaded areas.*

solved metal concentrations before entering Lower Moose Lake.

SAMPLING PROCEDURE

Four sample stations were established, two in acid waters and two in circumneutral waters (Figure 328.2). The acidic sites were located in the south end of Cranberry Lake (site A1) in 6.0 m of water and near the Fraser Mine Pond discharge (site A2) in 3.0 m of water. The pH level was 3.1 at both sites and remained constant over the 17-week sampling period. Neutral sampling stations were located in areas of Lower Moose Lake in 5–6 m of water. Site N1 was located above a narrow channel separating two arms of the lake, whereas site N2 was located below this channel (Figure 328.2). The pH level was more variable at these sites but stayed within a range of 6.5 to 6.9.

Test and control sampling slides were suspended (*in situ*) 1.5 m below an anchored buoy at each of the four sampling stations. Sampling slides consisted of strips of epoxy-impregnated Whatman No. 1 filter paper mounted in plastic 35 mm photographic slide binders (5.0 x 5.0 cm). Control slides were sandwiched between 0.22 μm nylon filters to inhibit microbial penetration to the support strips. Paired sets of test and control slides were recovered from each sample station after an initial *in situ* incubation of 1 week and at approximately 5-week intervals thereafter. Three 1.0 cm^2 subsamples were cut from the test and control strips using sterile scalpels. Two of these subsamples were retained for metal analyses and electron microscopy, whereas the third squares were transferred directly into sterile tubes containing M–9 salts for bacterial enumeration by serial dilution and plating.

Specimens for metal analyses were placed into small polypropylene bottles containing 1.0 ml of 2.0% (vol./vol.) HNO_3. Each square was leached for 2 weeks at 20°C before dilution to 10.0 ml with deionized distilled water. The concentrations of Mn, Fe, Co, Ni and Cu were determined using atomic absorption spectroscopy. Sample squares for electron microscopy were preserved in 1.0% (vol./vol.) glutaraldehyde in water from the corresponding sample station. Thin wedges cut from the specimen squares were embedded in Epon 812 using standard techniques (Hayat 1986). Thin sections were examined using transmission electron microscopy equipped with an energy-dispersive X–ray spectrometer (EDS). Mineral precipitates were also examined using selected area electron diffraction (SAED).

BIOFILM COLONIZATION AND GROWTH

Planktonic and adherent heterotrophic bacterial population density values increased at each station over the entire study period (Figure 328.3). Acidic site A1 in Cranberry Lake showed the highest initial counts for both planktonic and attached bacteria after 1 week (Figure 328.3C). Therefore, the data suggests, as one would expect, that the concentration of free-living bacteria plays an important role in the initial rate of surface colonization. Growth rates of the attached bacterial population appeared to be independent of planktonic populations after the first week. The adherent bacterial population density curves were generally hyperbolic as expected for systems controlled by cellular adsorption, growth and emigration of daughter cells (Caldwell *et al.* 1981; Lawrence *et al.* 1987). In contrast, the planktonic bacteria exhibited sinusoidal population curves characteristic of microbial population responses to increasing seasonal temperatures (Figure 328.3).

Biofilm growth increased rapidly at all four sites over the first 5 weeks. At neutral pH sites (Figure 328.3, A and B), biofilm growth rates decreased progressively throughout the sampling period. In contrast, a marked decrease in growth rate occurred at the acidic sites after week 5 along with a lower final population density. The lower population densities for the acidic sites suggest that bacterial growth was possibly stressed by the low pH levels and high dissolved metal concentrations.

Control strips covered with 0.22 μm nylon filters were found to be free of bacteria until the 11th week. However, bacterial counts from the controls at week 11 and at the final sampling were 10- to 100-fold lower than the corresponding values from the test strips.

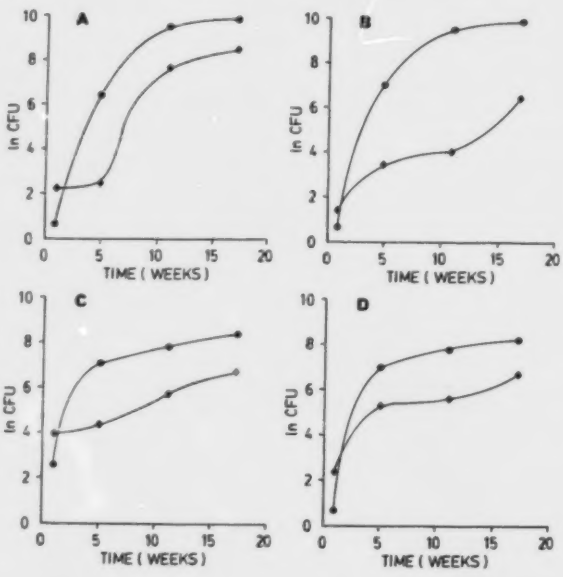

Figure 328.3. *Growth curves for attached bacteria (log CFU/cm² [●]) and planktonic heterotrophic bacteria (log CFU/ml [◆]) from neutral pH sites (A) N1, (B) N2, and acidic sites (C) A1, (D) A2.*

TABLE 328.3. MEAN AQUEOUS METAL CONCENTRATIONS FOR THE NEUTRAL AND ACIDIC SAMPLE STATIONS OVER THE 17-WEEK STUDY PERIOD.

Station	Concentration (ppm)* Mean ± SD				
	Mn	Fe	Co	Ni	Cu
N1	0.65 ± 0.14	2.71 ± 0.67	0.08 ± 0.02	2.10 ± 0.30	0.02 ± 0.01
N2	0.52 ± 0.16	12.56 ± 5.41	0.05 ± 0.04	2.08 ± 0.46	0.02 ± 0.01
A1	1.64 ± 0.02	37.23 ± 15.81	0.29 ± 0.11	5.57 ± 0.72	0.21 ± 0.11
A2	3.57 ± 0.60	62.50 ± 22.62	5.76 ± 2.76	62.92 ± 30.87	1.74 ± 0.65

* *Figures represent an average of at least five determinations for each sample plus or minus standard deviation of the mean (ppm, parts per million).*

TABLE 328.4. AMOUNT OF METAL ADSORBED BY CONTROL SURFACES AND BIOFILMS AFTER 17-WEEKS OF IN SITU INCUBATION.

Sample*	Amount of metal adsorbed ($\mu g/cm^2$)** Mean ± SD				
	Mn	Fe	Co	Ni	Cu
N1-C	0.15 ± 0.01	269.50 ± 29.90	0.05 ± 0.01	0.26 ± 0.04	0.09 ± 0.03
N1-B	0.17 ± 0.04	3145.00 ± 198.06	0.05 ± 0.02	1.98 ± 0.01	0.81 ± 0.10
N2-C	0.06 ± 0.02	238.50 ± 29.05	0.07 ± 0.02	0.24 ± 0.09	0.23 ± 0.01
N2-B	20.09 ± 0.10	11596.0 ± 238.45	0.25 ± 0.17	11.52 ± 0.36	2.18 ± 0.13
A1-C	0.06 ± 0.03	48.60 ± 9.30	0.01 ± 0.01	0.14 ± 0.03	0.01 ± 0.01
A1-B	0.18 ± 0.01	994.40 ± 137.09	NB	0.07 ± 0.02	0.16 ± 0.04
A2-C	0.09 ± 0.02	9.55 ± 1.65	0.03 ± 0.01	0.18 ± 0.05	0.06 ± 0.01
A2-B	0.10 ± 0.02	50.00 ± 21.25	NB	0.69 ± 0.31	0.09 ± 0.02

* *C, Control surface; B, Biofilm.*

** *Figures represent an average of at least five determinations ± standard deviation of the mean. Biofilm values are expressed in terms of metal adsorbed in excess of the corresponding control surface.*

NB, Not bound.

BACTERIAL METAL UPTAKE

Mean, aqueous metal concentration data (Table 328.3) reveals iron to be the most concentrated metal species at all four sites. Iron accounted for up to 83 mol percent of the five transition metals assayed. Nickel, manganese, cobalt and copper showed consecutively lower concentration levels, with a 3- to 100-fold concentration decrease for all metals in solution at the neutral sites.

Station A2, near the discharge of Fraser Mine Pond, had the highest aqueous metal concentrations of the two acidic sites. In contrast, Mn, Co, Ni and Cu concentrations were similar at both neutral pH sites (Table 328.3). However, iron was found to be approximately four times more concentrated at site N2. The high iron concentration at site N2 is believed to be a result of iron-rich anoxic water produced during summer stratification or partial meromictic conditions.

All metal species, except cobalt, were bound by the biofilms under acidic conditions. They were bound in excess of the amounts adsorbed by the corresponding control plates (Table 328.4). In general, metal adsorption was significantly enhanced at the neutral pH sites, particularly at site N2 where a thick coating of iron-oxide precipitated throughout the biofilm. No precipitates were evident on the control strips and only thin biofilm associated precipitates formed at the other sample stations.

BIOFILM MINERALIZATION

Biofilms examined in stained thin sections of the test strips material commonly revealed microcolonies of encapsulated bacteria. The polymeric capsular material surrounding the cell exhibits a fibrous structure which frequently contained an abundance of iron-

rich precipitates (Photo 328.6). These iron-rich precipitates exhibited a granular appearance in biofilms from neutral pH stations, whereas under acidic conditions clumps of acicular crystalloids developed (Photo 328.6, A and B). However, both of these crystalloid types generated the same diffuse prismatic diffraction pattern characteristic of ferrihydrite ($Fe_2O_3.nH_2O$) centered on d spacings of 0.25 and 0.15 nm.

In contrast, distinct differences in trace element composition was revealed by energy-dispersive X-ray spectroscopy (Figure 328.4). Precipitates formed under neutral pH conditions contained Al, Si and Cl, as minor indigenous element impurities while sulphur was incorporated under acidic conditions.

DISCUSSION AND CONCLUSIONS

Attached and planktonic heterotrophic bacterial population densities obtained here are similar to those recorded for other acid-stressed aquatic environments (Mills and Mallory 1987; Wassel and Mills 1983). Metal adsorption differences recorded for neutral and acidic pH sites can be partially attributed to the lower population densities at the acidic sites due to acid-induced stress. However, reactions between metallic ions and polymeric organic substrates are strongly influenced by pH levels (Stumm and Morgan 1981). Metal cations are adsorbed in smaller quantities at a low pH level due to a reduction of negatively charged sites on microbial surfaces such as carboxylates and phosphates. In contrast, at neutral pH levels metal adsorption is enhanced by an increase in the number of ionized acidic groups as reflected by the total amount of metal bound at the neutral sites.

Similarly, higher pH levels also cause cationic colloidal elements ($Fe(OH)^{2+}.5H_2O$ or $Fe(OH)^{+}.4H_2O$) to form via hydrolysis of ferric iron (Cotton and Wilkinson 1972). Once metal cations are complexed and immobilized by bacterial anionic polymers they can form precipitates at the cell surface by hydrolysis, a change in oxidation state, or through reactions with other ions in solution (Ferris *et al.* 1986). These bacterially induced precipitates undergo secondary growth via homogeneous crystal nucleation reactions and also play an important role in early diagenesis/authigenesis (Beveridge *et al.* 1983).

The importance of microbial biofilms in metal uptake and immobilization are highlighted by the current results. Natural metal-immobilizing biofilms are capable of removing significantly higher quantities of metal contaminants from solution than are inert surfaces. The current evidence indicates that there are clear differences in metal affinities by biofilms in acidic and neutral pH environments. However, the evidence also indicates that the capacity for metal binding by microbial biofilms is still greater than that of the control surfaces in either acidic or neutral environments.

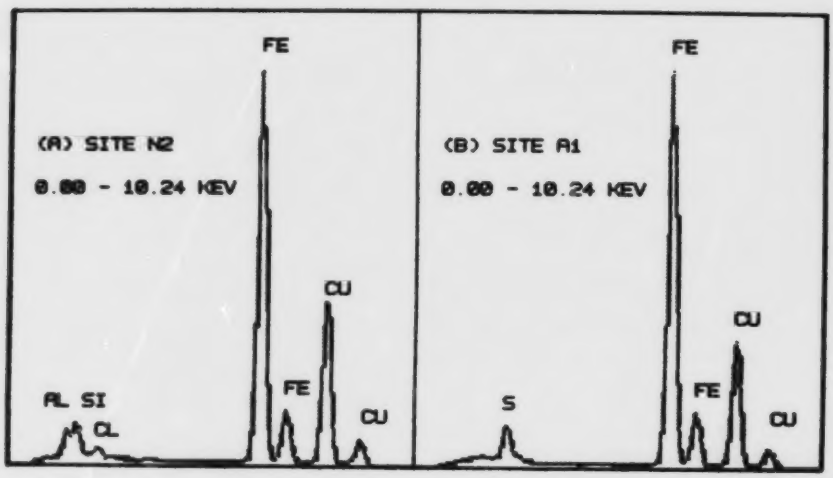

Figure 328.4. *Energy-dispersive X-ray spectra from ferrihydrite precipitates associated with microbial biofilms. (A) from neutral site N2 and (B) from acidic site A1. Fe (K_α and K_β), Al, Si, Cl, and S peaks are from the specimens, whereas Cu (K_α and K_β) peaks are from the supporting grids.*

Photo 328.6. *Thin-section transmission electron micrographs of mineralized biofilms. (A) Biofilm from neutral site N2 (bar scale = 250 nm). (B) Biofilm from acidic site A1 (bar scale = 1 μm).*

REFERENCES

Beveridge, T.J. and Fyfe, W.S.

1985: Metal Fixation by Bacterial Walls; Canadian Journal of Earth Sciences, Volume 22, p.1883-1898.

Beveridge, T.J., Meloche, J.D., Fyfe, W.S. and Murray, R.G.E.

1983: Diagenesis of Metals Chemically Complexed to Bacteria: Laboratory Formation of Metal Phosphates, Sulfides, and Organic Condensates in Artificial Sediments; Applied and Environmental Microbiology, Volume 45, p.1094-1108.

Caldwell, D.E., Brannan, J.D., Morris, M.E. and Betlach, M.R.

1981: Quantitation of Microbial Growth on Surfaces; Microbial Ecology, Volume 7, p.1-11.

Costerton, J.W., Irvin, R.T. and Cheng, K.J.

1981: The Bacterial Glycocalyx in Nature and Disease; Annual Review Microbiology, Volume 35, p.299-324.

Cotton, F.A. and Wilkinson, G.

1972: Advanced Inorganic Chemistry; John Wiley and Sons, Inc., New York.

Cowen, J.P. and Bruland, K.W.

1985: Metal Deposits Associated with Bacteria: Implications for Fe and Mn Marine Biogeochemistry; Deep-sea Research, Volume 32, p.253-272.

Cowen, J.P., Massoth, G.J. and Baker, E.T.

1986: Bacterial Scavenging of Mn and Fe in a Mid- to Far-Field Hydrothermal Particle Plume; Nature, Volume 322, p.169-171.

Ferris, F.G., Beveridge, T.J. and Fyfe, W.S.

1986: Iron-silica Crystallite Nucleation by Bacteria in a Geothermal Sediment; Nature, Volume 320, p.609-611.

Fletcher, M.

1985: Effect of Solid Surfaces on the Activity of Attached Bacteria; p.339-362 *in* Bacterial Adhesion, edited by D.C. Savage and M. Fletcher, Plenum Press, New York, 864p.

Forstner, U.

1982: Accumulative Phases for Heavy Metals in Limnic Sediments; Hydrobiologia, Volume 91, p.269-284.

Geesey, G.G., Mutch, R., Costerton, J.W. and Green, R.B.

1978: Sessile Bacteria: An Important Component of the Microbial Population in Small Mountain Streams; Limnology and Oceanography, Volume 23, p. 1214-1223.

Geesey, G.G., Richardson, W.T., Yeomans, H.G., Irvin, R.T. and Costerton, J.W.

1977: Microscopic Examination of Natural Sessile Bacterial Populations From an Alpine Stream; Canadian Journal of Microbiology, Volume 23, p.1733-1736.

Hayat, M.A.

1986: Basic Techniques for Transmission Electron Microscopy; Academic Press, New York, 411p.

Lawrence, J.R., Delaquis, P.J., Korber, D.R. and Caldwell, D.E.

1987: Behavior of *Pseudomonas fluorescens* Within the Hydrodynamic Boundary Layers of Surface Microenvironments; Microbial Ecology, Volume 14, p.1-14.

Leeder, M.R.

1982: Sedimentology: Process and Product; George Allen and Unwin, London, 344p.

Marszalek, D.S., Gerchakov, S.M. and Udey, L.R.

1979: Influence of Substrate Composition on Marine Microfouling; Applied and Environmental Microbiology, Volume 38, p.987-995.

Mills, A.L. and Mallory, L.M.

1987: The Community Structure of Sessile Heterotrophic Bacteria Stressed by Acid Mine Drainage; Microbial Ecology, Volume 14, p.219-232.

Mills, A.L. and Maubrey, R.

1981: Effect of Mineral Composition on Bacterial Attachment to Submerged Rock Surfaces; Microbial Ecology, Volume 7, p.315- 322.

Mittelman, M.W. and Geesey, G.G.

1985: Copper-Binding Characteristics of Exopolymers From a Freshwater-Sediment Bacterium; Applied and Environmental Microbiology, Volume 49, p.846-851.

Nissenbaum, A. and Swaine, D.J.

1976: Organic Matter-Metal Interactions in Recent Sediments: The Role of Humic Substances; Geochimica Cosmochimica Acta, Volume 40, p.809-816.

Palumbo, A.V., Boyle, M.A., Turner, R.R., Elwood, J.W. and Mulholland, P.J.

1987: Bacterial Communities in Acidic and Circumneutral Streams; Applied and Environmental Microbiology, Volume 53, p.337-344.

Rudd, T., Sterritt, R.M. and Lester, J.N.

1984: Formation and Conditional Stability Constants of Complexes Formed Between Heavy Metals and Bacterial Extracellular Polymers; Water Research, Volume 18, p.379-384.

Shimp, R.J. and Pfaender, F.K.

1982: Effects of Surface Area and Flow Rate on Marine Bacterial Growth in Activated Carbon Columns; Applied and Environmental Microbiology, Volume 44, p.471-477.

Stumm, W. and Morgan, J.J.

1981: Aquatic Chemistry: An Introduction Emphasizing Chemical Equilibria in Natural Waters, 2nd Edition; John Wiley and Sons, New York, 780p.

Tennissen, A.C.

1974: Nature of Earth Materials; Prentice-Hall, Inc., Englewood Cliffs, New Jersey, 439p.

Wassel, R.A. and Mills, A.L.

1983: Changes in Water and Sediment Bacterial Community Structure in a Lake Receiving Acid Mine Drainage; Microbial Ecology, Volume 9, p.155-169.

Weise, W. and Rheinheimer, G.

1978: Scanning Electron Microscopy and Epifluorescence Investigation of Bacterial Colonization of Marine Sand Sediments; Microbial Ecology, Volume 4, p.175-188.

Grant 329 The Expression of the Larder Lake Break in the Matachewan Area

W.G. Powell, C.J. Hodgson and J.A. Hanes

Department of Geological Sciences, Queen's University, Kingston

ABSTRACT

Evidence for a minimum of four deformational events was recognized in the Matachewan area:

1) D_1 structures, comprising east-northeast-trending zones of highly fissile rock, including the Larder Lake break, developed in the Archean rocks;
2) D_2 structures, comprising north-trending zones of crenulation cleavage or schistosity in zones of higher strain also developed during the Archean;
3) D_3 structures, comprising east-northeast-trending zones of spaced cleavage in the fine-grained beds of the Proterozoic Gowganda Formation, are spatially coincident with D_1 zones, including the Larder Lake break;
4) D_4 structures, comprising brittle faults.

Zones of D_3 strain directly overlie D_1 deformation zones and may be used as a guide in locating such zones, where the Archean basement is covered by Proterozoic rocks. It is well established that the major gold deposits of the Abitibi belt are spatially closely related to D_1 structures, such as the Larder Lake–Cadillac break. Using this relationship, several D_1 zones have been mapped through the arms of Huronian metasediments that lie across Cairo, Holmes, Burt and Flavelle townships.

INTRODUCTION

All of the large gold deposits of the southern Abitibi belt occur within a few kilometres of the two major breaks in the area, the Larder Lake–Cadillac break and the Porcupine–Destor break. Therefore, tracing these breaks is a major priority in gold exploration. The main objective of this project is to trace the Larder Lake–Cadillac break west from Kenogami Lake (approximately 15 km southwest of Kirkland Lake), through Matachewan, to the Halliday dome area. The method has involved structural mapping of Archean basement rocks and tracing zones of deformation from Archean rocks into the Proterozoic cover rocks.

This synoptic mapping project involved detailed structural analysis during a reconnaissance sweep of the study area. Follow-up mapping was then conducted in areas where strong photographic lineaments and/or deformation zones had been recognized. Initially, mapping of the Archean basement was conducted, in order to understand the distribution and nature of the Archean deformation. Subsequently, structures within the Proterozoic cover sedimentary rocks of the Gowganda Formation were mapped to ascertain whether late reactivation of underlying basement faults had affected the Gowganda Formation, allowing the detection of Archean structures through the overlying cover.

This paper describes the results of the 1988 mapping season, the first of two, and involves the eastern half of the intended study area (Eby, Burt, Holmes, Flavelle, Cairo and Powell townships) (Figure 329.1).

GENERAL GEOLOGY

The study area has been mapped previously by Lovell (1967, 1972) and Moore (1966). Figure 329.2 illustrates the general geology of the study area. Tholeiitic basalt and andesite flows (MERQ-OGS 1983) with minor iron formation and interflow sedimentary rocks form the bulk of the Archean supracrustal rocks. A sequence of sedimentary and alkalic volcanic rocks of the Timiskaming Group unconformably overlies the older volcanic rocks (Thomson 1946). Fluvial conglomerates and greywackes of the Timiskaming Group occur as thin bands spatially coincident with the Larder Lake–Cadillac break, a major structural zone controlling the distribution of gold mineralization along its strike length from Val d'Or, Québec, through Matachewan.

Several phases of intrusive activity have been documented. The earliest intrusions within the study area consist of small diorite bodies. A period of felsic intrusive activity followed. The Round Lake batholith, a composite intrusion is dominantly trondhjemite and tonalite but younger granodiorites have intruded along its margins (Jensen 1985). This early intrusive body is located along the southern extent of the study area. The latest felsic intrusive bodies are syenites. These include the Otto, Cairo, Holmes and Dixon Lake stocks.

Deformation associated with the Larder Lake–Cadillac break has been recorded in all of the Archean lithologies listed above.

Proterozoic rocks within the study area include diabase dikes of the Matachewan dike swarm, which cut the Archean stratigraphy but are overlain by the

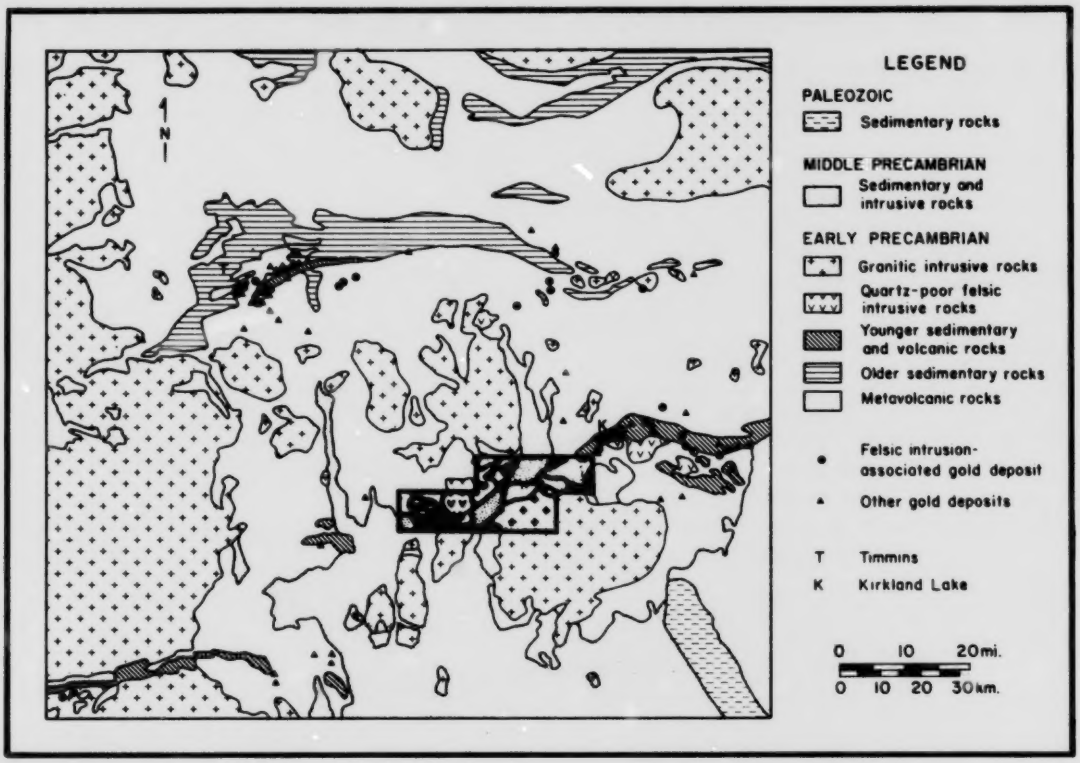

Figure 329.1. *Location of 1988 study area (shaded region). Modified from Cherry (1983, Figure 1).*

glaciogenic sedimentary rocks of the Coleman Member of the Gowganda Formation (Cobalt Group, Huronian Supergroup) (2240 ± 174 Ma; Fairbairn *et al.* 1969). The youngest rock unit in the area is the Nipissing diabase ($2219.4^{+3.6}_{-3.5}$ Ma) (Corfu and Andrews 1986).

STRUCTURAL GEOLOGY

The chronological classification of deformational events (i.e. D_1 through D_4) is based solely on field observations during the 1988 field season. No attempt has been made to correlate this classification with the nomenclature proposed in previous structural studies of the Abitibi belt (e.g. Hamilton 1986; Dimroth *et al.* 1983).

D_1 STRUCTURES

D_1 is the earliest cleavage-forming deformational event recognized in the study area. The D_1 fabric is a domainal schistosity trending in an east-northeast direction. S_1 is a schistosity defined by chlorite and actinolite in the mafic volcanic rocks (Photo 329.1), while muscovite and quartz ribbons define the fabric in the felsic intrusive and volcanic rocks. Linear fabrics defined by mineral orientations and clast elongation plunge westward in the plane of the foliation at angles of 60 to 75°. Kinematic indicators are uncommon and contradictory from location to location, suggesting a complex history of fault motion.

A number of subparallel, D_1, deformation zones have been identified, including the extension of the Larder Lake break (Figure 329.2). While these deformation zones are generally less than 20 m wide, the larger zones may be several hundred metres in width.

D_1 deformation zones are highly altered over much of their strike lengths. Carbonatization is widespread within the deformation zones as well as within permeable rock units lying outside of the zone of intense deformation. Calcite is the most widely distributed carbonate species, while ferroan carbonates are restricted to localized sites within the zones of high strain. Silica flooding, quartz veins and pyrite are also common. A number of gold showings are located along each of the D_1 zones that have been identified, including the past-producing Young–Davidson and Matachewan Consolidated mines north of the Matachewan townsite (e.g. Dyer 1936; Derry *et al.* 1948).

D_2 STRUCTURES

A north-northeast- to north-trending crenulation cleavage developed during the D_2 event. Locally, zones of intense D_2 strain exist, expressed as north-

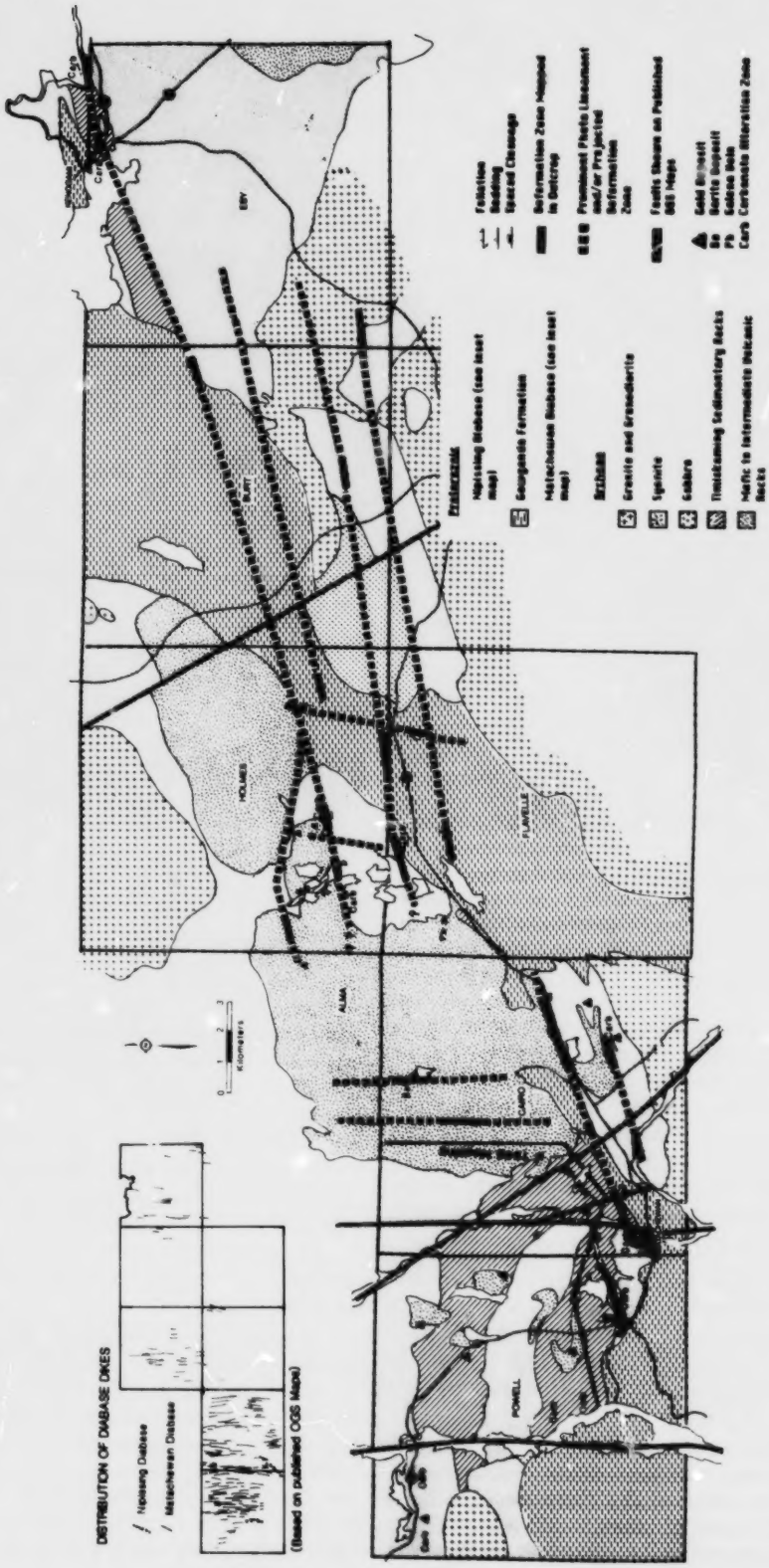

Figure 329.2. *Geological map of 1988 study area (Eby, Burt, Holmes, Flavelle, Cairo and Powell townships). After Lovell (1967, 1972) and Moore (1966).*

Photo 329.1. *Photomicrograph of carbonatized metabasalt (long dimension is 1.22 mm). S_1, the penetrative schistosity, is crenulated by the D_2 spaced cleavage.*

Photo 329.2. *Photomicrograph of a siliceous metasiltstone from the Gowganda Formation within a D_3 zone (long dimension is 4.9 mm). A pressure solution cleavage, produced during D_3, is defined by the accumulation of dark, insoluble material in the fine-grained matrix.*

trending schistose zones which cut S_1. Regionally, S_2 is a spaced crenulation cleavage (average spacing <1 cm) produced by pressure solution (Photo 329.1). Fabric development is best expressed in the highly altered schistose rock within D_1 zones. The D_2 fabrics were recorded over most of the study area but intensify westward towards Matachewan.

No pervasive alteration appears to be associated directly with this deformational event.

S_2 deforms the greenschist metamorphic minerals and carbonates associated with D_1 but was not identified in the overlying Proterozoic sedimentary rocks of the Gowganda Formation and appears to predate the Matachewan diabase. This suggests that D_2 was a very late Archean event.

There is a distinct correlation between the distribution of Matachewan diabase dikes and the development of S_2. In addition the orientation of S_2 is coincident with that of the local Matachewan diabase. These observations suggest that many of the diabase dikes within the Matachewan area may have been intruded into zones of weakness formed during the D_2 event.

D_3 STRUCTURES

East-northeast-trending air photo lineaments lie along strike of known D_1 zones, including the Larder Lake break, within the Gowganda sedimentary rocks. Where such lineaments cross favourable lithologies, structures associated with D_3 deformation have developed.

The most commonly observed expression of D_3 in the sedimentary rocks is a spaced cleavage oblique to the trend of the deformation zone defined by the air photo lineament. During compression, fine quartz particles in the sedimentary matrix dissolved, concentrating clays and white micas into planar to anastomosing bands of S_3 (Photo 329.2). Significant growth of white micas within the cleavage planes accompanied deformation. S_3, striking 045 to

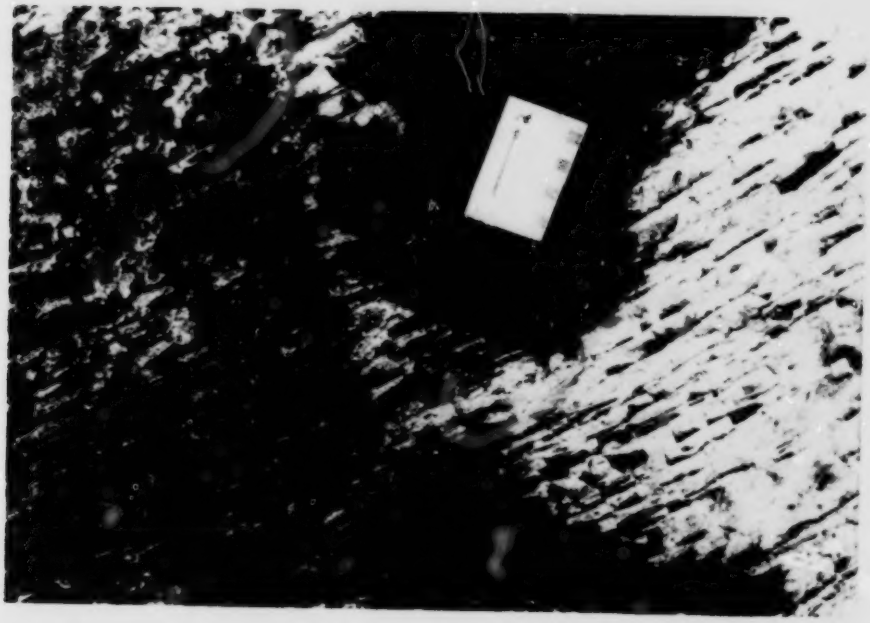

Photo 329.3. *Surface expression of D_3 within a Gowganda siliceous metasiltstone.*

060° and dipping steeply to the southeast (Photo 329.3), is axial planar to D_3 folds which plunge moderately in a northeasterly direction.

Grain size controls the degree of development of S_3, with deformation being most intense in the finest grained sedimentary rocks (siliceous argillite). S_3 is weakly developed in the fine-grained arkosic units and has not been observed at either mesoscopic or microscopic scales in the coarse-matrix conglomerates. Furthermore, the strain is best expressed in vertical sections of interbedded sandstone and argillite. In these exposures, sandy units interbedded with the argillite act as strain markers, tending to fold and/or disaggregate and overlap to accommodate the northwest-southeast horizontal shortening of the rocks. Photo 329.4 illustrates a vertical outcrop face where overlapping of a competent arkosic bed indicates a minimum horizontal shortening of 15%.

Increased dip of bedding planes within the Gowganda sedimentary rocks due to folding may be a useful field indicator of deformation, where cleavage development is not apparent. The Huronian cover rocks dip gently, less than 20° in most cases. It has been noted that within D_3 zones bedding planes commonly dip at angles of 45° or more.

Northerly trending zones of deformation, similar in appearance to those described above, have also been mapped in the Proterozoic. These are interpreted to overlie Archean D_2 zones which have also undergone reactivation after lithification of the Gowganda sediments; however, it has not been possible to observe Archean rocks along strike of these zones to confirm this hypothesis, due to lack of outcrop.

Geochronology

In a preliminary attempt to determine the age of D_3, a whole-rock sample of siliceous argillite from an east-northeast-trending D_3 zone in the Gowganda Formation was dated by the $^{40}Ar/^{39}Ar$ step-heating method. The sample was obtained from an outcrop situated just north of the Flavelle–Holmes townships boundary, 4 km east of Holmes Lake. An eight-step run yielded a disturbed age spectrum (Figure 329.3) with an integrated date of 1858 ± 9 Ma, that indicates argon loss, perhaps related to the D_3 event. Although the sample is a multi-reservoir system, the bulk of the ^{39}Ar gas-release (steps 2 to 5 in the spectrum) is attributed to the white mica. The 2.2–2.3 Ga dates for steps 4 and 5 may provide a crude estimate of either subgreenschist-facies regional metamorphism of the Gowganda sedimentary rocks, or the generation of the D_3 structures. Significant activity on the east-northeast-trending Ivanhoe Lake and Wakusimi River fault zones, 150 km to the northwest, at 2.25–2.3 Ga is indicated by Ar–Ar dates on biotite and muscovite from Archean basement rocks straddling these major structures (Archibald *et al.* 1989; 1986). The argon loss shown by the climb of the age spectrum from a date of ca. 1.2 Ga for step 2 (Figure 329.3) may be a result of Grenville-related fault activity. A component of minor, late movement on the Ivanhoe Lake fault zone has been dated (Ar–Ar) at ca. 1.1–1.2 Ga (Queen *et al.* 1989; Archibald *et al.* 1989). More detailed Ar–Ar analyses

Photo 329.4. *Vertical view (facing east) of a D_3 deformation zone. A strong, vertical, spaced cleavage has developed in the siliceous metasiltstone, while the arkosic bed in the centre has stacked in order to accommodate the horizontal shortening.*

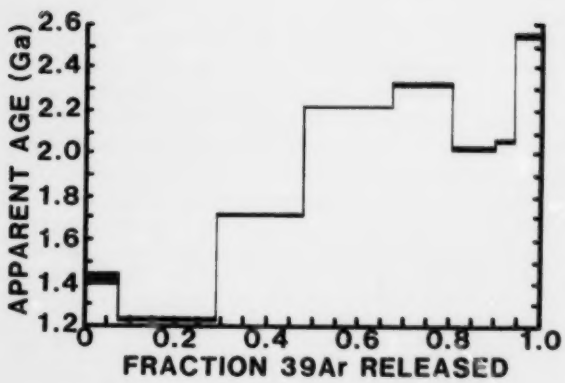

Figure 329.3. *$^{40}Ar/^{39}Ar$ age spectrum for Gowganda siliceous metasiltstone (whole-rock sample). Errors for each temperature step are ± 2 standard deviations (S.D.). Integrated date is 1858 ± 09 Ma (2 S.D.).*

of Gowganda sedimentary rocks in a transect across D_3 structures will clarify the timing of the formation of the structures.

D_4 STRUCTURES

These comprise all of the late, brittle faults with northerly and northwesterly trends, that cut across the study area. These include the Englehart River fault and the Montreal River fault. All of these correspond to major topographic lineaments.

No direct exposure of these structures was observed and more work is required to understand these faults.

METAMORPHISM

Archean lithologies south of the Larder Lake break have been metamorphosed regionally under greenschist facies conditions. Unaltered basaltic flows, the dominant lithology within the study area, contain the assemblage actinolite-epidote-chlorite. Intermediate volcanic and felsic plutonic rocks lack actinolite. Actinolite and chlorite define the D_1 schistosity and the D_1 mineral lineation, indicating metamorphism was synchronous with D_1.

Carbonate alteration spatially associated with the D_1 zones has modified the earlier greenschist assemblage which formed in the presence of a low CO_2 hydrous fluid. Increase in X_{CO_2} of the fluid has destabilized actinolite and epidote (Clark *et al.* 1986).

Assemblages observed within carbonate alteration zones include chlorite-biotite-carbonate and chlorite-carbonate along with muscovite, quartz and albite. D_2 has affected the carbonate, suggesting that the carbonatization was pre-D_2.

The Gowganda sedimentary rocks are of subgreenschist facies, containing assemblages of clays and white mica with quartz and feldspar.

DISCUSSION

Field and laboratory evidence indicates that a period of horizontal crustal shortening, possibly related to the Kapuskasing uplift event, is recorded in the Proterozoic cover rock. More specifically, the strain is found within discreet east-northeast-trending bands that correspond to photographic lineaments and along strike and updip extensions of known D_1 zones.

Based on the observation that D_3 zones in Proterozoic sedimentary rocks appear coincident with underlying Archean deformation zones attributed to D_1, these D_1 bands have been mapped through the arm of Gowganda Formation sedimentary rocks in Burt, Holmes and Flavelle townships as well as the spur of Proterozoic cover trending northeast from the Matachewan townsite. For example, strained Gowganda sedimentary rocks lie between the Larder Lake break along the southern contact of the Timiskaming sedimentary rocks south of Kenogami Lake, and the Galer Lake fault within Holmes Township.

FUTURE WORK

In the 1989 season, mapping of structural features will be continued westward to Midlothian Township. A significant portion of this area is overlain by Proterozoic sedimentary rocks so the applicability of D_3 strain as a marker for Archean deformation shall be tested further.

In addition, the metamorphic conditions attending deformation shall be examined.

ACKNOWLEDGMENTS

We wish to thank Len Cunningham for his informative field trip; Steve Jackson, Gary Grabowski and Gerhard Meyer for their helpful discussion; Helen Lasthiotakis and Sue Prinzen for their assistance and patience.

REFERENCES

Archibald, D.A., Farrar, E. and Hanes, J.A.

1986: An $^{40}Ar/^{39}Ar$ Study of the Eastern Boundary of the Kapuskasing Structural Zone, Ivanhoe Lake Cataclastic Zone and Contiguous Abitibi Greenstone Belt (abstract); Geological Association of Canada, Program with Abstracts, Volume 11, p.A41.

Archibald, D.A, Hanes, J.A., Queen, M., Ross, D. and Farrar, E.

1989: Summary of 40Ar/39Ar Geochronology in the Kapuskasing Uplift (abstract); Geological Association of Canada, Program with Abstracts, Volume 14, p.A103.

Cherry, M.E.

1983: The Association of Gold and Felsic Intrusions—Examples From the Abitibi Belt; p.48-55 *in* The Geology of Gold in Ontario, edited by A.C. Colvine, Ontario Geological Survey, Miscellaneous Paper 110.

Clark, M.E., Archibald, N.J. and Hodgson, C.J.

1986: The Structural and Metamorphic Setting of the Victory Gold Mine, Kambalda, Western Australia; p.243-254 *in* Proceedings of Gold '86, edited by A.J. Macdonald, Toronto, 1986.

Corfu, F. and Andrews, A.J.

1986: A U-Pb Age for Mineralized Nipissing Diabase, Gowganda, Ontario; Canadian Journal of Earth Sciences, Volume 23, p.107-109.

Derry, D.R., Hopper, C.H. and McGowan, H.S.

1948: Matachewan Consolidated Mine; p.638-643 *in* Structural Geology of Canadian Ore Deposits, Canadian Institute of Mining and Metallurgy, Special Volume 1.

Dimroth, E., Imreh, L., Goulet, N. and Rocheleau, M.

1983: Evolution of the South-Central Segment of the Archean Abitibi Belt, Quebec, Part II: Tectonic Evolution and Geomechanical Model; Canadian Journal of Earth Sciences, Volume 20, p.1355-1373.

Dyer, W.S.

1936: Geology and Ore Deposits of the Matachewan-Kenogami Area; Ontario Department of Mines, Annual Report for 1935, Volume 44, Part 2, p.1-55.

Fairbairn, H.W., Hurley, P.M., Card, K.D. and Knight, C.J.

1969: Correlation of Radiometric Ages of Nipissing Diabase and Huronian Metasediments with Proterozoic Orogenic Events in Ontario; Canadian Journal of Earth Sciences, Volume 6, p.489-497.

Hamilton, J.V.

1986: Structural and Stratigraphic Setting of Gold Mineralization in the Vicinity of Larder Lake, Southcentral Abitibi Greenstone Belt, Northeastern Ontario; unpublished MSc thesis, Queen's University, Kingston, Ontario, 156p.

Jensen, L.S.

1985: Stratigraphy and Petrogenesis of Archean Metavolcanic Sequences, Southwestern Abitibi Subprovince, Ontario; p.65-86 *in* Evolution of Archean Supracrustal Sequences, edited by L.D. Ayres *et al.*, Geological Association of Canada, Special Paper 28.

Lovell, H.L.

1967: Geology of the Matachewan Area, District of Timiskaming; Ontario Department of Mines, Geological Report 51, 61p. Accompanied by Maps 2109 and 2110.

1972: Geology of the Eby and Otto Area, District of Timiskaming; Ontario Department of Mines, Geological Report 99, 34p. Accompanied by Map 2239.

MERQ-OGS

1983: Lithostratigraphic Map of the Abitibi Subprovince; Ontario Geological Survey/Ministère de l'Énergie et des Ressources, Québec, catalogued as "Map 2484" in Ontario and "DV 83-16" in Quebec. Scale 1:500 000.

Moore, J.C.G.

1966: Geology of Holmes-Burt Area, District of Timiskaming; Ontario Department of Mines, Geological Report 44, 20p. Accompanied by Map 2078.

Queen, M., Hanes, J.A. and Archibald, D.A.

1989: $^{40}Ar/^{39}Ar$ Geochronology of Dykes and their Contact Aureoles in the Kapuskasing Uplift of the Canadian Shield (abstract); Geological Association of Canada, Program with Abstracts, Volume 14, p.A123.

Thomson, J.E.

1946: Kenogami Lake Area; Ontario Department of Mines, Map 1946-1.

Grant 331 Petrology of the Springpole Lake Alkalic Volcanic Complex

K.M. Barron, N.A. Duke and R.W. Hodder

Department of Geology, University of Western Ontario, London

ABSTRACT

The Springpole Lake alkalic volcanic complex is sited in the Birch Lake greenstone belt, approximately 110 km northeast of the town of Red Lake. The complex occurs midway between the Springpole Lake and Keigat Lake granite plutons. Volcanic members occur at the unconformity between older volcanic rocks and Temiskaming-type sedimentary rocks and therefore occupy a similar stratigraphic position to the alkalic rocks at Kirkland Lake. The alkalic volcanic rocks are well preserved and range from coarse porphyry flows with zoned K-feldspar phenocrysts up to 2.5 cm in diameter to graded pyroclastic deposits including vent proximal breccia, agglomerate, lapilli tuff, and ash tuff. Of particular interest for its petrological uniqueness is fluorite-bearing carbonatite, transgressing fenitized basement volcanic units. Minette-type lamprophyric dikes form the youngest member of the alkalic suite.

Bulk rock determinations of fenitized greenstone and volcanic rocks demonstrate high K_2O and anomalous Ba, F, and locally, Cl contents. The carbonatite is a sovitic type and also shows high Ba and F contents. Rare earth element (REE) plots of fenite, syenite, trachyte and carbonatite reveal extreme enrichment in the light rare earth elements (LREE) with the steepest profiles shown by carbonatite. Initial work on stable isotopes demonstrates considerable variation among differing carbonate species but the heaviest determination ($-5\ \delta^{13}C$) falls centrally in reported data on known carbonatite occurrences.

INTRODUCTION

This study was initiated by the renewed interest in a remnant alkalic volcanic centre at Springpole Lake, 110 km northeast of Red Lake (Figure 331.1) as a result of rejuvenated gold exploration. Gold was first discovered at Springpole Lake in 1928 (Harding 1936), but until recently the local geology remained largely unknown. Resumed mineral exploration activity in the area after a hiatus of some 40 years prompted two regional mapping studies by Ontario Geological Survey (OGS) staff (Good 1988; Beakhouse 1989) which have substantially aided research. The alkalic rocks of Springpole Lake were first documented by Harding (1936), who commented on the unusual porphyritic trachytoid textures and high alkalinity of several red-weathering outcrops. Thompson (1946) described "a remarkable extrusive rock of white unaltered feldspar phenocrysts" and stated that "fragments composed of rock very similar in appearance may be seen in nearby agglomerate and undoubted tuffs."

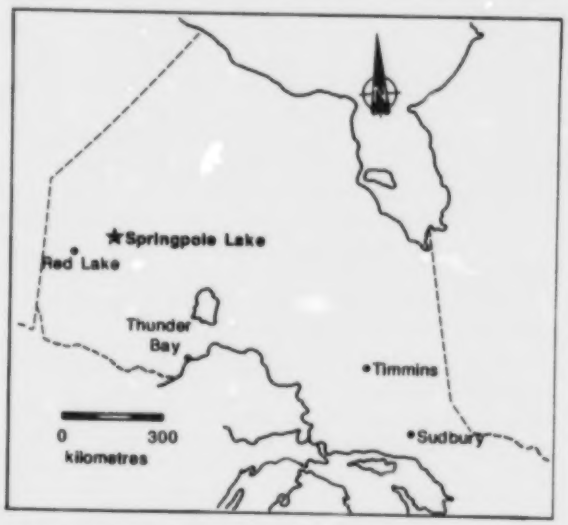

Figure 331.1. *Location map, Springpole Lake.*

The decision to mount the present detailed petrological study of the Springpole Lake alkalic rocks stemmed from the discovery of a large outcrop of massive calcite, hosting patchy disseminations and stringers of fluorite. Examination of the literature showed that non-pegmatitic occurrences of fluorite are rare in the Archean (Dawson 1985; Vos *et al.* 1987) and that fluorite/gold associations are likewise unusual. Follow-up detailed mapping of stripped outcrops at Springpole Lake through 1986–1987 revealed an irregular "carbonatite" breccia dike intruding strongly fenitized basement and overlying alkalic volcanic rocks. The members of this unique rock association are here named the Springpole Lake alkalic volcanic complex (SLC). This summary presents the results of the first year of detailed petrological study of the SLC employing detailed field mapping and petrographic examination supplemented by major and trace (including REE) element

geochemistry of the various rock types comprising the SLC.

Examples of Archean alkalic volcanic complexes are rare. Within the Superior Province they have been described in the Abitibi Subprovince at Kirkland Lake (Cooke and Moorhouse 1969) and at Chapais (Picard *et al.* 1984), in the Sachigo Subprovince (Brooks *et al.* 1982), and in the Wabigoon Subprovince (Shegelski 1980). In each case the alkalic volcanic activity appears late in greenstone belt evolution. Examples of Archean carbonatite are even more scarce and only a few are known worldwide. In overall distribution, carbonatites tend to follow major orogenic events (Woolley, in press). The oldest carbonatites dated fall late in the Archean Kenoran orogenic cycle: Siilinjarvi, Finland, at 2580 Ma (Pachett *et al.* 1981); Tupertalik, Greenland, at 2650 Ma (Larsen *et al.* 1983); Kaminak Lake, N.W.T., at 2545 Ma (Cavell *et al.* 1988); and Lac Shortt, Québec, at 2652 Ma (Morasse 1988). A fifth example of an Archean alkalic complex occurs at Sturgeon Narrows, northwestern Ontario (Trowell 1976).

Dating of disseminated galena separated from carbonatite collected by the authors from the SLC yielded a model lead isotope age of 2718 Ma while galena from a crosscutting quartz-carbonate vein yielded 2566 Ma (R. Thorpe, Geological Survey of Canada, Ottawa, personal communication, 1988-1989). U–Pb geochronological determinations of a syenite sample are currently being carried out at the Geological Survey of Canada (GSC) and should assign a precise age to the SLC. On the basis of current geochronological data it appears that the alkalic igneous activity at Springpole Lake compares well in age with other Superior Province alkalic volcanic occurrences such as Kirkland Lake at 2702 Ma (Basu *et al.* 1984). The SLC is therefore considered to be another example of a late-Kenoran alkalic volcanic centre with associated gold mineralization.

REGIONAL GEOLOGY

The SLC occurs midway between major northwest-trending fold structures separating the southerly Springpole Lake stock and northerly Keigat Lake pluton. A major sedimentary basin cores synclinal folds following Birch Lake, and the southern margin of the northeastern arm to this basin is exposed immediately north of the alkalic volcanic rocks. The SLC therefore occurs at the interface between younger sedimentary rocks and older mafic volcanic rocks of the Birch Lake greenstone belt.

The overlying sedimentary rocks are of Temiskaming-type with granite-cobble polymictic conglomerate interstratified with wacke and iron formation including characteristic magnetite-chert facies as well as hematite-jasper, carbonate and silicate members. Goodwin (1967) estimated this sedimentary succession to be 5000–10 000 feet thick. In the immediate study area the older volcanic rocks are of a type common to the upper cycles of greenstone belts with well developed Carlisle sequences. The amount of interstratified argillite–iron formation–wacke is unusually high. Tight synclinal infolds of siliceous wacke exposed immediately west of the SLC cap the greenstone succession. Contact relationships between this uppermost sedimentary facies of the greenstone belt and the alkalic volcanic rocks are obscure for lack of critical outcrop, but grading in the overlying tuffs consistently faces north, indicating a structural discontinuity. The alkalic volcanic rocks are thus identified as the lowest members of the north-facing sedimentary succession forming the south limb of the Birch Lake basin. The alkalic rocks at Springpole Lake therefore appear to occupy a stratigraphic position similar to the alkalic rocks at Kirkland Lake, which occur in the basal part of the type Temiskaming sedimentary succession.

In the immediate Springpole–Birch lakes area the regional northwest-trending structural grain is followed by late gabbro and syenite intrusions (Figure 331.2). The major Springpole Lake sill lying immediately south of the portage from Springpole Lake to Birch Lake, and a trend of syenite bodies along the northeast margin of Springpole Lake, broadly bracket the area of alkalic volcanic rocks. These intrusive belts occur on strike with the margins of a southeast-trending apophysis off the northern arm of the Birch Lake basin. Assuming the granitic clasts in the overlying polymictic conglomerates indicate unroofing of Kenoran granites, then the Springpole Lake alkalic complex is located within a zone of extension postdating granite emplacement. This domain was a site for gabbro and syenite injections, alkalic volcanism, and molasse deposition.

DETAILED GEOLOGY

The gross lithological distribution of rock types comprising the SLC is shown in Figure 331.2. The complex is cored by coarse trachyte porphyry and vent-proximal trachyte breccias. To the north, alkalic tuffs are interstratified with heterolithic volcanic breccia and debris deposits forming the southern margin to the Birch Lake sedimentary trough. Fluorite-bearing carbonatite dikes intrude this basin margin facies. The lateral extent of extrusive rocks is not well defined due to lake cover, but syenite intrusions persist at least 6 km southwestward into the northern part of Springpole Lake. Late lamprophyric dikes are common at the centre and were observed intruding the basement, alkalic volcanic rocks and slump breccias occurring at the northerly volcanic/sedimentary facies break.

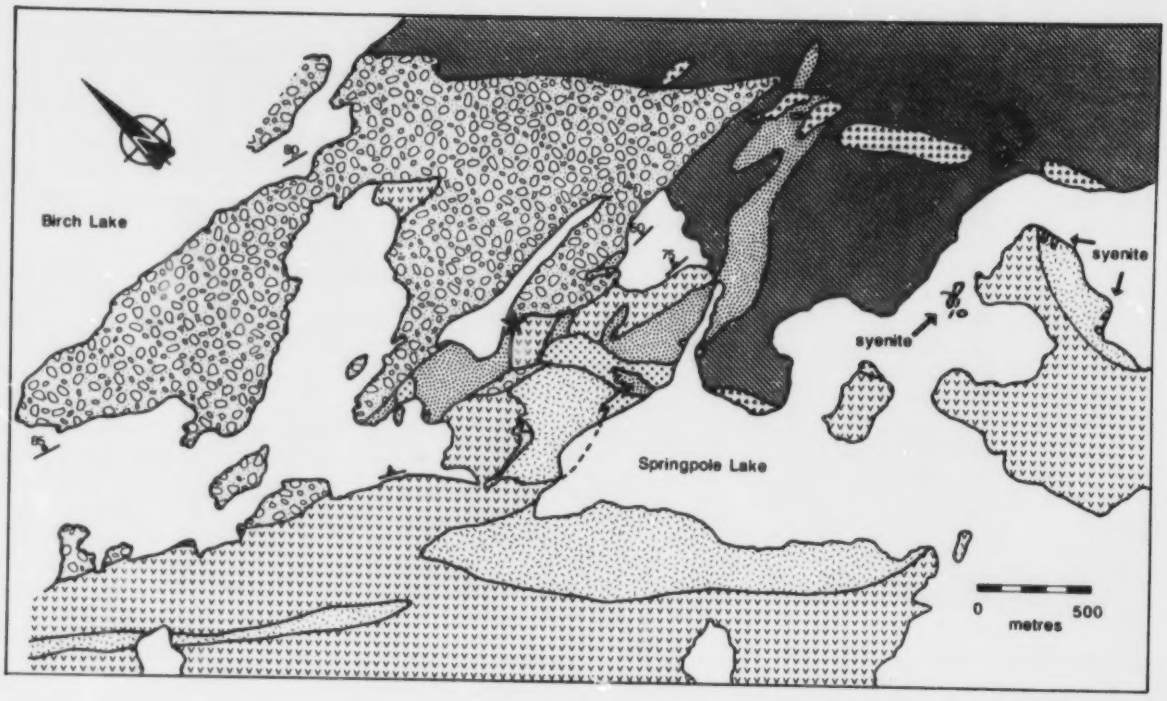

LEGEND

- fluorite–carbonatite outcrop
- trachyte tuff breccia
- trachyte
- trachytoid syenite
- gabbro
- polymictic conglomerate
- greywacke
- intermediate tuffs and flows
- mafic flows

Figure 331.2. *General geology of the Springpole Lake alkalic volcanic complex.*

LITHOLOGY

SUBVOLCANIC TRACHYTOID SYENITE AND TRACHYTE FLOWS

Porphyritic syenite and trachyte are the most voluminous members of the SLC. Trachytic flow textures defined by the alignment of crowded tabular orthoclase phenocrysts up to 5 cm in length are ubiquitous (Photo 331.1). In the absence of field relationships it is difficult to distinguish intrusive and extrusive variants due to textural convergence and alteration. Most samples collected and sectioned are carbonatized and pyritized to varying degrees and show partial to total replacement of groundmass by K-feldspar, muscovite and carbonate.

Away from the extrusive centre, syenite dikes are pink to deep red in colour due to finely disseminated hematite. Dike margins are rarely exposed due to selective erosion of intensely carbonatized contacts. Dike attitudes are generally difficult to ascertain. Where contacts are exposed no chill margins or contact metamorphic aureoles were ob-

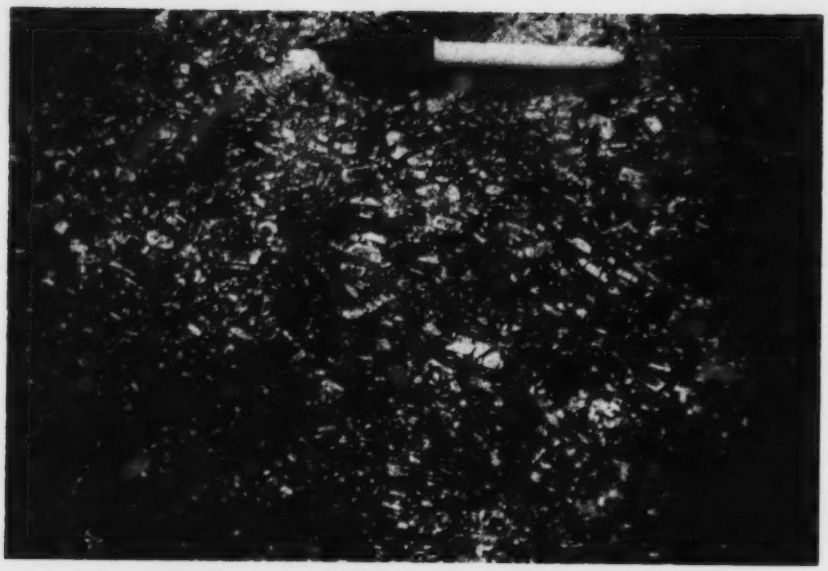

Photo 331.1. *Trachyte flow with orthoclase phenocrysts.*

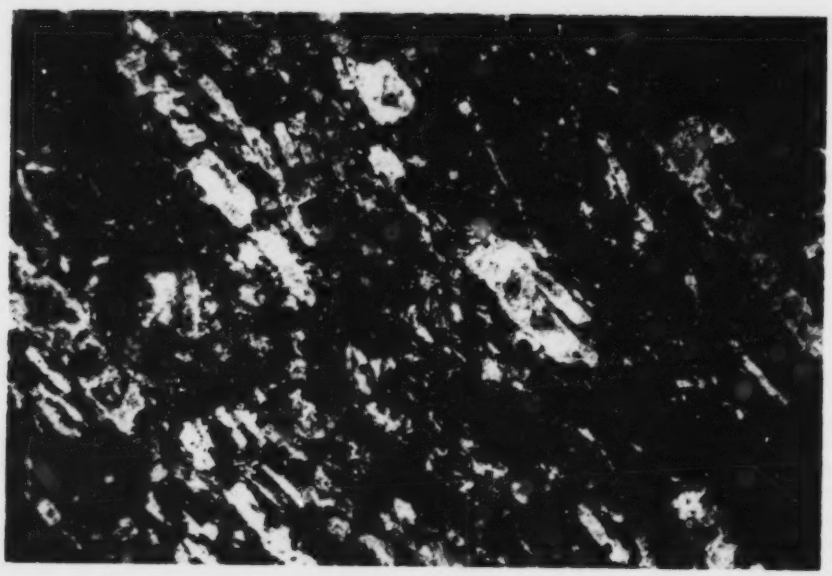

Photo 331.2. *Photomicrograph of trachytoid syenite showing aligned orthoclase phenocrysts in an albite groundmass (field of view 5.5 mm).*

served. Individual dikes generally range from 0.5 to 3 m in width and can only be traced a few tens of metres. The dikes defining a northwest trend east of the centre are somewhat larger.

In thin section the dike rocks consist essentially of strongly concentrically zoned, Carlsbad twinned, euhedral orthoclase phenocrysts in a groundmass of microcrystalline albite (Photo 331.2). Microprobe determinations show that phenocrysts often have sodic cores. The minor primary ferromagnesian mineral components are pseudomorphed by epidote, biotite, leucoxene, carbonate and pyrite. Relict euhedral grain outlines may indicate a primary pyroxene, which the distribution of alteration miner-

als suggests was also zoned. In one sample, aegirine veinlets were observed crosscutting trachytic syenite.

Trachyte flows are petrographically similar to dikes in that they too are strongly porphyritic and generally show increasing alignment of K-feldspar toward flow centres. The dikes probably represent feeders to highly viscous, laterally impersistent flows. Trachyte outcrops are pale brown or green depending on hematite content and the degree of sericitization. In contrast to intrusive syenite, where groundmass microlites are typically randomly oriented, in flows the trachytic alignment of feldspar laths persists down to the smallest grain size. The K-feldspar phenocrysts include clear untwinned orthoclase and cryptoperthite. Where sheared the trachyte flows take on the appearance of tuffs but under crossed polars adjacent phenocryst fragments retain their optical continuity. Where strongly bleached the trachyte flows are crosscut by anastomosing mica shears and quartz-carbonate veinlets and rarely, by veinlets containing fluorite.

ALKALIC PYROCLASTIC ROCKS

The alkalic pyroclastic deposits are well preserved and beautifully exposed in stripped outcrops northeast of the trachyte flows. These range from monolithic to heterolithic breccias and agglomerate to well graded lithic and crystal tuffs. Near the Springpole Lake shoreline, poorly sorted blocky breccias representing a proximal vent facies are comprised of textural variants of cognate trachytoid fragments up to 45 cm across (Photo 331.3). Fragments are non-vesicular, lithologically identical to underlying flows and cemented by tuffaceous matrix material. Clasts of repeatedly fragmented material are common. Agglomeratic units, hosting fine-grained bombs of vesicular trachyte up to 30 cm across, are occasionally interbedded with overlying lithic lapilli tuffs but are not common. The bombs often have bleached rims due to primary quenching and/or secondary alteration.

Up section, the poorly sorted tuff breccias give way to well sorted normally graded tuffs (Photo 331.4). Individual graded tuff bands are typically 1–2 m thick and some units may contain up to 10% exotic greywacke and greenstone clasts. Lithic lapilli are typically non-vesicular and finely porphyritic (Photo 331.5). K-feldspar phenocrysts are commonly broken. The tops of well graded units appear cherty. Microscopic examination reveals that some tops are composed of ultra-fine blocky glass shards and others are nearly monomineralic, consisting of abraded K-feldspar phenocrysts. Rare samples show concentrically zoned structures with hollow cores in a devitrified glass matrix. These are tentatively interpreted as accretionary lapilli.

With increased sorting up-section, tuffaceous units transit into an interbedded pyroclastic-epiclastic facies. Epiclastic units consist essentially of comminuted and reworked alkalic pyroclastic debris. With continued reworking and broader provenance, fine-grained chloritic argillaceous material begins to dominate. A zone of slumped epiclastic-pyroclastic debris caps the volcanic succession and floors over-

Photo 331.3. *Cognate lithic tuff, proximal breccia of trachytic clasts.*

Photo 331.4. *Photomicrograph of crystal lithic tuff with orthoclase phenocrysts (field of view 5.5 mm).*

Photo 331.5. *Normally graded, distal, crystal lithic tuff.*

lying pale green coloured wacke and conglomerate rich in mafic, granitic and iron formation cobbles but devoid of alkalic clasts.

FENITE

Where exposed, contacts between alkalic volcanic rocks and underlying fenitized greenstone are knife sharp, unconformable, and locally a site for intense K-feldspar veining. The main mass of fenite is developed between the alkalic volcanic rocks and the Springpole Lake gabbro sill. The interrelationship of sill emplacement, fenitization and alkalic volcanism is enigmatic. Relict pillows and locally unreplaced interflow sediment in the fenite prove, however, that alkali metasomatism did take place. This is borne out by geochemical and petrographic analysis and is similar to that seen adjacent to syenites in the Kirkland Lake camp (Jensen and Langford 1983). Although remnant gabbroic textures are locally preserved, the uniform fine-grained nature of these textural remnants indicates that the precursor rock stemmed from basal members of Carlisle sequences rather than the late Springpole Lake sill, which is characterized by moderately porphyritic and commonly trachytoid textures.

Bleached and rusty outcrops of classic "shock zone" fenite breccias occur in contact with carbonatite bodies (Figure 331.3). These are composed of non-rotated, *"in situ"*, brecciated mafic volcanic country rock (Photo 331.6); the intensity of brecciation diminishes away from carbonatite contacts. Open spaces are infilled with hematite, goethite and biotite. In thin section the fenite consists of a near-monomineralic mosaic of tabular turbid orthoclase grains pseudomorphing plagioclase. Pseudomorphs

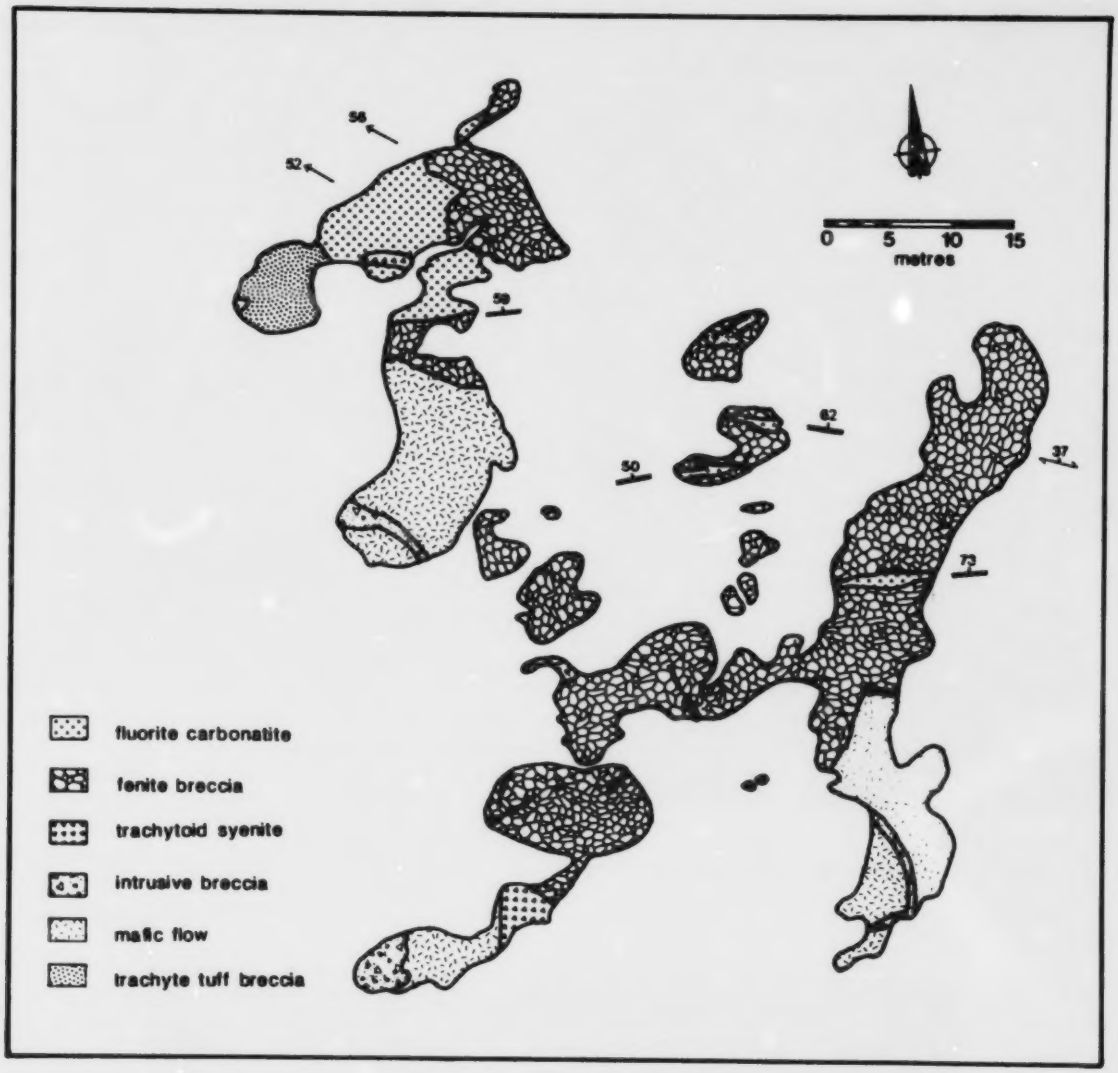

Figure 331.3. *Detailed map of carbonatite outcrops.*

occasionally show relict albite twinning in which individual twin lamellae are discontinuous or bent due to deformation. Microprobe determinations demonstrate that replacement orthoclase can contain up to 5 weight percent barium. The fenites are highly enriched in volatiles. Microprobe determinations have shown that biotite can contain up to 3 weight percent fluorine. This rock type highly resembles descriptions of "burnt rock" or "orthoclasite" from high-level, subvolcanic potassic fenite zones (Heinrich and Moore 1970; Vartiainen and Woolley 1976)

CARBONATITE

Of particular interest in terms of its petrological uniqueness is the occurrence of fluorite-bearing carbonatite. Volumetrically, such carbonatite makes up only a minor part of the SLC. It is exposed in outcrop only near the south shore of the east-trending pond (Figures 331.2 and 331.3), however it has been intersected in drilling over a 1.5 km strike length along the base of the overlying Temiskaming-type conglomerates. In drill core, carbonatite often shows strong overprinted shear fabrics. In outcrop the carbonatite is striking in appearance with incorporated wall rock xenoliths of syenite and mafic fenite standing up in weathered relief (Photo 331.7). Schlieren of entrained xenoliths or fluorite define a flow banding (Photo 331.8) (cf. Heinrich 1966). The outer margins of the carbonatite are quite siliceous, possibly due to the deposition of silica liberated through xenolith metasomatism, and strongly impregnated with purple fluorite. Brecciated fenite zones appear most intense adjacent to metre-wide

Photo 331.6. *"In situ", brecciated contact-zone fenite.*

dikes (Figure 331.3). Intrusive breccia bodies of angular syenite and mafic volcanic blocks are common near the carbonatite. Mineralogically the carbonatite consists of varying modal proportions of medium-grained equigranular calcite and fluorite with up to several modal percent barite and minor (0-5%) quartz. Both biotite and orthoclase are common trace constituents and accessory pyrite, galena and sphalerite were identified in several samples. In contrast to late ankerite veins, microprobe determinations reveal the only carbonate species in carbonatite as nearly end-member calcite.

LAMPROPHYRIC DIKES

Lamprophyric dikes are common and observed to crosscut all other members of the SLC except carbonatite. Individual dikes are up to 2 m thick and traceable across discontinuous outcrops for several hundred metres along strike. Most dikes are strongly carbonatized. Relict biotite phenocrysts in the least altered dike material indicate the SLC lamprophyres are minettes.

GEOCHEMISTRY

Whole-rock major and trace element analyses of representative samples from the SLC suite are presented in Table 331.1. The chemical signatures of the various members of the alkalic suite are demonstrated in Figures 331.4 and 331.5, depicting bulk rock alkalinity and REE profiles.

Samples of satellitic syenite dikes plot well within the alkalic field in Figure 331.4. In these rocks the K_2O/Na_2O ratio approximates unity (Table 331.1). The dikes are not peralkalic, as alumina is always in

Photo 331.7. *Carbonatite outcrop (carbonatite is light coloured).*

Photo 331.8. *Carbonatite showing schlieren of entrained xenoliths and fluorite.*

TABLE 331.1. CHEMICAL ANALYSES OF REPRESENTATIVE SAMPLES, SPRINGPOLE LAKE.

	Syenite	Trachyte	Breccia Fenite	F-rich Carbonatite	K-spar Tuff	Xenolithic Carbonatite
			weight percent			
SiO_2	64.40	59.30	54.06	19.50	54.50	12.87
TiO_2	0.14	0.26	1.04	0.06	0.63	0.37
Al_2O_3	19.20	17.80	16.72	1.55	17.50	4.59
Fe_2O_3	1.10	1.80	6.85*	4.02*	5.20*	2.07*
FeO	0.20	0.40	0.30	n.d.	n.d.	n.d.
MnO	0.02	0.05	0.06	0.26	0.10	0.15
MgO	0.18	1.99	1.61	0.73	1.61	0.67
CaO	0.69	0.96	0.20	46.18	2.73	43.65
Na_2O	6.50	0.30	0.47	0.10	3.70	0.12
K_2O	6.07	13.21	12.90	0.40	7.58	2.87
P_2O_5	0.03	0.17	0.20	<0.01	0.14	0.08
LOI	0.17	2.71	1.50	7.45	5.22	29.30
			ppm			
Ba	3569	2726	25000	31700	2096	2000
Sr	743	532	760	2300	496	730
Rb	103	375	590	<40	190	105
Zr	113	315	113	13	181	n.d.
F	460	3281	5800	27.5%	1813	2.9%
Cl	<100	<100	1210	59	<100	10

** Total Fe as Fe_2O_3*
n.d. not determined

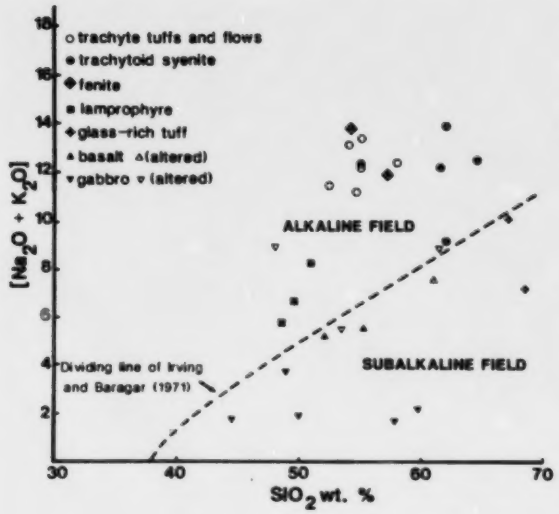

Figure 331.4. *Plot of total alkalies vs silica.*

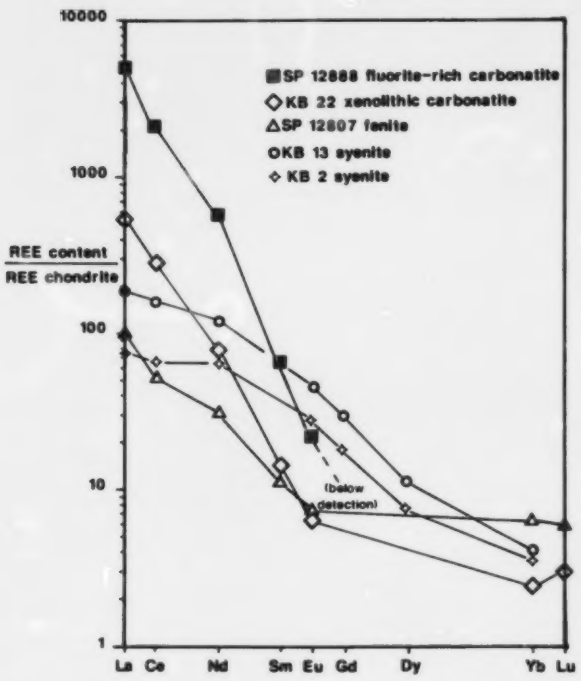

Figure 331.5. *Chondrite normalized rare earth plots.*

excess of total alkalies. Diagnostic features include low CaO, reflected in the absence of calcic plagioclase, low TiO_2 and Fe_2O_3 > FeO. The trachyte flows have bulk chemical signatures broadly similar to the syenite dikes. In flows, the alumina content still exceeds total alkalies, however, K_2O/Na_2O ratios can reach extreme values of 15:1. This is partly a consequence of K-fenitization which variably overprints all vent-proximal rocks. In rocks that are strongly sheared, K_2O contents reflect sericitization. Fenitization of basement has moved some mafic volcanic rocks and gabbro to well within the alkalic field (Figure 331.4). Breccia zone contact fenites illustrate strong fenitization by alkali and halogen rich fluids. Notable are the high chlorine and fluorine contents and the highest barium contents of any silicate rocks analyzed from the SLC (Table 331.1).

Chondrite normalized REE plots (Figure 331.5) of selected samples of fenite, syenite and carbonatite reveal extreme LREE, with the steepest profiles shown by carbonatite. The heavy rare earth elements (HREE's) are strongly depleted in all the analyzed samples. The profile of sample SP 12888 of carbonatite is incomplete because levels of HREE are below detection limits. This may be a function of analysis by neutron activation and interference between HREE's and barium. The more precise analytical technique by isotopic dilution (J. Franklin, Geological Survey of Canada, personal communication, 1989) is currently being carried out at the GSC to more accurately establish HREE abundances. Among the various members of the SLC suite, the carbonatites have the highest absolute REE abundances and La/Lu ratios. It is probable that most of the REE's reside in fluorite since the highest REE contents correlate well with high modal fluorite. It has been shown that REE levels in fluorite of differing paragenesis are greatest in samples from carbonatite (Moller and Morteani 1983). Such rare earth minerals as bastnaesite have not been detected.

Initial work on stable isotopes demonstrates considerable variation among differing carbonate species. However, the heaviest determination (−5.45 $\delta^{13}C$) falls centrally in reported data on known igneous carbonatite occurrences (Deines and Gold 1973). Samples identified as carbonatite but with $\delta^{13}C$ values in the −3 to −1 range have likely been subject to post-crystallization isotopic exchange as these exhibit crystalloblastic textures due to shearing. The lightest determinations are of carbonate species sited in late quartz veins and specify a late hydrothermal signature.

PETROGENETIC MODEL

The SLC is located in a zone of extension initiated by the intrusion of Kenoran plutons, possibly coinciding with the emplacement of the Springpole Lake pluton to the southeast. It appears to predate the emplacement of the Keigat Lake pluton to the northeast, responsible for the overprinting shear (Good 1988). The igneous activity accompanying the earliest stages of rifting entailed gabbro emplacement, syenitic injection, alkalic volcanism, and late fluorite-bearing carbonatite and minette dikes. The field relations indicate a rather small, short-lived alkalic volcanic centre. The alkalic volcanic rocks

TABLE 331.2. CHEMICAL ANALYSES OF SAMPLES FROM THE MONTANA ALKALINE PROVINCE.

	Little Rocky Mtns.		Bear Lodge Mtns.	
	Syenite	Trachyte	Alkali Trachyte Porphyry	Alkali Trachyte Porphyry
		weight percent		
SiO_2	65.7	65.3	57.16	50.90
Al_2O_3	16.4	19.4	22.79	18.46
Fe_2O_3	2.77	2.75	2.91	3.00
FeO	n.d.	n.d.	n.d.	n.d.
MgO	0.38	0.02	0.30	0.69
CaO	0.70	0.07	0.20	6.86
Na_2O	0.90	5.30	0.23	0.92
K_2O	13.1	8.5	12.96	11.35
TiO_2	n.d.	n.d.	0.44	0.62
P_2O_5	n.d.	n.d.	0.11	0.34
MnO	0.237	0.129	0.20	0.22

	Bear Paw Mtns.		N. Moccasin Mtns.	S. Moccasin Mtns.
	Syenite	Syenite	Syenite Porphyry	Alkali Syenite Porphyry
		weight percent		
SiO_2	47.33	56.86	63.5	62.8
Al_2O_3	17.76	24.45	16.6	17.6
Fe_2O_3	0.60	0.56	2.20	2.20
FeO	2.95	0.38	1.3	0.08
MgO	0.80	0.32	1.20	0.14
CaO	6.06	0.01	2.80	1.60
Na_2O	0.58	0.08	4.50	4.80
TiO_2	1.14	0.52	0.38	0.24
P_2O_5	0.31	0.07	0.15	0.05
MnO	0.32	0.00	0.10	0.06

n.d. not determined
Little Rocky Mtns., Montana (Rogers and Enders 1982) , Bear Lodge Mtns., Wyoming (Jenner 1984), Bear Paw Mtns., Montana (Pecora 1962), Moccasin Mtns. Montana (Lindsey 1980).

form the lowest members of a molasse-filled trough extending off the margin of the Birch Lake basin. The tectonic setting of the SLC can be broadly compared to sites of post-Laramide alkalic volcanism and molasse deposition in the US Cordillera. Geochemically, the alkalic rocks of the SLC best compare to the Tertiary age alkalic rocks of the Montana Alkaline Province (cf. Mutschler *et al.* 1985). Alkalic rocks from this region (Table 331.2) are characterized by similarly low TiO_2 and P_2O_5 and high Al_2O_3 and K_2O contents. The carbonatites at SLC, are unusual in that they do not carry apatite, magnetite or sodic amphibole. However, the absence of these minerals is not unknown among carbonatite occurrences and may reflect high level, subvolcanic emplacement of the dikes.

Though it is premature in our understanding of the SLC to assign a specific petrogenetic model, our data to date suggests that these alkaline rocks are examples of a shoshonitic igneous lineage (Morrison 1980). Notably, many of the examples of shoshonitic rocks identified in the Superior Province are spatially and temporally associated with lode gold deposits (Wyman and Kerrich 1988). Many of the alkaline centres from the Montana Alkaline Province, cited above for comparison, also have associated carbonatite and gold mineralization. The paleo-environment of the SLC is broadly similar to that of the youthful gold deposits of the US Cordilleran. Gold at Springpole may have originally been concentrated in a synvolcanic epithermal environment prior to remobilization into late shears.

ACKNOWLEDGMENTS

The authors would like to extend thanks to Bill Bond and Derek Barlett of Gold Fields Canadian Mining Ltd. for their support and permission to carry out this study. We are also grateful to Gary

Beakhouse of the Ontario Geological Survey for his interest and helpful advice. James Franklin and Ralph Thorpe of the Geological Survey of Canada are also thanked for assistance with REE and Pb isotope analyses, and for stimulating discussion.

REFERENCES

Basu, A.R., Goodwin, A.M. and Tatsumoto, M.

1984: Sm-Nd Study of the Archean Alkaline Rocks from the Superior Province of the Canadian Shield; Earth and Planetary Science Letters, Volume 70, p.40-46.

Beakhouse, G.P.

1989: Geology of the Western Portion of the Birch Lake Area, Kenora District, Patricia Portion; Ontario Geological Survey, Open File Report 5700, 106p.

Brooks, C., Ludden, J., Pigeon, Y. and Hubregste, J.J.M.W.

1982: Volcanism of Shoshonitic to High-K Andesite Affinity in an Archean Arc Environment, Oxford Lake, Manitoba; Canadian Journal of Earth Sciences, Volume 19, p.55-67.

Cavell, P.A., Baadsgaard, H. and Wijbrans, J.

1988: The Kaminak Lake Alkaline Complex—A Late Archean Intrusion in the Rankin-Ennadai Greenstone Belt; p.28-29 *in* Exploration Overview 1988, Northwest Territories, Indian and Northern Affairs Canada, Yellowknife.

Cooke, D.L. and Moorhouse, W.W.

1969: Timiskaming Volcanism in the Kirkland Lake Area, Ontario, Canada; Canadian Journal of Earth Sciences, Volume 6, p.117-132.

Dawson, K.R.

1985: Geology of Barium, Strontium and Fluorine Deposits in Canada; Geological Survey of Canada, Economic Geology Report 34, 136p.

Deines, P. and Gold, D.P.

1973: The Isotopic Composition of Carbonatite and Kimberlite Carbonates and their Bearing on the Isotopic Composition of Deep-Seated Carbon; Geochimica et Cosmochimica Acta, Volume 37, p.1709-1733.

Good, D.J.

1988: Geology of the East Half of the Birch Lake Area, Kenora District Patricia Portion; Ontario Geological Survey, Open File Report 5685, 119p.

Goodwin, A.M.

1967: Volcanic Studies in the Birch-Uchi Lakes Area of Ontario; Ontario Department of Mines, Miscellaneous Paper 6, 96p.

Harding, W.D.

1936: Geology of Birch-Springpole Lake Area; Ontario Department of Mines, Annual Report for 1936, Volume 45, Part 4, 33p.

Heinrich, W.M.

1966: The Geology of Carbonatites; Rand McNally, Chicago, 555p.

Heinrich, E.W. and Moore, D.G. Jr.

1970: Metasomatic Potash Feldspar Rocks Associated with Igneous Alkalic Complexes; Canadian Mineralogist. Volume 10, p.571-584.

Irvine, T.N. and Barragar, W.R.A.

1971: A Guide to the Geochemical Classification of the Common Volcanic Rocks; Canadian Journal of Earth Sciences, Volume 8, p.523-548.

Jenner, G.A. Jr.

1984: Tertiary Alkalic Igneous Activity, Potassic Fenitization, Carbonatite Magmatism and Hydrothermal Activity in the Central and Southeastern Bear Lodge Mountains, Crook County, Wyoming; unpublished MSc thesis, University of North Dakota, Grand Forks, North Dakota.

Jensen, L.S. and Langford, F.F.

1983: Geology and Petrogenesis of the Archean Abitibi Belt in the Kirkland Lake Area; Ontario Geological Survey, Open File Report 5455, 520p.

Larsen L.M., Rex, D.C. and Secher, K.

1983: The Age of Carbonatites, Kimberlites and Lamprophyres from Southern West Greenland: Recurrent Alkaline Magmatism during 2500 Million Years; Lithos. Volume 16, p.215-221.

Lindsey, D.

1980: Preliminary Geologic Map and Report on Selected Mineral Resources of the North and South Moccasin Mountains, Fergus County, Montana; United States Geological Survey, Open File Report 80-832 24p.

Morasse, S.

1988: Geological Setting and Evolution of the Lac Shortt Gold Deposit, Waswanipi, Quebec, Canada; unpublished MSc thesis, Queen's University, Kingston, Ontario.

Moller, P. and Morteani, G.

1983: On the Geochemical Fractionation of Rare Earth Elements During the Formation of Ca-Minerals and its Application to the Problems of the Genesis of Ore Deposits; p.747-791 *in* The Significance of Trace Elements in Solving Petrogenetic Problems and Controversies, edited by S.S. Augustithis, Theophratus Publications, Athens.

Morrison, G.W.

1980: Characteristics and Tectonic Setting of the Shoshonite Rock Association; Lithos, Volume 13, p.97-108.

Mutschler, F.E., Griffin, M.E., Stevens, D.S. and Shannon S.S. Jr.

1985: Precious Metal Deposits Related to Alkaline Rocks in the North American Cordillera; Transactions of the Geological Survey of South Africa, Volume 88, p.355-377.

Pachett, P.J., Kouvo, O., Hedge, C.E. and Tatsumoto, M.

1981: Evolution of Continental Crust and Mantle, and Mantle Heterogeneity: Evidence from Hf Isotopes; Contributions to Mineralogy and Petrology, Volume 78, p.279-297.

Pecora, W.T.

1962: Carbonatite Problem in the Bearpaw Mountains, Montana; p.83-104 *in* Petrologic Studies—A Volume to Honor A.F. Buddington, Geological Society of America.

Picard, C., Piboule, M. and Charbonneau, J.M.

1984: Pétrogènese des Volcanites Archéennes Hautement Potassique du Groupe d'Opémiska; p.35-47 *in* Chibougamau—Stratigraphy and Mineralization, edited by J. Guha and E.H. Chown, Canadian Institute of Mining and Metallurgy, Special Volume 34.

Rogers, L.M. and Enders, S.

1982: Syenite-Hosted Gold Deposits of the Little Rocky Mountains, Montana; unpublished paper presented at the 88th Annual Northwest Mining Association Convention, Spokane, Washington, December, 1982, 22p.

Shegelski, R.J.

1980: Archean Cratonization, Emergence and Red Bed Developmemt, Lake Shebandowan Area, Canada; Precambrian Research, Volume 12, p. 331-347.

Thomson, R.

1946: Report on the Springpole Lake Mines Ltd.; unpublished report on file, Ontario Ministry of Northern Development and Mines, Assessment Files, Red Lake, Ontario.

Trowell, N.F.

1976: Geology of the Quest Lake Area, Districts of Kenora and Thunder Bay; Ontario Division of Mines, Geoscience Report 154, 60p.

Vartiainen, H. and Woolley, A.R.

1976: The Petrography, Mineralogy and Chemistry of the Fenites of the Sokli Carbonatite Intrusion, Finland; Geological Survey of Finland, Bulletin 280, 87p.

Vos, M.A., Abolins, T., McKnight, R.L.W. and Smith, V.

1987: Industrial Minerals of Ontario; Ontario Geological Survey, Mineral Deposits Circular 26, 272p.

Woolley, A.R.

In Press: The Spatial and Temporal Distribution of Carbonatites; *in* Proceedings of the Second International Carbonatite Symposium, Ottawa, 1986, edited by K. Bell.

Wyman, D. and Kerrich, R.

1988: Alkaline Magmatism, Major Structures and Gold Deposits: Implications for Greenstone Belt Metallogeny; Economic Geology, Volume 83, p.454-461.

Grant 332 High-Resolution Magnetic-Susceptibility Logger and Dipmeter for Mineral Exploration Boreholes: Concept and Initial Progress

Alfred V. Dyck[1], Peter V. Auchincloss[1] and David L. Atherton[2]

[1]Department of Geological Sciences, Queen's University, Kingston

[2]Department of Physics, Queen's University, Kingston

ABSTRACT

The objectives of this project are to design, develop and test a prototype high-resolution magnetic-susceptibilty logger and three-arm dipmeter for use on diamond-drill cores and in drill holes. This will permit study of magnetic variations in greater detail than was before possible. Testing and comparison of the devices (field prototype) in mining-exploration environments are planned to gain an impression of the nature of high-resolution susceptibility variations and their potential utility in characterizing ore-deposition environments both lithologically and structurally.

The project is in its preliminary stages of design (computer aided) prior to fabrication of a laboratory prototype of a borehole tool. The immediate goal is to improve sensitivity (signal/noise ratio) to the extent that miniature Hall-effect sensors can be used, thus achieving a high spatial resolution of 5 mm necessary to detect minute variations in magnetic susceptibility along the wall of the hole.

INTRODUCTION

Mapping of spatial variations in the magnetic susceptibility of rocks is considered by many to be the single most useful geophysical tool in mineral exploration. Variations in susceptibility are common at all scales and reflect the concentration of magnetite (and in sulphide-rich environments, the concentration of pyrrhotite). The objective of this project is to develop a new method of susceptibility mapping using a high-resolution magnetic-susceptibility logger and three-arm dipmeter for use in exploration drill holes and on diamond-drill cores. The high spatial resolution of the susceptibility measurement will be achieved using powerful permanent magnets and miniature Hall-effect probes. Sensitivity of the proposed device to magnetic susceptibility variations, comparable to that of conventional susceptibility loggers, will render it useful in a wide range of rocks of interest in mineral exploration. The project brings together two areas of expertise ideally suited to this problem but not normally associated with one another, borehole geophysics and applied physics of pipeline inspection tools.

This method will provide the means to systematically search for and study characteristic magnetic signatures of mineral deposits and their environments. The orientation of planar magnetic features intersected by the drill hole should be able to be determined with respect to the hole. This development has the potential of yielding quantitative mineral-exploration data on the distribution and orientation of small but structurally important features like dikes and veins. Two such possibilities are mafic dike orientations and magnetite-bearing or magnetite-destructive alteration, both important in gold exploration.

The project has three phases: 1) initial-design phase (computer study); 2) construction of a prototype for laboratory testing using both a simulated drill hole and measurements on diamond-drill cores; and 3) design, fabrication and field testing of the drill-hole probe in mineral exploration environments (Sudbury and Timmins). The concept of this new device is described in greater detail. Initial results of the computer-aided design process are reported here, as well as a design of the laboratory test facilities required for phase two. A short field experiment was undertaken to demonstrate the potential application of small-scale variations in susceptibility to structural mapping. A contour map of susceptibility values at outcrop scale and a photograph of the outcrop are included here for comparison.

DESCRIPTION OF DEVICE

CONCEPT

The measurement of susceptibility is to be accomplished by D.C. (zero frequency) means, employing high-strength permanent magnets and miniature Hall-effect sensors. The magnets will be arranged so as to produce a primary magnetic field with axial symmetry (relative to the borehole). The Hall-effect sensor will be offset within the housing of the probe to be as near to the wall of the borehole as possible. As the probe is moved slowly along the hole on the end of a cable, the Hall-effect sensor will provide continuous output proportional to susceptibility vari-

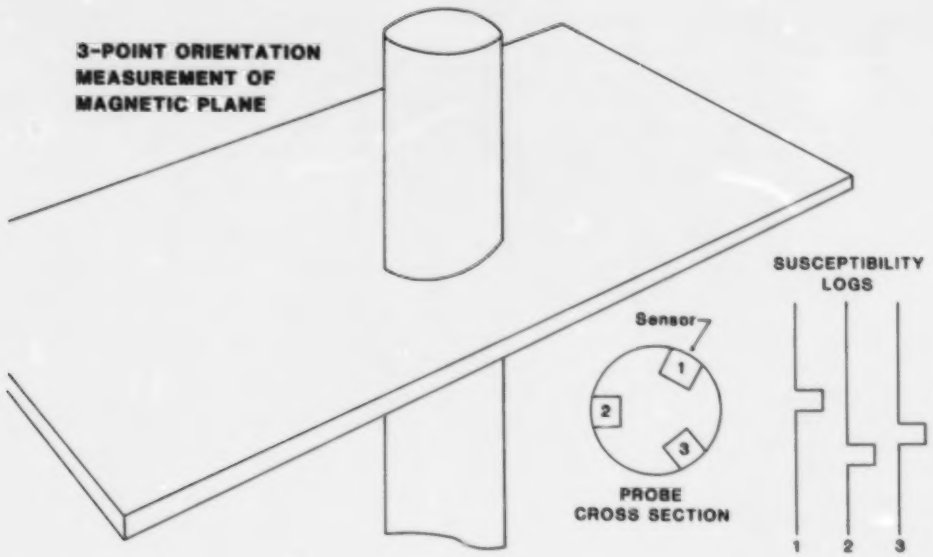

Figure 332.1. *The high-resolution magnetic-susceptibility logger, with a set of outputs from three sensors distributed at 120° intervals around the circumference of the tool. The pattern illustrates the tool's operation as a dipmeter.*

ations encountered in the rock. The concept is expected to be implemented in two forms:

1. A high-resolution device for mapping susceptibility along the wall of a drill hole will feature a three-arm design for determining orientation of planar geologic features of differing susceptibility from neighbouring rock, as described below.
2. An equivalent device for use on diamond-drill core.

The orientation, with respect to the drill hole, of planar magnetic features intersected by the hole, will be determined on the basis of the signature detected by each of the three arms. Relative displacement of the signature along the hole would be indicative of non-perpendicularity (with respect to the drill hole), as shown in Figure 332.1. This is similar in geometric principle to stratigraphic dipmeter devices, employed in hydrocarbon exploration, which operate on the physical principle of micro-resistivity determinations.

The practical challenge is that of achieving the necessary resolution through miniaturization. The technology is presently in use in the non-destructive testing of pipelines from the interior (Atherton and Daly 1987). We feel that miniaturization can be accomplished for borehole susceptibility measurements.

INTENDED APPLICATIONS

A valuable contribution of geophysics to exploration is the mapping of variations in the magnetic susceptibility of rocks. At the regional scale this commonly leads to the recognition of lithology and structural patterns not detected by normal mapping. At the detailed scale, variations in susceptibility may be caused by small-scale variations in rock and alteration type.

Susceptibility values are controlled primarily by the concentration of magnetite and, in sulphide-rich environments, by the presence of pyrrhotite. Figure 332.2 shows the ranges of values of magnetic susceptibility in common rock types. Borehole (and laboratory) susceptibility measurements show useful small-scale variability (e.g., Hillary and Hayles 1985; Glenn and Nelson 1979; Daniels *et al.* 1981; Lapointe *et al.* 1982). Clark (1983) pointed out that in the amphibolites of the Broken Hill (Australia) area, subtle lithologic variations, which are difficult to trace by conventional means, can be matched between holes on the basis of their magnetic susceptibility signature. This gives encouragement to search for and study characteristic magnetic patterns in rocks in further detail (i.e., with higher resolution).

Specifically, this research has the potential of providing quantitative data on the distribution and orientation of small but structurally important features like dikes and veins. Mafic dikes, for example, are ubiquitous in gold deposits, and commonly show structural patterns which are part of the larger structural system controlling ore deposition. Yet it is very difficult to determine the orientation of dikes from visual inspection of core. We feel that our downhole instrument has good potential for determining mafic dike orientations.

Measurements of the intensity and orientation of magnetite-bearing or magnetite-destructive alteration is also very important in gold exploration. In many

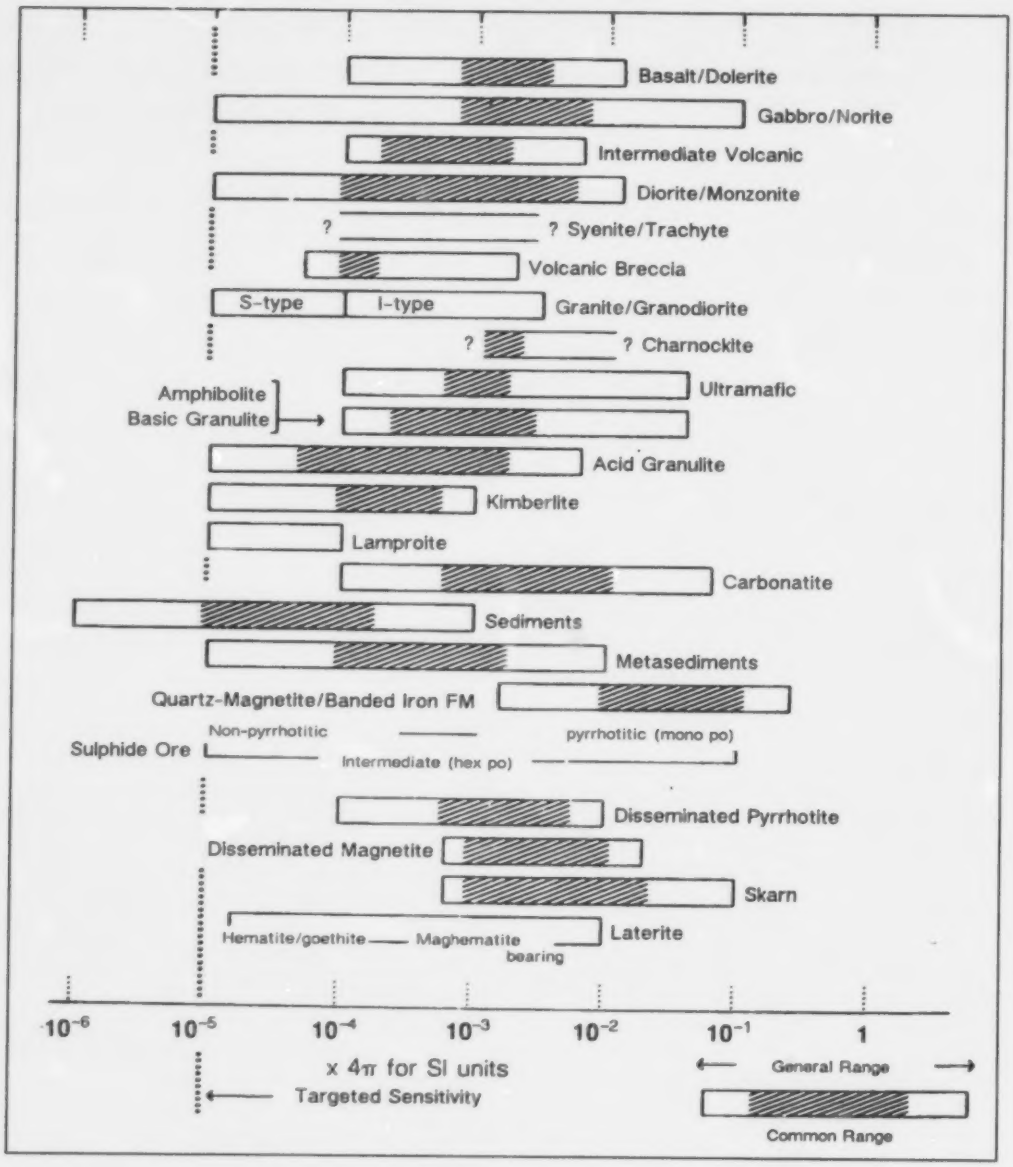

Figure 332.2. *Range of values of magnetic susceptibility in common rock types (after Clark 1983). The sensitivity thought to be achievable with a Hall-effect susceptibility probe is shown.*

gold environments in greenstone belts, secondary magnetite is formed in the outer parts of zones of progressive carbonatization, and destroyed in the inner parts of these alteration zones (e.g., Lac Shortt, Québec, Morasse *et al.* 1986; Victory Mine, Kambalda, Australia, Clark *et al.* 1986). Many massive base-metal sulphide deposits also have associated magnetite-bearing mineralization and/or alteration facies (e.g., Ansil deposit, Noranda, G. Riverin, Minnova Inc., personal communication, 1989; Corbet deposit, Knuckey and Watkins 1982).

This device will provide the means to study characteristics of mineral deposits on a systematic basis through their magnetic signatures. Detailed magnetic characterization will contribute to better geologic characterization of mineral deposits and their environments. This new instrument and method, for use at the small-scale extreme, will provide information which can be correlated directly with geological observations at that scale.

DESIGN CRITERIA

The drill-hole probe and core logger are intended for eventual independent use but during the research phase (this project) to test and prove the method (which will include comparison of the drill-hole response of magnetic features with that observed on core from the same hole), they are being designed to accommodate A-sized holes (47 mm diameter) and core.

The design incorporates the use of a steady (D.C.) magnetic field rather than alternating (A.C.) fields employed in conventional susceptibility systems. Advantages of a D.C. device are: 1) high spatial resolution because Hall sensors can be made very small, and 2) lack of interference from conductivity effects (through eddy-current induction).

The sensitivity will be comparable to present logging devices operating with alternating frequency in the kHz range. The design targets are a sensitivity to susceptibility values as small as 1.2×10^{-4} SI units, with a spatial resolution as small as 5 mm. The target sensitivity threshold would render the device useful in a wide variety of rocks of interest in mineral exploration according to the range of susceptibility variations in crystalline rocks shown in Figure 332.2. The target resolution will allow orientation of a magnetic plane to be determined to within $\pm 5°$ (with respect to the drill hole).

DESIGN PROGRESS

FINITE-ELEMENT CALCULATIONS

We have evaluated various designs of the borehole tool by calculating the tool's response to a thin magnetic layer (thickness = 5 mm, susceptibility = 2.4×10^{-4} SI) cut perpendicularly by a 47 mm diameter borehole. The parameter values of the layer represent the thresholds for detectability and resolution which we hope to achieve. Calculations have been carried out with the INFOLYTICA finite-element package, MAGNET (*see* Atherton and Daly 1987). Steps involved in solution of a problem are: 1) a geometric model of the tool is generated, without

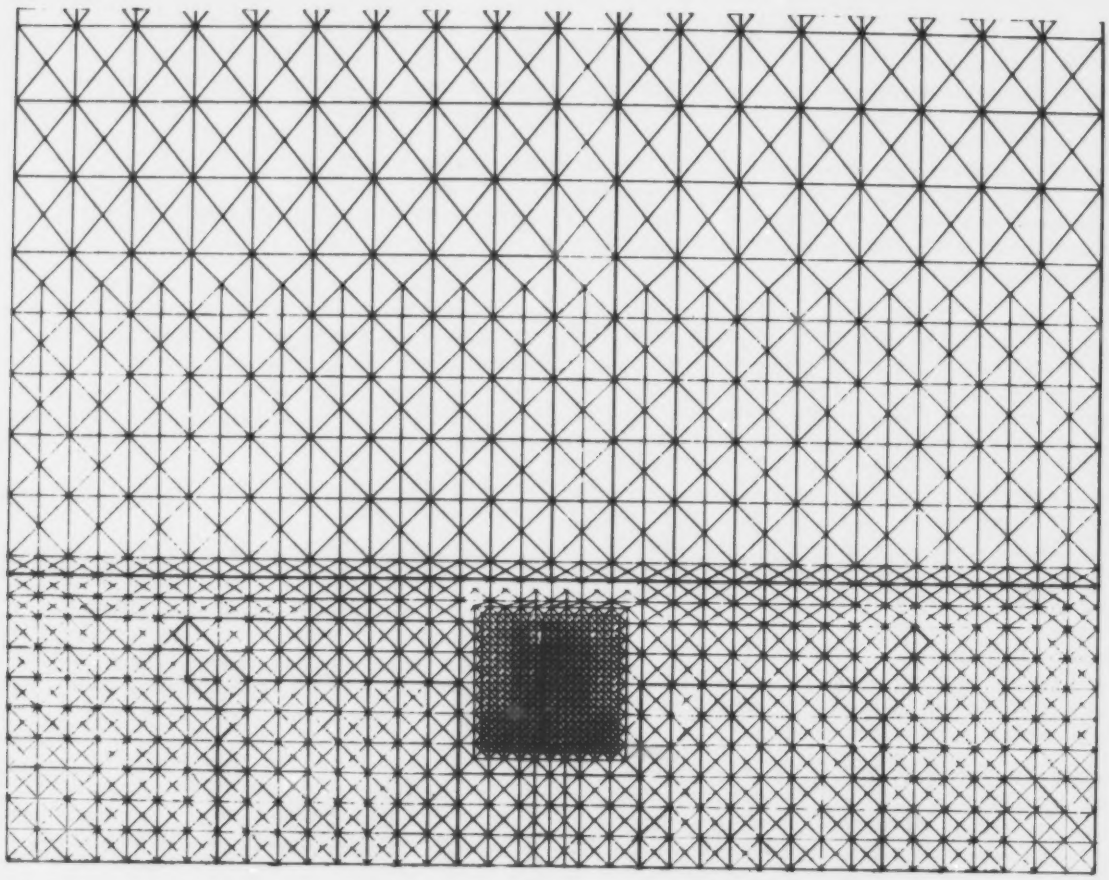

Figure 332.3. *Finite element mesh for design No. 3. Notice that mesh size approaches 5000 nodal points with high mesh density in the region of the measurement probe and magnetic layer.*

reference to any of the materials being used, by specifying a mesh containing groups of triangles (*see* Figure 332.3 for a sample mesh); 2) a library of magnetization curves is created, each member of which is assigned to a different material used in the design; 3) excitation and boundary conditions are specified; 4) the problem is solved in terms of a magnetic potential using a modified Newton iteration technique; and 5) calculations are displayed either as contour maps of the potential, or as profiles of magnetic flux.

At this stage of development of the tool, a two-dimensional permanent-magnet solver is being used to solve for the magnetic potential, A, which is related to the magnetic flux, B, by B = curl A. The coordinate system is shown in Figure 332.4a, which represents one-half of the section through the axis of the probe. In the 2-D case there is no flux spreading out of the plane so that $B_z = 0$ and the only component of A is A_z (perpendicular to the plane of the section. Therefore the axial and radial components of flux are represented by

$B_x = dA_z/dy$, and $B_y = -dA_z/dx$, respectively.

TOOL DESIGN

Results characterizing each of three designs are presented chronologically, outlining the tool's development. The tool consists of two strong permanent magnets whose orientations with respect to each other vary depending on the primary field desired. In designs 1 and 3, magnetically soft iron is used for flux shaping. The target magnetic layer is the only other medium of non-zero susceptibility. Anomalous fields were calculated by subtraction of the layer and layer-free solutions.

Design No. 1 (Figure 332.4). This is the original design. Two permanent magnets, separated by 47 mm, are oriented with their poles in line with one another so as to produce an axially dominant flux in the region of the layer. The presence of the soft-iron core between the magnets reduces the y-components of flux in the measurement region. The magnitudes of the anomalous flux (approximately 10^4 nT) are readily detectable with miniature Hall probes (sensitive down to 10^2 nT), except in the large background fields (5×10^7 nT) which exist in this design. The resulting 1/5000 signal/background can be increased to 1/1000 with the addition of a flux collector attached to the Hall sensor (not shown), but even greater improvement is required. Attempts to design a shield to exclude background field from the measurement region were unsuccessful.

Design No. 2 (Figure 332.5). Two permanent magnets are aligned with their poles opposing, thus producing a radially dominant flux in the region of the layer. The anomalous flux generated by this orientation of primary field has benefits in terms of improved spatial resolution. The anomalous flux magnitudes in this model are somewhat larger than in design 1 (by factors of 9 and 3 for the x and y components, respectively). However the background field has increased a comparable amount and no improvement in signal/background is achieved.

Design No. 3 (Figure 332.6). Two permanent magnets are oriented in line as for design 1. The main difference is that soft iron "arms" are introduced for flux shaping, the purpose of which is to direct more of the flux into the layer, while decreasing the flux in the measurement region. This leads to larger anomalous signals (by a factor of 2 over design 1) as shown in Figure 332.6c, accompanied by a slight reduction in background field. The shape of the flux concentrators is believed to be critical. It should be emphasized that design 3, as shown, is in the preliminary stages of evaluation and that reshaping of the iron is expected to yield further, significant improvement.

Signal/background must be increased to 0.02 or greater to allow use of Hall probes as flux detectors. We are confident that this is achievable, given the progress to date, and that the original design objectives can be met. The final stages of computer design will involve use of an axi-symmetric model as opposed to the 2-D model considered here. We anticipate a more favourable signal/background in that case because magnetic fringing effects are more severe and will naturally draw more flux away from the measurement region into the rock.

LABORATORY MEASUREMENT SYSTEM

A preliminary design for the complete measurement system is shown schematically in Figure 332.7. The final computer design will be tested with this setup. The laboratory prototype will afford the opportunity to evaluate various measurement conditions such as motion of the probe (relative to conductive material), effect of strong inducing fields, and thermal effects.

OUTCROP TEST

A short field experiment was undertaken to demonstrate the potential application of small scale variations in susceptibility to structural mapping. Approximately 1100 readings were taken on an outcrop face 0.9 m by 1.2 m in area, using a hand-held, commercially available susceptibility meter (EDA Model K-2). Readings were taken on a grid of 2 by 5 cm, these being the dimensions of the sensing head, and somewhat less than the spatial resolution of the instrument. Figure 332.8 shows a contour map of the susceptibility values, with a photograph of the outcrop for comparison (Photo 332.1).

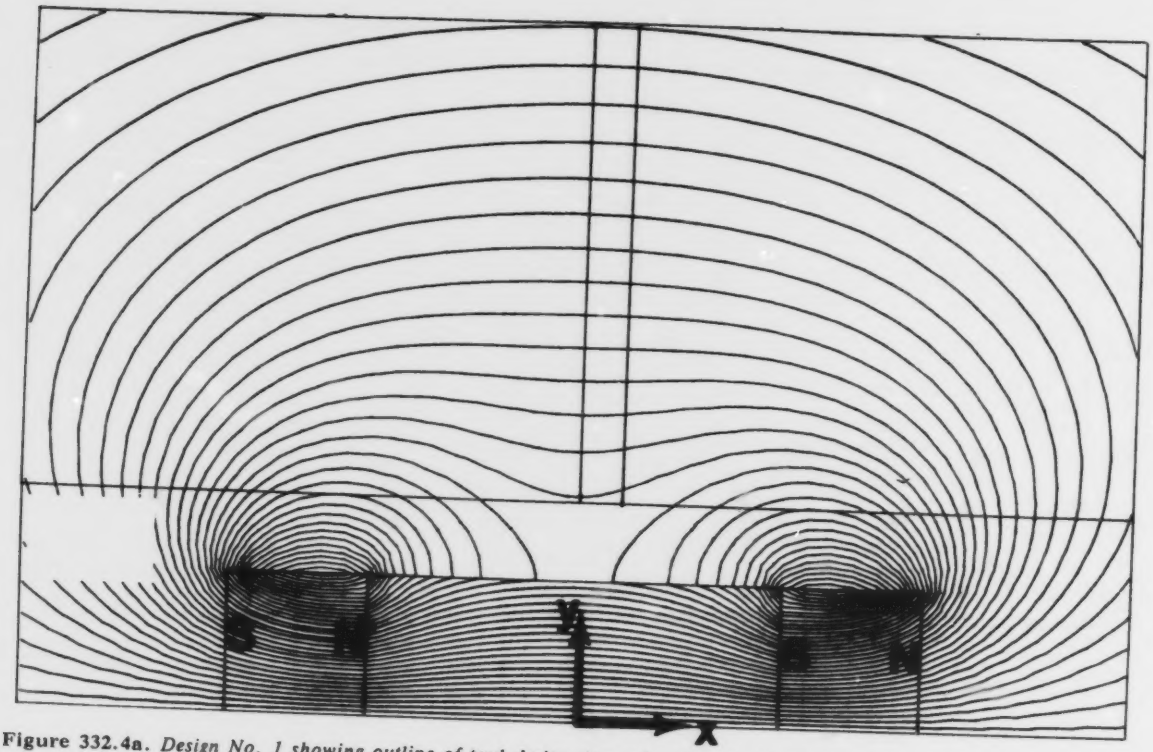

Figure 332.4a. *Design No. 1 showing outline of tool design situated within the borehole, position of the magnetic layer embedded in the wall rock (drawn to scale), and equipotential map for the total field (background plus anomalous).*

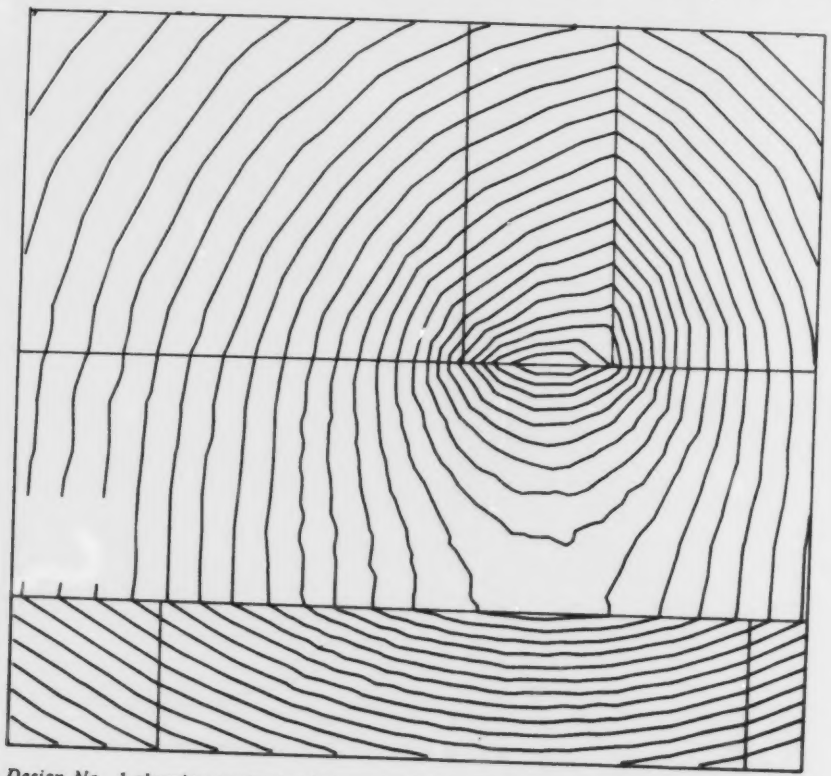

Figure 332.4b. *Design No. 1 showing equipotential map of the anomalous field (caused by the thin magnetic layer).*

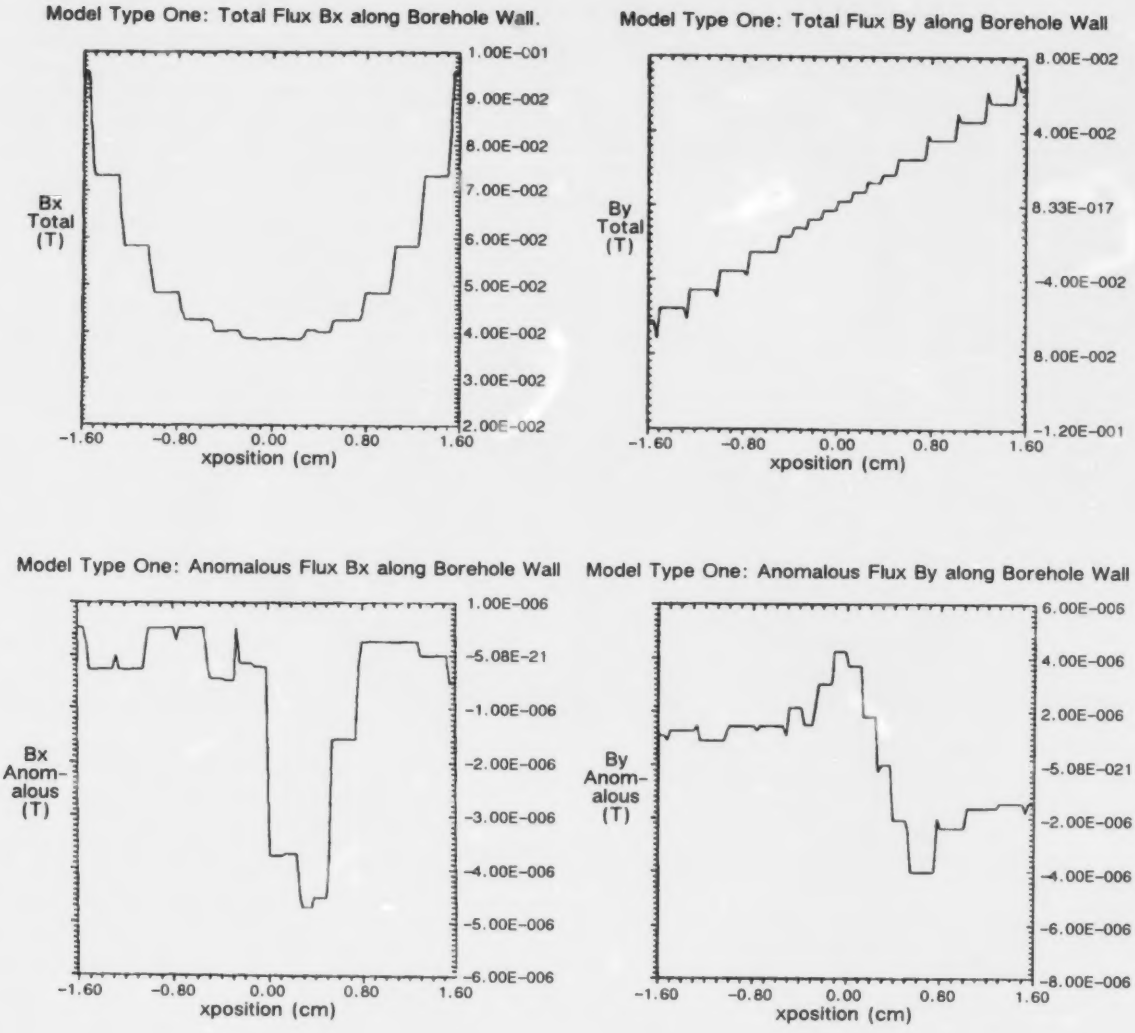

Figure 332.4c. *Design No. 1. Profiles of magnetic flux obtained as the tool is fed along the borehole past the thin magnetic layer: (top left) total axial component, (top right) total radial component, (lower left) anomalous axial component, and (lower right) anomalous radial component.*

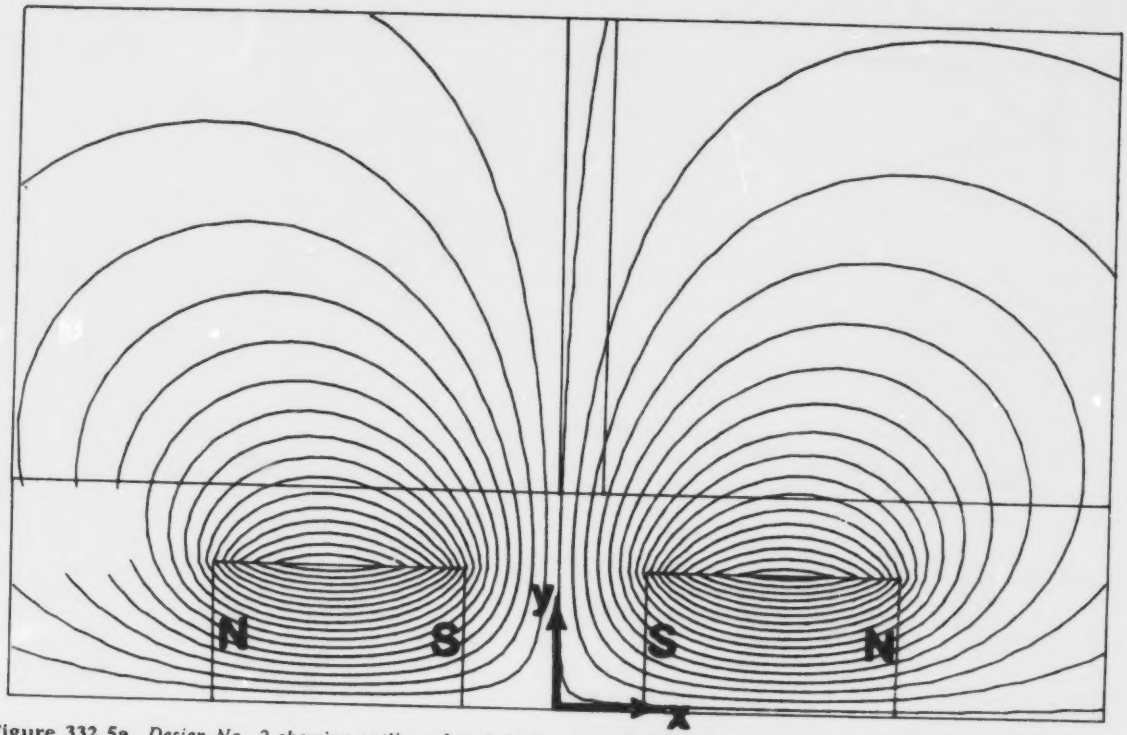

Figure 332.5a. *Design No. 2 showing outline of tool design situated within the borehole, position of the magnetic layer embedded in the wall rock (drawn to scale), and equipotential map for the total field (background plus anomalous).*

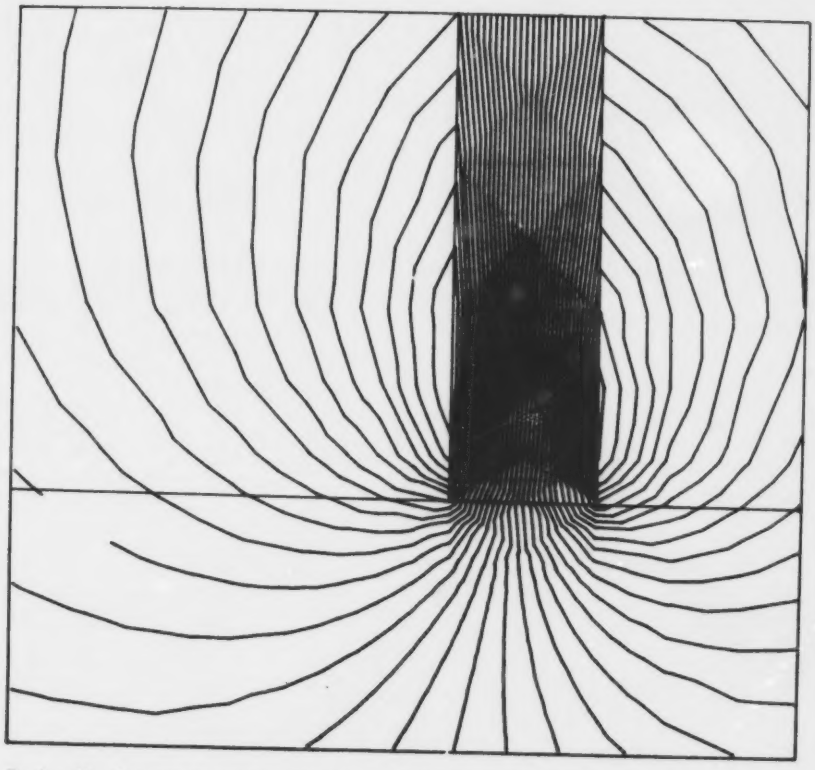

Figure 332.5b. *Design No. 2 showing equipotential map of the anomalous field (caused by the thin magnetic layer).*

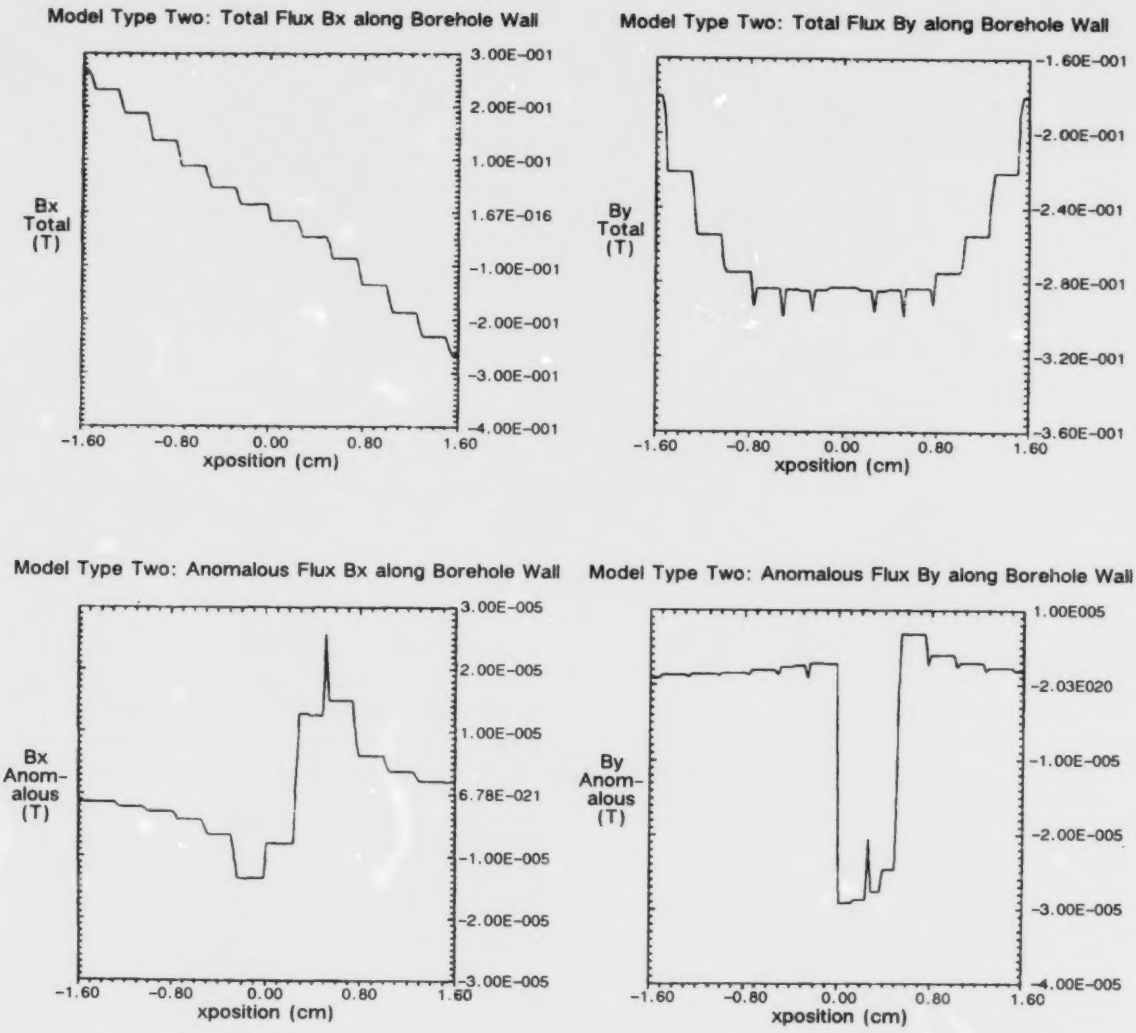

Figure 332.5c. *Design No. 2. Profiles of magnetic flux obtained as the tool is fed along the borehole past the thin magnetic layer: (top left) total axial component, (top right) total radial component, (lower left) anomalous axial component, and (lower right) anomalous radial component. Even though more flux is directed into the layer, no improvement in signal/noise is achieved.*

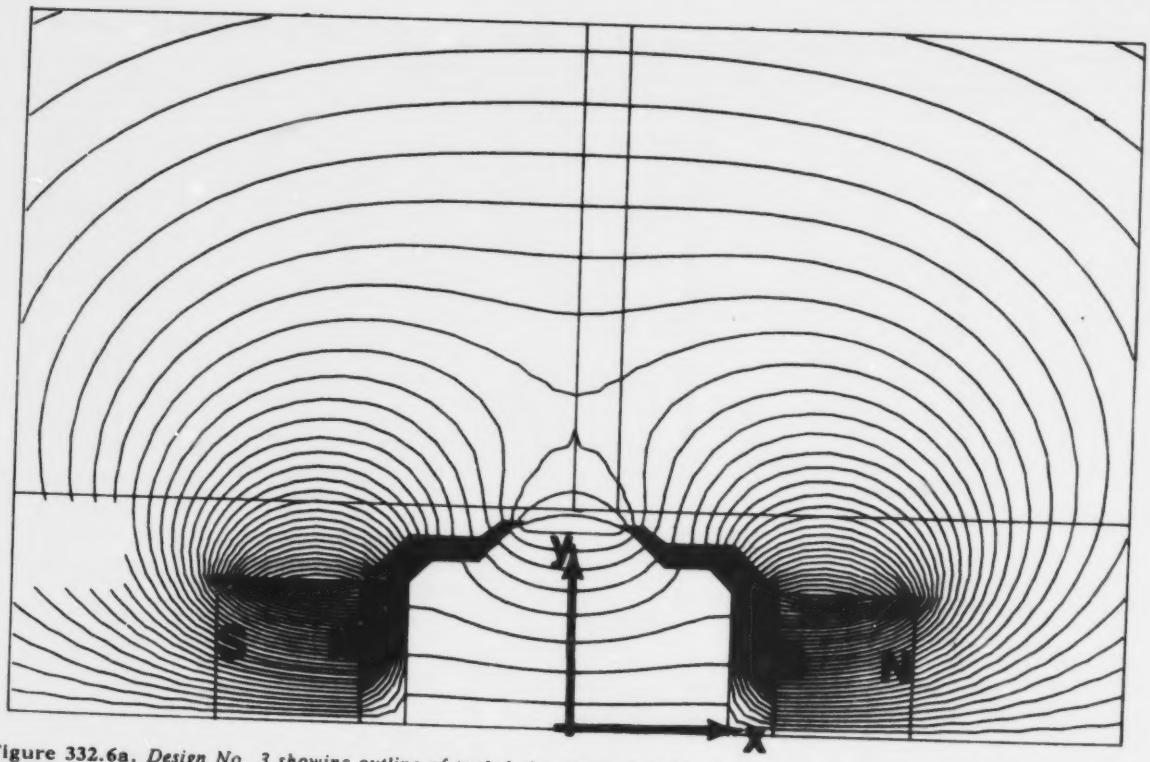

Figure 332.6a. *Design No. 3 showing outline of tool design situated within the borehole, position of the magnetic layer embedded in the wall rock (drawn to scale), and equipotential map for the total field (background plus anomalous).*

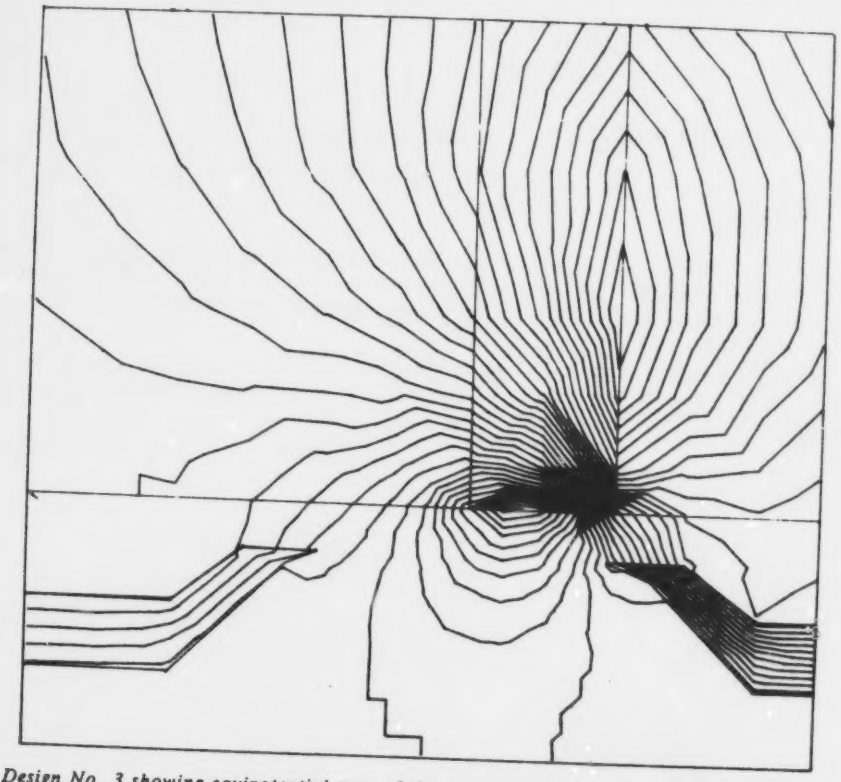

Figure 332.6b. *Design No. 3 showing equipotential map of the anomalous field (caused by the thin magnetic layer).*

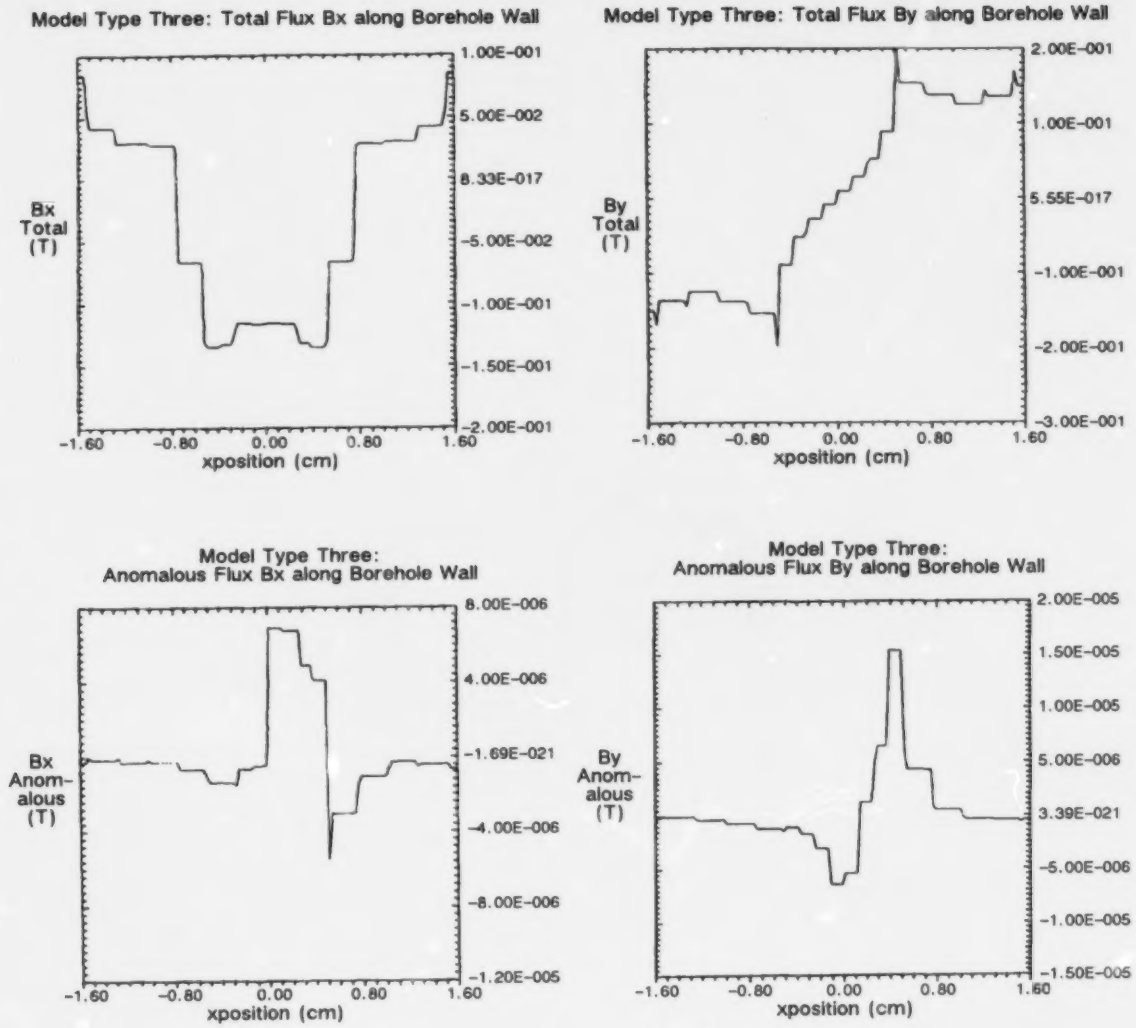

Figure 332.6c. *Design No. 3. Profiles of magnetic flux obtained as the tool is fed along the borehole past the thin magnetic layer: (top left) total axial component, (top right) total radial component, (lower left) anomalous axial component, and (lower right) anomalous radial component. Reshaping of the iron will yield even greater improvement in signal/noise than given by the design shown here.*

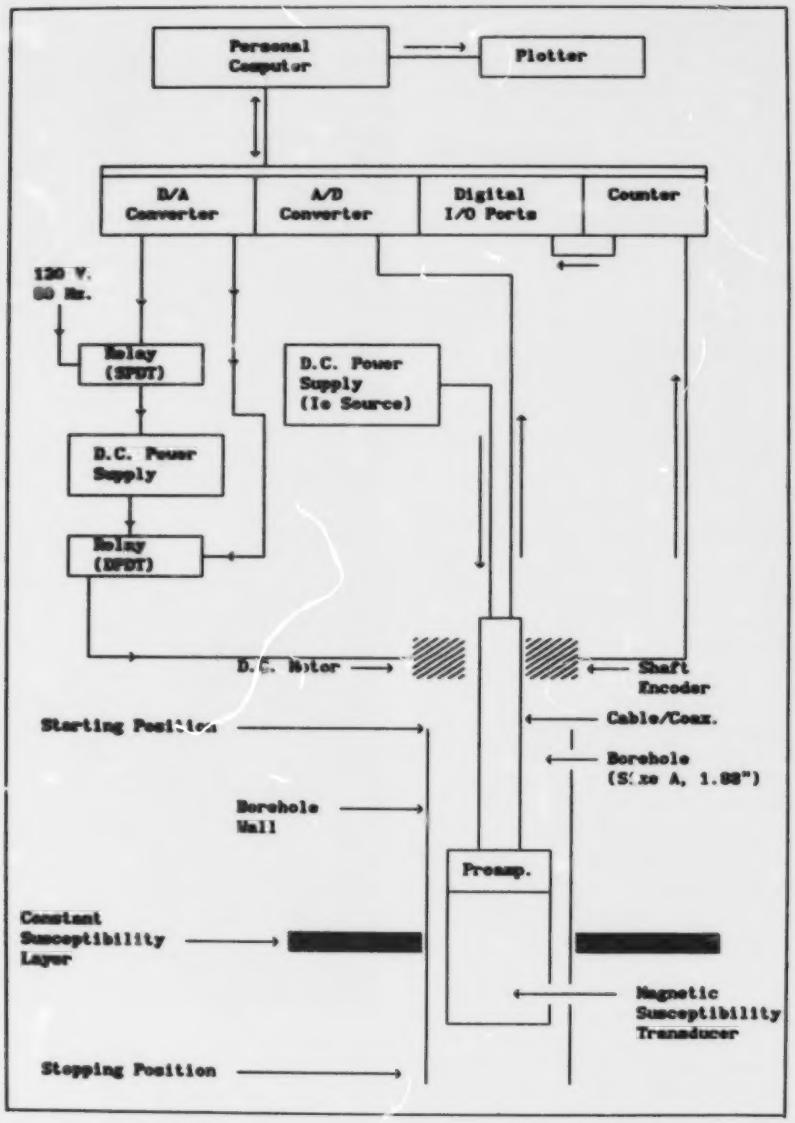

Figure 332.7. *Schematic diagram of the complete laboratory measurement system, showing the borehole tool, detection circuitry, and computer control/analysis system.*

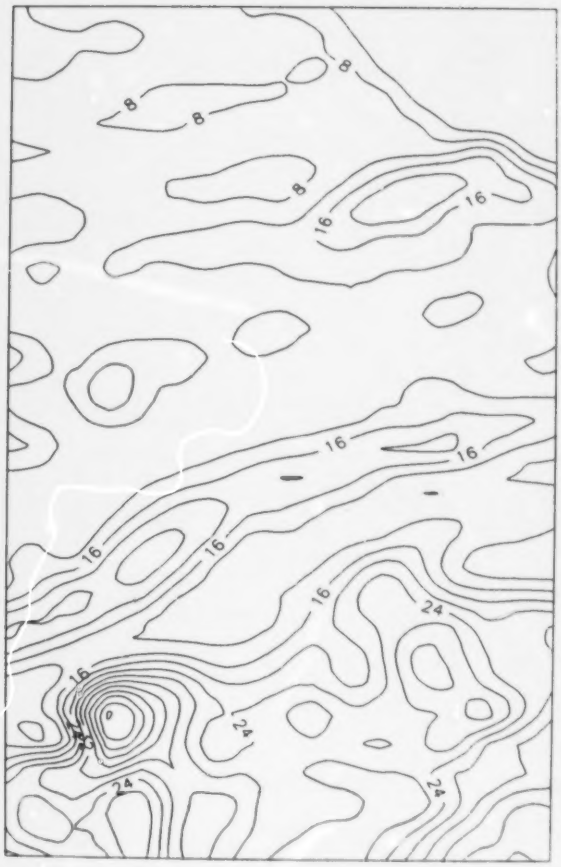

Figure 332.8. *Magnetic susceptibility values contoured at levels of 10^{-2} SI. See also Photo 332.1.*

Photo 332.1. *Outcrop of metasandstone (white outline defines border of magnetic susceptibility map in Figure 322.8).*

The rock is an outcrop of metasandstone of the Pinnacle Formation, Oak Hill group, and is located in the Four Corners area near Sutton, Québec. The Pinnacle Formation is characterized by visible bedding which serves as the primary structural indicator for field mapping in the area. Visibility of the bedding is caused largely by the uneven distribution of detrital-magnetite-bearing black sands. Discrete beds of black sands have been observed in nearby outcrops to be as thick as 20 cm and to have susceptibility values as high as 100 x 10^{-2} SI units. Some parts of the formation have values at or below the sensitivity threshold of the instrument, i.e. 10^{-4} SI. The highly magnetic character of the formation is expressed in magnetic striping which is visible in regional magnetic data, detailed ground magnetometer surveys, and as Figure 332.8 shows, at the outcrop level.

Susceptibility values for the outcrop range from 5 to 60 x 10^{-2} SI. Two distinct magnetic bands are visible, corresponding to grey beds within the outcrop. The upper 25% of the contour map is characterized by a more mottled, highly magnetic zone, but with some horizontal elongation of contours apparent. The dark area in the corresponding section of the photograph is the result of surface weathering and not the bedding which is, together with an unconformity, visible in the outcrop itself (D.C. Carmichael, Queen's University, personal communication, 1989). The distinct change in magnetic character correlates with the position of the unconformity, and is thought to be an expression of the observed younging direction, i.e., downwards in the photograph.

While this example is clearly a "most favourable" situation, it demonstrates the concept of using modern, high-resolution susceptibility instruments for detailed structural mapping, in addition to the more traditional approach of obtaining bulk susceptibility values for input into modeling routines during large-scale mapping exercises. We feel that this concept will prove even more valuable in drill-hole surveys.

CONCLUSIONS

A large number of finite-element calculations have been carried out. We have tested many variations of three basic designs, the simple design in the initial proposal, as well as two, more complex, designs. Sensitivity is as good or better than expected from the original calculations. A problem arises in that the measurement of anomalous field (signal) must be made in a region of high background flux. The immediate goal is to reduce the amount of background flux in the measurement zone, to improve signal/background ratio. There is little doubt that this is possible—the question is how sophisticated does the design have to become.

REFERENCES

Atherton, D.L. and Daly, M.G.

1987: Finite Element Calculation of Magnetic Flux Leakage Detector Signals; NDT International, Volume 20, p.235-238.

Clark, D.A.

1983: Comments on Magnetic Petrophysics; Bulletin of the Australian Society of Exploration Geophysicists, Volume 14, p.49-62.

Clark, M.E., Archibald, N.J. and Hodgson, C.J.

1986: The Structural and Metamorphic Setting of the Victory Gold Mine, Kambalda, Western Australia; p.243-254 *in* Proceedings of Gold '86, an International Symposium on the Geology of Gold, edited by A.J. MacDonald, Toronto, 1986.

Daniels, J.J., Scott, J.H. and Olhoeft, G.

1981: Interpreting Precambrian Metamorphic Geology from Geophysical Well Logs; Society of Professional Well Log Analysts, Proceedings of 22nd Annual Symposium, Paper T.

Glenn, W.E. and Nelson, P.H.

1979: Borehole Logging Techniques applied to Base Metal Ore Deposits; p. 273-294 *in* Geophysics and Geochemistry in the Search for Metallic Ores, edited by P.J. Hood, Geological Survey of Canada, Economic Geology Report 31.

Hillary, E.M. and Hayles, J.G.

1985: Correlation of Lithology and Fracture Zones with Borehole Geophysical Logs in Plutonic Rocks; Atomic Energy of Canada Limited, TR-343, Pinawa, Manitoba, 59 p.

Knuckey, M.J. and Watkins, D.J.

1982: The Geology of the Corbet Massive Sulphide Deposit, Noranda District, Quebec, Canada; p.297-317 *in* Precambrian Sulphide Deposits, H.S. Robinson Memorial Volume, edited by R.W. Hutchinson, C.D. Spence and J.M. Franklin, Geological Association of Canada, Special Paper 25.

Lapointe, P., Chomyn, B.A., Morris, W.A. and Coles, R.

1982: Significance of Magnetic Susceptibility Measurements from the Lac du Bonnet Batholith, Manitoba, Canada; *in* Geophysical Investigations in Connection with Geological Disposal of Radioactive Waste, Proceedings of a Workshop, Ottawa, September, 1982, published by Nuclear Energy Agency and the Organization for Economic Cooperation and Development.

Morasse, S., Hodgson, C.J., Guha, J. and Coulombe, A.

1986: Preliminary Report on the Geology of the Lac Shortt Gold Deposit, Demaraisville Area, Quebec, Canada; p.191-196 *in* Proceedings of Gold '86, an International Symposium on the Geology of Gold, edited by A.J. MacDonald, Toronto, 1986.

Grant 336 Residence Sites of Zinc in Weathered Till from the Clyde River Prospect in Eastern Ontario

Adrienne C.L. Larocque and H. Wayne Nesbitt

Department of Geology, University of Western Ontario, London

ABSTRACT

Chemical weathering of glacial sediments has resulted in redistribution of zinc among the various grain-size fractions in sediments at the Clyde River prospect. Furthermore, the degree of weathering influences the extent to which zinc is redistributed. There is, therefore, no single size fraction best suited to drift prospecting for sulphides unless the weathering intensity is considered. The most reliable and most economical procedure is to analyze bulk samples.

Specifically, redistribution of zinc results from the incorporation of zinc into limonite, which coats all grains in highly weathered sediments. Finer size fractions have progressively greater ratios of surface area to volume; therefore, in highly weathered sediments, concentrations of zinc increase dramatically as a function of decreasing grain size. Limonite is volumetrically significant in the clay fraction; therefore, clay fractions of sediments are greatly enriched in zinc (two to ten times), compared to bulk samples. In addition to redistributing metal, weathering appears to have concentrated metals in some samples, by decreasing sediment volume through dissolution of carbonate minerals.

INTRODUCTION

The practice of drift prospecting is gaining popularity with exploration companies as it becomes necessary to explore unexposed regions of the Canadian Shield for economic mineral deposits. A common problem in drift prospecting is the choice of representative grain-size fractions for analysis. Many studies of the distribution of ore minerals and elements in specific grain size ranges in till have been carried out (e.g., Shilts 1973, 1984; Ayras 1977; Klassen and Shilts 1977; DiLabio 1979, 1982, 1988). These and other studies have illustrated the tendency for metals to be enriched in the finer size fractions. The specific size fraction exhibiting this enrichment is determined by the grain size distribution of ore minerals in source bedrock (cf. Haldorsen 1977), the distance of glacial transport, the resistance of the minerals to comminution during transport (Dreimanis and Vagners 1971), and the susceptibility of the minerals to post-depositional alteration.

OBJECTIVES

The objectives of this study are as follows:

1. to determine the mineral phases in which metals in till reside;
2. to examine the relationship between mineralogy and grain size;
3. to compare weathered and unweathered samples with respect to mineral phases and partitioning, and to determine, if possible the processes responsible for variations (e.g., weathering reactions, exchange reactions).

This report presents compositional data for bulk-sample matrix and grain-size fractions of sediments collected in a zinc dispersal train in eastern Ontario. Several suggestions for sampling and analysis of drift for mineral exploration purposes are presented.

PREVIOUS WORK IN THE STUDY AREA

The Clyde River zinc prospect (Sinclair 1979) is located 5 km north of Hopetown, Ontario, approximately 80 km west of Ottawa (Figure 336.1). The study area is underlain by metadiorite, granite and interbedded calcitic and dolomitic marble of the Grenville Province (Reinhardt 1973; Sinclair 1979, 1986; Carter *et al.* 1980). The marble strikes northeast and dips moderately to the southeast.

Mineralization occurs as lenses of fine-grained sphalerite in the dolomitic layers. Fine-grained disseminated pyrite is present in small amounts. Mineralized boulders, which in part define the dispersal train, were first observed by prospector H.G. Pharoah in 1975. This discovery led Selco Mining Corporation to carry out drift sampling, trenching and drilling at the site (Sinclair 1979, 1986). The boulders were derived from a mineralized zone ap-

Figure 336.1. *Location of study area.*

proximately 2 m wide and 15 m long, which proved to be uneconomic. However, it is similar to larger economic deposits elsewhere in the Grenville Province (Brown 1976; Gauthier and Brown 1980).

The study area is located on a well drained, rolling upland surface, which slopes gently towards the Clyde River. Surficial cover comprises dominantly locally derived sandy till, up to 4 m thick. The till is overlain by a thin veneer of glaciolacustrine silt in some places (Sinclair 1979, 1986; DiLabio *et al.* 1982). Ice flow was from the north-northeast (Gadd 1980).

DiLabio *et al.* (1982) defined a classic dispersal train at this site on the basis of concentrations of Zn and Cd in the <2 μm fraction of till (Figure 336.2). For the present study, trenching and sampling were carried out in the dispersal train (Figure 336.2) in order to examine the distribution of zinc and sphalerite in fresh and weathered till.

METHODOLOGY

Four trenches were excavated using a small backhoe. The locations of the trenches relative to the dispersal train are shown in Figure 336.2. Trench 1 was located in a topographic low in the pasture. Trench 2 was located 20 m north-northeast of trench 1 on a gentle slope. Trench 3 was located approximately 100 m northeast of trench 1 on a south-facing slope. Trench 4 was located approximately 60 m northwest of trench 3, in the woods at the edge of the pasture, near the foot of a north-facing slope (Figure 336.3). The depths of the trenches ranged from 40 cm (trench 4) to 105 cm (trench 1). Short channel samples weighing approximately 2 kg were collected from vertical profiles on the walls of the trenches.

Samples were separated by dry-sieving, dispersion in a deflocculant (sodium hexametaphosphate), and wet-sieving to recover the following fractions: 5.6 to 4 mm, 4 to 2 mm, 2 to 1 mm, 1 to 0.5 mm, 0.5 to 0.25 mm, 0.25 to 0.125 mm, 0.125 to 0.063 mm and <0.063 mm. These fractions correspond to pebble, granule, very coarse sand, coarse sand, medium sand, fine sand, very fine sand, and silt plus clay fractions, respectively. The <0.063 mm (<63 μm) fraction was centrifuged to separate the <2 μm (clay) fraction. Major and trace element analyses of bulk samples (Table 336.1) and size fractions (Table 336.2) were carried out by X-ray fluorescence (XRF) at the University of Western Ontario. Analyses for H_2O, CO_2, FeO and S in sieved fractions were carried out by wet chemical methods at the Geological Survey of Canada (Table 336.2). Similar data for bulk samples are not yet available. Wavelength dispersive X-ray (WDX) analyses on polished thin sections of erratics (Table 336.3) and bulk till impregnated with epoxy were performed using the electron microprobe at the University of Western Ontario. Mineralogy of samples was determined by petrographic examination of thin sections and by X-ray diffraction (XRD) analysis. Separations of several fine size-fractions were made using a Frantz magnetic separator, in order to isolate and concentrate individual mineral species.

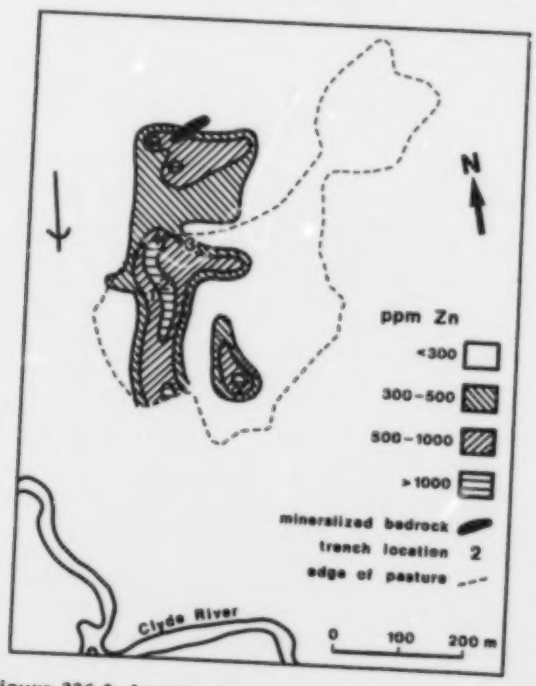

Figure 336.2. *Location of trenches relative to zinc dispersal train defined by DiLabio et al. (1982).*

STRATIGRAPHY, STRUCTURE AND TEXTURE OF SEDIMENTS

The stratigraphy of the trenches is summarized in Figure 336.3. Typical size frequency distributions in the sediments are shown in Figure 336.4. Textural characteristics and interpreted sediment types are summarized in Table 336.4. Coefficients of sorting (So) in Table 336.4 were calculated using the method of Pettijohn (1957, p.33-38).

Trenching did not reveal fresh sediments. Overburden is weathered to bedrock, and the intensity of weathering increases upwards. Weathered, rubbly bedrock was exposed in trenches 2 and 4. Compact, massive, olive-brown, silty sandy diamicton was exposed at the bases of trenches 1, 2 and 3. Poorly stratified, olive-brown, pebbly sand of variable thickness was exposed overlying the diamicton in trenches 2 and 3. The sand unit was not observed in trenches 1 and 4. The basal diamicton and overlying sand are overlain by olive-brown to orange-brown, bouldery sandy diamicton of variable thickness. In trench 1, the diamicton is overlain by a 35 cm thick sequence of well sorted sediments consisting of plane-bedded, olive-brown silt interbedded with thin, poorly stratified, brown, medium sand. The bedded sediments are overlain by poorly bedded, brown, fine sand and massive, olive-brown to brown,

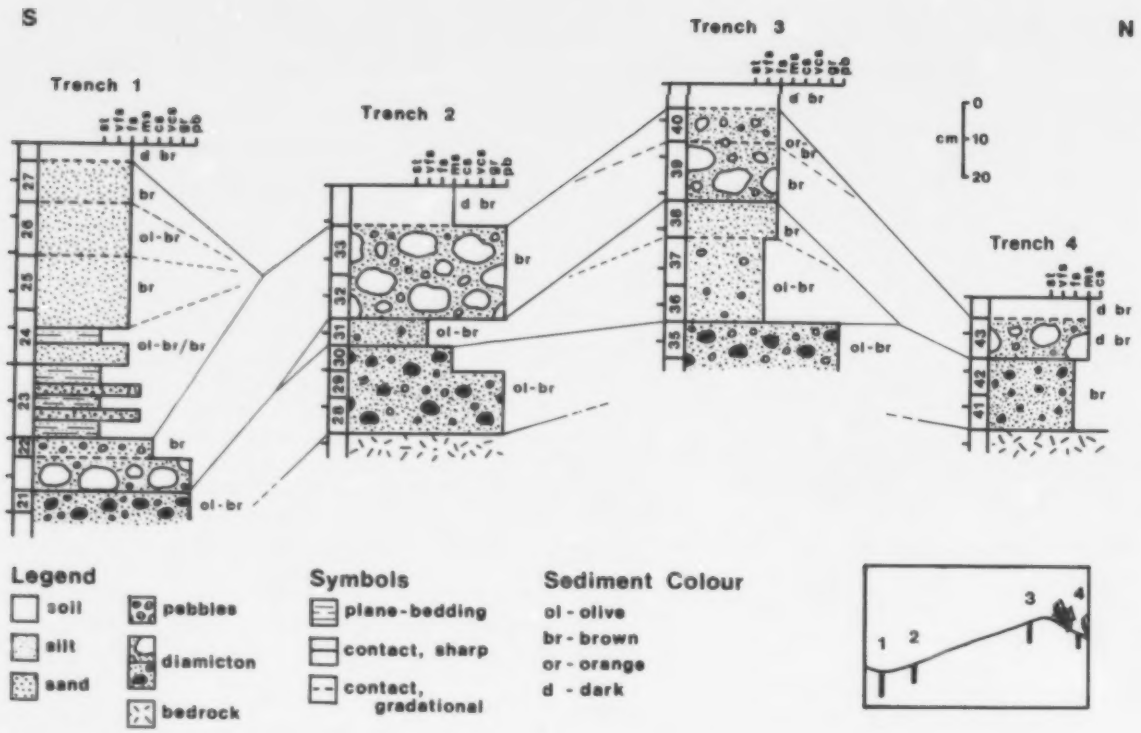

Figure 336.3. *Stratigraphy of trenches. Scale at top of each trench represents dominant sediment or matrix texture as follows: st = silt, vfs = very fine sand, fs = fine sand, ms = medium sand, cs = coarse sand, vcs = very coarse sand, gr = granule, pb = pebble. Symbol sizes are proportional to clast sizes. Inset: schematic of topographic positions of trenches.*

fine sand. In trench 4, pervasively weathered bedrock is overlain by 19 cm of compact, massive, brown, fine sand. This is overlain by poorly sorted, dark brown, bouldery medium sand. The sediments in each trench are overlain by A and B soil horizons.

Generally, the diamictons are characterized by poor sorting and strongly bimodal, nearly symmetrical, size frequency distributions with modes in both the pebble and medium or fine sand fractions (Figure 336.4, Table 336.4). The lower diamicton has coefficients of sorting (So) between 3.3 and 6.3 (most fall between 3.3 and 4.3). The sorting coefficients for the upper diamicton exhibit a slightly lower range, between 2.7 and 4.1. The size frequency distributions are slightly skewed towards coarser material. The lower diamicton in trench 4 and the upper part of the upper diamicton in trench 3 exhibit unimodal size distributions, with modes in the medium to fine sand fractions. The coefficient of sorting in both is 2.1. The size distributions in the sand units in trenches 2 and 3 range from unimodal to moderately bimodal, with first modes in the fine sand or very fine sand fraction. These sediments are better sorted (So between 2.2 and 2.9) than the lower and upper diamictons. Most of the massive and bedded sands in trench 1 exhibit unimodal size distributions, with modes in the fine sand fraction. The sands are well sorted (So between 1.8 and 2.2). The lowermost sample (23) exhibits a bimodal distribution with modes in the medium sand and silt fractions, due to mixing of sediment types during sampling. This mixing is evidenced by the high coefficient of sorting (2.6) in what are obviously interbedded, well sorted sediments.

In trenches 1, 2, and 3, several characteristics indicate that the lower diamicton is basal (also referred to as subglacial) till. These include: the position of the till at the base of each trench, immediately overlying bedrock (trench 2); the abundance of locally derived lithologies in the till; and the poor sorting and strongly bimodal, nearly symmetrical, size frequency distribution of the till. The colour, overall texture, and compactness of the basal till exhibits little variability laterally. However, there is some lateral variability in the specific size fractions exhibiting maxima in size frequency. In trenches 1 and 2, the second maximum occurs in the medium sand fraction; in trench 3, the second maximum occurs in the fine sand fraction. This variability is due to different provenance of the sediments in trenches 1 and 2 versus trench 3, as indicated by the different lithologies of the clasts. The basal till may have been deposited by meltout, although the compactness and fissility of the till are suggestive of deposition by lodgement. Both processes may have been involved in deposition of the till. Regardless of the actual

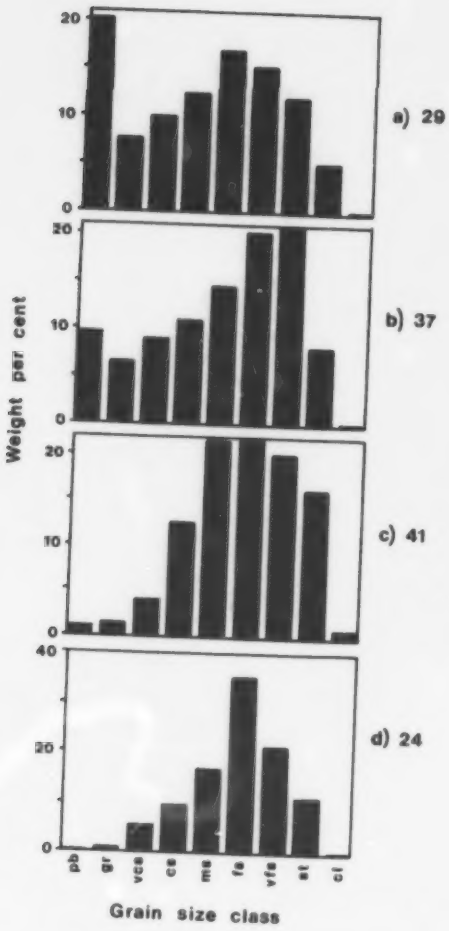

Figure 336.4. *Typical examples of size frequency distributions in* a) *slightly weathered basal and supraglacial tills;* b) *water-sorted deposits;* c) *highly weathered basal till;* d) *post-glacial fluvial deposits. Basal and supraglacial tills in trench 3 exhibit modes in pebble and fine sand fractions, whereas tills in trenches 1 and 2 have second modes in the medium sand fractions. Abbreviations are the same as those in Figure 336.2. Numbers are number of samples.*

mechanism of deposition, it is clear that the basal till was derived locally, and deposited subglacially with minimal reworking.

Characteristics of the upper diamicton indicate that it is supraglacial or surface ablation till (Dreimanis, in press). This till also is poorly sorted, although sorting is slightly better than that of the the basal till. The upper till has a strongly bimodal size frequency distribution; however, it commonly exhibits a higher proportion of coarser-grained material, especially boulder-size, than the underlying basal till. The lower frequency of fines and the crude bedding in the till are due to washing of the till by supraglacial meltwater. Lithologies of the clasts vary laterally, but are quite consistent with the basal till immediately below. This suggests that the supraglacial debris was derived locally, and sheared upwards under compressive-flow regime (Dreimanis in press, Appendix A). Thus, the upper and lower diamictons at the study site represent subunits of a single till unit.

The upper and lower till phases are separated by poorly bedded sediments. The lower coefficient of sorting (relative to the diamictons) and the skewness towards coarser material indicate that the sediments have been subjected to reworking by water. Reworking of glacial debris may have occurred in proglacial fluvial environments, or in subglacial cavities (cf. Dreimanis *et al.* 1986; Dreimanis 1988). The sediments may not extend continuously from trench to trench; however, they have been correlated in Figure 336.6 in order to distinguish them from the basal and supraglacial tills.

Stratified sand and silt were exposed at the top of trench 1. The silt interbeds possess well developed horizontal stratification. All of the sediments exhibit a high degree of sorting. These sediments were exposed only in trench 1, which is located in a depression. These characteristics suggest that the sediments were deposited by a post-glacial stream which occupied the lowlands (Sinclair 1986).

It is difficult to correlate the sediments in trench 4 with those in the other trenches. The former are extremely weathered, as is the upper part of the upper till in trench 3. It is likely that sediment colour and sedimentary structures in trench 4 were altered or destroyed by pervasive weathering. Textural characteristics also appear to have been modified during weathering (sediment sorting may have increased). Therefore, the sediments in trench 4 are correlated tentatively with those in the other trenches based on stratigraphic position and gross texture. The compact, massive sand overlying bedrock likely represents highly weathered basal till. The overlying bouldery sand is correlated with the boulder-rich supraglacial till in the other trenches (Figure 336.3).

MINERALOGY

ORE COMPOSITION

The compositions of sphalerite in dolomitic marble erratics collected near the trenching site are listed in Table 336.3. The ionic ratio of iron to zinc is low (approximately 1:7). Although large mineralized clasts were observed in the basal till, no fresh sphalerite was observed in any of the finer fractions of the samples.

SEDIMENT COMPOSITION

The basal till of trench 2 contains abundant clasts of weathered, mineralized dolomitic marble, as well as other local lithologies (granite and metadiorite). The basal and supraglacial tills in trenches 1 and 2 contain major quantities of dolomite, calcite, quartz, orthoclase, plagioclase, lesser amounts of amphibole, vermiculite and limonite, and minor quantities of ilmenite, magnetite, zircon, garnet, epidote and clay

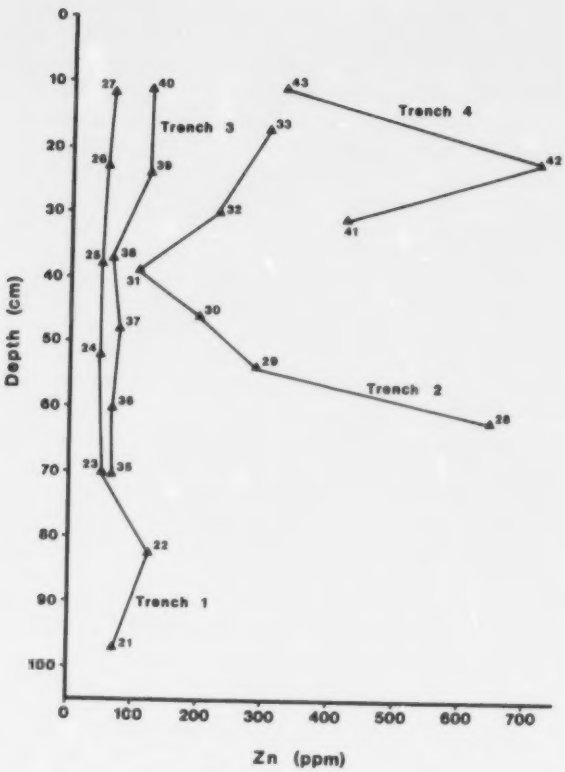

Figure 336.5. *Vertical distribution of zinc in bulk samples. Sample depths are plotted at the midpoint of the sample interval.*

minerals. The till ... ches 3 and 4 and the sand units contain little ... dolomite or calcite. Otherwise, the mineralogy is similar to the carbonate-rich sediments, although proportions of minerals vary. Limonite (identified optically) is present in varying amounts and abundant in weathered sediments.

GEOCHEMICAL RESULTS

GEOCHEMISTRY OF BULK SAMPLES

Trenches 2 and 4 were located in the most highly anomalous part of the dispersal train, whereas trenches 1 and 3 were excavated in moderately anomalous parts of the train (*see* Figure 336.2). The concentrations of zinc in bulk till samples (Figure 336.5) are consistent with the location of the trenches in the dispersal train defined by concentrations of zinc in clay fractions (*see* Figure 336.2). The zinc content of till is two to six times greater in trenches 2 and 4 than in trenches 1 and 3 (Table 336.1). However, stratigraphic variability also is apparent.

Although the colour, texture and compactness of the basal till is consistent throughout trenches 1, 2 and 3, the major and trace element compositions are variable (Table 336.1), indicating varying provenance. In trench 3, the basal till contains high SiO_2 content and relatively low loss-on-ignition (LOI). Size fractions containing little CO_2 (which is evolved during ignition of carbonate minerals) are characterized by similarly low LOI (Table 336.2). Although loss of water and sulphur contribute somewhat, LOI may be considered as a rough measure of carbonate content. Therefore, high SiO_2 content and low LOI indicate that the basal till in trench 3 was derived mainly from silicate lithologies such as local granite or metadiorite. This accounts for the low zinc content of the till, as sphalerite occurs locally in dolomitic marble. In trenches 1 and 2, the basal till exhibits lower concentrations of SiO_2 and higher LOI (Table 336.1), indicating that a large component of the till was derived from local marble. However, zinc concentrations in the till are much higher in trench 2 than trench 1. This may indicate derivation from mineralized and barren marble, respectively.

The major element compositions of the water-sorted sediments are consistent (Table 336.1). However, sample 31 exhibits a higher concentration of zinc than samples 36 to 38. The waterlaid deposits were produced by deposition and reworking of debris. The higher zinc content of sample 31 indicates that the sediments were derived from reworking of highly metalliferous basal debris and mixing with silicate detritus.

The major and trace element compositio... of the supraglacial till are variable (Table 336.1); however, the concentrations of zinc are consistently greater than 100 ppm, indicating that varying proportions of the debris were derived from mineralized marble. Variability of sediment compositions may have been caused by mixing during englacial transport of distally derived debris and proximally derived basal debris which had been sheared upwards.

The post-glacial fluvial sediments exhibit consistent major and trace element compositions (Table 336.1). They are characterized by high SiO_2 and low zinc concentrations. A slight increase in zinc concentrations in the uppermost samples (26 and 27) may be due to uptake of zinc by organics or decrease in sediment volume caused by weathering.

The compositions of sediments in trench 4 are very different from those in the other trenches. In trenches 1, 2 and 3, high zinc concentrations generally are associated with carbonate-rich till or sediments immediately derived from carbonate-rich till. In contrast, the sediments in trench 4 are characterized by high SiO_2 content, low LOI (i.e., low carbonate) and very high concentrations of zinc (Table 336.1). The most obvious difference between these sediments and those in trenches 1, 2 and 3 is the evidence of pervasive weathering in trench 4. Limonite is abundant throughout, and a 10 cm clast of limonite-cemented till was collected near the bedrock surface (Photo 336.1). A decrease in sediment volume due to dissolution of carbonate and other

minerals may have concentrated less mobile and immobile elements. Evidence for such concentration of elements is apparent in the distribution of Pb in the sediments (Table 336.1). Regardless of sediment type, the concentration of Pb ranges from 9 to 16 ppm in all sediments in trenches 1, 2 and 3, except sample 40 (which is highly weathered). The high Pb contents in sediments in trench 4 (38 to 111 ppm) indicate that concentration of metals due to removal of mobile constituents (such as carbonate minerals) occurred. The presence of flakes of galena in the clast of limonite-cemented till (Photo 336.2) indicates that some sulphide minerals persist, even in the most highly weathered sediments. Although none have been observed, grains of sphalerite also may persist, and may have been concentrated by weathering of the sediments. In contrast, Cu has not been concentrated in highly weathered sediments (Table 336.1), suggesting that it was leached during weathering.

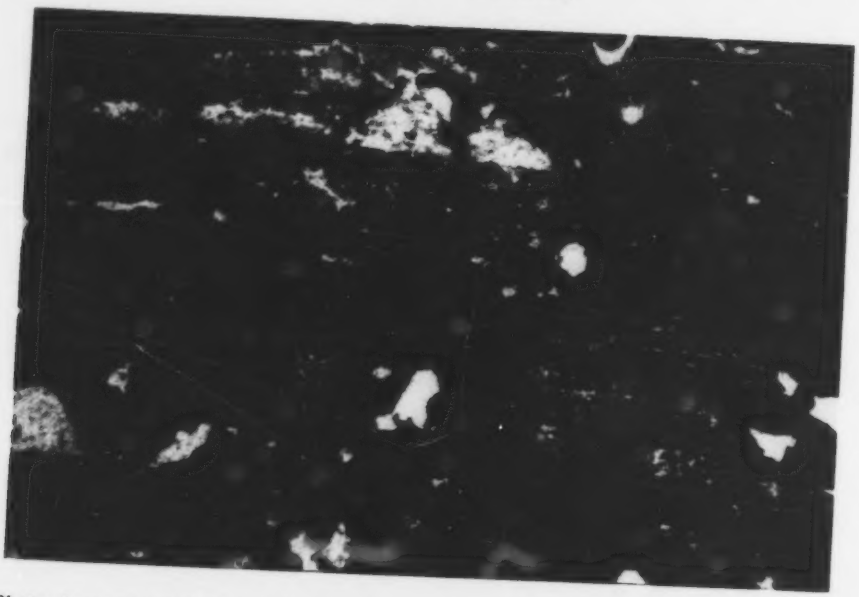

Photo 336.1. *Photomicrograph of highly weathered feldspars in limonite-cemented till from base of trench 4. Field of view is 5.2 mm.*

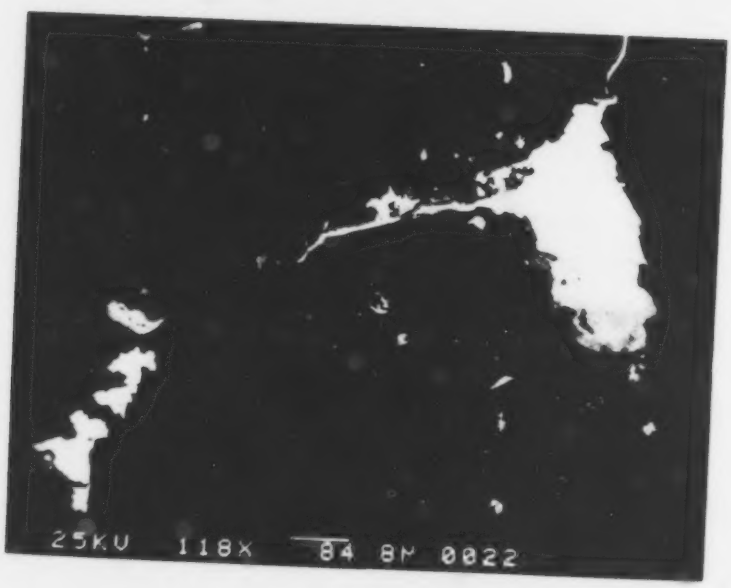

Photo 336.2. *Scanning electron micrograph showing bright galena flakes in limonite-cemented till.*

TABLE 336.1. MAJOR AND TRACE ELEMENT COMPOSITIONS OF BULK SAMPLES.

Trench No.	1	1	1	1	1	1	1
Sample No.	21	22	23	24	25	26	27
SiO_2	46.12	63.59	68.50	69.45	69.46	67.25	67.28
TiO_2	0.55	0.63	0.65	0.58	0.65	0.73	0.73
Al_2O_3	9.30	12.83	13.41	13.46	13.33	13.78	13.73
Fe_2O_3	4.33	6.00	4.56	4.16	4.39	4.86	4.99
MnO	0.09	0.13	0.09	0.08	0.08	0.08	0.08
MgO	7.57	4.58	2.05	2.03	2.10	2.03	1.78
CaO	13.74	3.91	3.20	3.16	3.16	2.94	2.88
Na_2O	1.23	2.66	3.21	2.87	2.65	2.64	2.33
K_2O	1.26	1.85	2.33	2.25	2.17	2.36	2.22
P_2O_5	0.16	0.20	0.20	0.19	0.19	0.19	0.18
LOI	15.60	4.10	1.80	1.80	1.70	2.90	3.80
TOTAL	99.95	100.48	99.99	100.03	99.91	99.75	100.01
Pb	13	14	16	13	12	14	13
Zn	71	124	49	45	46	56	64
Cu	19	26	22	21	18	13	11
Ni	18	21	16	16	15	16	15
Co	38	38	32	22	28	22	23
Cr	24	27	39	39	45	44	38
V	81	105	96	98	101	102	104
S	113	363	100	B.D.	B.D.	135	220

Trench No.	2	2	2	2	2	2
Sample No.	28	29	30	31	32	33
SiO_2	44.31	42.68	45.98	65.68	41.46	37.93
TiO_2	0.41	0.44	0.42	0.63	0.38	0.37
Al_2O_3	8.99	8.71	8.75	13.21	7.60	6.85
Fe_2O_3	3.75	3.85	3.67	4.73	2.94	3.28
MnO	0.08	0.07	0.08	0.10	0.06	0.08
MgO	7.27	7.82	7.31	2.88	7.36	10.71
CaO	15.66	15.88	14.26	4.32	17.54	18.49
Na_2O	1.72	1.42	1.51	2.74	1.17	1.13
K_2O	1.31	1.43	1.51	2.33	1.90	1.04
P_2O_5	0.14	0.13	0.18	0.22	0.10	0.10
LOI	16.00	17.90	16.00	2.80	19.20	20.10
TOTAL	99.64	100.33	99.69	99.62	99.72	100.09
Pb	9	10	12	11	12	10
Zn	645	283	196	106	223	302
Cu	11	14	14	17	8	12
Ni	10	12	12	15	10	12
Co	13	17	23	23	13	18
Cr	15	29	22	42	9	29
V	74	85	75	88	62	58
S	B.D.	85	67	77	B.D.	80

TABLE 336.1. CONTINUED.

Trench No.	3	3	3	3	3	3
Sample No.	35	36	37	38	39	40
SiO_2	64.75	65.48	61.28	68.79	64.2	63.71
TiO_2	0.87	0.80	0.97	0.46	0.8	0.79
Al_2O_3	14.32	14.30	15.34	13.90	14.19	14.70
Fe_2O_3	6.19	5.99	7.12	3.96	6.33	5.95
MnO	0.08	0.09	0.08	0.07	0.1	0.08
MgO	2.82	2.78	3.39	2.23	3.12	2.84
CaO	4.38	4.16	4.31	3.54	4.13	4.01
Na_2O	2.88	3.12	3.66	3.33	2.61	3.61
K_2O	1.92	2.36	1.83	2.11	1.73	1.79
P_2O_5	0.31	0.21	0.16	0.13	0.17	0.16
LOI	1.7	1.00	1.80	1.11	2.6	2.70
TOTAL	100.13	100.30	99.95	99.62	99.96	100.33
Pb	12	13	11	11	15	20
Zn	63	66	74	62	118	117
Cu	22	20	18	14	13	10
Ni	13	13	15	12	16	16
Co	65	47	46	44	46	39
Cr	19	30	18	27	32	43
V	137	126	145	94	122	134
S	B.D.	B.D.	73	B.D.	B.D.	131

Trench No.	4	4	4
Sample No.	41	42	43
SiO_2	65.67	59.46	63.05
TiO_2	0.83	0.86	0.85
Al_2O_3	14.32	14.06	13.93
Fe_2O_3	6.30	8.03	6.96
MnO	0.13	0.27	0.14
MgO	2.83	4.12	2.83
CaO	3.26	3.37	3.35
Na_2O	2.41	2.63	2.73
K_2O	2.25	1.88	1.97
P_2O_5	0.19	0.38	0.24
LOI	2.10	4.70	4.10
TOTAL	100.28	99.78	100.17
Pb	38	111	46
Zn	416	716	322
Cu	15	16	13
Ni	21	21	20
Co	39	34	37
Cr	47	34	44
V	122	145	140
S	73	192	141

TABLE 336.2. CHEMICAL COMPOSITION DATA FOR SIZE FRACTIONS.

Trench No.	1	1	1	1	1	1	1
Sample No.	21	21	21	21	21	21	21
Class	Pebble	Granule	VC Sand	C Sand	M Sand	F Sand	VF Sand
SiO_2	12.68	39.05	37.92	30.70	39.34	53.26	57.01
TiO_2	0.12	0.29	0.37	0.32	0.34	0.53	0.79
Al_2O_3	1.51	8.48	8.44	6.00	7.20	10.30	11.56
Fe_2O_3	1.03	3.11	3.43	2.57	2.95	4.01	5.47
MnO	0.07	0.06	0.06	0.05	0.06	0.07	0.10
MgO	16.77	8.95	9.07	11.04	9.56	6.68	5.29
CaO	27.95	17.53	17.76	21.64	17.23	10.57	8.10
Na_2O	0.00	1.09	1.52	0.86	1.29	1.38	2.72
K_2O	0.07	1.32	1.08	0.65	0.94	1.44	1.62
P_2O_5	0.02	0.07	0.06	0.03	0.03	0.10	0.20
LOI	39.60	20.10	20.30	25.90	21.10	11.60	7.50
TOTAL	99.83	100.05	100.00	99.77	100.04	99.93	100.35
FeO	0.8	1.5	1.6	1.3	1.4	1.9	2.5
H_2O	0.5	1.4	1.2	0.7	0.8	1.5	1.7
CO_2	39.1	18.4	19.4	26	20.6	10.2	6.8
S	0.01	0.01	0.01	0	0	0.01	0
Pb	B.D.	17	12	5	8	13	13
Zn	34	65	61	49	54	64	63
Cu	6	15	14	8	11	16	15
Ni	8	10	9	11	7	21	16
Co	B.D.	3	9	B.D.	5	6	16
Cr	17	11	1	20	10	23	33
V	B.D.	58	68	49	58	84	110
S	192	B.D.	B.D.	B.D.	B.D.	B.D.	B.D.
Wt % FRN	28.05	4.29	7.42	11.74	14.85	14.05	13.89
TRP Zn	17.96	5.25	8.52	10.83	15.10	16.93	16.48
TRP CO_2	49.74	3.58	6.53	13.84	13.87	6.50	4.28

NOTES
Compositional data is not available for all fractions.
Size fractions include pebble, granule, very coarse sand, coarse sand, medium sand, fine sand, very fine sand, silt and clay.
Wt% FRN = weight percent of size fraction.
TRP Zn, CO_2 = True relative percent Zn and CO_2 (explanation in text).
B.D. = below detection.
Size frequency distributions and true relative percents were calculated using data for all fractions; weight percents of fractions with no other data have been omitted.

TABLE 336.2. CONTINUED.

Trench No.	1	1	1	1	1	1	1
Sample No.	21	21	22	22	22	22	22
Class	Silt	Clay	Pebble	Granule	VC Sand	C Sand	M Sand
SiO_2	55.80	44.15	72.16	57.34	64.72	66.32	61.26
TiO_2	1.04	0.69	0.73	0.49	0.57	0.66	0.91
Al_2O_3	12.00	13.69	12.13	12.47	13.36	12.37	12.47
Fe_2O_3	6.98	13.10	3.34	3.90	4.80	5.11	6.78
MnO	0.15	0.44	0.04	0.06	0.07	0.07	0.11
MgO	5.37	9.91	1.55	5.14	3.94	3.75	4.57
CaO	8.09	2.12	3.68	6.60	4.29	4.44	5.67
Na_2O	2.49	1.92	2.67	3.55	2.73	3.18	2.97
K_2O	1.84	2.22	3.30	2.36	2.07	1.51	1.27
P_2O_5	0.34	2.03	0.02	0.10	0.11	0.11	0.11
LOI	6.20	9.70	0.90	7.80	3.60	2.50	3.90
TOTAL	100.30	99.98	100.54	99.82	100.25	100.03	100.03
FeO	3			2	2.5	2.7	3.4
H_2Ot	1.2			1.7	1.8	1.5	1.7
CO_2t	6.7			6	2.1	1.5	2.2
S	0			0.01	0.01	0	0
Pb	21	57	8	12	10	8	10
Zn	66	473	47	66	67	66	88
Cu	18	138	9	21	22	15	21
Ni	23	62	14	15	18	16	15
Co	25	60	B.D.	14	17	17	20
Cr	59	56	16	26	35	38	29
V	136	114	73	79	121	121	155
S	B.D.	B.D.	B.D.	147	B.D.	B.D.	B.D.
Wt % FRN	5.48	0.24	21.12	6.62	16.90	22.92	15.47
TRP Zn	6.81	2.12	14.49	6.38	16.52	22.08	19.87
TRP CO_2	1.66	0.00	0.00	20.77	18.55	17.97	17.79

Trench No.	1	1	1	1	1	1	1
Sample No.	22	22	22	22	23	23	23
Class	F Sand	VF Sand	Silt	Clay	VC Sand	C Sand	M Sand
SiO_2	57.52	53.62	50.52	46.04	67.80	71.28	72.49
TiO_2	1.44	1.61	1.08	0.83	0.63	0.56	0.50
Al_2O_3	12.62	12.77	12.17	16.51	14.14	12.54	12.84
Fe_2O_3	10.24	11.37	11.40	12.77	4.79	4.25	3.40
MnO	0.17	0.26	0.39	0.67	0.07	0.06	0.06
MgO	4.79	5.10	5.54	4.44	2.41	2.35	2.16
CaO	5.41	5.31	6.05	1.66	2.02	2.19	2.86
Na_2O	2.18	2.52	2.94	2.84	3.26	2.96	2.87
K_2O	1.09	1.30	1.47	3.41	2.18	1.86	1.92
P_2O_5	0.18	0.27	0.55	3.29	0.12	0.10	0.07
LOI	4.60	6.10	8.00	7.90	2.50	1.70	1.20
TOTAL	100.24	100.24	100.11	100.36	99.91	99.85	100.37
FeO	4.2	3.9	2.9		2.2	2.1	1.7
H_2Ot	3	4	3.5		2.1	1.7	1.2
CO_2t	2.1	2.9	5.4		0.2	0.2	0.2
S	0.01	0.01	0.01		0	0	0
Pb	11	19	22	42	10	13	11
Zn	129	161	136	312	48	45	44
Cu	44	76	96	135	14	16	9
Ni	24	35	43	57	21	21	12
Co	31	37	50	52	13	14	5
Cr	36	46	38	62	44	47	33
V	181	188	190	116	110	116	75
S	62	279	117	88	B.D.	B.D.	B.D.
Wt % FRN	8.99	5.32	2.48	0.17	6.37	16.15	20.12
TRP Zn	16.92	12.51	4.92	0.80	6.60	15.67	19.09
TRP CO_2	9.86	8.07	6.99	0.00	7.38	18.69	23.28

TABLE 336.2. CONTINUED.

Trench No.	1	1	1	1	1	1	1
Sample No.	23	23	23	24	24	24	24
Class	F Sand	VF Sand	Silt	VC Sand	C Sand	M Sand	F Sand
SiO_2	69.70	68.00	66.46	69.60	71.93	72.80	71.97
TiO_2	0.56	0.71	0.80	0.58	0.47	0.32	0.35
Al_2O_3	13.33	13.43	14.17	13.81	12.78	12.87	13.63
Fe_2O_3	3.95	4.81	5.12	4.40	3.59	2.47	2.67
MnO	0.09	0.11	0.11	0.09	0.06	0.05	0.05
MgO	2.30	2.31	2.04	2.34	1.71	1.49	1.91
CaO	3.58	3.69	4.10	1.62	1.83	2.17	3.08
Na_2O	2.87	2.82	3.39	3.64	3.51	4.01	3.45
K_2O	1.91	2.20	2.85	2.34	2.15	2.12	2.06
P_2O_5	0.11	0.18	0.33	0.11	0.09	0.06	0.07
LOI	1.40	1.50	1.10	2.00	1.70	1.20	0.80
TOTAL	99.78	99.76	100.46	100.54	99.83	99.56	100.03
FeO	1.7	1.9	2.2	1.9	1.7	1	1.2
H_2Ot	1.2	1.4	0.9	2	1.5	1.2	0.9
CO_2t	0.2	0.2	0.1	0.2	0.1	0.1	0.2
S	0.01	0	0	0	0	0	0
Pb	13	16	15	7	12	11	14
Zn	50	51	46	46	42	40	41
Cu	14	17	17	18	20	16	15
Ni	14	17	18	20	19	14	11
Co	12	13	10	11	7	B.D.	B.D.
Cr	36	39	46	43	31	24	22
V	83	100	100	102	107	56	60
S	B.D.	B.D.	B.D.	B.D.	B.D.	B.D.	B.D.
Wt % FRN	13.82	17.72	24.48	5.29	9.27	16.51	35.15
TRP Zn	14.90	19.48	24.27	5.82	9.31	15.80	34.48
TRP CO_2	15.99	20.50	14.16	0.54	0.47	0.84	3.58

Trench No.	1	1	1	1	1	1	1
Sample No.	24	24	25	25	25	25	25
Class	VF Sand	Silt	VC Sand	C Sand	M Sand	F Sand	VF Sand
SiO_2	66.96	65.45	68.67	72.28	72.86	70.74	66.30
TiO_2	0.88	0.86	0.63	0.54	0.42	0.53	1.00
Al_2O_3	13.20	13.84	14.02	12.50	12.84	13.17	13.23
Fe_2O_3	5.65	5.65	4.81	3.96	3.11	3.84	6.30
MnO	0.10	0.11	0.07	0.06	0.06	0.06	0.11
MgO	2.61	2.30	2.35	2.34	1.91	1.82	2.52
CaO	4.30	4.17	1.73	2.10	2.61	2.71	4.08
Na_2O	2.60	3.35	3.35	2.58	3.43	3.75	3.00
K_2O	2.06	2.71	2.35	2.05	1.95	2.00	1.99
P_2O_5	0.21	0.38	0.11	0.08	0.08	0.10	0.21
LOI	1.50	1.20	2.20	1.60	1.10	1.50	1.60
TOTAL	100.06	100.02	100.28	100.09	100.35	100.21	100.34
FeO	3	2.3	2.2	2	1.6	1.8	
H_2Ot	1.1	0.9	2.1	1.5	1.1	1.4	
CO_2t	8.6	0.2	0.2	0.1	0.2	0.2	
S	0.01	0	0	0	0	0	
Pb	15	13	11	12	15	14	11
Zn	48	38	45	43	40	43	46
Cu	14	13	20	16	13	11	14
Ni	16	15	21	17	14	14	21
Co	15	16	16	13	6	10	19
Cr	47	47	54	40	28	31	55
V	126	115	116	95	86	91	119
S	B.D.	B.D.	B.D.	B.D.	B.D.	B.D.	B.D.
Wt % FRN	21.36	11.07	3.90	11.37	24.28	35.01	21.03
WT% ZN	24.52	10.07	4.11	11.45	22.75	35.27	22.66
TRP CO_2	93.45	1.13	5.20	7.59	32.42	46.75	0.00

TABLE 336.2. CONTINUED.

Trench No.	1	1	1	1	1	1	1
Sample No.	25	26	26	26	26	26	26
Class	Silt	Granule	VC Sand	C Sand	M Sand	F Sand	VF Sand
SiO_2	64.02	64.20	66.68	70.86	73.00	70.94	67.31
TiO_2	1.11	0.55	0.71	0.59	0.41	0.53	0.99
Al_2O_3	13.44	19.00	14.34	12.98	13.80	13.69	13.33
Fe_2O_3	6.64	4.44	5.64	4.49	2.99	3.59	6.11
MnO	0.11	0.09	0.12	0.08	0.04	0.06	0.09
MgO	2.27	2.69	2.72	2.26	1.59	2.02	2.35
CaO	4.15	1.55	2.04	2.15	2.48	3.17	3.98
Na_2O	3.47	2.88	3.03	2.95	2.70	2.98	2.53
K_2O	2.52	2.21	2.30	2.03	2.04	2.06	2.07
P_2O_5	0.58	0.11	0.16	0.12	0.08	0.10	0.18
LOI	1.30	2.30	2.70	2.00	1.30	1.30	1.10
TOTAL	99.61	100.00	100.45	100.49	100.42	100.42	100.03
FeO	2.7		2.7	2.1	1.4	1.7	2.7
H_2Ot	1.2		2.4	2	1.3	1.2	1.4
CO_2t	0.3		0.6	0.6	0.5	0.5	0.6
S	0		0	0	0	0	0
Pb	15	14	12	11	10	15	14
Zn	40	50	54	47	41	48	52
Cu	14	5	13	11	6	12	12
Ni	16	26	20	14	9	11	16
Co	16	15	20	14	3	4	14
Cr	51	53	59	37	26	27	49
V	110	92	126	99	69	75	136
S	B.D.	B.D.	B.D.	B.D.	B.D.	B.D.	B.D.
Wt % FRN	4.01	1.84	5.40	8.20	15.74	29.24	22.35
TRP Zn	3.76	1.88	5.96	7.88	13.18	28.67	23.74
TRP CO_2	8.03	0.00	7.36	11.17	17.86	33.18	30.43

Trench No.	1	1	1	1	1	1	1
Sample No.	26	27	27	27	27	27	27
Class	Silt	VC Sand	C Sand	M Sand	F Sand	VF Sand	Silt
SiO_2	64.60	66.12	69.97	72.28	69.99	65.53	62.86
TiO_2	0.76	0.73	0.60	0.44	0.52	1.00	0.79
Al_2O_3	14.68	14.05	13.10	13.36	13.97	13.71	14.80
Fe_2O_3	5.17	5.75	4.65	3.25	3.64	6.51	5.35
MnO	0.08	0.14	0.09	0.04	0.06	0.09	0.06
MgO	2.19	2.55	2.27	1.51	1.79	2.25	2.11
CaO	2.99	2.01	2.17	2.46	2.93	3.79	2.93
Na_2O	2.56	3.33	2.80	3.11	3.33	3.01	2.90
K_2O	3.00	2.07	1.96	2.03	2.07	2.06	2.82
P_2O_5	0.50	0.16	0.12	0.08	0.08	0.17	0.75
LOI	3.50	3.20	2.30	1.80	1.90	2.40	5.00
TOTAL	100.04	100.10	100.02	100.36	100.27	100.52	100.36
FeO		2.6	2.1	1.7	1.7	2.8	
H_2Ot		2.7	2.2	1.6	1.6	2.1	
CO_2t		0.9	0.8	0.7	0.8	1.4	
S		0	0	0	0	0.01	
Pb	17	9	13	14	15	14	17
Zn	55	55	52	49	50	60	64
Cu	21	10	10	9	5	11	17
Ni	21	20	16	13	10	17	20
Co	16	19	15	4	2	20	17
Cr	50	45	47	35	29	57	53
V	97	129	105	75	69	146	103
S	61	70	68	B.D.	B.D.	104	74
Wt % FRN	16.64	5.55	7.27	16.34	27.55	22.80	18.61
TRP Zn	18.70	5.63	6.98	14.77	25.41	25.24	21.97
TRP CO_2	0.00	6.55	7.64	15.01	28.92	41.89	0.00

TABLE 336.2. CONTINUED.

Trench No.	2	2	2	2	2	2	2
Sample No.	28	28	28	28	28	28	28
Class	Pebble	Granule	VC Sand	C Sand	M Sand	F Sand	VF Sand
SiO_2	20.78	35.90	39.23	46.43	50.21	51.99	51.40
TiO_2	0.10	0.25	0.24	0.30	0.36	0.56	0.84
Al_2O_3	2.71	7.49	7.50	8.62	9.05	9.94	10.39
Fe_2O_3	1.61	2.61	2.59	2.80	3.01	4.16	5.51
MnO	0.07	0.07	0.07	0.05	0.06	0.08	0.11
MgO	15.95	9.37	7.66	6.63	6.11	5.59	5.43
CaO	25.59	18.99	19.10	15.64	13.66	11.87	11.67
Na_2O	0.53	1.39	1.58	2.44	2.13	2.50	2.40
K_2O	0.69	1.46	1.24	1.15	1.27	1.43	1.48
P_2O_5	0.02	0.06	0.06	0.05	0.05	0.11	0.18
LOI	32.00	22.30	20.50	16.20	14.20	11.90	10.50
TOTAL	100.04	99.88	99.75	100.31	100.10	100.12	99.90
FeO	0.8	1.3	1.3	1.4	1.4	2	2.7
H_2Ot	2.1	1.5	1.21	1.1	0.9	0.9	1
CO_2t	31.4	21.3	19.4	15.8	13.6	10.9	9.8
S	0.01	0.03	0.01	0.01	0.01	0.01	0
Pb	9	11	9	11	9	16	19
Zn	485	404	452	536	577	661	634
Cu	7	15	10	9	9	12	17
Ni	5	11	9	8	6	9	14
Co	B.D.	3	2	1	1	12	18
Cr	B.D.	10	17	5	1	11	34
V	3	47	40	58	63	98	106
S	300	467	265	175	66	110	168
Wt % FRN	22.43	8.67	8.84	11.94	16.22	14.02	11.49
TRP Zn	19.23	6.19	7.06	11.31	16.54	16.38	12.88
TRP CO_2	40.59	10.64	9.88	10.87	12.71	8.81	6.49

Trench No.	2	2	2	2	2	2	2
Sample No.	28	29	29	29	29	29	29
Class	Silt	Pebble	Granule	VC Sand	C Sand	M Sand	F Sand
SiO_2	46.38	27.28	31.70	36.57	41.00	47.45	53.82
TiO_2	0.73	0.12	0.26	0.27	0.26	0.34	0.48
Al_2O_3	10.11	4.62	6.40	7.25	7.36	8.43	10.34
Fe_2O_3	5.43	1.46	2.76	2.64	2.43	2.84	3.73
MnO	0.08	0.06	0.07	0.06	0.05	0.05	0.07
MgO	7.10	15.39	11.27	8.93	7.69	6.50	5.58
CaO	12.59	22.96	21.32	19.98	18.11	14.68	11.60
Na_2O	2.24	0.52	0.64	1.61	1.81	2.37	2.49
K_2O	1.69	0.89	1.15	1.21	1.10	1.22	1.49
P_2O_5	0.55	0.05	0.07	0.06	0.04	0.05	0.08
LOI	13.10	26.70	24.40	21.50	20.10	16.10	10.80
TOTAL	100.00	100.04	100.04	100.08	99.95	100.01	100.47
FeO		0.6	1.4	1.2	1.3	1.4	1.8
H_2Ot		1.5	1.7	1.4	1	0.9	0.9
CO_2t		27.7	23.7	21.4	19.5	15	10.7
S		0.02	0.02	0.01	0.01	0	0
Pb	20	7	13	8	8	11	14
Zn	959	135	271	230	217	240	295
u	16	6	14	13	10	9	12
Ni	17	4	5	9	7	6	10
Co	19	B.D.	3	1	1	2	11
Cr	46	3	B.D.	4	6	8	21
V	104	18	46	49	56	60	82
S	B.D.	331	209	305	103	80	B.D.
Wt % FRN	6.14	20.14	7.65	9.99	12.39	16.92	15.32
TRP Zn	10.40	11.27	8.60	9.52	11.15	16.83	18.74
TRP CO_2	0.00	32.39	10.53	12.41	14.03	14.73	9.52

TABLE 336.2. CONTINUED.

Trench No.	2	2	2	2	2	2	2
Sample No.	29	29	29	30	30	30	30
Class	VF Sand	Silt	Clay	Pebble	Granule	VC Sand	C Sand
SiO_2	53.73	49.00	40.84	21.74	36.49	37.20	42.88
TiO_2	0.72	0.81	0.66	0.16	0.32	0.31	0.36
Al_2O_3	10.76	10.53	13.76	4.09	7.71	7.47	7.99
Fe_2O_3	4.77	5.44	10.00	1.79	3.05	2.79	2.87
MnO	0.10	0.09	0.14	0.08	0.08	0.07	0.06
MgO	5.38	6.59	9.90	14.73	9.54	9.67	8.68
CaO	10.93	11.88	4.06	24.30	18.78	18.32	16.35
Na_2O	2.14	2.07	2.81	0.55	1.25	1.33	0.81
K_2O	1.60	1.68	2.40	0.99	1.44	1.40	1.19
P_2O_5	0.18	0.41	3.81	0.03	0.07	0.06	0.05
LOI	9.80	11.30	11.60	31.60	21.20	21.40	18.80
TOTAL	100.10	99.81	99.96	100.06	99.94	100.02	100.04
FeO	2.3			1	1.5	1.4	1.5
H_2Ot	1			1.7	1.6	1.4	1.1
CO_2t	9.1			30.6	20.4	20.7	18.1
S	0.01			0.03	0.01	0.01	0.01
Pb	15	19	34	11	11	10	10
Zn	277	345	2099	93	119	114	107
Cu	9	13	101	7	12	14	11
Ni	10	25	47	13	13	12	9
Co	16	16	36	B.D.	5	6	2
Cr	27	37	51	11	15	3	1
V	99	114	110	38	56	58	67
S	B.D.	B.D.	B.D.	1233	669	453	264
Wt % FRN	12.11	5.18	0.30	13.78	7.36	8.96	13.27
TRP Zn	13.91	7.41	2.57	10.00	6.84	7.97	11.08
TRP CO_2	6.40	0.00	0.00	27.52	9.80	12.11	15.68

Trench No.	2	2	2	2	2	2	2
Sample No.	30	30	30	30	30	31	31
Class	M Sand	F Sand	VF Sand	Silt	Clay	Pebble	VC Sand
SiO_2	49.45	54.85	56.12	52.20	41.83	57.00	65.03
TiO_2	0.40	0.53	0.79	0.90	0.68	0.40	0.43
Al_2O_3	8.85	10.43	10.99	11.09	13.83	13.59	14.71
Fe_2O_3	3.13	4.00	4.92	5.71	9.72	3.16	3.90
MnO	0.05	0.07	0.10	0.11	0.14	0.05	0.05
MgO	7.00	5.46	4.89	5.73	9.03	7.15	3.20
CaO	13.19	10.29	9.39	10.23	3.88	5.01	4.46
Na_2O	1.79	2.22	2.56	2.29	3.12	2.32	2.98
K_2O	1.42	1.57	1.75	1.79	2.44	3.05	2.27
P_2O_5	0.05	0.09	0.17	0.34	4.87	0.07	0.09
LOI	14.90	10.80	8.70	9.50	10.60	7.90	3.40
TOTAL	100.24	100.31	100.37	99.88	100.13	99.71	100.52
FeO	1.4	1.7	2.2				1.8
H_2Ot	1	1	1.1				1.4
CO_2t	14.1	9.6	7.9				1.8
S	0	0	0				0.01
Pb	14	18	18	17	44	13	15
Zn	128	143	145	136	1521	77	82
Cu	11	11	17	12	111	15	13
Ni	7	10	17	14	45	9	13
Co	B.D.	9	17	17	29	6	8
Cr	8	21	41	59	53	B.D.	12
V	72	87	114	130	102	65	94
S	103	186	248	B.D.	B.D.	1975	307
Wt % FRN	18.29	16.94	14.43	6.67	0.30	3.25	4.26
TRP Zn	18.28	18.90	16.33	7.08	3.52	2.70	3.77
TRP CO_2	16.84	10.62	7.44	0.00	0.00	0.00	6.87

TABLE 336.2. CONTINUED.

Trench No.	2	2	2	2	2	2	2
Sample No.	31	31	31	31	31	32	32
Class	C Sand	M Sand	F Sand	VF Sand	Silt	Pebble	Granule
SiO_2	66.23	66.45	69.14	67.62	63.63	26.92	31.99
TiO_2	0.25	0.32	0.46	0.64	0.84	0.23	0.29
Al_2O_3	14.46	13.81	13.13	13.55	13.80	5.62	6.71
Fe_2O_3	2.05	2.90	3.75	4.68	5.83	2.55	2.62
MnO	0.03	0.05	0.07	0.09	0.11	0.08	0.07
MgO	2.45	3.28	2.70	2.36	2.87	11.96	9.82
CaO	4.80	4.55	3.71	4.03	4.43	23.27	21.11
Na_2O	4.75	3.17	2.50	2.77	3.51	0.53	1.31
K_2O	1.45	1.65	2.06	2.26	2.30	0.53	1.22
P_2O_5	0.05	0.04	0.11	0.20	0.77	0.03	0.07
LOI	3.40	4.00	2.40	1.90	1.60	28.20	24.50
TOTAL	99.93	100.21	100.03	100.10	99.68	99.91	99.70
FeO	1	1.1	1.5	2.2		1.6	1.5
H_2Ot	0.9	1.5	1.6	1.6		1.2	1.4
CO_2t	2.5	2.8	1.2	1		27.9	25.8
S	0.01	0	0.01	0		0.04	0.06
Pb	11	13	15	18	19	7	12
Zn	52	75	97	105	109	123	168
Cu	8	9	14	16	16	2	9
Ni	7	11	12	15	22	11	10
Co	B.D.	1	7	13	16	5	1
Cr	2	12	22	44	67	3	8
V	37	44	71	98	114	42	47
S	144	185	234	119	B.D.	480	620
Wt % FRN	7.42	11.56	17.80	31.61	21.62	25.06	9.75
TRP Zn	4.17	9.37	18.66	35.87	25.46	15.96	8.48
TRP CO_2	16.62	29.02	19.15	28.34	0.00	37.33	13.43

Trench No.	2	2	2	2	2	2	2
Sample No.	32	32	32	32	32	32	33
Class	VC Sand	C Sand	M Sand	F Sand	VF Sand	Silt	Pebble
SiO_2	35.64	41.40	50.33	52.35	52.37	47.89	34.83
TiO_2	0.36	0.32	0.35	0.58	0.97	0.89	0.51
Al_2O_3	7.45	7.54	8.75	9.86	10.77	10.22	9.14
Fe_2O_3	2.91	2.46	2.82	4.37	6.47	7.88	2.89
MnO	0.07	0.05	0.05	0.08	0.11	0.10	0.06
MgO	8.92	8.16	6.80	6.01	5.50	5.97	10.43
CaO	20.24	17.97	13.52	12.02	10.96	11.24	18.64
Na_2O	1.08	1.30	1.22	1.67	1.91	2.35	1.18
K_2O	1.10	1.07	1.19	1.39	1.51	1.59	1.72
P_2O_5	0.06	0.04	0.05	0.12	0.24	0.83	0.13
LOI	22.40	19.70	14.60	12.00	9.60	10.80	20.80
TOTAL	100.23	100.00	99.68	100.44	100.40	99.76	100.34
FeO	1.5	1.3	1.4	2	2.4		1.6
H_2Ot	1.3	1	0.8	1	0.8		1.1
CO_2t	21.5	19.4	13.8	11.1	0.2		20.7
S	0.04	0.01	0	0.01	0		0.14
Pb	11	12	12	13	16	39	14
Zn	198	192	179	268	321	453	514
Cu	15	5	10	10	16	32	16
Ni	10	12	5	8	17	24	8
Co	5	B.D.	B.D.	5	21	28	7
Cr	15	11	15	30	33	50	19
V	65	47	56	87	116	120	63
S	425	58	100	B.D.	79	201	1312
Wt % FRN	11.40	15.05	18.41	11.70	5.95	2.45	28.31
TRP Zn	11.68	14.96	17.06	16.24	9.88	5.74	35.39
TRP CO_2	13.08	15.59	13.56	6.94	0.06	0.00	31.81

TABLE 336.2. CONTINUED.

Trench No.	2	2	2	2	2	2	2
Sample No.	33	33	33	33	33	33	33
Class	Granule	VC Sand	C Sand	M Sand	F Sand	VF Sand	Silt
SiO_2	26.11	30.14	35.45	43.84	50.23	52.12	46.75
TiO_2	0.18	0.35	0.48	0.50	0.76	1.19	1.05
Al_2O_3	4.61	6.59	7.18	8.12	10.11	11.04	10.47
Fe_2O_3	1.87	2.94	3.89	4.06	5.61	7.62	9.79
MnO	0.06	0.07	0.07	0.07	0.08	0.12	0.12
MgO	12.88	10.90	10.15	7.99	6.21	5.62	6.18
CaO	23.49	21.49	19.11	14.71	11.53	9.85	10.10
Na_2O	0.63	1.18	0.65	2.13	1.93	1.54	2.84
K_2O	0.81	0.87	0.77	1.01	1.30	1.45	1.47
P_2O_5	0.04	0.05	0.07	0.08	0.11	0.22	0.58
LOI	29.20	25.50	22.20	17.40	12.10	9.30	10.40
TOTAL	99.88	100.08	100.02	99.90	99.97	100.07	99.77
FeO	0.9	1.6	2.3	2.2	2.7	3.4	
H_2Ot	1.2	1.4	1.1	1.1	1.2	1.2	
CO_2t	28.8	24.9	21.5	16.4	10.8	7.8	
S	0.01	0.01	0.01	0	0.01	0.02	
Pb	12	13	10	8	13	14	40
Zn	202	240	259	378	501	572	869
Cu	9	8	6	8	17	19	37
Ni	6	8	6	8	11	15	27
Co	2	5	11	12	20	25	35
Cr	9	6	9	9	16	33	59
V	26	52	59	72	110	128	143
S	273	289	124	60	131	119	521
Wt % FRN	8.14	9.60	13.94	17.41	13.19	7.05	2.20
TRP Zn	4.00	5.61	8.47	16.00	16.07	9.81	4.65
TRP CO_2	12.73	12.98	16.26	15.50	7.73	2.99	0.00

Trench No.	3	3	3	3	3	3	3
Sample No.	35	35	35	35	35	35	35
Class	Pebble	Granule	VC Sand	C Sand	M Sand	F Sand	VF Sand
SiO_2	60.18	60.06	59.59	63.05	67.88	66.62	67.18
TiO_2	0.25	0.85	1.17	1.02	0.74	0.82	0.84
Al_2O_3	7.13	16.49	15.92	15.44	13.99	14.07	13.76
Fe_2O_3	3.05	7.15	8.41	7.01	5.25	5.97	5.45
MnO	0.06	0.07	0.07	0.06	0.06	0.09	0.11
MgO	12.03	3.05	3.45	3.00	2.12	2.56	2.36
CaO	14.28	4.86	5.28	5.13	4.23	4.08	4.21
Na_2O	0.72	2.60	2.55	2.77	2.62	2.12	2.27
K_2O	0.81	2.27	1.61	1.41	1.62	1.85	2.10
P_2O_5	0.12	0.21	0.13	0.12	0.11	0.18	0.23
LOI	1.70	2.10	2.00	1.40	1.30	1.30	1.40
TOTAL	100.31	99.71	99.68	100.40	99.92	99.67	99.90
FeO	1.8	3.5	4.4	3.7	2.5	2.6	2.4
H_2Ot	1.2	2	1.9	1.5	1.3	1.2	1.1
CO_2t	0.2	0.2	0.1	0.1	0.2	0.3	0.4
S	0.04	0.03	0.02	0.02	0	0	0
Pb	6	10	12	10	14	12	34
Zn	49	56	63	58	50	53	48
Cu	13	23	20	14	12	19	18
Ni	9	16	10	7	8	9	11
Co	2	23	26	19	13	27	27
Cr	4	B.D.	6	4	7	25	28
V	55	155	176	163	117	117	110
S	155	239	66	B.D.	B.D.	B.D.	B.D.
Wt % FRN	21.24	4.21	7.63	10.94	13.15	14.93	13.96
TRP Zn	20.08	4.55	9.28	12.25	12.69	15.27	12.93
TRP CO_2	21.63	4.29	3.89	5.57	13.39	22.80	28.44

TABLE 336.2. CONTINUED.

Trench No.	3	3	3	3	3	3	3
Sample No.	35	36	36	36	36	36	36
Class	Silt	Pebble	Granule	VC Sand	C Sand	M Sand	F Sand
SiO_2		67.10	62.79	58.86	62.67	64.11	68.90
TiO_2		0.71	0.80	1.21	0.97	0.98	0.62
Al_2O_3		16.53	15.67	15.99	15.38	14.56	13.95
Fe_2O_3		3.61	6.26	8.71	7.15	7.17	4.78
MnO		0.04	0.06	0.08	0.06	0.07	0.06
MgO		1.26	3.21	3.74	2.90	2.88	2.26
CaO		1.82	3.90	4.67	4.41	3.94	3.53
Na_2O		4.96	3.65	3.59	3.46	2.73	2.16
K_2O		3.40	2.53	1.52	1.37	1.45	1.94
P_2O_5		0.26	0.13	0.18	0.15	0.15	0.15
LOI		0.30	1.50	1.90	1.60	2.10	1.60
TOTAL		99.98	100.52	100.47	100.11	100.13	99.95
FeO		1.5	2.9	4.1	3.3	2.9	1.9
H_2O_t		0.7	1.6	1.8	1.6	1.7	1.2
CO_2t		0.1	0.1	0.1	0.1	0.2	0.3
S		0.01	0.01	0.01	0	0.01	0.01
Pb	17	11	13	9	11	11	13
Zn	49	50	59	65	59	69	57
Cu	26	4	10	12	8	14	13
Ni	14	6	16	9	8	9	8
Co	19	1	19	23	16	20	11
Cr	46	B.D.	46	12	15	12	12
V	128	48	122	157	129	128	85
S	B.D.	B.D.	B.D.	B.D.	B.D.	B.D.	B.D.
Wt % FRN	13.71	6.64	4.18	7.94	8.38	12.08	16.58
TRP Zn	12.96	5.71	4.23	8.87	8.49	14.33	16.24
TRP CO_2	0.00	2.97	1.86	3.54	3.74	10.79	22.20

Trench No.	3	3	3	3	3	3	3
Sample No.	36	36	37	37	37	37	37
Class	VF Sand	Silt	Pebble	Granule	VC Sand	C Sand	M Sand
SiO_2	68.02	63.90	63.21	64.94	61.80		68.03
TiO_2	0.66	1.20	0.83	0.66	0.92		0.69
Al_2O_3	14.05	14.01	13.92	15.70	15.83		14.11
Fe_2O_3	5.19	7.34	7.60	4.99	6.79		5.20
MnO	0.09	0.13	0.09	0.06	0.06		0.06
MgO	2.25	3.00	3.64	3.03	3.33		2.74
CaO	4.34	5.27	4.52	3.79	4.81		4.05
Na_2O	2.31	2.35	2.54	2.98	3.41		2.43
K_2O	2.12	2.10	1.51	2.21	1.72		1.69
P_2O_5	0.23	0.46	0.17	0.12	0.14		0.12
LOI	1.20	0.50	2.00	1.40	1.40		1.10
TOTAL	100.45	100.25	100.04	99.89	100.22		100.21
FeO	2.3			2.7	3.4	2.9	2.3
H_2O_t	1.1			1.5	1.7	1.3	1.2
CO_2t	0.4			0.1	0.1	0.2	0.2
S	0			0.01	0.01	0.01	0
Pb	14	14	9	10	10	7	10
Zn	57	53	62	56	66	59	59
Cu	15	13	20	7	7	8	12
Ni	12	17	13	12	10	7	10
Co	18	21	26	14	20	18	16
Cr	27	72	8	12	15	8	1
V	104	128	150	100	150	141	112
S	B.D.	B.D.	B.D.	B.D.	B.D.	B.D.	B.D.
Wt % FRN	30.73	13.19	9.61	6.49	8.97	10.89	14.52
TRP Zn	30.11	12.02	9.91	6.04	9.84	10.68	14.24
TRP CO_2	54.89	0.00	0.00	3.21	4.44	10.78	14.38

TABLE 336.2. CONTINUED.

Trench No.	3	3	3	3	3	3	3
Sample No.	37	37	37	38	38	38	38
Class	F Sand	VF Sand	Silt	Pebble	Granule	VC Sand	C Sand
SiO_2	68.12	66.14			66.38	65.27	71.89
TiO_2	0.66	0.78			0.41	0.32	0.34
Al_2O_3	13.79	13.89			16.48	17.14	13.82
Fe_2O_3	4.90	5.84			3.36	4.24	3.02
MnO	0.07	0.10			0.05	0.07	0.04
MgO	2.36	2.88			2.11	2.35	1.94
CaO	3.85	4.39			3.02	3.30	3.20
Na_2O	2.93	3.06			3.47	3.81	2.68
K_2O	1.88	2.00			3.03	2.23	2.00
P_2O_5	0.13	0.22			0.15	0.11	0.07
LOI	1.40	1.10			1.70	1.50	1.20
TOTAL	100.08	100.41			100.16	100.34	100.20
FeO	2.2	2.8	3.3	1.9	1.3	1.5	1.4
H_2Ot	0.9	1.2	1.2	1.4	1.4	1.3	1
CO_2t	0.2	0.3	0.4	0.1	0.1	0.2	0.2
S	0	0	0	0	0.01	0.01	0
Pb	12	10	14	8	12	13	11
Zn	61	60	59	48	47	50	48
Cu	10	14	15	6	7	5	6
Ni	11	13	18	14	7	10	6
Co	16	20	29	8	1	7	2
Cr	24	35	55	9	1	13	7
V	96	108	132	72	76	69	56
S	B.D.	B.D.	B.D.	B.D.	B.D.	B.D.	B.D.
Wt % FRN	20.16	20.83	8.23	3.94	3.87	6.85	9.53
TRP Zn	20.45	20.77	8.07	3.40	3.26	6.15	8.22
TRP CO_2	19.96	30.93	16.29	1.72	1.69	5.98	8.33

Trench No.	3	3	3	3	3	3	3
Sample No.	38	38	38	38	39	39	39
Class	M Sand	F Sand	VF Sand	Silt	Pebble	Granule	VC Sand
SiO_2	73.92	69.60	65.17		57.98	61.10	61.36
TiO_2	0.30	0.42	0.84		0.82	0.66	0.91
Al_2O_3	13.29	14.59	14.00		16.50	17.48	16.58
Fe_2O_3	2.48	3.56	6.51		7.91	5.83	6.67
MnO	0.04	0.06	0.11		0.07	0.08	0.08
MgO	1.83	2.14	3.04		3.65	3.37	3.32
CaO	2.99	3.73	4.90		4.44	5.23	4.81
Na_2O	2.64	3.04	2.16		4.31	2.79	2.54
K_2O	2.06	1.98	1.90		1.84	2.14	1.88
P_2O_5	0.08	0.12	0.23		0.13	0.13	0.15
LOI	0.70	0.90	0.90		1.90	1.70	1.70
TOTAL	100.34	100.15	99.77		99.57	100.51	99.98
FeO	1.1	1.9	3.2		4.1	2.9	3.2
H_2Ot	0.8	1	1.2		1.7	1.6	2.1
CO_2t	0.1	0.2	0.5		0.2	0.3	0.4
S	0	0	0.01		0.08	0.01	0.01
Pb	11	14	12	15	10	10	10
Zn	47	57	67	71	60	74	76
Cu	7	7	10	14	17	9	11
Ni	8	14	23	24	9	12	15
Co	B.D.	6	17	27	29	20	20
Cr	7	31	66	74	B.D.	13	21
V	48	70	113	135	176	125	128
S	B.D.	B.D.	B.D.	B.D.	855	406	465
Wt % FRN	19.41	29.10	22.15	4.81	9.22	4.92	8.00
TRP Zn	16.39	29.79	26.65	6.14	6.62	4.36	7.28
TRP CO_2	8.48	25.42	48.38	0.00	2.26	1.81	3.93

TABLE 336.2. CONTINUED.

Trench No.	3	3	3	3	3	3	3
Sample No.	39	39	39	39	39	40	40
Class	C Sand	M Sand	F Sand	VF Sand	Silt	Granule	VC Sand
SiO_2	64.95	66.59	64.49	61.31	58.94	58.68	
TiO_2	0.71	0.64	0.72	0.93	1.30	0.60	
Al_2O_3	15.42	14.32	14.73	14.08	14.06	20.90	
Fe_2O_3	5.85	5.35	5.79	7.43	8.77	4.74	
MnO	0.07	0.07	0.09	0.12	0.14	0.07	
MgO	2.77	2.98	2.99	3.66	3.60	2.84	
CaO	4.41	3.80	4.06	4.45	4.32	6.39	
Na_2O	2.21	2.43	2.46	2.63	2.47	2.45	
K_2O	1.61	1.68	1.80	1.77	1.91	1.14	
P_2O_5	0.10	0.12	0.17	0.24	0.65	0.10	
LOI	1.60	2.10	2.30	3.30	4.00	2.00	
TOTAL	99.69	100.09	99.60	99.91	100.16	99.91	
FeO	2.9	2.4	2.5	3			3.4
H_2Ot	1.7	1.8	2	2.5			2.1
CO_2t	0.4	0.6	0.9	2.1			0.6
S	0	0	0	0.01			0.01
Pb	10	12	14	16		13	17
Zn	70	84	100	116		75	100
Cu	7	9	12	17		8	7
Ni	12	12	18	20		11	12
Co	18	14	18	23		19	16
Cr	14	17	29	46		3	24
V	139	127	130	134		104	132
S	269	159	134	271		453	B.D.
Wt % FRN	11.89	19.95	22.02	18.26	5.54	2.78	5.26
TRP Zn	9.96	20.06	26.36	25.36	0.00	1.74	4.40
TRP CO_2	5.84	14.71	24.34	47.10	0.00	0.00	2.38

Trench No.	3	3	3	3	3	4	4
Sample No.	40	40	40	40	40	41	41
Class	C Sand	M Sand	F Sand	VF Sand	Silt	VC Sand	C Sand
SiO_2	65.49	67.27	64.93	61.93		63.18	67.38
TiO_2	0.71	0.64	0.81	1.12		0.75	0.70
Al_2O_3	15.39	14.18	14.14	14.27		15.73	13.95
Fe_2O_3	5.90	4.97	5.90	7.62		5.79	5.00
MnO	0.06	0.06	0.09	0.10		0.11	0.11
MgO	2.74	2.33	2.79	3.22		3.35	2.86
CaO	4.06	3.63	3.91	4.12		3.75	3.40
Na_2O	1.79	2.83	2.79	1.99		3.00	2.18
K_2O	1.56	1.69	1.77	1.83		1.80	1.77
P_2O_5	0.12	0.12	0.15	0.19		0.17	0.14
LOI	2.20	2.70	3.00	4.00		2.70	2.20
TOTAL	100.02	100.42	100.27	100.40		100.33	99.69
FeO	2.9	2.3	2.5	3.1		2.6	2.3
H_2Ot	2	1.9	2.3	3		2.3	1.7
CO_2t	0.6	1.1	1.5	3.1		0.5	0.5
S	0	0	0	0		0.01	0
Pb	16	15	18	20	27	19	22
Zn	94	100	126	144	166	212	188
Cu	4	5	6	5	9	6	5
Ni	11	12	13	18	19	12	11
Co	18	13	21	19	25	22	15
Cr	26	27	40	48	49	40	32
V	127	109	108	136	116	124	113
S	B.D.	B.D.	B.D.	B.D.	B.D.	B.D.	B.D.
Wt % FRN	11.70	22.39	25.17	19.42	11.53	4.04	12.61
TRP Zn	9.20	18.73	26.53	23.39	16.01	3.5[illegible]	9.88
TRP CO_2	5.29	18.55	28.44	45.34	0.00	3.7[illegible]	11.62

TABLE 336.2. CONTINUED.

Trench No.	4	4	4	4	4	4	4
Sample No.	41	41	41	42	42	42	42
Class	M Sand	F Sand	VF Sand	VC Sand	C Sand	M Sand	F Sand
SiO_2	68.31	66.22	63.81	61.74	65.71	65.82	60.48
TiO_2	0.62	0.85	1.07	0.84	0.76	0.68	0.86
Al_2O_3	13.49	13.82	13.82	14.91	14.01	13.64	13.44
Fe_2O_3	4.69	5.99	7.25	6.47	5.98	5.37	6.94
MnO	0.09	0.10	0.14	0.11	0.14	0.15	0.19
MgO	2.61	2.95	3.05	3.88	3.30	3.93	5.45
CaO	3.48	3.80	3.83	3.72	3.58	3.56	4.34
Na_2O	2.84	2.36	2.40	2.39	2.38	2.27	2.02
K_2O	1.76	1.82	2.04	2.00	1.69	1.61	1.53
P_2O_5	0.12	0.17	0.23	0.19	0.17	0.18	0.67
LOI	1.80	1.50	2.90	3.60	2.30	2.50	3.80
TOTAL	99.81	99.58	100.53	99.85	100.02	99.70	99.72
FeO	2	2.4	2.5	3.1	2.6	2.1	2.3
H_2Ot	1.6	1.4	2.2	3	2.2	2.2	3
CO_2t	0.5	0.5	1.2	0.8	0.9	0.9	1.9
S	0	0	0	0.02	0.01	0.01	0
Pb	21	19	30	38	32	33	46
Zn	210	266	355	310	292	325	471
Cu	8	7	11	5	6	6	9
Ni	12	12	16	16	13	14	15
Co	13	14	21	22	17	16	15
Cr	27	35	44	37	30	37	45
V	93	121	132	140	120	130	177
S	B.D.	B.D.	B.D.	B.D.	B.D.	B.D.	B.D.
Wt % FRN	21.61	21.76	20.21	4.59	14.11	21.73	20.76
TRP Zn	18.91	24.13	29.90	2.91	8.43	14.46	20.01
TRP CO_2	19.91	20.06	44.70	0.91	3.15	4.85	9.77

Trench No.	4	4	4	4	4	4	4
Sample No.	42	42	43	43	43	43	43
Class	VF Sand	Silt	Pebble	Granule	VC Sand	C Sand	M Sand
SiO_2	57.79	55.20	61.30	60.15	62.79	67.78	69.01
TiO_2	1.09	0.76	0.86	1.00	0.85	0.65	0.72
Al_2O_3	13.06	13.77	15.65	16.03	15.68	14.35	13.42
Fe_2O_3	9.34	9.99	7.88	7.64	6.44	4.90	4.93
MnO	0.33	0.41	0.16	0.16	0.10	0.08	0.09
MgO	4.06	2.65	3.40	4.18	3.61	2.57	2.61
CaO	4.09	2.69	5.79	3.98	3.47	3.03	3.39
Na_2O	1.54	2.26	1.92	1.91	2.82	2.77	1.98
K_2O	1.76	2.10	1.68	1.82	1.84	1.71	1.74
P_2O_5	0.59	0.68	0.12	0.27	0.21	0.16	0.11
LOI	6.20	9.50	1.30	2.70	2.50	2.30	1.80
TOTAL	99.85	100.00	100.05	99.83	100.31	100.29	99.81
FeO	2.4	1.1	0.9	3	2.3	2.3	2.8
H_2Ot	4.1	5.3	1.4	2.6	1.9	1.6	2.2
CO_2t	5.7	13.7	0.5	0.4	0.6	0.7	1.3
S	0.01	0.02	0	0	0	0	0.01
Pb	109	156	14	20	19	22	23
Zn	704	762	92	124	159	141	144
Cu	11	15	9	6	6	7	8
Ni	23	25	21	17	16	13	12
Co	25	26	28	27	23	14	13
Cr	51	49	48	44	44	36	31
V	150	108	151	141	126	101	109
S	183	206	B.D.	B.D.	B.D.	B.D.	B.D.
Wt % FRN	21.22	15.14	7.20	2.43	5.85	16.42	22.83
TRP Zn	30.57	23.61	3.42	1.56	4.81	11.96	16.99
TRP CO_2	29.96	51.37	4.18	1.13	4.08	13.35	34.47

TABLE 336.2. CONTINUED.

Trench No.	4	4	4
Sample No.	43	43	43
Class	F Sand	VF Sand	Silt
SiO_2	63.41	62.30	
TiO_2	0.99	1.24	
Al_2O_3	13.72	13.47	
Fe_2O_3	7.29	8.09	
MnO	0.12	0.13	
MgO	3.23	3.31	
CaO	3.84	4.05	
Na_2O	2.63	2.77	
K_2O	1.77	1.81	
P_2O_5	0.32	0.37	
LOI	3.10	2.60	
TOTAL	100.42	100.13	
FeO	3.1		
H_2Ot	2.1		
CO_2t	1.9		
S	0		
Pb	28	41	51
Zn	222	229	346
Cu	10	10	21
Ni	15	25	21
Co	19	21	18
Cr	41	56	54
V	127	157	115
S	B.D.	B.D.	110
Wt % FRN	19.39	11.32	14.31
TRP Zn	22.25	13.40	25.60
TRP CO_2	42.79	0.00	0.00

TABLE 336.3. ELECTRON MICROPROBE ANALYSES OF SPHALERITE IN ERRATICS.

	1	2	3	4	5
Zn	58.98	58.09	59.53	60.07	61.02
S	33.04	32.48	32.77	31.93	32.71
Cd	0.13	0.16	0.15	0.14	0.15
Mn	0.38	0.39	.036	0.34	0.36
Cu	0.00	0.00	0.00	0.00	0.00
Fe	6.76	6.84	6.46	6.65	6.46
Hg	0.00	0.00	0.00	0.00	0.00
Total	99.29	97.96	99.26	99.13	100.71
	6	7	8	9	10
Zn	59.53	59.46	59.24	59.73	60.51
S	32.21	32.18	32.81	32.35	32.69
Cd	0.17	0.17	0.15	0.16	0.15
Mn	0.40	0.42	0.36	0.40	0.41
Cu	0.00	0.00	0.00	0.00	0.00
Fe	6.89	6.94	6.48	6.91	6.64
Hg	0.00	0.00	0.00	0.00	0.00
Total	99.19	99.17	99.08	99.54	100.40

TABLE 336.4. TEXTURAL CHARACTERISTICS OF SEDIMENTS.

Sample Number	Size Frequency Distribution	First Mode	Second Mode	So*	Interpretation
21	bimodal	pebble	medium sand	6.3	basal till
22	bimodal	coarse sand	pebble	2.8	reworked supraglacial till
23	bimodal	silt	medium sand	2.6	mixed fluvial sediments
24	unimodal	fine sand		1.9	fluvial sediments
25	unimodal	fine sand		1.8	fluvial sediments
26	unimodal	fine sand		2.2	fluvial sediments
27	unimodal	fine sand		2.2	fluvial sediments
28	bimodal	pebble	medium sand	4.2	basal till
29	bimodal	pebble	medium sand	4.0	basal till
30	bimodal	medium sand	pebble	3.3	basal till
31	unimodal	very fine sand	pebble	2.2	water-sorted sediments
32	bimodal	pebble	medium sand	3.4	supraglacial till
33	bimodal	pebble	medium sand	4.1	supraglacial till
35	bimodal	pebble	fine sand	4.3	basal till
36	bimodal	very fine sand	pebble	2.9	water-sorted sediments
37	bimodal	very fine sand	pebble	2.8	water-sorted sediments
38	unimodal	fine sand		2.2	water-sorted sediments
39	bimodal	fine sand	pebble	2.7	supraglacial till
40	unimodal	fine sand		2.1	weathered supraglacial till
41	unimodal	fine sand		2.1	weathered basal till
42	unimodal	fine sand		2.1	weathered basal till
43	polymodal	medium sand	pebble	2.6	weathered supraglacial till

* *Coefficient of sorting*

GEOCHEMISTRY OF SIZE FRACTIONS

In trenches 1, 2 and 3, the samples of basal till and water-sorted sediments generally are characterized by slightly increasing concentrations of zinc as a function of decreasing grain size. In all size fractions coarser than clay-size, zinc concentrations are less than those in the bulk samples (Figure 336.6a,b,c). Available analyses indicate that clay fractions exhibit an order of magnitude higher concentration of zinc than the coarser fractions and the bulk samples (Figure 336.6a,b). The clay fractions also are enriched in Cu (Table 336.2).

In contrast, the supraglacial till samples exhibit substantially increasing concentrations of zinc as a function of decreasing grain size. Generally, fractions finer than medium or fine sand (inclusive) contain higher zinc concentrations than the bulk samples. The zinc content of the clay appears to be approximately double that of the silt fraction (Figure 336.6a). The weathered basal and supraglacial tills in trench 4 exhibit similar increases in zinc concentration as a function of decreasing grain size (Figure 336.6d). The fractions exhibiting higher concentrations of zinc than in the corresponding bulk samples vary from silt to fine sand (Table 336.2).

The post-glacial fluvial sediments exhibit a consistent distribution of zinc among the various size fractions (Figure 336.6a). Concentrations of zinc increase overall in some samples, and decreases in others; however, the variation is slight, and the fraction compositions are very similar to the bulk compositions (Tables 336.1, 336.2).

The pebble fraction is the most variable in terms of major and trace element composition. Some samples are enriched in zinc in the coarsest fraction, while others are depleted, relative to bulk sample concentrations (Figures 336.5, 336.6). This variability in the coarse fraction has been documented by many authors who have referred to the "nugget effect" (e.g., MacEachern and Stea 1985; DiLabio 1988). The nugget effect results from the small size of the fraction analyzed compared to the large average size of the detritus in that fraction, contributing to poor representativity of analyses.

DiLabio *et al.* (1982) documented the very high concentrations of zinc in the clay fraction of till at this site. Similar enrichments of other metals in fine fractions have been reported (e.g., DiLabio 1979, 1988; Gleeson *et al.* 1984; Shilts 1984; Shelp and Nichol 1987). However, the clay fraction is volumetrically small compared to the rest of the size fractions in each sample (Figure 336.4, Table 336.4). Therefore, although it is rich in zinc, the clay fraction accounts for only a small proportion of the total zinc in the sample. On the basis of weight proportion or true relative percent (TRP) (Vagners 1969) of zinc, the medium- to very fine-sand fractions contribute the greatest amount of zinc (Figure 336.7b). In contrast, the true relative percent of CO_2 in the samples (Figure 336.7c) is a maximum in coarser or finer fractions than the true relative percent of zinc.

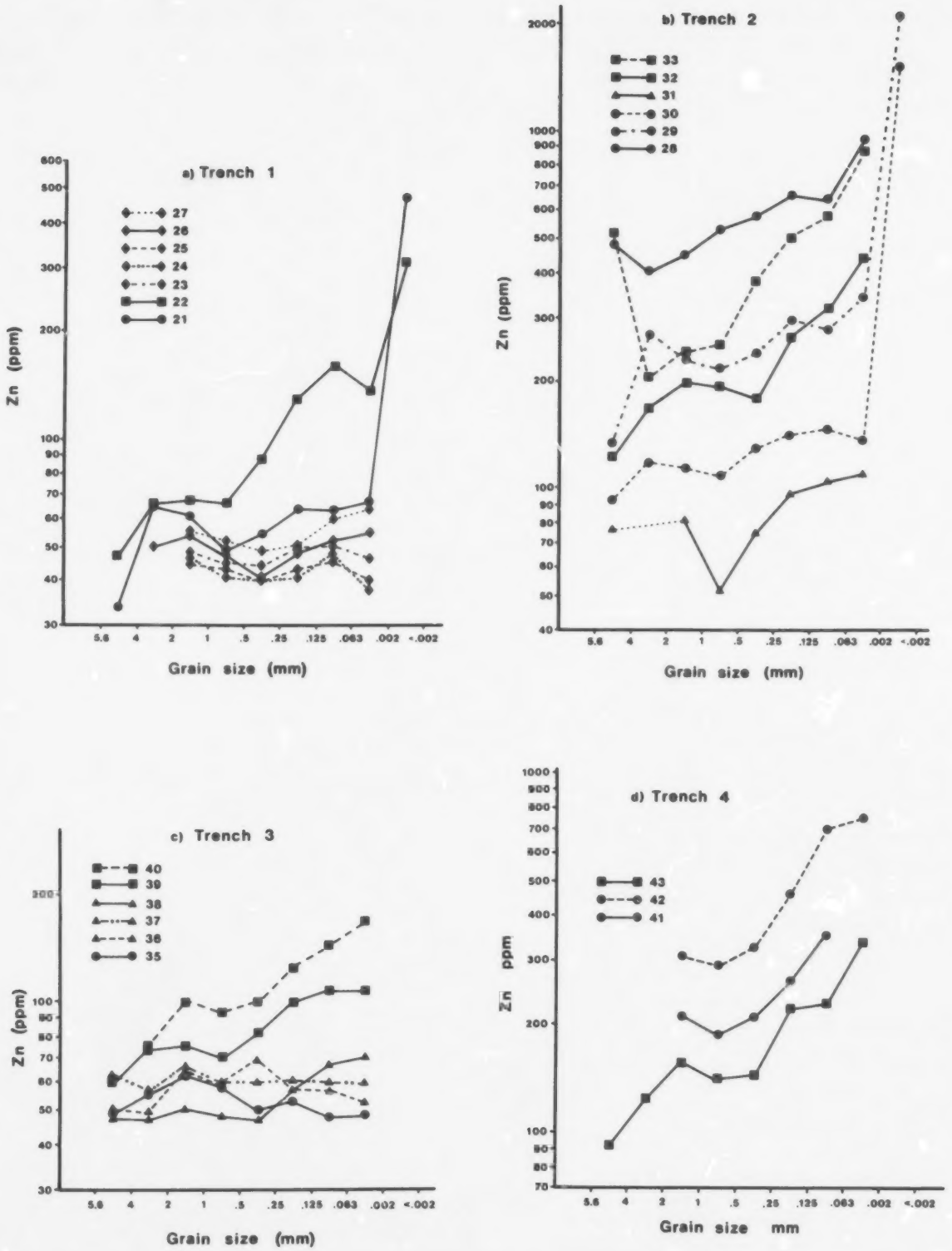

Figure 336.6. *Distribution of zinc in grain size fractions. Symbols represent sediment types as follows: circles = basal till, squares = supraglacial till, triangles = water-sorted sediments, diamonds = post-glacial fluvial deposits.*

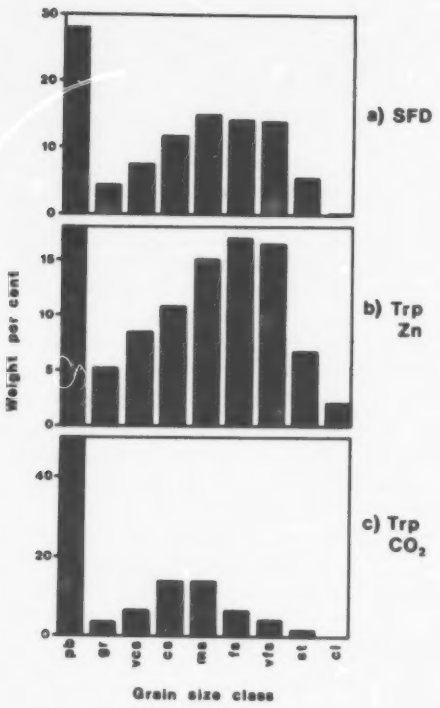

Figure 336.7. a) *Size frequency distribution (SFD) in basal till (sample 21).* b) *True relative percent (TRP) of zinc in sample 21.* c) *True relative percent of CO_2. Abbreviations are the same as those in Figure 336.2.*

Thus, although dolomitic marble is the host lithology for sphalerite, it does not appear to control the distribution of zinc in the various size fractions. No fresh sphalerite was observed in the fractions, indicating that grain size distribution of sphalerite inherited from the bedrock source is also not the controlling factor. True relative percents of zinc appear to correlate most closely with size frequency distributions in the sediments at this site.

PREDICTIONS

The differences in slope of the metal fractionation curves in Figure 336.6 may be due to differences in sedimentological processes. However, the slopes of the curves for the supraglacial till in trenches 1, 2 and 3 and for both the basal and supraglacial tills in trench 4 are similar. This similarity suggests that the slope of the curve is affected by the extent of weathering of the sediment (supraglacial till is stratigraphically higher and therefore subject to greater weathering than basal till except where drift is very thin). Similar distributions of gold (Gleeson *et al.* 1984) and palladium (DiLabio 1988) in size fractions of weathered till have been reported. At the Clyde River prospect, very highly weathered samples (41 to 43) contain fine-grained coatings of limonite on grains of all mineral species, in spite of wet-sieving of samples after dispersion in a deflocculant. Limonite is cryptocrystalline; concentrations of Fe_2O_3 (Table 336.2) indicate that limonite is volumetrically significant in the clay-sized fraction. Incorporation of zinc released during weathering into limonite may account for the very high concentrations of zinc in the clay fraction, as observed by Nikkarinen *et al.* (1984). It also accounts for the increasing zinc concentration with decreasing grain size, especially apparent in highly weathered samples, and the correlation between true relative percent of zinc and size frequency distribution. Grains in the finer fractions have greater surface area than the same weight of coarser grains, and therefore, may be coated by larger quantities of limonite. In less weathered samples, limonite generally is present as soft aggregates, rather than as coatings on all grains. These aggregates break down to clay-sized material during sample preparation; therefore, zinc is distributed uniformly among the coarser size fractions, and is enriched substantially in the clay fraction. Fluvial sediments were subjected to washing which destroyed the primary sulphides through oxidation during transport; therefore, they contain low concentrations of zinc.

We predict that slightly weathered basal till samples will exhibit an order of magnitude more zinc in the clay fraction than in the coarser fractions (5000–6000 ppm in sample 28, 500–600 ppm in sample 35). The clay fractions of the supraglacial till should exhibit approximately double the concentration of zinc in the silt fractions (800–1600 ppm in trench 2, 200–300 ppm in trench 3), as should those in trench 4 (700–1500 ppm). The water-sorted sediments have been reworked; therefore they are expected to exhibit a less pronounced increase in the clay fractions than the basal till (perhaps 200–400 ppm). The post-glacial fluvial sediments have been washed, and the concentrations of zinc in the bulk samples and size fractions are similar; therefore these sediments likely will not contain more than about 100 ppm Zn in the clay fractions. These predictions are based on few data; however, the predictions provide a testable hypothesis and a focus for further study.

CONCLUSIONS

Major and trace element compositions of bulk sediments at this site reflect stratigraphic variation defined by differences in provenance and sedimentology. In addition, weathering effectively has concentrated metals in some samples, by decreasing sediment volume. Although zinc has been released from primary sulphides during weathering, it appears to have been redistributed among the size fractions rather than removed in significant quantities from the bulk sediments.

All glacially deposited sediments at this site exhibit an overall increase in zinc content as a function

of decreasing grain size, whereas the fluvial sediments do not. The clay fractions of all sediments are enriched in zinc. The slopes of the metal fractionation curves are affected by the extent to which the sediments have been weathered. Slightly weathered basal sediments display curves with shallow positive slopes, and contain an order of magnitude more zinc in the clay fractions than in the silt fractions. Highly weathered sediments display curves with steep positive slopes, and contain twice as much zinc in clay fractions as in silt fractions.

In slightly weathered samples, limonite is present as soft aggregates and rarely coats other grains. In highly weathered samples, limonite coats and cements most grains, in spite of dispersion of samples in a deflocculant. This results in distribution of zinc throughout the size fractions, increasingly in finer size fractions which have greater surface area. Thus, weathering has resulted in an apparent redistribution of zinc among the size fractions. Although grains of sphalerite also may persist, the pronounced enrichment of zinc in the clay fraction suggests that zinc has been incorporated into limonite, which is volumetrically significant in the clay fraction.

IMPLICATIONS FOR MINERAL EXPLORATION

Drift prospecting may be an effective component of an exploration program if drift is sampled and analyzed systematically. As illustrated above, metal concentrations vary with sediment type. Therefore, field descriptions which include colour, structure, texture, compactness, depth, and degree of weathering of samples are valuable. The possibility that metals may be concentrated by weathering indicates that fresh sediments should be sampled in order to obtain accurate compositional data. However, this is not always possible, as at the Clyde River prospect.

If fresh drift is available for sampling, it may be useful in orientation surveys to analyze all size fractions, which may indicate metal residence sites in the host rock (DiLabio 1988). This approach is not practical for detailed sampling programs, however. In addition, the availability of unweathered drift is limited. The choice of a suitable size fraction for analysis is made difficult by the effect of weathering on metal fractionation. Highly weathered samples exhibit higher concentrations of zinc in silt and fine-sand sizes (relative to concentrations in bulk samples) than less weathered samples. Therefore, in a mixed population of weathered and unweathered sediments, analysis of the traditional <177 µm (<80 mesh) fraction may yield misleading results. Clay fractions of till at the Clyde River prospect exhibit pronounced enrichment of zinc; however, Nikkarinen *et al.* (1984) stated that clay fractions of fresh till are not strongly enriched in zinc. Therefore, analysis of clay-sized material, as suggested by Shilts (1984), also may be inappropriate. In addition, tills on the Canadian Shield generally are sandy, necessitating large sample size in order to provide sufficient clay-sized material for analysis. Since weathering apparently results in redistribution rather than removal of zinc, analyses of bulk samples may provide a more reliable indication of relative zinc content.

FUTURE WORK

1. Wet chemical analyses of bulk samples will be carried out. Major and trace element analyses of clay and pebble fractions present in insufficient quantities for XRF analyses will be carried out using secondary ion mass spectrometry (SIMS). The results will be compared with predicted compositions.
2. Clay fractions will be examined using SIMS, to determine the siting of metals (i.e., in secondary oxides/hydroxides/carbonates or adsorbed onto clay mineral surfaces).
3. Analyses of metalliferous drift from other regions will be examined in order to test predictions based on these data.

ACKNOWLEDGMENTS

This study is part of an in-progress MSc thesis project by the first author. The authors are grateful to R.N.W. DiLabio of the Geological Survey of Canada (Ottawa) for assistance with sampling, enlightening discussions and comments on the manuscript. Capable technical assistance was provided by Tsai-Way Wu, Bob Barnett, Dave Kingston, Mike Powell, Yu Chi Cheng, John Forth and Walt Harley of the Geology Department, University of Western Ontario, Ross Davidson of Surface Science Western, and Peter Belanger and Miriam Wygergangs at the Geological Survey of Canada. Norval Wilson of Hopetown, Ontario, kindly permitted sampling to be carried out on the property.

REFERENCES

Ayras, M.
1977: Statistical Observations on the Element Distribution in the Fine Material of Till, Sodankyla, Northern Finland; Geological Survey of Finland, Report of Investigation 14, 41p.

Brown, A.C.
1976: The Long Lake Zinc Mine, Frontenac County, Ontario; Exploration Research Institute, Montreal, Case History 76-2, 32 p.

Carter, T.R., Colvine, A.C. and Meyn, H.D.
1980: Geology of Base Metal, Precious Metal, Iron, and Molybdenum Deposits in the Pembroke-Renfrew Area; Ontario Geological Survey, Mineral Deposits Circular 20, 186p.

DiLabio, R.N.W.
1979: Drift Prospecting in Uranium and Base-Metal Mineralization Sites, District of Keewatin, Northwest Territories, Canada; p. 91-100 *in* Prospecting in Areas of Glaciated Terrain 1979, Institution of Mining and Metallurgy, London.

1982: Gold and Tungsten Abundance vs. Grain Size in Till at Waverley, Nova Scotia; p.57-62 *in* Current Research, Part B, Geological Survey of Canada, Paper 82-1B.

1985: Gold Abundances vs. Grain Size in Weathered and Unweathered Till; p.117-122 *in* Current Research, Part A, Geological Survey of Canada, Paper 85-1A.

1988: Residence Sites of Gold, PGE, and Rare Lithophile Elements in Till; p.121-140 *in* Prospecting in Areas of Glaciated Terrain—1988, edited by D.R. MacDonald and K.A. Mills, Canadian Institute of Mining and Metallurgy.

DiLabio, R.N.W., Rencz, A.N. and Eggington, P.A.

1982: Biogeochemical Expression of a Classic Dispersal Train of Metalliferous Till near Hopetown, Ontario; Canadian Journal of Earth Sciences, Volume 19, p.2297-2305.

Dreimanis, A.

1988: Tills: Their Genetic Terminology and Classification; p.17-83 *in* Genetic Classification of Glacigenic Deposits, edited by R.P. Goldthwait and C.L. Matsch, Balkema, Rotterdam.

In Press: Formation, Deposition, and Identification of Subglacial and Supraglacial Tills; *in* Handbook of Glacial Indicator Tracing, edited by R.Kujansuu and M. Saarnisto, Balkenia, Rotterdam.

Dreimanis, A., Hamilton, J.P. and Kelly, P.E.

1986: Complex Subglacial Sedimentation of Catfish Creek Till at Bradtville, Ontario, Canada; p.73-87 *in* Tills and Glaciotectonics, edited by J.J.M. Van Der Meer, Balkema, Rotterdam.

Dreimanis A. and Vagners, U.J.

1971: Bimodal Distribution of Rock and Mineral Fragments in Basal Tills; p.237-250 *in* Till—A Symposium, edited by R.P. Goldthwait, Ohio University Press, Columbus.

Gadd, N.R.

1980: Late-Glacial Regional Ice-Flow Patterns in Eastern Ontario; Canadian Journal of Earth Sciences, Volume 17, p.1439-1453.

Gauthier, M. and Brown, A.C.

1980: Lithologic and Stratigraphic Setting of Zinc Mineralization in Grenville Metasediments, Quebec; Mineralium Deposita, Volume 15, p.163-174.

Gleeson, C.F., Rampton, V.N., Thomas, R.D. and Paradis, S.

1984: Development and Adaptation of Geochemical Techniques to Gold Exploration in Glacial Drift; Ontario Geological Survey, Miscellaneous Paper 120, p.129-149.

Haldorsen, S.

1977: The Petrography of Tills—a Study from Ringsaker, South-Eastern Norway; Norges Geologiske Undersokelse, Nr. 336, 36p.

Klassen, R.A. and Shilts, W.W.

1977: Glacial Dispersal of Uranium in the District of Keewatin, Canada; p.80-88 *in* Prospecting in Areas of Glaciated Terrain 1977, Institution of Mining and Metallurgy, London.

MacEachern, I.J. and Stea, R.R.

1985: The Dispersal of Gold and Related Elements in Tills and Soils at the Forest Hill Gold District, Guysborough County, Nova Scotia; Geological Survey of Canada, Paper 85-18, 31p.

Nikkarinen, M., Kallio, E., Lestinen, P. and Ayras, M.

1984: Mode of Occurrence of Cu and Zn in Till over Th[illegible] Mineralized Areas in Finland; Journal of Geochemical Exploration, Volume 21, p.239-247.

Pettijohn, F.J.

1957: Sedimentary Rocks; Harper and Brothers, New York, 718p.

Reinhardt, E.W.

1973: Geology, Carleton Place, Ontario; Geological Survey of Canada, Map 1362A.

Shelp, G.S. and Nichol, I.

1987: Distribution and Dispersion of Gold in Glacial Till associated with Gold Mineralization in the Canadian Shield; p.315-336 *in* Geochemical Exploration 1985, edited by R.G. Garrett, Journal of Geochemical Exploration, Volume 28.

Shilts, W.W.

1973: Drift Prospecting: Geochemistry of Eskers and Till in Permanently Frozen Terrain, District of Keewatin, Northwest Territories; Geological Survey of Canada, Paper 72-45, 34p.

1984: Till Geochemistry in Finland and Canada; Journal of Geochemical Exploration, Volume 21, p.95-117.

Sinclair, I.G.L.

1979: Geochemical Investigation of the Clyde River Zinc Prospect, Lanark County, Ontario; p.487-495 *in* Geochemical Exploration 1978, edited by J.R. Watterson and P.K. Theobald, Association of Exploration Geochemists.

1986: The Use of Till Geochemistry as an Exploration Tool in Southeastern Ontario; Canadian Insitute of Mining and Metallurgy, Bulletin, Volume 79, p.75-78.

Vagners, U.J.

1969: Mineral Distribution in Tills of Southcentral Ontario; unpublished PhD Thesis, University of Western Ontario, London, Ontario, 277p.

Grant 341 PGE Study of the Geordie Lake and Marathon Cu–Ni–Precious Metal Deposits, Coldwell Alkalic Complex

D.J. Good and J.H. Crocket

Geology Department, McMaster University, Hamilton

ABSTRACT

The Geordie Lake gabbro contains several zones of Cu-sulphide mineralization associated with platinum-group element (PGE) mineralization. The mineralization occurs on both sides of a later crosscutting quartz syenite sill. A cross section of the gabbro shows a cyclical trend for trace element abundances indicative of periodic recharging of a crystallizing magma chamber. Mineralized samples are geochemically similar to unmineralized samples. Petrologically the mineralized samples are heterogeneous in grain size and composition, and commonly contain plagioclase which is rimmed or partially replaced by a symplectic growth of feldspar+clinopyroxene. Similar symplectic growths occur in the more fractionated unmineralized gabbro samples. There is no apparent relationship between the degree of alteration and the mineralized zones. For sulphide-bearing samples the Cu/Cu+Ni and Pd/Pt ratios are 0.919 ± 0.074 and 17.1 ± 6.3, respectively. The range of sulphur isotope values is between −1.75‰ and 2.77‰ and the average is 0.4‰. These observations are consistent with a model which involves the localized intrusion of evolved melts into partially crystallized cumulate layers. The evolved melt and crystalline pile must have been derived from the same parent magma. Sulphide saturation probably occurred late in the crystallization history of the intrusion allowing for considerable fractionation of Cu from Ni and perhaps Pd from Pt. There is, as yet, no evidence for the evolution of a volatile phase.

INTRODUCTION

This report summarizes the work completed during the first year of a project funded by Ontario Geoscience Research Grant 341. The project is a comparative study of platinum-group element (PGE) mineralization from within and at the intrusive margin of the Coldwell Alkalic Complex near Marathon, Ontario. Improved exploration strategies for evaluation of alkalic complexes for PGE mineralization should follow from an evaluation of the relative importance of magmatic and hydrothermal processes in transportation and concentration of PGE in alkalic complexes.

The deposits examined (Figure 341.1) are the Marathon deposit (Fleck Resources Ltd.) in the Two Duck Lake gabbro or the eastern margin of the Coldwell intrusion, and the MacRae occurrence within the Geordie Lake gabbro located well within the complex.

Figure 341.1. *Location map for the MacRae occurrence within the Geordie Lake gabbro and the Fleck deposit within the Two Duck Lake gabbro. The gabbroic bodies are relatively small segments of the larger Coldwell Alkalic Complex.*

To date, work has focussed on petrology and trace and major element analyses of the Two Duck Lake and Geordie Lake gabbros, and analyses for sulphur isotopes in the associated sulphides. Presented in this paper are the data and interpretation for the Geordie Lake gabbro and the sulphur isotope data for both deposits. An interpretation for the Two Duck Lake gabbro will follow in a later report.

GEOLOGY OF THE GEORDIE LAKE PROPERTY

A plan view of the geology of the Geordie Lake property is presented in Figure 341.2. The gabbroic and syenitic sills strike approximately north and dip moderately west. The mineralized zone lies within the Geordie Lake gabbro close to both the east and west contacts of the quartz syenite sill. Figure 341.3 is a detailed map of an outcrop located on Figure 341.2.

The quartz syenite sill intruded the Geordie Lake gabbro. Evidence for the relative timing of intrusion includes a decrease in grain size of the quartz syenite from very coarse grained in the centre of the

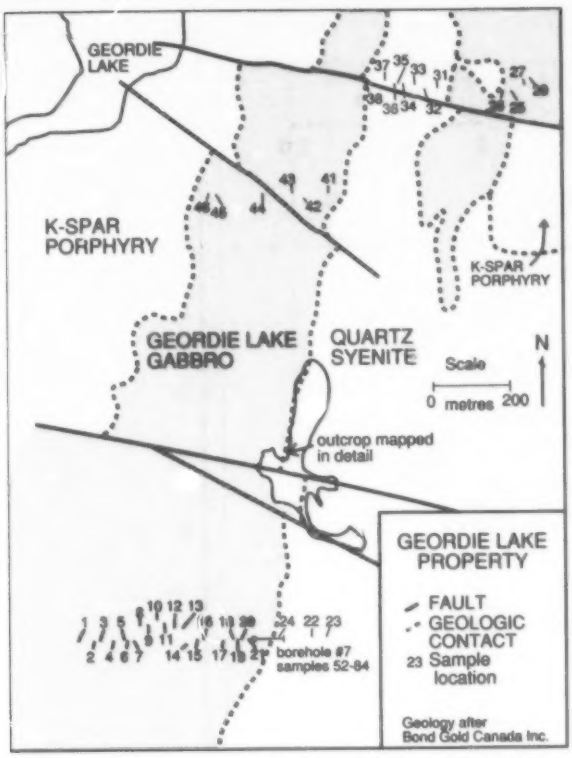

Figure 341.2. *Geology of the Geordie Lake property showing sample sites and the location of the outcrop mapped in detail shown in Figure 341.3. (After private company report by Bond Gold Canada Inc., Resident Geologist's files, Thunder Bay.)*

sill to fine grained at the contacts. There is no such systematic grain size change in the gabbro. More importantly, the gabbroic bodies at the east and west contacts of the syenite are geochemically and petrographically identical.

CIPW normative composition, combined with the igneous rock classification of Streckeisen (1976), is a useful means of grouping the rock types in the Geordie Lake gabbro. The normative abundances are in approximate agreement with estimated modal abundances, but there are some exceptions, e.g., no modal nepheline has, as yet, been identified. Despite some limitations the CIPW norms prove to be most useful for categorizing rocks with similar whole-rock major element abundances. This classification is further verified by similarities in trace element abundances and petrographic textures as described below.

A geochemical cross section of the Geordie Lake intrusion is presented in Figures 341.4a,b,c. Sample sites are located in Figure 341.2. Note that although all of the gabbroic rocks contain approximately 5–10% normative magnetite, 2–15% normative orthoclase and 1–5% normative apatite, the prefixes magnetite, monzo and apatite-bearing have been omitted from the rock names for simplicity.

Olivine gabbro is the most abundant rock type in the Geordie Lake gabbro. In general, the primary mineralogy consists of subhedral plagioclase and olivine, subophitic clinopyroxene, subhedral magnetite, and euhedral apatite. Textural relationships suggest apatite, olivine, magnetite, and plagioclase were contemporaneous cumulate phases, whereas clinopyroxene was post-cumulate. There are, however, some notable differences in textures between individual rock units of similar mineralogy which correspond to differences in trace element concentrations. For one, clinopyroxene in the entire section of olivine gabbro in Figure 341.4a (except samples 1 and 21) is not subophitic as in most of section 4b, rather it is subhedral and contains inclusions of apatite and magnetite only. The subhedral nature indicates early growth of clinopyroxene contemporaneous with olivine.

Another textural difference between the gabbros of Figures 341.4a and b is the common occurrence in the former section of aligned plagioclase laths which form a lineation approximately parallel to the dip direction of the basal contact.

There are, however, some similarities between samples from the two sections. Two samples of olivine gabbro (samples 80 and 1, Figures 341.4a and b) exhibit a symplectic relationship between clinopyroxene and feldspar (Photo 341.1) which may represent *in situ*, cotectic crystallization. These samples have trace element abundances higher, and presumably more fractionated, than other olivine gabbros.

Mineralized samples commonly contain plagioclase laths which are rimmed and partially replaced by symplectic feldspar+clinopyroxene (e.g., sample 65, Photo 341.2) similar to that found in samples 80 and 1, described above. Sample 65 contains lower trace element concentration than 80 and 1, and is, therefore, presumably less fractionated.

Two other samples of olivine gabbro (59 and 60; Figure 341.4b) contain elongated hopper olivine crystals which are intergrown with plagioclase (Photo 341.3). The two samples have lower trace element concentrations, lower normative albite contents and higher normative forsterite contents than the average olivine gabbro. Perhaps this texture is indicative of the least fractionated samples. Hopper olivine texture is not uncommon in layered intrusions and was described by Donaldson (1982) in the Rhum intrusion.

In other samples from Figures 341.4a–d the only significant difference between olivine gabbro and gabbro is that the latter contains less olivine and proportionately more clinopyroxene. Mela-olivine gabbro is distinguished by poikilitic olivine up to 2 cm in size.

Nepheline-bearing olivine gabbro and mela-olivine gabbro are essentially olivine+magnetite cumulates with subophitic plagioclase and subophitic to poikilitic clinopyroxene.

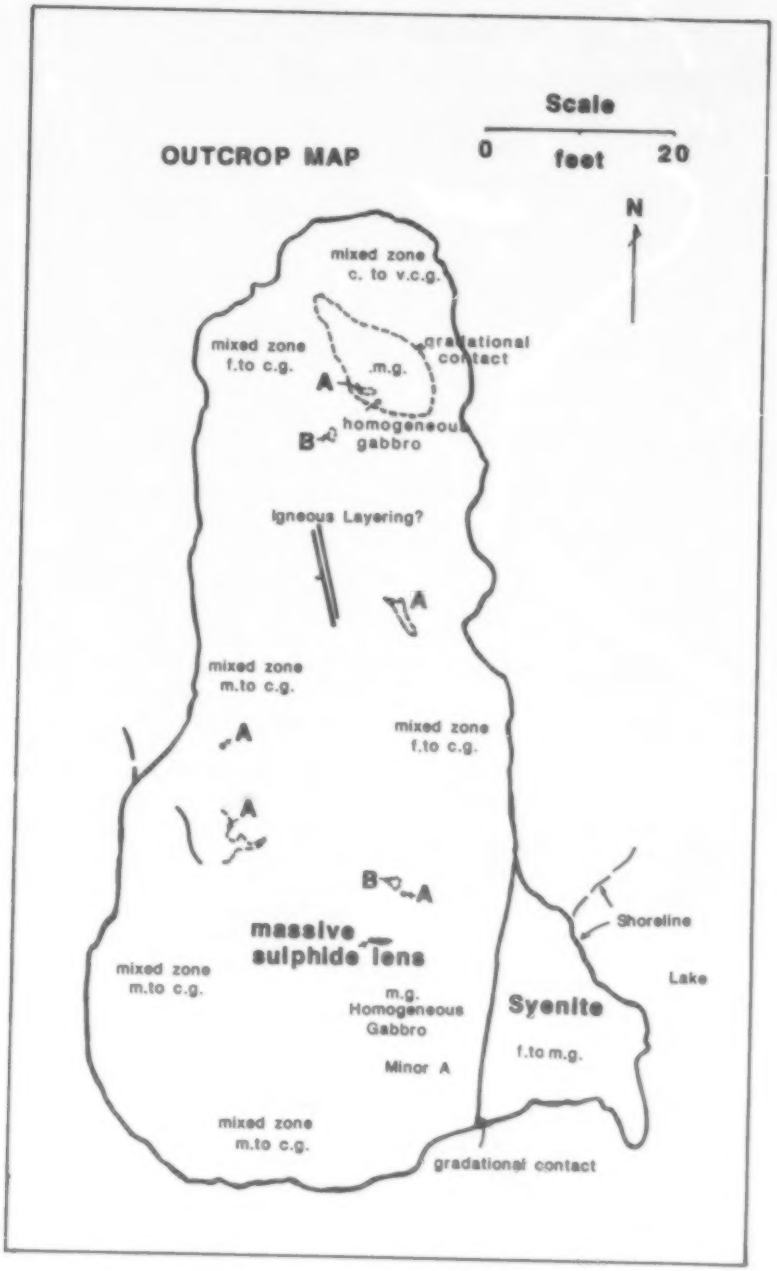

Figure 341.3. *Outcrop within the mineralized zone along the gabbro-quartz syenite contact. Areas labelled with 'A' or 'B' indicate pods of sulphide mineralization. Those labelled 'A' are zoned, irregularly shaped pods or dikelets, ranging in size from centimetres to metres. The centres of the zoned pods consist of fine- to medium-grained pink granular feldspar. The abundance of granular feldspar decreases rapidly away from the centres of the pods, giving way to coarse-grained subhedral plagioclase and anhedral hornblende which grades to medium-grained clinopyroxene+plagioclase. Areas marked 'B' indicate pods of coarser grained gabbro associated with sulphide and magnetite.*

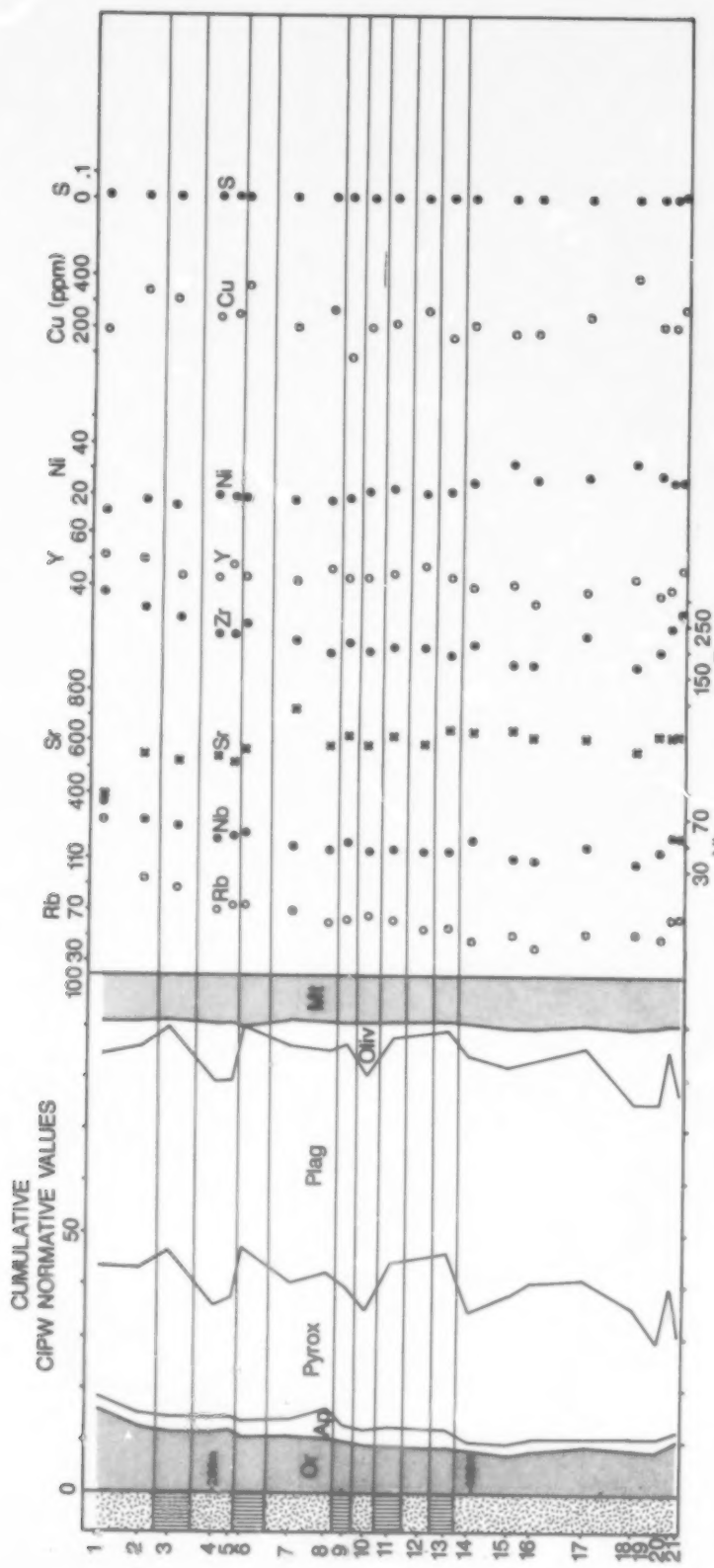

Figure 341.4a. *Geochemical cross-sections of the Geordie Lake gabbro. Sample sites are located in Figure 341.2. Samples were collected from outcrop. Rock types are based on the CIPW normative mineral abundances. The stipled zones outline sections of olivine gabbro; vertical hatching represents gabbro; horizontal hatching mela-olivine gabbro; left dipping hatching nepheline-bearing olivine gabbro; and right dipping hatching nepheline-bearing mela-olivine gabbro.*

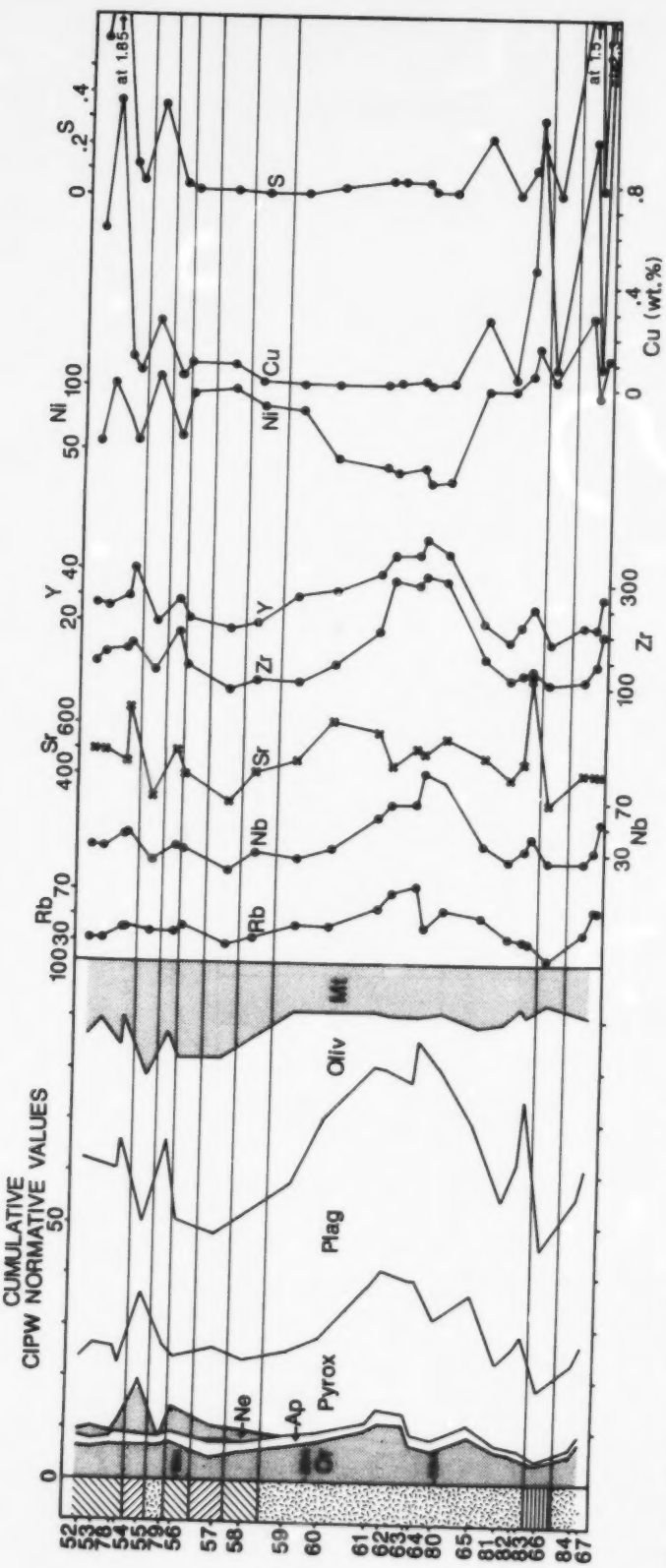

Figure 341.4b. *Geochemical cross-sections of the Geordie Lake gabbro. Sample sites are located in Figure 341.2. Samples were collected from diamond-drill core. Rock types are based on the CIPW normative mineral abundances. The stipled zones outline sections of olivine gabbro; vertical hatching represents gabbro; horizontal hatching mela-olivine gabbro; left dipping hatching nepheline-bearing olivine gabbro; and right dipping hatching nepheline-bearing mela-olivine gabbro.*

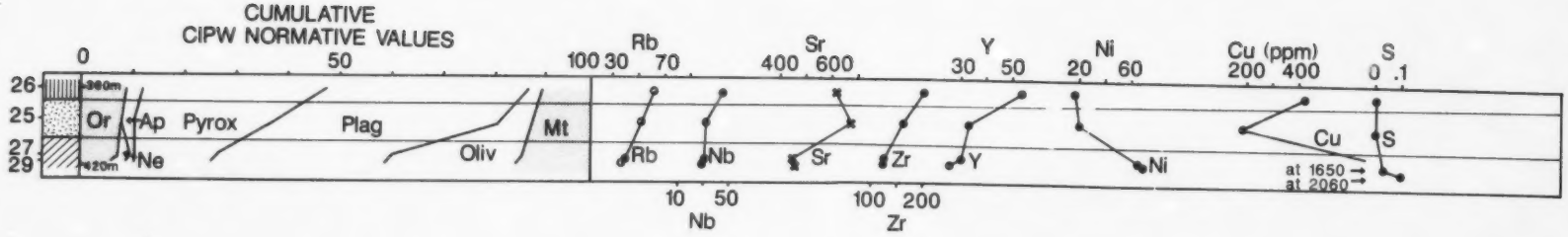

Figure 341.4c. *Geochemical cross-sections of the Geordie Lake gabbro. Sample sites are located in Figure 341.2. Samples were collected from outcrop. Rock types are based on the CIPW normative mineral abundances. The stipled zones outline sections of olivine gabbro; vertical hatching represents gabbro; horizontal hatching mela-olivine gabbro; left dipping hatching nepheline-bearing olivine gabbro; and right dipping hatching nepheline-bearing mela-olivine gabbro.*

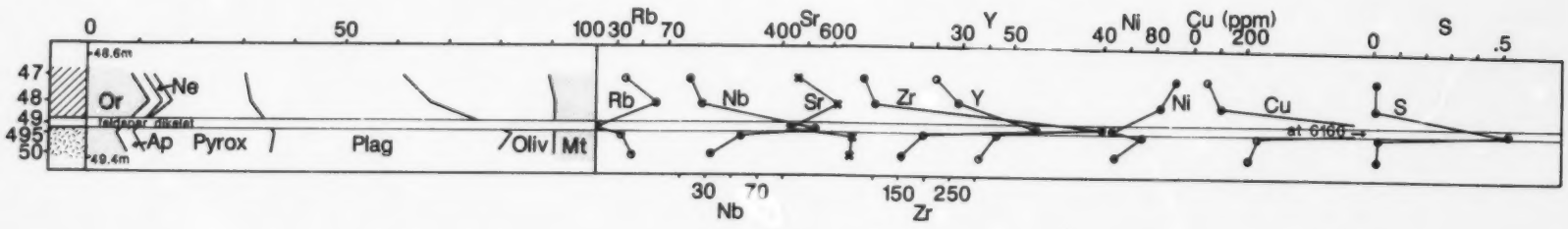

Figure 341.4d. *Geochemical cross-sections of the Geordie Lake gabbro. Sample sites are located in Figure 341.2. Samples were collected from diamond-drill core. Rock types are based on the CIPW normative mineral abundances. The stipled zones outline sections of olivine gabbro; vertical hatching represents gabbro; horizontal hatching mela-olivine gabbro; left dipping hatching nepheline-bearing olivine gabbro; and right dipping hatching nepheline-bearing mela-olivine gabbro.*

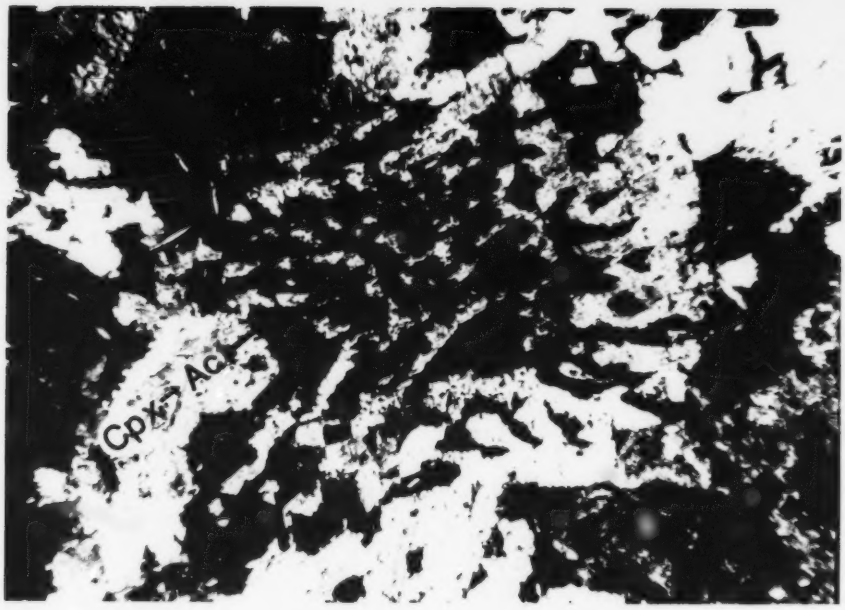

Photo 341.1. *Symplectic growth of feldspar and clinopyroxene in sample 1. The clinopyroxene is partially to completely altered to actinolite. Length of photo is 8 mm.*

Photo 341.2. *Mantling of plagioclase by symplectic feldspar+clinopyroxene in sample 65. The clinopyroxene is partially to completely altered to actinolite. Length of photo is 4 mm.*

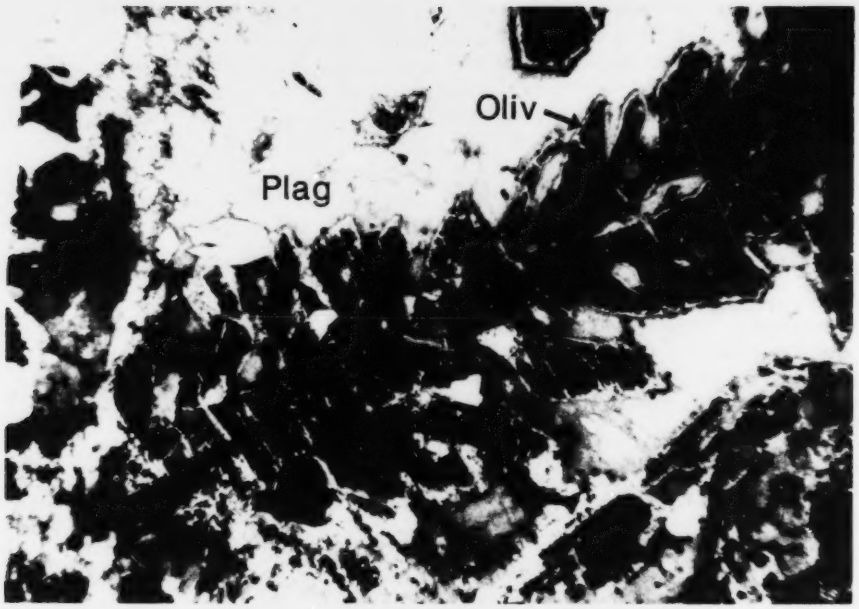

Photo 341.3. *Large, single, elongated hopper olivine intergrown with plagioclase in sample 59. Length of photo is 9 mm.*

Photo 341.4. *Mantling and partial replacement of plagioclase by symplectic feldspar+clinopyroxene in sample 52. Length of photo is 2.5 mm.*

Quartz syenite comprises perthitic orthoclase and lesser plagioclase+quartz, and minor, apparently secondary magnetite, amphibole and epidote. The mafic minerals occur in micro-veinlets and fractures. All of the observed sulphide mineralization in the quartz syenite is associated with these micro-veinlets and fractures. Close to the contact with the Geordie Lake gabbro, feldspar crystals in the syenite are overprinted by a 'net-like' pattern of micro-veinlets filled by an assemblage of indistinguishable secondary minerals. The deep red colour of the syenite is attributed to a pervasive distribution of <1 μm sized hematite flakes.

ALTERATION

Alteration of the primary mineralogy is similar in both degree and style across the Geordie Lake gabbro. There is no apparent relationship between the degree of alteration and the mineralized zones.

Clinopyroxene is variably altered to green actinolite and minor brown hornblende. Olivine is moderately to strongly altered to very fine aggregates of magnetite plus one or more of actinolite, chlorite or serpentine. Fresh olivine is uncommon, but olivine pseudomorphs are easily recognizable. Plagioclase is variably altered to sericite and commonly exhibits reddish-pink, cloudy patches or rims caused by concentrations of <1 μm sized hematite flakes.

GEOCHEMICAL TRENDS

The close resemblance of trace element abundances in samples of similar rock type from Figures 341.4a–d show that magmatic processes could be solely responsible for the distribution of rock types across the intrusion. This point is emphasized in order to downplay the role of metasomatism which could presumably be used to account for the mineralization event.

In these diagrams (Figures 341.4a–d) care must be taken to distinguish trace element trends which are produced by fractionation from those which are due to changes in the abundance of major minerals, i.e., changes in the bulk partition coefficients. An example of the problem in determining which process is dominant is the decrease in the trace element abundance from samples 63 and 64 to 57 and 58. This could be explained either by the large increase in the amount of normative olivine and decrease in plagioclase or by fractionation. In this section actual mineral compositions will have to be determined in order to depict fractionation trends.

In Figure 341.4a the trends of trace element enrichment or depletion across a 460 m thick sequence of gabbro and olivine gabbro correspond to those expected in a fractionating magma chamber. The incompatible elements Rb, Nb, Zr, Y and Cu all increase from the bottom to top, whereas the compatible elements Ni and Sr decrease. Surprisingly Nb, which is compatible in ilmenomagnetite, increases indicating its bulk partition coefficient must be less than 1.

The Cu and Ni concentrations are decreasing and increasing, respectively, from the bottom to top in the section in Figure 341.4a. Recall that this section is only a portion of the section across the entire intrusion. This trend is expected in a crystallizing magma chamber unsaturated in sulphides since Ni is compatible in olivine and clinopyroxene whereas Cu is strongly incompatible in silicates. This trend is dramatically different from that in the underlying sulphide-bearing layers.

In Figures 341.5a–c, Zr, Y and Nb are plotted against each other to show their near-coherent behaviour during fractionation in the magma chamber. The fields for two of the rock types, i.e., rock units which have similar bulk partition coefficients, are indicated to show the dependability of these diagrams in determining a priori values for some trace element concentrations.

Mineralized samples are also indicated in Figures 341.5a–c by the solid symbols. Note that the mineralized samples are evenly distributed among the unmineralized samples.

In Figure 341.5d Rb is plotted against Zr. The importance of this plot is to show that the mineralized samples (filled symbols) have Rb concentrations similar to unmineralized samples. If mineralization was related to metasomatism then one would expect that Rb, which is a relatively mobile element, would be systematically enriched or depleted with respect to the magmatic trend.

In Figure 341.5e Zr is plotted against the normative plagioclase content. The normative plagioclase content is a sensitive indicator of Na addition to the whole rock composition above what is normal for the degree of fractionation. Like Rb, Na is relatively mobile and susceptible to alteration. This diagram, like Figure 341.5e, indicates that mineralized samples are similar to unmineralized samples, and there is no evidence of metasomatism.

SULPHIDE-SILICATE RELATIONSHIPS

In the vicinity of sulphide mineralization, plagioclase, regardless of rock type, is commonly rimmed by feldspar and symplectic feldspar+clinopyroxene (Photos 341.4 and 341.2). These rims are apparently more susceptible to secondary alteration and, like the quartz syenite, are stained red by hematite flakes less than 1 μm in size. Rimmed plagioclase occurs in zones or patches commonly associated with gabbro of heterogeneous grain size and small pods or dikelets of fine- to medium-grained, equigranular orthoclase+plagioclase. These thin pods or dikelets of feldspar are commonly the focus of sulphide mineralization.

Figure 341.4d is a section across 1 m of a sulphide mineralized zone passing from olivine gabbro

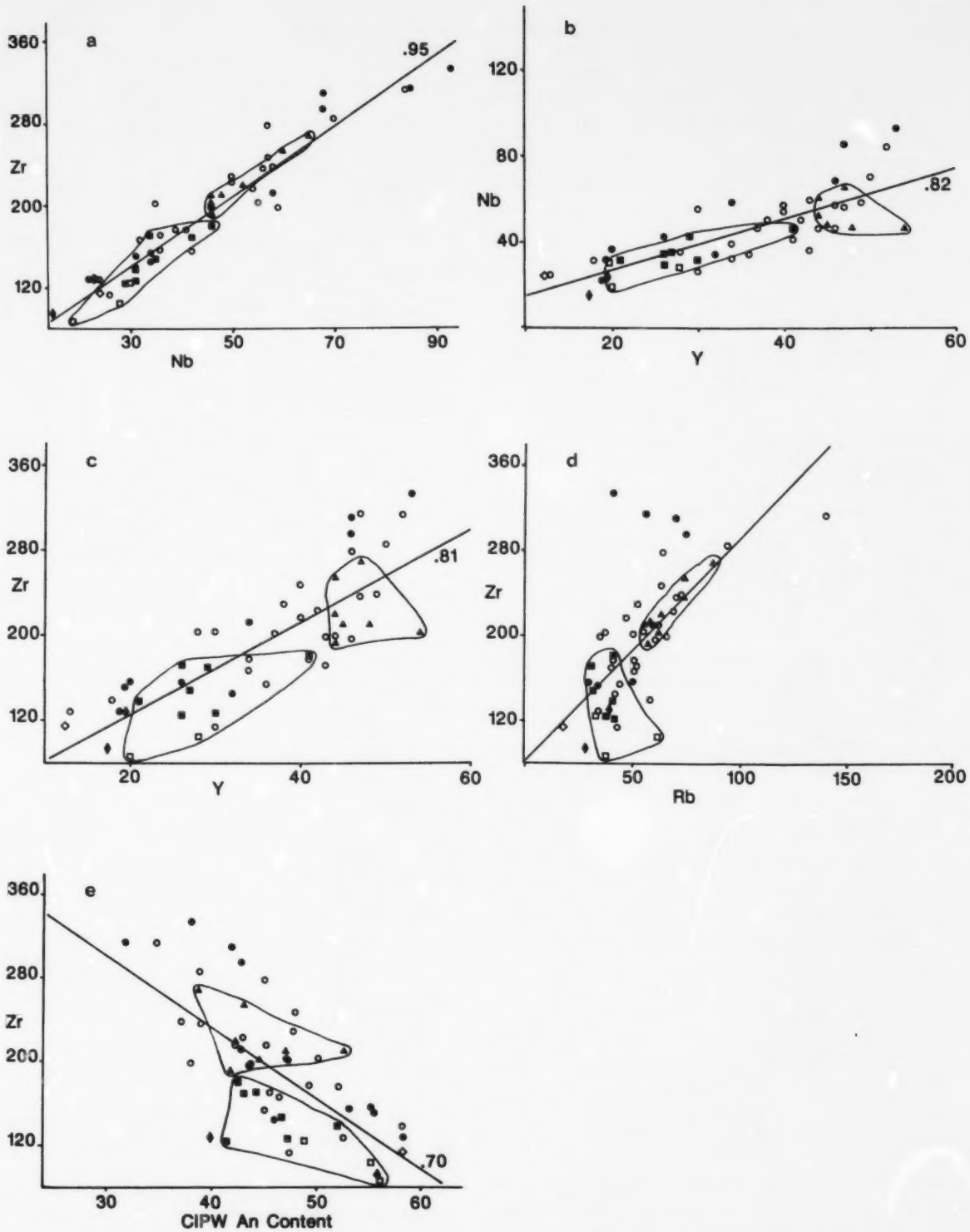

Figure 341.5. (a) – (d) *Trace element variation diagrams for all of the gabbroic samples shown in Figure 341.4.* (e) *Plot of Zr against normative plagioclase content for all of the gabbroic samples. Circles represent samples of olivine gabbro; triangles, gabbro; rotated square, mela-olivine gabbro; diamonds, nepheline-bearing mela-olivine gabbro; and squares, nepheline-bearing olivine gabbro. The filled symbols indicate samples with sulphide mineralization.*

(samples 495 and 50) with patches of rimmed plagioclase to a thin feldspar dikelet (sample 49) to nepheline-bearing olivine gabbro without rimmed plagioclase (samples 47 and 48). This section is important because it shows large variations in rock types across only 1 m and also shows that the abundance of trace elements in each of the gabbroic rocks is similar to the abundance in similar gabbroic rock types in unmineralized areas.

SULPHIDE MINERALIZATION

Sulphide mineralization occurs in the quartz syenite, and both east and west bodies of the Geordie Lake gabbro. To date the most significant zone lies within the western Geordie Lake gabbro along its contact with the quartz syenite.

Within the Geordie Lake gabbro there are three common sulphide mineral associations. These are 1) pervasive, trace, disseminated chalcopyrite; 2) fine- to medium-grained disseminated chalcopyrite-rich blebs; and 3) massive, stringer sulphides.

Throughout the unmineralized samples (e.g., samples 1 to 21) are <1 μm sized grains of chalcopyrite. This is attributed to localized post-cumulus diffusion of S and Cu from the trapped cooling magma to form the small grains.

The dominant form of sulphide mineralization is disseminations of chalcopyrite within heterogeneous gabbro, as described in the above section. Associated with the chalcopyrite is a large variety of tellurides, sulpharsenides and platinum-group minerals (Mulja and Mitchell 1988).

Massive stringer sulphides are uncommon and occur mainly along the contact with the quartz syenite. This form of sulphide mineralization could have resulted from late remobilization of the sulphides during cooling in the magma chamber or during the intrusion of the quartz syenite.

Sulphide mineralization within the eastern portion of the Geordie Lake gabbro is similar to that in the western portion.

Sulphide mineralization within the quartz syenite is associated with the mafic alteration mineral assemblage and occurs within blebs, fractures and microveinlets.

SULPHUR ISOTOPES

Sulphur isotope compositions were determined for sulphide mineralization in both the Geordie Lake and Fleck properties and are presented in Figure 341.6. Values are reported in per mil relative to the CDT standard.

At the Geordie Lake property, compositions were determined for the disseminated and stringer sulphide occurrences within the Geordie Lake gabbro and also the stringer and blebby sulphides within the quartz syenite. There is no distinguishable difference in sulphur isotopic values between any of these mineralized settings.

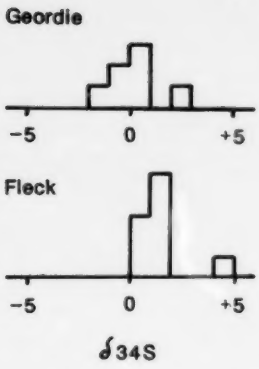

Figure 341.6. *Sulphur isotope compositions (per mil) for mineralized samples in the Fleck deposit and Geordie Lake gabbro.*

The values are equivalent to those expected for sulphur which was derived from the mantle. This is contrary to values determined in several sulphide-bearing major intrusive complexes, e.g., the Duluth, Sudbury, Noril'sk, and Bushveld igneous complexes, as summarized by Ohmoto (1986). For each of these intrusions the sulphur is thought to have been derived by assimilation from the country rock.

The tight grouping and primitive mantle signature of the sulphur isotope values suggests that the sulphur was mantle-derived. If this is so then sulphur saturation in the magma chamber may have been achieved at some point during crystal fractionation, perhaps by a combination of increasing sulphur concentration, decreasing temperature and/or a change in oxygen fugacity. Alternatively, it is possible that sulphur with mantle-like isotopic values from the Archean basement could have been assimilated during intrusion. However, the similar ranges of values for both deposits and the apparent association between sulphides and rather evolved magmas suggests that the former interpretation is more likely.

ORIGIN OF SULPHIDE MINERALIZATION

A model for sulphide mineralization in the Geordie Lake gabbro will have to account for the following observations:

1. The Cu/Cu+Ni ratio of all samples (n=24) containing greater than 0.2 weight percent S is 0.919±0.074. The Pd/Pt ratio for all samples (n=203) analysed by Bond Gold Canada Inc. (private company report, Resident Geologist's files, Ontario Ministry of Northern Development and Mines, Thunder Bay) with greater than approximately 50 ppb Pd is 17.1±6.3.

2. Sulphur isotope values for the Geordie Lake gabbro sulphides are all close to primitive mantle values.

3. Sulphide mineralization occurs in virtually all of the major rock types.

4. The geochemistry and mineralogy of the mineralized zones cannot be distinguished from that of unmineralized gabbro elsewhere in the Geordie Lake gabbro.

5. The grain size of gabbro associated with feldspar dikelets and pods in mineralized zones is heterogeneous.

6. In the vicinity of sulphide mineralization, plagioclase, regardless of rock type, is commonly rimmed by a symplectic intergrowth of feldspar and clinopyroxene. In absence of sulphides, similar symplectic relationships are only seen in the more fractionated gabbroic samples.

DISCUSSION

At this time we propose that the model which best fits all of the observations should involve the localized intrusion of evolved melts into partially crystallized cumulate layers. The evolved melt and crystalline pile must have been derived from the same parent magma. There is, as yet, no evidence for the evolution of a volatile phase.

With this model the partial replacement and rimming of plagioclase by the symplectic feldspar+clinopyroxene could then be explained by the disequilibrium between the evolved melt and early plagioclase. Also, the distribution of mineralized samples along the curves in Figures 341.5a–e would be akin to a straight mixing relationship.

The primitive mantle sulphur values and highly evolved Pd/Pt and Cu/Ni ratios would be expected in a magma whereby S saturation occurs late in the crystallization history. That the gabbros in Figure 341.4a (samples 1 to 21) exhibit fractionation of Cu from Ni is good evidence of significant fractionation of the magma prior to sulphur saturation.

The tight grouping of Cu/Ni and Pd/Pt ratios is typical of sulphides derived by magmatic processes in absence of hydrothermal fluids. Magmatic sulphides deposited in association with hydrothermal fluids typically have greater ranges for these ratios (e.g., Lac des Isles, Lawson and Macdonald 1987). Magmatic sulphides which are remobilized by hydrothermal fluids also tend to have widely varying ratios (e.g., Kanichee intrusion, Good 1988). As well, evidence of alteration related to hydrothermal fluids, as seen in the latter two deposits, is lacking in the Geordie Lake gabbro occurrence.

IMPORTANCE OF APATITE

Apatite occurs throughout the Geordie Lake gabbro as fine, euhedral cumulate grains included in clinopyroxene and less commonly in plagioclase and magnetite. The occurrence of apatite could be predicted by the systematics of apatite saturation determined by experimental work, as summarized by Watson and Harrison (1984). Its importance as a controlling factor in the fractionation of rare earth elements (REE) was highlighted by Watson and Capobianco (1981). Partition coefficients of Hf, Zr and REE between apatite and liquid are available (Fujimaki 1986). Therefore, in the Geordie Lake gabbro, apatite could prove to be a sensitive indicator of magma fractionation, particularly since other accessory phases are rare.

Apatite is a common accessory phase in the PGE ore zones of the Stillwater and Bushveld complexes (Boudreau *et al.* 1986). Boudreau *et al.* showed that these apatites were enriched in Cl relative to others found elsewhere in the intrusions, and concluded that a Cl-rich volatile phase may have been involved in the deposition of the PGE. This is consistent with thermodynamic modelling by Candela (1986) for the behaviour of F:Cl:OH ratios in apatite during magma fractionation and the evolution of a volatile phase. However, in both the Stillwater and Bushveld complexes the occurrence of apatite away from the ore zones is rare, making further study of apatite crystallization difficult. The Geordie Lake gabbro, however, contains ubiquitous apatite and its study with respect to the above principles could prove useful in relation to the evolution of PGE deposition.

APPLICATION TO EXPLORATION

There is reasonable evidence which supports the possibility that there are other Pd–Cu sulphide occurrences in the Geordie Lake gabbro besides those previously explored. The evidence includes the sulphide mineralization found on the east side of the quartz syenite and the irregular nature of the sulphide zones within the main mineralized zones. If sulphide mineralization resulted from the intrusion of evolved magma into a partially crystalline pile, as the above model postulates, then this could presumably have happened at any horizon in the intrusion. It's important to realize that the association between the mineralized zone and the quartz syenite is apparently coincidental.

The realization that the Geordie Lake gabbro is simply cut by and not bounded by quartz syenite means that the actual size of the gabbroic body might be much larger than previously expected. Therefore, additional regional mapping is highly recommended.

ACKNOWLEDGMENTS

We thank Mr. Mel Joa, prospector, Bond Gold Canada Inc. (formerly St. Joe Canada Inc.) and Fleck Resources Ltd. for access to their properties, accumulated geological information, and diamond drill core. We also thank Bernie Schnieders, Resident Geologist, and Mark Smyk, Staff Geologist, Schreiber–Hemlo District, Ministry of Northern Development and Mines, for introducing us to the Geordie Lake property and for their logistical support. Sulphur isotope compositions were determined at. McMaster University, in the laboratory of Dr. H.G. Thode.

REFERENCES

Boudreau, A.E., Mathez, E.A. and McCallum, I.S.

1986: Halogen Geochemistry of the Stillwater and Bushveld Complexes: Evidence for Transport of the Platinum-Group Elements by Cl-Rich Fluids; Journal of Petrology, Volume 27, Part 4, p.967-986.

Candela P.A.

1986: Toward a Thermodynamic Model for the Halogens in Magmatic Systems: an Application to Melt-Vapor-Apatite Equilibria; Chemical Geology, Volume 57, p.289-301.

Donaldson, C.H.

1982: Origin of some of the Rhum Harrisite by Segregation of Intercumulus Liquid; Mineralogical Magazine, Volume 45, p.201-209.

Fujimaki, H.

1986: Partition Coefficients of Hf, Zr, and REE between Zircon, Apatite, And Liquid; Contributions to Mineralogy and Petrology, Volume 94, p.42-45.

Good, D.J.

1988: Platinum-Group Element Distribution in the Kanichee Intrusion, District of Nipissing; Ontario Geological Survey, Open File Report 5705, 42p.

Lawson, G.E. and Macdonald, A.J.

1987: Relationships between Geology and the Statistical Distribution of Gold, Platinum and Palladium Grades in an Archean Noble Metal Deposit, Lac des Iles, Ontario, Canada (abstract); Geological Society of America, Abstracts with Programs, Phoenix, U.S.A.

Mulja, T. and Mitchell, R.H.

1988: Precious- and Base-Metal Mineralization in Gabbroic Rocks of the Geordie Lake Area, Coldwell Alkaline Complex, Ontario, Canada (abstract); Abstracts with Programs, Geological Society of America Annual Meeting.

Ohmoto, H.

1986: Sulfur Isotopes in Magmatic Systems; p.528-537 *in* Reviews in Mineralogy, Volume 16: Stable Isotopes in High Temperature Geological Environments, edited by Valley, Taylor and O'Neil, Mineralogical Society of America.

Streckeisen, A.

1976: To each Plutonic Rock its Proper Name; Earth-Science Reviews, Volume 12, p.1-33.

Watson, E.B. and Capobianco, C.J.

1981: Phosphorus and the Rare Earth Elements in Felsic Magmas: an Assessment of the Role of Apatite; Geochimica et Cosmochimica Acta, Volume 45, p.2349-2358.

Watson, E.B. and Harrison, T.M.

1984: Accessory Minerals and the Geochemical Evolution of Crustal Magmatic Systems: a Summary and Prospectus of Experimental Approaches; Physics of the Earth and Planetary Interiors, Volume 35, p.19-30.

Grant 342 Paleomagnetic Analysis of Regional and Contact Strains

C.J. Hale and P. Lloyd

Department of Geology, McMaster University, Hamilton

ABSTRACT

We have carried out alternating field (AF) and thermal demagnetizations on 136 samples from the Meen Lake–Dempster Lake greenstone belt (MD) and the neighbouring Dobie Lake Batholith to test the idea that a local block containing the Kawashe Lake Gabbro and accompanying metavolcanic rocks underwent a structural rotation between the northwest–trending zones of intense dextral shear that bound the northern and southern margins of this greenstone belt. Preliminary paleomagnetic results from the Dobie Lake Batholith define a magnetization with the following parameters: declination = 184°, inclination = −65°, K = 43, α_{95} = 19°. The Kawashe Lake Gabbro carries a reversed magnetization with the following parameters: declination = 314°, inclination = −70°, K = 14, α_{95} = 14°. Both normal and reversed polarities are represented in the Kawashe Lake data, probably because the Kawashe Lake Gabbro is partially overprinted by magnetic remanence dating from the intrusion of the Graniteboss Lake Stock (declination = 345°, inclination = 79°, K = 91, α_{95} = 10°). The similarity between the inclinations of the Dobie Lake and Kawashe Lake magnetizations is consistent with their having been acquired at nearly the same time. The discrepancy in declination suggests that a block containing the Kawashe Lake Gabbro may have rotated up to 130° clockwise with respect to the Dobie Lake Batholith. This clockwise rotation is consistent with the sense of subhorizontal motion in the shear zones but its magnitude may be overestimated if there has been a northward tilting of the Kawashe Lake Gabbro relative to the Dobie Lake Batholith.

INTRODUCTION

Paleomagnetism provides a unique combination of structural and temporal information. On one hand, the directions of the magnetizations recorded at various field localities can be correlated to show stability across crustal blocks and discrepancies can provide evidence of local block rotations. On the other, the magnetization directions can be compared with reference apparent-polar-wander paths (APWP's) to provide a chronology for intrusions and deformation on a regional scale. Studies of this type have been instrumental in the recognition of allochthonous terrains along the western margin of the North American Cordillera (e.g., Beck 1976). In our study, we are using paleomagnetism as an indicator of block rotations in the Meen Lake–Dempster Lake greenstone belt, in the central Uchi Subprovince. Such rotations are a feature of regional-scale shear, with important implications for economic geology.

Gold occurrences have been related in a preliminary way to the tectonic history of the Uchi Subprovince and this relationship has permitted Stott and Brown (1986) to suggest specific environments in which there is a likelihood of gold mineralization. Gold mineralization has been linked to two types of shear zones: contact shear associated with the intrusion of late stage plutons, and regional shear associated with a northwesterly directed transpression.

Gabbroic and basaltic rocks in the contact aureoles of late-stage plutons carry magnetizations which date from the time of pluton intrusion. If the gold mineralization is also related to the development of contact shear zones, then a paleomagnetic remanence that dates the reheating and shearing of the contact zone can be a useful guide to the timing of mineralization.

If a contact zone is dissected by a major regional shear, then comparison of the initially identical remanences across the shear zone provides a measure of the relative rotation of the adjacent structural domains.

GEOLOGICAL SETTING

The geological setting of our field area is shown schematically in Figure 342.1 which is simplified from the map by Stott and Wilson (1986).

The Meen Lake–Dempster Lake greenstone belt contains several bimodal cycles of mafic to felsic volcanic rocks including the Meen–Jacknife lakes cycle and the Dempster Lake cycle. These Archean metavolcanic rocks have been multiply intruded by the Dobie Lake Batholith ($2.747^{+0.003}_{-0.002}$ Ga), the Kawashe Lake Gabbro, the Kawashe Lake Stock ($2.720^{+0.006}_{-0.004}$ Ga) (U-Pb zircon, Corfu and Stott 1989) and the Graniteboss Lake Stock (2.699 ± 0.002 Ga) (F. Corfu, Royal Ontario Musem, personal communcation, 1989).

The greenstone belt is bounded on the north by a zone of intense shearing bordering the Dobie Lake Batholith, related to the regional-scale, northwest-trending, transcurrent Bear Head fault. The southern margin of the belt is also marked by a zone of intense shear. Thus, if a cordilleran analogy can be

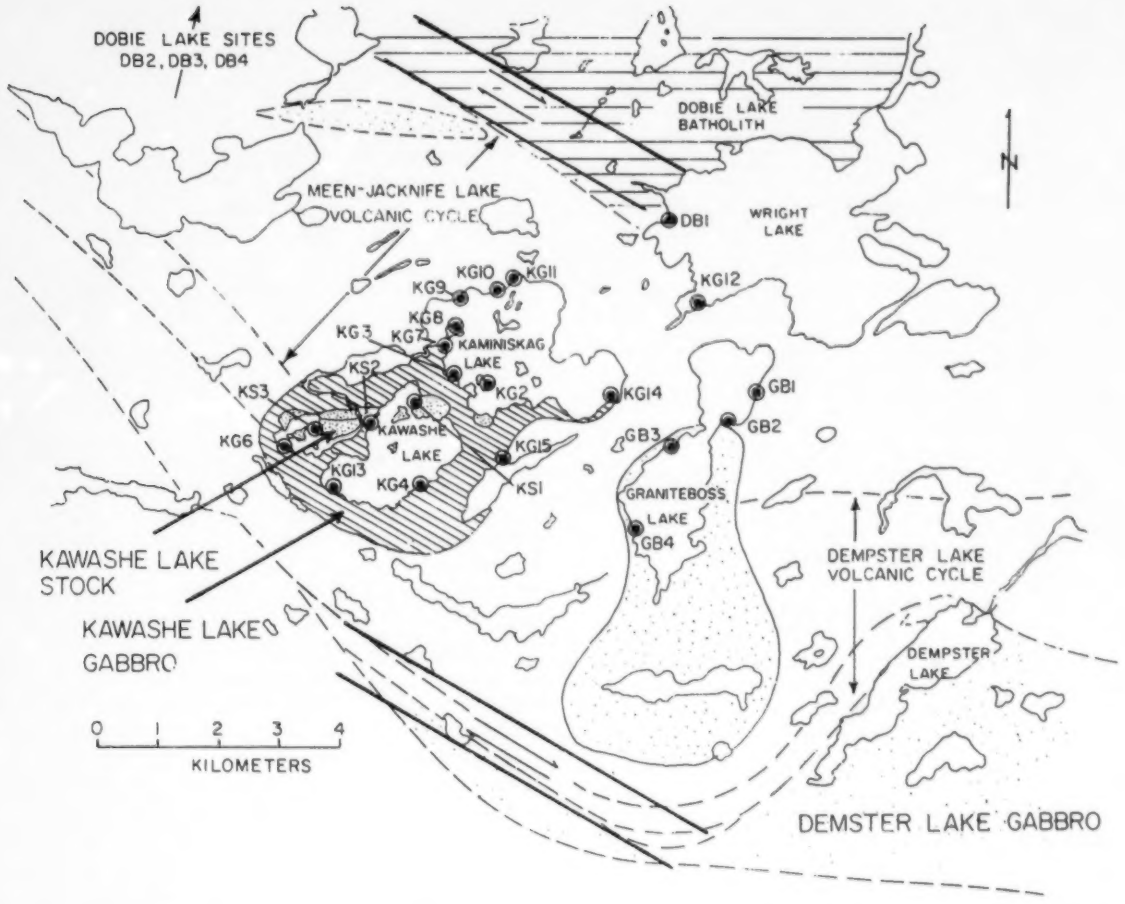

Figure 342.1. *Location of the sampling sites in the Meen Lake–Dempster Lake greenstone belt showing the relationship between the Dobie Lake Batholith, the Kawashe Lake Gabbro and the major shear zones which bound the block's northerly and southerly margins. The geology is simplified after Stott and Wilson (1986).*

applied, the volcanic rocks located between these zones are likely to have undergone block rotation in response to shearing. This area thus provides an excellent location in which to test whether cordilleran-type block rotations might also be a feature of late Archean tectonics.

The multiple intrusion history of the Meen Lake–Dempster Lake greenstone belt provides a series of dated thermal sources for contact remagetization studies. The Bear Head fault that provides the northern limit for the study area cuts through the Dobie Lake Batholith contact zone. We can thus compare the direction of magnetization in the Dobie Lake Batholith with the contact magnetization carried by metavolcanic rocks on the south side of this fault. The use of an intrusive body and its contact zone for such a comparison assures that the remanence was initially identical on both sides of the fault.

PALEOMAGNETIC SAMPLING

During the 1988 field season we collected 136 oriented hand samples from the sites shown in Figure 342.1. A typical site is represented by six independently oriented blocks. In all cases, orientation was determined by magnetic compass. The primary target for sampling was the Kawashe Lake Gabbro and its contact zone, including a radial traverse through the contact-baked mafic metavolcanic rocks that outcrop along the northern shore of Kaminiskag Lake. Samples from four additional sites were collected in the Graniteboss Lake Stock (GB2-4) or its contact zone (GB1). The Dobie Lake Batholith was sampled at three localities (DB2-4) on the western and southern shorelines of Dobie Lake and on an island in the east-central part of the lake.

Throughout the sampling, obviously sheared rocks were avoided in favour of the more massive parts of outcrops. This was particularly important in

the metavolcanic rocks from Kaminiskag Lake where most outcrops were found to contain both highly sheared and comparatively massive samples over a scale of only a few metres. A few highly strained samples that were collected invariably were found to be paleomagnetically unstable.

EXPERIMENTAL PROGRAM

All of the oriented hand samples were cored in the laboratory, yielding at least four specimens. At least one specimen from each sample was subjected to thermal demagnetization at 11 temperature steps spanning the range from 20 to 580°C. Demagnetizations were carried out in batches of 50 samples, in air, in a large non-inductive furnace. The residual magnetic field in the furnace was reduced to less than 10 nT with a double 3-axis (12 coil) Helmholtz coil system operated by a Schonstedt HCM-3 magnetic field controller.

At least one specimen was subjected to alternating field (AF) demagnetization at 14 steps up to 100 mT in a Schonstedt GSD-1 AF demagnetizer.

Measurements of remanence were made with a Schonstedt SSM-2 spinner magnetometer, interfaced to a Texas Instruments microcomputer for data archiving and processing.

Paleomagnetic directions were determined from the demagnetization records by three-dimensional, linear least-squares fitting to segments that appeared to be nearly linear on orthogonal vector plots. This process made use of Kirschvink's (1980) method in a computer program based on one originally provided by H. Hyodo.

PALEOMAGNETIC RESULTS

Figure 342.2 shows a histogram of the intensities of natural remanent magnetization (NRM) for the entire Meen Lake–Dempster Lake collection. Samples have been divided into three groups of lithologies. The mafic intrusive samples include the Kawashe Lake Gabbro and an associated minor pyroxenitic phase of the Kawashe Lake Stock. The basalt samples in the collection are largely from the Meen–Jacknife lakes volcanic cycle. Samples from felsic intrusions including tonalite from the Dobie Lake Batholith, granodiorite from the Kawashe Lake Stock and granite and granodiorite samples from the Graniteboss Lake Stock have been grouped under the general category of felsic rocks.

The NRM intensities span a wide range with little clear distinction on the basis of lithology. Within each category can be found both highly intense samples (J_{NRM} > 1 A/m) and others that challenge the lower sensitivity limit (10^{-3} A/m) of the spinner magnetometer. Median NRM intensities for mafic intrusive, basaltic and felsic groups all lie between 0.01 and 0.1 A/m.

Figure 342.3 shows the magnetic stability of the three major lithologies, as indicated by the median demagnetizing field (MDF) determined in alternating field demagnetization experiments. The mafic intrusive and basaltic samples are characterized by soft demagnetization spectra with MDF's typically less

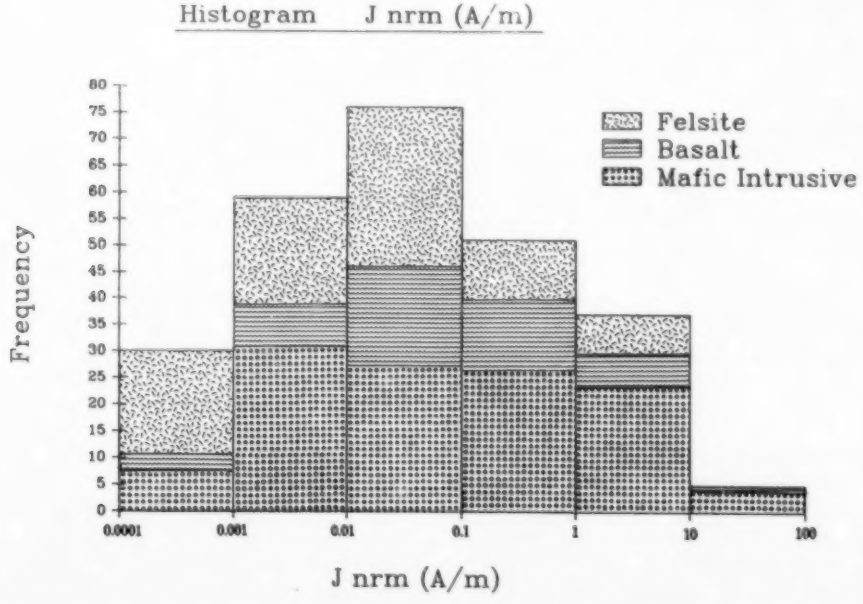

Figure 342.2. *Histogram of the intensity of natural remanent magnetization for all samples from the Meen Lake–Dempster Lake greenstone belt. All of the specimens from granitic, tonalitic and granodioritic plutons have been grouped in a single category labelled felsite.*

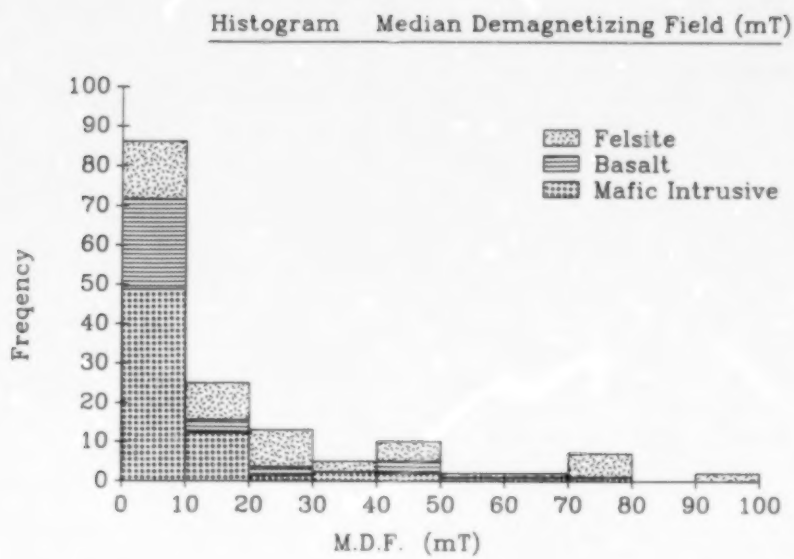

Figure 342.3. *Histogram of the median destructive fields determined in AF demagnetization experiments.*

than 10 mT. A few of the mafic intrusive samples are comparatively stable with MDF's as high as 70 or 80 mT. In general, the felsic intrusive samples are more stable than the mafic rocks. About half of the felsic samples have MDF's higher than 25 mT.

Figure 342.4 shows typical AF demagnetization spectra for samples from the Kawashe Lake Gabbro, the Graniteboss Lake Stock, the Dobie Lake Batholith and the Kawashe Lake Stock. For the Kawashe Lake Gabbro, Graniteboss Lake Stock and Kawashe Lake Stock, the curves have been selected to illustrate the maximum and minimum stabilities encountered in the collection.

The behaviour of the three major lithological types during thermal demagnetization is shown in Figure 342.5. The temperatures at which the NRM's of the samples are reduced to 50% of their initial value are presented as a histogram. The basaltic

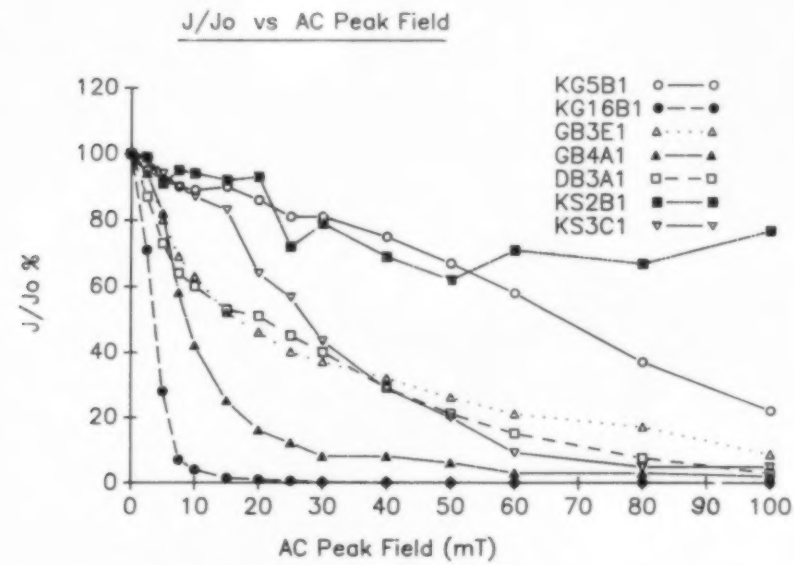

Figure 342.4. *Typical alternating field (AF) demagnetization obtained from the principal lithological types: KG5B1, Kawashe Lake Gabbro; KG16B1, metabasalt; GB3E1 and GB4A1, Graniteboss Lake granite; DB3A1, Dobie Lake hornblende tonalite; KS2B1 and KS3C1, Kawashe Lake Stock granodiorite.*

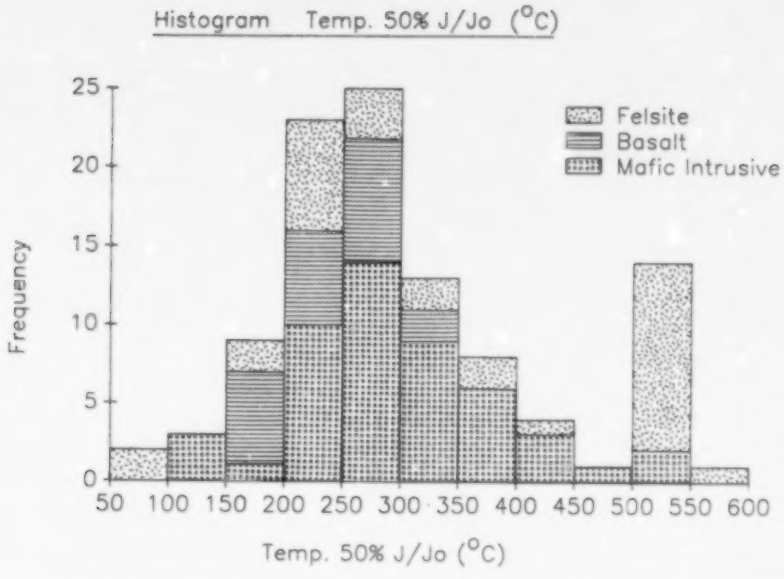

Figure 342.5. *Histogram of the temperatures at which NRM is reduced to half of its initial value in thermal demagnetization experiments. This provides a rough measure of the thermal stability of the paleomagnetic remanences.*

samples show a fairly narrow range of median unblocking temperatures from about 150°C to just over 300°C. The mafic intrusive samples show a comparatively wide distribution in median unblocking temperatures, centred around 270°C. The felsic intrusive samples can be divided into two populations. Most of the felsic rocks can be demagnetized to 50% at temperatures lower than 400°C but a number of the Graniteboss Lake samples show tightly grouped blocking temperatures in the range over 500°C.

PALEOMAGNETIC DIRECTIONS

Characteristic paleomagnetic directions have been obtained from the Kawashe Lake Gabbro, the Kawashe Lake Stock, the Dobie Lake Batholith and the Graniteboss Lake Stock. For each specimen, stable directions were obtained either by linear least-squares fitting of linear segments obtained on orthogonal vector plots or by reading stable end-point directions from stereonets. If no reasonably linear segment was recovered, a specimen was excluded from the subsequent averaging. Typical examples of the characteristic directions are presented in Figure 342.6. Both AF and thermal demagnetization spectra were obtained for all of the samples in the collection. Site averages were calculated using all of the specimens that yielded stable directions and these site averages in turn were averaged to yield the characteristic direction for each remanence type. The average direction for each of the characteristic remanences is shown in Figure 342.7 which includes both the site averages with their circles of confidence and the overall average for each remanence type.

Samples from the Kawashe Lake Gabbro carry one of two characteristic magnetizations. Those from the interior of the pluton carry a steep northwesterly magnetization with a negative inclination (declination = 314°, inclination = −70°, K = 14, α_{95} = 14°). For simplicity we shall refer to this as the Kawashe Lake reversed magnetization. The contact-baked metabasalts along the northwestern shore of Kaminiskag Lake carry a steep, positive magnetization (declination = 334°, inclination = 75°, K = 16, α_{95} = 14°). Again, for simplicity, we shall refer to this remanence as the Kawashe Lake normal magnetization. It is tempting to suppose that the normal and reversed magnetizations constitute a dual polarity record preserved in the Kawashe Gabbro, evidence that the magnetization is primary. Such an interpretation is premature, however, since the normal magnetization direction lies quite close to the direction of the present Earth's field and the possibility of viscous contamination cannot easily be ruled out.

Samples from the Kawashe Lake Stock also carry two steeply directed magnetizations with opposing polarities. All of the stable samples from site KS1 and about half of the samples from sites KS2 and KS3 carry a steeply downwards, northwesterly magnetization (declination = 304°, inclination = 67°, K = 47, α_{95} = 18°) while the remaining samples from sites KS2 and KS3 carry a westerly magnetization with a steep negative inclination (declination = 270°, inclination = −69°, K = 49, α_{95} = 36°) quite

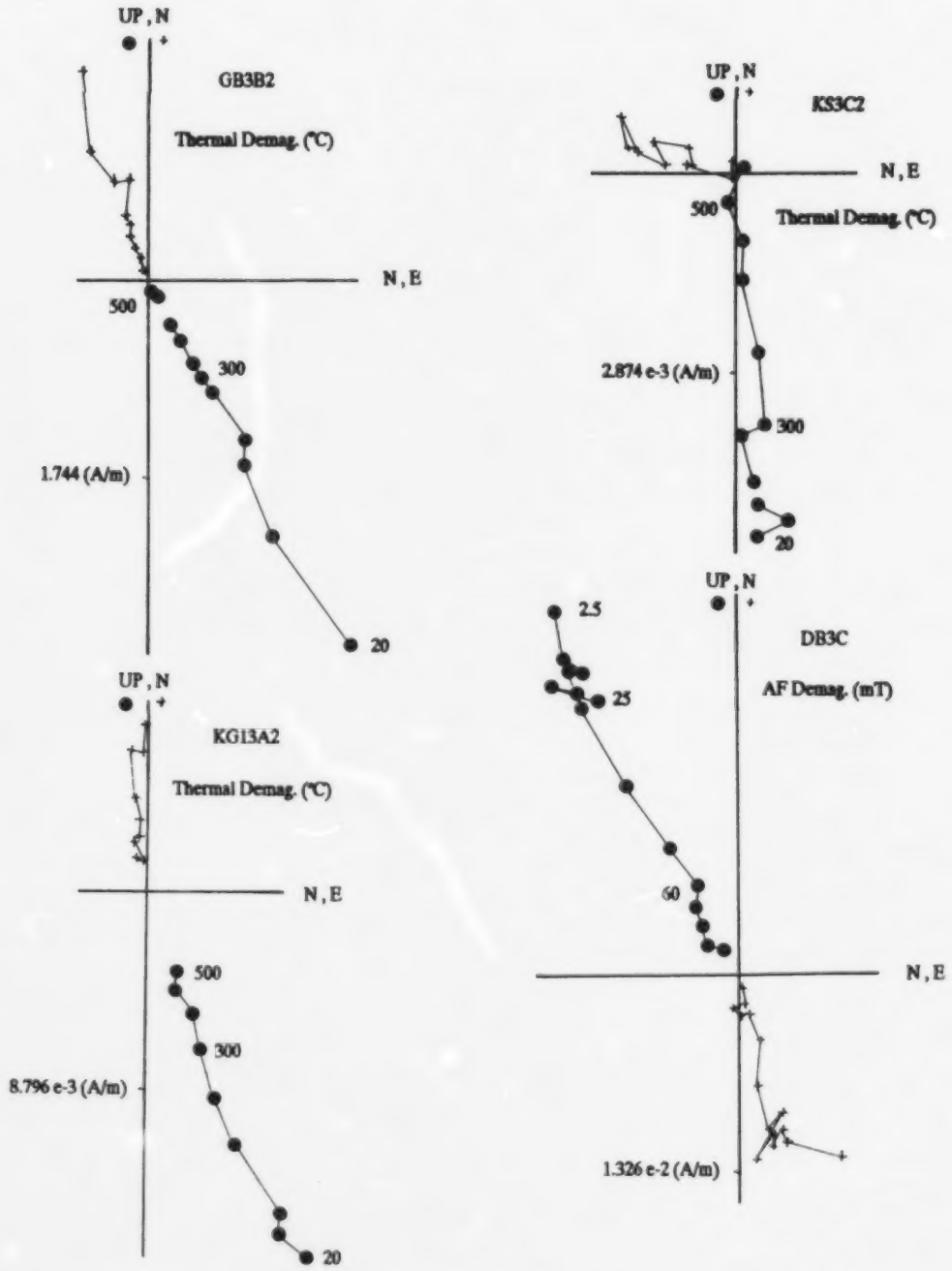

Figure 342.6. *Orthogonal vector plots of typical specimens illustrating the remanence types recovered.*

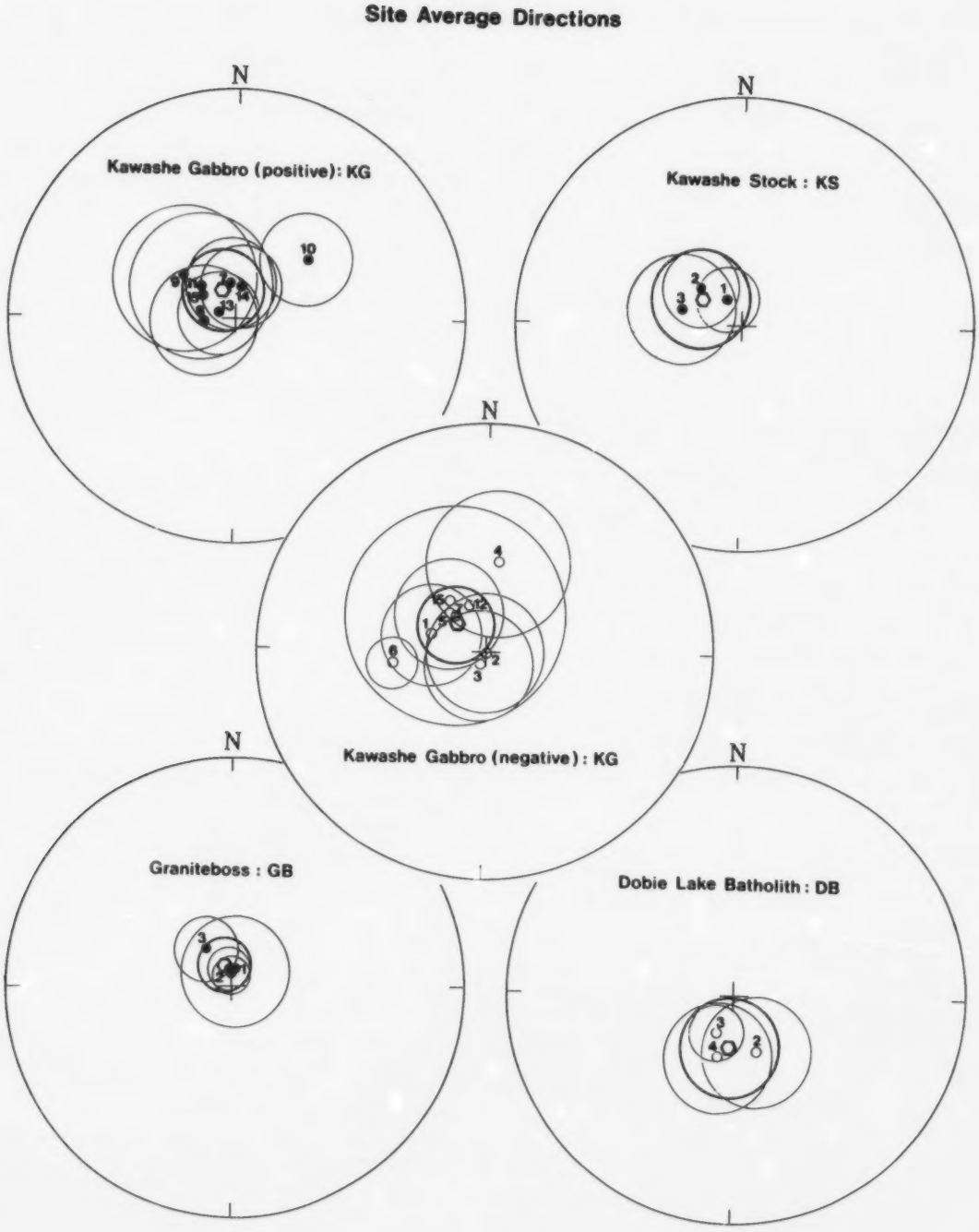

Figure 342.7. *Magnetization directions from the Kawashe Lake Gabbro, the Kawashe Lake Stock, the Dobie Lake Batholith and the Graniteboss Lake Stock. Open (closed) symbols indicate a point on the upper (lower) hemisphere of the stereonet. The average direction for each site is plotted along with its circle of 95% confidence. The heavy circle is the 95% confidence circle for the overall average direction, indicated by the hexagonal symbol.*

like the reversed magnetization recovered from the Kawashe Lake Gabbro.

Sites within the Graniteboss Lake Stock gave a steep, positive, northerly magnetization (declination = 345°, inclination = 79°, K = 91, α_{95} = 10°). In most samples, this magnetization was highly stable. Typically it could be recovered at demagnetization temperatures higher than 500° C and at AF strengths up to 100 mT. This characteristic Graniteboss Lake Stock magnetization is identical to the Kawashe Lake normal magnetization.

In common with the results reported above, the Dobie Lake Batholith yielded samples with both positively and negatively directed magnetizations. All of the stable samples from sites DB2 and DB3 and three samples from DB4 yielded a magnetization with a southerly declination and a steep negative inclination (declination = 184°, inclination = −65°, K = 43, α_{95} = 19°). This magnetization is distinct from the Kawashe Lake reversed direction. Although it has a nearly identical inclination, it differs in declination by about 130°.

All of the directions are presented in Table 342.1 and the paleomagnetic poles corresponding to these directions are compared with the APWP for North America, redrawn after Irving (1979) in Figure 342.8.

SIGNIFICANCE OF THE NEW PALEOMAGNETIC DATA

It is clear from a glance at Figure 342.8 that paleomagnetic poles from the Meen Lake–Dempster Lake greenstone belt do not plot on the previously drawn APWP for North America. Since these poles have been obtained from precisely dated plutons they can become preliminary tie points for a revised, Archean, apparent-polar-wander path. New paleomagnetic data from both the present study and work in progress in the Abitibi belt indicate that a new reference APWP is required for use either in paleomagnetic dating or structural studies.

The close correspondence between the Kawashe Lake normal magnetization and the normal magnetization of the neighbouring Graniteboss Lake Stock suggests that remanence of the Kawashe Lake Gabbro may have been partly overprinted during the intrusion of the Graniteboss Lake Stock at about 2.7 Ga.

This interpretation is strengthened by a recent re-evaluation of the contact relationship between a contemporaneous syenitic pluton located near Kirkland Lake, Ontario, and neighbouring diabase dikes of the Matachewan swarm. The paleomagnetic pole implied by the Otto Stock magnetization (OS, Figure 342.8) has recently been shown to predate the intrusion of the Matachewan dikes, probably with an age of 2.7 Ga (Buchan *et al.* 1989). The excellent agreement between the Otto Stock and Graniteboss/Kawashe normal poles, obtained from contemporaneous intrusions separated by several hundred kilometres, suggests that much of the Superior craton was stabilized by 2.7 Ga.

Although the agreement between the Otto Stock and Graniteboss Lake Stock poles is encouraging it must be treated with caution. Figure 342.8 also shows that the Graniteboss/Kawashe pole also agrees with a 2.1 Ga pole from the Nipissing Diabase (ND, Buchan *et al.*, in press) and thus the age assignment is in no way unique.

The close proximity of the Graniteboss/Kawashe pole and the present geomagnetic pole also raises the possibility that the Kawashe normal magnetization may reflect viscous contamination from the present Earth's field. Such viscous contamination is a well-known feature of Archean greenstones. It is not likely, however, that the highly stable normal remanence carried by some Graniteboss Lake Stock samples results from viscous contamination.

The reversed magnetization carried by the Kawashe Lake Gabbro cannot be the result of viscous contamination. The preservation of this possibly primary remanence in the Kawashe Lake Gabbro as well as the dual polarities recorded in the Kawashe Lake Stock and Dobie Lake Batholith hint that both the steep normal and steep reversed magnetizations may be Archean.

The reversed magnetization carried by the Kawashe Lake Gabbro is particularly intriguing. If the Kawashe Lake Gabbro is correlative with the Dempster Lake cycle of metavolcanic rocks, it was intruded at about 2.74 Ga (G.M. Stott, Ontario Geological Survey, Toronto, personal communication). This is contemporaneous with $2.747^{+0.003}_{-0.002}$ Ga U-Pb zircon and 2.734 ± 0.003 Ga titanite ages reported for the Dobie Lake Batholith by Corfu and Stott (1989). The directional discrepancy between the Dobie Lake Batholith southerly reversed magnetization and the Kawashe Lake Gabbro northwesterly reversed magnetization suggests clockwise rotation of a block containing the Kawashe Lake Gabbro. The Dobie Lake and Kawashe Lake reversed magnetizations share a common inclination implying that rotation must have occurred in response to essentially horizontal slip on the Bear Head fault extension. The 130° of relative rotation implied by a simple comparison of the reversed magnetizations is not unreasonably large when viewed beside typical cordilleran rotations (cf. Beck 1976) but this figure can be reduced drastically if a northward tilting of the Kawashe Lake Gabbro relative to the Dobie Lake Batholith is interpreted.

The apparent agreement between the Graniteboss Lake Stock and Otto Stock magnetizations requires that these movements must have taken place prior to 2.7 Ga.

TABLE 342.1. SITE AVERAGES OF PALEOMAGNETIC DIRECTIONS AND THEIR IMPLIED PALEOMAGNETIC POLES.

A. Site Average Directions

Site, Polarity	Values Averaged	Declination (°)	Inclination (°)	Fisher κ	α_{95} (°)
Kawashe Lake Gabbro					
KG 1 neg	5 of 9	288	-62.4	17.2	18.9
KG 2 neg	4 of 5	163	-88.9	15.9	23.7
KG 3 neg	4 of 6	199	-82.9	23.4	19.3
KG 4 neg	6 of 10	7.8	-46.5	6	29.7
KG 5 neg	6 of 9	315	-64.2	11.6	20.4
KG 6 neg	8 of 11	261.7	-45.8	36.2	9.3
KG 7 neg	4 of 10	319.7	-67	5.9	40.9
KG 7 pos	6 of 10	350	72.5	15.5	17.5
Kawashe Lake Gabbro Contact-Zone Metabasalts					
KG 8 pos	8 of 9	262	74	8.6	19.9
KG 9 pos	3 of 5	309	57	21.3	27.3
KG 10 pos	9 of 9	52	46	7.9	19.4
KG 11 pos	6 of 8	305	71	3.8	27
KG 12 neg	3 of 8	340	-66	3.8	74.5
KG 13 pos	8 of 10	288	82	13.6	15.5
KG 14 pos	8 of 11	10	75	13.1	15.8
KG 15 neg	1 of 2	323	-60		
KG 15 pos	1 of 2	312	67		
Dobie Lake Batholith					
DB 2 neg	8 of 9	157	-61	8.2	20.4
DB 3 neg	6 of 11	195	-59	12.9	19.3
DB 4 neg	3 of 11	205	-70	131	10
DB 4 pos	7 of 11	319	75	38.9	9.7
Kawashe Lake Stock					
KS 1 pos	6 of 7	329	75	36.6	11.2
KS 2 pos	6 of 11	312	63	22.3	14.4
KS 2 neg	4 of 11	293	-71	22.9	19.5
KS 3 pos	3 of 8	284	60	36.7	20.6
KS 3 neg	4 of 8	253	-64	8.9	32
Graniteboss Lake Stock					
GB 1 pos	4 of 10	12	81	21.6	20.2
GB 1 neg	4 of 10	27	-53	1.6	111
GB 2 pos	12 of 12	352	81	35.6	7.3
GB 3 pos	7 of 10	326	68	22.8	12.8
GB 4 pos	10 of 12	1	84	48.5	6.9
GB 4 neg	2 of 12	225	-47	820.8	8.7

B. Overall averages and their implied paleomagnetic pole positions

Formation	Average Dec.	Average Inc.	Fisher κ	α_{95}	Lat.	Long.	dp	dm
Kawashe Lake Gabbro (upwards magnetizations)	314	-70	13.9	14.3	22.0	-62.7	10.2	39.0
Kawashe Lake Gabbro (downwards magnetizations)	334	75	15.7	14.3	72.6	-134.1	26.8	16.3
Dobie Lake Batholith (upwards magnetizations)	184	-65	43.1	18.9	85.0	59.4	37.8	3.8
Kawashe Lake Stock (downwards magnetizations)	304	67	46.6	18.2	54.9	-159.4	27.6	27.1
Kawashe Lake Stock (upwards magnetizations)	270	-69	48.5	36.0	38.2	-38.4	40.1	80.7
Graniteboss Lake Stock	345	79	91.3	9.6	71.1	-107.2	17.8	16.2

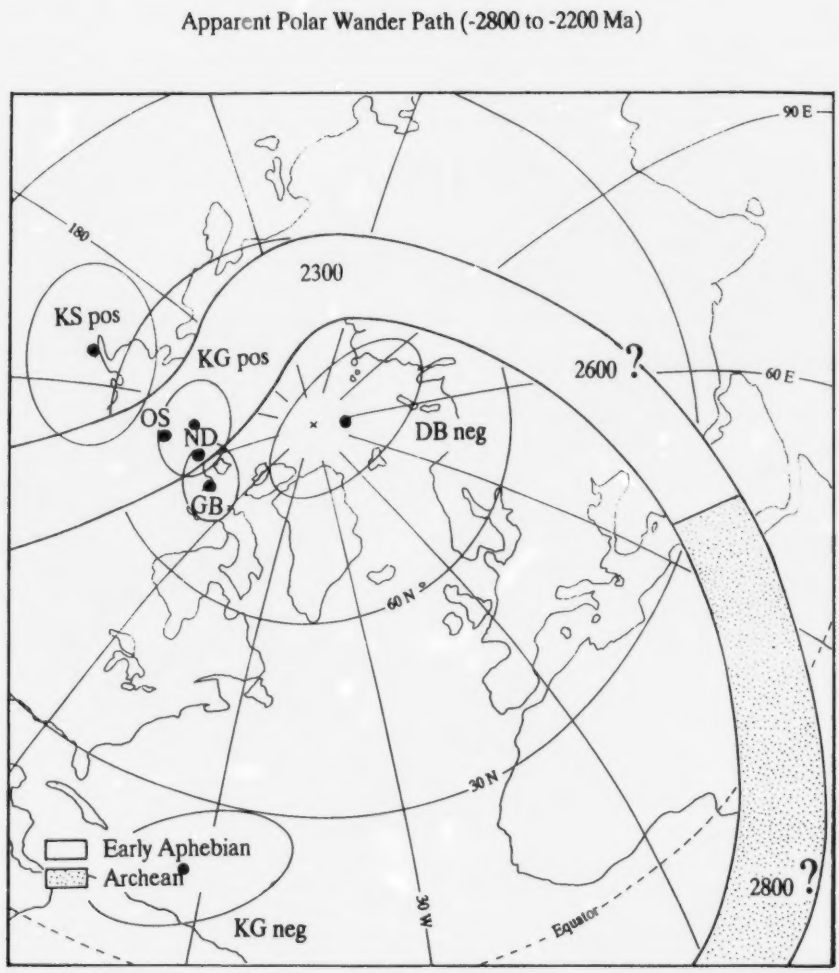

Figure 342.8. *Pole positions from the present study compared with apparent polar wandering path for North America, redrawn after Irving (1979). KG-Kawashe Lake Gabbro, KS-Kawashe Lake Stock, GB-Graniteboss Lake Stock, DB-Dobie Lake Batholith. For comparison, poles obtained from the Otto Stock (OS) (Buchan et al. 1989) and the Nipissing Diabase (ND) (Buchan et al.,* in press) *are also plotted.*

CONCLUSIONS

1. Stable magnetizations have been recovered from the Kawashe Lake Gabbro, the Dobie Lake Batholith, the Kawashe Lake Stock and the Graniteboss Lake Stock.
2. Both normal and reversed polarities have been recovered from each of the intrusions sampled. Normal polarity magnetizations carried by Kawashe Lake Gabbro samples may be partial thermal overprints acquired during intrusion of the nearby Graniteboss Lake Stock.
3. None of these magnetizations is consistent with the Archean APWP as it is conventionally drawn.
4. The remanence of metavolcanic rocks of the Meen–Jacknife lakes cycle is dominated by a steep, northerly, positive magnetization. This magnetization is likely a viscous contamination from the present Earth's field.
5. The Kawashe Lake Gabbro appears to have rotated clockwise with respect to the Dobie Lake Batholith. The magnitude of this rotation may be as high as 130° if no northward tilting has taken place.
6. All of the major deformations of the Meen Lake–Dempster Lake greenstone belt must have occurred prior to 2.7 Ga.

ACKNOWLEDGMENTS

This field locality was originally suggested by G.M. Stott who also participated in the collection of paleomagnetic samples. His familiarity with the structural details of the Meen Lake–Dempster Lake

greenstone belt has been a key component in this study and his help and encouragement are gratefully acknowledged. C. Holmden helped with the early phases of the study, notably in the field. A. Wiacek provided necessary modifications to H. Hyodo's software for the resolution of magnetic components. We acknowledge with thanks permission from F. Corfu, Jack Satterly Geochronology Laboratory, Royal Ontario Museum, to use an unpublished age of the Graniteboss Lake Stock.

REFERENCES

Beck, M.E. Jr.

1976: Discordant Paleomagnetic Pole Positions as Evidence of Regional Shear in the Western Cordillera of North America; American Journal of Science, Volume 276, p.694-712 .

Buchan, K.L., Card, K.D. and Chandler, F.W.

In Press: Multiple Ages of Nipissing Diabase Intrusion: Paleomagnetic Evidence from the Englehart Area, Ontario; Canadian Journal of Earth Sciences.

Buchan, K.L., Neilson, D. and Hale, C.J.

1989: Relative Ages of Matachewan Dykes and Otto Stock from Paleomagnetism (Abstract); Canadian Geophysical Union, 16th Annual General Meeting Program and Abstracts, p.75.

Corfu, F. and Stott, G.M.

1989: U-Pb Geochronology of the Central Uchi Subprovince, NW-Ontario (Abstract); Geological Association of Canada, Annual Meeting Program with Abstracts, p.A55.

Irving, E.

1979: Paleopoles and Paleolatitudes of North America and Speculations about Displaced Terrains; Canadian Journal of Earth Sciences, Volume 16, p.669-694.

Kirschvink, J.L.

1980: The Least-Square Line and Plane and the Analysis of Paleomagnetic Data; Geophysical Journal of the Royal Astronomical Society, Volume 62 p.699-718.

Stott, G.M. and Brown, G.H.

1986: Economic Geology of the Pickle Lake Metavolcanic Belt, District of Kenora, Patricia Portion; p.15-19 *in* Summary of Field Work and Other Activities, edited by P.C. Thurston *et al.*, Ontario Geological Survey Miscellaneous Paper 132.

Stott, G.M. and Wilson, A.C.

1986: Precambrian Geology of the Muskegsagagen-Bancroft Lakes Area, District of Kenora (Patricia Portion); Ontario Geological Survey, Map P.3049, Geological Series-Preliminary Map, scale 1:50 000. Geology 1984.

Grant 343 Structural Evolution of Central and East-Central Michipicoten (Wawa) Greenstone Belt, Superior Province

Z.G. Arias and H. Helmstaedt

Department of Geological Sciences, Queen's University, Kingston

ABSTRACT

The purpose of this project is to examine the structural evolution of the Archean Michipicoten greenstone belt with the ultimate aim of establishing the regional structural setting of vein-type gold mineralization.

Studies during the first field season (1988) concentrated on the structural style of clastic metasedimentary rocks underlying the central portion of the belt. Three sub-areas were mapped in detail.

The most prominent folds in all three areas are F_2 folds which have axial surfaces that approximately parallel the regional strike of the metasedimentary unit. Younging reversals along the F_2 axial surfaces indicate the presence of earlier folds (F_1). Overturned beds with opposed younging directions suggest pre-F_1 overturning of bedding. In all sub-areas, the latest cleavage (S_3) trends consistently northeastward.

In the Goudreau–Lochalsh area, early planar elements (S_0/S_1) within metavolcanics may have been transposed. A dominant east-northeast regional foliation trend (S_2), which is subparallel to lithologic contacts, appears to be associated with a major fold (F_2). Another northeast-trending cleavage (S_3) locally overprints the regional foliation trend.

Further research will focus on time relationships between the development of S_2/S_3 cleavages and local shear zones, as well as the nature of lithologic contacts within portions of the belt.

INTRODUCTION AND GEOLOGICAL SETTING

The Michipicoten (Wawa) greenstone belt is located within the Superior Province of the Canadian Shield, and extends approximately 110 km northeast from Michipicoten Harbour, at the eastern shore of Lake Superior (Figure 343.1).

The first regional geologic map (scale 1 inch to 2 miles) of the belt was produced and compiled by Goodwin (1963), who incorporated earlier mapping by Bruce (1940a). This was followed by the compilation of the Wawa–Manitouwadge map sheet at a scale of 1 inch to 4 miles (Milne *et al.* 1971). As a result of more detailed mapping by Sage and others (Sage *et al.* 1982a-e, 1984; Sage 1985a, in press), most of the belt has now been mapped at a scale of 1 inch to 1/4 mile (1:15 840) (*see also* reports by Sage 1979-1988). This excellent lithologic map base provides an opportunity to attempt a reconstruction of the structural development of the Michipicoten greenstone belt.

GENERAL GEOLOGY

Goodwin (1962) was the first to suggest a cyclic evolution of volcanism within the Michipicoten greenstone belt. Based on U–Pb zircon geochronology of metavolcanic and plutonic rocks (Turek *et al.* 1982, 1984, 1988; Sullivan *et al.* 1985; Frarey and Krogh 1986), and whole-rock geochemical analyses, Sage (1986) confirmed the existence of at least three volcanic packages, referred to by him as "cycles". Each cycle comprises mafic and felsic metavolcanic rocks with associated subvolcanic intrusions. These are overlain by chemical or clastic metasedimentary rocks. The two older packages yielded maximum ages of 2889 $\pm$ 9 Ma and 2749 $\pm$ 2 Ma, respectively, and the youngest has a minimum age of 2694 $\pm$ 5 Ma, from which Turek *et al.* (1988) suggested that the belt evolved over a time span of at least 195 Ma.

The mafic rocks of the oldest volcanic package are basaltic to peridotitic komatiite, whereas the mafic rocks of the two younger packages are tholeiitic (Sage *et al.* 1987). Mafic rocks consist mainly of massive or pillowed flows, and minor tuffs. The intermediate to felsic rocks of all three packages are rhyolites and dacites of calc-alkalic affinity (Sage *et al.* 1987), consisting of pyroclastic breccias, lapilli and ash tuffs, and minor flows. The chemical and/or clastic metasedimentary rocks of each package consist of siderite-, pyrite- or chert-magnetite iron formations, and/or turbiditic wackes and arenites, and conglomerates. Detailed descriptions of rock types are available in Sage (Open File Reports 5586, 5587, 5588, in press).

The supracrustal rocks are intruded by synvolcanic sills and dikes of gabbroic to quartz-dioritic composition, and granodiorite or quartz-feldspar porphyry stocks and dike complexes. Post-volcanic intrusions include various granitoid and syenitic

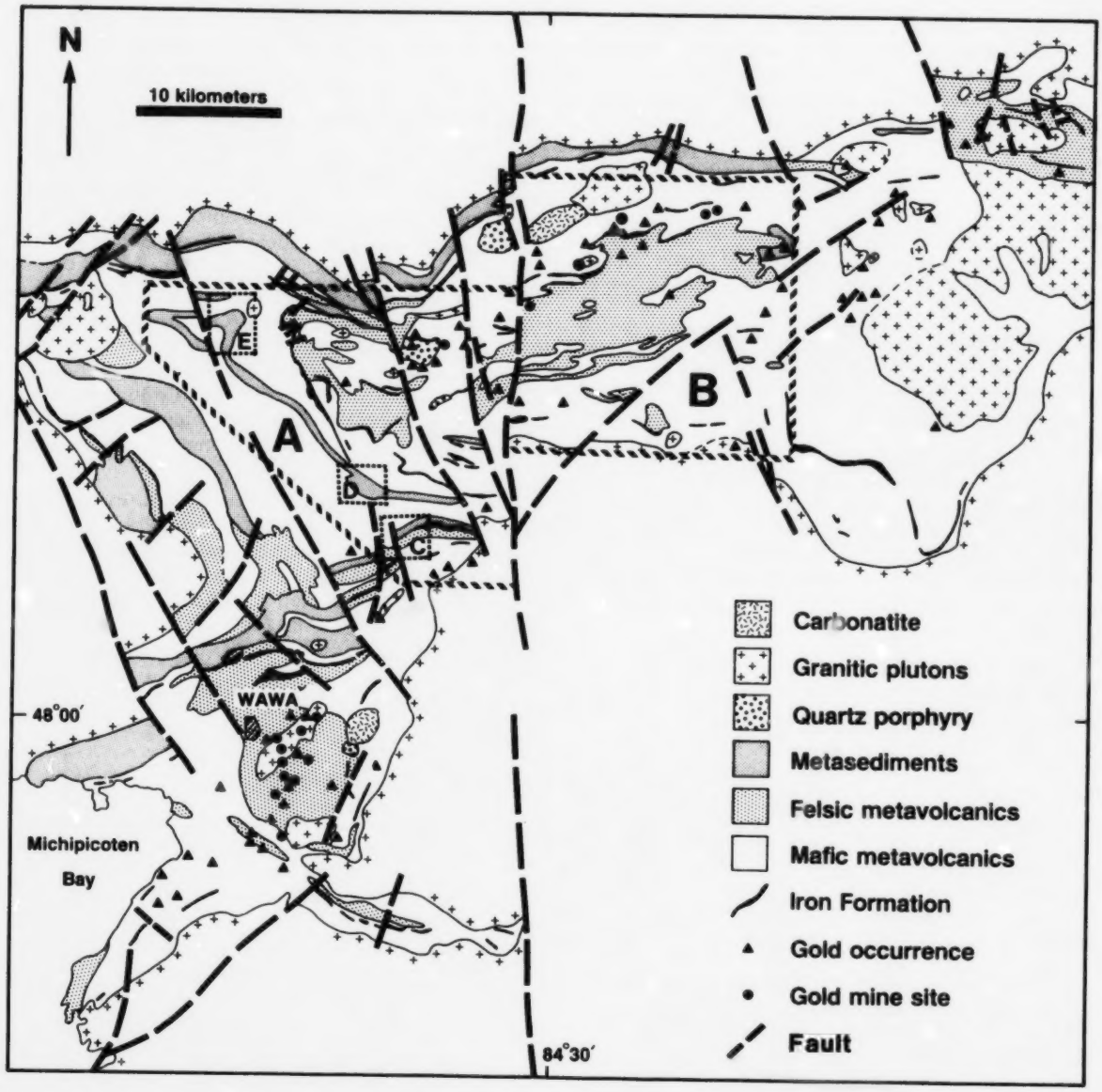

Figure 343.1. *General geology of the Michipicoten (Wawa) greenstone belt showing location of study area. A= Central belt area, B= East-central belt area (Goudreau-Lochalsh), C= Goetz Lake-Scott Lake area, D= West Andre Lake area, E= Kapimchigama Lake-Radford Lake area. (Compilation after Milne et al. 1971.)*

plutons. The youngest date within a granitoid intrusive phase is 2662 ± 5 Ma (Turek *et al.* 1984).

All supracrustal rocks have been regionally metamorphosed, exhibiting mineral assemblages characteristic of the greenschist facies. Rocks at the belt margins and in the immediate vicinity of large intrusions have undergone amphibolite-facies metamorphism. Late Archean and Proterozoic diabase dikes have intruded all Archean rock types.

PREVIOUS STRUCTURAL WORK

Early workers (Gledhill 1927; Frohberg 1935; Moore 1931, 1948) hypothesized that folding of the supracrustal rocks in the belt was associated with crustal disturbances related to batholithic intrusions. Frohberg (1935) suggested two major periods of folding, and Moore (1948) inferred that the northeast- to east-trending regional folds were formed during two distinct granitoid intrusive events.

Bruce (1940b), working in the Goudreau–Lochalsh area, recognized only a single folding event marked by a regional, upward-facing, east-plunging anticline. Goodwin (1962, 1963) documented belt-scale folding and, on the basis of a regional sinuous lineation pattern, concluded that east-trending upright folds are cross folded about northwest-trending axes.

Extensive mapping by Sage and others (Sage *et al.* 1982a-e, 1984; Sage 1985a, in press) did not confirm many of the fold axial traces shown on Goodwin's (1963) reconnaissance map, but supported Goodwin's (1962) interpretation of the existence of a second fold generation with a northwest-trending axial surface, in the central belt region (*see* Sage *et al.* 1984).

Based on stratigraphic facing and linear structures, R.P. Sage (Ontario Geological Survey, Toronto, personal communication, 1987) suggested that in the northwestern part of the central belt area (Figure 343.1, area A), a regional anticline faces downward to the northwest and plunges southeastward, defining an overturned panel with synformal geometry.

All authors recognized the existence of local shear zones and regional faults. Sage *et al.* (1987) suggested that sinistral shearing may have been coeval with regional folding in the central belt area, causing strong westward attenuation of the supracrustal rock units. In the Goudreau–Lochalsh area, Arias and Heather (1987) defined two regional heterogeneous zones of high strain that coincide broadly with major lithologic contacts, and are spatially associated with felsic intrusions. Shear zone geometry at a detailed (gold property) scale is discussed in Heather and Arias (1987).

Most authors and exploration geologists have noted the close association of gold mineralization with quartz-filled fractures and shear zones in the Goudreau–Lochalsh area, and other parts of the Wawa gold camp (Heather *et al.* 1988). Auriferous brittle fault breccia has also been recognized (Heather and Arias 1987), associated with major northwest-trending faults where they cut an east-northeast-trending high strain zone.

The presence of late faults has been noted by all workers. The faults of the most dominant set strike northwest and north. They cut the entire belt and show sinistral strike separation (Figure 343.1). The geometry and kinematic history of northeast-trending faults is more uncertain.

Arias (in preparation) presents a preliminary interpretation of the sequence of deformation preserved in the Goudreau–Lochalsh area. Additional work during 1988, to further constrain the structural development of the Goudreau–Lochalsh area, is presented in this paper.

The first detailed structural study of metasedimentary rocks in the belt was conducted by McGill and Shrady (1986) in a well-exposed area, north of Wawa. They recognized a multiphase deformation sequence and inferred that large-scale recumbent folding, possibly associated with thrust faults, occurred early in the structural evolution of the belt. This was followed by two periods of folding with axial planar cleavages oriented northwest and northeast, respectively. Local shearing was associated with the late regional faults.

The present study area encompasses portions of the central and east-central (Goudreau–Lochalsh) belt regions (areas A and B, Figure 343.1). The aim of the project is to establish the deformation history of a large part of the belt and should eventually lead to a definition of the relationship between the gold-hosting structures and the regional tectonic evolution.

The three-year study is designed to extend detailed structural studies (McGill and Shrady 1986) into the central and east-central belt region, and complements previous work in the Goudreau–Lochalsh area, conducted under affiliation with the Ontario Geological Survey (Arias and Heather 1987, Heather and Arias 1987, Arias, in preparation).

STRUCTURAL GEOMETRY AND DEFORMATION SEQUENCE

CENTRAL MICHIPICOTEN GREENSTONE BELT

Detailed work during the first field season has been conducted in three well-exposed areas, located along a folded unit of clastic metasedimentary rocks (Figure 343.1, areas C, D, and E). The local geometry and sequence of development of structural elements is described for each sub-area. This is followed by an attempt to correlate structures of all three areas, and to establish a regional early deformation history.

Goetz Lake–Scott Lake Area

This area is located at the border between Corbiere and Esquega townships (Figure 343.2; *see* Figure 343.1, area C), and is accessible along the railway track from Wawa to Hawk Junction. Bedrock exposure is excellent.

A composite stratigraphic section by Attoh (1980) shows that pillowed mafic volcanic flows of the area are overlain by felsic lapilli tuffs, and carbonate- and sulphide-facies iron formation in the northwest. A second unit of pillowed and massive mafic volcanic rocks overlies the iron formation southeast of Scott Lake (Figure 343.2), and is succeeded by bedded turbidites, outcropping along the shores of Goetz and Scott lakes. The turbidites in turn are overlain by a third unit of pillowed to massive mafic flows and ash tuffs underlying the northwestern part of the area (*see also* Sage *et al.* 1987).

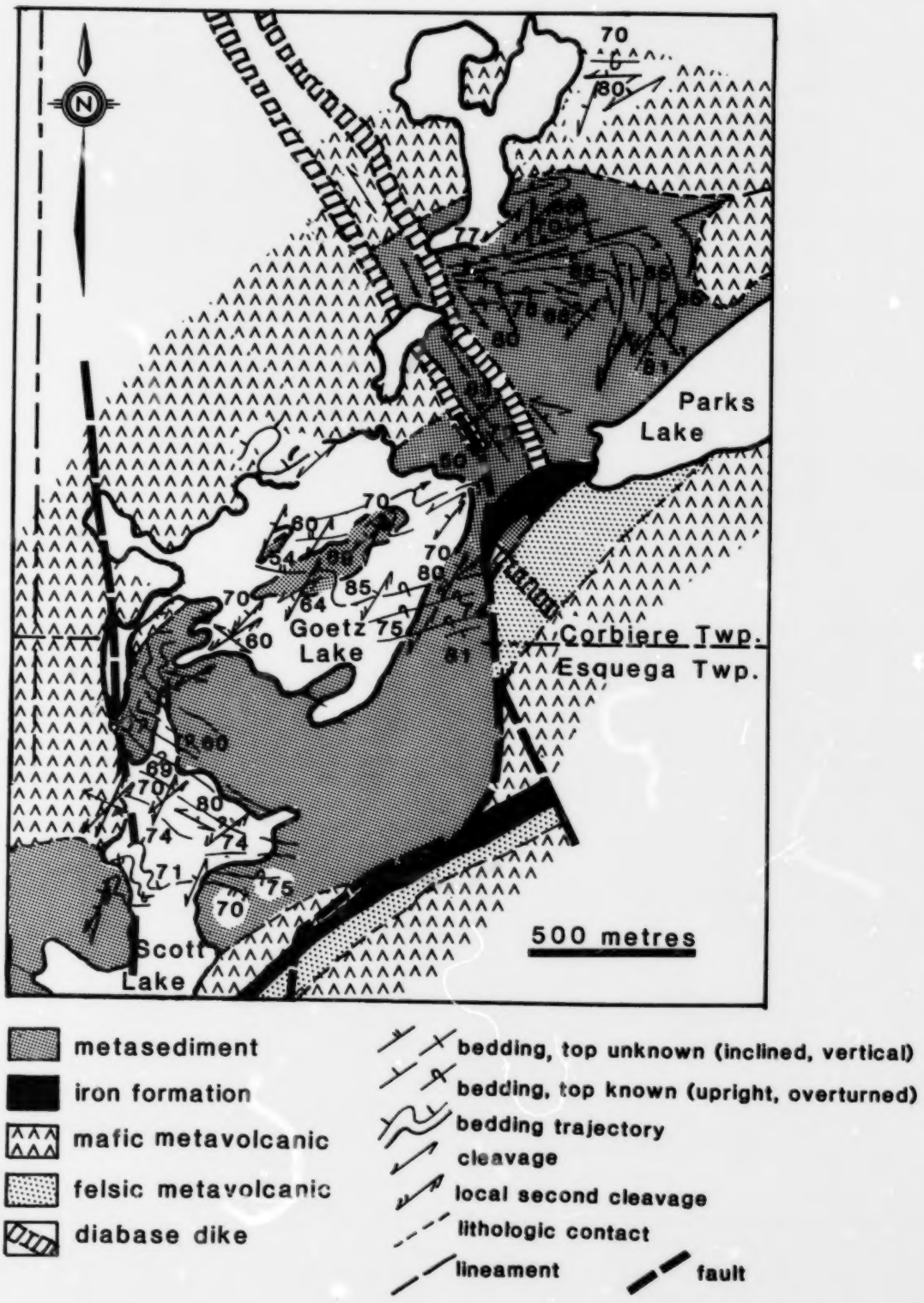

Figure 343.2. *Structural elements in metasediments in the Goetz Lake-Scott Lake area. Distribution of rock types after Sage et al. (1982b, 1984).*

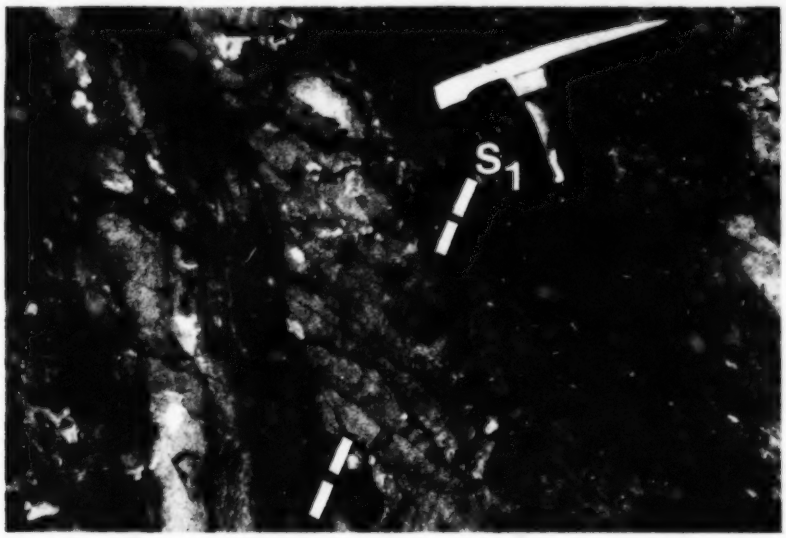

Photo 343.1. *Early cleavage (S_1) preserved at a moderate angle to bedding (S_0) in metaturbidites at Goetz Lake. Late northeast-trending cleavage (S_3) is strongly developed. (Plan view).*

Volcaniclastic pebble conglomerates occur along the contact between the clastic sediments and mafic volcanics northwest of Goetz Lake. This contact is sinistrally offset to the northeast along a northwest-trending fault zone infilled by diabase dikes. The conglomerates along the volcanic-sedimentary contact here comprise volcanic clasts, as well as banded chert, quartz and rare intrusive quartz porphyry clasts.

Lithologic contacts within the map-area trend dominantly to the northeast.

Sedimentary structures in the turbidites are well preserved, and younging directions were determined based on normal graded bedding, rippled bedforms, trough cross-bedding, primary truncation of bedding, reactivation of erosional surfaces, and flame structures. The map pattern shown is dominated by open to close folds of bedding (S_0) with overall Z-asymmetry. Mesoscopic fold closures are rarely preserved, and fold symmetry may be variable due to transposition. Bedding dips moderately to steeply and in places is overturned.

The earliest preserved tectonic planar fabric element (S_1) is rarely observed in outcrop, as it is commonly parallel to S_0. At Goetz Lake, where the overall trend of bedding is east-northeast, the S_1 fabric is preserved at several localities, trending west-northwest at a moderate angle to S_0 (Photo 343.1). On the microscopic scale, S_1 can be recognized even where parallel to bedding, as spaced, discontinuous seams of pressure solution residue (Photo 343.2).

At Scott Lake, bedding trends dominantly west-northwest, and an early planar fabric (S_1) parallel to bedding was recognized locally at both outcrop and thin-section scales. A large younging reversal along the axial surface of a northeast-trending fold (F_2), northwest of Parks Lake (Figure 343.2), suggests that the S_1 cleavage is associated with early folds (F_1). Local younging reversals at Scott Lake, and local dip variations and overturning across the strike of bedding in the area, support this interpretation. At only one locality, between Goetz and Scott Lakes, a west-northwest-trending mesoscopic fold was observed that is interpreted to be an F_1 closure with a strongly developed S_1 axial planar cleavage (Photo 343.3).

Overall younging along axial surfaces of steeply northeast-plunging mesoscopic- and map-scale folds (F_2) is to the northeast at about 050–060°. Associated with the F_2 folds is a steeply dipping axial planar cleavage (S_2) (Photo 343.4). At outcrop scale, bedding along the F_2 limbs appears to be largely transposed into the 055° S_2 orientation (Photo 343.4).

A similar relationship occurs at the map scale (Figure 343.2), where bedding within the metasediments is at a moderate angle to the 055°-trending lithologic contact between the youngest mafic volcanic unit to the northwest and the clastic sedimentary unit, and appears to be partially transposed into parallelism with this contact. Alternatively, the volcanic-sedimentary contact may truncate bedding within the turbidite sedimentary rocks. This contact was probably tectonically modified, as suggested by the presence of local shear fabrics and fault breccia (vein quartz fragments) in a pseudotachylite matrix,

Photo 343.2. *Photomicrograph of metagreywacke at Goetz Lake (plane light). Early cleavage (S_1), parallel to bedding (S_0), is marked by spaced, discontinuous seams of pressure solution residue.*

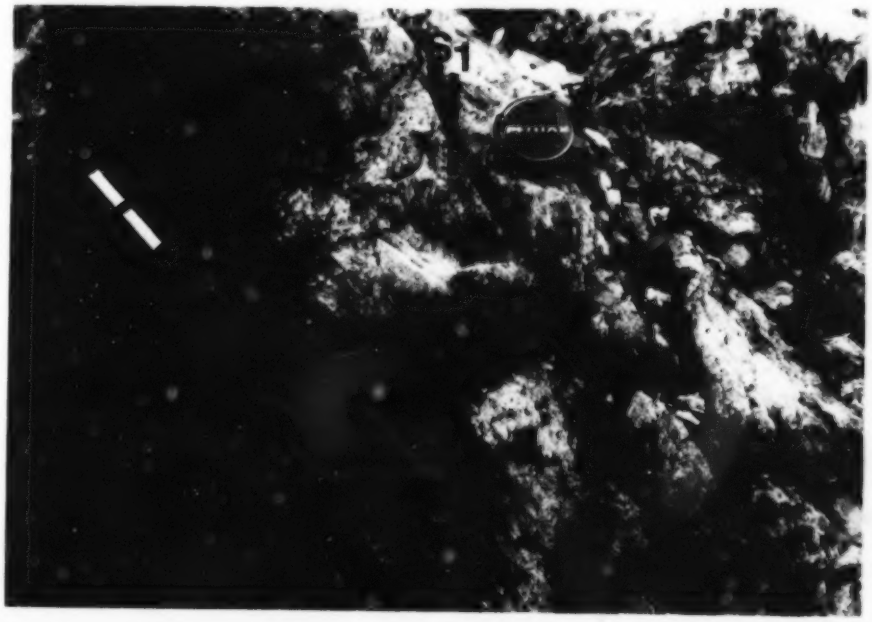

Photo 343.3. *Oblique cross-section view of F_1 fold with axial planar cleavage (S_1), marked by colour contrast, at the northern end of Scott Lake. S_1 is overprinted by a late northeast-trending cleavage (S_2 or S_3, white line).*

in the vicinity of the iron-carbonate-altered contact zone.

All earlier planar elements are overprinted by a moderately dipping, northeast-trending cleavage that forms the dominant planar fabric in the area (S_3). This cleavage is closely spaced and strongly developed within pelitic layers in turbidites, and is widely spaced and refracted within psammitic layers (*see* Photo 343.1). The 020–035°-trending S_3 cleavage can be distinguished from the axial planar S_2 where it cuts across tight 055°-trending folds (F_2), as

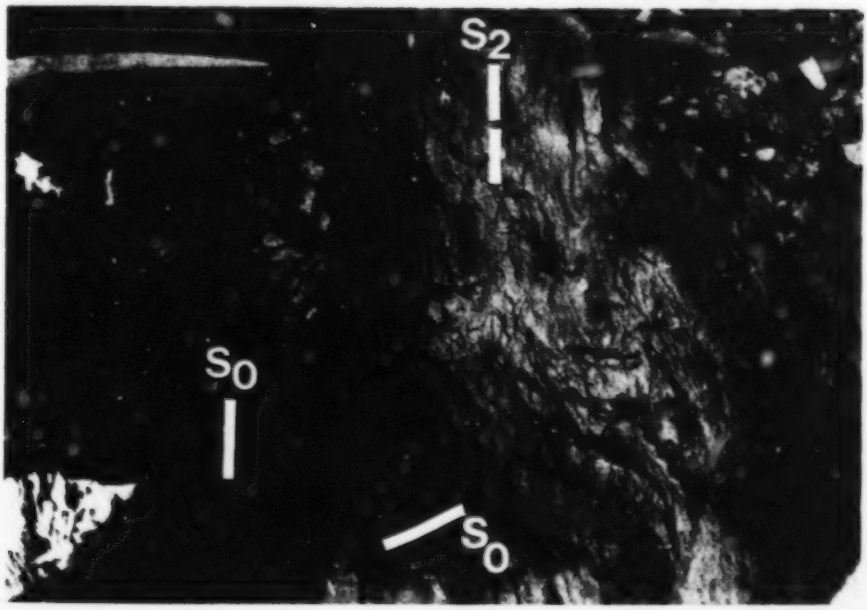

Photo 343.4. *F_2 fold with axial planar cleavage (S_2) at Goetz Lake. The fold is transected by the S_3 cleavage (plan view).*

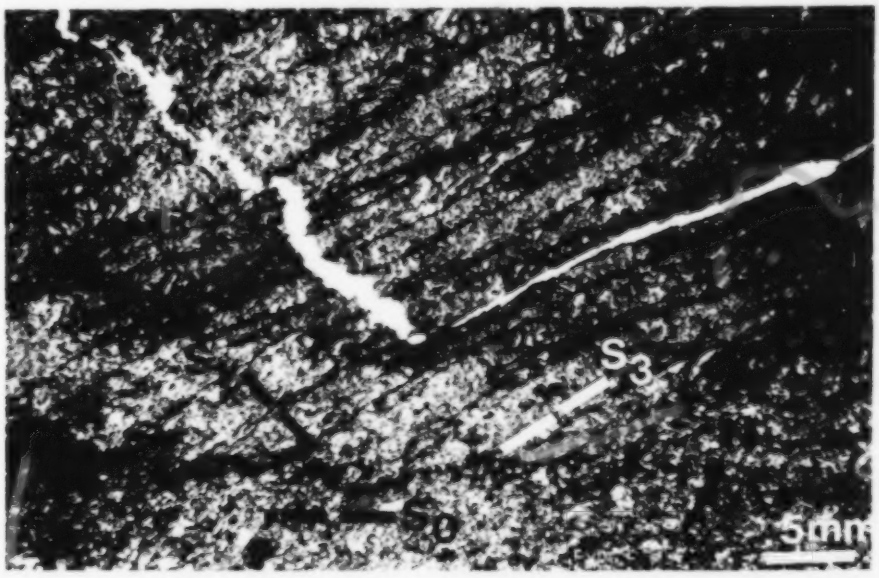

Photo 343.5. *Photomicrograph of metasiltstone at Goetz Lake (plane light). Early cleavage (S_1), oblique to bedding (S_0), is crenulated by strongly developed northeast-trending spaced cleavage (S_3). S_3 is axial planar to microfolds in extension fracture.*

shown in Photo 343.4. S_3 consistently overprints the 055°-trending S_2 cleavage where both are observed (Figure 343.2). In areas dominated by coarse-grained sedimentary rocks (psammites), the S_2 cleavage is refracted, and map-scale F_2 folds may exhibit axial surfaces trending 030°. S_3 is commonly associated with crenulations of bedding (F_3), but does not appear to be related to any major folds.

S_3 is axial planar to minor folds of northwest-trending extension fractures and quartz veins at mesoscopic and microscopic scales (Photo 343.5).

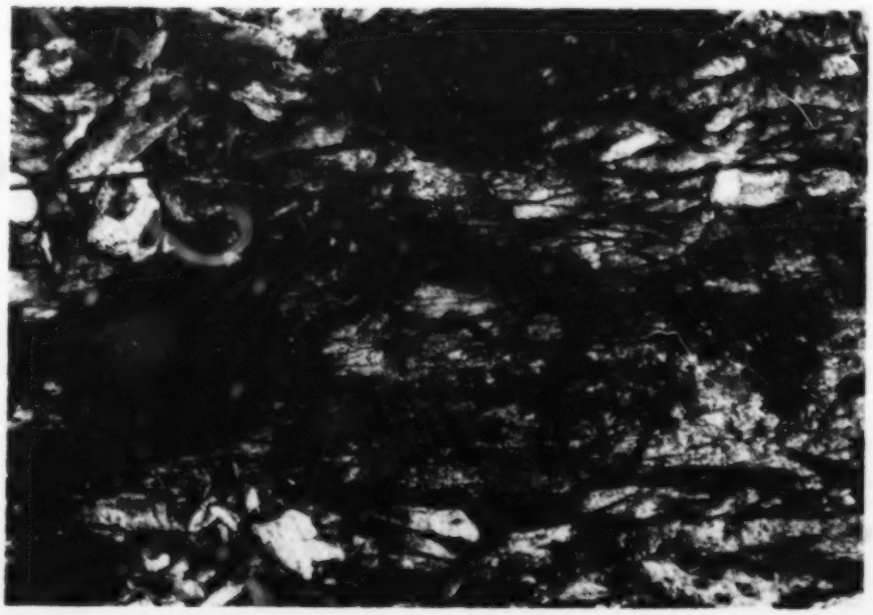

Photo 343.6. *Plan view of volcaniclastic metaconglomerate at the contact zone between metasediments and the youngest mafic volcanic unit (Goetz Lake). Fracture sets are parallel and at a low angle to the contact zone, forming a diamond-shaped pattern.*

This relationship is observed at least within mafic volcanic rocks and clastic sedimentary rocks at the top of the section. Dominantly mafic volcanic rocks and intrusions are crosscut by stockwork quartz veins and iron-carbonate-altered veins whose steep and flat northwest-trending, and steep west-trending, arrays indicate local northwest-southeast compression.

Centimetre-scale shear zones are more common within the mafic volcanic rocks, being concentrated in iron-carbonate-altered pillow selvages. *En echelon*, dominantly north-trending sigmoidal quartz vein arrays define sinistral shear zones within tuffaceous mafic volcanic rocks and turbiditic sedimentary rocks. Within volcaniclastic pebble conglomerates, late fracture sets exhibiting a diamond- or lozenge-shaped pattern (Photo 343.6) are oriented parallel and at low angles to the regional contact between volcanic and sedimentary rocks.

A structural discontinuity may exist in the northeastern part of the area, where an east-northeast-trending lineament separates overturned beds with opposed younging directions over a strike of at least 400 m (Figure 343.2). If this configuration of bedding represents an upside down syncline or a faulted version thereof, a pre-F_1 overturning of bedding is suggested. This event may be correlated with the early thrusting postulated by McGill and Shrady (1986) on the basis of similar overturned structures near Wawa.

West Andre Lake Area

This area is located in the southeastern part of Musquash Township and straddles the boundary with Corbiere Township (Figure 343.3; *see* Figure 343.1, area D). It is best reached by float-equipped aircraft from Hawk Junction.

According to Attoh (1980), the West Andre Lake area is located on the northern limb of a west-plunging syncline, such that a similar stratigraphic sequence as in the Goetz Lake–Scott Lake area is exposed (Figures 343.2 and 343.3). This would suggest that the northwesterly trending units face to the southwest. This interpretation (Attoh 1980) was based on the recognition of a west-plunging syncline between the Goetz Lake and West Andre Lake areas (Figure 343.1, areas C and D, respectively). Although the regional fold closure was not directly observed (Sage *et al.* 1984), Sage *et al.* (1982e, 1984) confirmed that the overall stratigraphic facing is to the southwest.

As in the Goetz Lake–Scott Lake area, primary structures within turbidites are well preserved. Abundant younging reversals across the west to northwest overall strike of bedding are present, and at every locality, mesoscopic fold closures with northwest-trending axial surfaces were traced.

Local younging reversals along the axial surfaces of the folds were observed, and an early S_1 cleavage may be preserved parallel to bedding (S_0), as shown in outcrop and thin section (Photos 343.7 and 343.8). This indicates that the S_1 cleavage predates

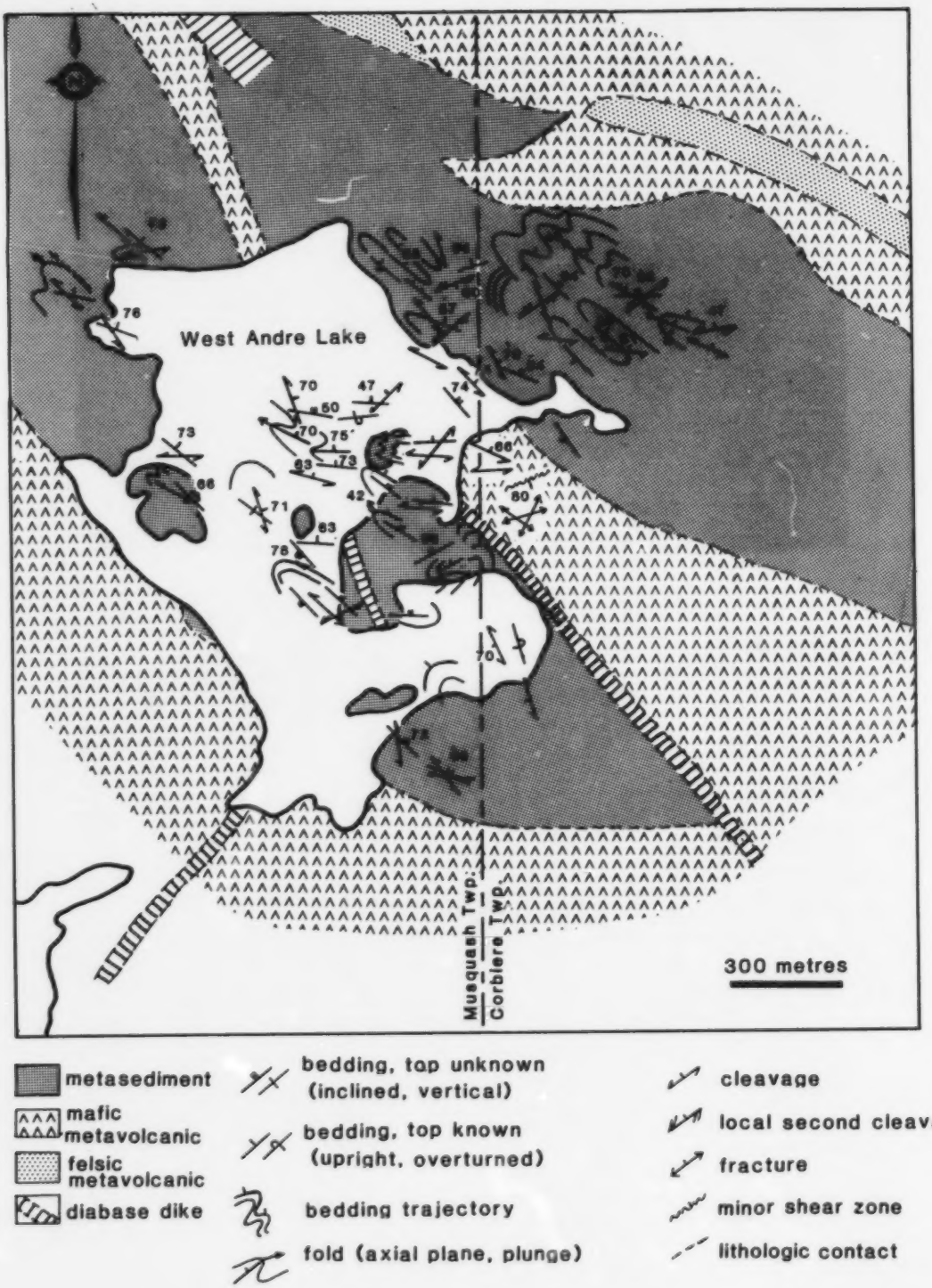

Figure 343.3. *Structural elements in metasediments in the West Andre Lake area. Distribution of rock types after Sage et al. (1982e, 1984).*

Photo 343.7. *Down-plunge view of northwest-trending F_2 fold showing early S_1 cleavage folded with bedding (S_0), northeast of West Andre Lake.*

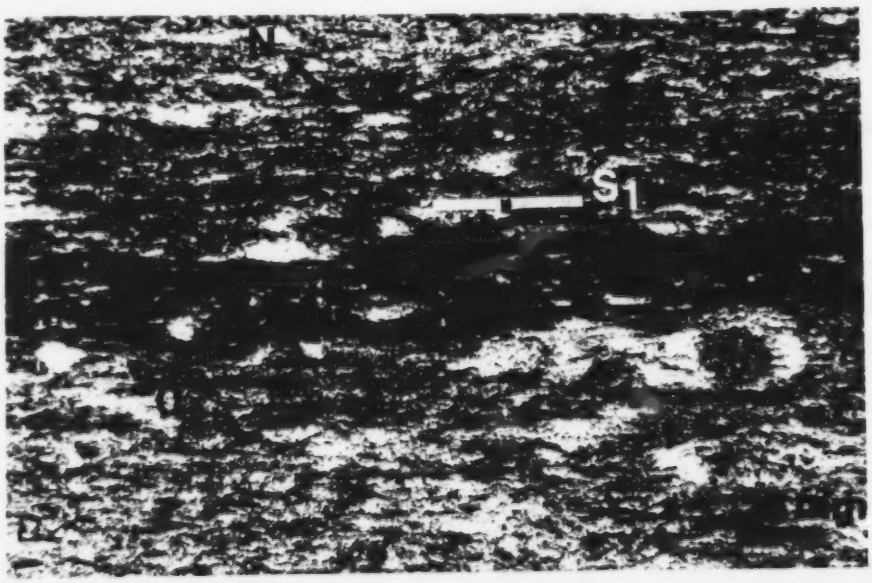

Photo 343.8. *Photomicrograph of metasiltstone in central West Andre Lake area (plane light). Early cleavage (S_1), parallel to S_0, is marked by flattening of detrital grains.*

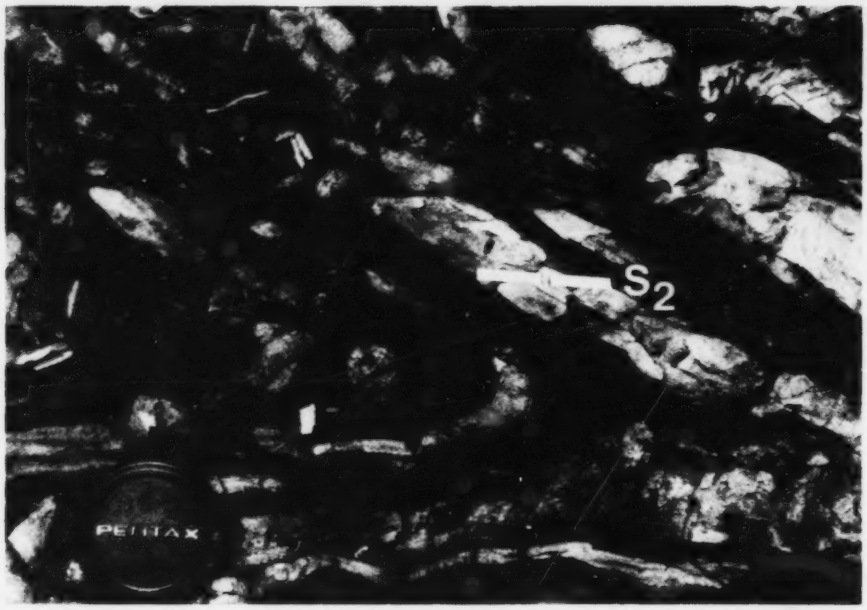

Photo 343.9. *Plan view of west-northwesterly trending F_2 fold with axial planar cleavage (S_2), northeast of West Andre Lake.*

the folds dominating the map pattern (F_2), and is associated with an earlier fold phase (F_1). A northwest-trending cleavage (S_2) is axial planar to these folds (Figure 343.3, Photo 343.9). Though normally well developed, the S_2 cleavage is not well preserved in some of the folds. The axial surface of the folds generally dips moderately to the north, causing overturning of the southern limbs. The plunge of folds varies from moderate to shallow to the northwest.

Interlimb angles vary widely from open to isoclinal. Fold symmetry was difficult to discern, as commonly only a single fold closure is preserved between northwest-striking beds. Limbs and portions of fold closures appear to be sheared off subparallel to their axial surfaces. Where discerned, folds exhibit variable symmetry, and it is tentatively concluded that the overall stratigraphic and structural facing within the turbiditic sediments is to the west-northwest and northwest, along the F_2 axial planar cleavage.

A northeast-trending cleavage (S_3) overprints and crenulates S_2 (Photo 343.10), and cuts across northwest-trending folds (F_2). Only one mesoscopic northeast-trending fold was observed.

Late deformation is expressed as various fracture sets and minor shear zones, and deciphering of their geometry requires more detailed work.

Kapimchigama Lake–Radford Lake Area

This area is located in the eastern part of Lalibert Township bordering into Leclaire Township (Figure 343.4; *see* Figure 343.1, area E). The geology of Leclaire Township was mapped by Sage and others (Sage 1985). Recent work within Lalibert Township is described by Sage (in press).

Clastic sedimentary rocks are the northwestern extension of the turbidite package studied at West Andre Lake (Figure 343.1). They are dominantly medium- to coarse-grained, thickly bedded psammites with minor pelitic interbeds, contrasting sharply with the thinly to thickly bedded turbidites that form part of the clastic sedimentary unit in the Goetz Lake–Scott Lake, and West Andre Lake areas. The sedimentary rocks in the Radford Lake area are also pervasively silicified, exhibiting a cherty appearance. Other rock types comprise massive to pillowed mafic volcanic rocks and a mafic biotite-hornblende-bearing porphyritic intrusion which is partly iron-carbonatized. East of the area (Figure 343.4) lies a granitoid intrusion, cut by northwest- and northeast-trending diabase dikes.

A large-scale, steeply northwest-plunging fold has been recognized in the northwestern part of the area, roughly conforming to the curvature of Radford Lake. At Radford Lake, bedding is dominantly overturned, younging to the southeast, defining a downward facing structure. This sharply contrasts with the upward, northwest-facing folds mapped in the West Andre Lake area.

A well developed cleavage (S_1) within pelitic interbeds in turbidites may predate the fold, as it appears to be folded with bedding. Likewise, reversals in younging direction along the axial surface of the

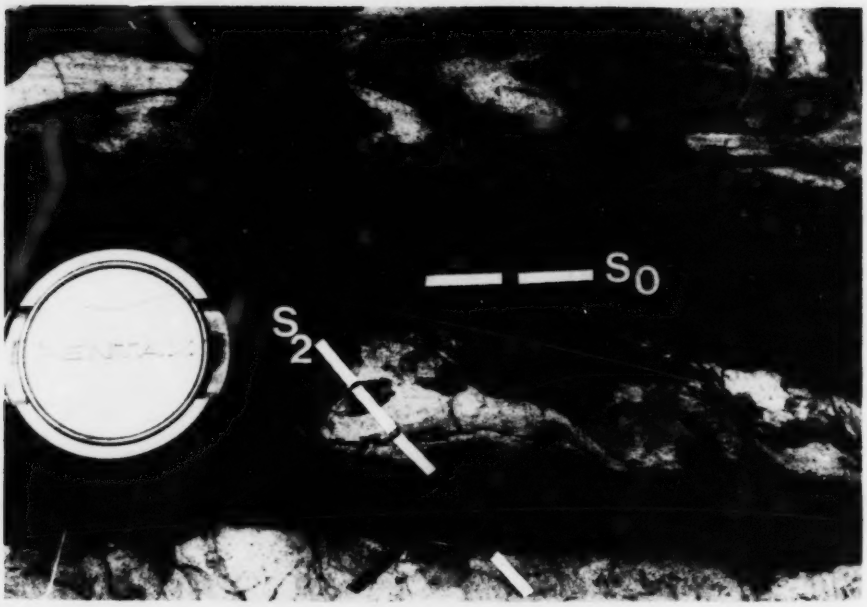

Photo 343.10. *Northwest-trending cleavage (S_2) is overprinted and crenulated by northeast-trending cleavage (S_3), northeast of West Andre Lake.*

regional fold indicate the presence of earlier folds. This was difficult to discern because only one mesoscopic early fold closure was observed. This U-shaped fold is upward facing and plunges moderately to the northwest. Lack of preservation of early structures may be attributed to the increased proportion of coarse psammites relative to pelites.

Locally, a second, northwest-trending cleavage (S_2) can be recognized which appears to be related to the regional fold closure (F_2). A later, northeasterly trending cleavage (S_3) was observed at the northern end of Kapimchigama Lake.

SUMMARY

Figure 343.5 schematically summarizes the sequence of early structural elements mapped within clastic metasediments of the three areas. The most prominent mesoscopic and megascopic folds in all subareas are F_2 folds which have axial surfaces that more or less parallel the regional strike of the metasedimentary unit. Earlier folds are indicated by younging reversals along the strike of the axial surfaces of F_2. The only planar fabric element that has a common orientation in all three areas is the northeasterly-trending S_3 cleavage.

EAST-CENTRAL MICHIPICOTEN GREENSTONE BELT (GOUDREAU–LOCHALSH)

Field work conducted during 1987 (Arias, in preparation) and 1988 indicates that the mafic and felsic metavolcanic and intrusive rocks underlying the Goudreau–Lochalsh area (Figure 343.1, area B) poorly preserve the early structural elements recognized in the metasediments within the central part of the belt. For example, only a single regional antiform has been recognized in the area. This interpretation is based on reversals in younging directions observed primarily within pillowed volcanic rocks where bedding could not be discerned readily. The rocks in the area may have experienced earlier folding, but evidence of this appears to have been largely transposed.

Regional foliation trajectories trend east to east-northeast, subparallel to lithologic contacts. Rare minor folds of a compositional colour banding or layering in intermediate to mafic tuffs are accompanied by a steeply dipping regional foliation. The layering may represent the transposed S_0/S_1, and the regional foliation may be an S_2 cleavage, axial planar to the earliest preserved regional fold (F_2).

A second northeast-trending planar fabric, subparallel to S_2 in plan, is preserved. These fabrics were originally interpreted as shear fabrics within

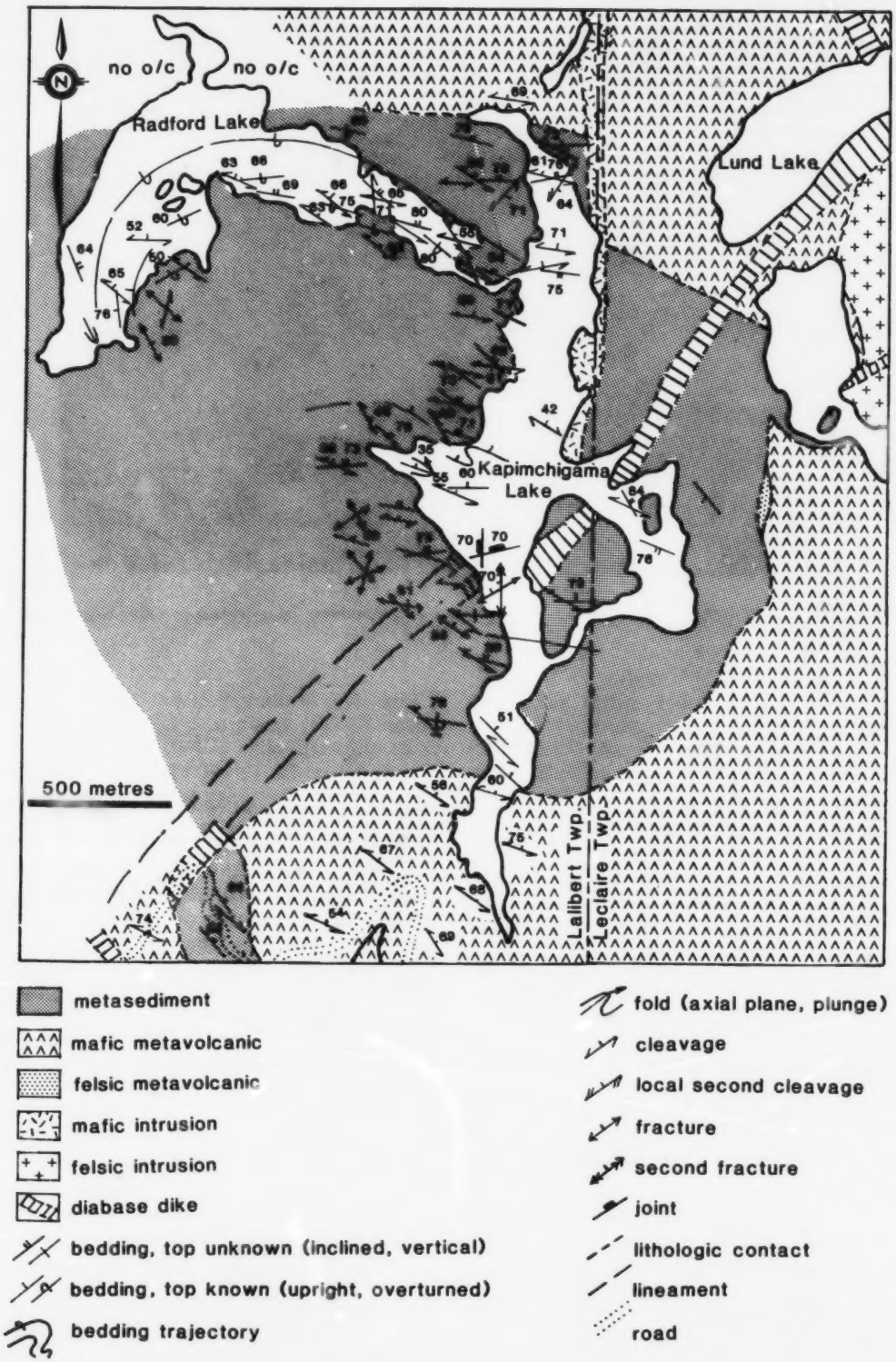

Figure 343.4. *Structural elements in metasediments in the Kapimchigama Lake–Radford Lake area. Distribution of rock types in Leclaire Township after Sage (1985a).*

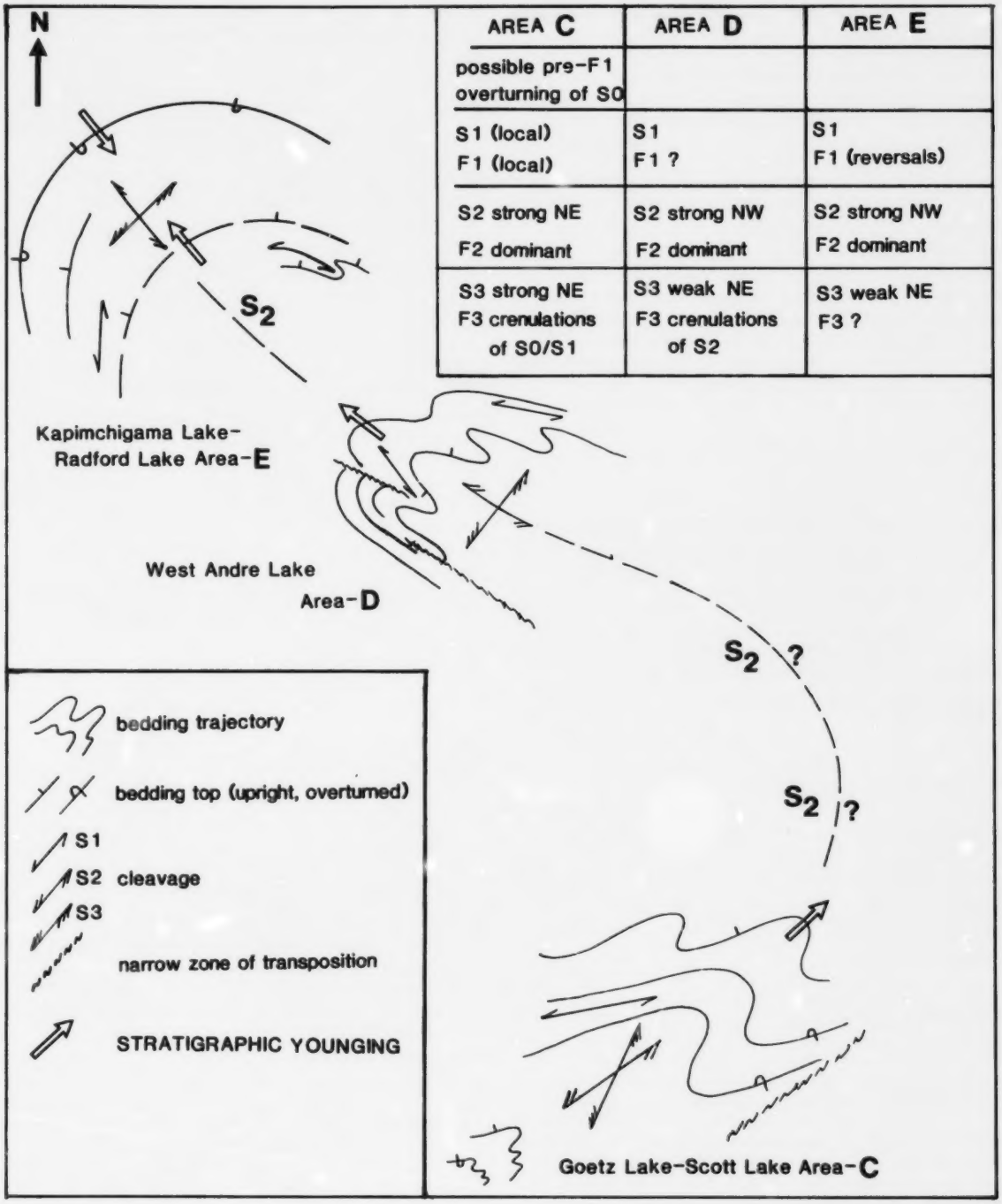

Figure 343.5. *Sketch of regional correlation of structural elements, showing geometry and early structural evolution along the metasedimentary unit in the central Michipicoten greenstone belt area (Figure 343.1, area A, and sub-areas C, D, E). Not to scale.*

broad zones of shearing. However, shear zones in the area are characteristically narrow, from centimetre-scale to a maximum of tens of metres wide. The two northeast-trending cleavages can be distinguished locally in cross section, where a moderately north-dipping cleavage (S_3) crenulates the S_2 cleav-

age. Generally, both cleavages dip steeply to the north. It is concluded that these cleavages formed in response to regional flattening, rather than to localized simple shear.

The northeast-trending S_3 cleavage in the Goudreau–Lochalsh area may be related to that preserved in the central belt area, but time relationships with the local shear zones have yet to be established.

Based on a qualitative study of deformation intensity in the rocks, two zones of high strain were delineated (Arias and Heather 1987). These coincide with major lithologic contacts, and consist of systematically oriented narrow shear zones and well developed planar fabrics within weakly deformed areas. The heterogeneous nature of the high strain zones makes it difficult to determine whether flattening and shearing were distinct events or were part of a single progressive deformation.

FURTHER RESEARCH

As shear zones and shear fractures locally host quartz-tourmaline and quartz-carbonate veins, some of which are auriferous, further work is planned to elucidate the position of the shear zones within the structural sequence.

Future studies will also concentrate on a correlation between structures mapped within the metasediments and those observed within the metavolcanics in the central part of the Michipicoten greenstone belt.

ACKNOWLEDGMENTS

We gratefully acknowledge the assistance, interest, and enthusiasm of R.P. Sage (Ontario Geological Survey, Toronto), D. Tortosa (Resident Geologist, Wawa), and E. Frey (Resident Geologist's Office, Ministry of Northern Development and Mines, Wawa).

REFERENCES

Arias, Z.G.

In Prep: Regional Structural Geology of the Goudreau-Lochalsh Area; *in* Geological Setting of Gold Mineralization in the Goudreau–Lochalsh District, Michipicoten Greenstone Belt, Ontario Geological Survey, Open File Report.

Arias, Z.G. and Heather, K.B.

1987: Regional Structural Geology Related to Gold Mineralization in the Goudreau–Lochalsh Area, District of Algoma; p. 107-109 *in* Summary of Field Work and Other Activities, 1987, by the Ontario Geological Survey, edited by R.B. Barlow, M.E. Cherry, A.C. Colvine, Burkhard O. Dressler and Owen L. White, Ontario Geological Survey, Miscellaneous Paper 137, 429p.

Attoh, K.

1980: Stratigraphic Relations of the Volcanic-Sedimentary Successions in the Wawa Greenstone Belt, Ontario; Geological Survey of Canada, Paper 80-1A, p.101-106.

Bruce, E.L.

1940a: Goudreau–Lochalsh Area, District of Algoma, Ontario; Ontario Department of Mines, Map 49G, scale 1:31 680 or 1 inch to 1/2 mile.

1940b: Geology of the Goudreau–Lochalsh Area; Ontario Department of Mines, Annual Report, Volume 49, part 3, p.1-50.

Frarey, M.J. and Krogh, T.E.

1986: U–Pb Zircon Ages of Late Internal Plutons of the Abitibi and Eastern Wawa Subprovinces, Ontario and Québec; p.43-48 *in* Current Research, Part A, Geological Survey of Canada, Paper 86–1A.

Frohberg, H.

1935: The Ore Deposits of the Michipicoten Area; Ontario Department of Mines, Annual Report, Volume 44, Part 8, p.39-83.

Gledhill, T.L.

1927: Michipicoten Gold Area, District of Algoma; Ontario Department of Mines, Annual Report, Volume 36, Part 2, p.1-49.

Goodwin, A.M.

1962: Structure, Stratigraphy and Origin of Iron Formations, Michipicoten Area, Algoma District, Ontario, Canada; Geological Association of America, Bulletin, Volume 73, p.561-586.

1963: Michipicoten Area Compilation Sheet; Ontario Department of Mines, Preliminary Geological Map P.184, scale 1 inch to 2 miles.

Heather, K.B. and Arias, Z.G.

1987: The Geological Setting of Gold Mineralization in the Goudreau–Lochalsh Area, District of Algoma; p.155-162 *in* Summary of Field Work and Other Activities, 1987, by the Ontario Geological Survey, edited by R.B. Barlow, M.E. Cherry, A.C. Colvine, Burkhard O. Dressler and Owen L. White, Miscellaneous Paper 137, 429p.

Heather, K.B., Arias, Z.G. and Sage, R.P.

1988: The Geological Setting of Gold in the Wawa Gold Camp, Ontario, Canada, Abstract Number 23; p.20-22 *in* Bicentennial Gold '88, Extended Abstracts Poster Programme, Volume 1, Geological Society of Australia Incorporated.

Heather, K.B. and Buck, S.

1988: The Geological and Structural Setting of Gold Mineralization in the Missanabie-Renabie District of the Michipicoten Greenstone Belt, Wawa, Ontario; p. 257-270 *in* Summary of Field Work and Other Activities, 1988, by the Ontario Geological Survey, edited by A.C. Colvine, M.E. Cherry, Burkhard O. Dressler, P.C. Thurston, C.L. Baker, R.B. Barlow and Chris Riddle, Ontario Geological Survey, Miscellaneous Paper 141, 498p.

McGill, G.E. and Shrady, C.H.

1986: Evidence for a Complex Archean Deformational History; Southwestern Michipicoten Greenstone Belt, Ontario; Journal of Geophysical Research, Volume 91, no. B13, p.E281-E289.

Milne, V.G., Giblin, P.E., Bennett, G., Thurston, P.C., Wolfe, W.J., Giguere, J.F., Leahy, E.J. and Rupert, R.J.

1971: Manitouwadge-Wawa Sheet; Ontario Department of Mines, Geological Compilation Series, Map 2220, scale 1:253 440 or 1 inch to 4 miles.

Moore, E.S.

1931: Goudreau and Michipicoten Gold Areas, District of Algoma; Ontario Department of Mines, Annual Report, Volume 40, Part 4, p.1-54.

1948: Structure of the Michipicoten-Goudreau Area; p.414-419 *in* Structure of Canadian Ore Deposits, Geology Division, Canadian Institute of Mining and Metallurgy.

Sage, R.P.

1979: Wawa Area, District of Algoma; p.48-53 *in* Summary of Field Work, 1979, by the Ontario Geological Survey, edited by V.G. Milne, Owen L. White, R.B. Barlow and C.R. Kustra, Ontario Geological Survey, Miscellaneous Paper 90, 245p.

1980: Wawa Area, District of Algoma; p.47-50 *in* Summary of Field Work, 1980, by the Ontario Geological Survey, edited by V.G. Milne, Owen L. White, R.B. Barlow, J.A. Robertson and A.C. Colvine, Ontario Geological Survey, Miscellaneous Paper 96, 201 p.

1981: Josephine Area, District of Algoma; p.37-40 *in* Summary of Field Work, 1981, by the Ontario Geological Survey, edited by John Wood, Owen L. White, R.B. Barlow and A.C. Colvine, Ontario Geological Survey, Miscellaneous Paper 100, 255p.

1982: Josephine Area, District of Algoma; p.28-33 *in* Summary of Field Work, 1982, by the Ontario Geological Survey, edited by John Wood, Owen L. White, R.B. Barlow and A.C. Colvine, Ontario Geological Survey, Miscellaneous Paper 106, 235p.

1983: Josephine Area, District of Algoma; p.45-49 *in* Summary of Field Work, 1983, by the Ontario Geological Survey, edited by John Wood, Owen L. White, R.B. Barlow and A.C. Colvine, Ontario Geological Survey, Miscellaneous Paper 116, 313p.

1984: Josephine-Goudreau Area, District of Algoma; p.56-63 *in* Summary of Field Work, 1984, Ontario Geological Survey, edited by Owen L. White, R.B. Barlow and A.C. Colvine, Ontario Geological Survey, Miscellaneous Paper 119, 309 p.

1985a: Precambrian Geology of Leclaire Township, District of Algoma; Ontario Geological Survey, Geological Series - Preliminary Map, P.2636, scale 1:15 840 or 1 inch to 1/4 mile.

1985b: Goudreau-Lochalsh Area, District of Algoma; p.90-94 *in* Summary of Field Work and Other Activities, 1985, Ontario Geological Survey, edited by John Wood, Owen L. White, R.B. Barlow and A.C. Colvine, Ontario Geological Survey, Miscellaneous Paper 126, 351p.

1986: Stratigraphic Correlation in the Wawa Area; p.62-68 *in* Volcanology and Mineral Deposits, edited by John Wood and Henry Wallace, Ontario Geological Survey, Miscellaneous Paper 129, 183p.

1987: Geology of the Goudreau-Lochalsh and Kabenung Lake Areas, District of Algoma; p.134-137 *in* Summary of Field Work and Other Activities, 1987, by the Ontario Geological Survey, edited by R.B. Barlow, M.E. Cherry, A.C. Colvine, Burkhard O. Dressler and Owen L. White, Ontario Geological Survey, Miscellaneous Paper 137, 429p.

1988: Geology of the Kabenung Lake Area, District of Algoma; p.242-248 *in* Summary of Field Work and Other Activities, 1988, by the Ontario Geological Survey, edited by A.C. Colvine, M.E. Cherry, Burkhard O. Dressler, P.C. Thurston, C.L. Baker, R.B. Barlow and Chris Riddle, Ontario Geological Survey, Miscellaneous Paper 141, 498p.

In Press: Geology of Chabanel, Esquega, Lastheels and McMurray Townships, District of Algoma; Ontario Geological Survey, Open File Report 5586.

In Press: Geology of Abotossaway, Corbiere, Leclaire and Musquash Townships, District of Algoma; Ontario Geological Survey, Open File Report 5587.

In Press: Geology of Aguonie, Bird, Finan and Jacobson Townships, District of Algoma, Ontario Geological Survey, Open File Report 5588.

In Press: Precambrian Geology of Lalibert Township, District of Algoma, Ontario Geological Survey, Geological Series - Preliminary Map, scale 1:15 840 or 1 inch to 1/4 mile.

Sage, R.P., Thorpe, R. and Berdusco, E.

1987: Field Trip Guidebook—Geology and Stratigraphy of the Michipicoten Iron Formation; Institute on Lake Superior Geology, Thirty-third Annual Meeting, Wawa, Ontario, May 1987, Volume 33, Part 3, 93 p.

Sage, R.P., Rebic, Z., Abercrombie, S., Neale, K., MacMillan, D., England, D. and Calvert, T.

1982a: Precambrian Geology of Chabanel Township, District of Algoma; Ontario Geological Survey, Geological Series - Preliminary Map, P.2439, scale 1:15 840 or 1 inch to 1/4 mile.

Sage, R.P., Rebic, Z., Abercrombie, S., Neale, K., MacMillan, D. and Calvert, T.

1982b: Precambrian Geology of Esquega Township, Wawa Area, District of Algoma; Ontario Geological Survey, Geological Series - Preliminary Map P.2440, scale 1:15 840 or 1 inch to 1/4 mile.

Sage, R.P., Sawitsky, E., Turner, J., Leeselleuer, P. and Sagle, E.

1982c: Precambrian Geology of McMurray Township, Wawa Area, District of Algoma; Ontario Geological Survey, Geological Series - Preliminary Map P.2441, scale 1:15 840 or 1 inch to 1/4 mile.

1982d: Precambrian Geology of Lastheels Township, Wawa Area, District of Algoma; Ontario Geological Survey, Geological Series - Preliminary Map P.2442, scale 1:15 840 or 1 inch to 1/4 mile.

Sage, R.P., England, D. Calvert, T., Oudkerk, G., Worona, R. and Kosciusko, K.

1982e: Precambrian Geology of Musquash Township, District of Algoma; Ontario Geological Survey, Geological Series - Preliminary Map P.2569, scale 1:15 840 or 1 inch to 1/4 mile.

Sage, R.P., Calvert, T., Epstein, R., England, D., Kosciusko, K., Worona, R., Oudkerk, J., Inasi, J., Lockwood, M. and Thomas, D.

1984: Precambrian Geology of Corbiere Township, District of Algoma; Ontario Geological Survey, Geological Series - Preliminary Map P.2607, scale 1:15 840 or 1 inch to 1/4 mile.

Sullivan, R.W., Sage, R.P. and Card, K.D.

1985: U-Pb Zircon Age of the Jubilee Stock in the Michipicoten Greenstone Belt near Wawa, Ontario; Geological Survey of Canada, Current Research, Part B, Paper 85-1B, p.361-365.

Turek, A., Smith, P.E. and Van Schmus, W.R.

1982: Rb-Sr and U-Pb Ages of Volcanism and Granite Emplacement in the Michipicoten Belt - Wawa, Ontario; Canadian Journal of Earth Sciences, Volume 19, p.1608-1626.

1984: U-Pb Zircon Ages and the Evolution of the Michipicoten Plutonic-Volcanic Terrain of the Superior Province, Ontario; Canadian Journal of Earth Sciences, Volume 21, p.457-464.

Turek, A., VanSchmus, W.R. and Sage, R.P.

1988: Extended Volcanism in the Michipicoten Greenstone Belt, Wawa, Ontario; p. 127 *in* Program with Abstracts, Geological Association of Canada - Mineralogical Association of Canada Joint Annual Meeting, Volume 13.

Grant 351 Stratigraphy and Sedimentology of the Upper Ordovician Georgian Bay Formation, Manitoulin Island and Bruce Peninsula

M. Byerley and M. Coniglio

Department of Earth Sciences, University of Waterloo, Waterloo

ABSTRACT

The Georgian Bay Formation is a shallowing-upward, Upper Ordovician shelf succession composed of four principal lithofacies. Shales at the bottom of the formation are overlain by interbedded limestones and shales, argillaceous limestones and then dolostones at the top. Measured sections across Manitoulin Island can be correlated lithostratigraphically but detailed correlation with coeval strata on the Bruce Peninsula remains problematical.

Skeletal grainstones, packstones and wackestones are the dominant carbonate sediments with local bryozoan, stromatoporoid and coral biostromal floatstones. Outcrops and polished slabs display scoured surfaces, load structures, graded beds, megaripples, amalgamated beds, hardgrounds and hummocky cross-stratification. Abundant trace fossils from the *Skolithos* and *Cruziana* ichnofacies are present. The spectrum of sedimentary structures and ichnofabrics indicates deposition in a shallowing subtidal setting subjected to increasing storm influence. Biostromes near the top of the sequence resulted from storm winnowing as well as *in situ* accumulation. Hardground formation, early aragonite dissolution, silicification and pyrite precipitation are recorded in the interbedded limestones and shales and in the shale-dominated lower parts of the sequence. The carbonate-dominated upper part of the formation is characterized by dolomitized and leached allochems and late-stage saddle dolomite and gypsum. Comparison of the Georgian Bay Formation to similar Ordovician strata in central eastern North America suggests that storm effects were the dominant control on shelf sedimentation in Paleozoic epicontinental seas.

INTRODUCTION

Strata of the Upper Ordovician Georgian Bay Formation are widespread, undeformed and well exposed in roadside outcrops and wave-cut terraces of the northeastern Lake Huron area. The formation extends from Manitoulin Island on the northeastern margin of the Michigan Basin along the east side of the Bruce Peninsula and over the Algonquin Arch to Toronto where it disappears due to post-Paleozoic erosion (Figures 351.1 and 351.2). Georgian Bay strata are correlative to sequences exposed in Manitoba, Michigan, Ohio, Kentucky, Indiana, West Virginia, upper New York State and eastern Ontario (Table 351.1).

The primary goal of this project is to integrate stratigraphic and sedimentological information from outcrop and existing subsurface cores to improve regional correlation and clarify local facies relationships. A second aim is to understand the role of storms in the deposition of the Georgian Bay Formation. The depositional model that is proposed will assist in better understanding the origin of storm-influenced, mixed carbonate-siliciclastic shelf sequences occurring throughout the Lower Paleozoic of eastern North America. This study will also briefly examine the diagenesis of the Georgian Bay Formation, especially where fracture dolomitization has occurred. Local dolomitization is closely associated with hydrocarbon occurrences in other carbonate strata in southwestern Ontario, although sedimentary rocks of the Georgian Bay Formation are generally not considered to be good reservoir rocks (Bailey 1984; Coogan and Parker 1985).

This progress report is based upon examination of outcrop of the Georgian Bay Formation on Manitoulin Island and at the type area on the Bruce Peninsula. Field work was carried out between April and June of 1988. Over 50 stratigraphic sections were measured. Major section locations are shown in Figure 351.2. Grid locations of significant measured sections are listed in Table 351.2. Approximately 500 oriented samples were collected. To date 200 petrographic thin sections have been examined using cathodoluminescence, epifluorescence and staining. An additional 100 stained slabs and acetate peels have also been studied.

GEOLOGIC SETTING AND STRATIGRAPHY

The gentle (less than 1°) regional dip (Caley 1936) and favourably oriented outcrop created by the Niagara Escarpment results in excellent exposure of the Georgian Bay Formation throughout the northeastern Lake Huron area (Figure 351.2). On Manitoulin Island, outcrop occurs along the northern and eastern shores. Outcrop on the Bruce Peninsula extends from Cape Crocker to Meaford.

The Georgian Bay Formation is up to 150 m thick. This mixed carbonate-siliciclastic succession

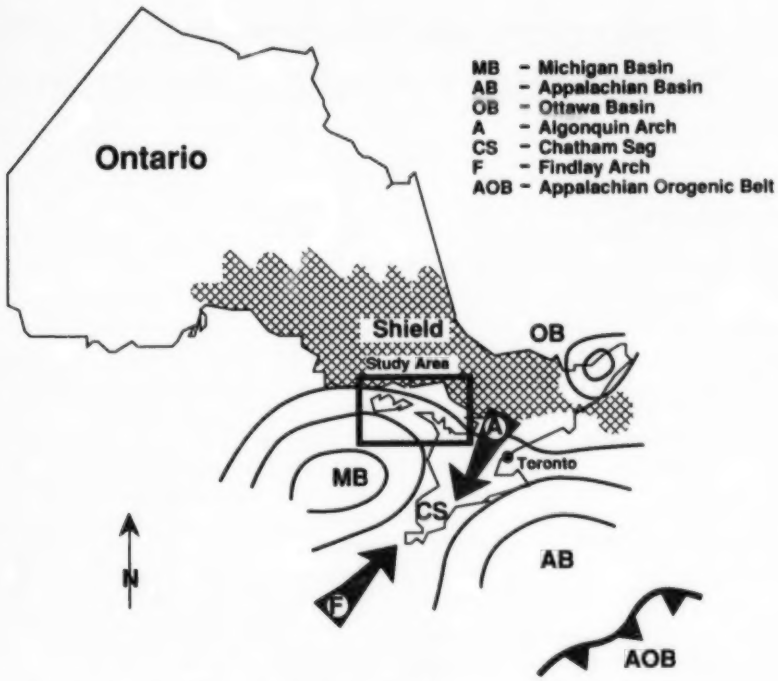

Figure 351.1. *Geologic setting of study area. Study area is enlarged in Figure 351.2.*

TABLE 351.1. EASTERN NORTH AMERICAN STRATA EQUIVALENT TO THE GEORGIAN BAY FORMATION.

Location	Formation (Listed in order of decreasing age)			
S Manitoba[1] (Wiliston Basin)	Upper Red Creek (R)	Stony Mountain (R)	Stonewall (G)	
Upper Michigan Peninsula[2] (Michigan Basin)	Bill's Creek (M/R)	Stonington & Big Hill (R)		Manitoulin (S)
Manitoulin Island[3]	Blue Mountain (M)	Georgian Bay (R)		Manitoulin (S)
SW Ontario[2,3]	Blue Mountain (M)	Georgian Bay (R)	Queenston (R)	Manitoulin (S)
SE Ohio[4]	Oregonia (M)	Waynesville, Liberty, Whitewater & Saluda (R)		
Kentucky and S Ohio[4]	Oregonia (M)	Waynesville, Liberty, Whitewater & Drakes (R)		
Indiana[4]	Oregonia (M)	Waynesville, Liberty, Whitewater & Elkhorn (R)		
New York State[2,5] (Appalachian Basin)	Whetstone Gulf (M)	Reedsville (R)	Martinsburg (R)	Whirlpool (S)
West Virginia[5,6]		Reedsville (R)	Martinsburg (R)	
E Ontario[1] (Ottawa Basin)	Billings (M)	Carlsbad (R)	Russell/= Queenston (R)	

(M) Maysvillian Series *(R) Richmondian Series*
(G) Gamachian Series *(S) Silurian System*
(M/R) Maysvillian to Richmondian */= Lateral Facies equivalents*

1- Barnes et al. 1981; 2- Liberty and Bolton 1971; 3- Johnson and Telford 1981a; 4- Tobin 1982; 5- Horst 1978; 6- Kriesa 1981

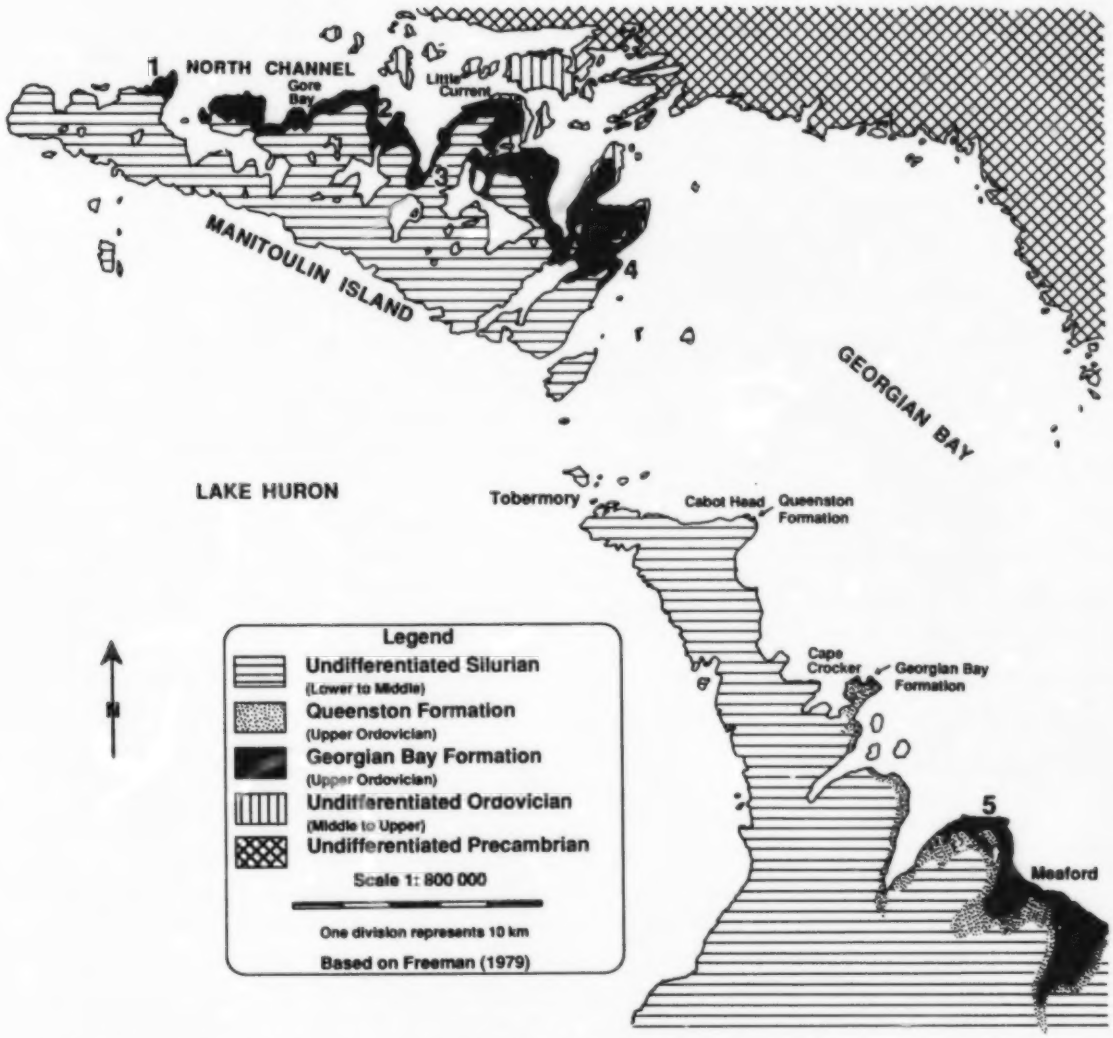

Figure 351.2. *Location map showing geographic extent of the Georgian Bay Formation and the location of measured sections discussed in text.*

conformably overlies organic-rich shales of the Blue Mountain Formation (Figure 351.3). On Manitoulin Island the Georgian Bay Formation is unconformably overlain by the pervasively dolomitized strata of the Manitoulin Formation (Lower Silurian). On the Bruce Peninsula the carbonates at the top of the Georgian Bay Formation pass laterally into time-equivalent, fine-grained, siliciclastic strata of the Queenston Formation (Figure 351.3).

The Georgian Bay Formation was deposited during Richmondian time at approximately 15°S paleolatitude in a broad epicontinental sea covering the eastern portion of North America (Bambach *et al.* 1980). Paleogeographic reconstructions indicate that the North American craton was moving southward and was rotated about 45° clockwise from its present orientation (Bambach *et al.* 1980). Major regression occurred towards the conclusion of Richmondian time. The resulting hiatus at the top of the Georgian Bay Formation represents the entire Gamachian Stage (Barnes and Bolton 1988) and was marked by intermittent subaerial exposure on the Bruce Peninsula.

Most studies of the Georgian Bay Formation (Foerste 1912, 1924; Caley 1936; Williams 1937; Copper 1971, 1978; Horst 1978) have concentrated on its fauna. Mapping by Liberty (1957, 1969, 1972) and Liberty and Bolton (1971) was based upon lithostratigraphy, but faunal occurrences were used in the regional correlation. Johnson and Telford (1981a, 1981b, 1985) provide the most recent

TABLE 351.2. GRID LOCATIONS OF SIGNIFICANT MEASURED SECTIONS.

Locality Name	Locality Number	NTS Grid Reference (Easting-Northing)
Manitoulin Island		
Cyril Cove (BP)	5/17/2	3558-50915
E Cape Roberts (BP)	5/17/1	3590-50930
[1]Cape Roberts Bluffs	5/23/1	3603-50910
Creighton Pt Bluffs	4/30/3	3693-50907
Beer Point Bluffs	4/30/2	3715-50908
Gore Bay Airport	4/19/10	3782-50835
Janet Head Bluffs	4/14/4	3840-50890
Gore Bay Village (RC)	4/19/2	3865-50845
East Bluff Falls (WF)	5/01/8	3896-50900
McDougal Falls (WF)	5/01/7	3917-50915
McRae Beach Bluff	5/30/1	3919-50919
Maple Pt Cottages (BP)	4/17/4	3995-50930
Jacksonville Road (RC)	5/01/1	3995-50894
[2]Sextant Falls (RC & WF)	4/17/5	3995-50889
Grey Pt Lookout (RC)	5/01/3	3994-50882
Kagawong W Quarry	5/04/1	4001-50831
Lebar Lookout	5/01/1	4009-50852
St. Paul's Church (RC)	5/26/2	4024-50838
Bridal Veil Falls (WF)	4/19/1	4026-50837
Mudge Bay Hill (RC)	5/01/6	4029-50852
Kagawong E (RC)	5/19/2	4030-50831
West Bay E (RC BP)	5/25/2	4090-50780
[3]West Bay East (RC)	4/30/5	4106-50742
Honora Pt Rd (RC)	5/04/2	4143-50832
McLean Mt Falls (WF)	5/02/3	4253-50893
McLean Mt Stream (WF/BP)	5/09/2	4268-50880
McLean Mt E (RC/BP)	4/21/7	4268-50869
Conc Rd IV & Hwy 6 (BP)	4/21/8	4294-50869
Manitoulin Island (cont.)		
Hwy 6 & Conc Rd 15 (RC)	5/07/2	4310-50808
Ten Mile Pt @ Conc Rd X (RC)	5/10/4	4339-50785
Bay Estates Rd (RC)	5/12/2	4335-50787
Manitoulin Airport (RC)	5/10/1	4339-50770
High Falls (WF)	4/18/10	4339-50720
Bidwell Rd & Hwy 6 (RC)	4/20/2	4339-50673
Sunova Beach (BP)	4/20/1	4370-50664
Two O'Clock (RC)	4/18/9	4400-50650
N Wiky (BP)	4/18/7	4594-50770
Kaboni Water Falls (WF BP)	4/18/2	4450-50646
Cape Smith Road (BP)	4/18/5	4473-50687
[4]Clay Cliffs Bluffs	5/03/1	4540-50670
Clay Cliffs Water Fall (WF)	5/04/1	4547-50672
Bruce Peninsula		
Cabot Head Bluff	6/13/2	4773-50100
Benjamin Pt Bluff	6/15/5	4980-49794
[5]Clay Banks Bluff	6/16/1	5517-49230
Black Pt Bluff (&BP)	6/14/1	5298-49465
Lower Workman's Ck (SC)	6/17/1	5350-49378
Upper Workman's Ck (SC)	6/17/2	5350-49370

Superscripts (1) match the section numbers used in Figure 351.5.
Bluff - an extended lateral and vertical section
(WF) - Water fall exposure (BP) - Bedding plane
(RC) - Road cut (WF BP) Water fall and bedding plane
(SC) - Stream bank and stream bedding plane exposure
Beach - laterally extensive wave cleared bedding plane

lithostratigraphic information on the Georgian Bay Formation (Figure 351.3).

The Georgian Bay Formation, as currently recognized by Johnson and Telford (1985), includes three previously established formations: Wikwemikongsing, Meaford and Kagawong. Each of these formations was defined biostratigraphically by Foerste (1912, 1924). The Wikwemikongsing Formation consists of 46–100 m of light grey fossiliferous shale with scattered fossiliferous carbonate beds. The lower contact with shales of the Whitby Formation (now Blue Mountain Formation) in southern Ontario is placed at the first carbonate 'hardband' (Caley 1936). On Manitoulin Island, however, this definition is problematic because carbonate layers occur in outcrop of the Blue Mountain Formation. The overlying Meaford Formation is an 11–15 m thick fissile shale containing beds of limestone that increase upwards in abundance throughout the upper two-thirds of the unit. The Kagawong Formation was described as a 22–31 m thick argillaceous limestone with interbedded shale. Parts of this unit are biostromal (Foerste 1924; Copper 1971, 1978; Horst 1978; Johnson and Telford 1985). These strata appear to be stratigraphically equivalent to the siliciclastic-dominated Queenston Formation of central southern Ontario.

Liberty (1972) redefined the Georgian Bay Formation to consist of a Lower Member (Wikwemikongsing strata) and an Upper Member which was subdivided further into a Lower Submember (Meaford strata) and an Upper Submember (Kagawong strata, Figure 351.3).

The relationship of the type area on the Bruce Peninsula to outcrop on Manitoulin Island is uncertain because Liberty's report for the Ontario Department of Mines was never published. In addition, the reference section in the type area near Meaford is ambiguously located and exposures in this area are discontinuous. The best exposure in the type area occurs at Clay Banks within the Meaford Tank Range of the Department of National Defence.

CORRELATION

For convenience, an informal nomenclature is adopted in this report to refer to the submembers of the Upper Member of the Georgian Bay Formation.

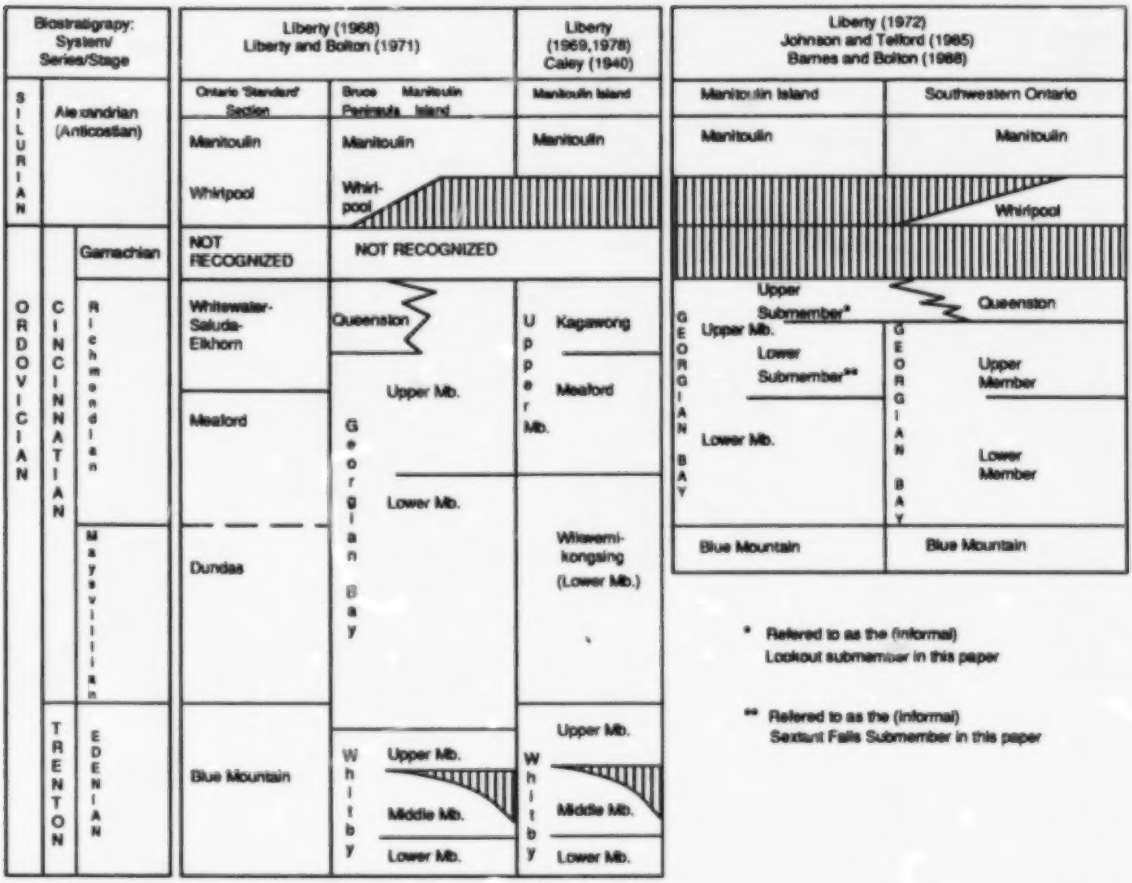

Figure 351.3. *Stratigraphic nomenclature for the Georgian Bay Formation. Additional sources include Barnes et al. (1981) and Russell and Telford (1983).*

The Lower and Upper Submembers are referred to as the Sextant Falls and Lookout submembers after localities where they are well exposed on Manitoulin Island. Recognition of these units on Manitoulin Island is based upon several criteria (Figure 351.4). The Lower Member–Sextant Falls submember contact occurs at the base of the first sequence of interbedded bioclastic argillaceous wackestone and shale in which shale beds are less than 50 cm in thickness. The Sextant Falls–Lookout submember contact is placed at the base of first 1 m thick, pervasively dolomitized carbonate interval. Above this contact, shale and argillaceous carbonates are minor. The Lookout submember is further characterized by the widespread occurrence of silicified bryozoans and brachiopods, as well as late-phase pore-filling gypsum cement.

Five stratigraphic sections are correlated from west to east across the study area (Figure 351.5). The Clay Cliffs section at the southeastern end of Manitoulin Island is the most complete exposure of the Lower Member. It also contains approximately 9 m of the Sextant Falls submember. The Sextant Falls–Lookout submember contact is not present at this locality. Cape Roberts exposes the full Sextant Falls submember as well as 3.5 m of the underlying Lower Member. The upper part of the section at Cape Roberts correlates to the lower part of the Sextant Falls section. At Sextant Falls a prominent stromatoporoid biostrome 3.6 m above the base marks the transition from shale-dominated sediment to interbedded wackestone and shale. The base of the Lookout submember lies 2 m from the top of this section. The Sextant Falls–Lookout submember contact is not exposed at the West Bay road cut, but a prominent stromatoporoid horizon can be correlated based on bedding style and diagenetic features. A series of discontinuous outcrops of the Sextant Falls submember is found in a drainage ditch immediately below the West Bay section.

The Sextant Falls and Lookout submembers show only minor thickness variations across Manitoulin Island. There is, however, a gradual increase in the argillaceous content of the Sextant

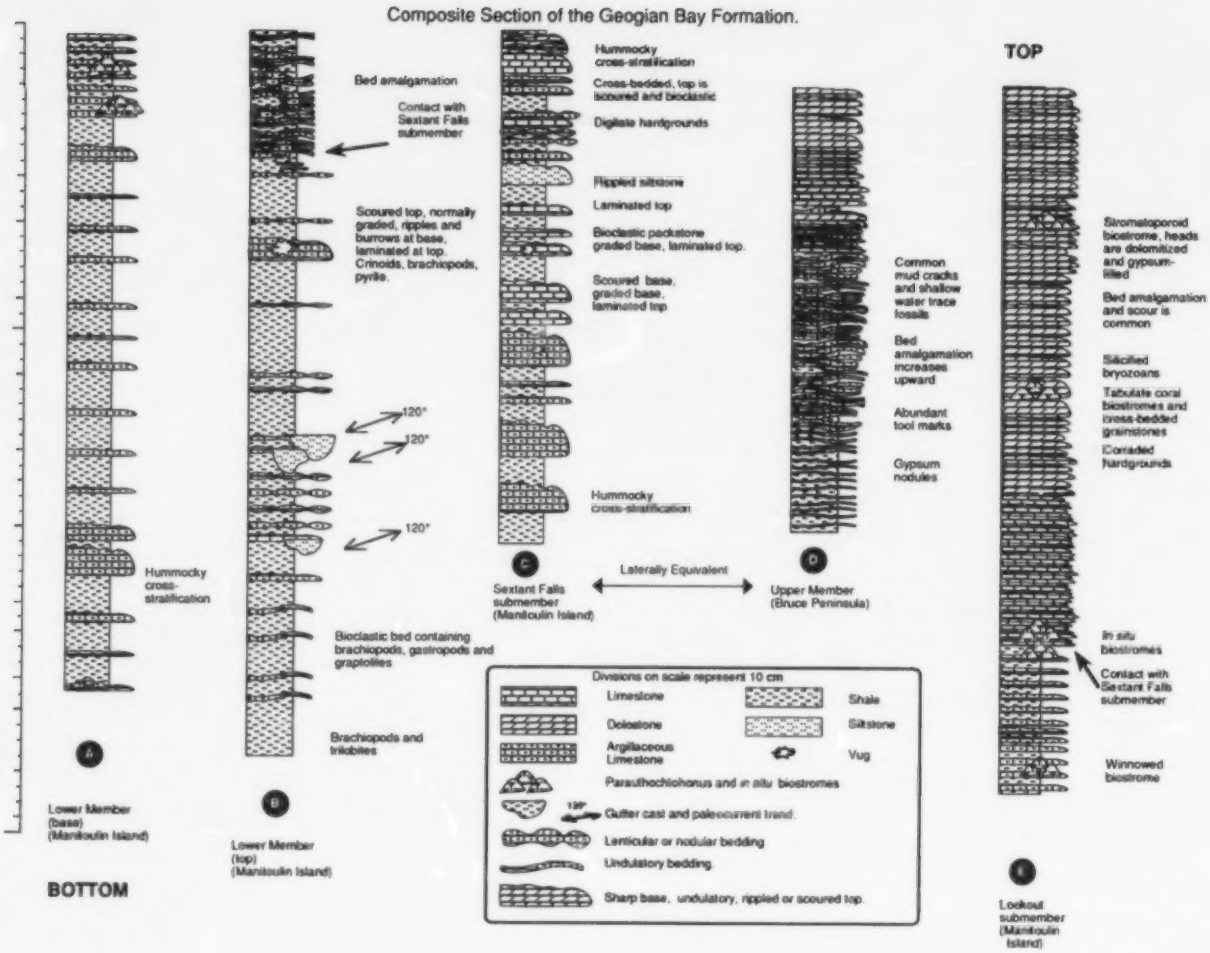

Figure 351.4. *Composite lithologic section of the Georgian Bay Formation. Various features, including unusual fossil occurrences, are described in marginal notes and are based on actual sections. Sections A-E are representative of the lithofacies in which they occur. The entire thickness of the formation is not indicated.*

Falls submember from the west to east. The base of the Georgian Bay Formation is poorly exposed, outcropping at only one locality on Manitoulin Island. It is not certain whether the regional thickness of the Lower Member changes.

Correlation of these strata to the Bruce Peninsula is possible only on a broad scale. The Clay Banks section at Meaford (Figure 351.2, 351.5) contains the Lower Member which is overlain by Upper Member strata (Sextant Falls submember equivalent) followed by the Queenston Formation. The equivalence of the Queenston Formation on the Bruce Peninsula and the Lookout submember of Manitoulin Island is difficult to demonstrate other than through their stratigraphic position.

SEDIMENTOLOGY

The Georgian Bay Formation can be divided into four main lithofacies. In ascending order these are: 1) finely laminated siliciclastic mudstones and siltstones; 2) interbedded bioclastic limestones and shales with minor biostromes; 3) argillaceous bioclastic limestones with minor biostromes; and 4) dolomitized bioclastic dolostones (Figure 351.4). Limestones include bioclastic wackestones, packstones and floatstones with grainstones being significant locally.

SEDIMENTARY STRUCTURES

A wide variety of primary sedimentary structures are seen within the carbonates of the Georgian Bay For-

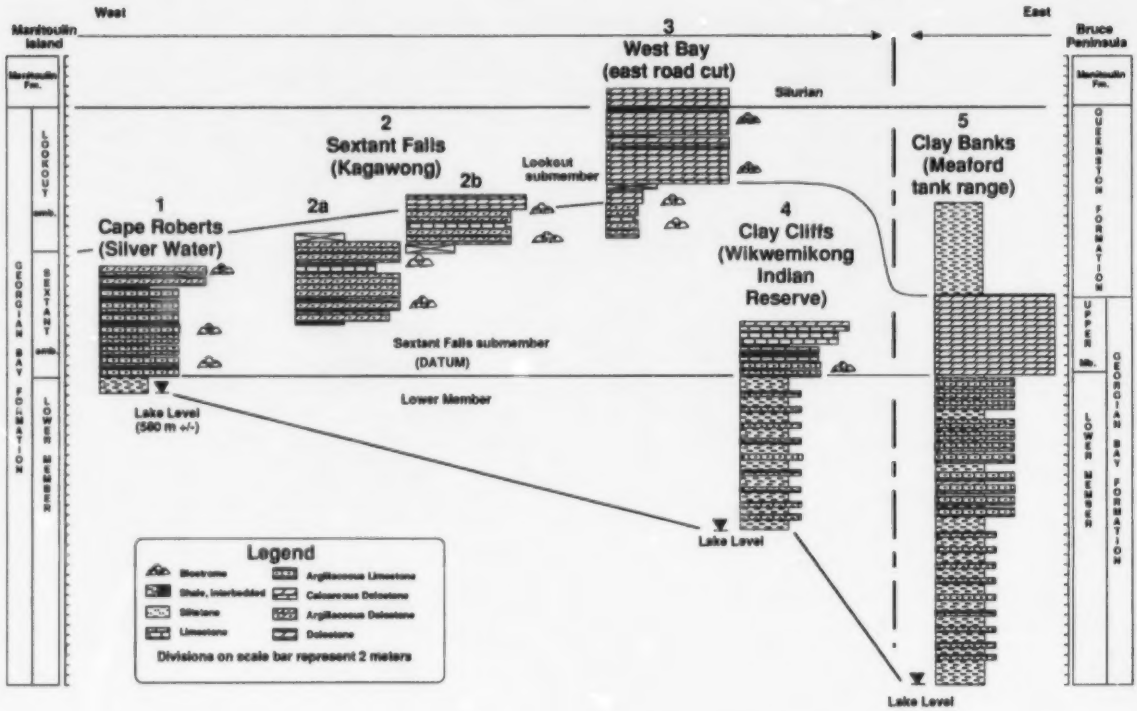

Figure 351.5. *Regional correlation of measured sections. Sections are located in Figure 351.2.*

mation. Scours, gutter casts with imbricated or graded fills and current-generated sole marks are abundant. Graded beds which fine upwards from bioclastic packstone to laminated siltstone and then shale are present but not common. Unidirectional paleocurrents measured from elongation of gutter casts, channels, current ripples and megaripples indicate southward flow. Orientation of wave ripple crests suggest east-west trending currents. Hummocky cross-stratification is rare but clearly displayed in a few outcrops. Distinct beds that are followed laterally can be observed to merge into single, amalgamated beds. Mudcracked and bioturbated surfaces occur near the top of the section on the Bruce Peninsula.

BIOSTROMES

Biostromes generally increase in thickness towards the top of the section. Two distinct types are recognized. The most common are winnowed and transported rugose and tabulate coral-bryozoan-brachiopod biostromes. These biostromes demonstrate considerable evidence of current action. Ramose bryozoans and rugose corals rest within the troughs of ripples; scattered beds contain imbricated bivalve and brachiopod valves; tabulate coral and stromatoporoid heads lie overturned; and elongate fossils, such as nautiloids, bryozoans and rugose corals, show parallel alignment. Fossils typically demonstrate little evidence of abrasion, disarticulation or bioerosion although rare rugose corals show borings. This suggests these biostromes were rapidly buried and represent parautochthonous accumulations rather than life assemblages.

Other biostromes consist of local, *in situ* accumulations of stromatoporoids with variable amounts of tabulate corals, gastropods and calcareous algae (*Girvanella* oncolites and encrustations and rounded nodules of *Solenopora*). In contrast to the winnowed biostromes, the abundance of hemispherical stromatoporoid heads in growth position suggest that these stromatoporoid-dominated biostromes were preserved as life assemblages. Fossil breakage indicates that periodically energetic currents must have disturbed the stromatoporoid community.

HARDGROUNDS

Hardgrounds are locally prominent in the upper Georgian Bay Formation. Two distinct hardground morphologies are recognized. Highly irregular, digitate hardgrounds occur within the interbedded shales and argillaceous limestones and dolostones of the Sextant Falls submember. Digitate hardgrounds exhibit numerous overhangs and pinnacles with vertical relief of 5–10 cm. Corroded hardgrounds with sharp truncated surfaces occur within pervasively dolomitized packstones and grainstones of the Lookout submember. Surface relief is typically less than

TABLE 351.3. TRACE FOSSIL OCCURRENCE AND LIFESTYLE (OSGOOD 1970; EKDALE *ET AL.* 1984).

Ichnofacies	Trace Fossil	Dwelling	Locomotion	Resting	Feeding	Escape
S	*Skolithos*	X				
S	*Skolithos delicatus*	X				
S	*Corophioides biclavata*	X				
S	*Corophioides cincinnatiensis*	X				
C	*Phycodes*	X			X	
C	*Chondrites type A, type B*	X			X	
C	*Trichophycus*				X	
C	*Rusophycus carleyi*			X		
C	*Rizocorallium*		X			
S	*Lockeia siliquaria*	X				
S	*Rhabdoglyphus*		X			
S	*Diplocraterion*	X				
C	*Tiechichnus*	X				
C	*Planolites*		X		X	
C	*Paleophycus*		X		X	
C	*Paleophycus striatum*		X		X	
C	*Paleophycus type C*		X		X	
?	Unlined vertical traces					X

S = Skolithos C = Cruziana

1–2 cm. Numerous vertical *Trypanites* borings approximately 3 mm in diameter and 4–8 mm deep truncate burrows and allochems.

TRACE FOSSILS

Trace fossils from the *Cruziana* and *Skolithos* ichnofacies are abundant throughout the Georgian Bay Formation (Table 351.3). Many burrows are unbranched and exhibit backfilling structures. Surface traces are more diverse than burrows.

DIAGENESIS

Several stages of diagenesis are currently recognized in the Georgian Bay Formation. The early stages of diagenesis in these strata comprise seafloor dissolution of aragonite, hardground cementation and precipitation of iron sulphides and silica. Silicification is restricted to portions of Manitoulin Island west of West Bay, whereas pyritization is limited to the Little Current area and the Bruce Peninsula. Late-stage dolomitization related to jointing occurs near West Bay whereas exposures at Janet Head show strong stratigraphic control on dolomitization. Later events include the precipitation of calcite, dolomite and gypsum cement in a variety of pore types.

INTERPRETATION

Sediments of the Georgian Bay Formation form a general shallowing upward sequence. The preservation of delicate traces on interference wave-rippled bedding surfaces at the base of the Lower Member of the formation indicates sedimentation below fair-weather wave base. Wave-rippled bioclastic grainstones/packstones in the overlying Sextant Falls submember contain no preserved surface traces. This is interpreted to reflect deposition in shallower water, probably above fair-weather wave base. In addition the Lookout submember contains abundant lenses of cross-bedded grainstone. Mud cracks and *Lockeia siliquaria*, the dwelling structure of an intertidal pelecypod, indicate intermittent subaerial exposure at the top of the section in the Bruce Peninsula. The lack of fine terrigenous material in the upper parts of the section can be explained through winnowing by frequent storm events that allowed clastics to bypass this shallow, agitated environment.

Recent studies of storm depositional systems (e.g., Kreisa 1981; Aigner 1985; Haines 1988) have shown that storms sporadically transfer large volumes of sediment between different shelf environments as well as transport nearshore sediments into deeper environments. Preliminary analysis of sedimentary structures, hardgrounds and biostromes in the Georgian Bay Formation on Manitoulin Island and the Bruce Peninsula demonstrates that deposition was significantly influenced by storms. A model for the deposition of tempestites in the Georgian Bay Formation based on Aigner (1985) is shown in Figure 351.6.

In the Georgian Bay Formation, gutter casts, cross-beds, scours and sole marks are interpreted to be the products of strong currents. Graded beds were deposited from waning currents. Hummocky

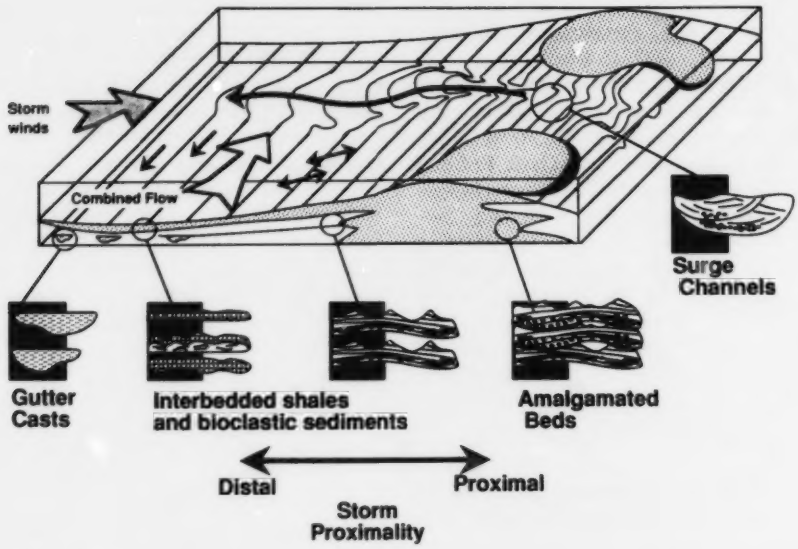

Figure 351.6. *Schematic diagram of seafloor topography, current paths and proximality trends for a storm-dominated, shallow, marine shelf (modified from Aigner 1985). Contours show bottom topography. Stippled areas are spillover lobes or shoals. The channel between the shoals was generated and maintained by the ebbing surge from set-up storm currents. Arrows represent idealized current vectors, those running parallel to the shoreline are geostrophic currents. Combined flow is the resultant of wind and wave vectors. The tops of the shoals and constantly winnowed areas are sites where hardgrounds are likely to form. The schematic sedimentologic profiles show the lateral changes in storm-generated structures. Note that bedding thickness, bed truncation/amalgamation, sediment grain size and flow energy all decrease with distance from shore.*

cross-stratified sediments were deposited at depths above storm wave base and below the limit of fair-weather wave base (Aigner 1985). Escape burrows are common throughout the entire formation. They cut entirely through single beds, confirming the tempestite origin of these layers.

Bed amalgamation in the Georgian Bay Formation is further evidence of storm activity. In shallower-water sediments at the top of the section, repeated storms could erode and rework sediments, amalgamating them into single homogeneous beds. In deeper water, the lower frequency and intensity of storm waves resulted in less common bed amalgamation.

Early seafloor cementation also played an important role in the depositional and preservational evolution of storm deposits in the Georgian Bay Formation. The formation of firm substrates that were resistant to mechanical and biological erosion influenced the faunal content of the sediment. Storm processes in turn assisted hardground formation (Aigner 1982, 1985; Brookfield and Brett 1988). Exposure of sediment surfaces by winnowing or creation of topographic relief increased pore fluid circulation and aided early cementation. Carbonate sediment production may also have been slowed by an influx of terrigenous muds leaving sediments for longer lengths of time in an active marine cementation zone.

SUMMARY

Preliminary analysis of the Georgian Bay Formation has shown that four dominant lithofacies comprise this formation. In ascending order these are shales, interbedded limestones and shales, argillaceous limestones, and dolostones. Scattered biostromes consisting of both winnowed and *in situ* fossil assemblages and hardgrounds punctuate the upper part of the succession. Lithostratigraphic correlation is possible across Manitoulin Island although it is more problematical across to the Bruce Peninsula. The general shallowing-upwards nature of this sequence is indicated by such features as preserved delicate traces in the lower part of the section and mud-cracked horizons near the top.

Sedimentary structures include various unidirectional current- and wave-generated structures that indicate a tempestite origin for many of the carbonate beds. Mixed carbonate and siliciclastic sediments such as the Georgian Bay Formation allow recognition of storm deposits more easily than in pure carbonate deposits. These storm features are better developed in the Lower Member and Sextant Falls submember where shale interbeds help define bioclastic storm tempestites clearly. Pervasive dolomitization in the Lookout submember and the high degree of bed amalgamation make storm beds more difficult to recognize.

RECOMMENDATIONS

Johnson and Telford's (1985) restatement of Liberty's (1957, 1968, 1969, 1972) stratigraphy was based upon drill core and a stratotype has yet to be established. We propose a composite stratotype based on stratigraphic sections located at the Clay Cliffs (Wikwemikong Indian Reserve), Cape Roberts (north of Silver Water), Sextant Falls (on Maple Point north of Kagawong), and the West Bay outcrop (road cut on Highway 540, east of the village of West Bay). The Clay Banks section at the Meaford Tank Range is suggested as the Bruce Peninsula reference section. The terms Wikwemikongsing, Meaford and Kagawong should be restricted to biostratigraphic use. Adoption of the informal nomenclature used in this report for the submembers of the Upper Member would avoid confusion with biostratigraphic units.

Future work will better define the relation between the informal Sextant Falls and Lookout submembers used in this report and earlier established lithostratigraphic and biostratigraphic terminology. Detailed petrographic analysis of tempestite and hardground layers will provide clearer recognition of the processes involved in their formation. Refinement of the proposed depositional model will assist in better understanding the origin of storm-influenced, mixed carbonate-siliciclastic shelf sequences occurring throughout the Lower Paleozoic of eastern North America.

ACKNOWLEDGMENTS

The authors thank J.L. Perron of Meaford Training Area of CFB Borden for granting safe access to sections within the Meaford Tank Range; the Chiefs and Band Councils of the Wikwemikong, Sheshegwaning and Cape Crocker Indian Reserves for permission to study their land; S. McRae and G. Huttinger for access to key localities on Manitoulin Island; and E.C. Jowett, University of Waterloo, for use of computer drafting facilities. Able field assistance was provided by J.S. Cameron. Funding was provided through Ontario Geoscience Research Grant 351 and Natural Sciences and Engineering Research Council funding to M. Coniglio.

REFERENCES

Aigner, T.

1982: Calcareous Tempestites: Storm-Dominated Stratification in Upper Muschelkalk Limestones (Middle Trias, SW Germany); p.180-198 *in* Cyclic and Event Stratification, edited by G. Einsele and A. Sielacher, Springer-Verlag, Berlin,.

1985: Storm Depositional Systems: Dynamic Stratigraphy in Modern and Ancient Shallow-Marine Sequences; Lecture Notes in Earth Sciences, Springer-Verlag, Berlin, 174p.

Bailey, B.

1984: The Hydrocarbon Potential of the Cambrian, Ordovician, and Devonian of Ontario; 23rd Annual Ontario Petroleum Institute Conference, Volume 23, 41p.

Bambach, R.K., Scotese, C.R. and Ziegler, A.M.

1980: Before Pangaea: the Geographies of the Paleozoic World; American Scientist, Volume 68, p.26-38.

Barnes, C.R. and Bolton, T.E.

1988: The Ordovician-Silurian Boundary on Manitoulin Island, Ontario, Canada; Bulletin British Museum Natural History (Geology), Volume 43, p.247-253.

Barnes, C.R., Norford, B.S. and Skevington, D.

1981: The Ordovician System in Canada, Correlation Chart and Explanatory Notes; International Union of Geological Sciences, Publication No. 8, 26p.

Brookfield, M.E. and Brett, C.E.

1988: Paleoenvironments of the Mid-Ordovician (Upper Caradocian) Trenton Limestones of Southern Ontario, Canada: Storm Sedimentation on a Shoal-Basin Shelf Model; Sedimentary Geology, Volume 57, p.75-105.

Caley, J.F.

1936: The Ordovician of Manitoulin Island, Ontario; Geological Survey of Canada, Memoir 202, pt. 2, p.21-92

1940: Paleozoic Geology of the Toronto-Hamilton Area, Ontario; Geological Survey of Canada, Memoir 224.

Coogan, A.H. and Parker, M.M.

1985: Six Potential Trapping Plays in Ordovician Trenton Limestone, Northwestern Ohio; Oil and Gas Journal, Nov. 26, p.112-127.

Copper, P.

1971: Geology of Manitoulin Island and Adjacent Islands; Field Trip 8, Geological Association of Canada - Mineralogical Association of Canada, p.1-37.

1978: Paleoenvironments and Paleocommunities in the Ordovician-Silurian Sequence of Manitoulin Island; p.47-62 *in* Geology of the Manitoulin Area, edited by J.T. Sanford and R.E. Mosher, Michigan Basin Geological Society, Special Paper No. 3.

Ekdale, A.A., Bromley, R.G. and Pemberton, S.G. (editors)

1984: Ichnology: Trace Fossils in Sedimentology and Stratigraphy; Society of Economic Paleontologists and Mineralogists, Short Course No. 15, 316p.

Foerste, A.F.

1912: The Ordovician Section in the Manitoulin Area of Lake Huron; Ohio Naturalist, Volume 13, p.37-48.

1924: Upper Ordovician Faunas of Ontario and Quebec; Geological Survey of Canada, Memoir 138, 51p.

Freeman, E.B. (editor)

1979: Geological Highway Map, Southern Ontario; Ontario Geological Survey, Map 2441.

Haines, P.W.

1988: Storm-Dominated Mixed Carbonate/Siliciclastic Shelf Sequence Displaying Cycles of Hummocky Cross-Stratification, Late Proterozoic Wonka Formation, South Australia; Sedimentary Geology, Volume 58, p.237-254.

Horst, R.

1978: Paleoecology and Stratigraphy of Late Ordovician (Ashgillian) Biostromes of Manitoulin Island, Ont-

ario; unpublished MSc thesis, Laurentian University, Sudbury, Ontario, 155p.

Johnson, M.D. and Telford, P.G.

1981a: Preliminary Results of 1980 Drilling Programme, Manitoulin Island Limestone-Dolostone Assessment Project; Ontario Geological Survey, Open File Report 5364, 44p.

1981b: Preliminary Results of the Northern Ontario Geological Survey Programme, Manitoulin Island Limestone-Dolostone Assessment Project; Ontario Geological Survey, Open File Report 5360, 81p.

1985: Paleozoic Geology of the Little Current Area, District of Manitoulin; Ontario Geological Survey, Geological Series Preliminary Map P. 2670, scale 1:50 000, Geology 1979-81.

Kreisa, R.D.

1981: Storm-Generated Sedimentary Structures in Subtidal Marine Facies with Examples from the Middle and Upper Ordovician of Southwestern Virginia; Journal of Sedimentary Petrology, Volume 51, p.823-848.

Liberty, B.A.

1957: Manitoulin Island, District of Manitoulin, Ontario; Geological Survey of Canada, Map 20-1957.

1968: Ordovician and Silurian Stratigraphy of Manitoulin Island, Ontario; p.14-37 *in* Guidebook for 1968 Annual Field Conference, edited by B.A. Liberty and F.D. Shelden, Michigan Basin Geological Society.

1969: Paleozoic Geology of the Lake Simcoe Area, Ontario; Geological Survey of Canada, Memoir 355, 173p.

1972: Little Current Area, Manitoulin District; Ontario Division of Mines, Map 2247, scale 1:63 360.

1978: Ordovician Nomenclature of Manitoulin Island; p.43-45 *in* Geology of the Manitoulin Area, edited by J.T. Sanford and R.E. Mosher, Michigan Basin Geological Society, Special Paper No. 3,.

Liberty, B.A. and Bolton, T.E.

1971: Paleozoic Geology of the Bruce Peninsula Area, Ontario; Geological Survey of Canada, Memoir 360, 163p.

Osgood, R.G.J.

1970: Trace Fossils of the Cincinnati Area; Palaeontographica Americana, Paleontological Research Institution, Ithaca, New York, 444p.

Russell, D.J. and Telford, P.G.

1983: Revisions to the Stratigraphy of the Upper Ordovician Collingwood Beds of Ontario—a Potential Oil Shale; Canadian Journal of Earth Sciences, Volume 20, p.1780- 1790.

Tobin, R.C.

1982: A Model for Cyclic Deposition in the Cincinnatian Series of Southwestern Ohio, Northern Kentucky, and Southeastern Indiana; unpublished PhD thesis, University of Cincinnati, Cincinnati, Ohio, 483p.

Williams, M.Y.

1937: General Geology and Petroleum Resources of Manitoulin and Adjacent Islands, Ontario; Geological Survey of Canada, Paper 37-25.